An Integrated Approach to Damage Ship Survivability Assessment

©Andrzej Jasionowski

The Ship Stability Research Centre
Department of Ship and Marine Technology
University of Strathclyde

Submitted as partial requirements for the degree of
Doctor of Philosophy, February 2001.

The copyright of this thesis belongs to the author under the terms of the United Kingdom Copyrights Acts as qualified by University of Strathclyde Regulation 3.49. Due acknowledgement must always be made of the use of any material contained in, or derived from, this thesis.

"We write in order to understand,
not in order to be understood"

- *C. Day Lewis, [213]*

Table of content

Appendix 1 Parameterisation of rigid body motion

Appendix 2 Validation studies on numerical predictions of intact ship hydrodynamics

Appendix 3 Study into the accuracy of modelling of damage vessel hydrodynamics

Appendix 4 Testing of survivability of the Passenger Ro-Ro vessel PRR1

Abstract

This research concentrates on damage ship stability and means for assessing dynamic ship performance in this state. A consolidation of many approaches for tackling damage ship dynamics has been undertaken, culminating in the development of a numerical tool for simulating ship behaviour while accounting for progressive flooding and the ensuing effects of floodwater motion. General features that have been accounted for in a new purposely developed numerical program PROTEUS3 include the following:

- Linear concepts regarding intact ship hydrodynamics based on strip theory and Rankine source method (RSM). These are further utilised by convolution and spectral transformations in deriving relevant time domain force realisations.
- Non-linear excitation/restoring forces calculated from pressure integration up to the instantaneous undisturbed wave profile.
- Non-linearities in hydrodynamic properties arising from variation of mean underwater geometry due to occurrence of non-stationary asymmetries in mass distribution are taken into account by a database approach.
- Forward speed in arbitrary heading.
- Progressive flooding through a ship with any internal subdivision and floodwater motion simulations based on free-mass-on-potential-surface (FMPS) model.
- Non-linear treatment of the effects of cargo shift or floodwater motions on the overall ship dynamic behaviour.

The underlying modelling has been explained by rigorous derivation of all the relevant equations from first principles. Validity of the model has been tested comprehensively through comparison with available physical model tests data. A thorough investigation on the new effects of modelling advancements concerning the accuracy of the developed model has been undertaken and the results are presented and discussed.

Despite the introduction of simplifying assumptions concerning floodwater behaviour, the predictions show consistency with physical experimental data. It is believed that this pragmatic approach constitutes a very efficient tool for predictions of vessel performance in extremely adverse conditions. This effectiveness has been demonstrated by undertaking forensic analysis of two of the most controversial accidents of the last two decades, namely the loss of MV Derbyshire and the MV Estonia disaster.

Acknowledgements

I would like to express my immense gratitude to many people that helped in making this dream come true. In particular I would like to single out my parents, Zygmunt and Mirosława, for life long support and love, my wife Kasia for friendship and love, my daughter Klaudia for just being there. She has turned this work into a sweet experience by spending countless hours on my knees in front of the computer and tirelessly asking the most philosophical of questions: "why?".

Professor Dracos Vassalos for his all-round-support, encouragement, friendship and most valuable hours of discussions.

Professor Maciej Pawłowski for his introduction to the most exciting science of ship dynamics in the undergraduate courses.

The University of Strathclyde for the studentship award.

All colleagues from The Ship Stability Centre for their fellowship.

Nomenclature

L, Lpp	Lift force, Ship length between perpendiculars
B	Ship beam
B_e	Linear viscous damping coefficient
T	time, period, ship draught
D	Rotation matrix, Ship displacement
CB	Block coefficient
D^*	Rotation matrix
M, M_s, M_w	Mass (total), ship mass, floodwater mass, cargo mass
m_i	Mass of a unit, e.g. particle, floodwater in compartment I
$\vec{F}$	A force (total) vector
f	Function of, or a force component
$\vec{M}_O, \vec{M}_A$	Moments vector (total) relative to a given point "O" or "A"
$\vec{P}$	Linear momentum
$\vec{K}_O, \vec{K}_A$	Angular momentum relative to point "O" or "A"
K_0	Wave number
K_{jk}	Impulse response function
K	Correction coefficient
$\vec{v}$	(Body) Velocity vector
$\vec{u}$	(Fluid) Velocity vector
$\vec{r}$	Position vector
i, j, k	Numerators
$\vec{i}, \vec{j}, \vec{k}$	Unit directional vectors
x, y, z	Coordinates
$\vec{\omega}$	Rotational velocity vector
ω_0	Circular frequency of incident wave
ω_E	Circular frequency of encountered wave
ω_φ	Natural roll frequency
λ	Wave length

I	Inertia matrix
ρ	Density of water
$\vec{n}$	Normal vector to a surface
$\vec{g}$	Gravity vector
μ	Viscosity coefficient
Φ	Fluid velocity potential (time dependent)
ϕ	Amplitude of fluid velocity potential (time independent)
p	Pressure
ξ	Free surface elevation
U	Ship speed
t	Time
G	Source strength
$S_F, S_B, S_+, S_-, S_\infty$	Control surfaces
$S(\omega)$	Wave energy spectrum
a_{jk}, b_{jk}	Sectional hydrodynamic coefficients (added mass, damping)
A_{jk}, B_{jk}	3D hydrodynamic coefficients for 3D hull (added mass, damping)
a_i	Amplitude of wave harmonic component
A	Denotation of amplitude
A^I	Amplitude of incident wave
A^R	Amplitude of reflected wave
A_F	Plan-form area
δ	Denotation of phase angle or boundary layer thickness
$\Re$	Real part of
q_j	j^{th} mode of motion
β	Ship heading angle, or fin attachment angle
$H(\omega)$	Impulse response function
$W(\omega)$	Windowing function
$y(t)$	Finite Impulse Response (FIR) function
C_d	Drift coefficient
C_c	Current coefficient

φ_A	Roll amplitude
C_L	Lift coefficient
R_N	Reynolds number
E	Stabilising fin effectiveness
α	Fin incidence angle
∇	Differential operator (space derivative)
$\frac{\partial}{\partial x}, \frac{\partial}{\partial y}, \frac{\partial}{\partial z}$	Space derivatives
$\frac{D}{Dt}$	Global time derivative
$\frac{d}{dt}$	Local time derivative

1 Introduction

Technical evolution, the result of untamed progression of humankind innovation, has grown at an ever-increasing rate in the last one hundred years, facilitating creation of the most complex engineering systems on one hand but leaving the implications of their widespread utilisation unexplored on the other. The lack of full disclosure of the consequences of technological advances has mainly been the result of a quest for economical benefits deriving directly from the performance and therefore treatment of the safety considerations as a secondary issue.

Perhaps, for clarity, it would be worthwhile at this stage to ponder on what safety means. As is generally perceived and recognised, the term "safety" does not have a plain definition derived from etymological considerations. "Freedom from danger", as the word is simplistically referred to in the Oxford Dictionary, does not encompass far-reaching scope of the expression nor does it specify a precise state in absolute terms, as it cannot do anyway.

Safety is the measure of the *relative* freedom from risks or dangers. Safety is the *degree* of freedom from risks and hazards in any environment. Safety is relative - nothing is 100% safe under *all conditions*. There is *no absolute safety* in mathematical probability terms. These quotes reflect just a few more attempts to apprehend the complexity of the meaning of the word in a single expression. Even narrowing any reference to safety as only made in the context of dangers deriving from utilisation of technology, as is intended in this thesis, one can hardly find satisfaction in these explanations.

It is because of this feeling of uneasiness pervading the public and demanding additional and new avenues to be explored that lead to evolution of a separate field of scientific endeavour aiming at making available any new scientific findings, knowledge, and methods of research devoted to the prevention of accidents by unveiling of their causes and consequences. The path, which finally led to the *Science of Safety*, constitutes an inevitable and necessary process, which now and in the future, must be carefully shaped and controlled as this discipline is still at the beginning of its development. An "infancy" state, as the progression of the science of safety could be reasonably described, derives from the fact that many basic concepts it must use have not been fully determined, neither have they been universally recognised. Whilst it is easy to suggest criteria, such

as "intrinsically safe", "safe by design", "fail safe", "safe by procedure", and so on, in practice the exact definitions and meanings of these are not always, indeed hardly ever, clearly definable.

In an attempt to address these disputable qualities, the ultimate goal of the science of safety sets to hold to an *absolute minimum* any damaging effects from handling modern technology, or, at least, to keep them within *tolerable limits*. In so doing, it is a special task of safety science to determine "the present state of the art in technology" under the aspects of safety and to submit it to critical examination. Science of safety, in short, is the research and doctrine of safety.

The principles of safety do not find straightforward implementations, however, even if derived from advanced scientific considerations, due to afore mentioned debatable nature of the levels of safety educing from its relativity. It is the economical implication of safety enhancements that leads to safety relativity in the societal perception sense, as is demonstrated in Figure 1.

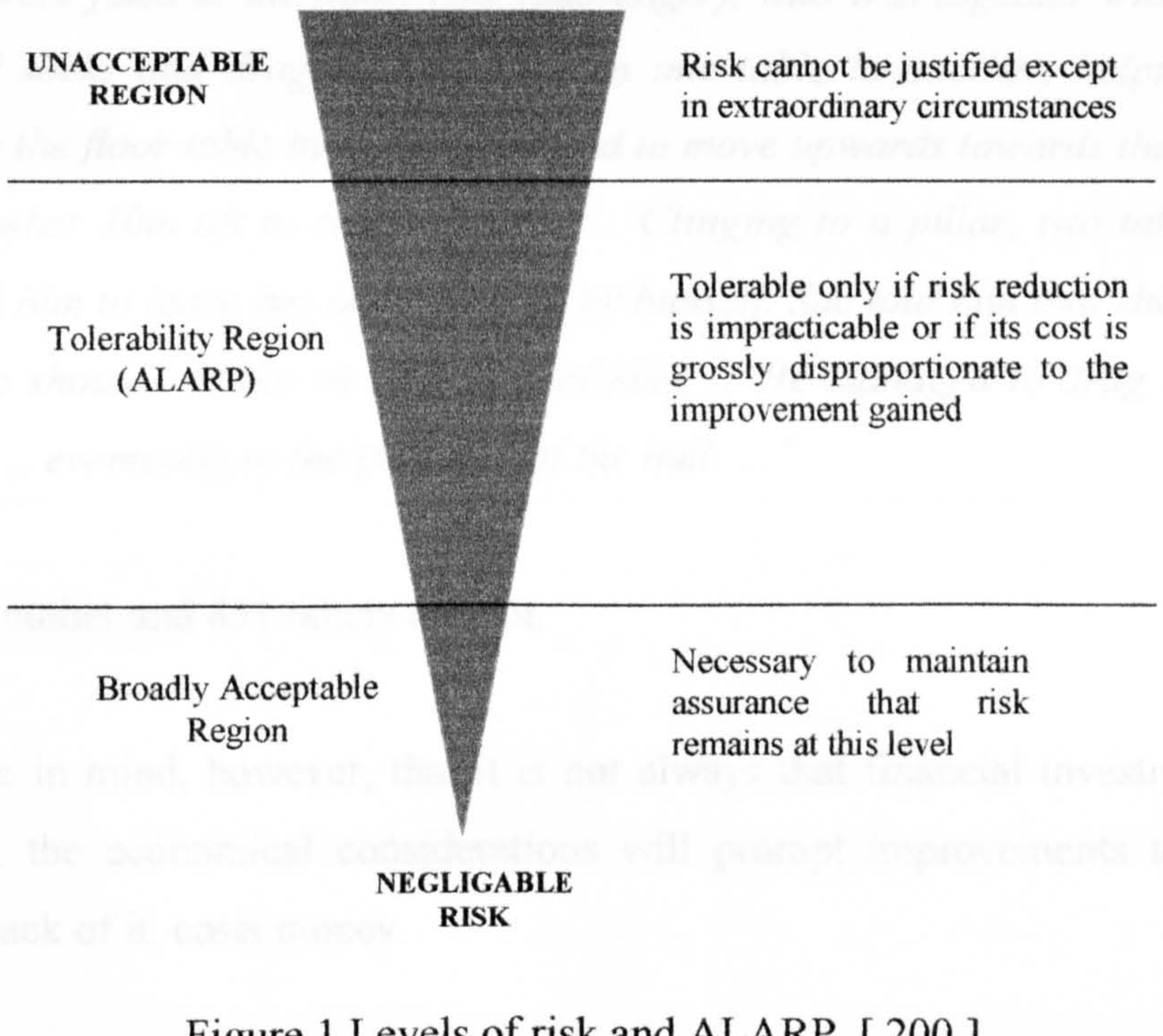

Figure 1 Levels of risk and ALARP, [200]

Although, the intuitively preferable frequency of any hazard state and consequences of it materialising are that of the "NEGLIGABLE RISK", to achieve an economically viable design, a compromise must be established. This compromise constitutes the *acceptability* of a given safety level and is mostly a result of debate between ethical and economical considerations.

It is a fact that the ethical considerations as derived from human psychology have always been motivated mostly by accidents of catastrophic nature, distinctive example being that of ship disasters. The established explanation lies in the fact that the difference in the psychological reaction between one, ten or one thousand people being killed simultaneously due to the same cause and in the same place is highly non-linear.

Light could be shed upon the ethical aspects by the following excerpt from the report on one of the most tragic maritime accident of the last decade, [188], which also highlights a need for critical revision of the safety levels currently prevailing in the world-wide shipping industry. To elucidate the scale of the problem it is also worth mentioning that about 1500 marine accidents and dangerous incidents to vessels and personnel are reported each year in the UK alone, [210].

" ...A few (passengers) lay down on the floor and started to drag themselves up to the doors using the tables which were fixed to the floor. One (passenger), who was together with his mother, took off his shoes and socks and dragged himself from one table to another, helping his mother by pulling her across the floor table by table. They had to move upwards towards the centre line of the ship and then another 10m aft to reach a door. ... Clinging to a pillar, two tables from the port doors, she begged him to leave her and continue by himself. She told him that she did not have any more strength. He shouted at her in vain to continue. ... He managed to drag himself out to the open aft deck and ... eventually to the port side of the hull. ... "

He survived. His mother and 851 others did not.

It should be borne in mind, however, that it is not always that financial investments limit safety, quite the reverse, the economical considerations will prompt improvements towards safety, as safety, particular lack of it, costs money.

Avoiding engaging in any further moralising about the relative merits of duty and inclination, it is worth to summarise that safety is an entity subject to design, where common sense optimisation procedures seeking compromise between a series of conflicting determinants, is the engine towards future safety enhancements in a cost-efficient manner. Such balancing of cost, efficiency, reliability, time and other constraints with regards to safety is, however, a very complex process and general methodologies, especially applicable in naval architecture, have only recently started emerging, not

least because of their elaborate and interdisciplinary character, but also because of the prevailing design philosophies. Safety in ship design is treated superficially, for being a minimum requirement of rule-conformant it is not an integrated part of the design process, and therefore by approach ships are not safety-oriented and safety-optimised.

This currently dominant deterministic approach is directly challenged by statistical deductions, which demonstrate that most of the accidents are caused by an event or physical phenomenon entirely predictable at the concept design stage. Therefore it is the design stage where the safety must be inherently catered for, see Figure 2.

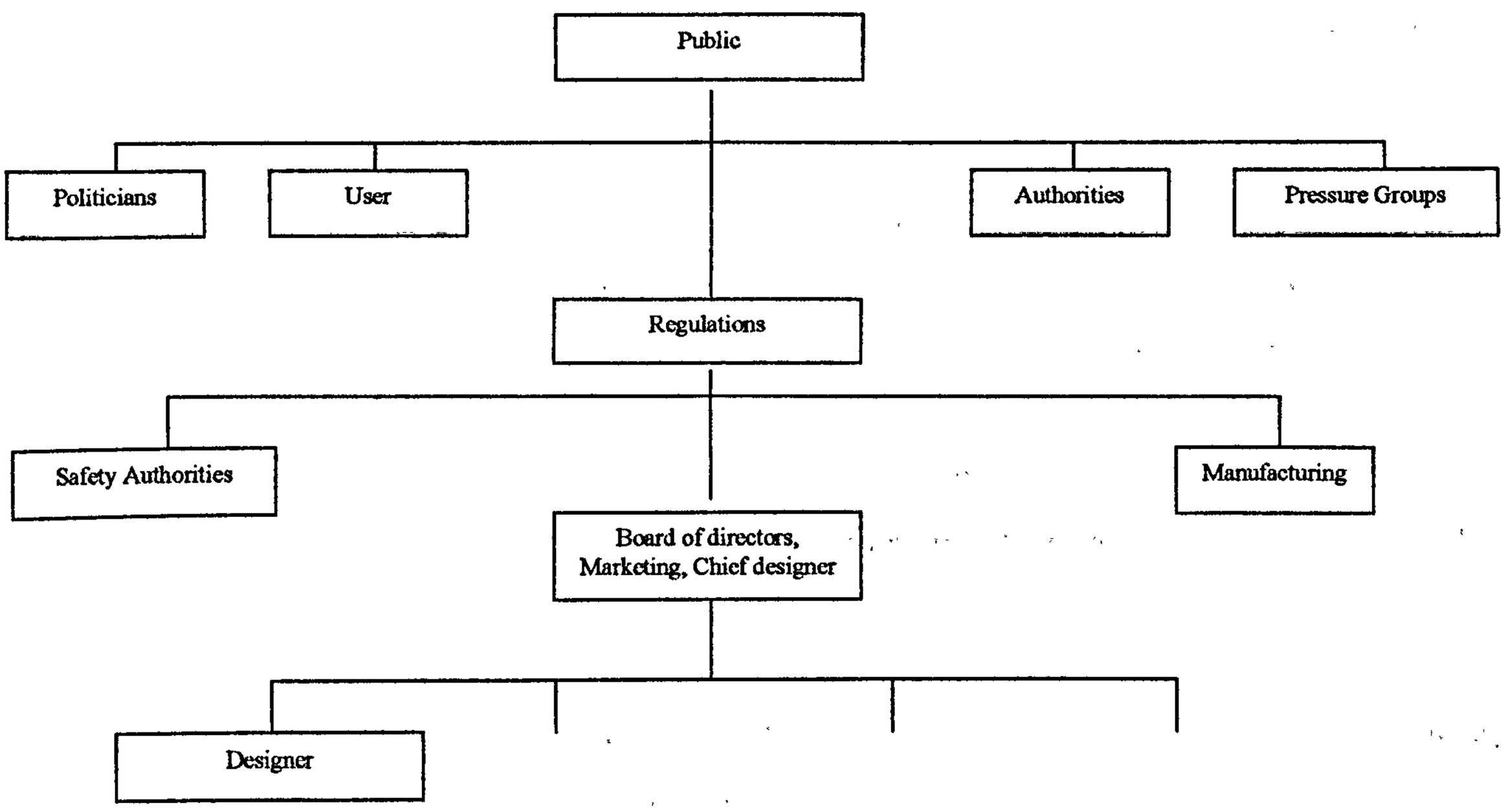

Figure 2 Safety comes down to the designer "in the end", [199]

Designers should use available methods to recognise the hazards inherent in their design, and design the hazards out of the ship. Safety should be designed into a ship right from the start, rather than being tackled after accident data have pointed out the designer's original mistakes. Therefore the key to safety is a proper design, where the recognition of hazards and determination of levels of severity in the early design stages is one of the primary themes of the design process.

Prime example of this philosophy advocated for ship design is the *Design for Safety* as demonstrated by practical implementation in an integrated software environment (blackboard system), [207], where the emphasis put is on linking three interdependent actions allowing safety to be inherently catered for during the design stage. These are:

(a) Safety performance prediction through the utilisation of appropriate technical tools.
(b) Safety assessment deriving from risk-based methodologies.
(c) Disparate design activities and issues.

Association of these three elements permits formalisation of the design for safety methodology, which by adopting iterative solution scheme allows for balancing between different performance qualities (resistance, seakeeping, survivability, structural design, passenger evacuation, stability, etc.) while efficiently compromising between risks and costs.

It is important to emphasise again that the mentioned risk assessment addresses both the frequency and consequences of an undesirable event occurring and risk reductions would involve both of these elements. Obviously since the level of reduction relates to costs some acceptance criteria need to be established. It is postulated in [207] that although the level of risk can be reduced by reduction in frequency of occurrence of undesirable events (mainly fatality), there will be a level of consequences that cannot be tolerated. Therefore some maximum tolerable consequences must also be defined.

In view of the above reasoning it becomes clear that technical tools for performance assessment, also applicable for estimations of consequences must be developed.

This thesis sets to actively support the evolution of the above discussed goal of implementing safety in a ship at the design process by providing designers with high level consequence analysis tools for assessment of ship dynamic stability while in limit state conditions and exposed to extreme environments.

Full use will be made of the knowledge generated since 18^{th} century, which by integration into a specific model addressing ship dynamics, will form the core of the delineated safety assessment methodology and therefore contribute to the increase of quality and safety of life.

Following the renowned early works of Newton, Euler, Froude, Stokes, Green, Rayleigh and other advancers of mostly fundamental sciences, an era of modern approaches to ship dynamic response in a random seas can be distinguished with an advent of the superposition principle by St Denis and Pierson in 1953. This was followed by the first ship motion theories suitable for numerical computing introduced in fifties, notably by Grim or Korvin-Kroukovsky and Jacobs in 1957. Middle of the century has seen countless number of such advances contributing to developments of intact ship motion prediction tools: multipole expansion method of Ursell 1949, Kim's application of the Ursell's method to Lewis forms in 1969, close-fit method of Frank, 1967, 5dof strip theory with forward speed of Salvesen at al 1970, pioneering calculations of 3D hydrodynamics of semi-submerged heaving sphere by Havelock in 1955, first successful applications of an integral equation techniques in 3D by Hess & Smiths in 1958 or Yeung application of this method for arbitrary 3D bodies oscillating on free surface in 1970.

It is eighties that can be considered the time of extended efforts on numerical modelling of the dynamics of ships in waves in flooded conditions, such as techniques to deal with water on deck developed by Dillingham in 1981, or Turan numerical model of Ro-Ro vessel dynamic stability and survivability, 1993. The latter approach, has attracted great interest from the ferry industry, who were keen on seeking optimal stability-criteria-conforming design and cost-effective retrofitting solutions to meet new strict rules.

Such numerical treatment of damage stability is deemed to evolve into a viable alternative of physical model testing, once fuller understanding of the overly complex processes involved in ship foundering is gained and reliable methods for modelling them become adequately validated. Henceforth these tools, by achieving widespread utilisation in routine design practices would contribute significantly to ship safety improvements, as by enabling systematic identification of stability deficiencies and survivability assessment, they would allow safety to become an inherent feature of new designs.

This research addresses fundamental advances in modelling techniques achieved in the pursuit of the aforementioned goals, by detailed explanation of the underlying theoretical considerations. In so doing, after statements of aims in §2, literature review in §3 and an outline of the approach adopted in §4, the first technical chapter §5 Ship dynamics, explains principles adopted in modelling of floodwater or cargo shifting effects on the ship behaviour. §6 Ship hydrodynamics, addresses in great detail the issue of modelling of ship hydrodynamics for a damaged ship whilst §7 Internal

effects, explains key points in modelling actual motions of floodwater or cargo shift. Key aspects of numerical implementation are discussed in §8 Numerical algorithms. Finally §9 demonstrates validation studies undertaken to provide confidence in the use of the developed tools, together with its practical application. §10 offers a review of the research presented in this thesis and §11 concludes the study performed.

2 Aims of research

The primary aim of this research work is to *advance* the existing state-of-the-art in mathematical modelling of the dynamic behaviour of damaged ships undergoing progressive flooding and exposed to random extreme seas by addressing the key elements pertinent to limit state performance in these conditions.

Building on the wealth and variety of available knowledge and experimental data concerning predictions of ship performance, the specific objectives of the project are formulated as follows:

- To resolve existing ambiguities in the development of the generalised mathematical ship motion model.
- Enable the model to account for speed effects by including the relevant non-linearities arising in the equation of ship dynamics.
- Model cargo shifting as a dynamic phenomenon, taking place during extreme motions.
- Develop a methodology for simulating ship response when exposed to extreme environmental conditions whilst accounting for extreme undesirable events.
- Develop techniques for predictions of internal fluid motions allowing for interactions with ship dynamics.
- Study the effects of these advancements on the quality of ship performance assessment by comparison with experimental data.
- Demonstrate through case studies the potential and practicalities of the developed tools.

Deriving from the above stated aims the review of the relevant literature available is carried out in the next chapter.

3 Literature review

Exploration of the published literature pertaining to the aims of this work, can only be addressed to a greatly limited extent given the enormity of the progress that has been achieved as regards ship dynamic responses in a seaway in intact or damaged conditions. Therefore, rather selective appraisal was completed, targeting mainly key issues deemed of fundamental importance in meaningful representing phenomenon of ship dynamics. Three general themes encompassing such details were identified as is discussed below.

3.1 Predictions of interactions between ship and the external fluid

Modelling techniques of the interaction between the fluid and the submerged rigid hull is the very essence of a science of predicting motions of a ship in seaway, or shortly seakeeping theory. The literature, [27] - [76], addressing the subject of ship hydrodynamics, the prime element of ship motion predictions process, provides a plethora of choices for application purposes with varying degree of prediction accuracy and modelling complexity. Only the theories deriving from the assumption of an ideal fluid model will be discussed here.

There are two types of approach for prediction of the interactions between ship and sea that can be distinguished: classical seakeeping theory based on linear potential flow and the recent advances in explicit time domain simulations, accounting to some extent for body-geometrical and free surface non-linearities.

The origin of classical seakeeping theory could be attributed to the work of Grim [38], and Korvin-Kroukovsky and W.R. Jacobs, 1957, who provided the first usable method for calculating the coupled heave and pitch motions of rigid ship in regular, deep water sinusoidal waves, [42]. Their pioneering approach used slender-body theory as a basis for predicting the hydrodynamic properties of a series of sections (strips) along the rigid hull of a vessel. The ensuing "strip theories", most classical examples being [50] or [66] developed on the basis of scientific and pragmatic considerations, [42], have evolved to an adequate level for practical use within a range of parameters deriving from the inherent assumptions. The most recent review of the slender body theories has been presented in [48] together with some discussion on their accuracy, see Figure 3.

Theory	Applicable region
Strip Theory	**2**
Rational Strip Theory	**2,3**
High Speed Slender Body Theory	**2,3,4**
Unified Theory	**1,2**

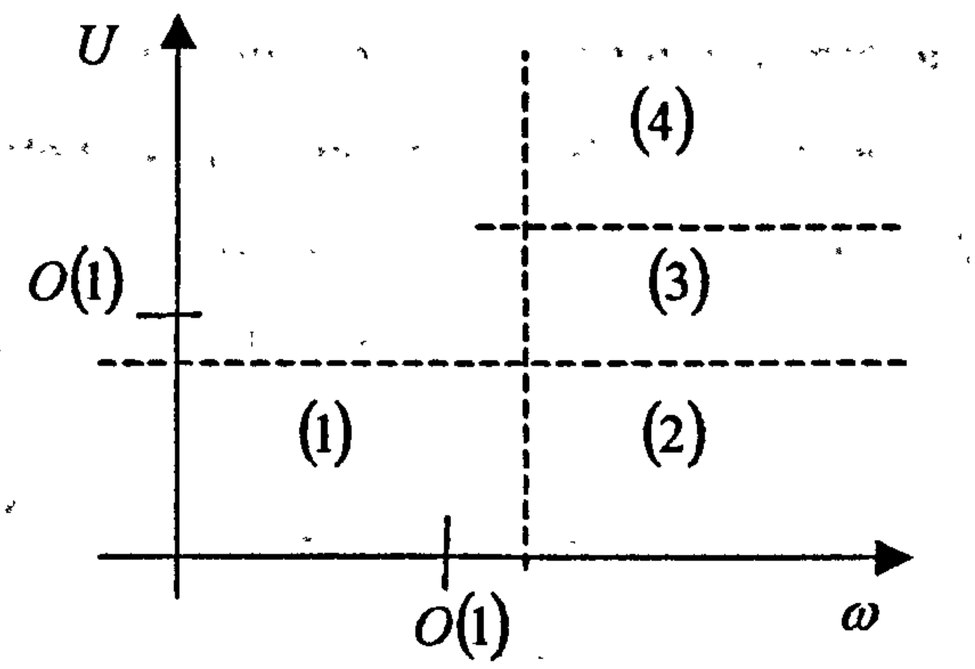

Figure 3 Order of parameters valid for various slender body theories, [48].

The free surface boundary condition $\left(i\cdot\omega_E - U\cdot\frac{\partial}{\partial x}\right)^2\phi + g\cdot\frac{\partial\phi}{\partial z} = 0$, can be considered in order to highlight recommended limitations of strip theories, which should not be applied when the expression containing operator $\frac{\partial}{\partial x}$ in the first part of this equation becomes predominant. Firstly large values of the gradient operator itself (blunt-shaped ships) would directly violate the main assumption of small longitudinal gradient of the velocity potential. High speed would accentuate this expression even if the longitudinal gradient of the velocity potential was small. Low frequency range, $\omega_E \sim 0$, renders the first expression very small in comparison to the second one. Therefore, most of the strip theories should not be applied for cases of high speed, to hulls that are not slender or for long waves. Note, however, that in the latter case hydrostatic forces dominate the motions and therefore the error in using strip theories at low frequency is negligible. Also the reported success of strip theories, e.g. [47],[48],[50], to predict motions at zero to low speeds even for non-slender hull forms supports the robustness of the strip theories and their practicability for ship motion predictions.

To summarise it is worth underlining that the main source of any inferiority in the prediction of ship hydrodynamics by strip theory as compared to more sophisticated 3D-based approaches derives from the inherent assumption of small longitudinal gradient of the velocity potential as well as no interaction between the vessel strips (longitudinal component of vector normal to body surface ignored and velocity potential solved separately for each strip). Figure 4 to Figure 6 demonstrate quantitative comparison between different approaches mentioned in Figure 3, 3D techniques and

experimental results, [48]. As exemplified by the radiation coefficients in yaw in Figure 4 for the zero speed case, the unified theory overcomes any deficiencies deriving from these assumptions. Furthermore, the enhanced unified theory of [48], validated for low speeds (Fn<0.3-0.4) takes into account the 3D wave diffraction effects in x-direction near the ship ends. In case of higher Froude numbers (Fn>0.3-0.4) the high-speed slender-body theory seems to be adequate, Figure 6.

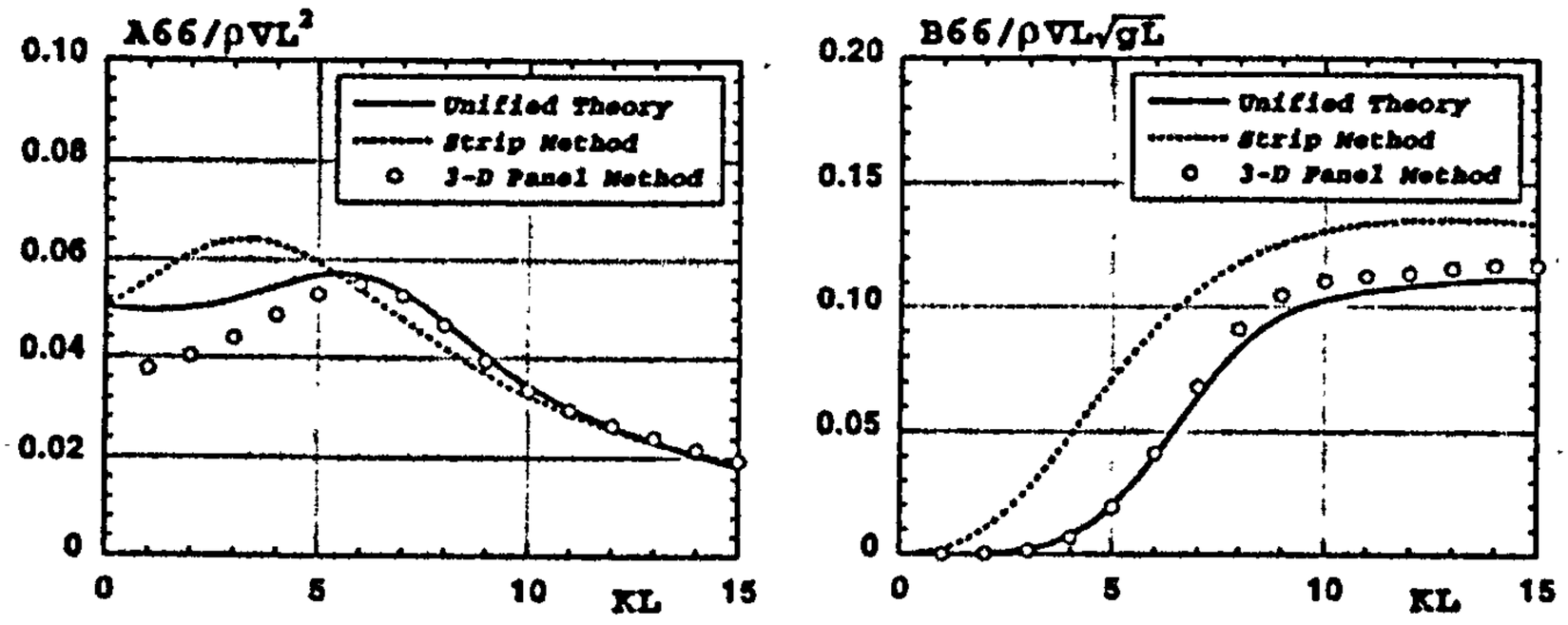

Figure 4 Added-moment of inertia and damping coefficient in yaw of a half-immersed spheroid of L/B=5 at zero speed, [48]

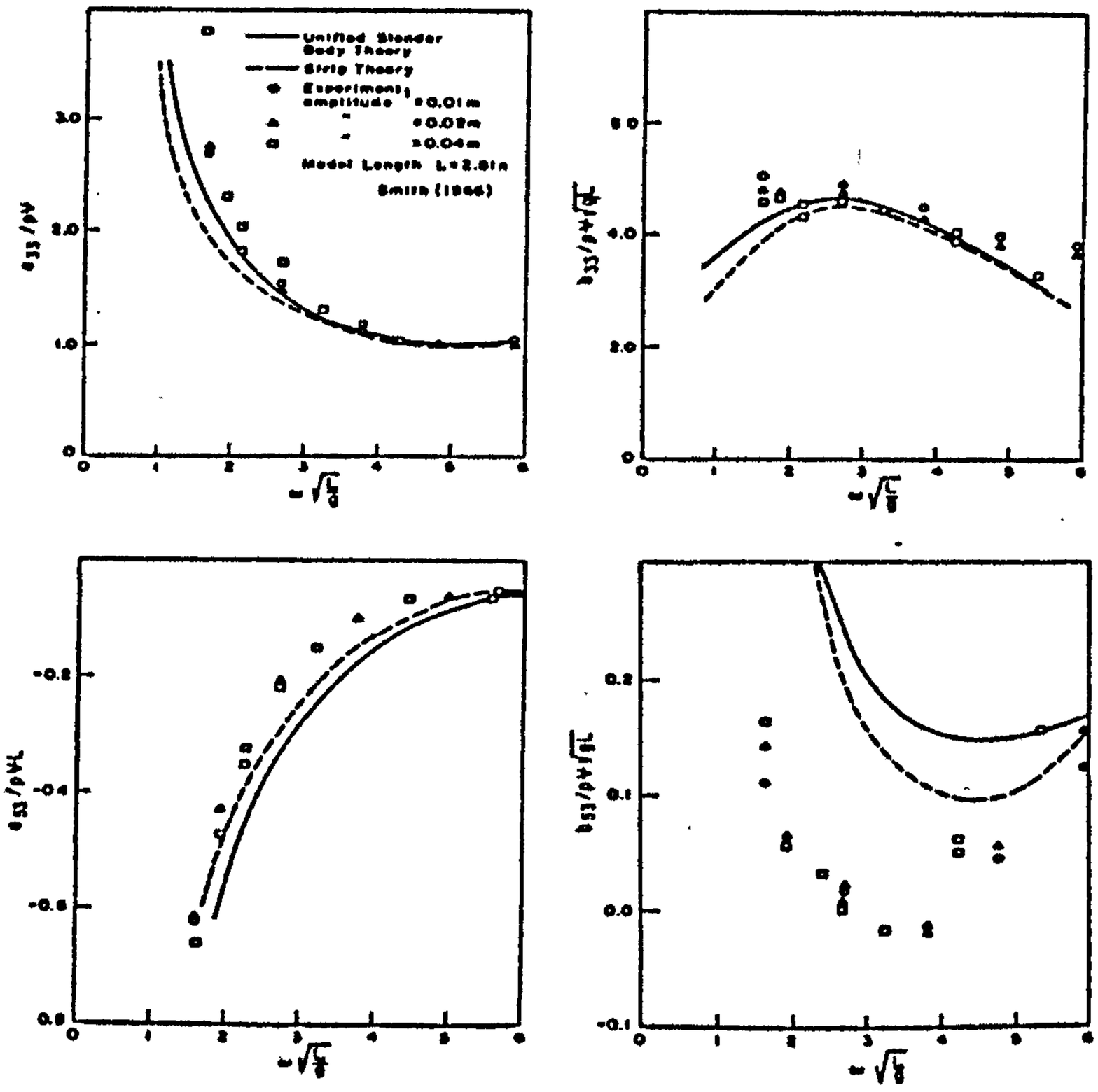

Figure 5 Radiation force coefficients of a frigate hull (CB=0.55) due to heaving at Fn=0.35 (computed by Newman and Sclavounos (1980) using unified theory), [48]

It can only be concluded that strip theories shall be recognised as practical calculation methods.

As can be found in some published studies, strip theories have even found application for predictions of the effects of the damage opening on the flow over the hull. In the work presented in [127], a strip method with the hull bound perturbation flow concept is used to predict hydrodynamic pressure on the hull surface for a damaged ship in a seaway, in which a two dimensional Green function approach is applied to determine flow parameters around hull sections including normal and damage sections. The main aim was prediction of the wave loads encountered by the damaged ship hull. The computational results showed that these loads are of identical order as for the intact ship case. This implies little effect of the opening on the fluid flow over the hull in oscillatory vessel motions. This research, however, has not been backed up by any experimental data.

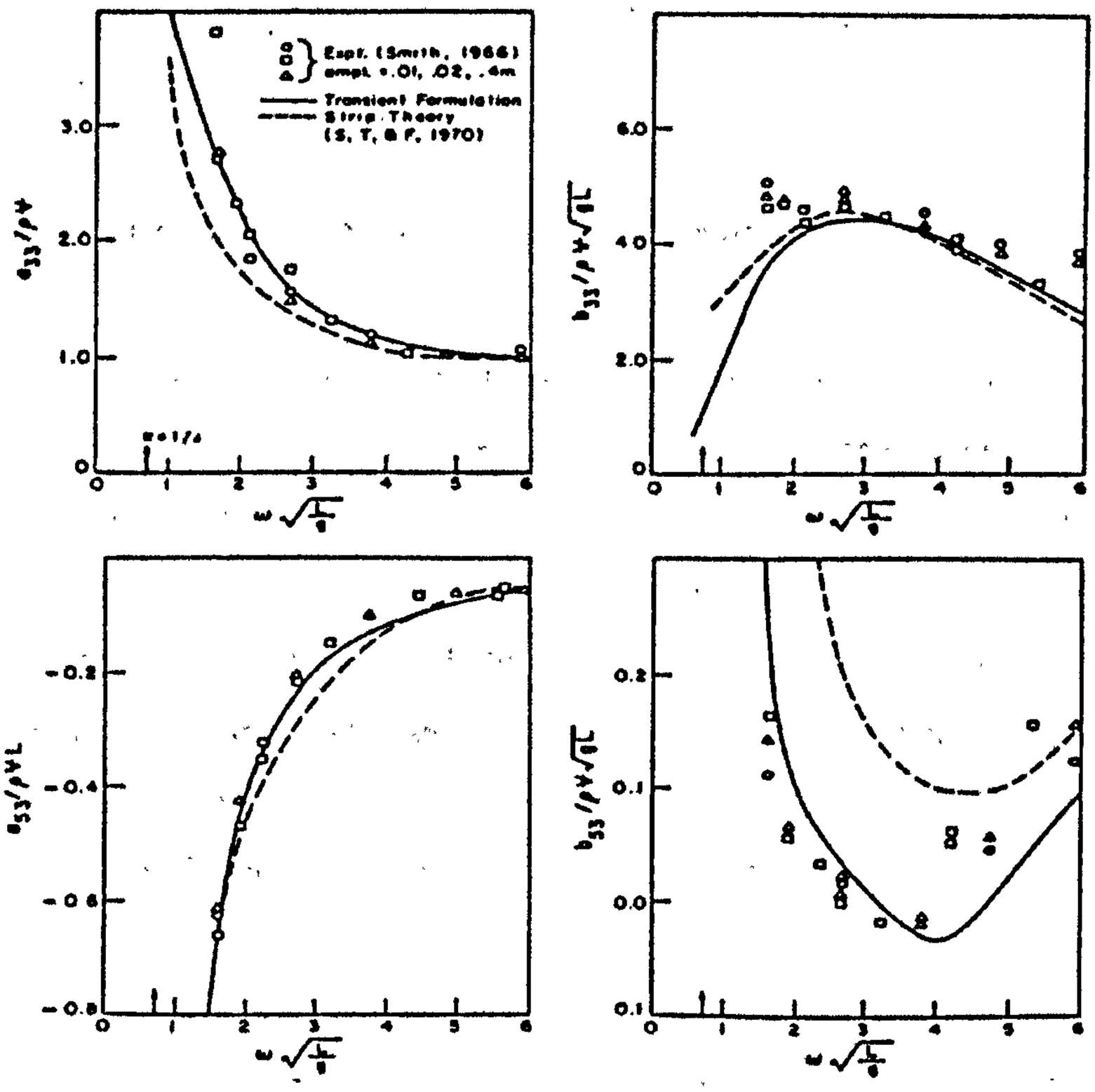

Figure 6 Radiation force coefficients of a frigate hull (CB=0.55) due to heaving at Fn=0.35 (computed by Yeung and Kim (1981) using high-speed slender-body theory), [48]

The recently emerging class of solutions to the problem of hydrodynamics due to interaction between floating body and fluid, performed explicitly in the time domain, can be further divided into two techniques: one employing complex time-dependent pulsating source distribution and the second relying on Rankine singularities. Prime example of the first application is the work [28] where studies into transient motions of floating bodies at zero speed have been performed. The method allows taking into account geometrical non-linearities arising from large amplitude motions but linear free surface condition is retained. Techniques with Rankine source distribution, for instance [31], [32], [37], allow in principle to account for all of the non-linearites including those of the free surface condition and therefore become more and more popular, [77]. In fact potential flow predictions based on Rankine source distribution have recently been applied in work of [49] for studies on hydrodynamics of a damaged ship involving instantaneous water ingress/egress, where the mixed Eulerian-Lagrangian (MEL) time stepping technique is used to predict linear hydrodynamics of the hull and the interaction between the internal and external fluid flows in time domain simulation is achieved by domain partition. The approach has been successfully compared with experimental data.

3.2 Hybrid time domain motion simulations and ship damaged state

The time-domain solutions of the mentioned type, however, have a common feature preventing them from widespread application in routine design practices. Namely, they are both difficult to use, require extensive pre- and post- processing effort, and are computationally demanding.

Therefore, to resolve the problem of predicting ship behaviour in a seaway in an efficient yet considerably meaningful manner, another class of approaches evolved based on what can be referred to as hybrid modelling. The problem is solved in two steps: predictions of ship hydrodynamics based on linear potential flow theory, and then via spectral and convolution techniques (impulse response function) a general non-linear model of ship dynamics is set and solved in time domain. A comprehensive overview of the state of the art concerning modelling of intact ship dynamics in this fashion available in 90s is given in [95], where common resolutions to many problems in such modelling are discussed.

Early application of this motion prediction technique in developments addressing assessment of the effects of water on deck on the vessel motions were undertaken by Dillingham [146], where the seakeeping characteristics of a small fishing vessel with large flat deck and possibility of water ingress/egress were investigated. The vessel was considered as a two-degree-of-freedom system and the equations of motion in sway and roll were formulated in the time domain using the mentioned impulse response technique. An approximate solution to a non-linear hyperbolic system of equations describing the flow of the water on deck was obtained numerically using the random-choice method, also known as Glimm's method. From this solution the static and dynamic forces exerted on the vessel by the deck water were computed and then added to the external wave excitation forces to obtain a complete time-domain solution for the motion of the vessel and the deck water. Water ingress/egress was modelled by Bernoulli's equation with empirical discharge coefficient. The model was successfully verified by available experimental data.

Another such approach focusing more on the ro-ro type damage ship survivability was developed by [117] where the hydrodynamic reaction forces were taken for one frequency, corresponding to the peak of the sea spectrum, and the linear excitation was simulated based on the spectral approach. The water ingress/egress was again modelled by Bernoulli's equation with a purposefully derived coefficient. The linearised equations of sway-heave-roll motions were solved simultaneously with a simplified floodwater motion model, where the latter was based on two assumptions: that the free surface is flat and it rotates in phase with the ship rotations. Gravity forces as well as change in inertia due to the floodwater were accounted for. Despite great simplicity of the approach, the numerical simulations were used to derive the physical measure of ship resistance against capsize in terms of significant wave height, the boundary survivability curves, [134], and successfully compared with experiments.

Different hybrid combination was employed in [138], where again the focus of the research was to determine the vessel's dynamic response when water is present on deck. A numerical 3DOF ship motion model, sway-heave-roll, was built, where the fluid forces were derived based on linear strip theory, and the water sloshing was simulated by means of the non-linear shallow water wave equation solved by random choice method (Glimm's method). Although the model was only developed for testing in regular harmonic waves, useful conclusions were drawn. Correlation of numerical predictions of ship responses with experiment was also shown.

An interesting reasoning on the dynamics of a ship with flooded compartments in a seaway was presented by [135], the aim of which study was the discussion of peculiarities of the analytical calculation technique for predicting the forced motions of a ship with flooded compartments in regular beam waves. Three types of compartment flooding were considered namely fully flooded, partially flooded and compartment with an opening to the sea. It was assumed that three-degree of freedom (sway-heave-roll) harmonic ship motions and liquid sloshing in flooded compartment are linear. The linear hydrodynamic coefficients in the equations of ship motions were considered for geometry resulting from asymmetrical flooding. The essence of the technique was introduction of additional terms (corrections) in frequency-domain equations of motions due to floodwater mass motion as well as variation. The analytical corrections addressed inertia, restoring (in terms of metacentric height), damping as well as wave excitation. The results presented correlated with the experiment.

The model introduced by [119] and detailed later in [120] was the first known attempt to take into account all six degree of freedom ship motions, whilst in damaged state. Building on the experience of [117], the model featured linearised to some extent general set of ship motions equations with terms accounting for derivatives of mass variation. The model in the form of two vectors for linear and angular motions is summarised below:

Linear	Angular
$M_w \cdot \left[\frac{d}{dt} \overrightarrow{v_{GsGw}} + \left(\frac{d}{dt} \overrightarrow{\omega} \right) \times \overrightarrow{r_{GsGw}} \right] +$	$M_w \cdot \left[\overrightarrow{r_{GsGw}} \times \left(\frac{d}{dt} \overrightarrow{v_{GsGw}} + \frac{d}{dt} \overrightarrow{v_{Gs}} \right) \right] +$
$+ \left(\frac{d}{dt} M_w \right) \cdot \left(\overrightarrow{v_{GsGw}} \right) +$	$+ \left(\frac{d}{dt} M_w \right) \cdot \left[\overrightarrow{r_{GsGw}} \times \left(\overrightarrow{v_{Gs}} + \overrightarrow{v_{GsGw}} \right) \right] +$
$+ \left(M_s + M_w \right) \cdot \left(\frac{d}{dt} \overrightarrow{v_{Gs}} \right) + \left(\frac{d}{dt} M_w \right) \cdot \overrightarrow{v_{Gs}} = \vec{F}$	$+ \left(I_s + I_w \right) \cdot \frac{d}{dt} \overrightarrow{\omega} + \left(\frac{d}{dt} I_w \right) \cdot \overrightarrow{\omega} = \overrightarrow{M_{Gs}}$

(1)

The floodwater ingress/egress as well as the fluid behaviour was modelled in similar manner as [117]. A step forward was made in an attempt to account for non-linearities due to hull asymmetries arising from progressive flooding and asymmetric floodwater distribution. This has been tackled by a DATABASE approach, whereby a set of hydrodynamic forces and coefficients are pre-calculated from the aforementioned linear potential flow theory and the corresponding

values are instantaneously interpolated from the storage. No firm conclusions have been reached as to the effect of inclusions of these non-linearities other than that they are qualitatively small for a typical mono-hull vessel. Also, no distinctive differences between [120] and [117] in derived aggregate result of ship survivability predictions were obtained.

Another development addressing full six-degrees-of-freedom ship motion in irregular seaways model was presented by [94]. The simulation combined non-linear equations for roll and surge motions with a linear treatment of heave, pitch, sway and yaw, using the strip method. The volume of water in each damaged compartment was corrected at each time step. Special emphasis was placed on simulating realistically the motion of water on deck. Similar to [146] application of Glimm's method was used for simulations of floodwater motions for low tank filling ratios and single degree of freedom for rotation of the liquid free surface assumed plane. The forces and moments due to the interior fluid motion in partly flooded rooms and on the vehicle deck were determined and added to the other moments due to wave excitation, etc. The simulation method was comprehensively validated by comparisons with model tests.

Noteworthy is the research of [145], where deterministic chaos analysis of flooded ship motions were performed. The mathematical model used was a single degree of freedom roll motion of a two-dimensional box-shaped ship with free water, where the water motion was described by an equivalent pendulum equation and no water ingress/egress was considered. Based on the results derived and verified by physical experiment, the authors concluded that such simplified modelling is meaningful and that chaos control techniques can be applied for studies on capsize prevention.

The work presented in [130][131] and [132] is yet another example of growing variability and sophistication of dealing with ships in damaged state, where in a similar approach to the above mentioned work of [120] (floodwater treated as rigid body), an innovative treatment of floodwater behaviour has been proposed. It was still assumed that the floodwater free surface is flat, but its motion was represented as a free mass moving on a prescribed trajectory. The results showed good correlation with experimental data.

Even more sophisticated advances have been achieved taking advantage of the hybrid modelling where the floodwater behaviour and effects on motions have been represented by RANS techniques. A good example has been given by the work published in [126] where physical and numerical experiments with water held captive on the deck of an inshore type-fishing vessel were undertaken.

Particular emphasis in the tests was placed on ensuring that numerical simulations could be compared to the experimental results with minimum of uncertainty in the conditions of the model and its dynamics. The results of the tests were compared to those of a time domain simulation code (MOTSIM) used in conjunction with a 3-dimensional Navier-Stokes solver (FLOW3D). Apparent problems with numerical simulations of manoeuvrability of the vessel in waves were observed. An ad-hoc procedure was adopted to mend the differences between ship heading onto the waves, namely a mean yaw correction term was applied. This proved to solve the discrepancy. The experiments themselves showed a peculiar effect of water on deck for ship in astern seas, where the vessel rolled with amplitude of approximately 22 [deg] when there was no water on deck but only 2 [deg] when some amount of water on the deck was allowed. Numerical simulation showed the same trend.

To gain more understanding of the dynamics involved in the ship foundering process due to progressive flooding, a number of experiments have been executed and results made available.

For instance in the research [125] an investigation on the dynamic effects on a Ro-Ro ship due to entrained water on deck and ensuing consequences on stability and survivability in beam sea conditions was undertaken. The emphasis was put on investigating the water motion without the effects of progressive flooding and that of the opening on ship hull hydrodynamics. A standard Ro-Ro ship in 1:60 scale was built and tested at SOLAS damage with 0.5 m of water on the closed deck. The experiments confirmed analytically derived values of liquid oscillation frequency. Interesting to note were the dynamic pressures of double amplitude of the corresponding static values. The vessel survived sea states of Hs=9.0m with 0.5m of water on the ro-ro deck.

Another research shown in [129] presents experimental and numerical research on the fluid dynamics related to progressive flooding and sloshing inside a typical ship compartment. Model tests have been carried out to investigate transient flooding following the occurrence of sudden damage. Forced oscillation tests were carried out with the same compartment geometries as for the transient flooding tests. The compartment geometries consisted of several engine room layouts and accommodation spaces including cross-flooding arrangements. The experimental results provide validation data for a numerical model to simulate the dynamics of a damaged ship. The authors underlined that indeed little is known about the internal flow dynamics and about the interaction with ship motions, especially during the initial stages of flooding, during which process the ship may experience large amplitude transient roll not considered by current regulations.

3.3 Water ingress/egress

Whilst dealing with predictions of damaged ship behaviour in the manner described above, a very complex problem commonly approximated by all models is the water ingress/egress. The applied steady flow continuity equation corrected by an empirical coefficient by no means can be accepted as the ultimate procedure. Many problems remain not addressed, e.g. the influence of the circular velocity of fluid particles due to progression of waves, the radiation and diffraction fields introduced by the presence of the ship body, ship kinematics, highly non-steady flow character, etc.

There does not seem to be much of a direct research aiming at devising procedures for more in-depth modelling of water ingress/egress where these effects would be catered for. However, studies like the work presented in [124] could be made use of. In this work a method of predicting the duration of inflow onto the deck and the thickness of the inflow layer over the bulwark top are sought after. The proposed method makes use of the linear potential theory (based on Lewis forms) for prediction of diffracted wave amplitude and this is used to simulate the dynamic swell-up effects. The calculated values agreed reasonably well with the experiment. The key factor was the correct prediction of wave elevation relative to the deck edge and then the derivation of a flooding coefficient, which in this case proved to be K=0.583. The estimated quantity of the shipping water on the deck using the duration and the thickness for fixed two-dimensional bodies in beam seas was successfully compared with a purposely designed experiment.

3.4 Summary

Taking into consideration of the literature review, as presented above, a preferred general outline of the sought cluster of methods to be implemented in the modelling emerges.

It is felt that to arrive at a practical model, the fully non-linear time domain solutions to waves-body interaction cannot be applied and therefore the linear, frequency domain solutions seem to be the suitable choice. Moreover, the 2D approach instead of the 3D appears to be a good compromise between efficiency (for instance perceived data pre-processing) and accuracy. However, the applied technique would have to address the cases of geometry asymmetries and speed. Furthermore, an

option can be facilitated to evaluate the exciting F-K and restoring forces up to the instantaneous wave profile for prediction of motions in extreme environments.

Also for the modelling of floodwater behaviour it does not seem to be feasible within the time constraints of this work duration to aim at fully non-linear CFD simulations of water motion. Instead a simplified approach can be pursued involving a combination of floodwater flat free-surface and independent mechanism for its behaviour.

The equations of motion of ship dynamics in all 6dof can be resolved and all the resultant terms retained for the sake of accuracy and completeness of the mathematical model.

4 Approach adopted

In addressing the goal of development of robust modelling techniques capable of representing damaged ship dynamics with sufficient accuracy and hence allowing for routine utilisation in design, exploration of approaches derived from first principles is of vital importance. However to "exactly" model ship dynamics a multitude of physical phenomena has to be considered, each of which needs development of highly sophisticated mathematical representation with even more elaborate numerical coding, an approach one can easily deem impractical for the sheer costs involved. Therefore, for this modelling to integrate into an application for use in practical naval architecture, adoption of simplifications, which by their very nature are more or less disputable, becomes necessary. Here literature offers an extensive set of options for implementation and, therefore, the choice by necessity driven by pragmatism leaves a large scope for creativity, consequences of which are numerical tools for simulation of ship dynamics with acceptable accuracy.

Deriving from this philosophical preamble, the following specific tasks, chosen techniques and appropriate simplifications are adopted to address the set objectives of this work.

- Full set of equations for modelling of intrinsic effects of floodwater dynamics on ship behaviour, to be re-derived based on rigid body motion theory, with emphasis on retaining all arising non-linearities.
- Treatment of non-linear damaged vessel hydrodynamics based on intact hull properties tackled by database approach to be improved by development of efficient strip-theory for asymmetric geometries.
- Flooding process modelled by stationary fluid momentum equations with empirically derived correction coefficients.
- The ensuing floodwater behaviour to be predicted by a pendulum-like motion equation (free mass constrained by surface motion) resolved in Cartesian coordinate system. The motion space to be formulated by appropriate geometrical database.
- Cargo shifting to be formulated as a point-mass planar motion due to acceleration field.
- Non-linear flow phenomena such as viscous flows or higher order effects addressed by empirical formulations.

5 Ship dynamics

For advanced description of rigid body motions rigorous derivation of equations from first principles is required. This chapter deals with basic dynamics theorems and geometrical issues, aiming to establish a basic mathematical model for the description of ship motions whilst accounting for free mass (floodwater and cargo) shifting effects.

5.1 Inertial Coordinate Systems

In nonrelativistic dynamics it is assumed that there is an absolute space, which is Euclidean, and an absolute time, which is independent of space, [97, p.3]. A coordinate system must be employed to measure and describe a motion. It was Galileo who showed that there exists a preferred reference system for which the acceleration has its simplest possible form. Such a reference frame is called an inertial- or Galilean- coordinate system. The acceleration measured with respect to inertial coordinate system can be called absolute, and hence the frame can be referred to as absolute or global.

An inertial frame of reference may be defined as a coordinate system that does not rotate and whose origin is either fixed in space or if it translates, then it moves in a straight line at a constant velocity. The nearest one can come to a "fixed" reference system is the primary inertial system or astronomical frame of reference, [107, p.222], which is an imaginary set of axes attached to the fixed stars. All other reference systems, then, are considered to move in space, including any reference system attached to the moving earth. The accelerations of points attached to the earth as measured in the primary system are quite small, however, and can normally be neglected for most earth-surface measurements. For example the acceleration of the centre of the earth in its near-circular orbit around the sun considered fixed is 0.00593 m/s^2.

Deriving from the above, the earth-fixed, "inertial" reference frame $EX^EY^EZ^E$ is assumed to delineate space. The EX^EY^E plane is fixed on the calm water level and the EZ^E axis points upwards, see Figure 7.

Ship motions can be decomposed into two components: steady and unsteady, the first denoting the ship moving forward with constant velocity at a given mean position and the second 6dof

oscillations around her mean position. Following this, to simplify the motion description, a second inertial co-ordinate system OXYZ can be adopted. The OXY plane is placed on the calm water level, and the OZ axis points upwards, see Figure 7. This system moves with the mean, rectilinear motion of the ship, i.e. in case of no ship oscillations, the origin 'O' of the system is located at the intersection between water-plane, centre-line-plane and mid-ship-plane of the ship, see Figure 8. The OX axis points towards the bow of a ship and OY to port side. The angle between the EX^E and OX axes, β, defines the heading of the ship with respect to the oncoming waves, the propagation direction of which is assumed to be along the EX^E axis.

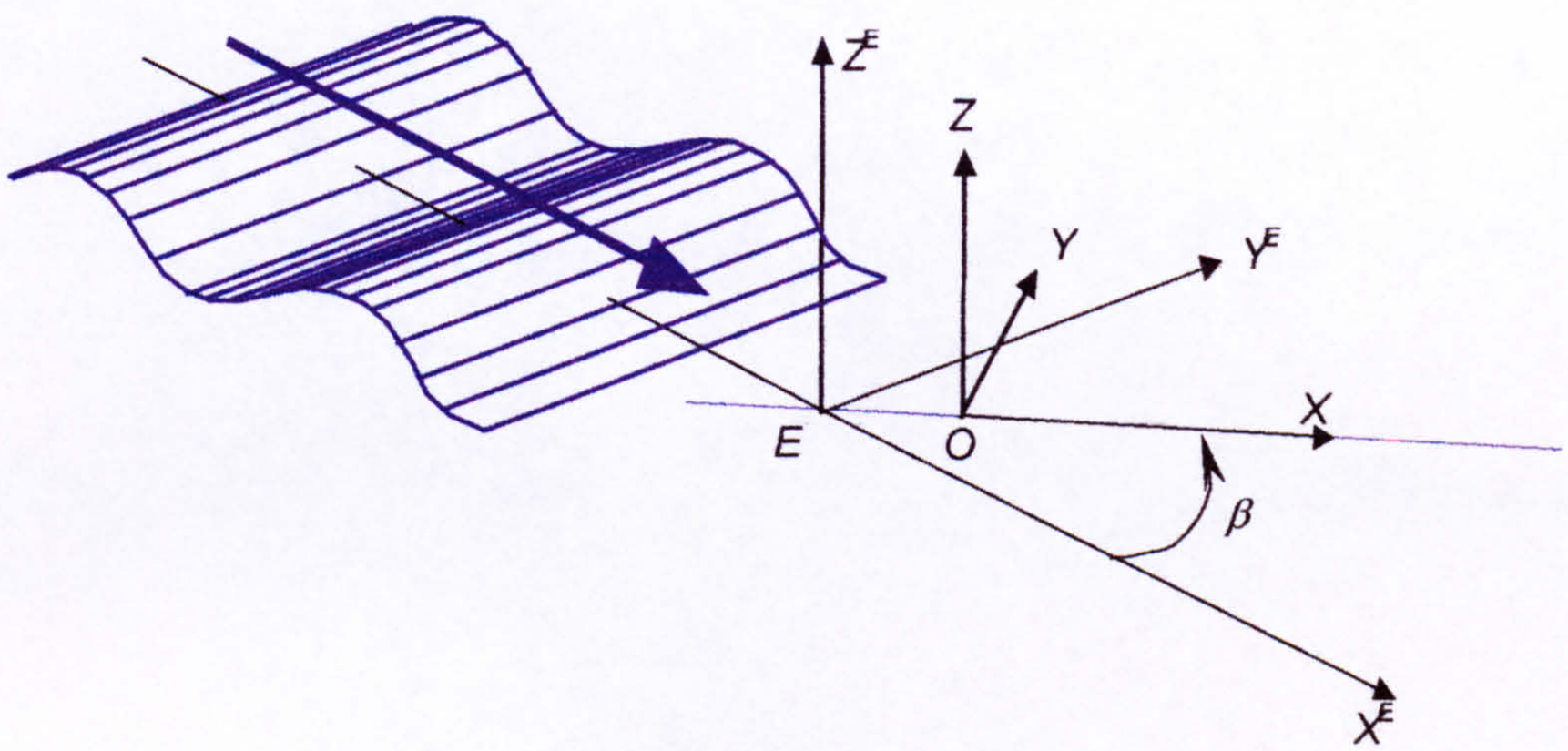

Figure 7 Definition of inertial co-ordinate systems

The ship-environment interaction will be expressed in the OXYZ co-ordinate system. Note here that the predicted vessel motions will be expressed in this coordinate system at its initial position (t=0), and for convenience this system will be referred to as $O^0X^0Y^0Z^0$, see Figure 23.

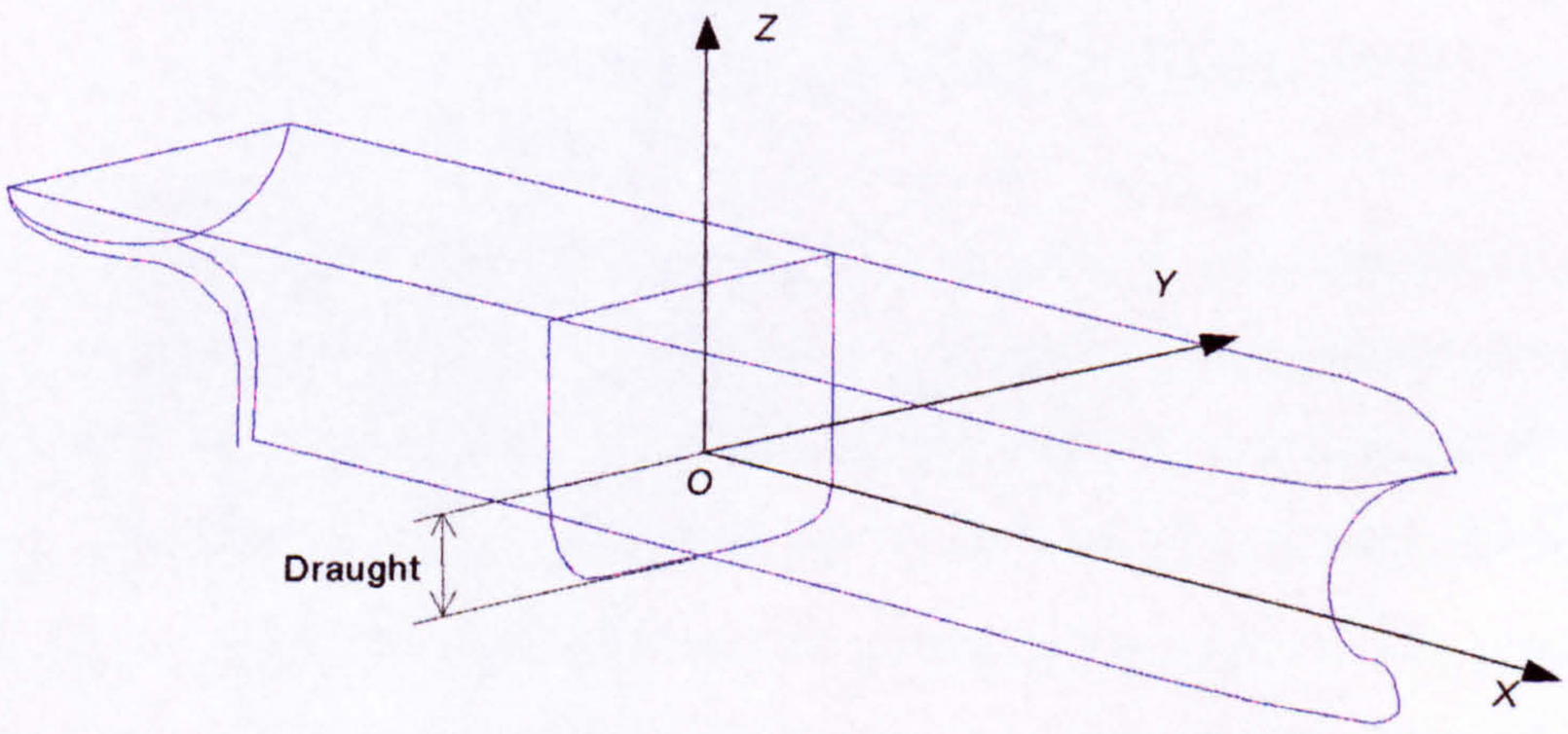

Figure 8 Inertial co-ordinate system in relation to ship with no oscillations

5.2 Ship as a rigid body

Classical definition of a rigid body describes it as a system of n mass points, with masses m_i, which are joined by rigid links. The major implication of this assumption is that elastic or plastic deformation of a given body is ignored in both the interaction of material particles between each other as well as interaction between the body as a whole with the surrounding environment. The former is of major interest for engineering dealing with fatigue whereas the later is a main study subject for vibration and hydro-elasticity. Both these aspects, however, are beyond the scope of this thesis and will not be addressed here. Therefore, the assumption of rigidity of the ship will hold throughout this work. Moreover, this definition will be extended onto any "free mass" within the ship like floodwater or shifting cargo, where such masses will be generalised as separate rigid bodies of given mass. The theory on kinematics and dynamics of multi-body systems will then be used to model the mutual interactions between ship and free masses.

Deriving from the above, the mass of the system composed of the ship and any free mass, treated as rigid bodies, will be assumed to be:

$$M = \sum_i m_i = \sum_i m_{is} + \sum_i m_{iw} = M_s + M_w \qquad (2)$$

Where:

M_s	Total mass of an intact ship
M_w	Total free mass (e.g. flood water or cargo)

It should be noted that unless otherwise indicated, the index "i" corresponds to a single fluid particle. It is worth highlighting it due to indeterminable discretisation resolution that can be used in defining ship spaces that could undergo flooding and which spaces would intuitively be identified by the index "i". Therefore for the sake of simplicity in the derivation process, the term M_w from now on should be interpreted as a composition of a number of particles "i" into one body of mass M_w and that the body represents one flooded/loaded space within the ship. Naturally there will be many such units within the ship.

5.3 Conservation of momentum

Motion of any rigid body in space can be described by virtue of conservation of momentum, the general theorem of classic dynamics.

$$\frac{D}{Dt}\vec{P} = \vec{F} \qquad \text{Conservation of linear momentum} \qquad (3)$$

$$\frac{D}{Dt}\vec{K}_O = \vec{M}_O \qquad \text{Conservation of angular momentum} \qquad (4)$$

Where:

$\vec{F}, \vec{M}_O$ — Resultant of all external forces and moments relative to point O, acting on the body

$$\vec{P} = \sum_i m_i \cdot \vec{v}_i \qquad \text{Linear momentum of the translating body} \qquad (5)$$

m_i — Mass of a single, finite element of the body (mass point)

$\vec{v}_i$ — Total velocity of the mass point

$$\vec{K}_O = \sum_i \vec{r}_{Oi} \times m_i \cdot \vec{v}_i \qquad \text{Angular momentum relative to point O of the translating and rotating body} \qquad (6)$$

$\vec{r}_{Oi}$ — Position vector of the mass point

Note that all vectors are expressed in the inertial co-ordinate system OXYZ. It is easily noticeable that equation (3) with definition (5) is fairly simple to solve numerically. It is difficult or impossible, however, to instantaneously determine the position vector $\overrightarrow{r_{Oi}}$ and velocity $\vec{v}_i$ of each single particle of the system, denoted by equation (6), relative to the origin of the inertial co-ordinate system OXYZ. For this reason, derivations of solvable equations of motions will be carried out starting with identity (4) and (6) first.

To simplify equation (6), the motion of the body can be decomposed into its rotation around an arbitrarily chosen point A and its linear displacement relative to the point O, see Figure 10.

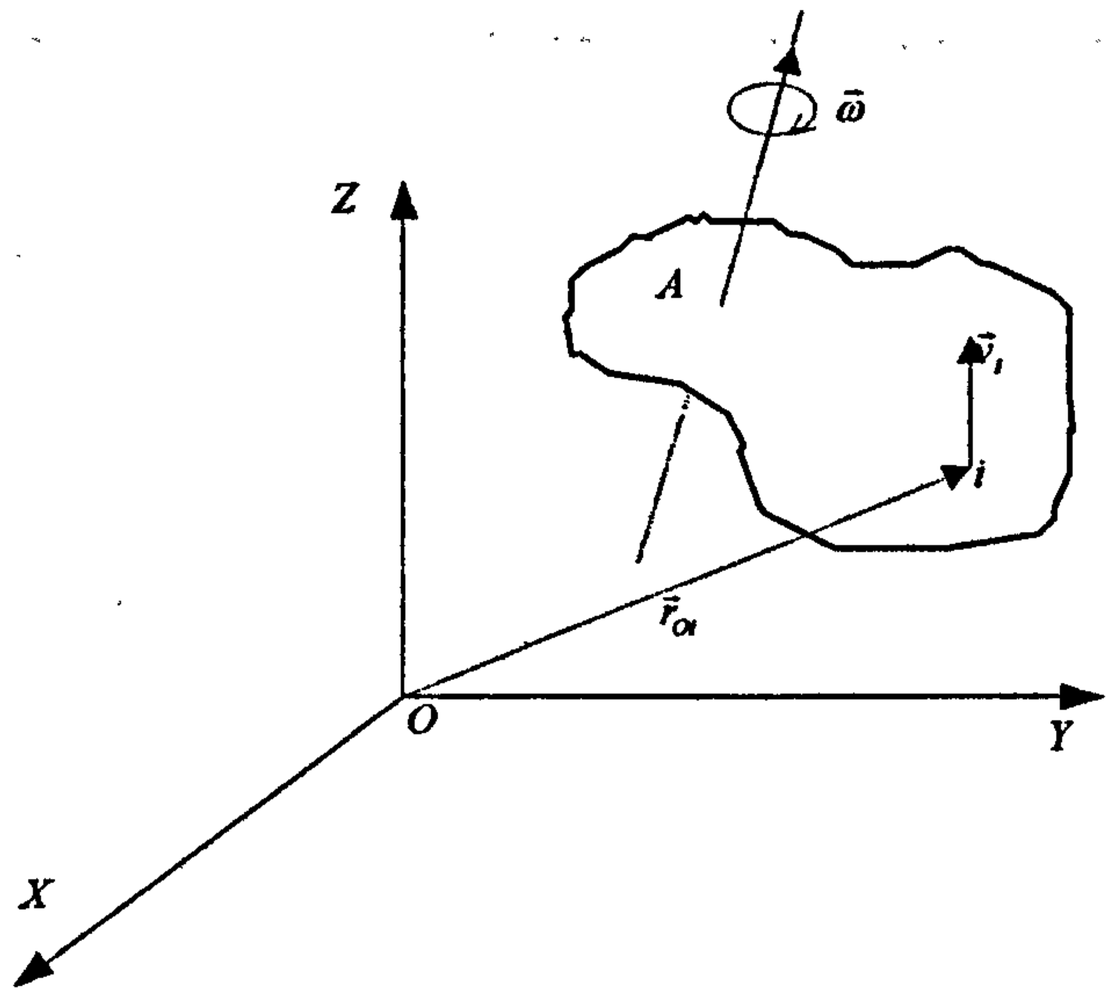

Figure 9 Body moving in the inertial co-ordinate system

The position vector may then be rewritten as:

$$\vec{r}_{Oi} = \vec{r}_A + \vec{r}_i \qquad (7)$$

Hence applying (7) to equation (6) leads to the following:

$$\vec{K}_O = \sum_i (\vec{r}_A + \vec{r}_i) \times m_i \cdot \vec{v}_i$$

$$\vec{K}_O = \left(\vec{r}_A \times \sum_i m_i \cdot \vec{v}_i\right) + \left(\sum_i \vec{r}_i \times m_i \cdot \vec{v}_i\right) \qquad (8)$$

Applying further definitions (5) and (6) to equation (8) gives:

$$\vec{K}_O = \vec{r}_A \times \vec{P} + \vec{K}_A \qquad (9)$$

Where:

$$\vec{K}_A = \sum_i \vec{r}_i \times m_i \cdot \vec{v}_i$$

Angular momentum of the rotating body but now relative to point A (10)

When equation (9) is inserted into equation (4) the following is obtained:

$$\frac{D}{Dt}\vec{K}_O = \frac{D}{Dt}\left(\vec{r}_A \times \vec{P} + \vec{K}_A\right) = \vec{M}_O$$

$$\vec{v}_A \times \vec{P} + \vec{r}_A \times \frac{D}{Dt}\vec{P} + \frac{D}{Dt}\vec{K}_A = \vec{M}_O$$

$$\vec{v}_A \times \vec{P} + \frac{D}{Dt}\vec{K}_A = \vec{M}_O - \vec{r}_A \times \frac{D}{Dt}\vec{P}$$

$$\vec{v}_A \times \vec{P} + \frac{D}{Dt}\vec{K}_A = \vec{M}_A \qquad (11)$$

Where use has been made of equation (3):

$$\vec{M}_O - \vec{r}_A \times \frac{D}{Dt}\vec{P} = \vec{M}_O - \vec{r}_A \times \vec{F} = \vec{M}_A$$

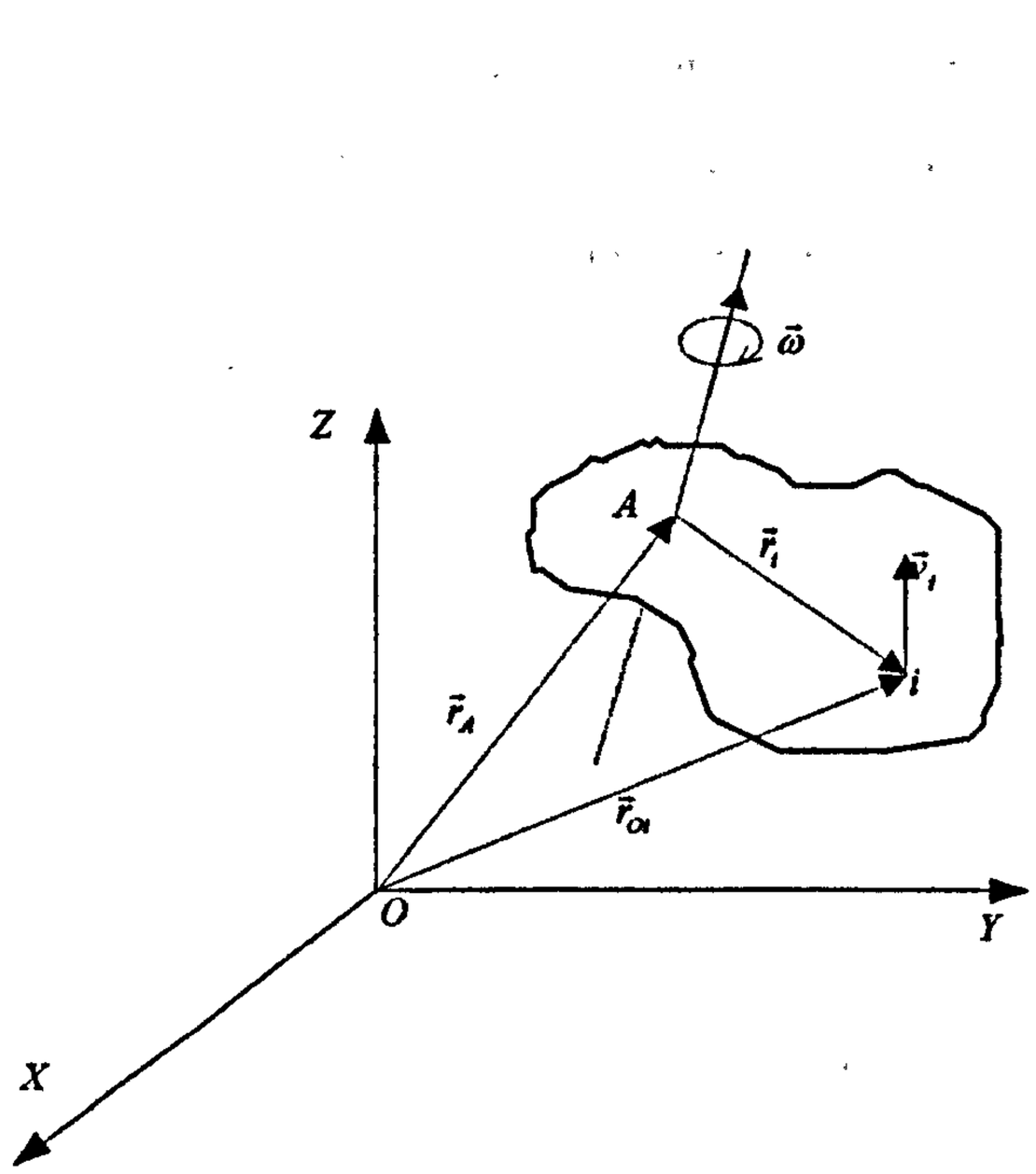

Figure 10 Decomposition of motion of the body into rotation around point A and its displacement with respect to point O

5.4 Absolute velocity vector

For equation (11) to be further elaborated, the absolute velocity vector, $\vec{v}_i$, seen in both definitions (5) and (10) must be explored in more detail. In an inertial co-ordinate system this velocity can be found as:

$$\vec{v}_i = \frac{D}{Dt}\vec{r}_{Oi} = \frac{D}{Dt}(\vec{r}_A + \vec{r}_i)$$

$$\vec{v}_i = \frac{D}{Dt}\vec{r}_A + \frac{D}{Dt}\vec{r}_i = \vec{v}_A + \frac{D}{Dt}\vec{r}_i \qquad (12)$$

Where equation (7) has been made use of. Due to the rotation of the rigid body the vectors $\vec{r}_i$ and their derivatives, $\frac{D}{Dt}\vec{r}_i$, seen in equation (12), are still too difficult to express instantaneously in the inertial co-ordinate system OXYZ, see Figure 10. It is known, however, [113, p.59], that the position of these points in space can be described in any coordinate system, provided their orientation with respect to the inertial system is known. So, to overcome this difficulty let some co-ordinate system be fixed to the rotating body with the origin located at the arbitrarily chosen point A. Unit vectors, denoted as $\vec{i}',\vec{j}',\vec{k}'$, describing uniquely this system in the inertial (OXYZ) one can be found from the following relation:

$$\begin{aligned} \vec{i}' &= D^{-1}\cdot\vec{i} \\ \vec{j}' &= D^{-1}\cdot\vec{j} \\ \vec{k}' &= D^{-1}\cdot\vec{k} \end{aligned} \qquad (13)$$

Where the definition of the time-dependent rotation tensor $D = D(t)$, [113, p.63], can be found in Appendix 1. The unit vectors $\vec{i},\vec{j},\vec{k}$ (also called vector basis for the space, [113, p.44]), used above and describing the inertial co-ordinate system OXYZ are defined as follows:

$$\vec{i} = [1 \quad 0 \quad 0]^T$$
$$\vec{j} = [0 \quad 1 \quad 0]^T \qquad (14)$$
$$\vec{k} = [0 \quad 0 \quad 1]^T$$

Vector $\vec{r}_i$ can now be expressed in two ways:

$$\vec{r}_i = x \cdot \vec{i} + y \cdot \vec{j} + z \cdot \vec{k} \qquad (15)$$

Or:

$$\vec{r}_i = x' \cdot \vec{i}' + y' \cdot \vec{j}' + z' \cdot \vec{k}' \qquad (16)$$

where its coordinates in the second definition, x', y' and z' are now expressed with respect to the body-fixed reference system. It can be shown that:

$$x \cdot \vec{i} + y \cdot \vec{j} + z \cdot \vec{k} = x' \cdot \vec{i}' + y' \cdot \vec{j}' + z' \cdot \vec{k}'$$

$$x \cdot \vec{i} + y \cdot \vec{j} + z \cdot \vec{k} = x' \cdot D^{-1} \cdot \vec{i} + y' \cdot D^{-1} \cdot \vec{j} + z' \cdot D^{-1} \cdot \vec{k}$$

$$x \cdot \vec{i} + y \cdot \vec{j} + z \cdot \vec{k} = D^{-1} \cdot \left(x' \cdot \vec{i} + y' \cdot \vec{j} + z' \cdot \vec{k} \right) \qquad (17)$$

And by denoting:

$$\vec{r}'_i = x' \cdot \vec{i} + y' \cdot \vec{j} + z' \cdot \vec{k} \qquad (18)$$

equation (17) can be written as

$$\vec{r}_i = D^{-1} \cdot \vec{r}'_i$$ Orthogonal transformation operation, [112 ,p.52] (19)

See also equation (227). Equation (17) to (19) are shown at this moment for clarification purposes only but are useful later. The main interest is in equation (16). If for simplicity, this definition of vector $\vec{r}_i$ is used, the second term of equation (12) can be written as:

$$\frac{D}{Dt}\vec{r}_i = \frac{D}{Dt}\left(x'\cdot\vec{i}'+y'\cdot\vec{j}'+z'\cdot\vec{k}'\right)=\left(\frac{d}{dt}x'\right)\cdot\vec{i}'+\left(\frac{d}{dt}y'\right)\cdot\vec{j}'+\left(\frac{d}{dt}z'\right)\cdot\vec{k}'+$$
$$+x'\cdot\left(\frac{d}{dt}\vec{i}'\right)+y'\cdot\left(\frac{d}{dt}\vec{j}'\right)+z'\cdot\left(\frac{d}{dt}\vec{k}\right) \qquad (20)$$

which follows from the fact that the unit vectors of body-fixed coordinate system are now time dependent, see equations (13) contrary to equations (14)! Based on the analysis of infinitesimal rotations in Appendix 1, the time derivatives of unit vectors of body-fixed reference system seen in equation (20) take the following form:

$$\frac{d}{dt}\vec{i}'=\vec{\omega}\times\vec{i}'$$
$$\frac{d}{dt}\vec{j}'=\vec{\omega}\times\vec{j}' \qquad (21)$$
$$\frac{d}{dt}\vec{k}'=\vec{\omega}\times\vec{k}'$$

Where:

$\vec{\omega}=\omega'_x\cdot\vec{i}'+\omega'_y\cdot\vec{j}'+\omega'_z\cdot\vec{k}'$ Cartesian rotational velocity vector (22)

See equations (238) and (243) of **Appendix 1.** Once equations (21) are inserted into equations (20) the following is derived:

$$\frac{D}{Dt}\vec{r}_i=\frac{d}{dt}\vec{r}_i+\vec{\omega}\times\left(x'\cdot\vec{i}'+y'\cdot\vec{j}'+z'\cdot\vec{k}'\right)$$
$$\frac{D}{Dt}\vec{r}_i=\frac{d}{dt}\vec{r}_i+\vec{\omega}\times\vec{r}_i \qquad (23)$$

Where, $\frac{d}{dt}$ denotes differentiation only over vector co-ordinates expressed in the body-fixed system of reference. The above can now be used to express equation (12) as follows:

$$\vec{v}_i = \vec{v}_A + \frac{d}{dt}\vec{r}_i + \vec{\omega} \times \vec{r}_i \qquad (24)$$

Note that the vectors $\vec{r}_i$, $\frac{d}{dt}\vec{r}_i$ and $\vec{\omega}$ are expressed from now on by equation (16) and (22), respectively. Although their coordinates are expressed in body-fixed reference frame, the vectors correspond to global coordinate system, OXYZ, because of definitions (13)!

The terms in equation (24) can be interpreted in the following way:

$\vec{v}_A$	Velocity of translation of point A relative to point O.
$\frac{d}{dt}\vec{r}_i$	Velocity of translation of mass point "i" relative to point A, which results from differentiation only of coordinates of $\vec{r}_i$ vector, expressed in body-fixed reference system. Because of definition (13) this vector is expressed in the OXYZ system.
$\vec{\omega} \times \vec{r}_i$	Velocity of translation of mass point "i" due to rotation around point A, which results from differentiation of unit vectors of body-fixed reference frame. Again, because of definition (13) and (22) this vector is expressed in the OXYZ system.

Note that the coordinate system OXYZ can translate with some constant velocity $\vec{v}_0 = [U \quad 0 \quad 0]^T$ and in this case the translation vector should account for this: $\vec{v}_A = \vec{v}_A + \vec{v}_0$.

Following the logic of equation (2) and inserting equation (24) into (5) and (10), which are to be used for further elaboration of equation (11), the following is obtained:

$$\vec{v}_A \times \vec{P} = \vec{v}_A \times \sum_i m_i \cdot \vec{v}_i = \vec{v}_A \times \sum_i m_i \cdot \left[\vec{v}_A + \frac{d}{dt}\vec{r}_i + \vec{\omega} \times \vec{r}_i \right] =$$

$$= \left[\vec{v}_A \times \vec{v}_A \cdot \sum_i m_i \right] + \left[\vec{v}_A \times \sum_i m_i \cdot \frac{d}{dt}\vec{r}_i \right] + \left[\vec{v}_A \times \left(\vec{\omega} \times \sum_i m_i \cdot \vec{r}_i \right) \right]$$

$$\vec{K}_A = \sum_i \vec{r}_i \times m_i \cdot \vec{v}_i = \sum_i \vec{r}_i \times m_i \cdot \left[\vec{v}_A + \frac{d}{dt}\vec{r}_i + \vec{\omega} \times \vec{r}_i \right] =$$

$$= \left[\sum_i m_i \cdot \vec{r}_i \times \vec{v}_A \right] + \left[\sum_i \vec{r}_i \times m_i \cdot \frac{d}{dt}\vec{r}_i \right] + \left[\sum_i \vec{r}_i \times (\vec{\omega} \times m_i \cdot \vec{r}_i) \right]$$

Where:

$$\vec{v}_A \times \vec{v}_A \cdot \sum_i m_i = \vec{0} \qquad (25)$$

$$\vec{v}_A \times \sum_i m_i \cdot \frac{d}{dt}\vec{r}_i = \vec{v}_A \times \left(M_s \cdot \frac{d}{dt}\vec{r}_{AGs} + M_w \cdot \frac{d}{dt}\vec{r}_{AGw} \right) = \vec{v}_A \times M_w \cdot \frac{d}{dt}\vec{r}_{AGw} \qquad (26)$$

Note here, that $\frac{d}{dt}\vec{r}_{AGs} = \vec{0}$ as both of the points, *A* and *Gs* belong to the same rigid body and hence the distance between them is always constant. Note also the following definition:

$$\sum_i m_i \cdot \vec{r}_i \equiv M \cdot \vec{r}_G$$

In a similar manner the remaining equations can be expanded:

$$\vec{v}_A \times \left(\vec{\omega} \times \sum_i m_i \cdot \vec{r}_i \right) = \vec{v}_A \times \left[\vec{\omega} \times \left(M_s \vec{r}_{AGs} + M_w \cdot \vec{r}_{AGw} \right) \right] \qquad (27)$$

$$\sum_i m_i \cdot \vec{r}_i \times \vec{v}_A = \left(M_s \cdot \vec{r}_{AGs} \times \vec{v}_A \right) + \left(M_w \cdot \vec{r}_{AGw} \times \vec{v}_A \right) \qquad (28)$$

$$\sum_i \vec{r}_i \times m_i \cdot \frac{d}{dt}\vec{r}_i = \left(\vec{r}_{AGs} \times M_s \cdot \frac{d}{dt}\vec{r}_{AGs} \right) + \left(\vec{r}_{AGw} \times M_w \cdot \frac{d}{dt}\vec{r}_{AGw} \right) = \vec{r}_{AGw} \times M_w \cdot \frac{d}{dt}\vec{r}_{AGw} \qquad (29)$$

$$\sum_i \vec{r}_i \times (\vec{\omega} \times m_i \cdot \vec{r}_i) = \vec{k}_A \qquad (30)$$

All equations (25) to (30) except (29) are the result of a simple mathematical deduction. Equation (29), however, requires some justification as it is not mathematically correct averaging of a summation of cross product of two discrete vectors. Physically it implies that the **sum** of angular

momenta with respect to point A resultant from motions of mass points m_i relative to point A with velocities $\frac{d}{dt}\vec{r}_i$ can be **approximated** by an angular momentum with respect to point A of a single mass point M_w undergoing motion with average velocity $\frac{d}{dt}\vec{r}_{AGw}$. For justification of this operation it should be reminded that the index "i" denotes here fluid particle and the term "M_w" corresponds to single flooded space within the ship (or single shifting mass unit). These two subtle points already indicate that the error in making assumption (29) will be of limited importance as it will be confined to this single shifting unit. Figure 11 demonstrates motions of two fluid particles in a flooded space. Although the particles are assumed to belong to the same rigid body, their motion is independent as it relies on geometrical constraints imposed by the space. Here already for this reason it can be clearly seen that the equation is imprecise. This imprecision, however, will be ignored in this study, as it seems that it will be locally limited to single flooded compartments.

For the case of a shifting cargo, which unlike the ideal model of point mass assumed here has some dimension and therefore space mass distribution, the same equation will not be correct in the situation of cargo undergoing rotations with respect to body fixed system of reference as in this case each particle of the cargo would have different velocity. However, in this work the moving cargo will undergo only rectilinear motions with respect to body-fixed system, and therefore equation (29) is valid.

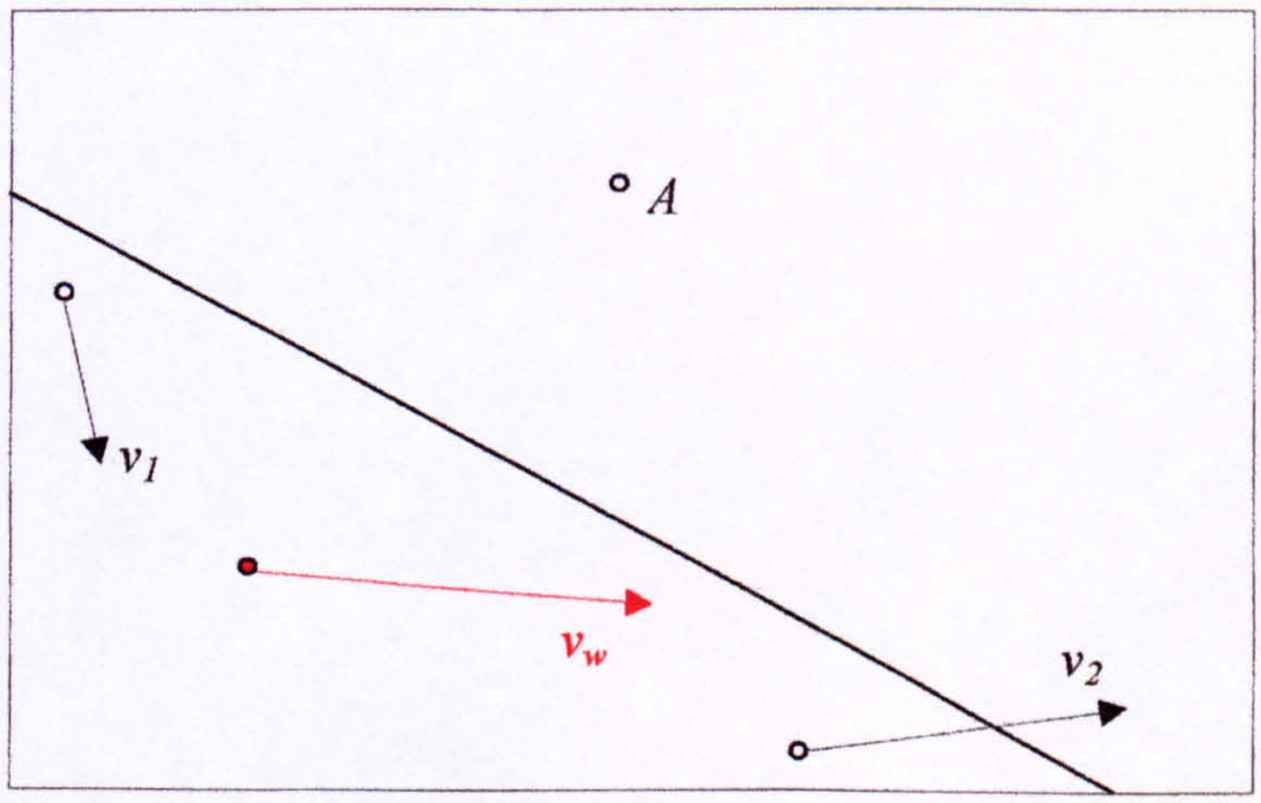

Figure 11 Motion of fluid particles in a closed tank

Note furthermore, that equation (30) can be expressed in more convenient form by applying identity (47):

$$\vec{k}_A = \sum_i \vec{\omega} \cdot m_i \cdot (\vec{r}_i \cdot \vec{r}_i) - \sum_i \vec{r}_i \cdot m_i \cdot (\vec{\omega} \cdot \vec{r}_i) \qquad (31)$$

It is worth to write equation (31) in a scalar form for better clarity:

$$k_{Ax} = \omega_x \cdot \left[\sum_i m_i \cdot r_i^2\right] - \sum_i m_i \cdot x_i \cdot (x_i \cdot \omega_x + y_i \cdot \omega_y + z_i \cdot \omega_z)$$

$$k_{Ay} = \omega_y \cdot \left[\sum_i m_i \cdot r_i^2\right] - \sum_i m_i \cdot y_i \cdot (x_i \cdot \omega_x + y_i \cdot \omega_y + z_i \cdot \omega_z)$$

$$k_{Az} = \omega_z \cdot \left[\sum_i m_i \cdot r_i^2\right] - \sum_i m_i \cdot z_i \cdot (x_i \cdot \omega_x + y_i \cdot \omega_y + z_i \cdot \omega_z)$$

After simple manipulations it can be further rewritten as:

$$\begin{bmatrix} k_{Ax} \\ k_{Ay} \\ k_{Az} \end{bmatrix} = \begin{bmatrix} \sum_i m_i \cdot (y_i^2 + z_i^2) & -\sum_i m_i \cdot x_i \cdot y_i & -\sum_i m_i \cdot x_i \cdot z_i \\ -\sum_i m_i \cdot y_i \cdot x_i & \sum_i m_i \cdot (x_i^2 + z_i^2) & -\sum_i m_i \cdot y_i \cdot z_i \\ -\sum_i m_i \cdot z_i \cdot x_i & -\sum_i m_i \cdot z_i \cdot y_i & \sum_i m_i \cdot (x_i^2 + y_i^2) \end{bmatrix} \cdot \begin{bmatrix} \omega_x \\ \omega_y \\ \omega_z \end{bmatrix}$$

And when the following is introduced:

$$I_A = \begin{bmatrix} I_{xx} & I_{yx} & I_{zx} \\ I_{xy} & I_{yy} & I_{zy} \\ I_{xz} & I_{yz} & I_{zz} \end{bmatrix} = \begin{bmatrix} \sum_i m_i \cdot (y_i^2 + z_i^2) & -\sum_i m_i \cdot x_i \cdot y_i & -\sum_i m_i \cdot x_i \cdot z_i \\ -\sum_i m_i \cdot y_i \cdot x_i & \sum_i m_i \cdot (x_i^2 + z_i^2) & -\sum_i m_i \cdot y_i \cdot z_i \\ -\sum_i m_i \cdot z_i \cdot x_i & -\sum_i m_i \cdot z_i \cdot y_i & \sum_i m_i \cdot (x_i^2 + y_i^2) \end{bmatrix} \qquad (32)$$

Equation (30) can be written in matrix form as follows:

$$\vec{k}_A = I_A \cdot \vec{\omega} \qquad (33)$$

5.5 Equations of motion

When equations (25) to (30) and (33) are inserted into equation (11), the following equation of angular motion is achieved:

$$\left(\vec{v}_A \times M_w \cdot \frac{d}{dt}\vec{r}_{AGw}\right) + \vec{v}_A \times \left[\vec{\omega} \times \left(M_s \cdot \vec{r}_{AGs} + M_w \cdot \vec{r}_{AGw}\right)\right] +$$

$$+ \frac{D}{Dt}\left[\left(M_s \cdot \vec{r}_{AGs} \times \vec{v}_A\right) + \left(M_w \cdot \vec{r}_{AGw} \times \vec{v}_A\right) + \left(\vec{r}_{AGw} \times M_w \cdot \frac{d}{dt}\vec{r}_{AGw}\right) + \left(I_A \cdot \vec{\omega}\right)\right] = \vec{M}_A \qquad (34)$$

Some steps can be undertaken for more simplification before further differentiation. Firstly, the mass moment of inertia matrix I_A, seen in the above equation needs attention. Applying the reasoning of assumption (2) into equation (32), the inertia matrix with respect to the chosen rotation point A of the system can be decomposed into two parts, one corresponding to intact vessel and the second describing inertia of all the moving objects on the vessel.

The first will be time independent, as the rotation point, *A*, is assumed fixed to the intact vessel i.e. inertia is constant. The later varies with time, but can be easily traced in the coordinate system fixed to the intact vessel with origin at point A, since this mass will be composed of a finite number of moving points. It is further preferable, here solely for the purpose of presentation of the derivation process, to locate the rotation point, *A*, (again, in reference to which matrix (32) is evaluated) in the centre of gravity of the intact ship, see Figure 12, as the axes of coordinate system passing through this point can be assumed central and hence the intact ship inertia matrix will have the easiest possible form. Note, however, that for practical reasons it is more convenient to express the equations in a coordinate system, the origin of which is located at an arbitrary location within the ship (this location will usually be a point for which the hydrodynamic forces are evaluated). Further details will be given in §5.5.1 below.

$A \to G,\ I_G = I_s + I_w,\ I_s \cong \begin{bmatrix} I_{xx} & 0 & 0 \\ 0 & I_{yy} & 0 \\ 0 & 0 & I_{zz} \end{bmatrix}$, and where I_w is given by equation (32). Note, however, that the indexing "i" in equation (32) here corresponds to flooded spaces or shifting masses.

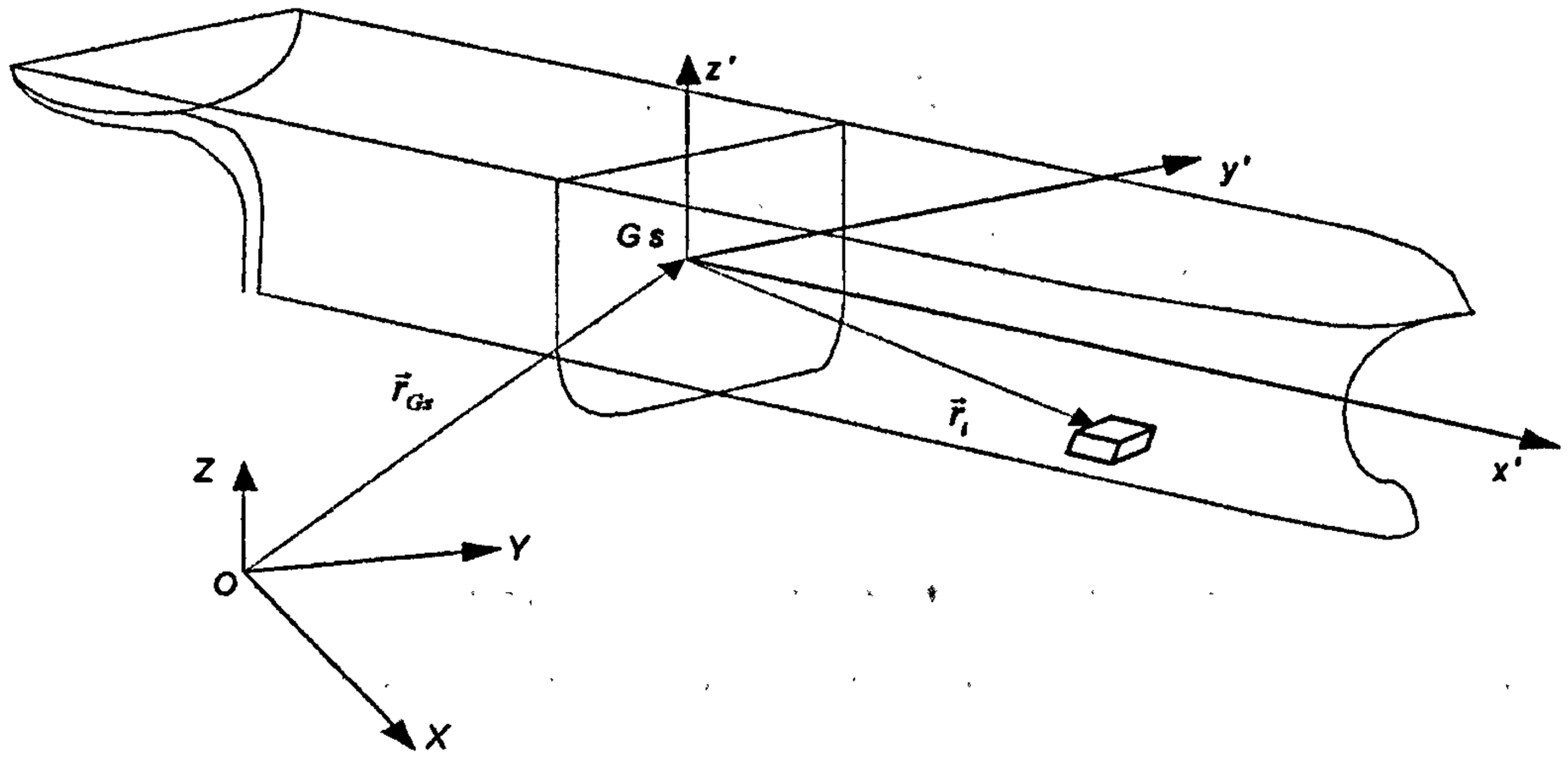

Figure 12 Coordinate system fixed to the centre of gravity of the intact vessel

Implementing the above mentioned assumptions transforms equation (34), expressing the conservation of angular momentum theorem, into the following form:

$$\left[\vec{v}_{Gs}\times M_w\cdot\frac{d}{dt}\vec{r}_{GsGw}\right]+\vec{v}_{Gs}\times\left(\vec{\omega}\times M_w\cdot\vec{r}_{GsGw}\right)+$$
$$+\frac{D}{Dt}\left[\left(M_w\cdot\vec{r}_{GsGw}\times\vec{v}_{Gs}\right)+\left[\vec{r}_{GsGw}\times M_w\cdot\frac{d}{dt}\vec{r}_{GsGw}\right]+\left(\left(I_s+I_w\right)\cdot\vec{\omega}\right)\right]=\vec{M}_{Gs} \qquad (35)$$

Furthermore, before embarking on further differentiation of the above equation one must realise the concept of the system with variable mass, to which general conservation of momentum theorem (4) cannot be applied, [220][107], as in such case the force due to mass variation will be dependent on the *relative* velocity between the system under consideration and the mass entering or leaving this system. However, establishing what is the actual velocity of the mass entering or leaving the system (the ship), is very complex and will not be addressed here. Instead it will be assumed the time derivative of the mass is proportional to the velocity of the centre of gravity of the ship, which implies that the mass that enters or leaves the system has zero velocity. To what extent this assumption is correct remains to be established.

Deriving from the above and remembering that all the vectors are expressed by means of formulae (16) i.e. having the global derivative expressed by equation (23) the following is obtained:

$$(\vec{v}_{Gs} \times M_w \cdot \vec{v}_{GsGw}) + \vec{v}_{Gs} \times (\vec{\omega} \times M_w \cdot \vec{r}_{GsGw}) +$$

$$+ \frac{d}{dt} M_w \cdot (\vec{r}_{GsGw} \times \vec{v}_{Gs}) + M_w \cdot (\vec{v}_{GsGw} + \vec{\omega} \times \vec{r}_{GsGw}) \times \vec{v}_{Gs} + (M_w \cdot \vec{r}_{GsGw}) \times \frac{D}{Dt} \vec{v}_{Gs} +$$

$$+ (\vec{\omega} \times \vec{r}_{GsGw}) \times (M_w \cdot \vec{v}_{GsGw}) + \vec{r}_{GsGw} \times \left(\frac{D}{Dt} M_w \cdot \vec{v}_{GsGw} \right) + \vec{r}_{GsGw} \times M_w \cdot \left(\frac{d}{dt} \vec{v}_{GsGw} + \vec{\omega} \times \vec{v}_{GsGw} \right) +$$

$$+ \frac{D}{Dt} ((I_s + I_w) \cdot \vec{\omega}) = \vec{M}_{Gs}$$

Let $\vec{a}$ indicate the whole left-hand side vector of the above equation. Prior to the final rearrangement it is worth to follow the logic of (17) so to remove the time dependent tensor still present in $\vec{a}$, accordingly to adopted definition (16) with (13).

$$\begin{aligned} &\vec{a} = \vec{M}_{Gs} \\ &D^{-1} \cdot \vec{a}' = \vec{M}_{Gs} \\ &\vec{a}' = D \cdot \vec{M}_{Gs} \\ &\vec{a}' = \vec{M}'_{Gs} \end{aligned} \qquad (36)$$

All the vectors can now be interpreted according to definition (18), i.e. having their constant now basis considered the same as in (14). After algebraic rearrangements the conservation of angular momentum theorem takes the form:

$$M_w \cdot \left[(\vec{\omega}' \times \vec{r}'_{GsGw}) \times \vec{v}'_{GsGw} + \vec{r}'_{GsGw} \times \left[\frac{d}{dt} \vec{v}'_{Gs} + \frac{d}{dt} \vec{v}'_{GsGw} + \vec{\omega}' \times (\vec{v}'_{Gs} + \vec{v}'_{GsGw}) \right] \right] +$$

$$+ \frac{d}{dt} M_w \cdot [\vec{r}'_{GsGw} \times (\vec{v}'_{Gs} + \vec{v}'_{GsGw})] + \qquad (37)$$

$$+ (I'_s + I'_w) \cdot \frac{d}{dt} \vec{\omega}' + \left(\frac{d}{dt} I'_w \right) \cdot \vec{\omega}' + \vec{\omega}' \times [(I'_s + I'_w) \cdot \vec{\omega}'] = \vec{M}'_{Gs}$$

To derive the corresponding solution to equation (3), definition (24) should be inserted into equation (5):

$$\frac{D}{Dt} \left[\sum_i m_i \cdot \left(\vec{v}_{Gs} + \frac{d}{dt} \vec{r}_i + \vec{\omega} \times \vec{r}_i \right) \right] = \frac{D}{Dt} \left(\sum_i m_i \cdot \vec{v}_{Gs} \right) + \frac{D}{Dt} \left(\sum_i m_i \cdot \frac{d}{dt} \vec{r}_i \right) + \frac{D}{Dt} \left(\sum_i m_i \cdot \vec{\omega} \times \vec{r}_i \right)$$

Where:

$$\frac{D}{Dt}\left(\sum_i m_i \cdot \vec{v}_{Gs}\right) = \frac{D}{Dt}\left((M_s + M_w)\cdot \vec{v}_{Gs}\right) = (M_s + M_w)\cdot \frac{D}{Dt}\vec{v}_{Gs} + \frac{D}{Dt}M_w \cdot \vec{v}_{Gs}$$

$$\frac{D}{Dt}\left(\sum_i m_i \cdot \frac{d}{dt}\vec{r}_i\right) = \frac{D}{Dt}\left(M_w \cdot \vec{v}_{GsGw}\right) = \frac{D}{Dt}M_w \cdot \vec{v}_{GsGw} + M_w \cdot \left(\frac{d}{dt}\vec{v}_{GsGw} + \vec{\omega}\times\vec{v}_{GsGw}\right)$$

$$\frac{D}{Dt}\left(\sum_i m_i \cdot \vec{\omega}\times\vec{r}_i\right) = \frac{D}{Dt}M_w \cdot \left(\vec{\omega}\times\vec{r}_{GsGw}\right) + \frac{d}{dt}\vec{\omega}\times M_w \cdot \vec{r}_{GsGw} + \vec{\omega}\times M_w \cdot \left(\vec{v}_{GsGw} + \vec{\omega}\times\vec{r}_{GsGw}\right)$$

Again, after some rearrangements and application of (36), the equation expressing conservation of linear momentum takes the following final form:

$$M_w \cdot \left[\frac{d}{dt}\vec{v}'_{GsGw} + 2\cdot\vec{\omega}'\times\vec{v}'_{GsGw} + \frac{d}{dt}\vec{\omega}'\times\vec{r}'_{GsGw} + \vec{\omega}'\times\left(\vec{\omega}'\times\vec{r}'_{GsGw}\right)\right] +$$

$$+\frac{d}{dt}M_w \cdot \left(\vec{v}'_{GsGw} + \vec{\omega}'\times\vec{r}'_{GsGw}\right) + \qquad (38)$$

$$+\left(M_s + M_w\right)\cdot\frac{d}{dt}\vec{v}'_{Gs} + \frac{d}{dt}M_w \cdot \vec{v}'_{Gs} + \vec{\omega}'\times\left(M_s + M_w\right)\cdot\vec{v}'_{Gs} = \vec{F}'$$

Expressions (37) and (38) compose now a solvable system of 6 equations describing motions of a ship with effect of cargo shifting and water displacement within the vessel as well as their mass variations accounted for and where all the component vectors are expressed in a body-fixed reference frame. Note also the difference between these equations and equations (1) derived by [120]. Here all the non-linear terms discarded by [120], on the grounds that the ship had no forward velocity, have been retained. Also the process of equations derivation seems more transparent than that of [120], elucidating for instance the consequences of assumption of floodwater behaving as a single mass point, see (39).

In case when there is no motion of cargo relative to the ship or, say, no flooding takes place, the equations of intact ship motions, deriving from (37) and (38) take the commonly known form:

$$I'_s \cdot \frac{d}{dt}\vec{\omega}' + \vec{\omega}' \times I'_s \cdot \vec{\omega}' = \vec{M}'_{Gs}$$

$$M_s \cdot \frac{d}{dt}\vec{v}'_{Gs} + \vec{\omega}' \times M_s \cdot \vec{v}'_{Gs} = \vec{F}'$$

5.5.1 Choice of the origin of a body-fixed system of reference

As mentioned in the foregoing the choice of origin of the system of reference where the equations are solved will be dictated by practical considerations. Namely, the right hand side of the equations (37) and (38) constitute an extensive computational effort, as discussed throughout §6. Since the derived moments will be a function of the origin of the body-fixed coordinate system, it is desirable to account for the eventual variation of the centre of gravity of the intact vessel (particularly VCG), in the LHS of these equations, rather than have the hydrodynamic forces re-evaluated each time the VCG varies. The missing terms accounting for the distance between an arbitrarily chosen origin and the centre of gravity of the intact vessel (equal to zero otherwise) can be obtained either by deriving the solvable equations from equation (34) (as an example for angular momentum) or by reconsidering equations (37) and (38) and substituting subscripts: A for Gs, Gs for Gw, s for w, and so on. The complete equations are presented below. The angular momentum equation can be derived as:

$$\begin{aligned}
&M_s \cdot \left(\vec{r}'_{AGs} \times \left(\frac{d}{dt} \cdot \vec{v}'_A + \vec{\omega}' \times \vec{v}'_A \right) \right) + \\
&+ M_w \cdot \left[\left(\vec{\omega}' \times \vec{r}'_{AGw} \right) \times \vec{v}'_{AGw} + \vec{r}'_{AGw} \times \left[\frac{d}{dt}\vec{v}'_A + \frac{d}{dt}\vec{v}'_{AGw} + \vec{\omega}' \times \left(\vec{v}'_A + \vec{v}'_{AGw} \right) \right] \right] + \\
&+ \frac{d}{dt} M_w \cdot \left[\vec{r}'_{AGw} \times \left(\vec{v}'_A + \vec{v}'_{AGw} \right) \right] + \\
&+ \left(I'_s + I'_w + I'_{AGs} \right) \cdot \frac{d}{dt}\vec{\omega}' + \left(\frac{d}{dt} I'_w \right) \cdot \vec{\omega}' + \vec{\omega}' \times \left[\left(I'_s + I'_w + I'_{AGs} \right) \cdot \vec{\omega}' \right] = \vec{M}'_A
\end{aligned} \qquad (39)$$

Where I'_{AGs} can be calculated from (32), with x,y,z being the components of a vector between points A and Gs. The linear momentum equation will take the following form:

$$
\begin{aligned}
&M_s \cdot \left(\frac{d}{dt}\vec{\omega}' \times \vec{r}'_{AGs} + \vec{\omega}' \times \left(\vec{\omega}' \times \vec{r}'_{AGs} \right) \right) + \\
&+ M_w \cdot \left[\frac{d}{dt}\vec{v}'_{AGw} + 2 \cdot \vec{\omega}' \times \vec{v}'_{AGw} + \frac{d}{dt}\vec{\omega}' \times \vec{r}'_{AGw} + \vec{\omega}' \times \left(\vec{\omega}' \times \vec{r}'_{AGw} \right) \right] + \\
&+ \frac{d}{dt} M_w \cdot \left(\vec{v}'_{AGw} + \vec{\omega}' \times \vec{r}'_{AGw} \right) + \\
&+ \left(M_s + M_w \right) \cdot \frac{d}{dt}\vec{v}'_A + \frac{d}{dt} M_w \cdot \vec{v}'_A + \vec{\omega}' \times \left(M_s + M_w \right) \cdot \vec{v}'_A = \vec{F}'
\end{aligned}
\qquad (40)
$$

Having the mathematical model describing dynamics of a ship, capable of taking into account any displacements of internal mass within the ship and relatively to the ship, the remaining task is to determine the right hand sides in equations (39) and (40), or F_j^A in equation (219), the external forces and moments.

Apart from the obvious gravity forces, only the fluid forces will be evaluated in this research, leaving possible effects of wind or perhaps collision with other objects for later investigations. This will be the subject of the following chapter.

6 Ship hydrodynamics

The success of predictions of ship responses to the action of random seas relies ultimately on the robustness and accuracy in modelling of ship hydrodynamics in such conditions. The burden of dealing with confused seas, however, has been resolved to a great extent by the introduction in 1953 of the principle of superposition to the ship-motion problem by St. Denis and Pierson. They hypothesised that the responses of a ship to irregular waves can be considered as the summation of the responses to regular waves of all frequencies. This approach has been followed for most practical issues addressing ship motions for nearly half a century since inception of their idea, as the complex problem of ship hydrodynamics had to be solved for greatly simplified regular sinusoidal wave cases. As has been discussed in §3.1, numerous approaches have been devised to assess ship hydrodynamics in frequency domain. The strip theory technique has been chosen in this thesis for its perceived simplicity and sufficient documented accuracy. The fundamental principles and assumptions made in building the model of the interaction between the ship and the outside water are discussed in this chapter.

6.1 Basic assumptions and notations

The very basic physical theorems and their mathematical treatments are well founded in the literature. For thorough understanding of the problem at hand, however, it is very useful to carry out the process of derivation and underlying interpreting here, so direct reference to assumptions made can be given. The assumptions concerning the fluid model are as follows:

- The water is an ideal fluid i.e. *homogeneous, incompressible, inviscid* and its flow is *irrotational.*
- The flow change in time has harmonic character (see the discussions below).
- The external force field acting on fluid particles is confined to the gravity force.
- The continuity equation and the conservation of momentum (Euler's) equation define fluid behaviour.

Let consider all the coordinate systems, adopted in this work and shown in Figure 7 and Figure 12.

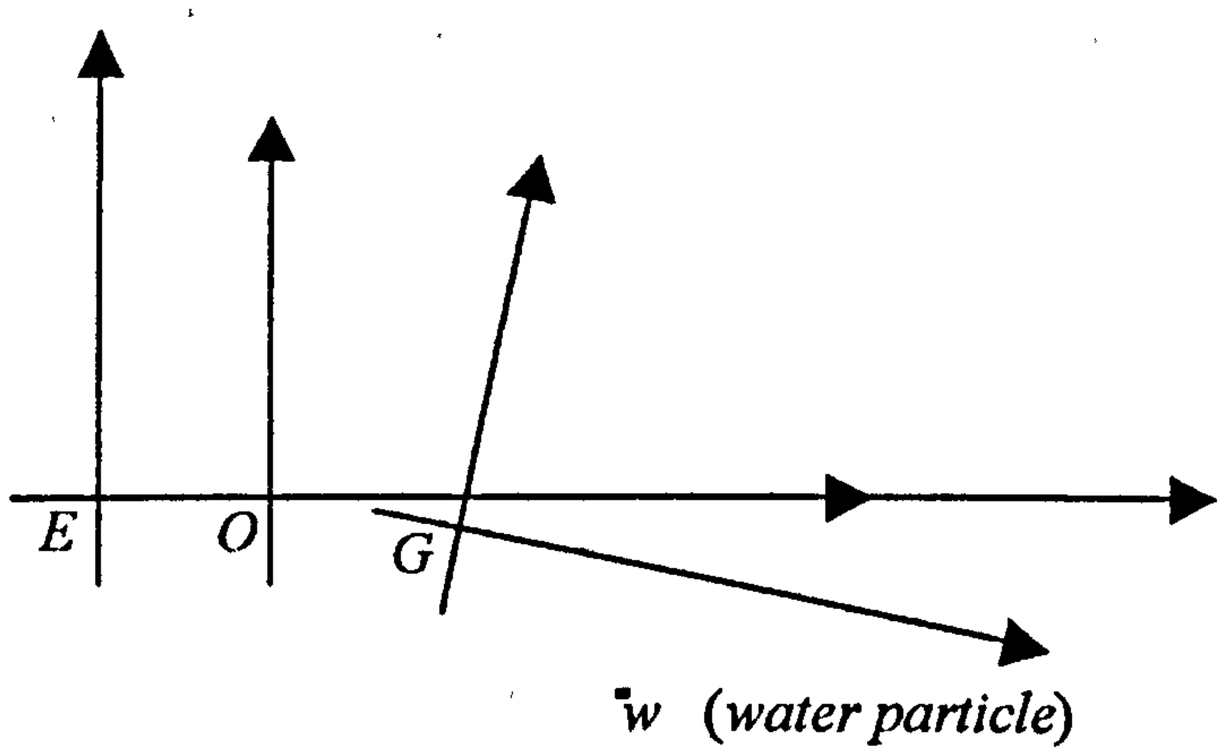

Figure 13 Overview of coordinate systems used

Motion of a water particle can be described in absolute coordinate system EXYZ, by position vector and **absolute velocity**:

$\vec{r}_{Ew}$

$$\frac{D}{Dt}\vec{r}_{Ew} = \vec{u}$$

The same motion can be expressed employing inertial coordinate system OXYZ provided its motion with respect to EXYZ is known:

$$\vec{r}_{Ew} = \vec{r}_{EO} + \vec{r}_{Ow}$$

$$\vec{u} = \vec{u}_O + \vec{u}_w$$

If the oscillatory moving and rotating coordinate system Gxyz is adopted, fluid motion description can be further decomposed:

$$\vec{r}_{Ew} = \vec{r}_{EO} + \vec{r}_{OG} + \vec{r}_{Gw}$$

$$\vec{u} = \vec{u}_O + \vec{u}_G + \vec{u}_w + \vec{\omega} \times \vec{r}_{Gw}$$

Where $\vec{\omega}$ is an angular velocity vector, see Appendix 1 for more details. Generalising, the absolute fluid particle velocity can be expressed as:

$$\vec{u} = \vec{u}_e + \vec{u}_w \qquad (41)$$

Where:

$\vec{u}_e$ Absolute velocity of a coordinate system where the motion is analysed

$\vec{u}_w$ Particle velocity relative to the origin of a coordinate system where the motion is analysed

Let some function of location in space and time be defined $\vec{f} = \vec{f}(\vec{r}, t)$. Its absolute time derivative will be expressed as:

$$\frac{D}{Dt}\vec{f} = \frac{d}{dt}\vec{f} + \left(\frac{d\vec{r}}{dt} \cdot \frac{\partial}{\partial \vec{r}}\right)\vec{f}$$

Where:

$$\frac{\partial}{\partial \vec{r}} = \vec{i} \cdot \frac{\partial}{\partial x} + \vec{j} \cdot \frac{\partial}{\partial y} + \vec{k} \cdot \frac{\partial}{\partial z} = \nabla$$ Differential operator acting directly on any expression on right hand side to the operator

Utilising now different coordinate systems yields:

$$\frac{D}{Dt}\vec{f} = \frac{d}{dt}\vec{f} + (\vec{u} \cdot \nabla)\vec{f}$$ $\vec{f}$ in absolute EXYZ, $\vec{r} = \vec{r}_{Ew}$, $\vec{u}_e = \vec{0}$ (42)

$$\frac{D}{Dt}\vec{f} = \frac{d}{dt}\vec{f} + (\vec{u}_w \cdot \nabla)\vec{f}$$ $\vec{f}$ in moving with mean speed fixed to the body OXYZ, $\vec{r} = \vec{r}_{Ow}$ (43)

$$\vec{u}_e = \vec{u}_O$$ (44)

$$\frac{D}{Dt}\vec{f} = \frac{d}{dt}\vec{f} + \vec{\omega} \times \vec{f} + (\vec{u}_w \cdot \nabla)\vec{f}$$ $\vec{f}$ in oscillating, fixed to the body Gxyz $\vec{r} = \vec{r}_{Gw}$, (45)

$$\vec{u}_e = \vec{u}_O + \vec{u}_G + \vec{\omega} \times \vec{r}_{Gw}$$ (46)

Some note worthy identities:

$$\vec{a} \times (\vec{b} \times \vec{c}) = \vec{b} \cdot (\vec{a} \cdot \vec{c}) - \vec{c} \cdot (\vec{a} \cdot \vec{b})$$ (47)

$$(\vec{a} \cdot \vec{b}) \cdot \vec{c} = \vec{a} \cdot (\vec{b} \otimes \vec{c}) = (\vec{b} \otimes \vec{c})^T \cdot \vec{a}$$ (48)

$$\vec{b} \otimes \vec{c} = \begin{bmatrix} b_x \cdot c_x & b_x \cdot c_y & b_x \cdot c_z \\ b_y \cdot c_x & b_y \cdot c_y & b_y \cdot c_z \\ b_z \cdot c_x & b_z \cdot c_y & b_z \cdot c_z \end{bmatrix}$$ (49)

$$\vec{a} \times (\nabla \times \vec{c}) = \vec{a} \cdot (\nabla \otimes \vec{c})^T - \vec{a} \cdot (\nabla \otimes \vec{c})$$ (50)

6.2 Continuity equation

For the description of fluid behaviour the first theorem to summon is that of conservation of mass:

$$\frac{D}{Dt}\int_{V(t)} \rho \cdot dV = 0 \qquad (51)$$

Where ρ is the fluid density. The left hand side of equation (51) needs difficult integration over time-dependent volume domain. An assumption is usually adopted that the volume considered is always composed of the same fluid particles, hence variation of volume in time can be accounted for by applying the transport theorem, [54]. Then the time derivative of the function inside the integral will be derived with the assumption that the volume does not move, i.e. no change in space is considered. Hence the left hand side of equation (51) can be expanded as:

$$\frac{D}{Dt}\int_{V(t)} \rho \cdot dV = \int_{V(t)} \frac{d}{dt}\rho \cdot dV + \int_{S(t)} (\vec{n} \cdot \vec{u}) \cdot \rho \cdot dS \qquad (52)$$

By virtue of Gauss theorem, the surface integral can be rewritten as volume integral:

$$\int_{S(t)} \vec{n} \cdot \rho \cdot \vec{u} \cdot dS \equiv \int_{V(t)} \nabla(\rho \cdot \vec{u}) \cdot dV \qquad (53)$$

And thus equation (51) can be expressed as:

$$\int_{V(t)} (\frac{d}{dt}\rho + \nabla(\rho \cdot \vec{u})) \cdot dV = 0 \qquad (54)$$

Since the volume in question is an arbitrary quantity, the volume integral in (54) can be omitted. Hence the continuity equation will be expressed by the partial differential equation, which will be simplified further when the following assumptions are adopted: the fluid is *homogeneous* ($\nabla\rho = 0$) and *incompressible* ($\frac{d}{dt}\rho$). Thus the continuity equation takes the form:

$$\nabla\vec{u} = 0 \qquad (55)$$

6.3 Fluid motion equation

This equation is derived in absolute coordinate system from the conservation of momentum equation:

$$\frac{D}{Dt}\int_{V(t)} \rho \cdot \vec{u} \cdot dV = \int_{V(t)} (\nabla \vec{P} + \vec{F}) \cdot dV \qquad (56)$$

Where:

$\nabla \vec{P} = -\nabla p + \mu \cdot \nabla^2 \vec{u}$ Stress tensor in the Newtonian fluid domain

$p = \begin{bmatrix} p & 0 & 0 \\ 0 & p & 0 \\ 0 & 0 & p \end{bmatrix}$ Normal pressure stress tensor

μ Viscosity coefficient

$\vec{F} = \rho \cdot \vec{g} = \nabla(-\rho \cdot g \cdot z)$ Vector of external mass forces acting on the fluid

$\vec{g} = \begin{bmatrix} 0 \\ 0 \\ -g \end{bmatrix}$ Gravity acceleration, $g = 9.81 \frac{m}{s^2}$ (57)

Since the fluid is assumed *incompressible* and *homogeneous* the density ρ can be taken outside of the left hand side integral of the equation (56), which can be rewritten as:

$$\frac{D}{Dt}\int_{V(t)} \vec{u} \cdot dV = \int_{V(t)} \frac{d}{dt} \cdot \vec{u} \cdot dV + \int_{S(t)} (\vec{n} \cdot \vec{u}) \cdot \vec{u} \cdot dS \qquad (58)$$

The surface integral can then be rewritten as:

$$\int_{S(t)} (\vec{n} \cdot \vec{u}) \cdot \vec{u} \cdot dS = \int_{S(t)} \vec{n} \cdot (\vec{u} \otimes \vec{u}) \cdot dS = \int_{V(t)} \nabla(\vec{u} \otimes \vec{u}) \cdot dV =$$

$$= \int_{v(t)} \left(\nabla\left(\vec{u}^c \otimes \vec{u}\right) + \nabla\left(\vec{u} \otimes \vec{u}^c\right) \right) \cdot dV = \int_{V(t)} \left(\nabla \cdot \vec{u}^c\right) \vec{u} + \left(\nabla \vec{u}\right) \cdot \vec{u}^c \cdot dV =$$

$$= \int_{V(t)} \left(\vec{u} \cdot \nabla\right) \vec{u} \cdot dV$$

Where the superscript "c" denotes "no differentiation", accordingly to Leibnitz rule of differentiation. Note that equation (55) has been applied.

Again, since the volume in question is an arbitrary quantity, the integrals can be replaced by the partial differential equations. Hence the momentum equation (56) can be expressed as the well known Navier-Stokes equation [54]:

$$\frac{d}{dt}\vec{u} + \left(\vec{u} \cdot \nabla\right) \vec{u} = -\nabla \frac{p}{\rho} + \nu \cdot \nabla^2 \vec{u} + \frac{\vec{F}}{\rho} \qquad (59)$$

Where $\nu = \frac{\mu}{\rho}$ is the kinematic viscosity coefficient. The following steps will be undertaken to further simplify the fluid flow description. Firstly, the fluid is assumed to be *inviscid* so that $\nu = 0$. Secondly, the left hand side of equation (59) can be interpreted as absolute derivative of $\vec{u}$ expressed in absolute coordinate system $EX^EY^EZ^E$, see equation (42). For simplicity, the fluid behaviour can be analysed in the inertial system OXYZ, moving with the mean forward speed of the ship, see Figure 14. The left hand side of equation (59) will take the form of expression (61).

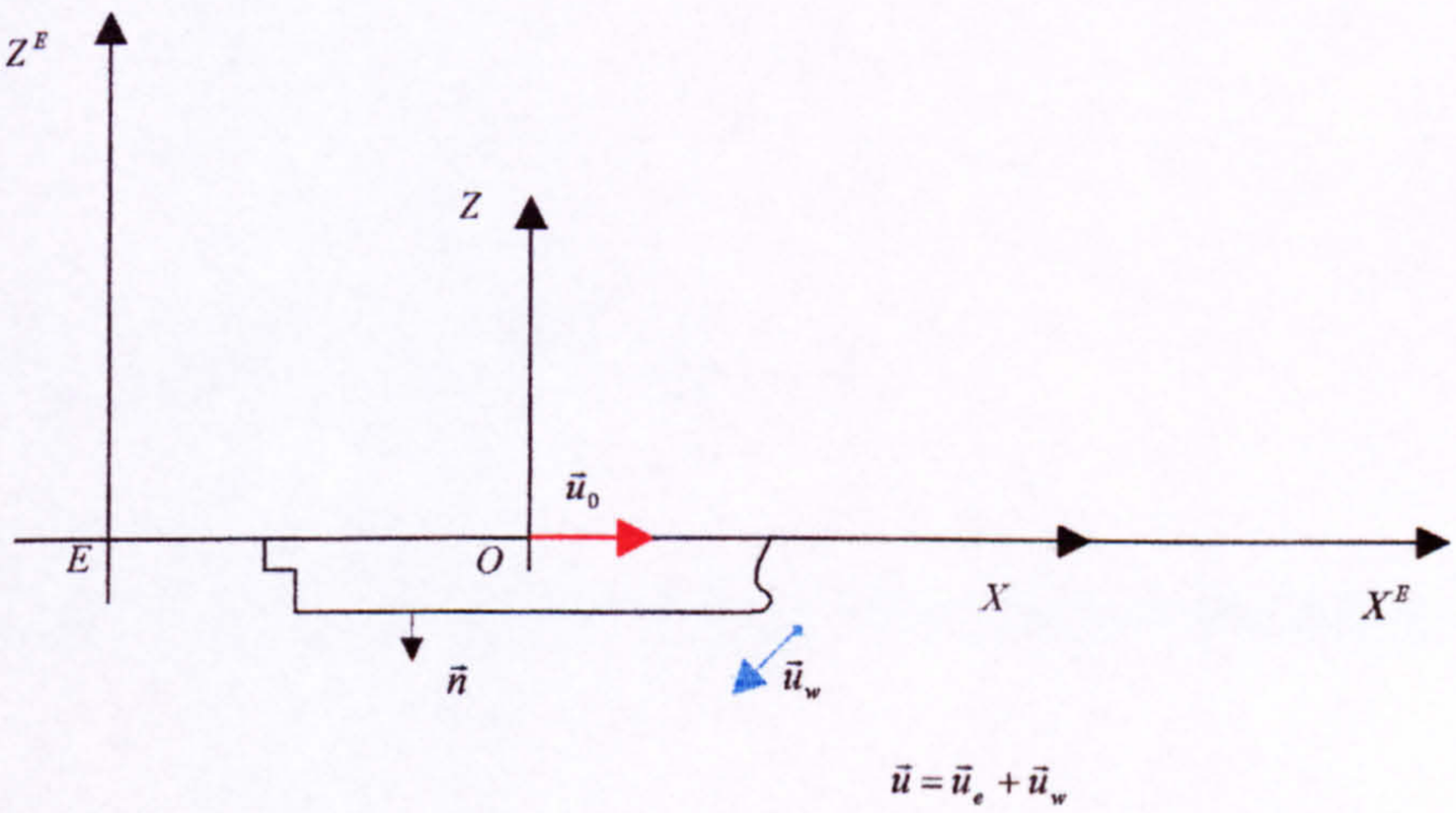

Figure 14 Fluid flow description in inertial system of reference moving with mean speed of the ship

$$\vec{u}_e = \vec{u}_0 = \begin{bmatrix} U & 0 & 0 \end{bmatrix}^T \tag{60}$$

Where U is the forward speed of the ship.

$$\frac{d}{dt}\vec{u} + (\vec{u}_w \cdot \nabla)\,\vec{u} \tag{61}$$

Where $\vec{u}_w$ is defined by equation (41) with (44), respectively, i.e. $\vec{u}_w = \vec{u} - \vec{u}_e$. The second term of expression (61), can be rewritten in the form:

$$(\vec{u}_w \cdot \nabla)\,\vec{u} = \vec{u}_w \cdot (\nabla \otimes \vec{u}) = \vec{u}_w \cdot (\nabla \otimes \vec{u}) - \vec{u}_w \cdot (\nabla \otimes \vec{u})^T + \vec{u}_w \cdot (\nabla \otimes \vec{u})^T$$

Now, applying identities (47) - (50) we can write:

$$\vec{u}_w \cdot (\nabla \otimes \vec{u}) - \vec{u}_w \cdot (\nabla \otimes \vec{u})^T = -\vec{u}_w \times (\nabla \times \vec{u})$$

$$\vec{u}_w \cdot (\nabla \otimes \vec{u})^T = (\nabla \otimes \vec{u}) \cdot \vec{u}_w{}^c = \nabla(\vec{u} \cdot \vec{u}_w{}^c) = \nabla(\vec{u} \cdot \vec{u}^c - \vec{u} \cdot \vec{u}_e^c) = \nabla\left(\frac{\vec{u}^2}{2} - \vec{u} \cdot \vec{u}_e^c\right)$$

Introducing of all of the above into the equation (59) will produce:

$$\frac{d\vec{u}}{dt} + \nabla\left(-\vec{u}_e^c \cdot \vec{u} + \frac{\vec{u}^2}{2}\right) - \vec{u}_w \times (\nabla \times \vec{u}) = -\nabla\left(\frac{p}{\rho} + g \cdot z\right) \tag{62}$$

Or:

$$\frac{d\vec{u}}{dt} + \nabla\left(-\vec{u}_e^c \cdot \vec{u} + \frac{\vec{u}^2}{2} + \frac{p}{\rho} + g \cdot z\right) = \vec{u}_w \times (\nabla \times \vec{u}) \tag{63}$$

The final assumption introduced is that of *irrotational* flow, which means that the vorticity will be zero:

$$\nabla \times \vec{u} = \vec{0}$$

Hence, through Helmholt'z theorem, [54], velocity can be expressed as a gradient of a scalar function, the velocity potential:

$$\vec{u} = \nabla\Phi \tag{64}$$

Note that now $\frac{d\vec{u}}{dt} = \frac{d\nabla\Phi}{dt} = \nabla\frac{d\Phi}{dt}$. Hence equation (63) will be expressed as:

$$\nabla\left(\frac{d\Phi}{dt} - \vec{u}_e \cdot \nabla\Phi + \frac{(\nabla\Phi)^2}{2} + \frac{p}{\rho} + g \cdot z\right) = \vec{0} \tag{65}$$

Or equivalently, integral with respect to the tree space variables x, y and z, in (65) is constant:

$$\frac{d\Phi}{dt} - \vec{u}_e \cdot \nabla\Phi + \frac{(\nabla\Phi)^2}{2} + \frac{p}{\rho} + g \cdot z = const. \tag{66}$$

Equations (66), also known as Bernoulli's equation, together with (55) and (64) describe *unsteady* and *irrotational* motion of *inviscid*, *homogeneous* and *incompressible* fluid as seen from a coordinate system moving with mean ship velocity (60).

6.4 Boundary conditions

To resolve given fluid behaviour, i.e. to find a solution to equations (55) and (66), the undefined thus far fluid domain must be precisely defined and the corresponding boundary conditions set. In case of predictions of flow past the ship the domain is confined by:

- Free surface
- Ship surface
- Bottom surface
- Some finite control surfaces within fluid

Despite assumptions introduced in §6.2 and §6.3 confining the mathematical model of the fluid to that of an ideal one, the problem of determining the flow about the ship is extremely complex because of the mentioned boundaries and complexities arising in modelling them. Therefore, a further set of assumptions and methods associated with boundary conditions must be introduced in order to arrive at practical solutions. This is the subject of the following paragraphs.

6.4.1 Free surface boundary

Kinematic boundary conditions contain the right amount of information regarding the fluid motion, provided the boundary is known, [54, p.110]. In case where velocity and position of the boundary are unknown, additional information must be given. For free surface the relevant information is the pressure on the free surface is equal to that of atmospheric, giving rise to the dynamic free surface condition derived from Bernoulli's equation (66).

Let the free surface be defined in OXYZ reference frame as a function of horizontal coordinates and time as:

$$z = \xi \text{ where } \xi = f(x(t), y(t), t) \qquad (67)$$

The following boundary conditions can be determined on this surface:

6.4.1.1 Kinematic free surface condition

Kinematic boundary condition requires that the fluid particles on the free surface stay on the free surface, which can be expressed as:

$$\frac{D}{Dt}(z-\xi) = \frac{d}{dt}(z-\xi) + \vec{u}_w \cdot \nabla(z-\xi) = 0$$

$$-\frac{d}{dt}\xi + (\nabla\Phi - \vec{u}_e)\cdot\left(-\frac{\partial\xi}{\partial x}, \quad -\frac{\partial\xi}{\partial y}, \quad 1\right) = 0 \qquad (68)$$

6.4.1.2 Dynamic free surface condition

Dynamic free-surface condition requires the water pressure to be equal to the constant atmospheric pressure on the free surface. Choosing constant in equation (66) to be $\frac{p}{\rho}$ at $z = \xi$ gives:

$$\frac{d\Phi}{dt} - \vec{u}_e \cdot \nabla\Phi + \frac{(\nabla\Phi)^2}{2} + g \cdot \xi = 0 \qquad (69)$$

6.4.1.3 Combined free surface condition

It is convenient to have the free surface condition given by a single expression. Here the combined kinematic and dynamic free surface condition can be obtained either by combining equations (68) and (69) or by requiring the absolute pressure to be constant. Absolute derivative of pressure, in inertial coordinate system OXYZ moving with mean ship forward velocity, has the expression:

$$\frac{D}{Dt}p=\frac{d}{dt}p+(\vec{u}_w\cdot\nabla)p=0 \qquad (70)$$

Pressure anywhere in the fluid domain will follow from Bernoulli's equation (66):

$$\frac{d\Phi}{dt}-\vec{u}_e\cdot\nabla\Phi+\frac{(\nabla\Phi)^2}{2}+\frac{p}{\rho}+g\cdot z=\frac{p_a}{\rho} \qquad (71)$$

Solving for the total pressure at any point of the fluid will yield:

$$-\frac{p-p_a}{\rho}=\frac{d\Phi}{dt}-\vec{u}_e\cdot\nabla\Phi+\frac{1}{2}\cdot(\nabla\Phi)^2+g\cdot z \qquad (72)$$

Applying (72) in (70) will result in an equation:

$$\left(\frac{d}{dt}+(\nabla\Phi-\vec{u}_e)\cdot\nabla\right)\left(\frac{d}{dt}\Phi-\vec{u}_e\cdot\nabla\Phi+\frac{1}{2}\cdot(\nabla\Phi)^2+g\cdot z\right)=0$$

Which after carrying out differentiation, results in the exact within the potential-flow theory, combined kinematic-dynamic free surface boundary condition expressed in moving OXYZ reference frame:

$$\begin{aligned}&\frac{d^2\Phi}{dt^2}+g\cdot\frac{\partial\Phi}{\partial z}+\vec{u}_e\cdot\nabla(\vec{u}_e\cdot\nabla\Phi)+2\cdot(\nabla\Phi-\vec{u}_e)\cdot\nabla\frac{d\Phi}{dt}+\\&+\frac{1}{2}\cdot(\nabla\Phi-\vec{u}_e)\cdot\nabla(\nabla\Phi)^2-\nabla\Phi\cdot\nabla(\vec{u}_e\cdot\nabla\Phi)=0\end{aligned} \qquad (73)$$

Again, this equation is valid if $z=\xi(x,y,t)$, i.e. (67) condition applies, which means that:

$$\Phi = \Phi(x, y, \xi, t) \qquad (74)$$

6.4.1.4 Linearisation of combined free surface condition

Expression (73) is a highly non-linear partial differential equation expressed on an unknown free surface $z = \xi(x, y, t)$ to which numerical solutions are too complex to constitute a practical tool. Therefore the following assumptions are commonly introduced, [45]:

The values of the searched velocity potential on the free surface can be determined using the Taylor formula, by the values of the function on the horizontal waterplane, i.e. z=0:

$$\Phi(x, y, \xi, t) = \Phi(x, y, 0, t) + \frac{\partial \Phi}{\partial z} \cdot \xi \Big|_{z=0} + \frac{1}{2} \cdot \frac{\partial^2 \Phi}{\partial z^2} \cdot \xi \Big|_{z=0} + \ldots + \frac{1}{n!} \cdot \frac{\partial^n \Phi}{\partial z^n} \cdot \xi \Big|_{z=0} + R_n \qquad (75)$$

Where R_n is the residual of the Taylor formulae. Assuming, furthermore, that the generated waves are of small amplitudes, higher order terms in equation (75) will have negligible values and can therefore be discarded. This constitutes a great simplification as the velocity potential is now being sought on the known surface z=0, $\Phi(x, y, \xi, t) = \Phi(x, y, 0, t)$.

However, the non-linear terms in (73) are still too cumbersome for numerical tackling and therefore a further simplification is introduced, namely that all the quadratic terms being of smaller order than $\nabla\Phi$ can be as well discarded following an assumption of small wave amplitudes. Then the free surface boundary condition takes the well known linearised form, e.g. [42]:

$$\frac{d^2\Phi}{dt^2} + g \cdot \frac{\partial \Phi}{\partial z} + U^2 \cdot \frac{\partial^2 \Phi}{\partial x^2} - 2 \cdot U \cdot \frac{d}{dt} \frac{\partial \Phi}{\partial x} = 0 \qquad (76)$$

Or once expressed in more concise form:

$$\left(\left(\frac{d}{dt} - U \cdot \frac{\partial}{\partial x} \right)^2 + g \cdot \frac{\partial}{\partial z} \right) \Phi = 0 \qquad (77)$$

6.4.1.5 Harmonic oscillations

The free surface condition (77) is still, however, not a trivial task to model. Indeed, there are still no unique solutions and numerical schemes approved universally which allow predicting properties of the fluid flow about the translating and oscillating ship in waves.

Therefore, one more simplification is introduced, deriving also from the St. Denis and Pierson approach to dealing with random sea excitation by superimposing of solutions for separate frequency components. It is assumed that no transient effects in the flow due to forward speed or initial conditions are present, i.e. the flow has reached steady state mode (induced by external steady excitation conditions) and hence it has a time harmonic character. This allows separation of the time from the amplitude of the velocity potential, hence:

$$\Phi = \phi \cdot e^{i \cdot \omega_E \cdot t}$$

Where the frequency of oscillation ω_E referred to as frequency of encounter, is the steady excitation frequency ω_0 as given in absolute $EX^EY^EZ^E$ reference frame, expressed here in inertial OXYZ coordinate system:

$$\omega_E = \omega_0 \cdot \left(1 - U \cdot \frac{\omega_0}{g} \cdot \cos(\beta)\right) \tag{78}$$

Then finally the free surface linearised condition will be expressed in the form:

$$\left(i \cdot \omega_E - U \cdot \frac{\partial}{\partial x}\right)^2 \phi + g \cdot \frac{\partial \phi}{\partial z} = 0 \tag{79}$$

6.4.2 Linearised velocity potential

There are further consequences of expression (75) and the assumption discarding higher order terms, leading thereby to linearisation of the velocity potential, namely that the superposition principle can now be used. This implies that the total velocity potential can be expressed as a sum of the potentials due to different modes of fluid flow: resulting from action of exciting wave, diffraction and radiation by the moving ship as well as ship steady forward motion. The radiation problem for all 6 degrees of freedom and the diffraction problem can be solved separately and the total solution can be superimposed. Therefore the total velocity potential can be written as:

$$\Phi(t) = \phi_0 + \left(\phi_I + \phi_D + \sum_j \phi_J \right) \cdot e^{i \cdot \omega_E \cdot t} \qquad (80)$$

Where:

ϕ_0	Stationary potential due to ship forward motion
ϕ_I, ϕ_D	Excitation and diffraction potentials due to action of the incident wave
ϕ_J	Radiation potential due to ship motion in j-th mode

Boundary conditions leading to solution for each of the fluid flow problems expressed in (80) will be discussed in the paragraphs below.

6.4.3 Body boundary

Only the kinematic boundary conditions at the ship hull are required, as the boundary itself is known. This condition requires impermeability of the ship body, that is the *relative* normal velocity of the fluid flow at the wetted surface must be zero:

$$\vec{u}'_w \cdot \vec{n}' = 0 \qquad (81)$$

The very complexity implicit in equation (81) is that the vector normal to the ship surface, (82), is known conveniently in ship-fixed coordinate system whereas the fluid velocity is described preferably in inertial coordinate system OXYZ, see for instance equation (41).

$$\vec{n}' = \begin{bmatrix} n_x & n_y & n_z \end{bmatrix}^T \qquad (82)$$

Therefore, the derivation of conditions (81) will be quoted here rather than derived. As mentioned above each of the problems will be solved separately following a linearisation processes.

The linearised diffraction condition must satisfy:

$$(\vec{n} \cdot \nabla)(\phi_I + \phi_D) = 0 \qquad (83)$$

And the radiation problem for each of the modes of motion will become:

$$(\vec{n} \cdot \nabla)\phi_j = i \cdot \omega_E \cdot n_j + U \cdot m_j \qquad (84)$$

Where:

$$n_j = \begin{Bmatrix} \vec{n} \\ \vec{r} \times \vec{n} \end{Bmatrix} \qquad (85)$$

With $\vec{r} = \vec{P} - \vec{A}$ a vector between the assumed point of rotation and any given point $\vec{P}$ on the body surface.

Note that the normal vector can now be considered as expressed in either of the coordinate systems, body fixed or inertial OXYZ, which derives from the linearisation procedure. The ship motions are assumed to be small and hence boundary conditions are expressed for the ***mean*** ship attitude.

The m_j terms and the solution to speed dependent part of conditions (84) are adopted according to strip theory formulation by [66] where the effects of the steady ship motion on the fluid flow are approximated by a uniform flow stream.

6.4.4 Conditions at infinity

For unique solution to the set of governing equations additional condition must be imposed, insuring that the waves generated due to presence of the ship are propagating away from the body. In case of ship progressing with some speed, the problem is complicated further by the three-dimensionality of the generated waves. However, since the strip theory will be adopted to solve the set of governing equations for given boundary conditions, the conditions at infinity can be set for zero speed case and in two dimensions. As work of [75] demonstrated, these conditions can be applied with good approximation at some finite distance from the oscillating body, and this method will be adopted in this thesis. The approach to achieve this is to apply the Green's theorem to the unknown potential and to the source function for an unbounded fluid over fluid domain bounded by the body, the free surface, the bottom and a control surface over which the radiation condition will be applied. The radiation conditions to be insured on the control surfaces for 2D case are given in the mentioned work [75, p.26]: $\frac{\partial \phi}{\partial n} = \pm\, i \cdot K \cdot \phi$, where $\pm$ signifies positive and negative sides of the ship.

6.5 Boundary Element Method (BEM)

Following the general introduction to models of fluid flow in the foregoing, the boundary element method for solving for the unknown velocity potential will be shown next. The technique adopted has been first inspired in [46] and is essentially the same as that of [75]. The main merit of the technique is a very simple source function.

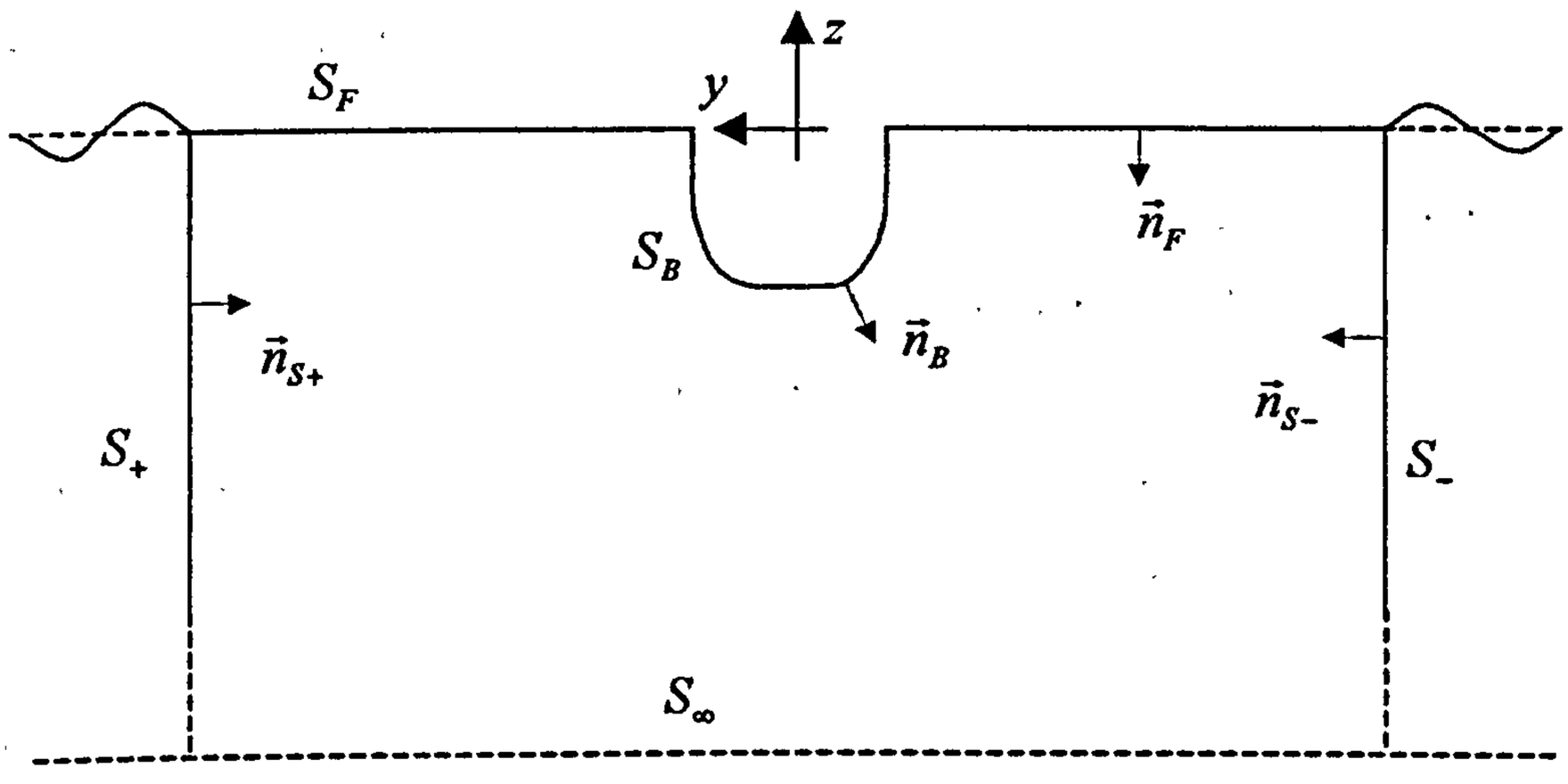

Figure 15 The fluid boundary control surfaces

The 2D velocity potential can be found based on the Green's Second Identity, e.g. [34]:

$$\int_{S_+ S_- S_F S_B S_\infty} \left(\phi \cdot \frac{\partial G}{\partial n} - G \cdot \frac{\partial \phi}{\partial n} \right) dS = 0 \qquad (86)$$

Where ϕ is the unknown velocity potential and G is the known singularity of the form (87). Both functions satisfy the 2D fluid continuity condition (55) anywhere in the fluid domain except the singular points. The singularities are distributed on the control surface.

$$G_{ij} = \ln(r_{ij}) \qquad (87)$$

The control surface is composed of the linearised free surface, body mean surface, far field surface and sea bottom surface. Equation (86) can be rewritten for convenience as:

$$I_{S_+} + I_{S_-} + I_{S_F} + I_{S_B} + I_{S_\infty} = 0 \qquad (88)$$

Since it is assumed that the water depth is infinite, the contribution from sea bottom will be zero:

$$I_{S_\infty} = 0 \qquad (89)$$

6.5.1 Far field solution, S+, S-

The far field refers to the region where no singularities will be distributed and instead the solution of the flow also in this region will be obtained by imposing of radiation condition on control surfaces in the fluid set at finite distance from the ship. Practically, the finite distance is set to one wavelength from the ship but not less than the equivalent ship beam. The magnitude of the velocity potential of a unit-amplitude wave propagating along "$\pm$y" direction can be written as:

$$\phi_\pm = \frac{b_\pm \cdot g}{\omega} \cdot e^{K \cdot z} \cdot e^{\mp i \cdot K \cdot y} \qquad (90)$$

Where $\pm$ corresponds to positive and negative sides of "y" axis. Considering the normal derivative to S+:

$$\frac{\partial}{\partial n} = -\frac{\partial}{\partial y} \qquad (91)$$

A confirmation of the required radiation condition can be obtained:

$$\frac{\partial \phi_+}{\partial n} = i \cdot K \cdot \frac{b_+ \cdot g}{\omega} \cdot e^{K \cdot z} \cdot e^{-i \cdot K \cdot y} \qquad (92)$$

In 2D the position vector can be rewritten using complex number notation as:

$$\vec{r} = (z_c - z) + i \cdot (y_c - y) \qquad (93)$$

Where:

z_c, y_c are the coordinates of a control point

z, y are the coordinates of a source point

Inserting (87) and (92) into (86), leads to the following equation, which can be compared with the equation 3-17, p.39 of [75]:

$$I_{S_+} = \frac{b_+ \cdot g}{\omega} \cdot e^{-i \cdot K \cdot y} \cdot \int_{-\infty}^{0} \left(e^{K \cdot z} \cdot (-1) \cdot \frac{\partial}{\partial y} \ln(r) - \ln(r) \cdot i \cdot K \cdot e^{K \cdot z} \right) dz \qquad (94)$$

Or for convenience:

$$I_{S_+} = B_+ \cdot e^{-i \cdot K \cdot y} \cdot (A_1 + A_2) \qquad (95)$$

Where:

$$B_+ = \frac{b_+ \cdot g}{\omega}$$

$$A_1 = (-1) \cdot \int_{-\infty}^{0} e^{K \cdot z} \cdot \frac{\partial}{\partial y} \ln(r) \cdot dz \qquad (96)$$

The logarithmic expression of (96) can be expanded by making use of (93) :

$$\begin{aligned} \frac{\partial}{\partial y} \ln(r) &= \frac{1}{2} \cdot \frac{\partial}{\partial y} \cdot \ln((z_c - z) + i \cdot (y_c - y)) + \frac{1}{2} \cdot \frac{\partial}{\partial y} \cdot \ln((z_c - z) - i \cdot (y_c - y)) = \\ &= \frac{1}{2} \frac{-i}{(z_c - z) + i \cdot (y_c - y)} + \frac{1}{2} \frac{i}{(z_c - z) - i \cdot (y_c - y)} \end{aligned} \qquad (97)$$

Inserting (97) into (96) and substituting complex number (98) for variable z in (96) allows to express (96) as (99):

$$t = K \cdot \left((z - z_c) \pm i \cdot (y - y_c) \right)$$

$$dt = K \cdot dz \qquad (98)$$

$$z = 0 \;\rightarrow\; t = K \cdot \left((-z_c) \pm i \cdot (y - y_c) \right)$$

$$A_1 = \frac{1}{2} \cdot i \cdot e^{-K \cdot (-z_c + i \cdot (y - y_c))} \cdot \int_{-\infty}^{K \cdot (-z_c + i \cdot (y - y_c))} \frac{e^{K \cdot ((z - z_c) + i \cdot (y - y_c))}}{K \cdot \left((z_c - z) + i \cdot (y_c - y) \right)} dt + \qquad (99)$$

$$-\frac{1}{2} \cdot i \cdot e^{-K \cdot (-z_c - i \cdot (y - y_c))} \cdot \int_{-\infty}^{K \cdot (-z_c - i \cdot (y - y_c))} \frac{e^{K \cdot ((z - z_c) - i \cdot (y - y_c))}}{K \cdot \left((z_c - z) - i \cdot (y_c - y) \right)} dt$$

Now the second part of expression (95) can be expanded:

$$A_2 = (-i \cdot K) \cdot \int_{-\infty}^{0} e^{K \cdot z} \cdot \ln(r) \cdot dz = \begin{vmatrix} \ln(r) & \frac{\partial}{\partial z} \ln(r) \\ \frac{1}{K} \cdot e^{K \cdot z} & e^{K \cdot z} \end{vmatrix} =$$

$$= (-i \cdot K) \cdot \left(\frac{1}{K} \cdot e^{K \cdot z} \cdot \ln(r) \Big|_{-\infty}^{0} - \frac{1}{K} \cdot \int_{-\infty}^{0} e^{K \cdot z} \cdot \frac{\partial}{\partial z} \ln(r) \cdot dz \right) = \qquad (100)$$

$$= (-i) \cdot \left(\ln(r_c) - \int_{-\infty}^{0} e^{K \cdot z} \cdot \frac{\partial}{\partial z} \ln(r) \cdot dz \right)$$

Where:

$$r_c = z_c^2 + (y_c - y)^2$$

Similarly as (97), the logarithmic part of (100) can be further rewritten:

$$\frac{\partial}{\partial z} \ln(r) = \frac{1}{2} \cdot \frac{-1}{(z_c - z) + i \cdot (y_c - y)} + \frac{1}{2} \cdot \frac{-1}{(z_c - z) - i \cdot (y_c - y)} \qquad (101)$$

Again, inserting (101) and (98) into (100) leads to the following:

$$A_2 = (-i)\cdot\ln(r_c) + (-i)\cdot\frac{1}{2}\cdot e^{-K\cdot(-z_c+i\cdot(y-y_c))}\cdot\int_{-\infty}^{K\cdot(-z_c+i\cdot(y-y_c))}\frac{e^t}{-t}dt + (-i)\cdot\frac{1}{2}\cdot e^{-K\cdot(-z_c-i\cdot(y-y_c))}\cdot\int_{-\infty}^{K\cdot(-z_c-i\cdot(y-y_c))}\frac{e^t}{-t}dt \quad (102)$$

Now combining (99) and (102) into (95) produces the solution expressing contribution from S+:

$$I_{S_+} = B_+\cdot e^{-i\cdot K\cdot y}\cdot(-i)\cdot(E(Z_+)+\ln(r_c)) \quad (103)$$

Where:

$$E(x) = e^x\cdot\int_{-\infty}^{-x}\frac{e^t}{-t}dt \quad (104)$$

$$Z_\pm = K\cdot(z_c \pm i\cdot(y-y_c)) \quad (105)$$

Following the same procedure for contribution from S-

$$I_{S_-} = B_-\cdot e^{i\cdot K\cdot y}\cdot(-i)\cdot(E(Z_-)+\ln(r_c)) \quad (106)$$

6.5.2 Near field solution, S_F, S_B

The near field refers to the region where the singularities are distributed, that is the surfaces S_F, S_B.

6.5.2.1 Free surface boundary

The linear free surface condition derived for the 2D case, where only transverse waves are considered to be generated i.e. longitudinal variation of potential is negligible, ignoring in effect the speed-dependent terms (convective terms) in (79) is:

$$-\omega_E{}^2 \cdot \phi + g \cdot \frac{\partial \phi}{\partial z} = 0 \qquad (107)$$

Noting that on the free surface

$$\frac{\partial}{\partial z} = -\frac{\partial}{\partial n}$$

$$\frac{\partial \phi}{\partial n} = -K \cdot \phi$$

The surface integral (86) will be expressed as:

$$I_{S_F} = \int_{S_F} \left(\frac{\partial G}{\partial n} + K \cdot G \right) \cdot \phi \cdot dS = 0 \qquad (108)$$

6.5.2.2 Body boundary

Deriving from (84) and (83), the 2D radiation and diffraction boundary conditions can be expressed as:

$$\frac{\partial \phi_j}{\partial n} = i \cdot \omega_E \cdot n_j \qquad (109)$$

And

$$\frac{\partial \phi_D}{\partial n} = -\frac{\partial \phi_{FK}}{\partial n} \qquad (110)$$

Or generalising the body boundary conditions will read:

$$\frac{\partial \phi}{\partial n} = U_n$$

The boundary integral over the body surface will take the following form:

$$I_{S_B} = \int_{S_B} \left(\phi \cdot \frac{\partial G}{\partial n} - G \cdot U_n \right) dS \qquad (111)$$

6.5.3 Matching scheme of inner and outer solutions

The integral (108) is solved for the unknown velocity potential on the free surface, and with normal velocity known through free surface condition (107). By setting additional condition that the normal velocity on the **last** segment of the free surface on both sides of the ship is equal to the normal velocity to the radiation boundaries, $S_{\pm}$, the unknown amplitudes of the outgoing waves, B_+ and B_-, seen in (103) and (106), will be removed from the matrix of influence coefficients resulting from numerical solution of (86).

$$\frac{\partial \phi_{last\pm}}{\partial n} = \frac{\partial \phi_{S\pm}}{\partial n}$$

Where:

$$\frac{\partial \phi_{last\pm}}{\partial n} = -K \cdot \phi_{last\pm} \text{ and } \frac{\partial \phi_{S\pm}}{\partial n} = -\frac{\partial \phi_{S\pm}}{\partial z} = -K \cdot B_{\pm} \cdot e^{K \cdot z}\Big|_{z=0} \cdot e^{\mp i \cdot K \cdot y_{\pm}}$$

Hence the matching takes the form:

$$-\phi_{last\pm} + B_{\pm} \cdot e^{\mp i \cdot K \cdot y_{\pm}} = 0 \qquad (112)$$

Equation (88) with (89), (103), (106), (108), (111) and (112) is a complete boundary element method set-up for a given ship section to solve for unknown 2D velocity potential ϕ on the control surfaces and dependent on imposed body boundary conditions (109) or (110). The numerical algorithm is shown in §8.

Validation of the presented approach for prediction of hydrodynamic coefficients for 2D sections is demonstrated in Appendix 2 with experimental data deriving from research presented in [36], [57] and [68].

6.6 Fluid forces

The technique for resolving of the fluid flow has been discussed in the foregoing. The ensuing fluid pressures deriving from Bernoulli's equation can be integrated over the body surface and fluid forces be obtained.

$$p - p_a = -\rho \cdot \left(\frac{d}{dt} - U \cdot \frac{\partial}{\partial x} \right) \cdot \Phi - \rho \cdot g \cdot z \qquad (113)$$

Following the superposition principles deriving from (80) the total hydrodynamic force will be composed of Restoring, Radiation (added mass and potential damping), Incident Wave and Diffraction components. Numerical schemes for integration of (113) for each of these components and their time domain representation will be discussed in the following paragraphs.

Additionally, a series of empirical formulations aiming at inclusion of non-linear (higher order) effects, such as drift or viscosity terms, will be presented.

Unless otherwise stated, the forces are always expressed in the inertial coordinate system OXYZ, and for the purpose of time simulation they are transformed to the body-fixed system by applying the theory discussed in Appendix 1.

6.6.1 Restoring forces

The hydrostatic forces and moments (restoring forces) are derived by integration of hydrostatic water pressure over the submerged mean ship geometry:

$$F_{Restoring_j} = -\int_{S_B} p_S \cdot n_j \cdot dS \qquad (114)$$

Where the six component normal vector n_j is given by (85).

The hydrostatic pressure derives from linearised Bernoulli equation (113) where only the last static term is taken into account:

$$p_S = -\rho \cdot g \cdot z \qquad (115)$$

Note, that consistent with the assumption of linearity of the free surface condition this pressure is evaluated up to the mean water plane level:

$$-\infty < z < 0 \qquad (116)$$

However, in order to account for non-linearities arising from geometrical variations due to large amplitude motions and bearing in mind that hydro static forces are the predominant component of the total hydrodynamic forces in estimation of ship dynamic behaviour, this pressure is evaluated for the instantaneous vessel attitude, i.e. $S_B = f(t)$. The integral in (114) can be evaluated either by direct 3D or 2D approach.

6.6.2 Radiation forces: Added Mass & Potential Damping

The radiation forces and moments can be obtained from integration of the fluid pressure over the wetted surface of the ship, S_B:

$$F_{Radiation\,j} = -\int_{S_B} p_R \cdot n_j \cdot dS$$

The radiation forces will be evaluated by a strip theory formulation, as discussed in §6.5. That is the 2D pressure distribution due to harmonic body oscillations is first evaluated from linearised momentum equation (72) by only considering dynamic terms and neglecting the convective terms, ignoring therefore any influence of the radiation velocity potential in longitudinal direction:

$$p_R = -\rho \cdot \frac{d\Phi_R}{dt}$$

$$\Phi_R = \phi \cdot e^{i\cdot\omega_E\cdot t} \longrightarrow \quad \frac{d\Phi_R}{dt} = i \cdot \omega_E \cdot \phi \cdot e^{i\cdot\omega_E\cdot t}$$

The force amplitude in j direction due to motion in k mode can be derived:

$$T_{jk} = \rho \cdot i \cdot \omega_E \cdot \int_S \phi_k \cdot n_j \cdot dS \qquad (117)$$

Velocity potentials ϕ_k in (117) are solution to boundary element method (86) with boundary conditions (109).

Sectional added mass and damping force coefficients are found according to the following:

$$a_{jk} = \frac{\mathrm{Re}(T_{jk})}{\omega_E^2} \qquad b_{jk} = \frac{\mathrm{Im}(T_{jk})}{-\omega_E} \qquad (118)$$

The sectional coefficients are integrated along the length of the ship. To account for speed and "end" effects according to strip theory formulation the following corrections have been applied as derived in [66]:

6.6.2.1 Added mass

$$A_{33} = \int a_{33}dx - \frac{U}{\omega_E^2} \cdot b_{33}^A \quad (119)$$

$$A_{35} = \int -x \cdot a_{33} \cdot dx - \frac{U}{\omega_E^2} \cdot B_{33}^0 + \frac{U}{\omega_E^2} \cdot x_A \cdot b_{33}^A - \frac{U^2}{\omega_E^2} \cdot a_{33}^A \quad (120)$$

$$A_{53} = \int -x \cdot a_{33} \cdot dx + \frac{U}{\omega_E^2} \cdot B_{33}^0 + \frac{U}{\omega_E^2} \cdot x_A \cdot b_{33}^A \quad (121)$$

$$A_{55} = \int x^2 \cdot a_{33} \cdot dx + \frac{U^2}{\omega_E^2} \cdot A_{33}^0 - \frac{U}{\omega_E^2} \cdot x_A^2 \cdot b_{33}^A + \frac{U^2}{\omega_E^2} \cdot x_A \cdot a_{33}^A \quad (122)$$

$$A_{22} = \int a_{22} \cdot dx - \frac{U}{\omega_E^2} \cdot b_{22}^A \quad (123)$$

$$A_{24} = \int a_{24} \cdot dx - \frac{U}{\omega_E^2} \cdot b_{24}^A \quad (124)$$

$$A_{42} = \int a_{42} \cdot dx - \frac{U}{\omega_E^2} \cdot b_{42}^A \quad (125)$$

$$A_{26} = \int x \cdot a_{22} \cdot dx + \frac{U}{\omega_E^2} \cdot B_{22}^0 - \frac{U}{\omega_E^2} \cdot x_A \cdot b_{22}^A + \frac{U^2}{\omega_E^2} \cdot a_{22}^A \quad (126)$$

$$A_{62} = \int x \cdot a_{22} \cdot dx - \frac{U}{\omega_E^2} \cdot B_{22}^0 - \frac{U}{\omega_E^2} \cdot x_A \cdot b_{22}^A \quad (127)$$

$$A_{44} = \int a_{44} \cdot dx - \frac{U}{\omega_E^2} \cdot b_{44}^A \quad (128)$$

$$A_{46} = \int x \cdot a_{24} \cdot dx + \frac{U}{\omega_E^2} \cdot B_{24}^0 - \frac{U}{\omega_E^2} \cdot x_A \cdot b_{24}^A + \frac{U^2}{\omega_E^2} \cdot a_{24}^A \quad (129)$$

$$A_{64} = \int x \cdot a_{42} \cdot dx - \frac{U}{\omega_E^2} \cdot B_{42}^0 - \frac{U}{\omega_E^2} \cdot x_A \cdot b_{42}^A \quad (130)$$

$$A_{66} = \int x^2 \cdot a_{22} \cdot dx + \frac{U^2}{\omega_E^2} \cdot A_{22}^0 - \frac{U}{\omega_E^2} \cdot x_A^2 \cdot b_{22}^A + \frac{U^2}{\omega_E^2} \cdot x_A \cdot a_{22}^A \quad (131)$$

6.6.2.2 Damping coefficients

$$B_{33} = \int b_{33}dx + U \cdot a_{33}^A \quad (132)$$

$$B_{35} = \int -x \cdot b_{33} \cdot dx + U \cdot A_{33}^{0} - U \cdot x_A \cdot a_{33}^{A} - \frac{U^2}{\omega_E^2} \cdot b_{33}^{A} \quad (133)$$

$$B_{53} = \int -x \cdot b_{33} \cdot dx - U \cdot A_{33}^{0} - U \cdot x_A \cdot a_{33}^{A} \quad (134)$$

$$B_{55} = \int x^2 \cdot b_{33} \cdot dx + \frac{U^2}{\omega_E^2} \cdot B_{33}^{0} + U \cdot x_A^2 \cdot a_{33}^{A} + \frac{U^2}{\omega_E^2} \cdot x_A \cdot b_{33}^{A} \quad (135)$$

$$B_{22} = \int b_{22} \cdot dx + U \cdot a_{22}^{A} \quad (136)$$

$$B_{24} = \int b_{24} \cdot dx + U \cdot a_{24}^{A} \quad (137)$$

$$B_{42} = \int b_{42} \cdot dx + U \cdot a_{42}^{A} \quad (138)$$

$$B_{26} = \int x \cdot b_{22} \cdot dx - U \cdot A_{22}^{0} + U \cdot x_A \cdot a_{22}^{A} + \frac{U^2}{\omega_E^2} \cdot b_{22}^{A} \quad (139)$$

$$B_{62} = \int x \cdot b_{22} \cdot dx + U \cdot A_{22}^{0} + U \cdot x_A \cdot a_{22}^{A} \quad (140)$$

$$B_{44} = \int b_{44} \cdot dx + U \cdot a_{44}^{A} \quad (141)$$

$$B_{46} = \int x \cdot b_{24} \cdot dx - U \cdot A_{24}^{0} + U \cdot x_A \cdot a_{24}^{A} + \frac{U^2}{\omega_E^2} \cdot b_{24}^{A} \quad (142)$$

$$B_{64} = \int x \cdot b_{42} \cdot dx + U \cdot A_{42}^{0} + U \cdot x_A \cdot a_{42}^{A} \quad (143)$$

$$B_{66} = \int x^2 \cdot b_{22} \cdot dx + \frac{U^2}{\omega_E^2} \cdot B_{22}^{0} + U \cdot x_A^2 \cdot a_{22}^{A} + \frac{U^2}{\omega_E^2} \cdot x_A \cdot b_{22}^{A} \quad (144)$$

6.6.2.3 Asymmetric hull geometry:

In order to account for the mean variation of ship underwater geometry, additional terms will have non-zero values, as the XZ-plane symmetry will no longer exist. The following terms have been additionally assessed:

$$A_{23} = \int a_{23} \cdot dx \qquad B_{23} = \int b_{23} \cdot dx \quad (145)$$

$$A_{32} = \int a_{32} \cdot dx \qquad B_{32} = \int b_{32} \cdot dx \quad (146)$$

$$A_{34} = \int a_{34} \cdot dx \qquad B_{34} = \int b_{34} \cdot dx \qquad (147)$$

$$A_{43} = \int a_{43} \cdot dx \qquad B_{43} = \int b_{43} \cdot dx \qquad (148)$$

Note however, that these coefficients do neither account for end- or speed-effects, and cannot, therefore, be applied for speeds deviating "far" from zero.

6.6.3 Convolution techniques

Having derived the hydrodynamic radiation forces in frequency domain, a question now arises of expressing these forces in the time domain. The solution is offered by [33] with its methodology generally referred to as convolution technique and recently applied in [120].

$$F_{Radiation\,j}(t) = A_{\infty} \cdot \frac{d}{dt} u_j(t) + \int_{t-lag}^{t} K_{jk}(t-\tau) \cdot u_j(\tau) \cdot d\tau \qquad (149)$$

$$K_{jk}(\omega) = \frac{2}{\pi} \cdot \int_{0}^{\infty} B_{jk}(\omega) \cdot \cos(\omega \cdot t) \cdot d\omega \qquad (150)$$

Where:

$u_j = \begin{Bmatrix} \vec{v}_A \\ \vec{\omega} \end{Bmatrix}$ Generalised velocity vector in inertial coordinate system, j=1 .. 6

B_{jk} Damping coefficients matrix, k=1 .. 6

A_{∞} Added mass matrix for frequency of oscillation $\omega \rightarrow \infty$

$lag = 15s$ Length of convolution

Examples of kernel functions for test vessel PRR1 are shown in Figure 16 to Figure 20 below.

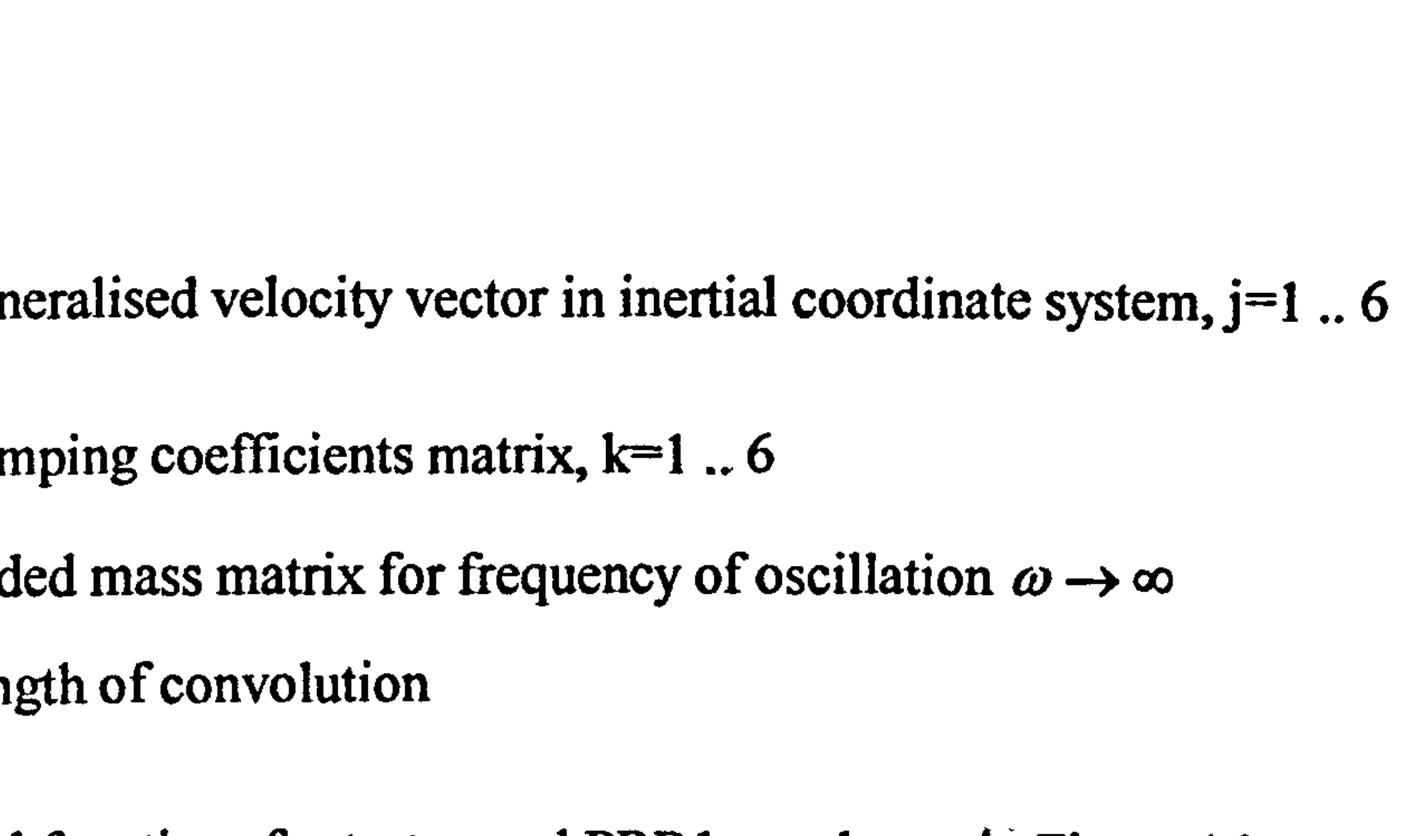

Figure 16 Kernel function for sway mode of motion (the two curves overlap). The "3D (Ha)" corresponds to solution with the code developed by [39].

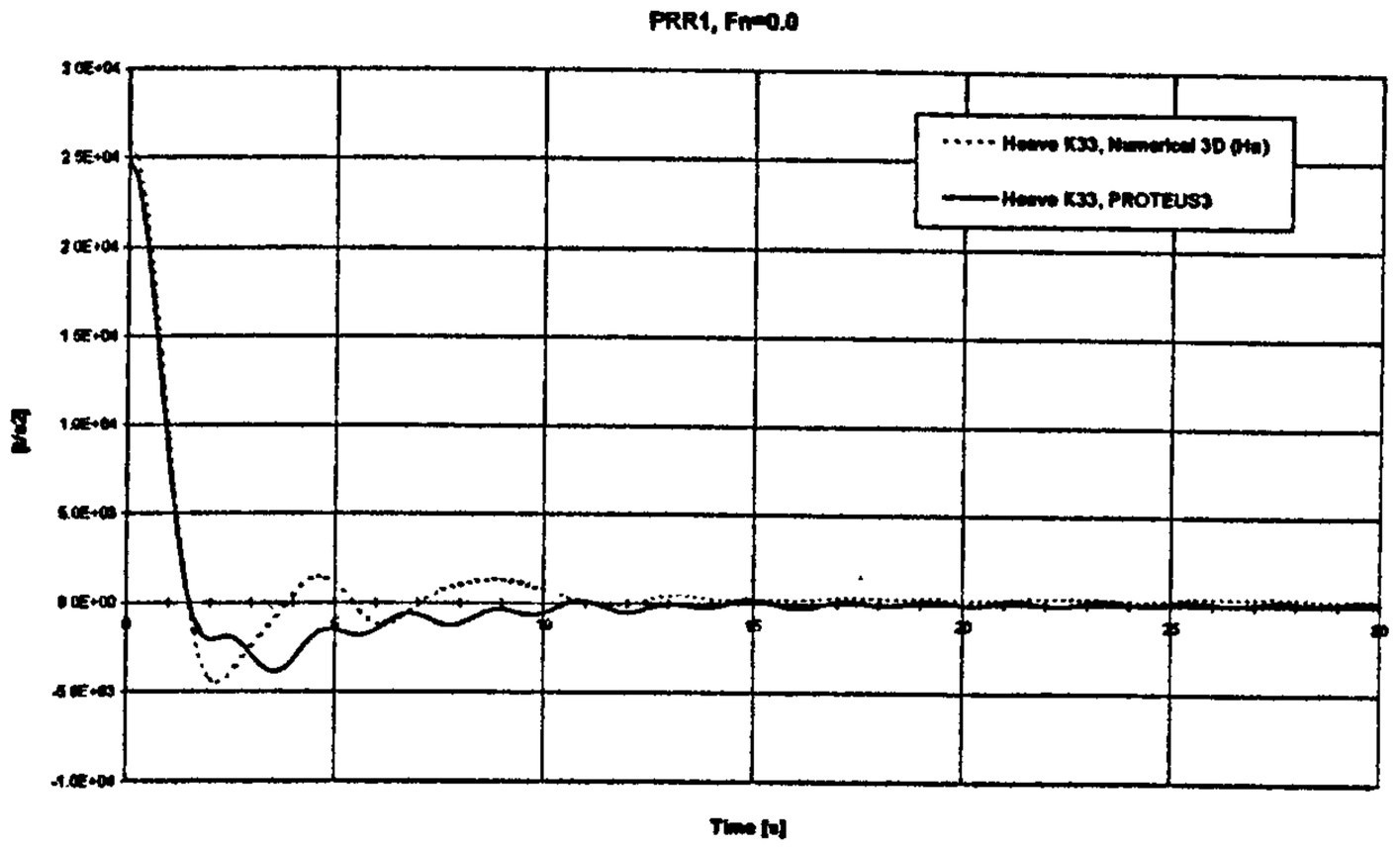

Figure 17 Kernel function for heave mode of motion The "3D (Ha)" corresponds to solution with the code developed by [39].

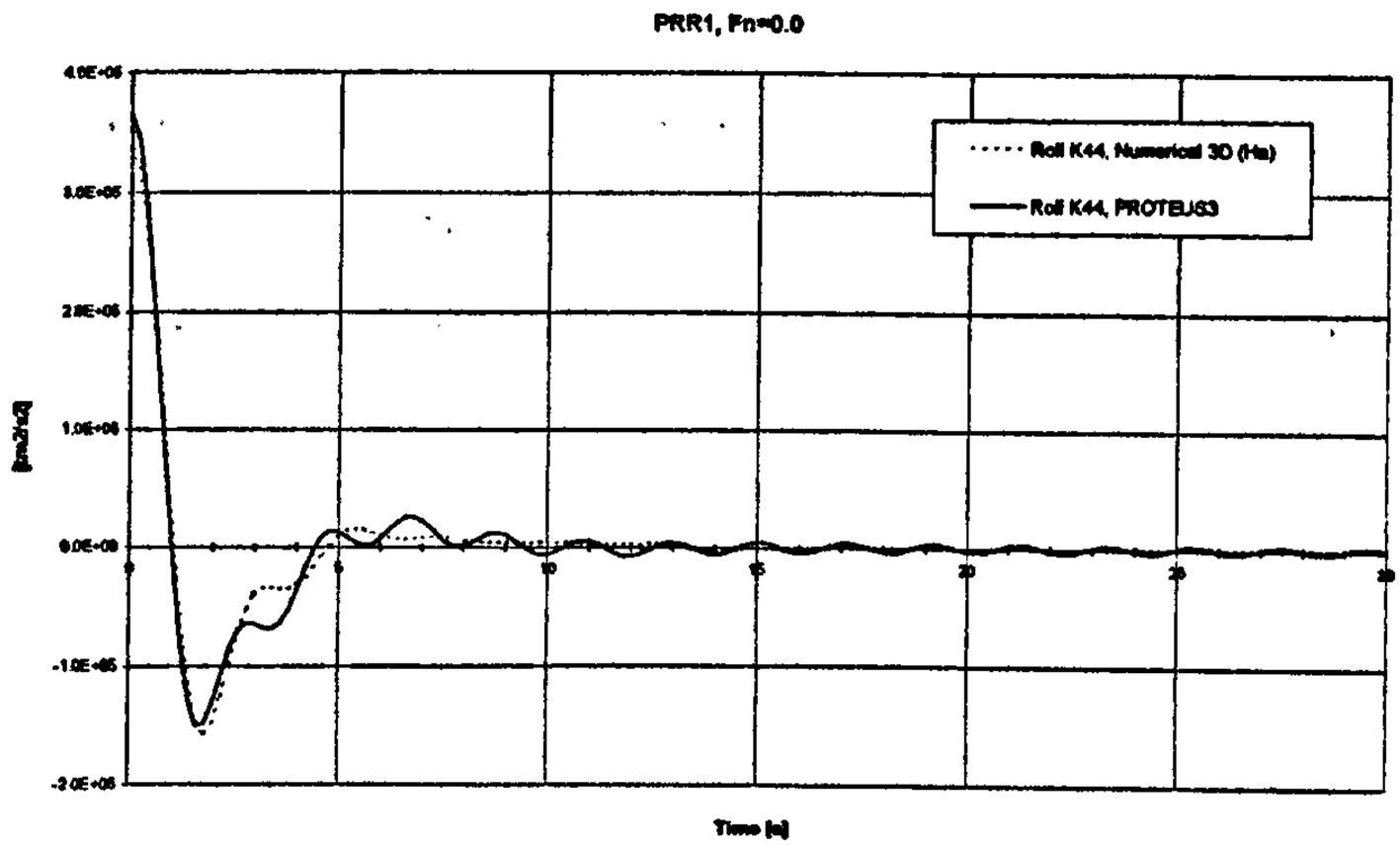

Figure 18 Kernel function for roll mode of motion The "3D (Ha)" corresponds to solution with the code developed by [39].

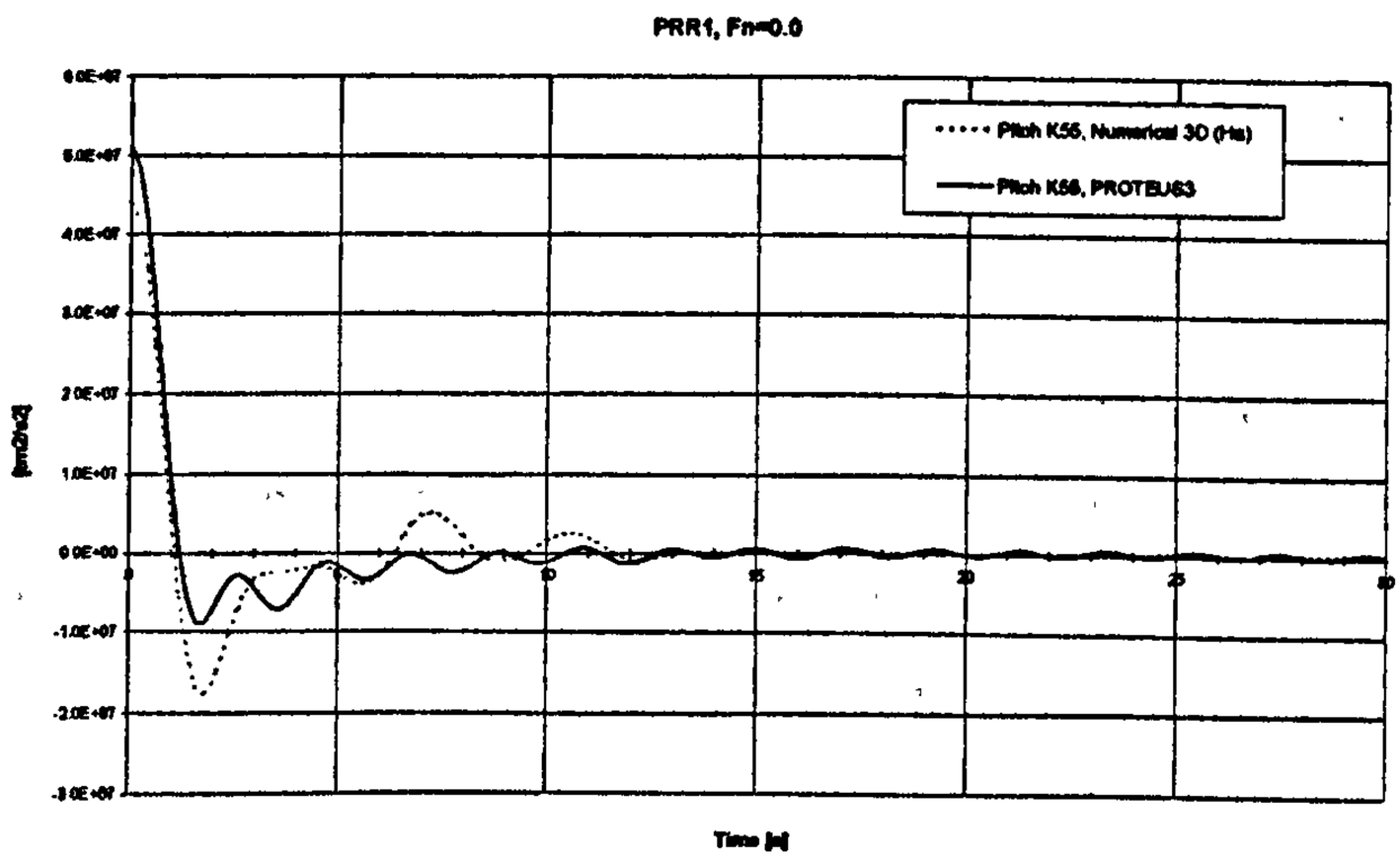

Figure 19 Kernel function for pitch mode of motion The "3D (Ha)" corresponds to solution with the code developed by [39].

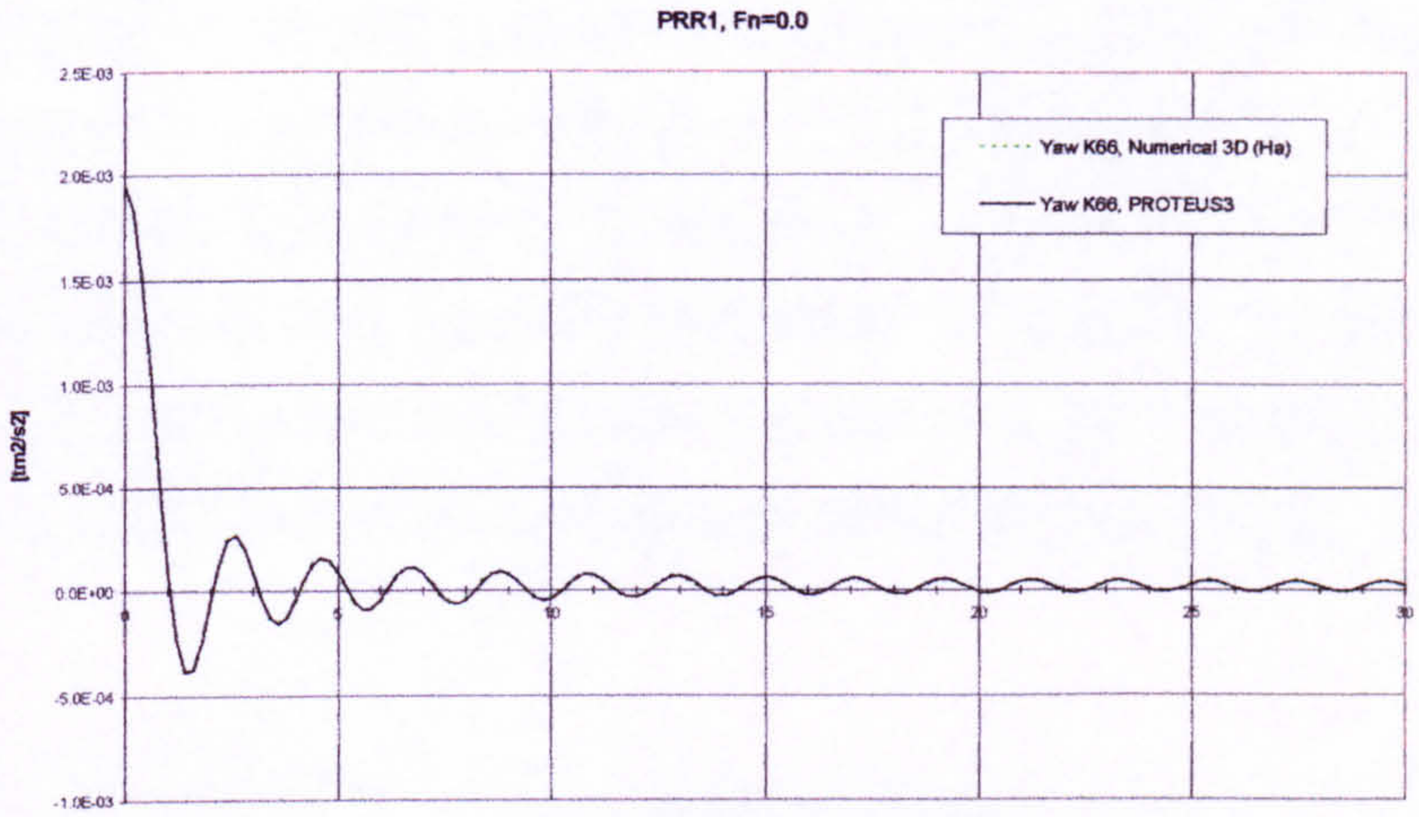

Figure 20 Kernel function for yaw mode of motion. The "3D (Ha)" corresponds to solution with the code developed by [39].

Note that both equations (149) and (150) are expressed in the inertial coordinate system OXYZ and will need, therefore to be transferred to the body-fixed system of reference. Transformation of these forces, however, is not straightforward and needs additional discussion to that in Appendix 1.

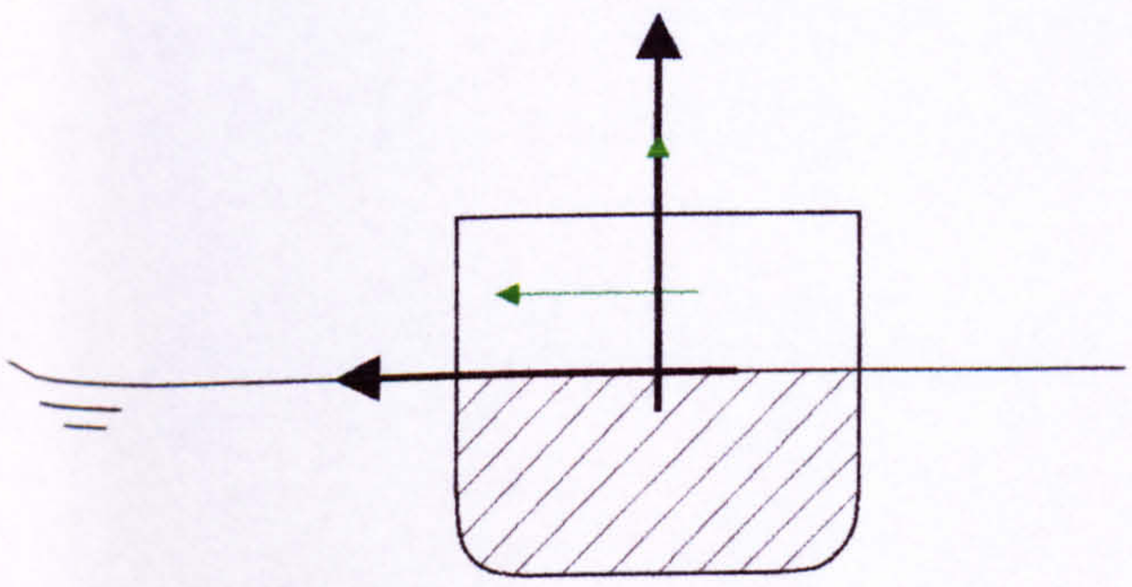

Figure 21 The hydrodynamic coefficients are obtained for the mean immersed ship geometry

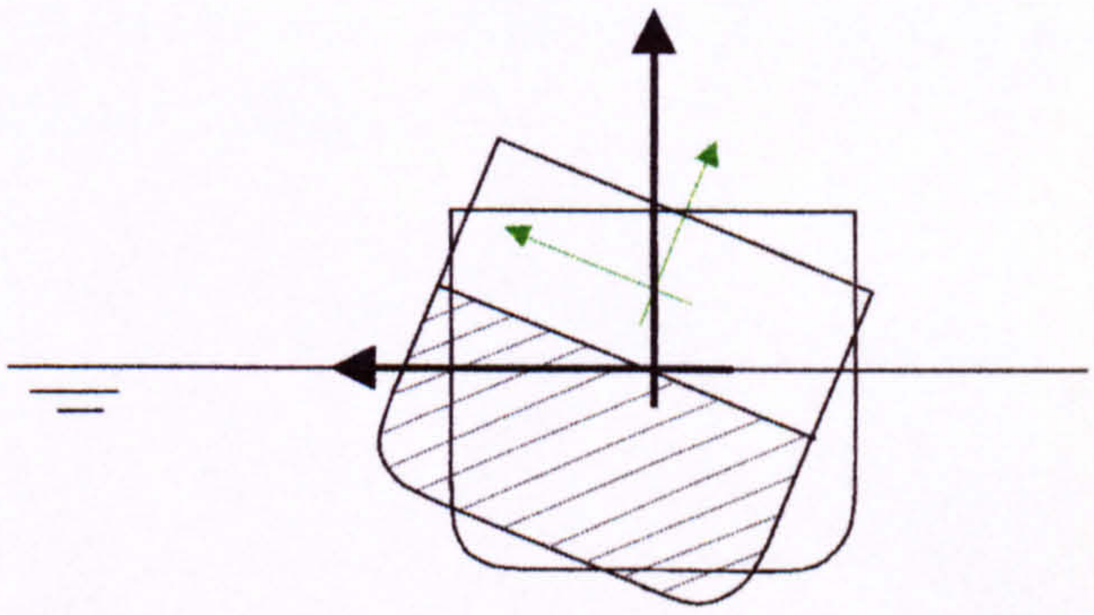

Figure 22 During time domain simulation of ship response the hydrodynamic forces are assumed to be constant and corresponding to the mean attitude.

As is shown in Figure 21, the coefficients are evaluated for stationary ship attitude, which follow an assumption that the motions are of small amplitude. However, the equations of motion must be

solved in a system fixed to the body and bearing in mind that the actual motion amplitudes the vessel can undergo can be significant, say roll of 10-20deg amplitude, these forces should be expressed in this system. The solution to boundary value problem instantaneously is very expensive, indeed impractical, and hence the coefficients are assumed to be constant for the ship oscillating around its mean position. What this assumption implies is that the expression of the radiation forces in inertial or body-fixed systems will depend only on the velocity vector, see Figure 22:

$$f_3 = A_{33} \cdot \ddot{v}_3 \qquad \text{inertial system}$$

$$f'_3 = A_{33} \cdot \ddot{v}'_3 \qquad \text{body-fixed system} \qquad (151)$$

Therefore the kernel functions (150) will be assumed constant, i.e. transferable between body-fixed or inertial coordinate systems without any rotation-related operations.

6.6.4 Incident wave excitation (Froude-Krylov) forces

The excitation forces and moments are derived by integrating the pressure resulting from incident wave acting on the mean hull surface:

$$F_{FKj} = -\int_{S_B} p_{FK} \cdot n_j \cdot dS \qquad (152)$$

The pressure on the hull boundary resulting from action of gravity-waves described by velocity potential (159) satisfying the free surface condition (79), and expressed in the inertial coordinate system OXYZ, can be derived from (66) while considering only dynamic and linear terms of that equation:

$$p_{FK} = -\rho \cdot \left(\frac{d\Phi_{FK}}{dt} - U \cdot \frac{\partial \Phi_{FK}}{\partial x} \right) \qquad (153)$$

After substitution of (161) and (162) into (153), the pressure distribution in any point (known in OXYZ system of reference) of the fluid and due to the action of undisturbed incident waves will be expressed by (155). Note that the pressure due to the action of incident wave has the same complex amplitude in either $EX^EY^EZ^E$ or OXYZ coordinate systems.

$$p_{FK} = -\rho \cdot i \cdot \left(\omega_E + U \cdot K_0 \cdot \cos(\beta)\right) \cdot \phi_{FK} \cdot e^{i \cdot \omega_E \cdot t} \qquad (154)$$

$$p_{FK} = g \cdot \rho \cdot e^{K_0 \cdot z} \cdot e^{-i \cdot S} \cdot e^{i \cdot \omega_E \cdot t} \qquad (155)$$

Where:

$$S = K_0 \cdot (x \cdot \cos(\beta) - y \cdot \sin(\beta)) \qquad (156)$$

$$K_0 = \frac{\omega_0^2}{g} \qquad (157)$$

x, y, z Coordinates of offset points of the mean hull geometry or of any point expressed in OXYZ system of reference. Note that OXYZ system here is considered same as $O^0X^0Y^0Z^0$ i.e. OXYZ for t=0 in (178).

Note also that deriving from (78), the encounter frequency can be expressed as:

$$\omega_E = \omega_0 - U \cdot K_0 \cdot \cos(\beta) \qquad (158)$$

The potential of incident gravity waves satisfying the free surface condition (79), [66], can be expressed as follows:

$$\Phi_{FK} = \phi_{FK} \cdot e^{i \cdot \omega_E \cdot t} \qquad (159)$$

Where time independent amplitude of the potential per unit wave amplitude is:

$$\phi_{FK} = \frac{i \cdot g}{\omega_0} \cdot e^{K_0 \cdot z} \cdot e^{-i \cdot S} \qquad (160)$$

The time derivative of incident wave velocity potential (159) can be easily found as:

$$\frac{d\Phi_{FK}}{dt} = i \cdot \omega_E \cdot \phi_{FK} \cdot e^{i \cdot \omega_E \cdot t} \qquad (161)$$

And the gradient of this potential in inertial coordinate system OXYZ follows:

$$\frac{\partial \phi_{FK}}{\partial x} = \frac{i \cdot g}{\omega_0} \cdot e^{K_0 \cdot z} \cdot e^{-i \cdot S} \cdot (-i) \cdot K_0 \cdot \cos(\beta) \qquad (162)$$

$$\frac{\partial \phi_{FK}}{\partial y} = -\omega_0 \cdot \sin(\beta) \cdot e^{K_0 \cdot z} \cdot e^{-i \cdot S} \qquad (163)$$

$$\frac{\partial \phi_{FK}}{\partial z} = i \cdot \omega_0 \cdot e^{K_0 \cdot z} \cdot e^{-i \cdot S} \qquad (164)$$

The final force corresponding to the excitation by wave of frequency ω_0 will be composed of real and imaginary parts, or what has more physical meaning, the amplitude and the phase lag with respect to the exciting wave:

$$F_{FK_J}(t,\omega_E)=\Re\left(\left(f^R_{FK_J}(\omega_0)+i\cdot f^I_{FK_J}(\omega_0)\right)\cdot e^{i\cdot\omega_E\cdot t}\right) \qquad (165)$$

Or:

$$F_{FK_J}(t,\omega_E)=\Re\left(f^A_{FK_J}(\omega_0)\cdot e^{i\cdot\omega_E\cdot t+i\cdot f^\delta_{FK_J}(\omega_0)}\right) \qquad (166)$$

Where:

$\Re$	denotes real part of
f^R_{FK}, f^I_{FK}	frequency dependent incident wave excitation forces and moments in a complex format derived from (152)
$f^A_{FK}=\sqrt{\left(f^R_{FK}\right)^2+\left(f^I_{FK}\right)^2}$	amplitude of the force
$f^\delta_{FK}=\arctan\left(\frac{f^I_{FK}}{f^R_{FK}}\right)$	phase lag angle of the force

It is also important to derive an equation describing the wave elevation profile in earth-fixed coordinate system $EX^EY^EZ^E$, which follows from linearised condition (69) with (161) expressed here in this system:

$$\xi^E=\Re\left(-\frac{1}{g}\cdot\frac{d\Phi}{dt}\right) \qquad (167)$$

$$\xi^E=\Re\left(-\frac{1}{g}\cdot\left(i\cdot\omega_0\cdot\left(\frac{i\cdot g}{\omega_0}\cdot e^{K_0\cdot z}\cdot e^{-i\cdot K_0\cdot X^E}\right)_{z=0}\cdot e^{i\cdot\omega_0\cdot t}\right)\right) \qquad (168)$$

$$\xi^E=\Re\left(e^{i\left(\omega_0\cdot t-K_0\cdot X^E\right)}\right) \qquad (169)$$

$$\xi^E=\cos\left(\omega_0\cdot t-K_0\cdot X^E\right) \qquad (170)$$

6.6.5 Diffraction forces

The diffraction force is derived similarly by integrating the diffraction pressures over the mean immersed hull geometry, i.e.:

$$F_{Dj} = -\int_{S_B} p_D \cdot n_j \cdot dS \qquad (171)$$

As in the case of radiation forces, diffraction forces will be found based on the 2D approach where the pressure will be evaluated for each strip and integrated along her length. The convective terms will again be dropped and resulting speed and end terms will be added as derived in [50].

The 3D-pressure expression is as follows:

$$p_D = -\rho \cdot \left(\frac{d\Phi_D}{dt} - U \cdot \frac{\partial \Phi_D}{\partial x} \right) \qquad (172)$$

Disregarding the convective terms and accounting for (175) the pressure expression for the 2D strip follows:

$$p_D = -\rho \cdot i \cdot \omega_E \cdot \phi_D \cdot e^{i \cdot \omega_E \cdot t} \qquad (173)$$

The diffraction potential will be written in the following form:

$$\Phi_D = \phi_D \cdot e^{i \cdot \omega_E \cdot t} \qquad (174)$$

With the time derivative:

$$\frac{d\Phi_D}{dt} = i \cdot \omega_E \cdot \phi_D \cdot e^{i \cdot \omega_E \cdot t} \qquad (175)$$

Where ϕ_D is a solution to boundary element method (86) with boundary conditions (110) and where the velocity components in z- and y- directions are defined by (163) and (164), respectively.

The additional end and speed terms may be expressed as:

$$f_D^{speed} = \frac{U}{i \cdot \omega_E} \cdot \begin{bmatrix} 0 \\ 0 \\ 0 \\ 0 \\ F_{D3} \\ -F_{D2} \end{bmatrix} \qquad f_D^{end} = \frac{U}{i \cdot \omega_E} \cdot \begin{bmatrix} 0 \\ f_2^{end} \\ f_3^{end} \\ f_4^{end} \\ -x \cdot f_3^{end} \\ x \cdot f_2^{end} \end{bmatrix}$$

Similar to (165) the diffraction forces in time domain will be of the form:

$$F_{D_J}(t, \omega_E) = \Re\left(f_{D_J}^A(\omega_E) \cdot e^{i \cdot \omega_E \cdot t + i \cdot f_{D_J}^\delta(\omega_E)} \right) \qquad (176)$$

Having applied, in the foregoing, techniques for predicting hydrodynamic excitation (FK+D) forces and moments for a given incident wave frequency, speed and heading, a well known method will now be briefly discussed, allowing for representation of these forces for long-crested confused seas.

6.6.6 Spectral techniques

The principle of superposition proposed by [157] applicable to the ship motions problem will be applied in this work. It hypothesises that responses of ship to irregular waves can be considered as the summation of responses to regular waves of all frequencies. The validity of this approach has been considered proven for the past three decades, [66]. Considering the coordinate systems employed, see Figure 23 below, and the harmonic forces and moments resulting from incident wave excitation and diffraction, the forces and moments exerted on a ship advancing in a seaway can be predicted based on the spectral techniques.

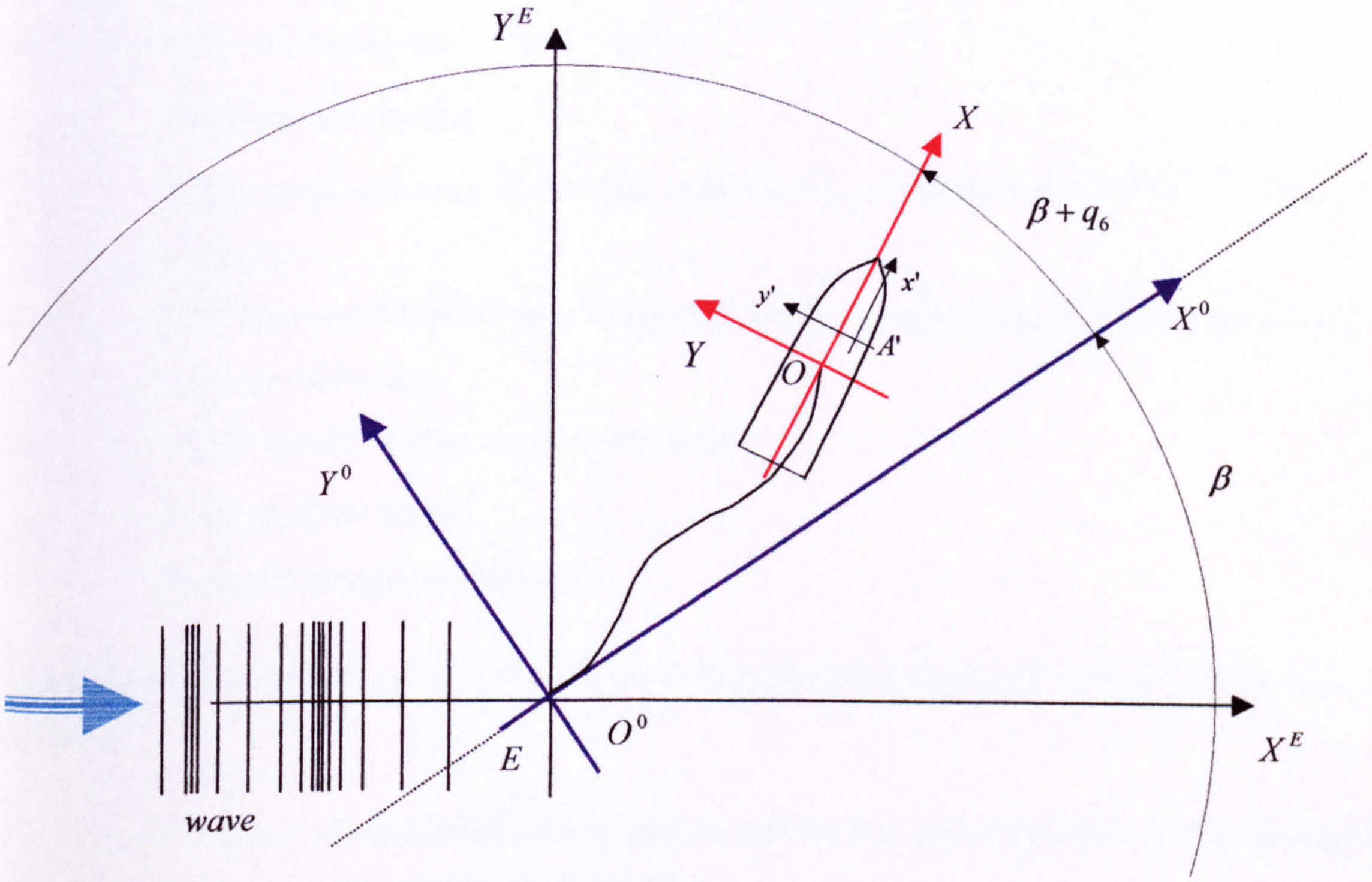

Figure 23 Conventions used for environment description, the coordinate systems: inertial earth fixed $EX^EY^EZ^E$, inertial initial $O^0X^0Y^0Z^0$, inertial moving with mean ship speed OXYZ, non-inertial body-fixed Ax'y'z'. See also Figure 7 and Figure 12.

The random wave elevation in the earth fixed coordinate system $EX^EY^EZ^E$ is composed of a series of harmonic components (170) and hence is given as:

$$\xi^E = \sum_i a_i \cdot \cos\left(\omega_{0i} \cdot t - K_{0i} \cdot X^E + \sigma_i\right) \qquad (177)$$

Where, accounting for the vessel motions to any position X^0, Y^0 in the inertial coordinate system $O^0X^0Y^0Z^0$ as well as aiming to define the wave elevation at any position x, y, z in the inertial coordinate system OXYZ, the longitudinal coordinate in the earth fixed system X^E can be expressed:

$$X^E = X^0 \cdot \cos(\beta) - Y^0 \cdot \sin(\beta) + (x \cdot \cos(\beta + q_6) - y \cdot \sin(\beta + q_6)) \qquad (178)$$

Where further:

β	Initial heading
q_6	Yaw mode of motion
$\beta + q_6$	Instantaneous heading
X^0, Y^0	**Mean** surge and sway of the ship, respectively, predicted in the $O^0X^0Y^0Z^0$ system of reference
x, y, z	Coordinates of offset points of the hull geometry or of any point expressed in the OXYZ system of reference.
a_i	Amplitude of wave harmonic components
σ_i	Random phase angle
i	Harmonic component numeral

Thus substitution of (178) into (177) will yield wave elevation expressed in the OXYZ system of reference.

Note that the number of harmonics used should be sufficient to avoid repetition of the simulated wave record. The repetition time can be found from:

$$t_{signal\_repetition} = \frac{1}{\Delta f}$$

The total incident wave excitation and diffraction forces due to the action of confused sea will be found from:

$$F^E(t) = \sum_i a_i \cdot \left(f^A_{FK+D}\right)_i \cdot \cos\left(\omega_{0i} \cdot t - K_{0i} \cdot X^E + \sigma_i + \left(f^\delta_{FK+D}\right)_i\right) \qquad (179)$$

Again, substituting (178) into (179) will yield the force expressed in OXYZ system of reference. However, care must be taken in applying (179) for predicting forces in time domain, where the speed as well as the heading of the vessel can change. Namely that each force harmonic component corresponds to a given ship heading and speed, and therefore once the ship changes its mean speed and heading, these forces (F-K with heading, diffraction with both heading and speed) must be updated. This technique will be discussed together with the treatment of the effects of mean ship geometry variations in §6.6.8.

The amplitudes and phase angles, a_i and σ_i, respectively, of each wave harmonic component is usually found from a given wave energy spectrum and through digital random number generators, which procedure is broadly discussed in literature.

6.6.7 Forces up to instantaneous wave elevation

Sometimes a need arises to simulate ship motions in high seas, where the prevalent sea components are of high amplitudes (approaching ship draught) as well as long with respect to ship length ($\lambda >> L$). An approach will be shown allowing approximations of hydrodynamic forces and moments resulting in large amplitude ship motions. It has been deemed impractical to solve the whole problem of non-linear fluid-ship interactions. Bearing in mind that the hydrostatic and incident wave (F-K) forces are the prevalent components in high seas, these forces will be evaluated up to the instantaneous wave elevation. It should be noted that despite the theoretical limitations, linear wave theory applied to large amplitude waves in deep water has been found to yield quite adequate results as regards wave profile, water particle kinematics and pressure, [96], therefore this approach is expected to be satisfactory for predictions of wave excitation forces and moments for large amplitude motions.

The radiation and diffraction forces will be predicted as discussed in the foregoing based on linear prepositions.

The total hydrostatic and Froude-Krylov force will be expressed as follows:

$$F_{FK+Restoring_j} = -\int_{S_B} (p_S + p_{FK}) \cdot n_j \cdot dS \qquad (180)$$

Note that the restoring forces are not evaluated by (114) anymore as these forces are now included in (180). The hydrostatic pressure is evaluated from:

$$p_S = -\rho \cdot g \cdot z \qquad (181)$$

The instantaneous pressure due to oncoming random waves will be obtained by the superposition principle discussed in the §6.6.6, with the velocity potential of each harmonic component given by the real part of (159). The resultant pressure distribution will be expressed as:

$$p_{FK} = \rho \cdot g \cdot \sum_i a_i \cdot e^{K_0(z_i)} \cdot \cos(\omega_{0i} \cdot t - K_{0i} \cdot X^E + \sigma_i) \qquad (182)$$

Where in order to account for the effects of the wave excitation integrated up to the instantaneous elevation the vertical coordinate should be taken as:

$$-\infty < z < \xi^E \qquad (183)$$

The wave elevation ξ^E is given by (177). The integral (180) can be evaluated based on 3D geometry of the hull.

Note that in this work the exponential part of (182) is assumed to be constant above the mean water level in accordance with linear wave theory, [34]:

$$z_1 = \begin{cases} z & if\ z \le 0 \\ 0 & if\ z > 0 \end{cases}$$

6.6.8 Hydrodynamics for a damaged ship

As has been discussed in the foregoing, the fluid exciting and reaction forces are assessed based on an ideal fluid model, undergoing potential flow and confined by the linearised free surface and mean ship immersed geometry boundaries. Despite especially the last two critical assumptions, requiring in effect that the ship oscillates with small amplitude and the free surface undergoes only limited disturbances, the theory in the case of intact ship conditions shows encouragingly good correlation with experimental or full scale measurements even for environmental conditions outside those permissible by the theory.

This agreement verifies that the predominant constituents influencing ship behaviour are modelled with sufficient accuracy and that the higher order non-linear effects are normally of limited importance for the prediction of ship dynamic behaviour.

It is on this basis that the approach initiated in [120] is pursued further in this research, which borrows the underlying potential hydrodynamics theory for intact ship conditions and applies it to the damaged ship case.

There are two phenomena associated with ship foundering that will influence the flow field around the ship geometry. Firstly the breach in the ship hull will change the flow in the vicinity of the opening due to the ensuing ingress/egress of water and although the real extent to which such a hull discontinuity could have on the overall mean forces is not known accurately, it is disregarded in this research based on the supposition that the effect will be partly addressed while (a) modelling water ingress/egress and (b) accounting for the effects of floodwater on the ship dynamics by applying rigid body theory. As will be discussed in further part of this thesis, the flow disturbance outside the ship due to the damage opening, not addressed in this work in any way, needs more research attention in future.

The second phenomenon addresses the ship wetted surface. The mean hull geometry around which the ship oscillates will vary significantly violating thereby the assumptions introduced in §6.4, equations (83) and (84), allowing predictions of fluid exciting and reaction forces. Disregarding from the beginning the instantaneous solution to the boundary value problem, this effect will be accounted for by the "database" approach were the forces will be evaluated for a range of

anticipated ship sinkage, trim and heel, before the time simulation and the coefficients for the "relevant" attitude will be found by linear interpolation. The content of the database (added mass, potential damping, Froude-Krylov and diffraction forces) will be compiled with the use of the theory underlined in §6.6. An extensive study on the effects of the ship attitude on fluid forces is presented in Appendix 3.

There are two aspects associated with the DATABASE approach that need careful implementation, finding the "mean" ship attitude instantaneously and expressing the actual radiation forces in time domain based on the coefficients contained in this DATABASE.

6.6.8.1 Filtering of the signals

Finding the mean response of the ship in the time-domain solution relies on processing of a continuous data stream instantaneously so that the filtered output is obtained in parallel. There are a number of techniques available, from Fourier transform-based filters to moving averages, but having experimented with a few, the following Finite Impulse Response (FIR) filter has been designed and applied in this work:

$$y(t) = \frac{1}{K} \cdot \int_{-T/2}^{T/2} x(t-\tau) \cdot h(\tau) \cdot d\tau \qquad (184)$$

Where:

$x(t)$	time-domain signal to be analysed
$h(t) = W(t) \cdot \frac{1}{2 \cdot \pi} \cdot \int_{-\omega_{cut}}^{\omega_{cut}} H(\omega) \cdot e^{-i \cdot \omega \cdot t} \cdot d\omega$	time-domain impulse response function
$H(\omega) = 1$ if $\omega < \omega_{cut}$	parameters of the filter
$H(\omega) = 0$ if $\omega >= \omega_{cut}$	
$W(t) = \cos^2\left(t \cdot \frac{\pi}{2 \cdot T}\right)$	windowing function
$K = \int_{-T/2}^{T/2} h(\tau) \cdot d\tau$	correction coefficient
$\omega_{cut} = 0.1$ [rad/s]	low-pass band of the filter

$T = 30$ [s] span of the signal $x(t)$ to be filtered

Note that the signal (184) has some time lag behind the original signal as shown in Figure 24.

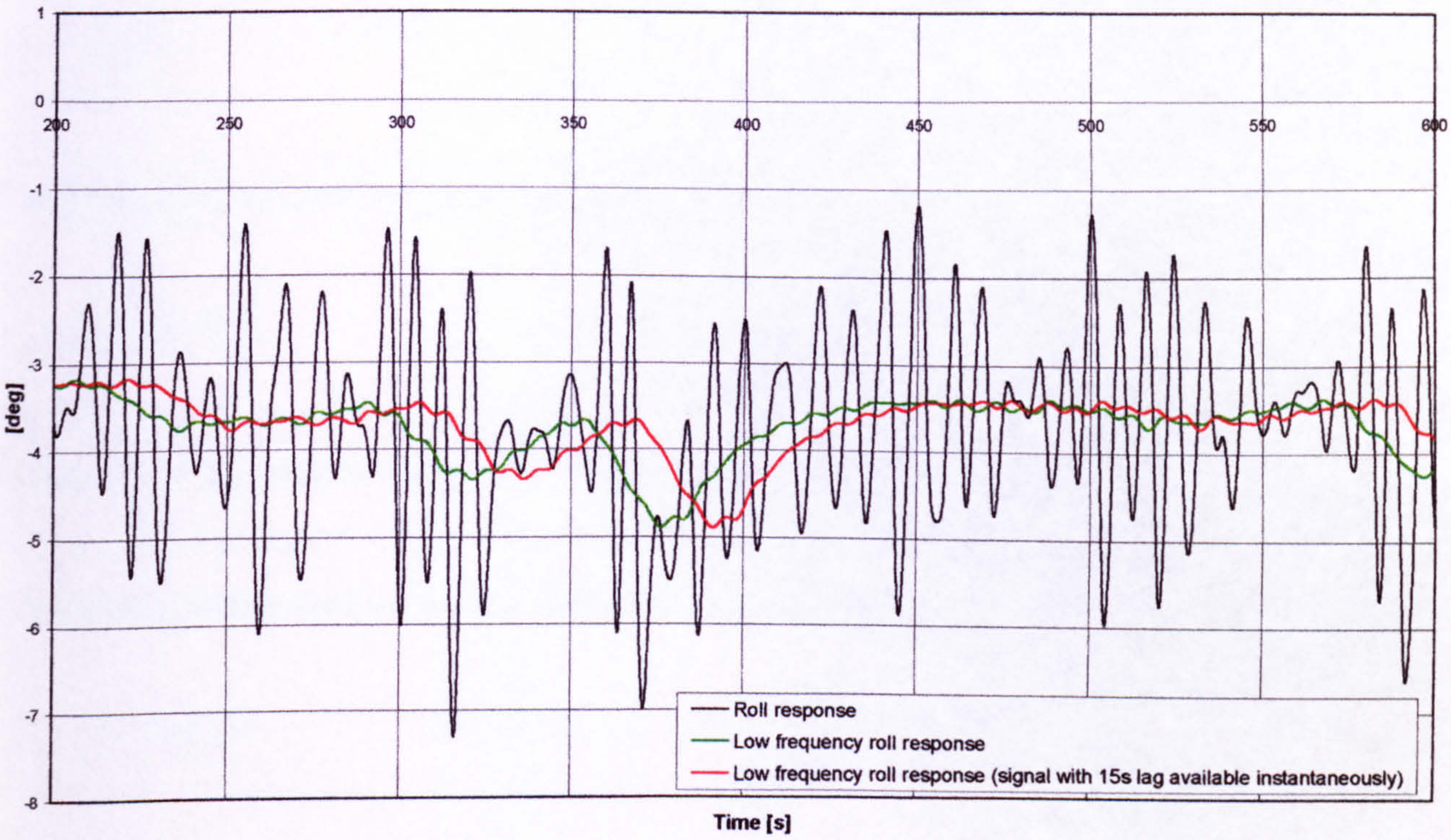

Figure 24 Sample of low-pass filtering of the time-domain-solution data stream

6.6.8.2 Radiation forces for mean varying geometry

As discussed in §6.6.3, while simulating radiation forces, the hydrodynamic coefficients are kept constant in either body-fixed or inertial coordinate systems with the resultant force expression resolved in either of the systems depending on the resolution of the velocity vector. The problem occurs, however, in case the mean ship attitude deviates significantly, from that of the up-right one, see Figure 25. In this case the boundary value problem is still set up in a system with its vertical axis perpendicular to calm water level whereas the ship-bound vertical axis, designating e.g. the ship heave motion mode, is transformed. Obviously all the modes of motion are affected.

Therefore the coefficients must be transformed to the coordinate system that designates the mean ship attitude, and then kept constant for the oscillatory motions around that attitude. This is shown below based on the added mass coefficients.

The force in the inertial coordinate system, Figure 25, is written:

$$F_j = A \cdot \ddot{u}_j$$

The corresponding force in a system fixed to "mean" ship attitude could be obtained:

$$F_j^* = D^* \cdot \left(A \cdot \ddot{u}_j\right)$$

Where $D^* = D(heel, trim)$, with the D matrix explained in Appendix 1.

The forces in body-fixed system can then be derived similarly as (151):

$$F'_j = \left(D^* \cdot A\right) \cdot \ddot{u}'_j$$

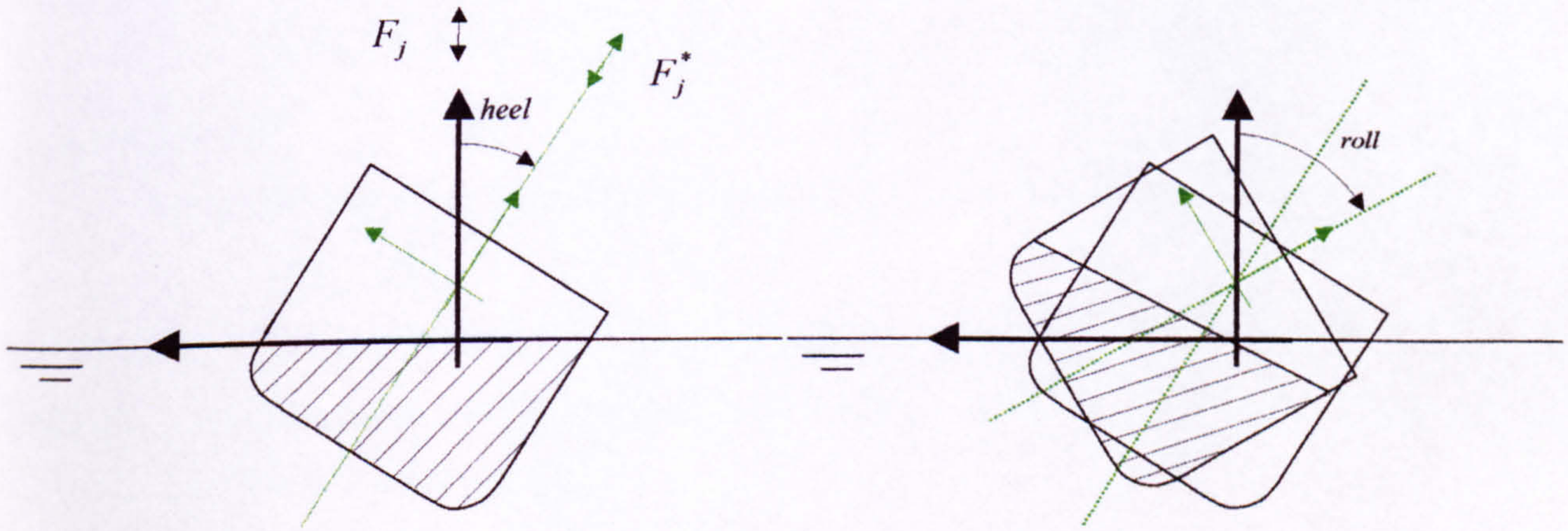

Figure 25 For the damaged ship, the mean attitude results from the equilibrium after flooding

Figure 26 Ship deviations from mean attitude are assumed to be small and hence the coefficients are kept constant but corresponding to the mean attitude.

6.6.9 Drift and current forces

Higher order effects, such as the mean drift forces, might be a subject of separate dissertation due to the complex nature of this phenomenon. Resulting from non-zero mean pressure due to oscillating fluid flow past the body, drift forces are subject to non-linear analysis. The problem is usually solved by applying perturbation analysis with the wave amplitude as a small parameter and solving the potential problem to second-order in incident wave amplitude. The result of this approximation are mean forces, and forces oscillating with difference and sum frequencies in addition to the linear solution, [34]. This powerful approach proves very useful in a multitude of ocean engineering problems.

However, for the purpose of this research, rigorous treatment of mean wave forces has been discarded on the preposition of significantly lower order of magnitude (~ 10 to 100 times lower), [34], than the resultant first order incident wave forces. Instead, for the sake of simplicity, approximate parametric methods described in [120] will be employed here.

The drift forces in OXYZ coordinate system can be derived from:

$$\vec{F}_{Drift} = \frac{1}{2} \cdot \rho \cdot g \cdot \begin{bmatrix} C_{dx} \cdot B \\ C_{dy} \cdot L \\ 0 \\ 0 \\ 0 \\ C_{dn} \cdot L^2 \end{bmatrix} \cdot A^1 \qquad (185)$$

Where:

$$C_{dx} = \cos(\beta) \cdot |\cos(\beta)| \cdot C_{dx}^{S} \qquad (186)$$

$$C_{dy} = -\sin(\beta) \cdot |\sin(\beta)| \cdot C_{dy}^{S} \qquad (187)$$

$$C_{dn} = -\sin(2 \cdot \beta) \cdot C_{dn}^{S} \qquad (188)$$

C_{dx}^{S}, C_{dy}^{S} and C_{dn}^{S} are vessel geometry and wave-length dependent coefficients:

$$C_{dx}^{S} = 0.62 \cdot \sin^2\left(\frac{\pi \cdot \lambda}{1.6 \cdot L}\right),\ C_{dx}^{S} = 0.0 \text{ if } \lambda / L > 1.6 \qquad (189)$$

$$C_{dy}^{S} = \left| -1.1414 - 0.10235 \cdot \frac{L}{B} + 12.559 \cdot \frac{\sqrt{B \cdot T}}{\lambda} - 132.01 \cdot \frac{(B \cdot T)^2}{\lambda^4} + 0.06374 \cdot \frac{\lambda}{\sqrt{B \cdot T}} \right| \qquad (190)$$

$$C_{dy}^{S} \le 1.0$$

$$C_{dy}^{S} = 1.0 \text{ if } \lambda / L < 0.3$$

$$C_{dy}^{S} = 0.0 \text{ if } \lambda / L > 1.5$$

$$C_{dn}^{S} = 0.16 \cdot \sin^2\left(\frac{\pi \cdot \lambda}{L}\right),\ C_{dn}^{S} = 0.0 \text{ if } \lambda / L > 1.0 \qquad (191)$$

Visual presentation of variation of drift force components with the ship heading is shown in Figure 27 below.

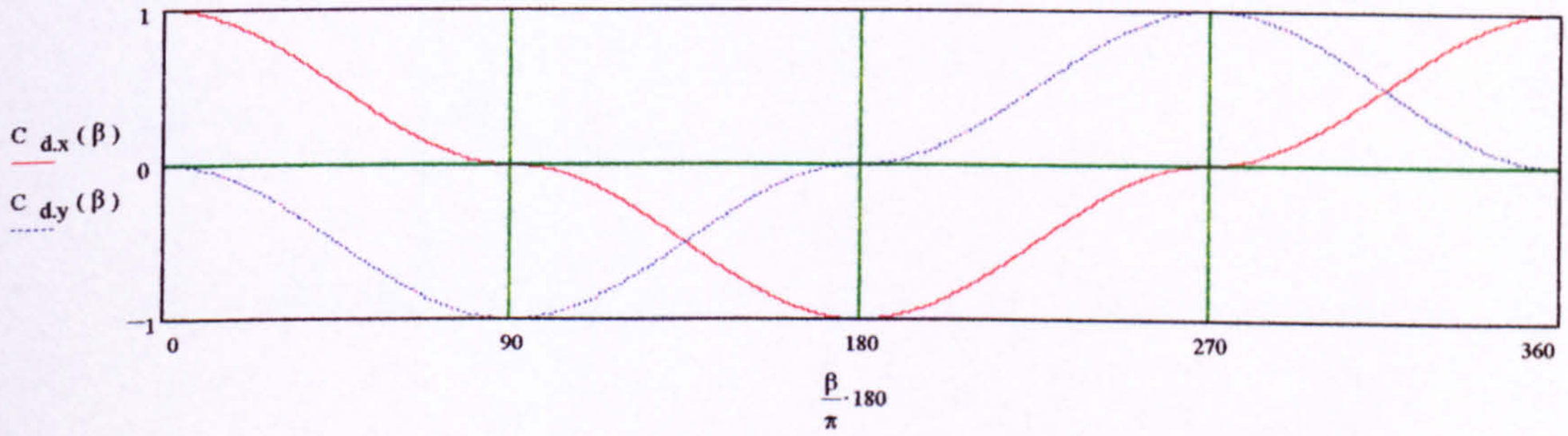

Figure 27 Drift forces coefficients with geometrical/wave coefficients taken as unity

The incident wave amplitude A^I and length λ, seen in equations (185) and the coefficients, are taken in a discrete manner as the properties of the last wave passing through the ship, and kept constant until the next wave passage.

With implementation of the drift forces one more consideration must be given to the associated effects they have on the vessel motions. Namely, integrating the mean unbalanced forces, in this case for planar motions where no restoring is present, will result in a constant acceleration along the direction of forcing vector. This obviously does not take place in reality. The ship exposed to beam incident wave train will attain fairly constant velocity, this being the result of balance of mean

forces. This implies that an additional component must be defined and in this case it will be the drag force (or slow-drift damping moment) resulting from the ship mean planar motion. As the ship accelerates due to the mean drift forces, the drag force starts counteracting to the point where a balance is reached. The ship then drifts with constant mean velocity in the direction of drift force vector.

This drag force will be a combined result of normal (wave-making) and tangential (viscous) flow past the body, with a number of parameters influencing it, such as free-surface effects, beam-draught ratio, bilge radius, bilge keel dimensions, Reynolds number, three-dimensional effects, and so on. Hence predictions by theoretical means are overly complex and resorting to empiricism is most often the preferred option. Indeed, these forces will be modelled here, similarly as the drift forces, by a simplified parametric formulation, borrowed from the methods for predicting the effect of current forces, [120]. Denoted as $\vec{F}_{Current}$, the drag forces will be expressed as follows:

$$\vec{F}_{Current} = \frac{1}{2} \cdot \rho \cdot T \cdot L \cdot \begin{bmatrix} C_{cx} \\ C_{cy} \\ 0 \\ 0 \\ 0 \\ C_{cn} \cdot L \end{bmatrix} \cdot V_{cr}^2 \qquad (192)$$

Where:

$$V_{cr} = \sqrt{v_x^2 + v_y^2} \qquad (193)$$

$$C_{dx} = -\cos(\beta) \cdot C_{dx}^S \cdot \frac{-v_x}{|v_x|} \qquad (194)$$

$$C_{dy} = \sin(\beta) \cdot C_{dy}^S \cdot \frac{-v_y}{|v_y|} \qquad (195)$$

$$C_{dn} = \sin(2 \cdot \beta) \cdot C_{cn}^S \cdot \frac{-\omega_z}{|\omega_z|} \qquad (196)$$

With the ship-geometrical coefficients given as follows:

$$C_{cx}^{S} = \left| 1.264 \cdot 10^{-4} \alpha - 0.08466 \cdot \frac{B}{T} - 0.0368 \cdot \frac{L}{T} + 0.06545 \cdot \frac{L}{B} \right| \quad (197)$$

$$C_{cy}^{S} = \left| 1.765 \cdot 10^{-3} \cdot \alpha - 1.549 \cdot \frac{B}{T} + 0.09031 \cdot \frac{L}{T} + 5.897 \cdot C_B \right| \quad (198)$$

$$C_{cn}^{S} = \left| 1.291 \cdot 10^{-3} \cdot \alpha - 0.02154 \cdot \frac{B}{T} + .003413 \cdot \frac{L}{T} - 0.04181 \cdot C_B \right| \quad (199)$$

$$\alpha = \beta \cdot \frac{180}{\pi}, \text{ if } \alpha > 180 \text{deg} \text{ then } \alpha = 360 - \alpha$$

The velocity components in (194) to (196) are expressed in the inertial coordinate system $O^0X^0Y^0Z^0$.

6.6.10 Viscous forces

A fairly critical assumption in the development of the fluid model has been introduced in the fluid momentum equation (59), where fluid viscosity has been neglected thereafter, leading to (66). The ensuing modelling of ship-fluid interaction by decomposing the total fluid force into a number of autonomous components, each of which result from potential flow as shown in §6.6, of necessity ignores the effect of fluid viscosity. This simplification has not as big an impact on the accuracy of prediction of ship seakeeping qualities, however, for the prevailing fluid excitation/reaction is due to normal forces (i.e. wave making properties of the ship hull geometry) rather than fluid internal friction. Therefore the techniques involving solutions to equation (59), referred to usually as RANS (Reynolds Averaged Navier-Stokes) techniques have not been widely utilised in the ship industry as have the ubiquitous potential flow theories.

However, viscosity effects are of an immense importance for motion modes where fluid separation occurs, resulting in damping forces with order of magnitude approaching or exceeding those resulting from wave radiation. Apart from the slow-drift motions discussed in the foregoing, where viscous flow has been accounted for implicitly in the empirical formulations, ship roll is such a mode of motion. Despite this importance, however, there are no simple prediction methods alternative to RANS techniques other than empirical formulations. The techniques presented in [78], and referred to as Ikeda's method hereafter, is the most commonly used and so they will be applied in this research.

In Ikeda's approach, the viscous damping moment is divided into several components: friction, eddy shedding, lift, wave and bilge keel, and the total force is obtained by a superposition of all these components. Detailed expressions for each of these forces are presented in [78] and will not be reproduced here. However some discussion on the application will follow.

The total, non-linear damping can be represented by a kind of linearised damping coefficient:

$$B_{\varphi}(\dot{\varphi}) = B_e \cdot \dot{\varphi} \qquad (200)$$

Where disregarding the linear wave component, the aforementioned pseudo-linearised damping coefficient is a superposition of the other components:

$$B_e = B_F + B_E + B_L + (B_{NBK} + B_{HBK} + B_{WBK}) \quad (201)$$

Where:

B_F	Friction damping
B_E	Eddy damping
B_L	Lift damping
B_{NBK}	Normal Bilge-Keel damping
B_{HBK}	Hull-Pressure Bilge-Keel damping
B_{WBK}	Wave Bilge-Keel damping

Accordingly to the technique derived in [78] this coefficient shows high dependency on roll amplitude φ_A, see example predictions for the PRR1 study ship geometry in Figure 28, and additionally on frequency ω_φ and ship speed U, that is:

$$B_e = B_e(\varphi_A, \omega_\varphi, U) \quad (202)$$

Application of this formulation becomes unclear for the case of time domain solution, as the roll amplitude cannot be known *a priori*. It becomes even less obvious in the case of estimation of ship roll response to irregular seas. A number of approaches have been suggested. For instance the following is proposed:

$$B_e = B_1 + \sqrt{\frac{8}{\pi}} \cdot B_2 \cdot \sigma_{\dot{\varphi}} \quad (203)$$

Where the variance of roll angular velocity can be expressed as a function of roll natural frequency and variance of roll motion:

$$\sigma_{\dot{\varphi}} = \omega_{\varphi natural} \cdot \sigma_\varphi \quad (204)$$

The coefficients B_1 and B_2 are found by regression analysis based on comparison of quadratic expansion of equation (200) with equation (201).

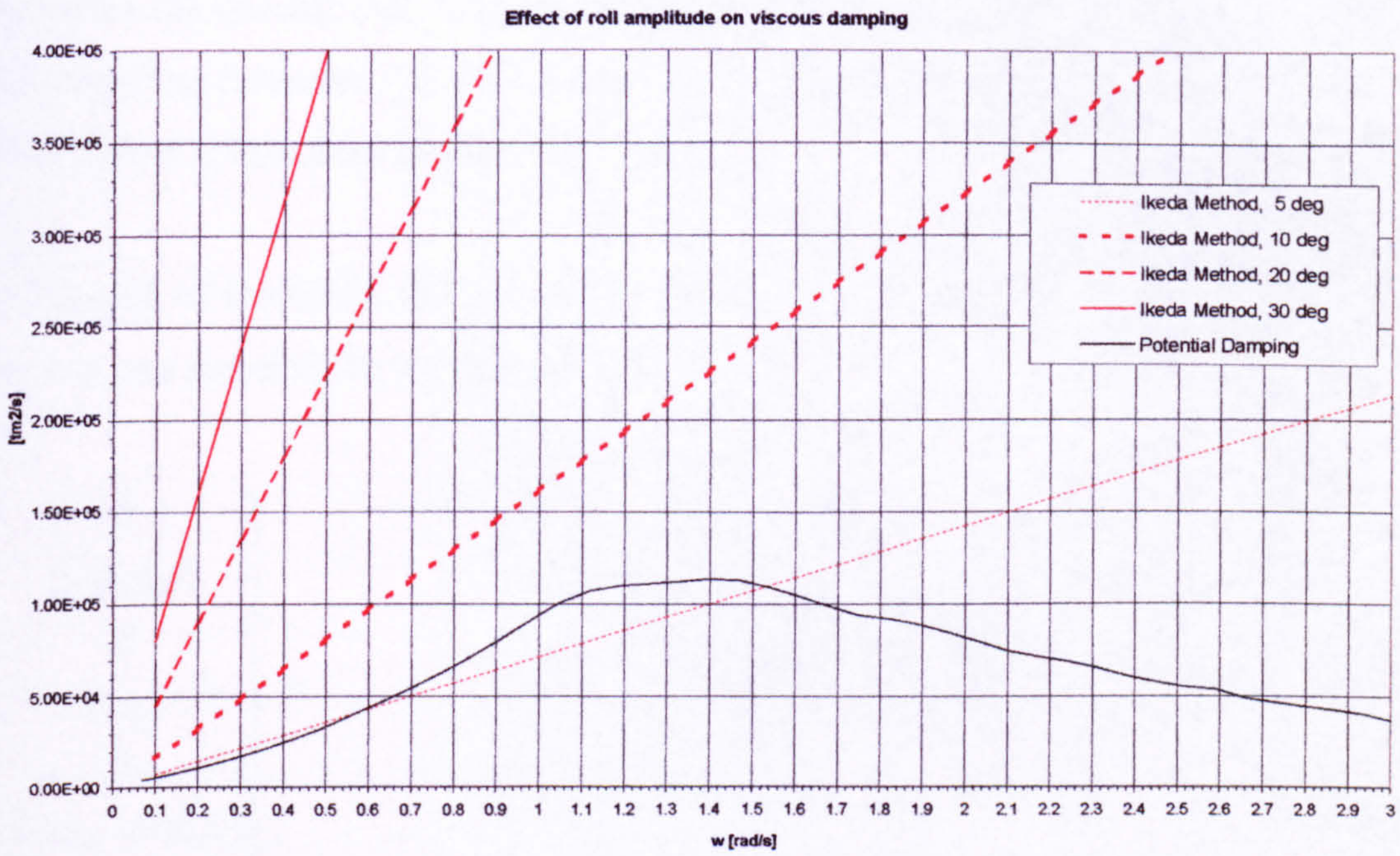

Figure 28 Effect of roll amplitude on viscous damping

This approach, however, is said to fail for the case of e.g. bare hull, where damping is less non-linear and can not be expressed in a form like (203). Also expression (204), derived on a preposition that roll motion occurs largely in a narrow band near the natural frequency, is questionable, especially when the damping attains high values (e.g. due to large bilge keels) leading to high responses at the peaks of incident wave energy spectra.

In this research, a discrete piece-wise constant treatment of equation (202) is proposed, whereby the coefficient is evaluated for the wave spectrum peak frequency and amplitude evaluated as the amplitude of the last half roll cycle. In this approach the viscous roll damping will vary as the time marching progresses in a kind of iterative manner, constantly adjusting to the current roll amplitude.

It is finally worth noting that the presented and applied method has only been confirmed to work for well established monohull forms, and hence should be applied with caution in case of hull geometry deviating from this (e.g. hard chine, double propeller, multihulls, etc.).

6.6.11 Stabilising fins

For a ship progressing in waves at speed the appendages such as stabilising fins, can contribute significantly to the overall roll damping moments. The forces can be evaluated in numerous of ways, but empirical formulae can give adequate accuracy, as is suggested in [214]. The following prediction method is therefore applied in this work.

For small angles of incidence the lift coefficient increases more or less linearly with the angle of incidence and can therefore be written as follows:

$$\vec{F}_{Fin} = \begin{bmatrix} 0 \\ 2 \cdot \sin(\beta) \\ 0 \\ 2 \cdot r_{GF} \\ 0 \\ 2 \cdot x_{GF} \cdot \sin(\beta) \end{bmatrix} \cdot L$$

Where:

$L = E \cdot \frac{\partial C_L}{\partial \alpha} \cdot \alpha \cdot \frac{1}{2} \cdot \rho \cdot U^2 \cdot A_F$ Lift force

$E = E_{BL} \cdot E_{IBK}$ Overall fin effectiveness

$E_{BL} = 1 - 0.21 \cdot \frac{\delta}{b}$ Hull boundary layer loss

$E_{IBK} = 0.84$ Fin-bilge keel interference loss

$\delta = 0.377 \cdot x_{FP} \cdot (Rn)^{-0.2}$ Boundary layer thickness on the hull

$R_N = \frac{\rho \cdot U \cdot x_{FP}}{\mu_w}$ Local Raynolds number

$\mu_w = 1.14 \cdot 10^{-6}$ Kinematic viscosity coefficient $\frac{m^2}{s}$

x_{FP} Longitudinal location of the fin (from midship)

$$C_L = \frac{\partial C_L}{\partial \alpha} \cdot \alpha$$ Lift coefficients

$$\frac{\partial C_L}{\partial \alpha} = \frac{1.8 \cdot \pi \cdot a}{1.8 + \sqrt{a^2 + 4}}$$ The lift curve slope

$$a = \frac{4 \cdot b}{c_r + c_t}$$ The fin aspect ratio

$$A_F = \frac{b}{2} \cdot (c_r + c_t)$$ Planform area

α Incidence angle

β

x_{GF}

r_{GF}

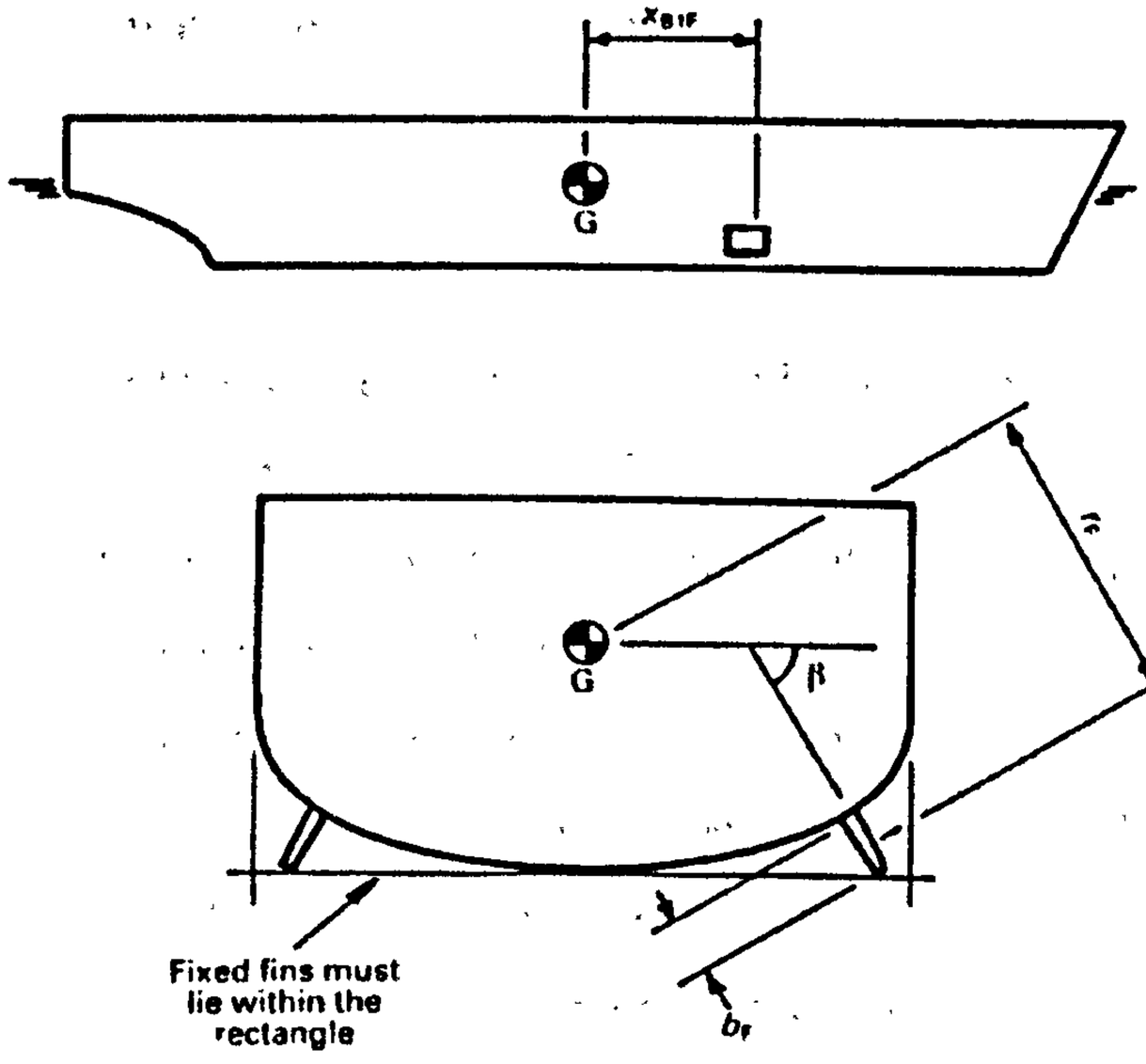

Figure 29 Stabilising fins. Note on the drawing $x_{GF} = x_{B1F}$ and $r_{GF} = r_F$

7 Internal effects

As was assumed in §5.2 and followed in the ensuing derivation of the equations of ship motion, the effects of floodwater and cargo shifting are accounted for based on rigid body theory. This assumption, initiated in [117] to [120], allows for relatively simple yet accurate prediction of dynamic effects of any free mass within the ship on her response. This derives from the fact that the major contributors to the forces are resulting from (a) influence of gravity field (b) variation of inertia and (c) relative velocity and acceleration. All of these are catered for by the theory applied in §5.

However, in case of floodwater, a major source of inaccuracies, understanding of the seriousness of which is still not established, derive from mathematical modelling techniques employed for describing the actual behaviour of the free masses in the ship. The free-mass motion will be affected not only by the ship behaviour in the seaway but also by their inherent dynamic properties, good example of which is floodwater sloshing. Furthermore, having adopted a mathematical technique, a very generalised problem in computer modelling arises in defining of the level of discretisation of the flooded volume.

Idealising, the fluid onboard the ship could be represented with the accuracy reaching fluid particles resolution, i.e. defined by thousands of small cells, and its behaviour determined from a series of fluid flow theorems (continuity, momentum, heat transfer, etc). The ensuing displacement, velocity and acceleration of each single cell could be used in the model presented in this thesis and the resultant forces would be similar to those derived from direct pressure integration. The latter force determination method, the pressure integration, has been already applied with some success when used in hybrid models, [25], i.e. the floodwater onboard the ship is discretised and its motion predicted by RANS techniques. The derived forces are then used in a general seakeeping model to predict the total response. This quite sophisticated technique, however, requires considerable computation power and high level of expertise for practical applications.

Therefore, aiming at a mathematical model that could be easily used in practise, the approach pursued in this thesis attempts to address the two mentioned questions. Such an approach will be adopted here based, again, on expertise gained in **[117]** to **[120]** with innovative treatment of floodwater motion description, inspired by [132]. The floodwater free surface will be

approximated by a flat surface and a pendulum-type resolution of motion of the water will be adopted, whereby the centre of its discrete volume will be exposed to an acceleration field and the ensuing movement, constrained by the potential motion space, predicted. This model is hereby referred to as Free-Mass-in-Potential-Surface (FMPS). Following this, the discretisation can be minimised to a few sets of compartments within the ship, simply so that geometrical properties of vessel interiors would be modelled accurately. The whole mass of water in the compartment can then be treated as a single point mass, thus the simplification introduced in equation (29) can be justified.

Modelling of cargo shifting is considerably simpler, as the possible displacements can be easily confined to a flat plane and the displacements themselves result purely from a balance of forces, each of which is known. The numerical model will be discussed below.

Finally the issue remains of the water ingress/egress modelling. Comprehensive discussion on this can be found in [120]. An ideal fluid momentum equation was utilised for this purpose with an empirical coefficient for any potential energy losses derived from a series of purposely conducted experiments. This model has been adopted here, see discussion below, with some refinements to take into account the relative motion between ship and oncoming waves.

7.1 Floodwater motions

The floodwater motion is modelled in this work as a free mass point moving due to the acceleration field restrained geometrically by predetermined potential surfaces of the centre of buoyancy for given amounts of floodwater, see for example Figure 38. This model, inspired by work in [132] and derived from simple rigid body motion consideration as is detailed by equations (212) to (215) is summarised below and illustrated in Figure 30:

$$\begin{cases} \dfrac{d}{dt}\vec{r}'_{AW} = \vec{v}'_{AW} - \left(\vec{v}'_{AW}\cdot\vec{n}\right)\cdot\vec{n} \\ \dfrac{d}{dt}\vec{v}'_{AW} = \vec{a}_f - \left(\vec{a}'_f\cdot\vec{n}\right)\cdot\vec{n} \end{cases} \qquad (205)$$

Where:

$\vec{r}'_{AW}$	Position vector of the centre of buoyancy "W" of floodwater in a body-fixed reference system with origin at A
$\vec{v}'_{AW}$	Velocity of the above point "W"
$\vec{a}'_f = \vec{g}' - \vec{a}'_s - 2\cdot\vec{\omega}'\times\vec{v}'_{AW} - \mu^*\cdot\vec{v}'_{AW}$	Total forcing acceleration vector
$\vec{g}'$	Gravity acceleration vector expressed in the body-fixed system of reference
$\vec{a}'_s = \dfrac{d}{dt}\vec{v}'_A + \dfrac{d}{dt}\vec{\omega}'\times\vec{r}'_{AW} + \vec{\omega}'\times\left(\vec{v}'_A + \vec{\omega}'\times\vec{r}'_{AW}\right)$	Ship motion-related acceleration vector expressed in body-fixed system of reference, see also equations (212) to (215).
$\vec{n}$	Instantaneous normal vector to the potential surface of floodwater motion, determined from a damage compartment geometry database

μ^*

A coefficient representing damping of floodwater motion based on a supposition that such damping is opposing motion velocity. Here it has been taken as 0.15 following studies addressed by Figure 43. Further verification is necessary, especially the dependence of μ^* on permeability (i.e.) obstructions in a flooded compartment.

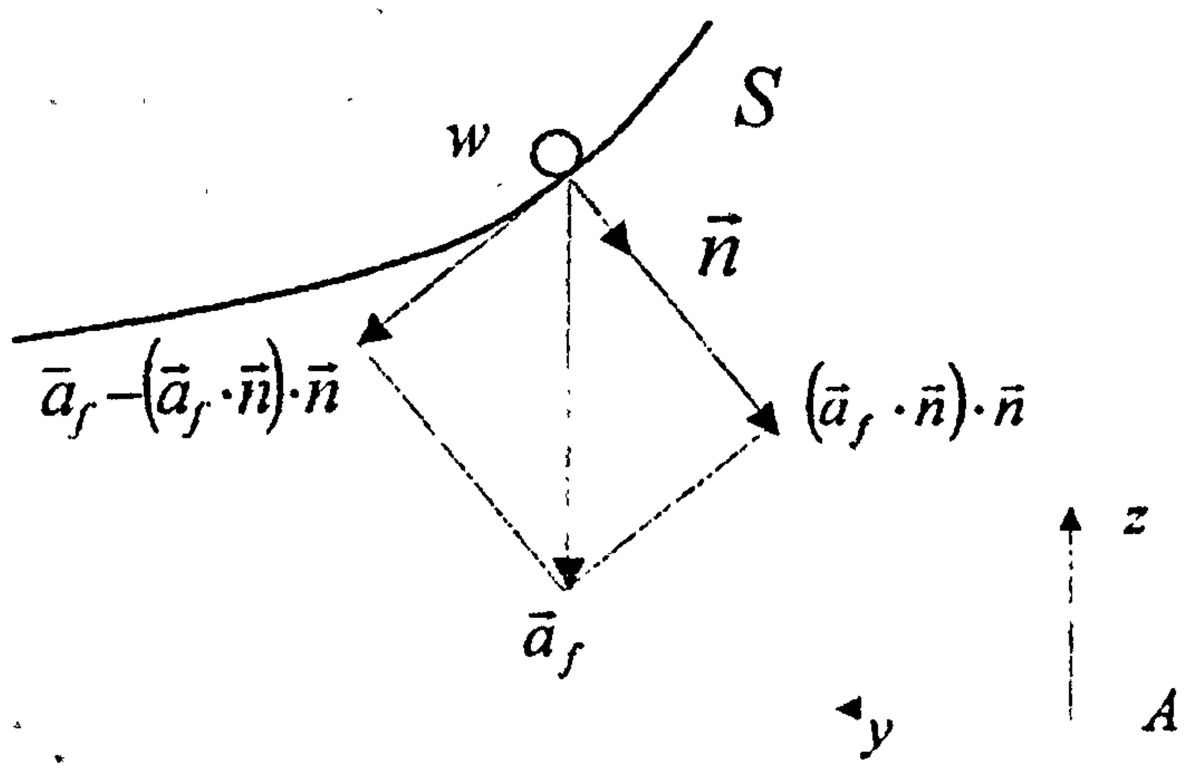

Figure 30 Fluid particle "w" (centre of buoyancy) in acceleration field $\vec{a}_f$ moving on the potential surface S. All the vectors are resolved in *Axyz* system of reference.

As can be envisaged, the mathematical model of the damage ship motion becomes a multi-body multi- degrees-of-freedom (dof) system, where in addition to six modes of ship motion, equations (40) and (39), there are another 3dof, equation (205), for each ship compartment considered flooded.

7.2 Water ingress/egress

As can be easily envisaged, fluid flow in the vicinity of the hull damage opening is of a very complex nature. However, following the adopted model of ideal fluid, Bernoulli's equation can be used to represent fluid flow, with a flow loss coefficient derived from experimental studies.

Examining carefully model experiments of a damaged ship, however, a question arises on the possible effects of the dynamics of the system: ship and oncoming waves, see for instance the distribution of fluid velocities at the free surface, Figure 32. These would address the wave swell-up at the hull surface and relative velocity between the opening facet and the fluid particles undergoing oscillatory motions, see Figure 31.

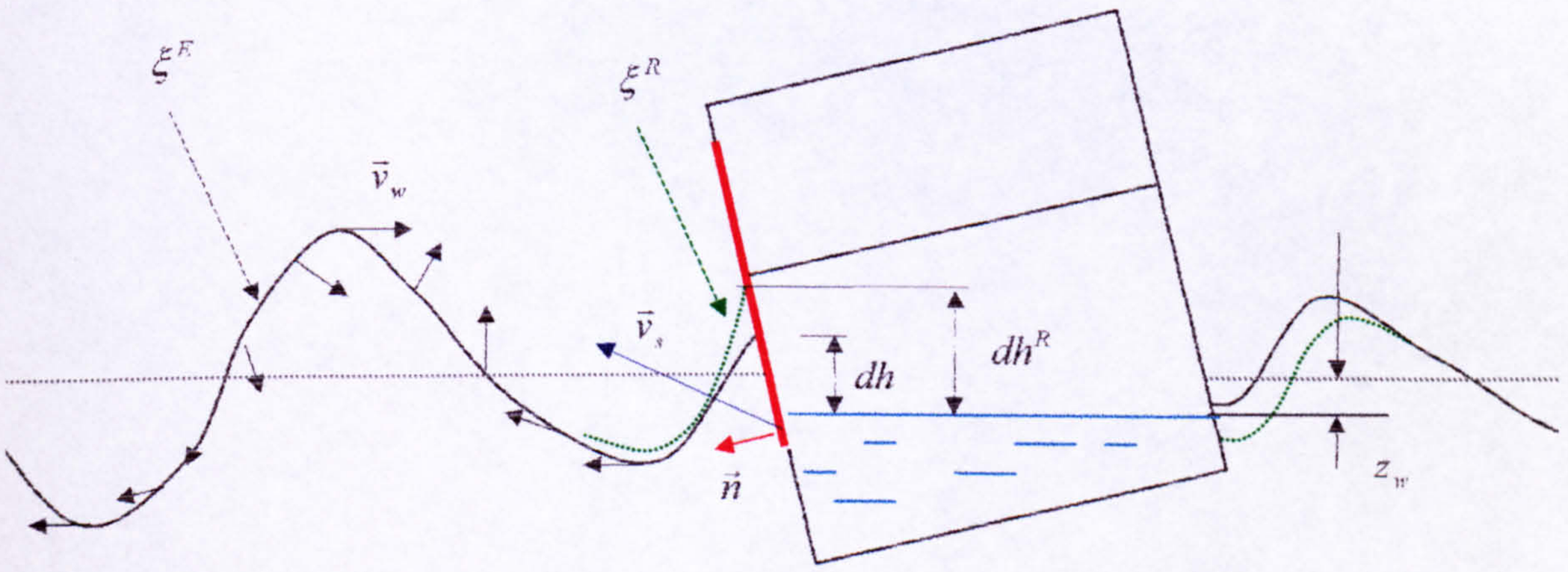

Figure 31 Water ingress/egress modelling

Accounting for these effects will lead to the following inflow rate expression:

$$\frac{dQ}{dt} = \mathrm{sgn}(dh) \cdot K \cdot v_f \cdot dA \qquad \left[\frac{m^3}{s}\right] \qquad (206)$$

$$v_f = \sqrt{2 \cdot g \cdot dh} + (\vec{v}_s \cdot \vec{n}) - (\vec{v}_w \cdot \vec{n}) \qquad (207)$$

Where:

$$K = 0.6 \qquad [122] \qquad (208)$$

$$dh = \xi^R - z_w \qquad (209)$$

$$\xi^R = \xi^E \cdot \left(1 - \mathrm{sgn}(C_d) \cdot \sqrt{C_d}\right) \qquad (210)$$

$$C_d = C_{dx} \cdot n_x + C_{dy} \cdot n_y \qquad (211)$$

With C_{dx} and C_{dy} is given by (186) and (187), respectively, and the wave elevation ξ^E is given by equation (177).

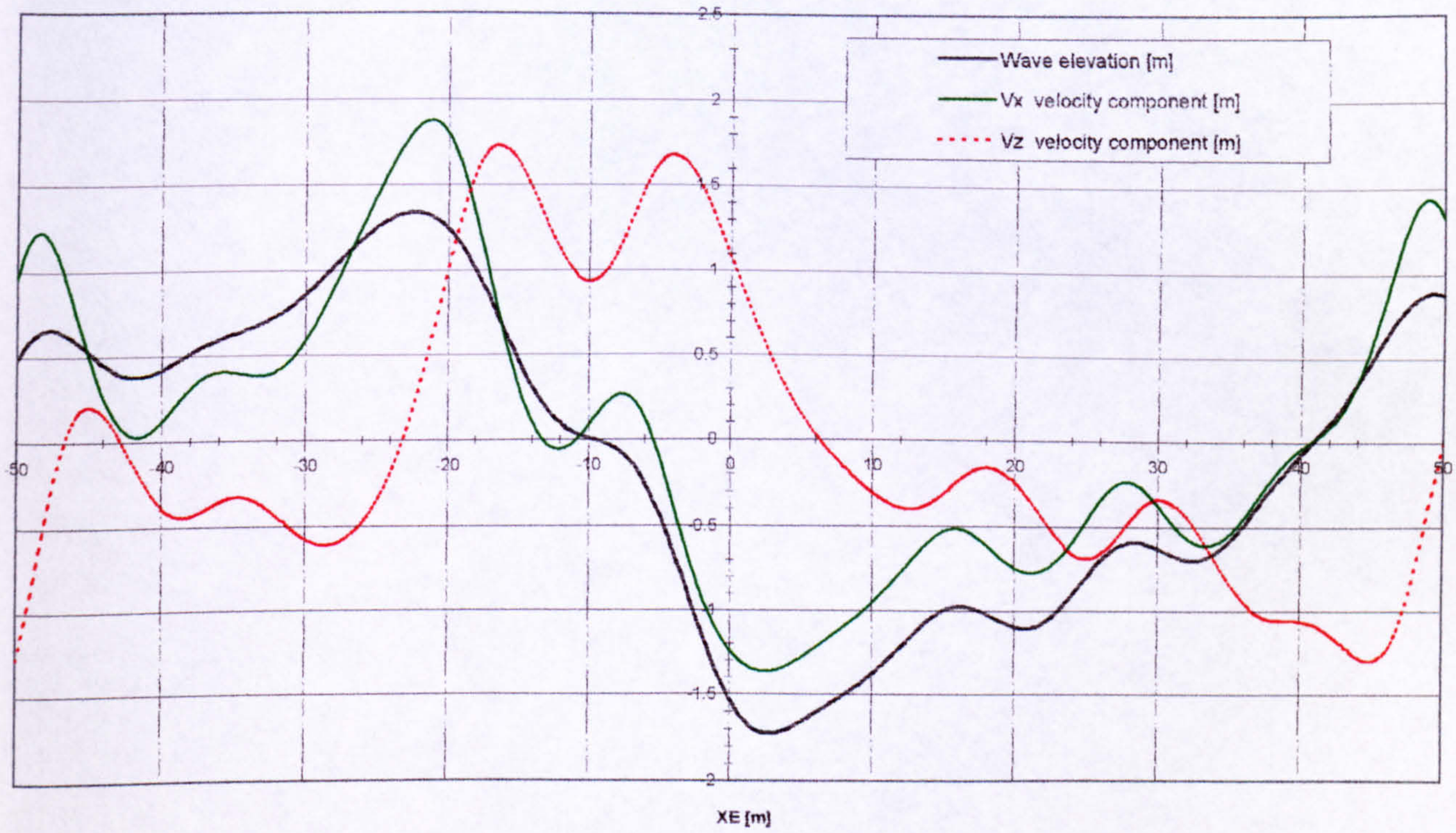

Figure 32 Example of kinematics of a long-crested irregular wave, Hs=4.0m, To=6.25s.

The swell-up equation (210) has been derived by [215] and follow generalisation of Morison equation, which states that the 2D mean drift force for a ship in beam seas is proportional to square amplitude of the reflected waves:

$$F_2 = \frac{1}{2} \cdot \rho \cdot g \cdot A_R^2$$

Deriving from (185) and the above equation it can be shown that:

$$A_R^2 = C_J \cdot A_I^2$$

That is the amplification of the wave at the ship surface can be given by (210).

Although it could be argued that these effects are accounted for in the flooding coefficient, K, it is suggested here, that such averaging of the flow leads to coefficient K being test-specific, i.e. valid only for conditions the experiments were carried out at. Moreover, as has been discussed and demonstrated in [120] the value of this coefficient can vary from 0.6 to 1.4 depending on the flow mode (fluid on-one/on-both sides of the opening), which by all means is a considerable scatter. Therefore, it is believed that much more fundamental study is required to quantify these effects in a more representative and general manner. The approach outlined is an attempt to step into this direction.

7.3 Cargo Shift model

None of the model experimentation undertaken to date on ship survivability addresses the potential consequences that cargo shifting could have on the survivability of a ship. In many cases the cargo in question can be generalised as a unit point mass lashed to the deck and this representation has been the premise for the numerical model of cargo shifting described in this section.

When considering cargo shifting, a set of equations expressing conservation of linear momentum, see equation (3), in inertial coordinate system must be summoned. To initiate the derivation of these equations, the position of the centre of gravity of a single point mass, P, in the inertial coordinate system OXYZ can be determined, see equation (7), by:

$$\vec{r}_{OP} = \vec{r}_G + \vec{r}_{GP}$$

The easiest system to describe the cargo movements, however, is in a body-fixed system of reference. It is recommended, therefore, to express the elements of the above equation utilising the property of this system as explained in the foregoing, formulae (13) to (23) . Deriving from this, the velocity and acceleration can be expressed as:

$$\frac{D}{Dt}\vec{r}_{OP} = \frac{D}{Dt}\vec{r}_G + \frac{d}{dt}\vec{r}_{GP} + \vec{\omega} \times \vec{r}_{GP}$$

$$\frac{D}{Dt}\vec{v}_{OP} = \frac{D}{Dt}\vec{v}_G + \frac{D}{Dt}\vec{v}_{GP} + \frac{d}{dt}\vec{\omega} \times \vec{r}_{GP} + \vec{\omega} \times \frac{d}{dt}\vec{r}_{GP} + \vec{\omega} \times \left(\vec{\omega} \times \vec{r}_{GP}\right)$$

Finally it is worth to apply the logic of (36) to express all vectors in the body-fixed system according to formula (18) i.e. with its unit vectors constant:

$$\frac{D}{Dt}\vec{v}'_{OP} = \frac{d}{dt}\vec{v}'_G + \vec{\omega}' \times \vec{v}'_G + \frac{d}{dt}\vec{v}'_{GP} + \vec{\omega}' \times \vec{v}'_{GP} + \frac{d}{dt}\vec{\omega}' \times \vec{r}'_{GP} + \vec{\omega}' \times \vec{v}'_{GP} + \vec{\omega}' \times \left(\vec{\omega}' \times \vec{r}'_{GP}\right)$$

When the exciting acceleration resultant from ship motions is separated from acceleration directly describing motion of cargo P within the ship then the above equation can be rewritten as:

$$\frac{D}{Dt}\vec{v}'_{OP} = \vec{a}'_S + \vec{a}'_P \qquad (212)$$

Where:

$$\vec{a}'_S = \frac{d}{dt}\vec{v}'_G + \frac{d}{dt}\vec{\omega}' \times \vec{r}'_{GP} + \vec{\omega}' \times \left(\vec{v}'_G + \vec{\omega}' \times \vec{r}'_{GP}\right) \qquad (213)$$

$$\vec{a}'_P = \frac{d}{dt}\vec{v}'_{GP} + 2 \cdot \vec{\omega}' \times \vec{v}'_{GP} \qquad (214)$$

Equation (212) with (213) and (214) define absolute acceleration of the point mass resultant from the motion of the ship as well as the cargo within the ship, expressed in the body-fixed coordinate system. An unknown here is: cargo velocity and its displacement $\vec{v}_{GP}, \vec{r}_{GP} = f(t)$ with respect to the vessel and induced by both external forces as well as the ship motions. The external forces acting on the point mass cargo on board the ship are gravity, surface friction, lashing forces and impact forces by other objects. Disregarding the effect of external objects impact, the total equation of motion, again, following from (3) can be written as:

$$\vec{a}'_S + \vec{a}'_P = \vec{a}'_{lash} + \vec{a}'_{friction} + \vec{g}' \qquad (215)$$

where both the lashing as well as the friction force direction always counteracts gravity and ship motion resultant acceleration:

$$\mathrm{sgn}(\vec{a}'_{lash}, \vec{a}'_{friction}) = -\mathrm{sgn}(\vec{g}' - \vec{a}'_S)$$

where:

$$\vec{a}'_{friction} = f(\mu, (\vec{g}' - \vec{a}'_{,})_z)$$

μ Friction coefficient [-]

The two critical assumptions made for adoption of the above model for cargo shifting predictions are the ones concerning impact of other shifting objects. Firstly it is assumed that the impact has plastic character, i.e. the energy loss is maximum. It follows from the fact that the masses/inertias

are the prevalent forces and the cargo is pliant, hence plastic deformations rather than "bouncing off" are expected. It implies that after the contact between a number of objects, some of which are still lashed, takes place, their common velocity according to conservation of momentum rule, will be:

$$\vec{v}' = \frac{\sum_i m_i \cdot \vec{v}'_i}{\sum m_i}$$

Secondly, the duration of an impact impulse is taken ad-hoc as a constant value equal to $t_{impulse} = 0.05s$ (this value needs further study). Hence the lashing breaking condition is:

$$|\vec{b}| > |\vec{a}'_{lash}|$$

Where:

$$\vec{b} = \frac{\vec{v}'}{t_{impulse}} + (\vec{g}' - \vec{a}'_s) + \vec{a}'_{friction}$$

Once this condition is true the lashing is assumed to be broken and the post-impact initial velocity for cargo shifting can be approximated as:

$$\vec{v}'_{post\_impact} = \frac{\vec{b}}{|\vec{b}|} \cdot \left(|\vec{b}| - |\vec{a}'_{lash}|\right) \cdot t_{impulse}$$

The ensuing cargo shift can then be determined from integration of the following set of first order coupled integral equations:

$$\begin{cases} \frac{d}{dt}\vec{r}'_{GP} = \vec{v}'_{GP} \\ \frac{d}{dt}\vec{v}'_{GP} = \vec{g}' - \vec{a}'_s + \vec{a}'_{friction} - 2 \cdot \vec{\omega}' \times \vec{v}'_{GP} \end{cases} \quad (216)$$

With initial values for velocity taken as:

- Zero if the object starts shifting
- Velocity from the previous integration time step if the object were shifting
- $\vec{v}'_{post\_Impact}$ in case of impact/contact with other objects and lashing present
- $\vec{v}'$ in case of impact/contact with other objects and no lashing

It is to be noted that there is no modelling of tipping phenomenon at present! Furthermore, in the numerical code, the force for breaking off lashing is assumed in one direction only i.e. if there are lashings on both sides of the track each having break force of 50kN, then the net force assumed for a lashing breaking condition is 100kN.

8 Numerical algorithms

As mentioned in the §4 of this thesis, development of a numerical code is associated with making choices of the numerical algorithms and schemes available for solution of the particular mathcmatical formulation developed. Summary of essential details of the numerical implementation is given in this chapter.

The basic equations of motions are given by two vectors (**39**) and (**40**), for three rectilinear and three angular modes of motion respectively. These equations can be rearranged as is shown below:

$$
\begin{aligned}
&M_s\cdot\left(\vec{r}'_{AGs}\times\left(\frac{d}{dt}\cdot\vec{v}'_A\right)\right)+M_w\cdot\left[\vec{r}'_{AGw}\times\left[\frac{d}{dt}\vec{v}'_A\right]\right]+\\
&+\left(I'_s+I'_w+I'_{AGs}\right)\cdot\frac{d}{dt}\vec{\omega}'=\vec{M}'_A+\\
&\qquad -M_s\cdot\left(\vec{r}'_{ACis}\times\left(\vec{\omega}'\times\vec{v}'_A\right)\right)+\\
&\qquad -M_w\cdot\left[\left(\vec{\omega}'\times\vec{r}'_{ACiw}\right)\times\vec{v}'_{ACiw}+\vec{r}'_{ACiw}\times\left[\frac{d}{dt}\vec{v}'_{ACiw}+\vec{\omega}'\times\left(\vec{v}'_A+\vec{v}'_{ACiw}\right)\right]\right]+\\
&\qquad -\frac{d}{dt}M_w\cdot\left[\vec{r}'_{AGw}\times\left(\vec{v}'_A+\vec{v}'_{AGw}\right)\right]+\\
&\qquad -\left(\frac{d}{dt}I'_w\right)\cdot\vec{\omega}'-\vec{\omega}'\times\left[\left(I'_s+I'_w+I'_{AGs}\right)\cdot\vec{\omega}'\right]
\end{aligned}
\tag{217}
$$

$$
\begin{aligned}
&M_s\cdot\left(\frac{d}{dt}\vec{\omega}'\times\vec{r}'_{AGs}\right)+M_w\cdot\left[\frac{d}{dt}\vec{\omega}'\times\vec{r}'_{AGw}\right]+\\
&+\left(M_s+M_w\right)\cdot\frac{d}{dt}\vec{v}'_A=\vec{F}'+\\
&\qquad -M_s\cdot\left(\vec{\omega}'\times\left(\vec{\omega}'\times\vec{r}'_{AGs}\right)\right)+\\
&\qquad -M_w\cdot\left[\frac{d}{dt}\vec{v}'_{AGw}+2\cdot\vec{\omega}'\times\vec{v}'_{AGw}+\vec{\omega}'\times\left(\vec{\omega}'\times\vec{r}'_{AGw}\right)\right]+\\
&\qquad -\frac{d}{dt}M_w\cdot\left(\vec{v}'_{AGw}+\vec{\omega}'\times\vec{r}'_{AGw}\right)+\\
&\qquad -\frac{d}{dt}M_w\cdot\vec{v}'_A-\vec{\omega}'\times\left(M_s+M_w\right)\cdot\vec{v}'_A
\end{aligned}
\tag{218}
$$

Furthermore, the equations can be rewritten in matrix form (219), where all the terms associated with the rigid body dynamics are expressed as a six component force and moment vector, F_j^{Gyro}.

$$M_{i,j} \cdot \ddot{q}_j = F_j^A - F_j^{Gyro} \qquad i,j = 1...6 \qquad (219)$$

The second order time derivatives of the six respective motions can be found as:

$$\ddot{q}_j = M_{i,j}^{-1} \cdot f_j \qquad f_j = F_j^A - F_j^{Gyro} \qquad i,j = 1..6$$

This equation can be expressed as equivalent 12 first-order differential equations of motions:

$$\begin{aligned} &\frac{d}{dt} q_j = \dot{q}_j \\ &\frac{d}{dt} \dot{q}_j = M_{i,j}^{-1} \cdot f_j \end{aligned} \qquad i,j = 1...6 \qquad (220)$$

Remembering that for $j = 4,5,6$ the relation (248) must be used, the above set of equations is solved in time domain by the Runge-Kutta-Feldberg adaptive-step numerical integration scheme. The same scheme was also applied to six equations (205) and four equations (216). This technique has been chosen for its good and stable performance leaving the speed of the solution as a secondary issue. It is strongly recommended that other methods such as extrapolation Bulirsch-Stoer or multi-step Adam's schemes be explored. It should be mentioned that the twelve equations of ship motions are solved independently from the six equations (205) for each floodwater free mass and four equations (216) for each shifting cargo point. The interaction between these models is established at each simulated motion step, as is explained in Figure 33.

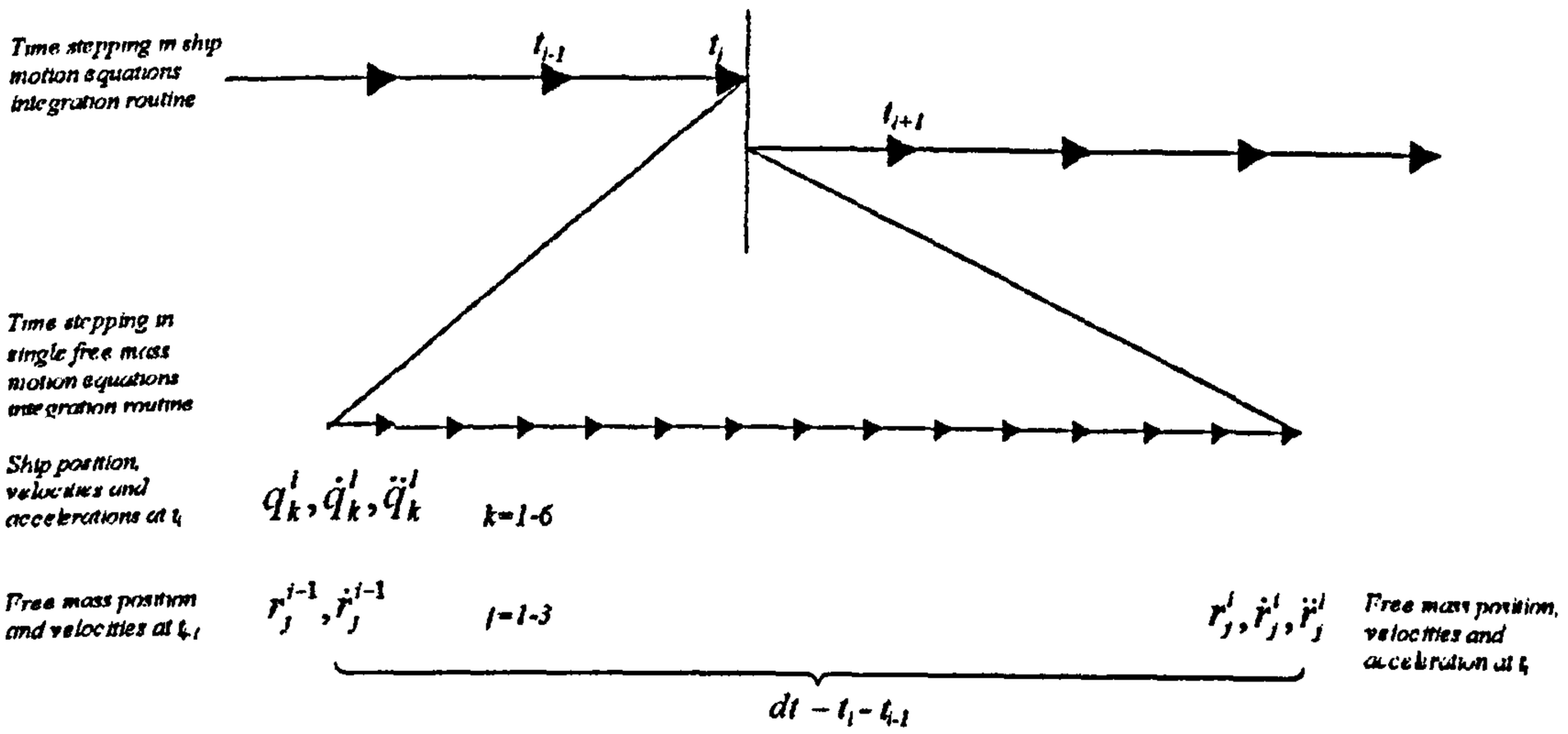

Figure 33 Numerical integration of coupled *systems* of equations

The BVP given by equation (86) and appropriate boundary conditions is solved numerically by approximating the body section contour as well as the free surface by total of N straight lines (plus two elements representing control surfaces S+ and S-), and assuming constant density sources distribution on each of the segments. The boundary conditions were satisfied on mid position of each segment. Therefore equation (86) can be rewritten as:

$$\int_S \left(\phi \cdot \frac{\partial G}{\partial n} - G \cdot \frac{\partial \phi}{\partial n} \right) \cdot dS = \sum_{j=1}^{N} \int_{S_j} \phi \cdot \frac{\partial G}{\partial n} \cdot dS_j - \sum_{j=1}^{N} \int_{S_j} G \cdot \frac{\partial \phi}{\partial n} \cdot dS_j = 0$$

Or after matrix arrangement:

$$A_{j,k} \cdot \phi_k = C_k \qquad j,k = 1..N+2 \qquad (221)$$

Where:

$$A_{j,k} = \begin{cases} \int_{S_k} \frac{\partial}{\partial n_k} \ln(r_{j,k}) \cdot dS_k & \text{for } j,k \in S_B \\ \int_{S_k} \frac{\partial}{\partial n_k} \ln(r_{j,k}) \cdot dS_k - K \cdot \int_{S_k} \ln(r_{j,k}) \cdot dS_k & \text{for } j,k \in S_F \\ B_{\pm} \cdot e^{\mp i \cdot K \cdot y} \cdot (-i) \cdot \left(E(Z_{\pm}) + \ln(r_{j\pm}) \right) & \text{for } j = 1..N \text{ and } k = N+1 \\ -1 & \text{for } j = 1..N \text{ and } k = N+2 \\ & \text{for } j = N+1 \text{ and } k @ y_+ \\ & \text{for } j = N+2 \text{ and } k @ y_- \\ B_{\pm} \cdot e^{\mp i \cdot K \cdot y_{\pm}} & \text{for } j = N+1 \text{ and } k = N+1 \\ & \text{for } j = N+2 \text{ and } k = N+2 \end{cases}$$

$$C_k = \begin{cases} \left(\int_{S_k} \ln(r_{j,k}) \cdot dS_k \right) \cdot U_{n_k} & \text{for } j,k \in S_B \\ 0 & \text{for } j,k \notin S_B \end{cases}$$

Furthermore:

$$K = \frac{\omega_E^2}{g}$$

r_{jk} Radial distance between mid points of segments j and k

$r_{j\pm}$ Radial distance between mid point of segment j and finite horizontal location $y_{\pm}$ of control surface in fluid domain on positive or negative sides

$Z_{\pm} = K \cdot (z_j \pm i \cdot (y_{\pm} - y_j))$

$B_{\pm} = 1$ The amplitude of the waves generated due to ship presence in the fluid can be taken arbitrarily, as it does not effect the sought velocity potential values on the body.

U_n for each body section element is given by (109) for three modes of forced motion and (110) for diffraction problem.

Solution to a set of linear algebraic equations of the form: $[A] \cdot [B] = [C]$, where either real (220) or complex (221) matrix B is the unknown, is solved by Jordan-Gauss method.

All the geometrical integrations have been based on the trapezoidal rule for the sheer reliability. It has been found that the accuracy of this most basic of all integration schemes is sufficient enough for the problems modelled in this work. Moreover, since the ship shapes can be very versatile, no particular attention for geometry discretisation is required, simplifying the usually manual input data pre-processing.

Iterative methods are unavoidable for solutions of complicated mathematical functions or engineering problems. The Newton-Raphson multi-variable procedure has been implemented for all such problems in this thesis.

Much effort has been put into handling of the input/output information and internal data pre-processing for use in the overall solutions, for instance for the problem (86). This has proved to be extremely beneficial in practical application of the code, which most of the time detects possible errors and informs the user of the problem origin.

Depending on the level of geometry modelling complexity, which is only restricted by a computer storage capacity, the typical speed of computation can vary between 1-20 real simulation seconds per computed second on now-days average-power personal computer (PII 200MHz).

9 Case studies

The study addressed herein aims to test different elements of the modelling discussed above and therefore establish level of capability of the developed software PROTEUS3 for predictions of ship motions in random seas subject to progressive flooding. In addressing this issue considerably detailed validation studies have been undertaken as discussed below, followed by demonstration of the application of the software to realistic problems.

9.1 Validation studies on ship hydrodynamics predictions

Testing the accuracy of predicting ship hydrodynamics has been carried out based on two hull forms, Wigley1 and Series60, with the basis for comparison derived from published model experiments as well as by use of more sophisticated 3D numerical prediction methods, [39] and [63]. This study also addressed the hydrodynamics of asymmetric geometries being a consequence of vessel attitude variation due to progressive flooding and ensuing stability deterioration. Predictions for the latter conditions have been validated in a qualitative manner, by comparison with one of the 3D-based techniques, that of [39], using a model of a passenger RO-RO vessel denoted as PRR1, [26]. The summary of the study is given below with more details reported in **Appendix 2 & 3.**

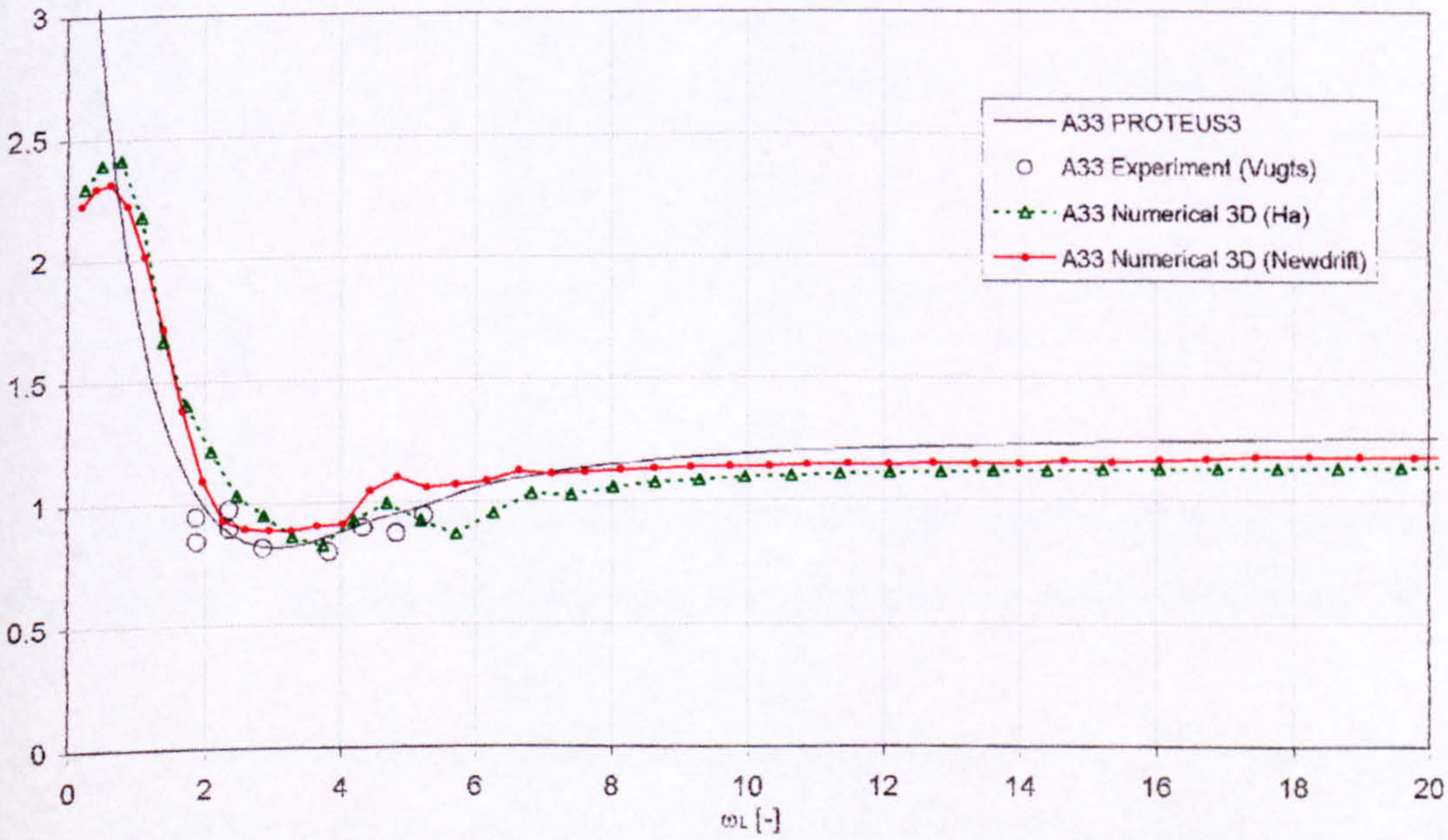

Figure 34 Dimensionless added mass in heave mode for 3D Series 60, CB=0.7 hull form, comparison between predictions by strip theory, 3D panel methods and experiments, Fn=0.2

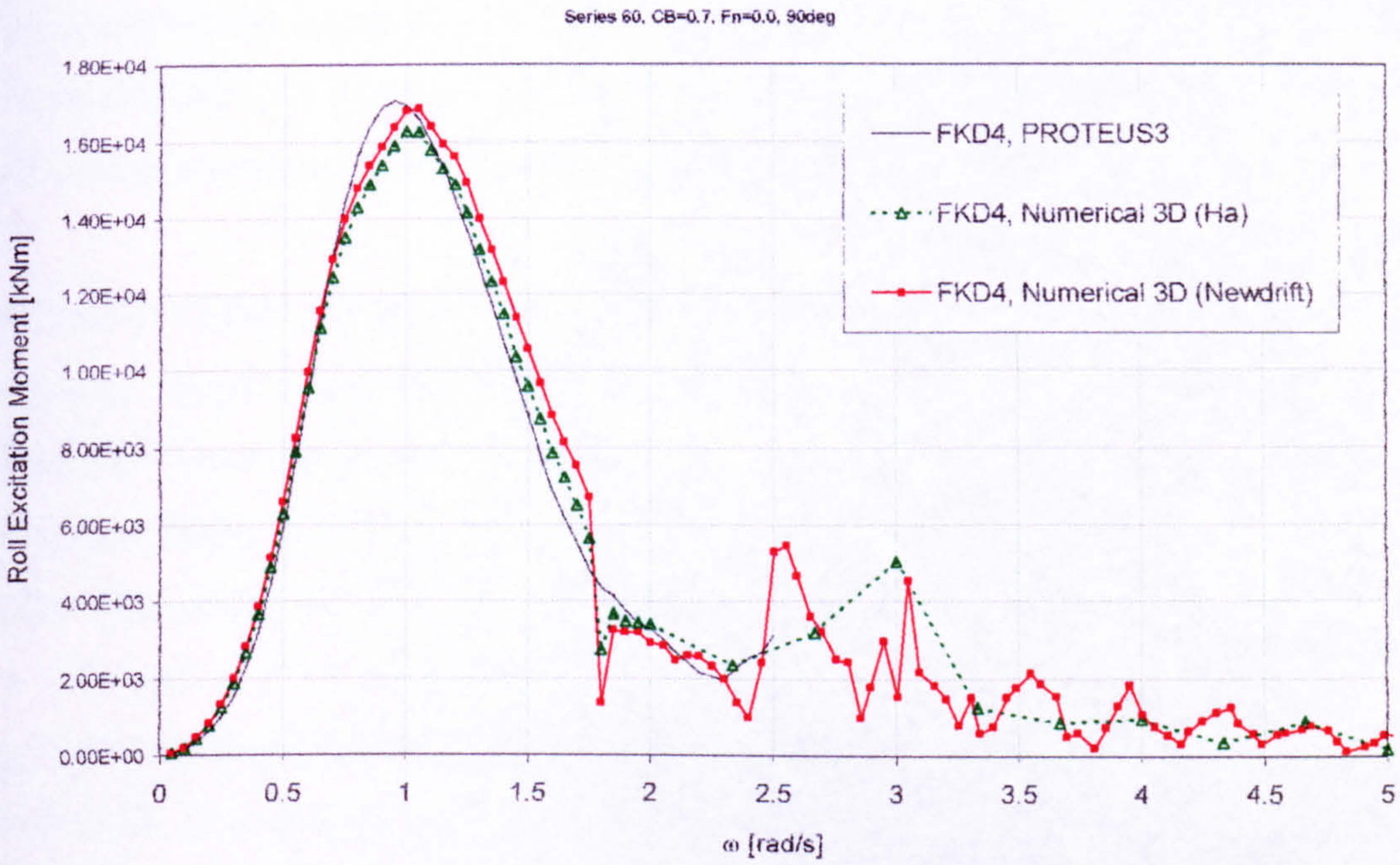

Figure 35 Excitation moment in roll mode for 3D Series 60, CB=0.7 hull form, comparison between predictions by strip theory and 3D panel methods, Fn=0.0, Heading 90deg

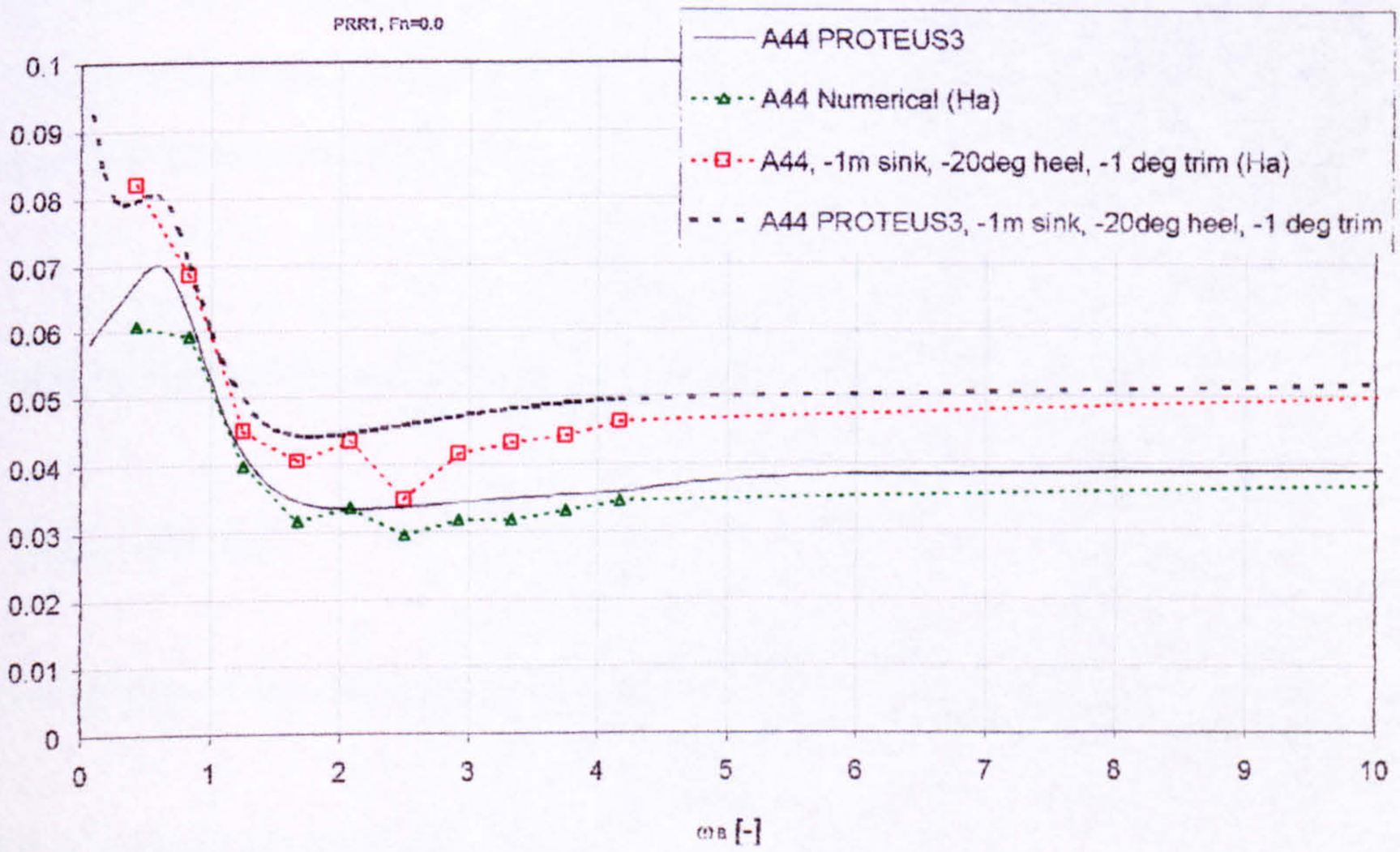

Figure 36 Dimensionless added mass in roll mode for 3D PRR1 hull form, effect of –1m sinkage, -20deg heel and –1deg (aft) trim, derived by strip theory and 3D panel methods, Fn=0.0

Based on results such as shown in Figure 34 or Figure 35 and taking other that displayed some degree of inconsistency between the numerical methods themselves and the experiment on one hand, but taking into account the experience of the last few decades showing that the potential

theory approach is very successful in resolving many engineering issues involving ship motion problems, on the other, it was concluded that the strip theory applied in this thesis is sufficiently accurate for predicting intact ship hydrodynamic properties.

Also the validity of the 2D approach for predictions of hydrodynamics in damaged conditions has been confirmed. All the predicted values of hydrodynamic coefficients, forces and moments as derived by either 2D or 3D methods, unlike expected, showed exactly the same trends dependent on the ship mean attitude, see for example Figure 36. Moreover, the study indicated quite a profound effect of the heel attitude on all the quantitative values of hydrodynamic properties of the monohull geometry. Therefore it is recommendable, that demonstrated non-linearity of hydrodynamic properties of the damaged ship deriving from variation of mean attitude due to progressive flooding, be included in the time domain solution of equations of motions. Such effects can be accounted for, most efficiently, by DATABASE approach, where these properties are predicted for a series of anticipated attitudes, and the relevant values interpolated.

Summarising, this study concluded that the techniques addressing ship hydrodynamics problem derived in §6 are sufficiently accurate and, therefore, could be confidently relied upon when applied to studies on dynamics of damaged ship.

9.2 Calibration of free mass motion models

9.2.1 Water sloshing

The prototype testing of the mathematical model (205) was performed for three cases:

- Simulation of the point-pendulum motion
- Predictions of natural frequencies of water sloshing in a rectangular box
- Simulations of sloshing loads in a rectangular box

The set-up and the result for the first of the tests are given in Figure 39 and Figure 40, respectively. For this purpose a compartment of spherical shape has been defined and free fall of some amount of floodwater from the initial position has been simulated. Note that the initial position refers here to

some inclination of the floodwater free surface with respect to absolute horizontal plane. It represents directly, thereby, free motion of a pendulum, which motion has a simple analytical solution. The comparison shown in Figure 40 is fully satisfactory.

For the second of the tests, a rectangular box of large height to breadth (H/b) ratio has been used, see Figure 41. Similarly, the free fall from an initial position has been simulated in order to establish the first natural frequency of the water motion in the box, known also from theoretical considerations as is shown by equation (222), e.g. [150]:

$$\omega_s = \sqrt{\frac{g \cdot \pi}{b} \cdot \tanh\left(\frac{h \cdot \pi}{b}\right)} \qquad (222)$$

Where the components of the above equation have been elucidated in Figure 37.

Strictly speaking, a comparison of the natural period as derived from modelling the water motion based on rigid-body considerations with formulae (222) is not fully representative of the prediction accuracy, as the solution (222) represents frequency, at which the amplitude of the sloshing water waves inside the tank and generated by forced oscillation has the highest value. Model (205), on the other hand represents the motion of the centre of buoyancy of the water inside the tank, as the disturbances to the free surface are only represented by its inclination with respect to earth horizontal plane.

It is for this reason, that Figure 42 shows discrepancies, but simply because it presents two different physical phenomena, i.e. internal wave propagation versus pendulum motion. It is clear that for a closed container and for the amount of floodwater approaching the capacity of the tank the natural frequency tends to zero if it represents motion of the centre of buoyancy along the possible geometrical surface, which for a full compartment becomes one point. This trend is not seen in the theoretical solution which shows that the natural period has an asymptotic value and varies very little for large ratios of water height to tank breadth.

The merit of the test is in demonstrating that despite disregarding the wave generation in the tank, the natural period of the motion is close enough to theoretical prediction of the real natural period for low ratio of water heights to tank breadth ($h/b<0.5$), which is the case for most tank geometries modelled in a damaged ship. It is anticipated, therefore, that the resultant forces predictions based on FMPS theory are representative of most of the effects of the real water sloshing.

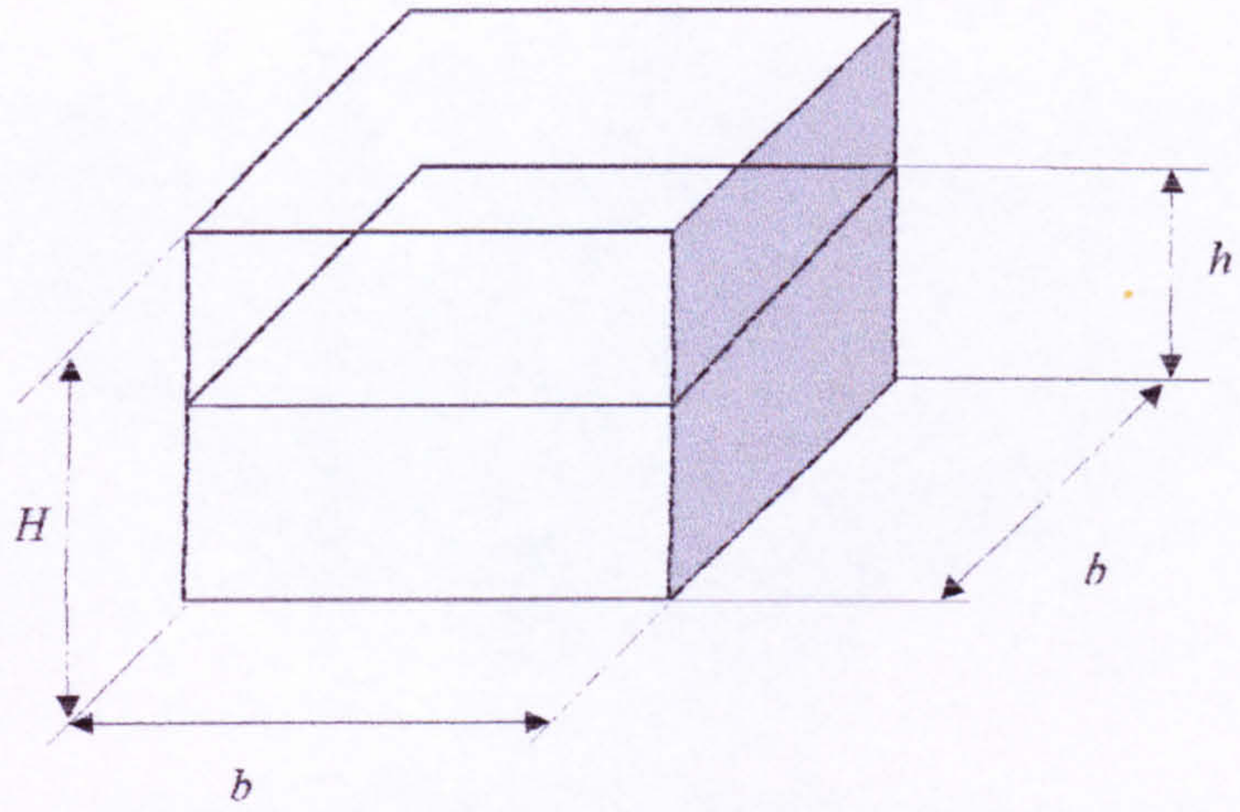

Figure 37 Prototype rectangular compartment used for verification studies of water sloshing

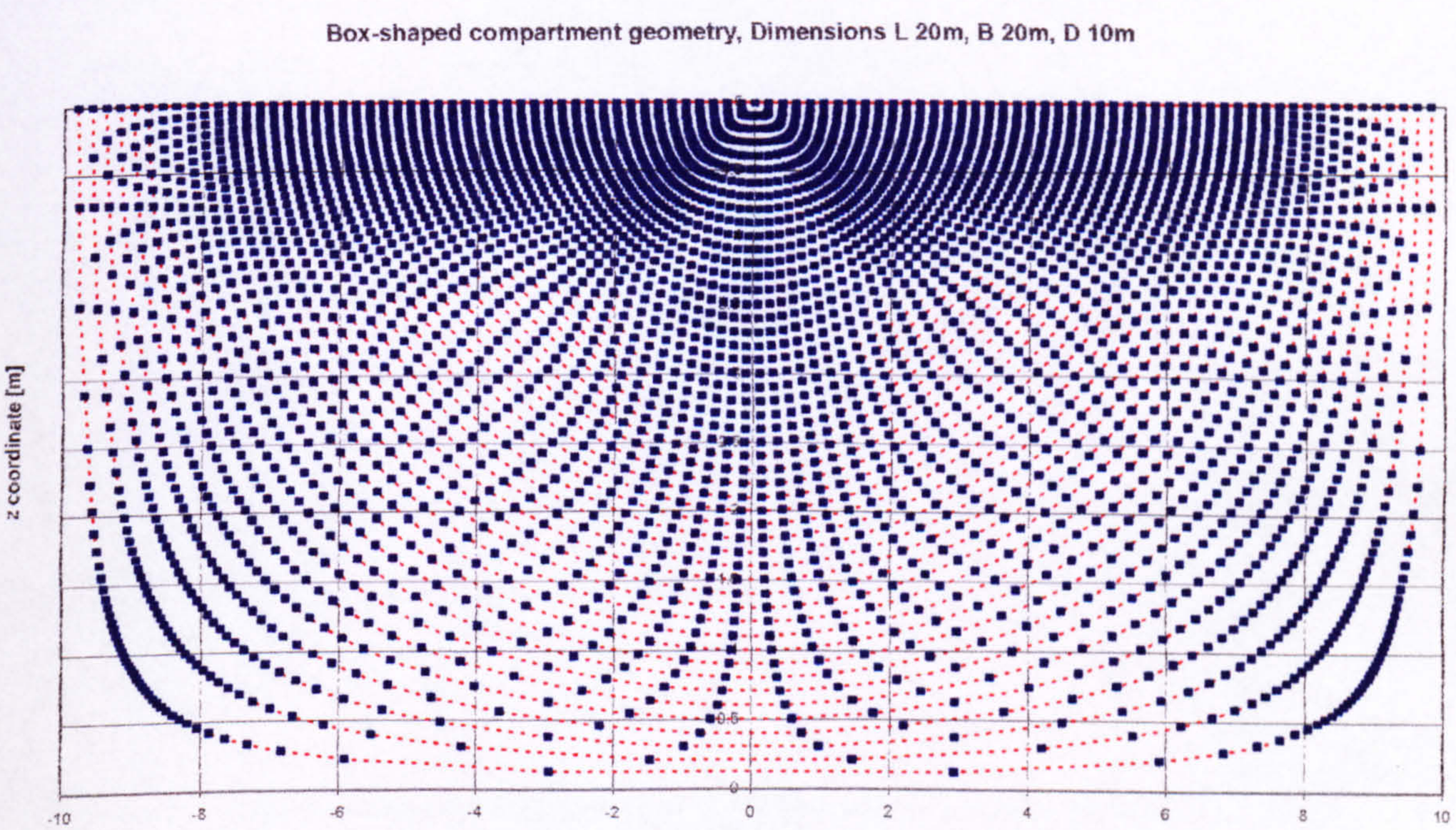

Figure 38 Damage compartment geometry database. The curves designate limiting paths of transverse displacement of a centre of buoyancy for various amounts of floodwater. Values in between are interpolated.

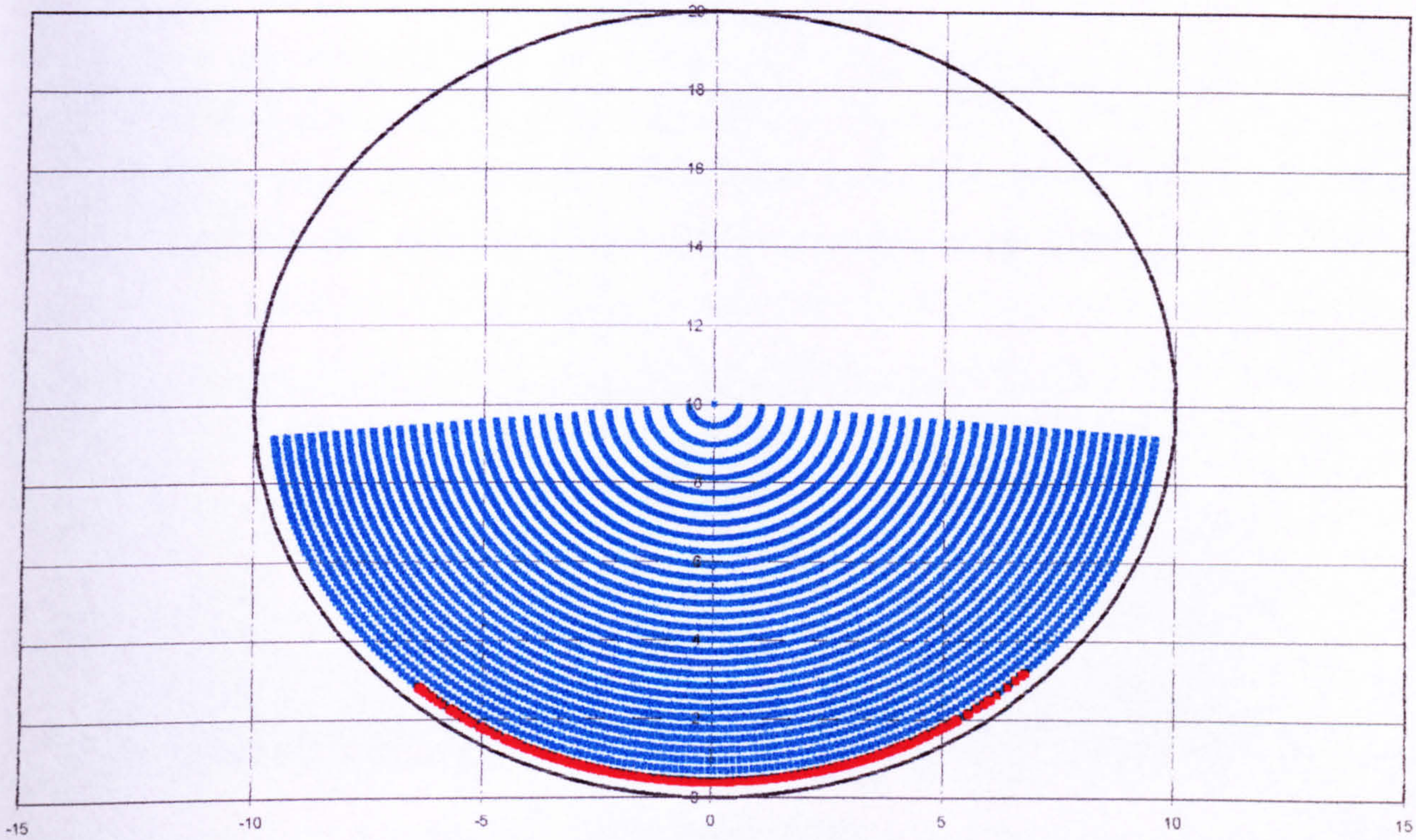

Figure 39 Sphere-shaped discretised compartment

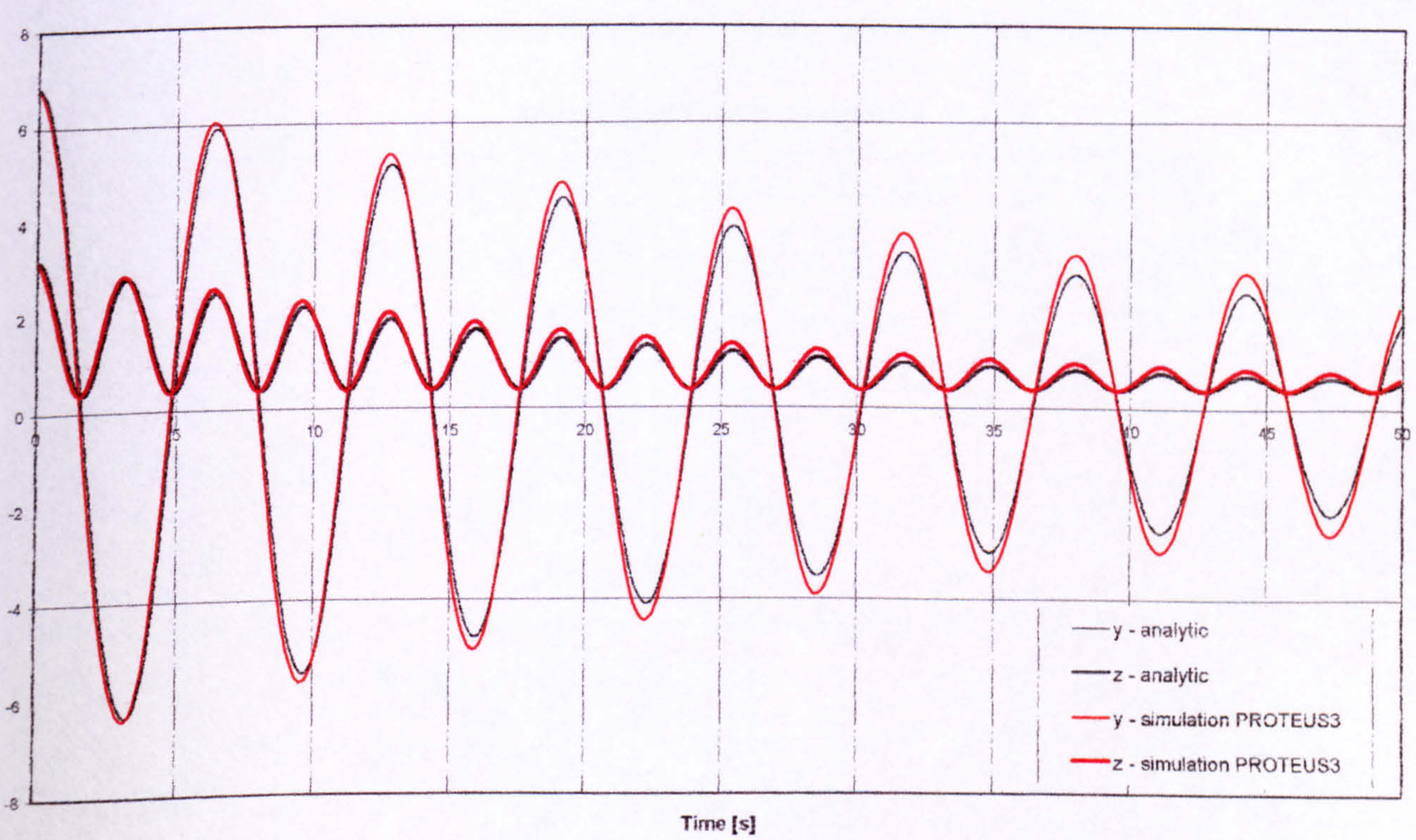

Figure 40 Simulation of the free motion of a mass point compared with the analytic solution

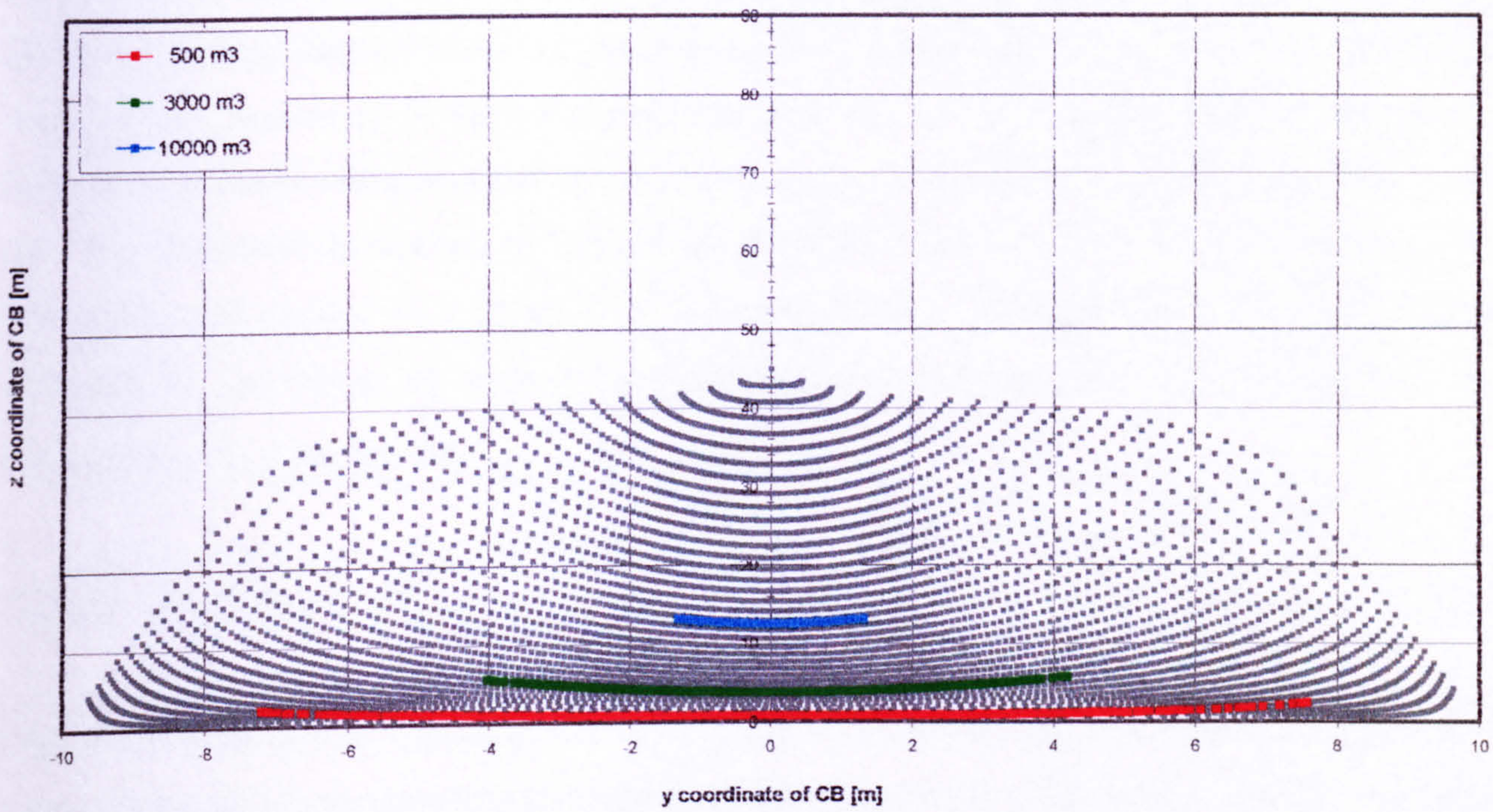

Figure 41 Geometry database for a box 20x20x90 m with sample of simulated patterns of motions of fluid centre of buoyancy for different amounts of fluid.

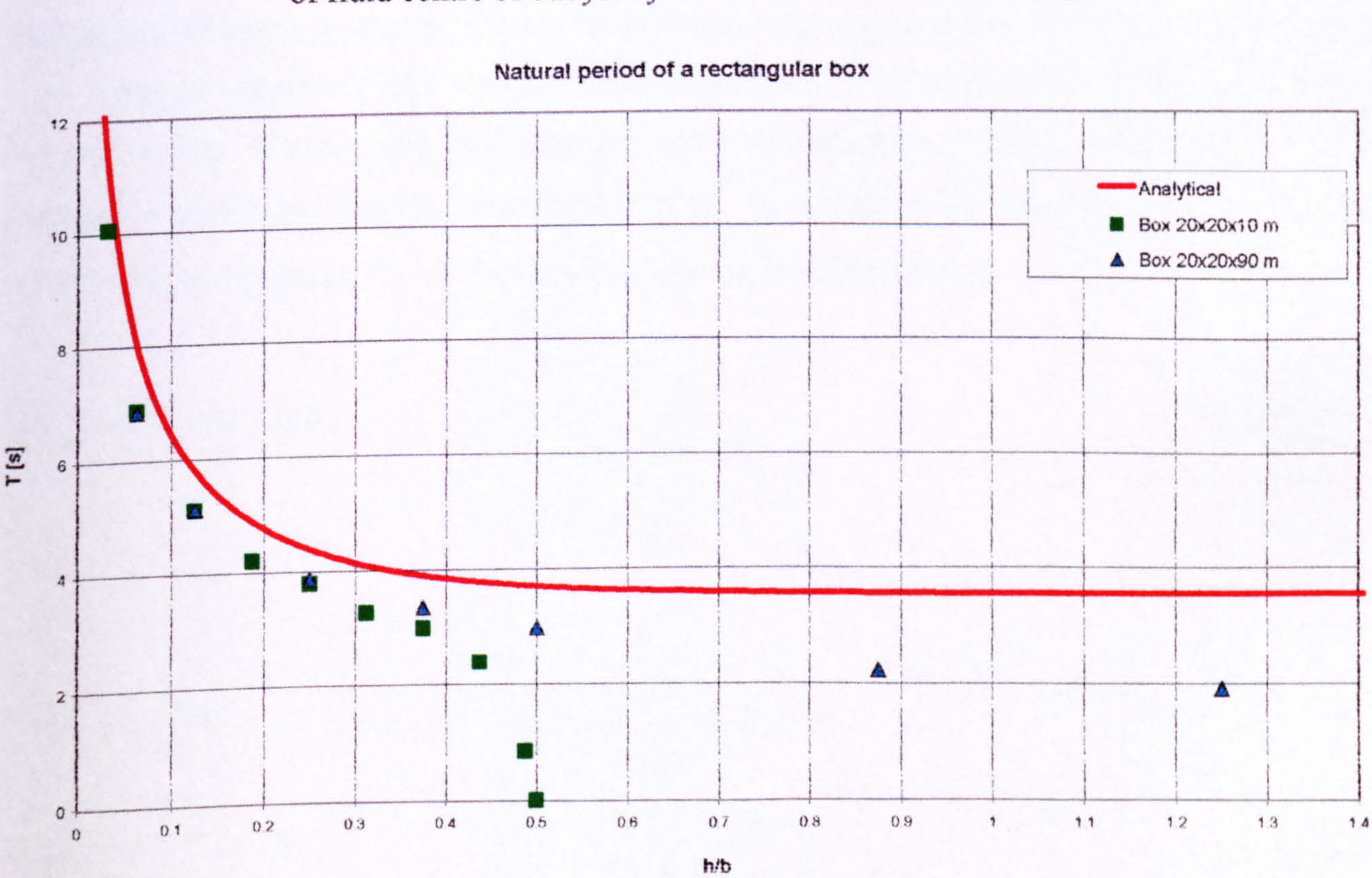

Figure 42 A comparison between the theoretical natural period for a rectangular box and the simulated natural period of fluid motion based on the FMPS model.

The third set of tests was found to be the most insightful into the ability of the approach adopted for estimations of fluid motion effects on the ship response. Experiments performed by de Bosch and Vugts, [148], have been the basis for studies on loads due to fluid sloshing. In their experimental research, they performed a series of bench testing on the behaviour of the fluid in the box-shaped tank. The tank, with dimensions of 0.1m in length, 1.0m in breadth and 0.5m in depth, was filled with water, and excited at a range of rotation amplitudes and frequencies. The tank moment amplitude, K_a, as well as the angle ε by which the moment lags behind the rolling was recorded. The moment was expressed as:

$$m_{wat}(t)\big|_x = K_a \cdot \sin(\omega \cdot t - \varepsilon)$$

Since the flow behaviour in such conditions displays very complex nature, as mentioned earlier on, it was perceived of great interest to quantify to what degree the fluid loads can be predicted by simplified methods such as discussed in this thesis.

For demonstration purposes, the moment vector extracted from equation (39) is used and presented in the form of equation (223), where three components are distinguished to represent inertial moment, gravity moment and non-linear moment, see equations (224), (225) and (226), respectively. Note here that the fluid inertia matrix, I'_w, contains only the inertia of a single mass point located at a position $\vec{r}'_w$ in the ship-fixed system of reference at A.

$$\vec{M}'_{wat} = \vec{M}'_I + \vec{M}'_g + \vec{M}'_N \qquad (223)$$

Where:

$$\vec{M}'_I = I'_w \cdot \frac{d}{dt}\vec{\omega}' \qquad (224)$$

$$\vec{M}'_g = M_w \cdot \vec{r}'_{ACw} \times \vec{g}' \qquad (225)$$

$$\vec{M}'_N = M_w \cdot \left[\left(\vec{\omega}' \times \vec{r}'_{AGw} \right) \times \vec{v}'_{AGw} \right] +$$
$$+ M_w \cdot \left[\vec{r}'_{AGw} \times \left[\frac{d}{dt} \vec{v}'_{AGw} + \vec{\omega}' \times \left(\vec{v}'_{AGw} \right) \right] \right] + \qquad (226)$$
$$+ \left(\frac{d}{dt} I'_w \right) \cdot \vec{\omega}' + \vec{\omega}' \times \left[\left(I'_w \right) \cdot \vec{\omega}' \right]$$

Harmonic oscillations were imposed to estimate the tank response in terms of forces generated by the fluid. Figure 43 and Figure 44 show amplitudes and phases, respectively, of the total moment (223) around rotation axis x. Notable in these figures is the effect of the damping coefficient μ^*, the value for which thereafter has been adopted as 0.15. For lower values of this coefficient, the predicted moment shows characteristics of an under-damped spring-mass system. With the damping adjusted as mentioned, however, the predicted moment amplitude and phase compare very favourably with the measurements. Although the calculated amplitude curve shows slight difference, as it resembles typical damped spring-mass systems behaviour, it is the accurate estimation of the phase angle, which renders the modelling a very reliable tool for sloshing estimations. Since the filling ratio is relatively low, the natural period is predicted also quite accurately.

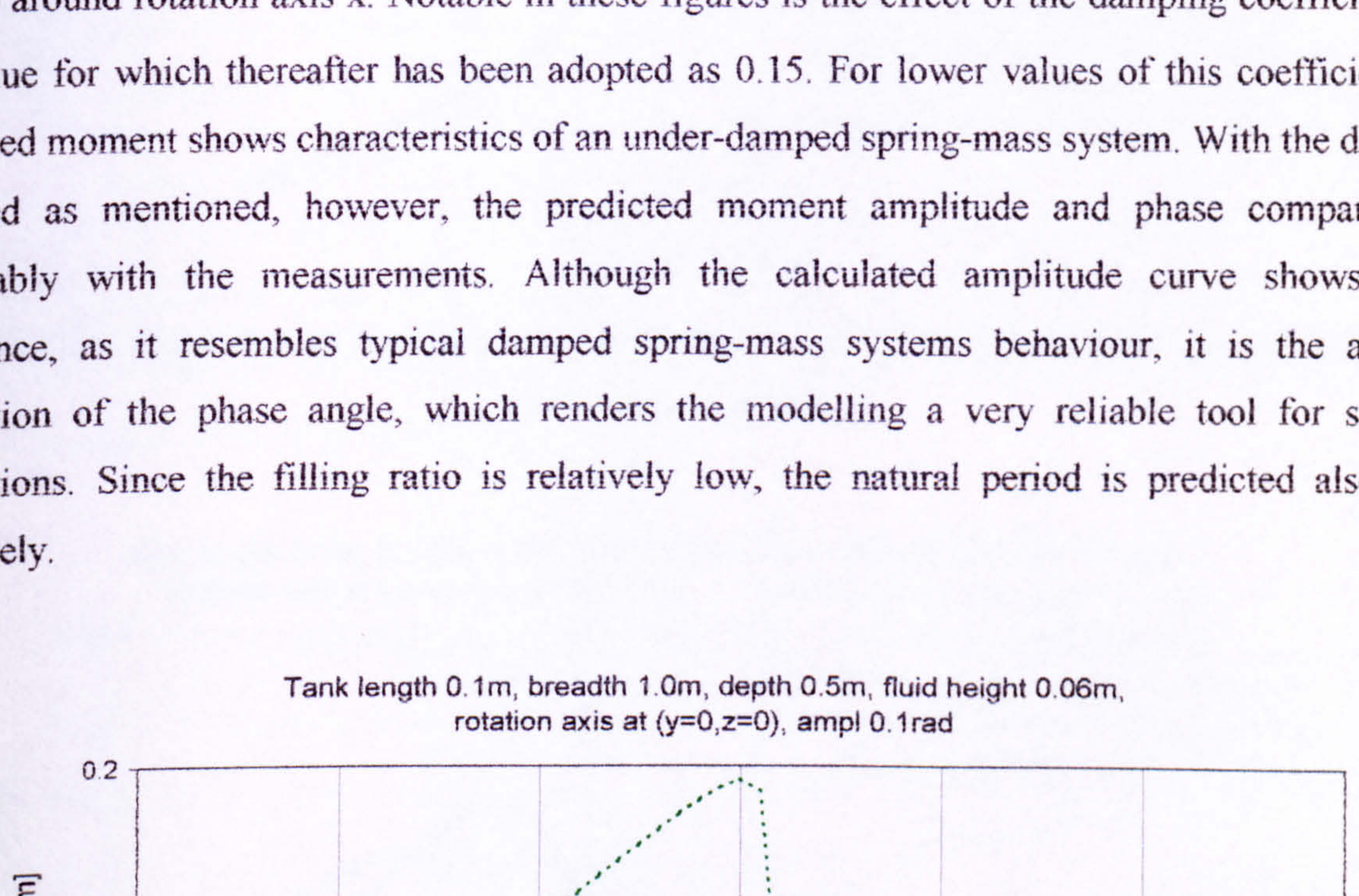

Figure 43 Comparison of fluid moment amplitudes derived by experiments and in-phase and FMPS sloshing models

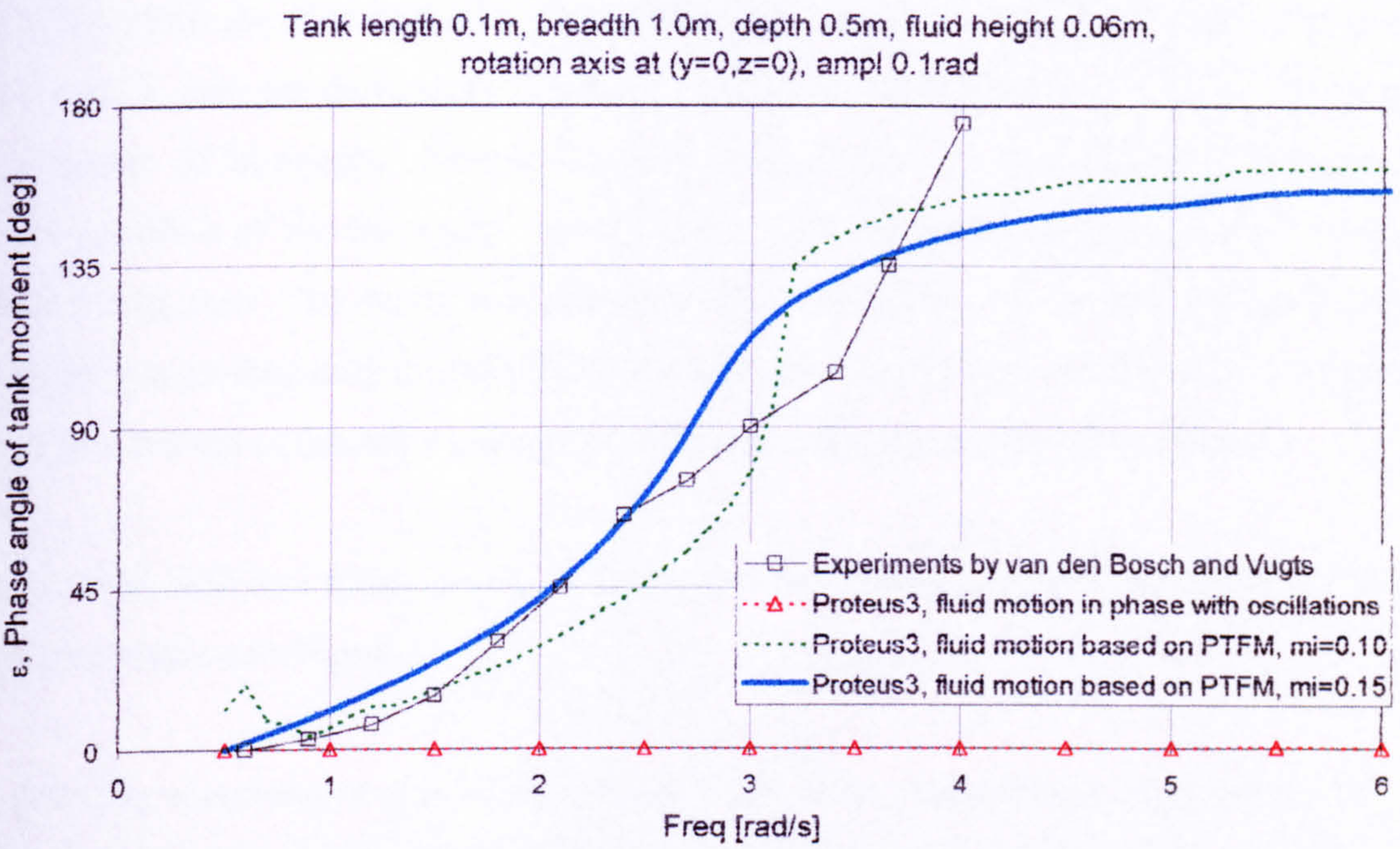

Figure 44 Comparison of fluid moment phase angles derived by experiments and in-phase and FMPS sloshing models

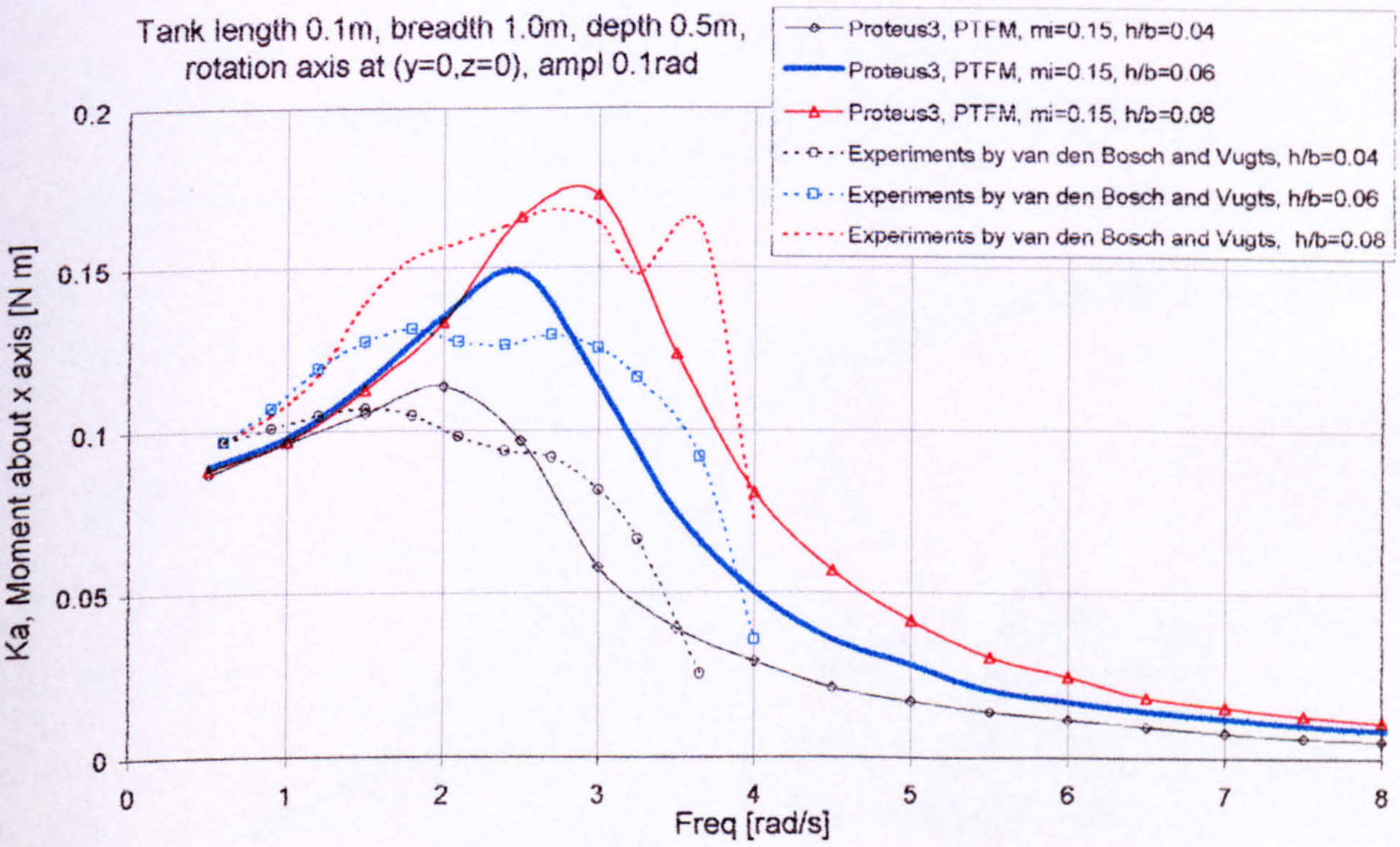

Figure 45 Comparison of fluid moment amplitudes derived by experiments and FMPS sloshing models. Effect of filling ratio.

Figure 43 also shows results from a simpler model where the floodwater free surface is assumed to move in phase with the ship rotations. Note that in this case the velocity and acceleration vectors, seen in (226), can be derived by means of backward differentiation on the instantaneously estimated centre of buoyancy. As can be seen from Figure 43, the moment remains virtually constant irrespective of the frequency of oscillation, with the phase angle shown in Figure 44, by assumption being zero. The moment amplitudes are considerably lower than the values measured experimentally or predicted by model (205) for most of the frequency range, implying that the free surface slopes derived in the latter are consistently exceeding the rotation amplitudes.

Simulations with different filling ratios confirm consistent predictions of the amplitudes of the tank moments, as is shown in Figure 45.

Finally, partially surprising it was discovered that the most predominant component of the water sloshing moment in this case is due to gravity, as is shown in Figure 47. However, some further testing showed that the non-linear terms are of considerable importance for greater filling ratios (h/b~0.25), which is demonstrated in Figure 48.

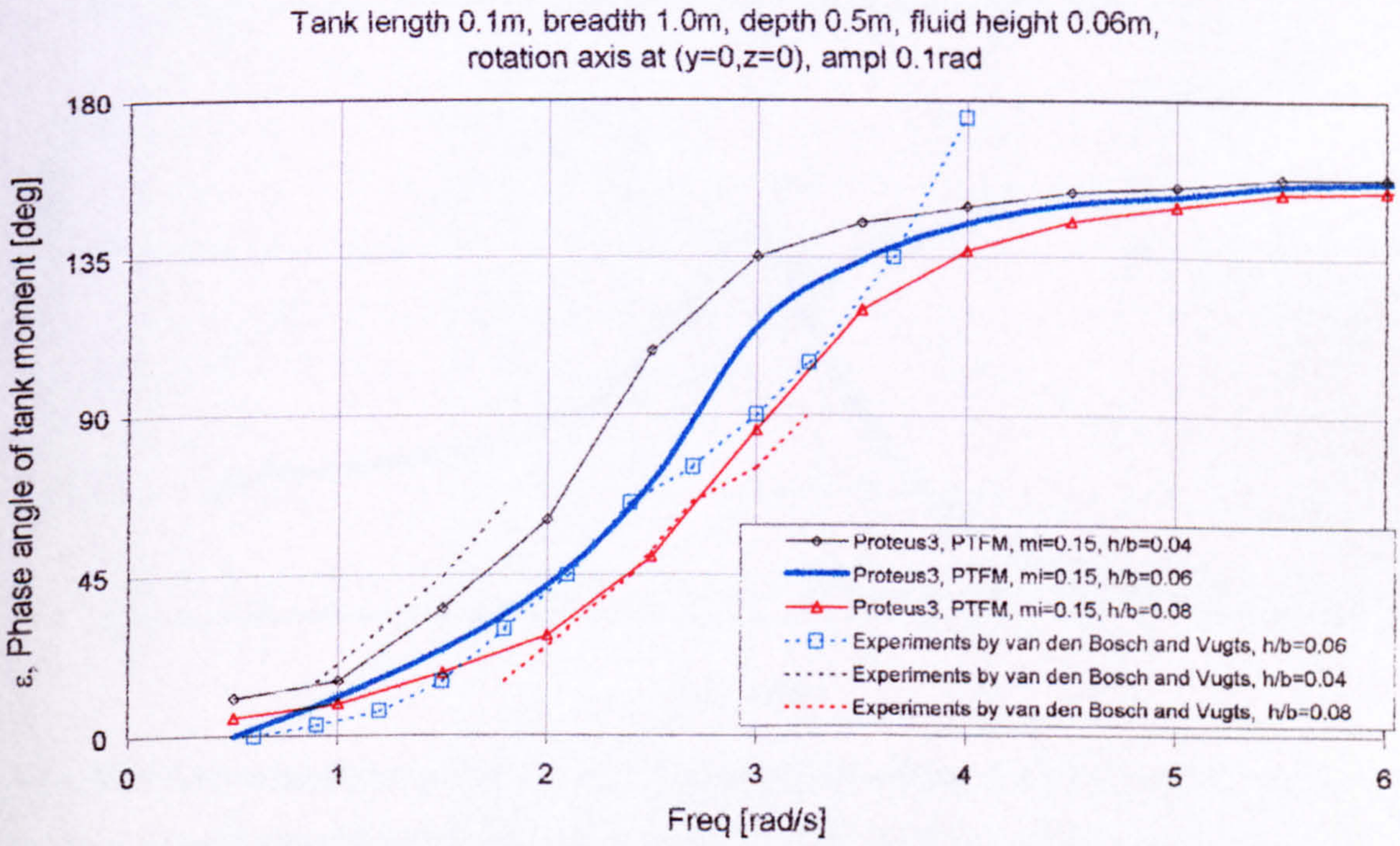

Figure 46 Comparison of fluid moment phase angles derived by experiments and FMPS sloshing models. Effect of filling ratio.

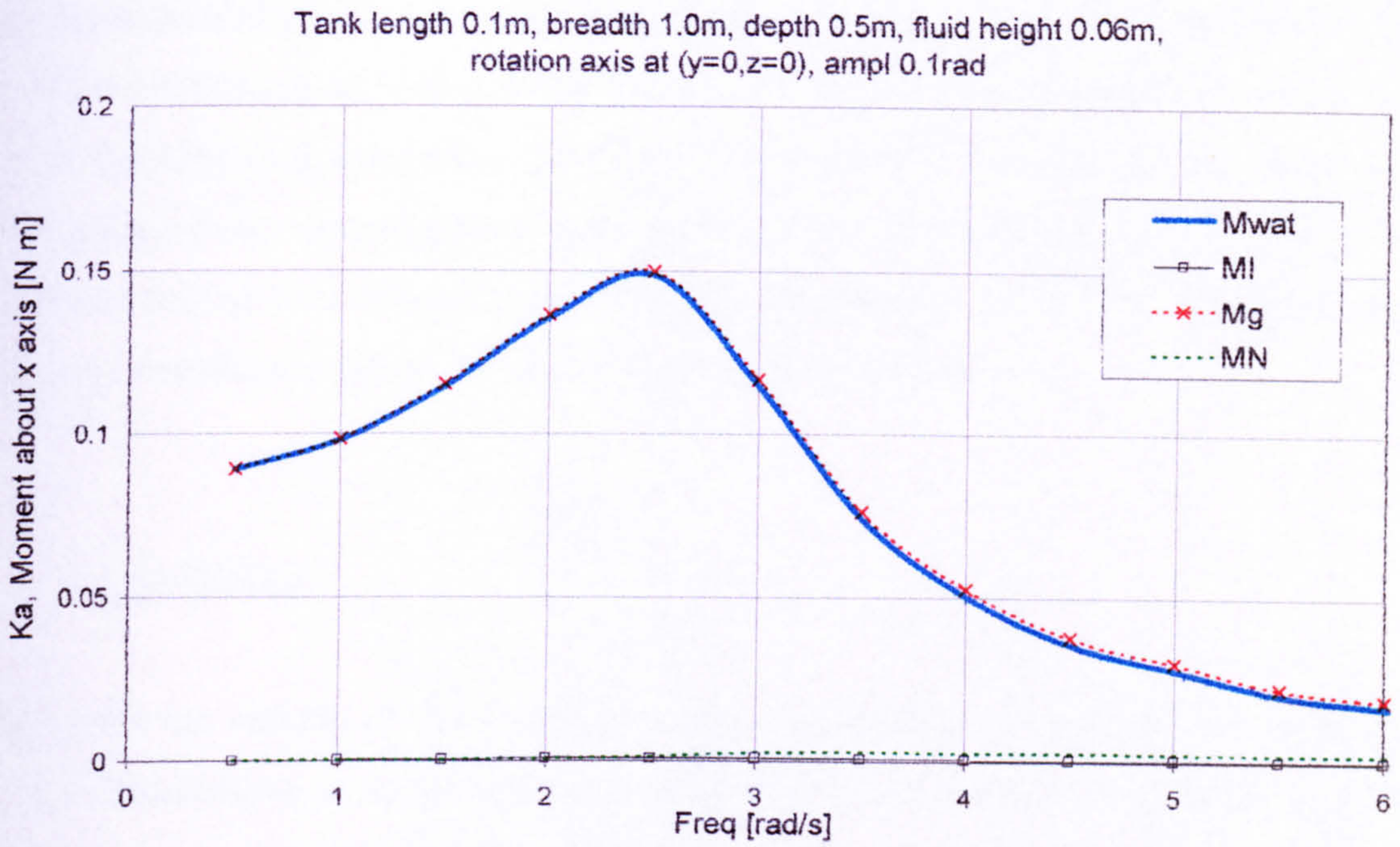

Figure 47 Fluid moment amplitudes derived by FMPS sloshing model. Comparison between different moment components. For low filling ratio, the gravity moment is the predominant component

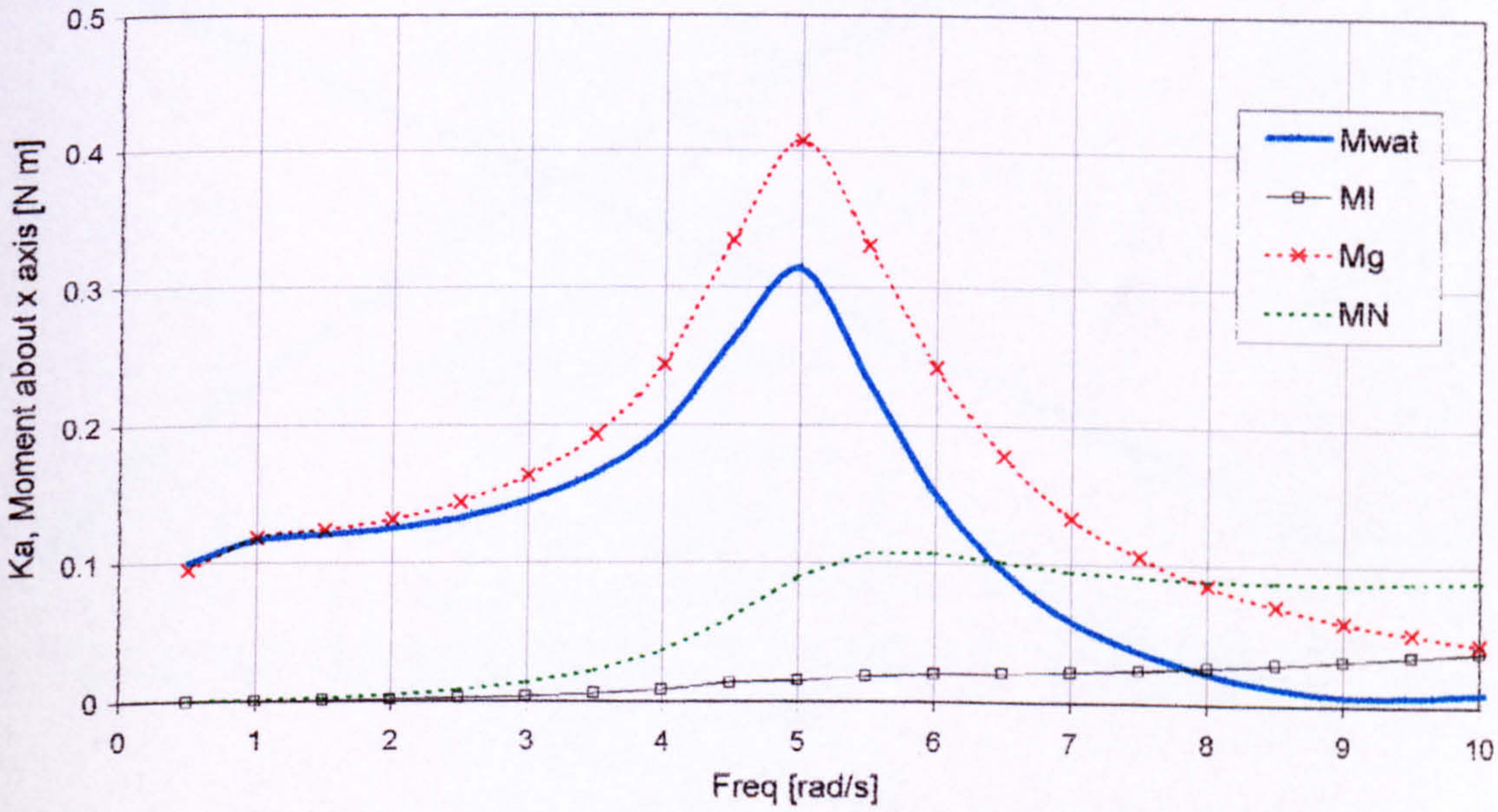

Figure 48 Fluid moment amplitudes derived by FMPS sloshing model. Comparison between different moment components to elucidate importance of non-linear terms for higher fill ratios (h/b~0.25)

The very fundamental case studies discussed above demonstrate that the techniques presented in this thesis for predictions of fluid sloshing and its effects can be confidently applied for examining the dynamic stability of flooded ships. This derives from the fact that the main load components due to fluid transfer can be modelled from most basic of dynamic laws, and that the highly non-linear effects present during water sloshing are of minor importance, perhaps relevant for more focused studies on e.g. impulsive loads on localised elements of tank structures.

9.2.2 Cargo shifting

To demonstrate the validity of the numerical code developed on the basis of the model for cargo shifting presented above, a set of basic examples have been produced as shown in Figure 49 to Figure 52. As can be seen the numerical predictions match the analytical solutions.

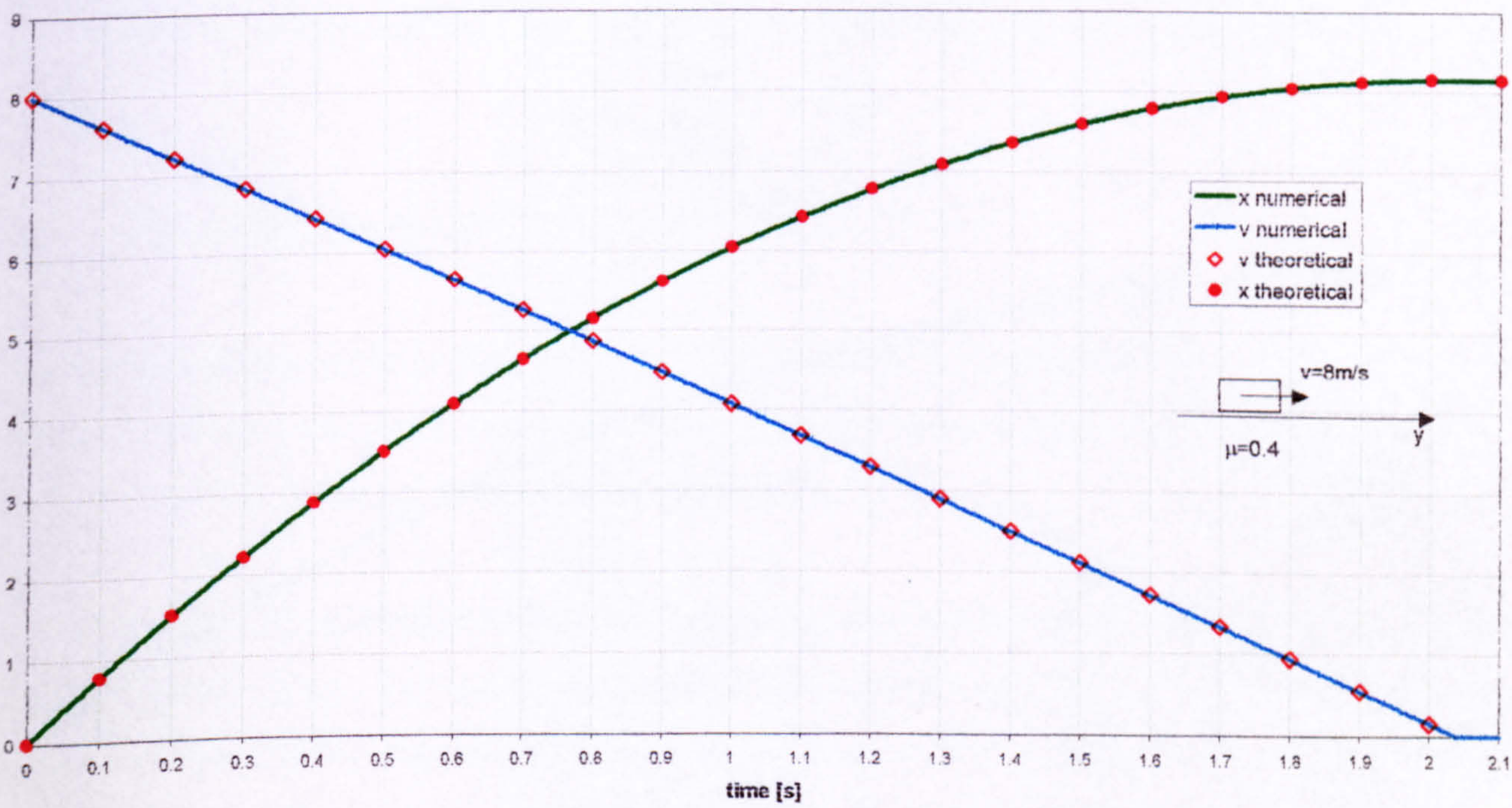

Figure 49 Test1, horizontal Plane, Initial v=8[m/s], Friction 0.4

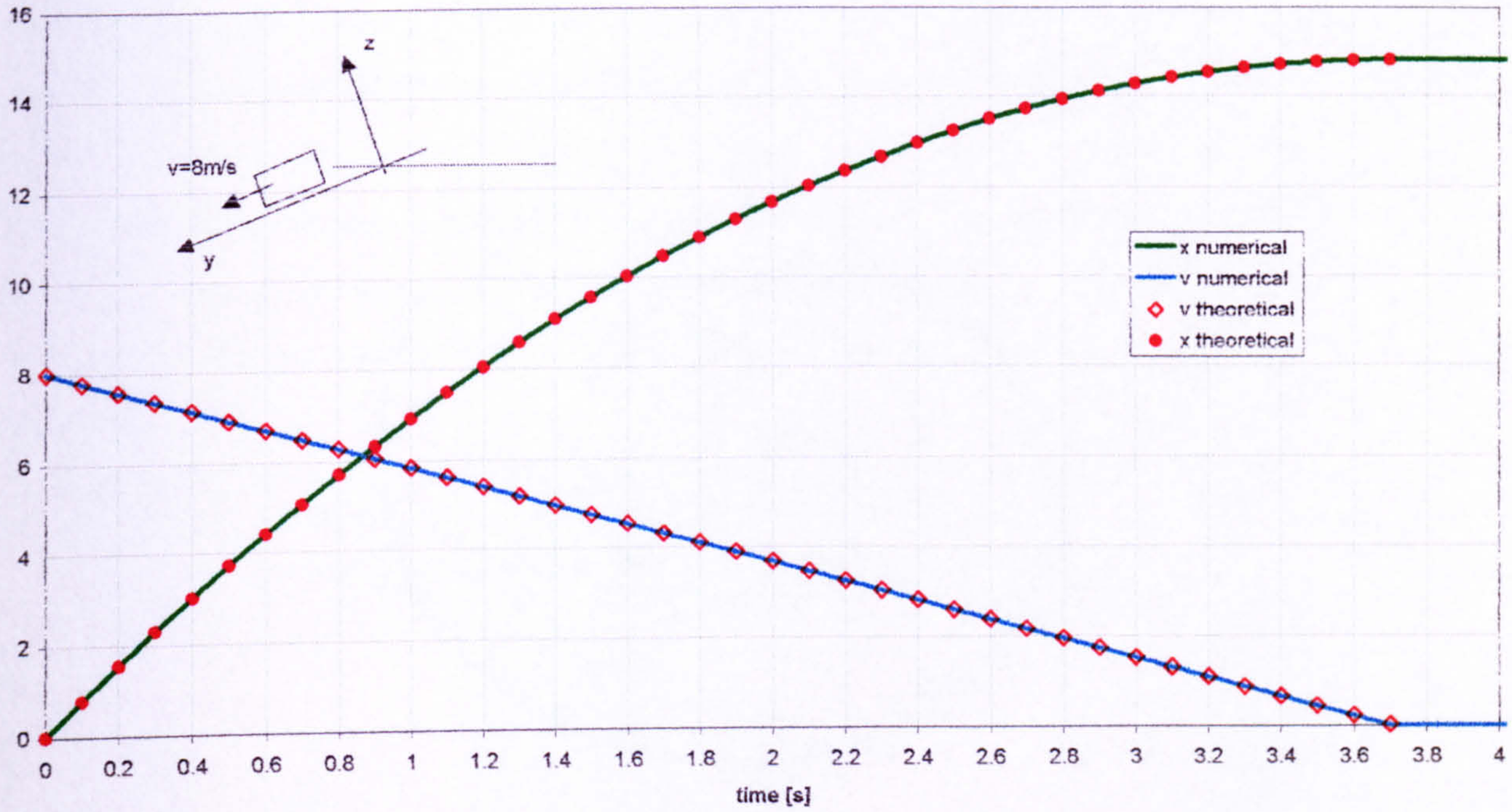

Figure 50 Test2, slope –10deg, Initial v=8[m/s], Friction 0.4

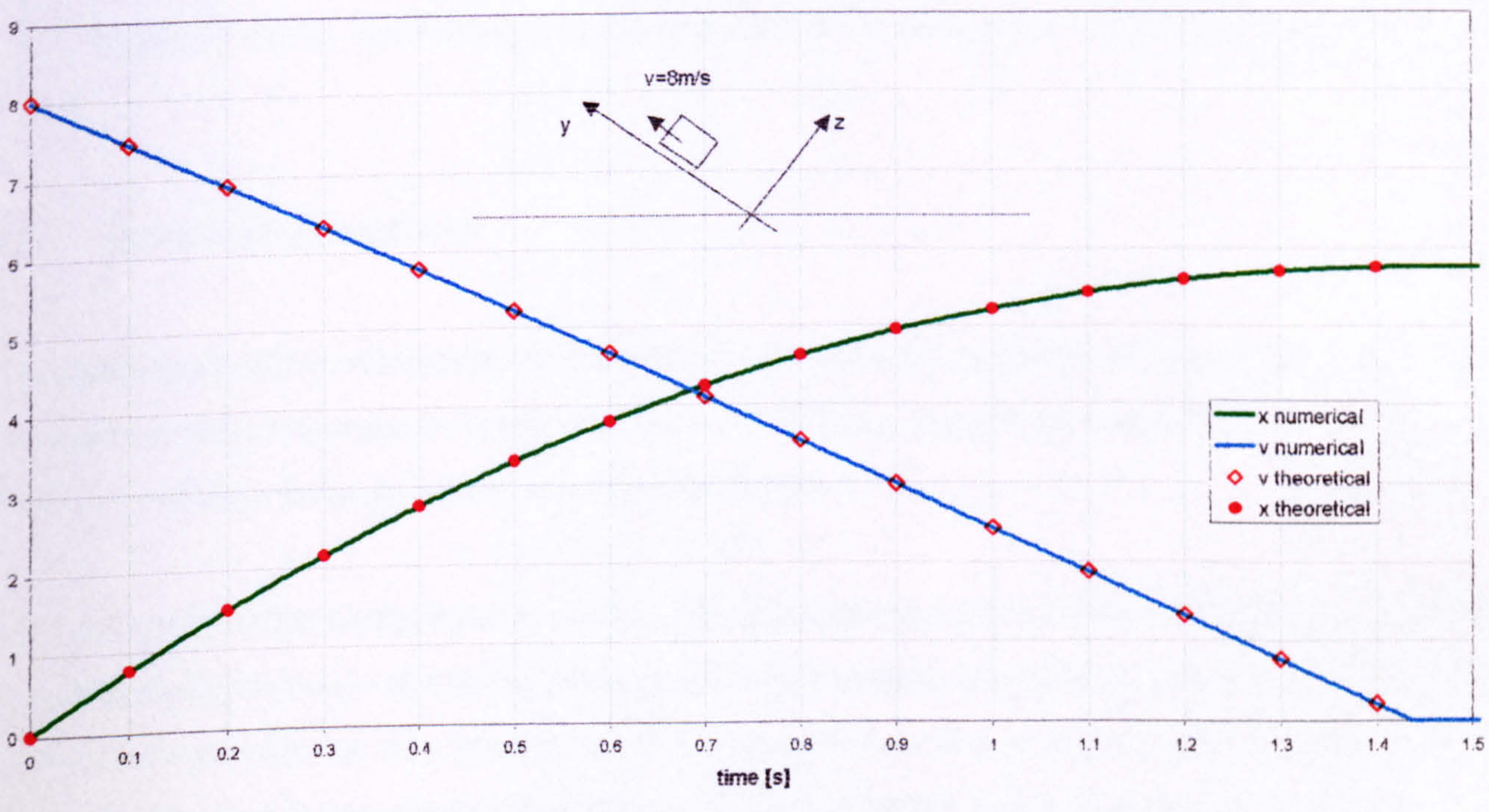

Figure 51 Test3, slope 10deg, Initial v=8[m/s], Friction 0.4

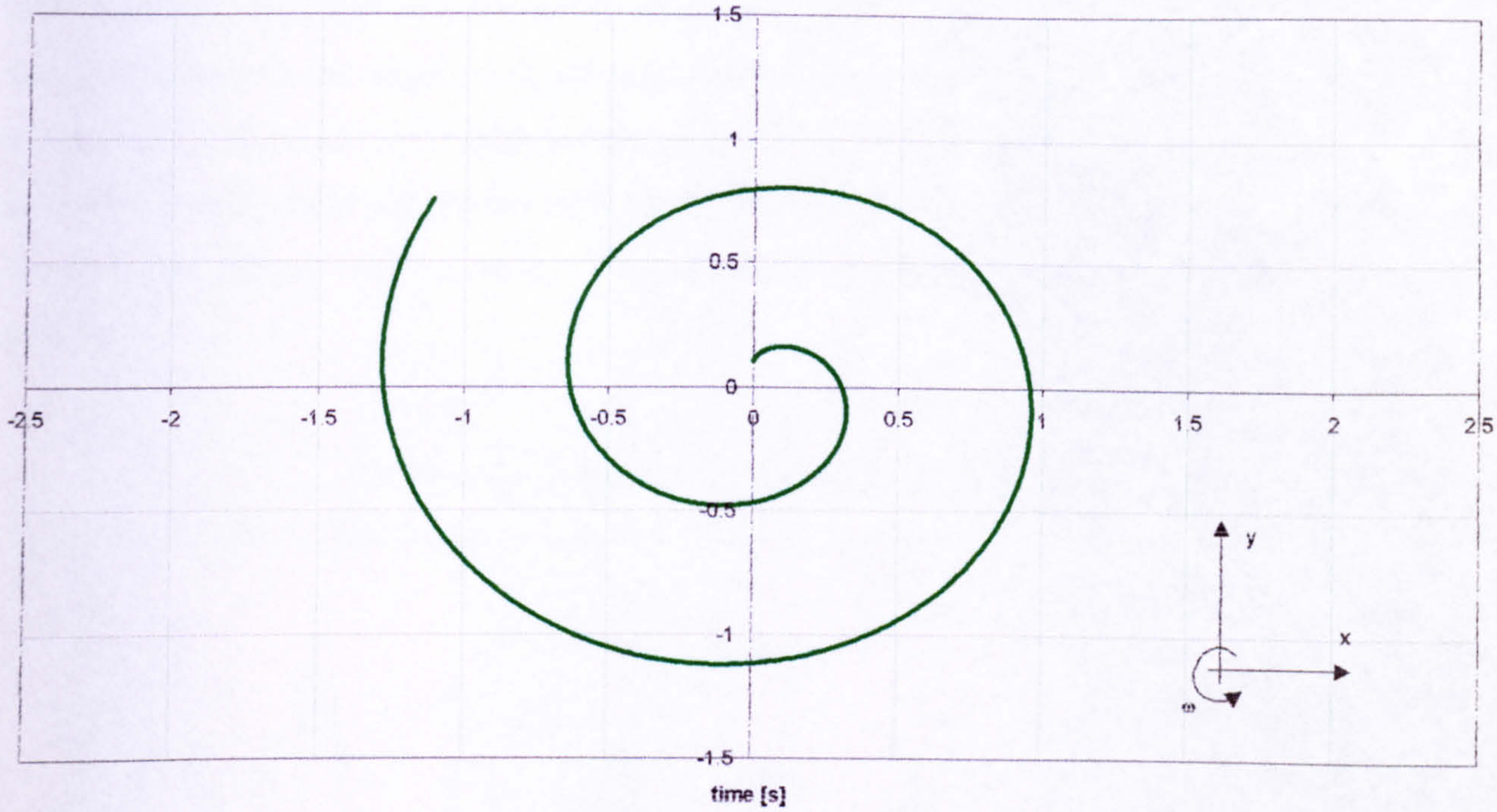

Figure 52 Test4, horizontal plane rotating around OZ axis with ω=1[rad/s], Friction 0.4

9.3 Intact ship motions

The main emphasis in the testing of time-domain solution to equations of intact ship motions has been put on ship responses in beam seas. A series of tests undertaken, including free roll test, roll RAO and motions in irregular seas are discussed below.

The University of Strathclyde has recently undertaken an extensive model testing campaign aiming at quantification of survival time of passenger RO-RO vessels subject to progressive flooding. This exercise has provided a very comprehensive database of quality records of ship motions, relative wave elevations and quantitative measurements of floodwater amount and motions with respect to the ship, [30]. Some of these data corresponding to intact ship conditions, have been used here to demonstrate correlation between experimentally and numerically derived dynamic behaviour of the intact ship.

Three types of tests have been carried out for the PRR1 ship in intact conditions: free rolling, motions in harmonic regular wave and motions in irregular seas. As can be seen from Figure 53, the correlation between the experiment and numerical simulation for the ship in intact conditions while not exposed to the wave excitation, is very good. This demonstrates that the basic ingredients of the code such as numerical integration schemes, hydrodynamic forces predictions (restoring, radiation) or non-linear effects such as viscous roll damping are modelled properly and with acceptable accuracy.

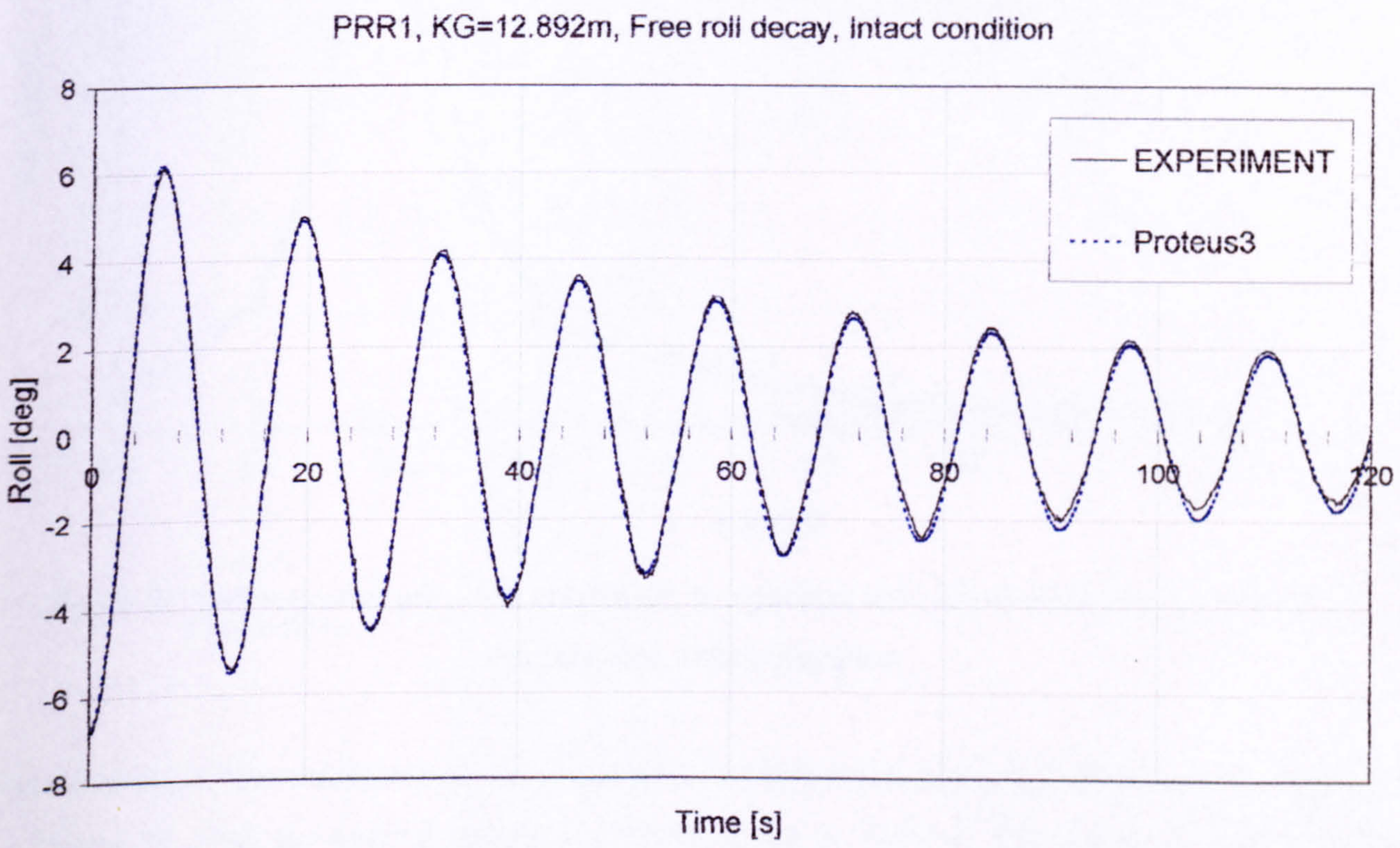

Figure 53 Free roll decay curve for PRR1, intact condition

The results of experimentation in regular waves are shown in Figure 54. As can be seen, roll response derived in experiments shows noticeable scatter at the natural roll frequency. This could be a result of the non-linear character of the viscous effects varying with the roll amplitude, which will be dependent on the actual excitation amplitude, here taken as 0.6 or 1.2m. The numerically derived roll response for wave of unit amplitude falls in between the two curves, accuracy of which response at the natural frequency is mostly attributable to the non-linear viscous forces modelling. This confirms that the empirical technique employed for predictions of this very complex phenomenon is accurate enough. The predicted response at frequencies higher and lower than the

natural roll frequency (approximately 0.49 rad/s) is also consistent with the experiments, which verifies that basic elements of ship motion dynamics (e.g. restoring) are correctly represented.

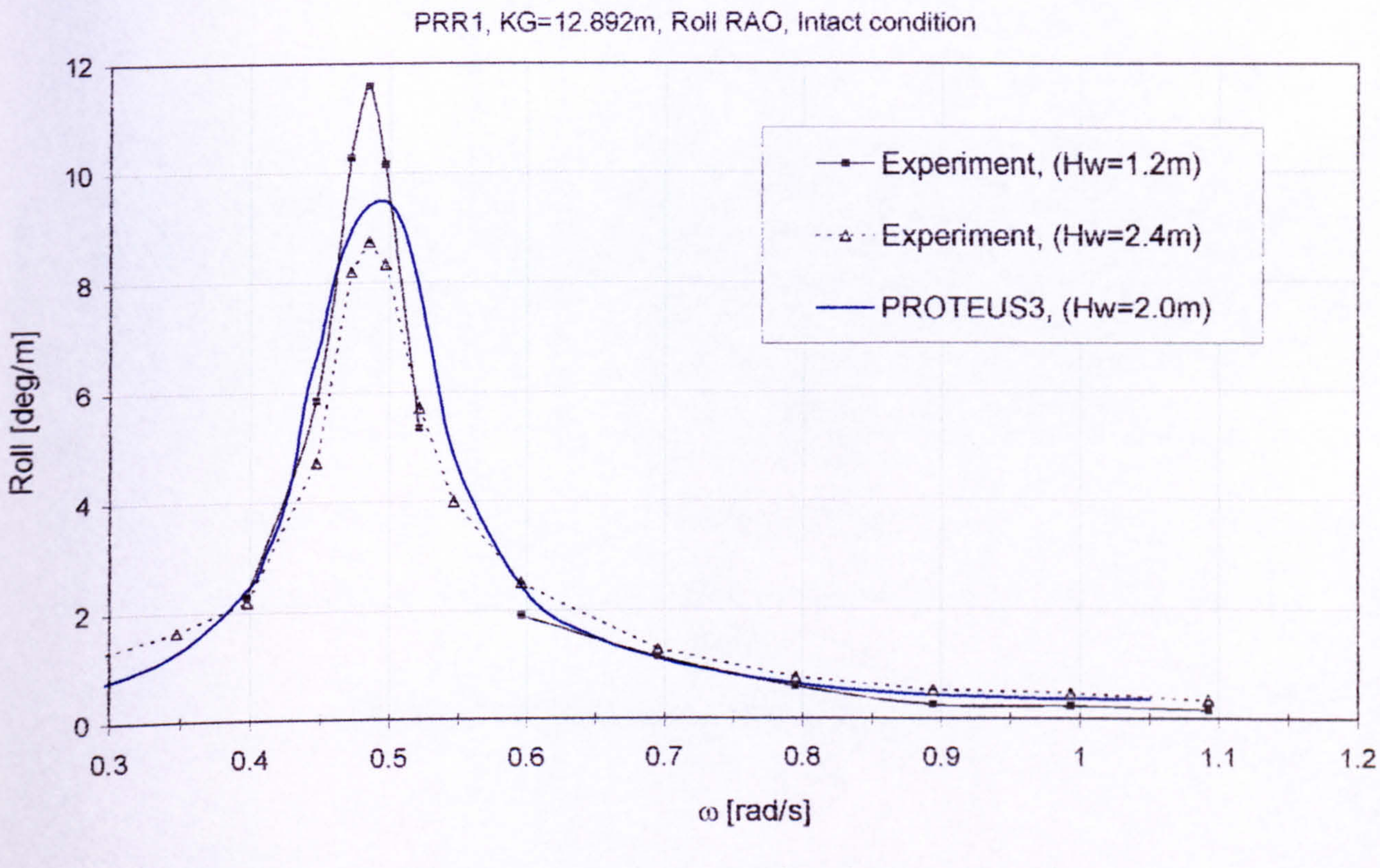

Figure 54 Roll response per wave amplitude, comparison between experiment and numerical simulations, intact condition

The outcome of the simulation of the vessel response in irregular seas is demonstrated in Figure 55 to Figure 58, with the general statistical analysis given in Table 1. This result indicates that the capability of the numerical model for predicting of ship behaviour in confused seas is reliable enough for addressing the problem of ship survivability.

Table 1 Underlying statistics of the test

PROTEUS3

	Heave[m]	Roll[deg]	Pitch[deg]
4Stdev	3.579	4.946	0.21
T02	8.045	10.508	7.936
T01	8.135	10.766	8.744

EXPERIMENT R16

	Heave[m]	Roll[deg]	Pitch[deg]
4Stdev	3.776	5.043	0.636
T02	8.171	10.339	7.484
T01	8.541	10.638	9.099

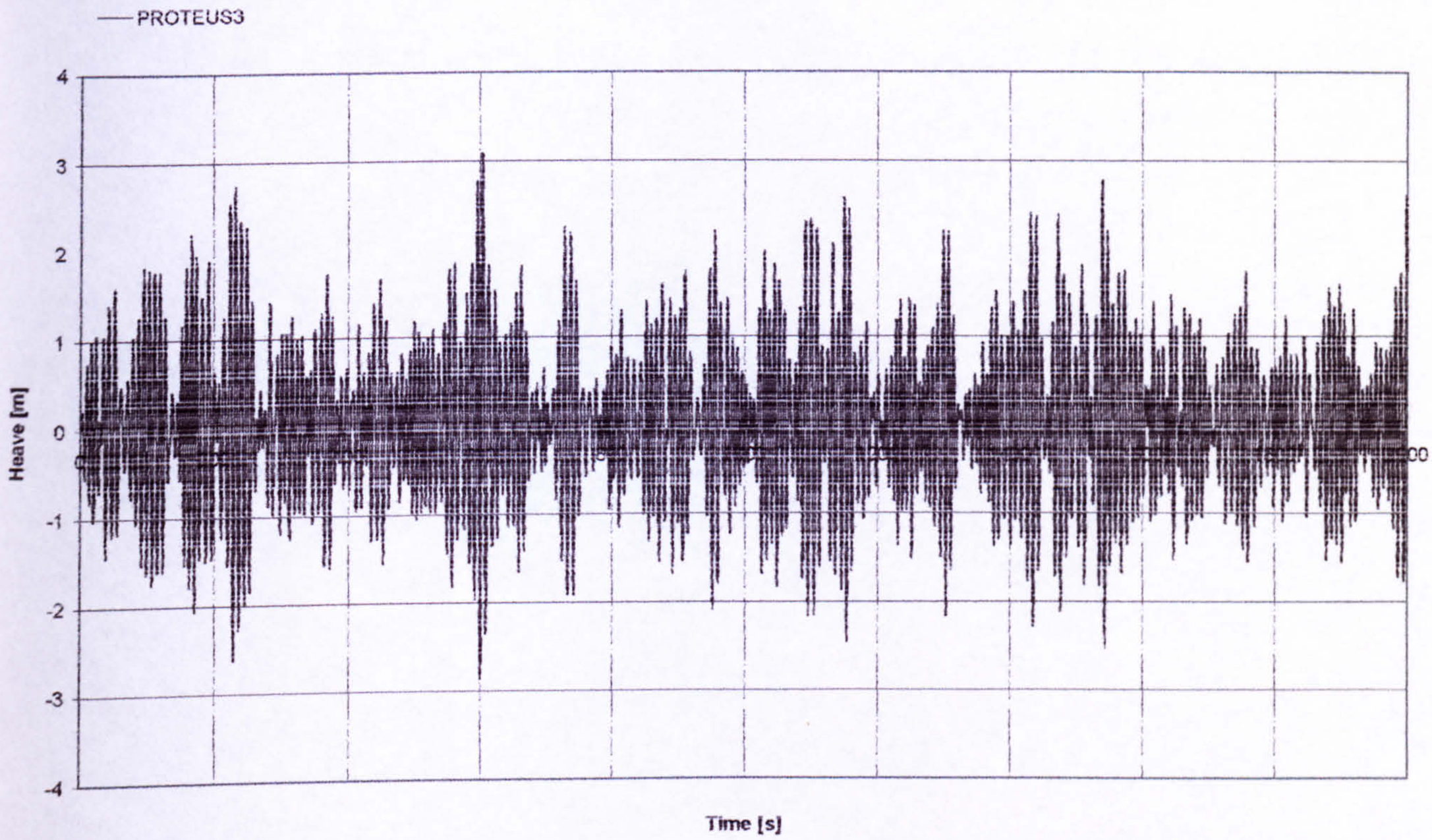

Figure 55 Heave response, PROTEUS3, Hs=4.0m

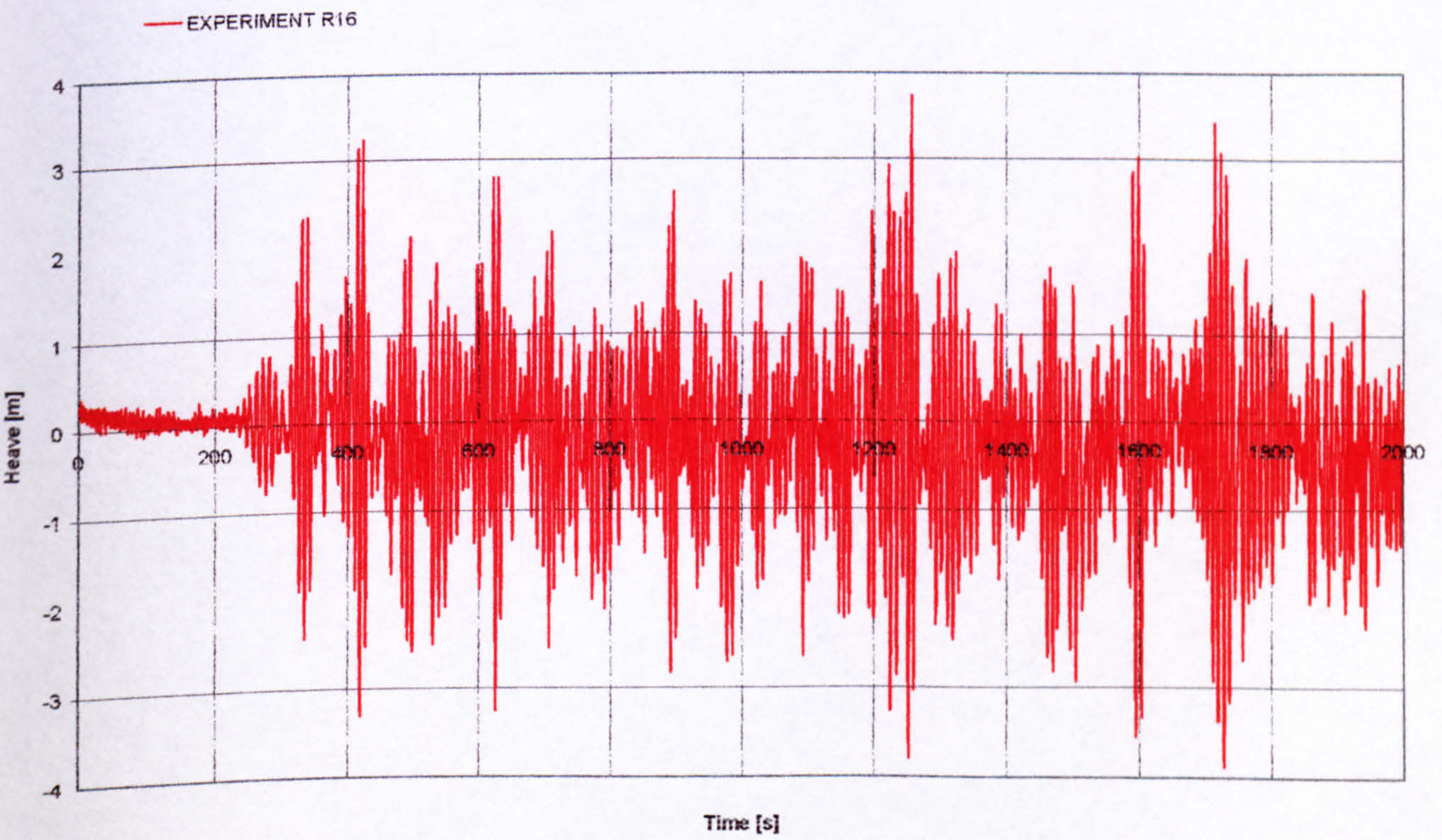

Figure 56 Heave response, experiment, Hs=4.0m

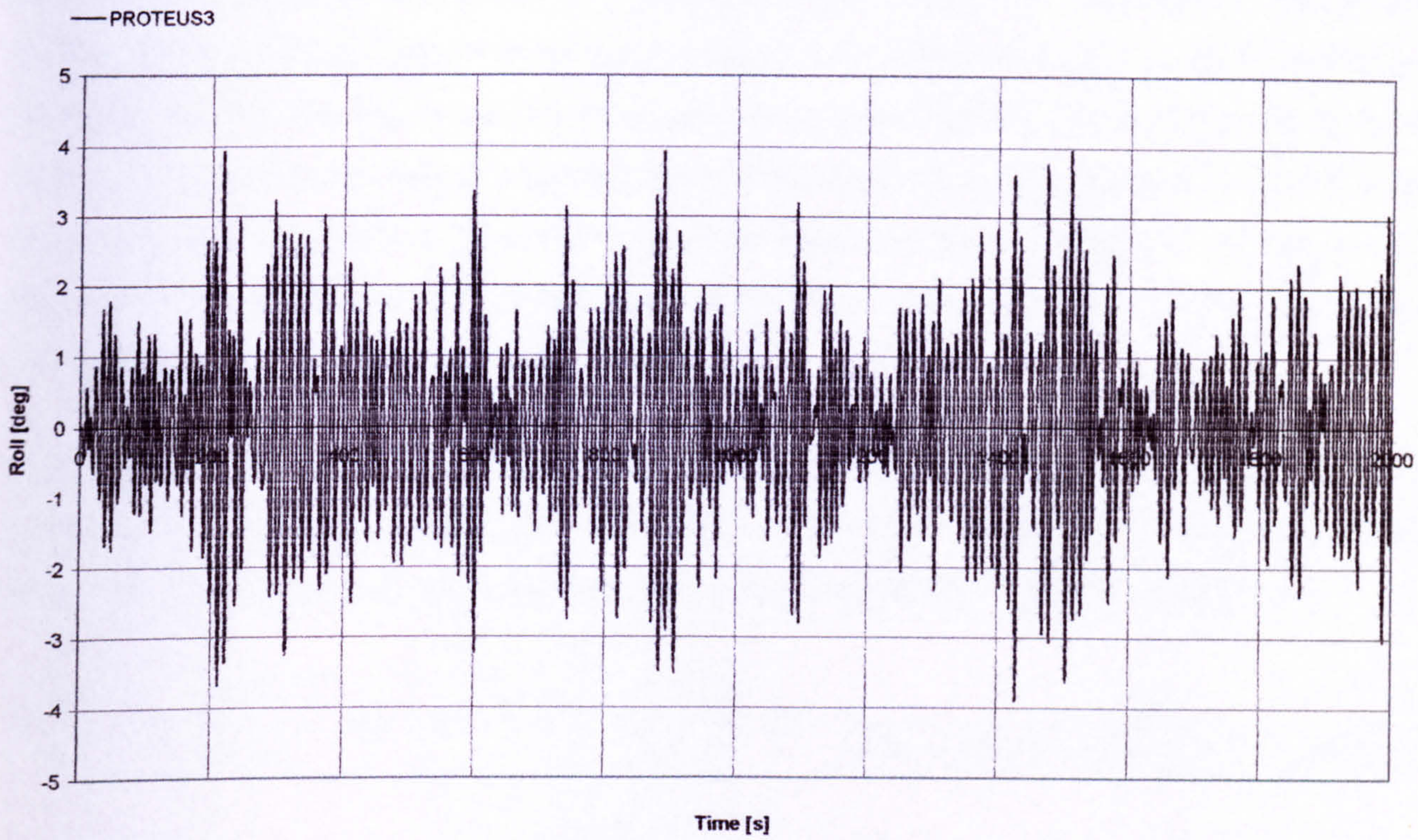

Figure 57 Roll response, PROTEUS3, Hs=4.0m

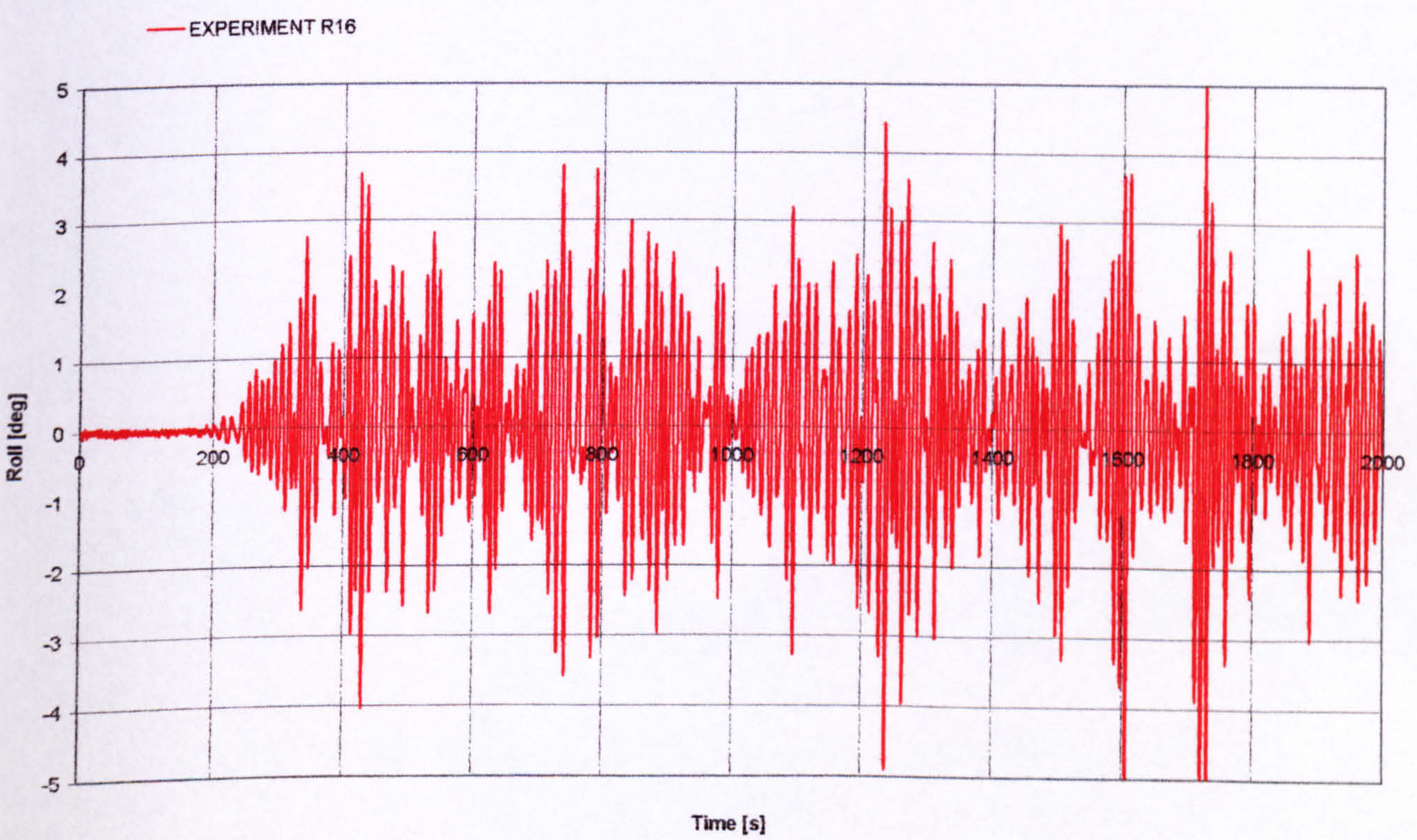

Figure 58 Roll response, experiment, Hs=4.0m

Furthermore, systematic testing has been carried out to identify the relationship between the severity of the excitation environment and the capability of the software to cope with motions predictions in these extreme conditions, limit state. A comparison of the calculations when applying the classical treatment of the ship hydrodynamic forces and moments evaluated up to the mean water plane level as well as approximation of the excitation forces/moments evaluated for the geometry under the actual undisturbed wave profile have led to interesting conclusion, as is discussed next.

The extreme environment has been modelled accordingly to JOHNSWAP wave energy spectrum, generated accordingly to linear theory of random processes, as adopted in the main body of the thesis. The parameters of the spectrum were determined accordingly to the following relations:

$$\alpha = \frac{Hs}{\lambda},\ Tp = \sqrt{\frac{2\cdot\pi\cdot\lambda}{g}},\ Tp = C\cdot\sqrt{Hs},\ C = \sqrt{\frac{2\cdot\pi}{g\cdot\alpha}},\ Tz = \frac{Tp}{1.49 - 0.102\cdot\gamma + 0.0142\cdot\gamma^2 - 0.00079\cdot\gamma^3}$$

The input parameters are: the wave steepness α chosen as 1/25, the spectral peakness parameter γ chosen as 3.3, and significant wave height here being the variable, taken in the range of Hs=2-14.0m. The spectrum was defined by:

$$\omega_p(Hs) := \frac{2\cdot\pi}{C\cdot\sqrt{Hs}}$$

$$\tau(\omega, Hs) := \text{if}\left(\omega > \omega_p(Hs), 0.09, 0.07\right)$$

$$S(\omega, Hs) := \frac{0.0624}{0.23 + 0.0336\gamma - \frac{0.185}{1.9+\gamma}}\cdot Hs^2\cdot\frac{\omega^5}{\omega_p(Hs)^{-4}}\cdot e^{-\frac{5}{4}\left(\frac{\omega_p(Hs)}{\omega}\right)^4}\cdot\gamma^{e^{\left[\frac{-\left(\omega-\omega_p(Hs)\right)^2}{2\cdot\tau(\omega,Hs)^2\cdot\omega_p(Hs)^2}\right]}}$$

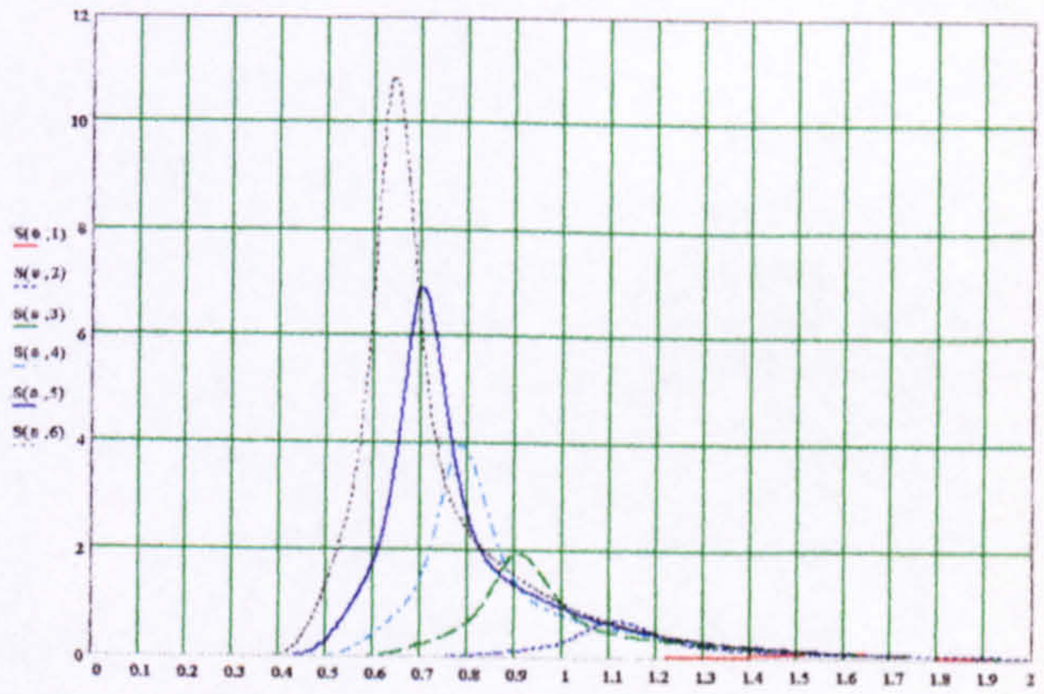

Figure 59 JOHNSWAP wave energy spectrum. $\omega[rad/s]$

For the PRR1 vessel considered, there is no noticeable difference in predicted motions as derived by either of the methods, for sea states with significant wave height, Hs, not exceeding the vessel draught of 6.25m, see Figure 60 and Figure 61. Above this level, the predicted motions, in particular roll, appear to diverge between the two methods, with the vessel ultimately capsizing at sea state of Hs~9.0m when the forces are evaluated up to the mean water level. The option of accounting for forces considering the actual wave profile thus demonstrates its superiority and usefulness when predictions in extreme environmental conditions are of interest.

Considering the studies on intact ship responses discussed above, it can be concluded, that despite some discrepancies noticed in predictions of ship hydrodynamics discussed in §9.1 and Appendix 2 and 3, the overall predictive capabilities of the ship behaviour in random seas is satisfactory for the cases considered.

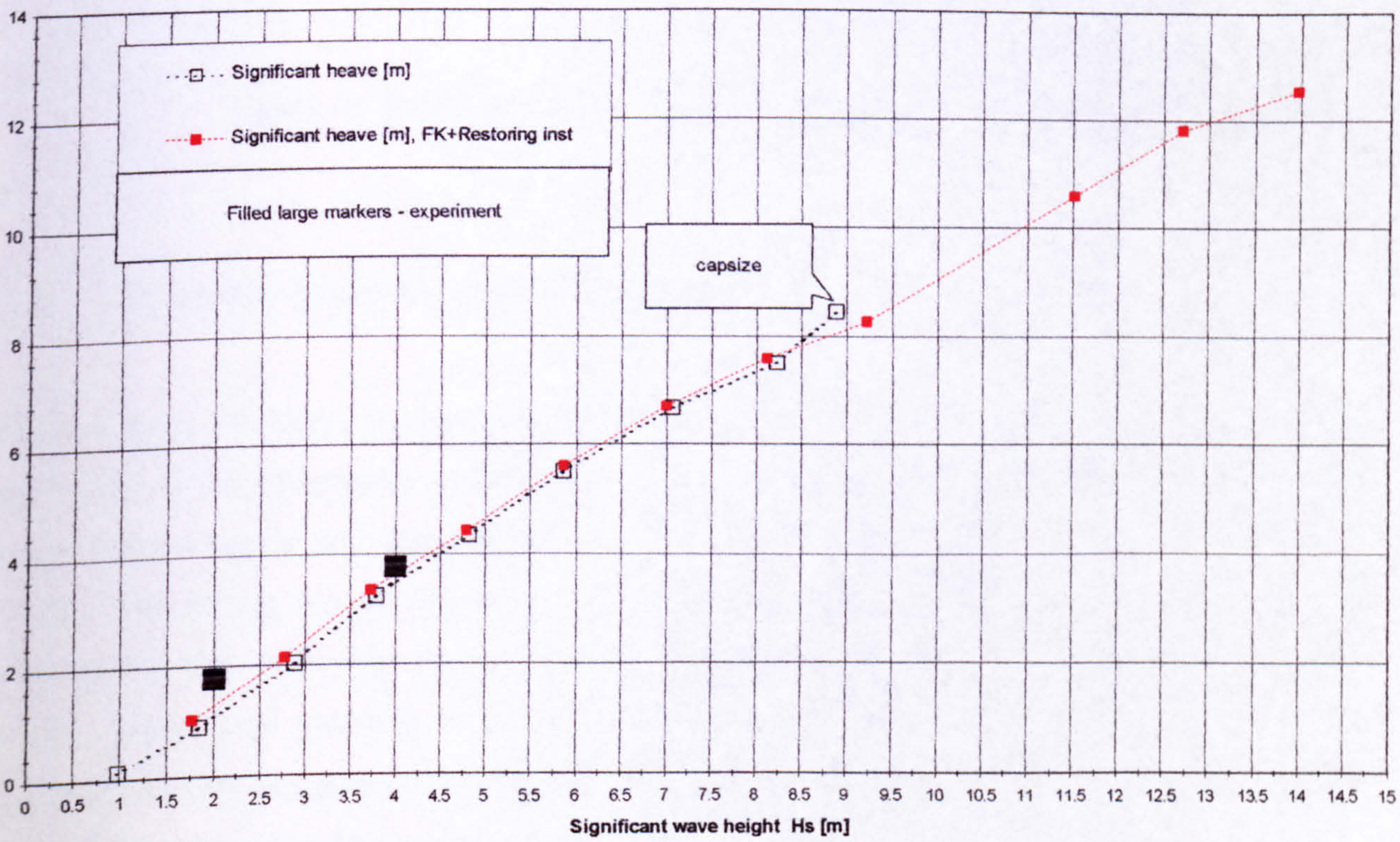

Figure 60 Significant values of heave motions in extreme environment

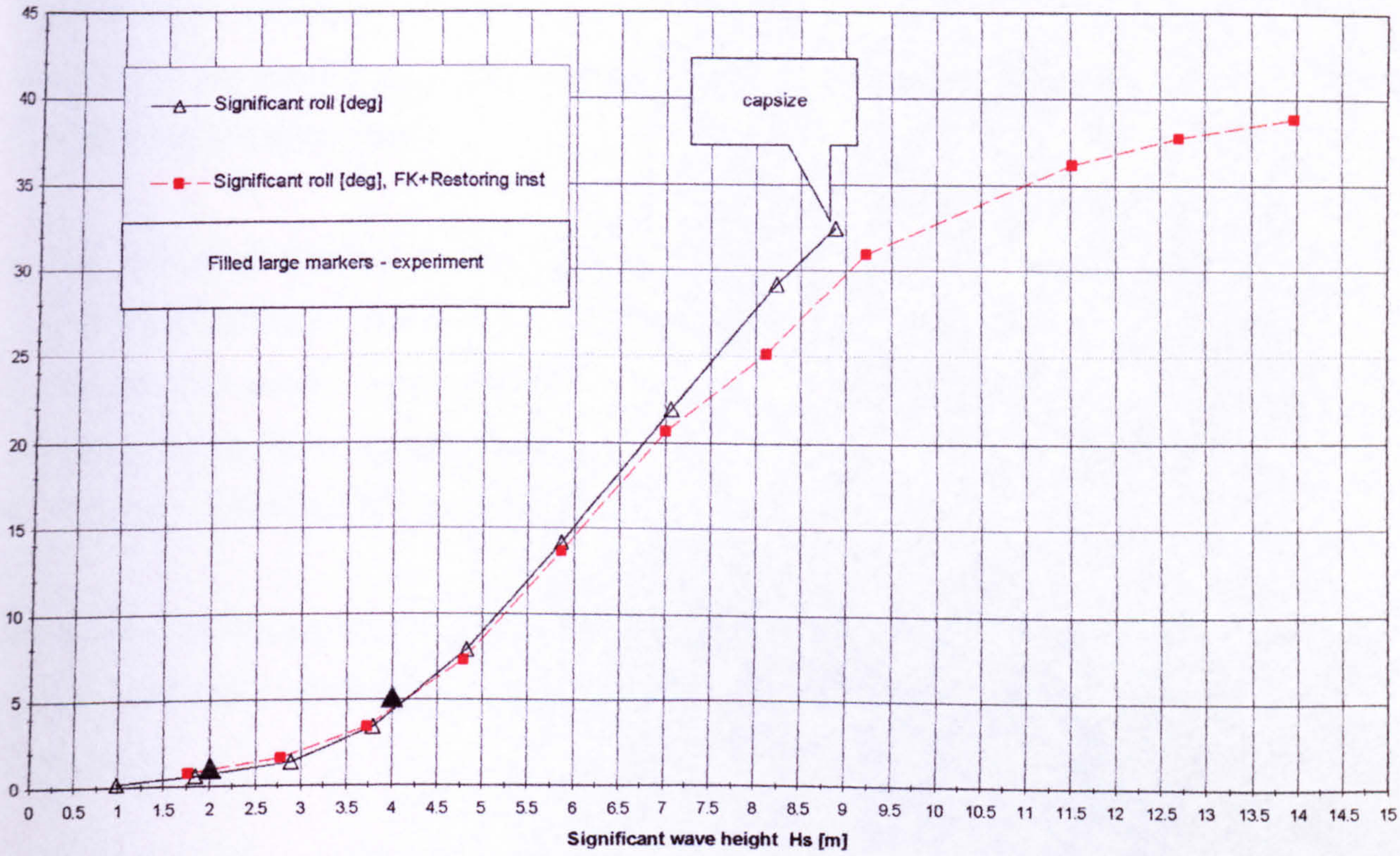

Figure 61 Significant values of roll motions in extreme environment

9.4 Dynamic behaviour in damaged conditions

Extending on the above studies, similar testing strategy was adopted addressing the accuracy of modelling of the phenomena associated with the ship damage state and resulting from continuous water ingress/egress and ensuing non-linear dynamic interactions between floodwater and the vessel. This testing was mainly concentrated on beam seas, because (a) this is the most onerous state for the ship transverse dynamic stability and therefore most difficult to simulate and (b) there exists a very large database of reliable physical model experiment measurements, [26]. The undertaken study comprised again the free roll and frequency response curves as well as responses in irregular seas with ultimate determination of the ship survivability.

As can be seen from the Figure 62 and Figure 63, the numerical predictions in either of the tests do not match the experiment. Considering the study presented in §9.3 as a convincing evidence of the capabilities of the software to predict ship responses in intact conditions, the prime source of the discrepancy noted in this study is associated with the ship damage state. Furthermore, in view of the

rather positive validation of the numerical FMPS-system-based representation of floodwater dynamics, as discussed in §7.1, the following hypotheses have been deduced as to the predominant cause of the noted discrepancy:

- The effects of sloshing water on the motion of the ship derive from complex free surface behaviour leading to generation of internal waves.
- Continuous water ingress/egress has a considerable influence on the damaged ship hydrodynamic forces and moments.
- Other, e.g. reliability of the experiment, etc.

Verification of either of these hypotheses requires, as a starting point, performing of further set of experimental tests, which is beyond the scope of this research and is therefore recommended as a future study.

The reliability of the experiment was questioned in view of studies on behaviour of the damaged ship in irregular seas, which seem to somewhat contradict the main point noted in Figure 62 and Figure 63, that the natural frequency of damaged ship is lower than the natural frequency of intact ship. As is shown in Figure 64 below as well as by a number of more examples attached in **Appendix 4**, the Fourier analysis seem to suggest that the roll natural frequency in damaged condition is in fact not only not lower than the natural frequency of 0.49 rad/s derived in intact condition, but indeed seems higher. The behaviour simulated numerically shows consistently the natural frequency occurring as second peak in the Fourier analysis at frequency of approximately 0.49 rad/s, i.e. as is seen on the frequency response curve in Figure 63. No explanation has been established to date on this inconsistency in the experimental data, which could as well be a result of some physical phenomenon. In this case the numerical simulations seem unable to represent it. It also seems to be confirmed that the level of roll damping in numerical simulations is lower than in the actual physical test, which conclusion is based on the energy of the roll response at the natural frequency. It is for these reasons perhaps, that despite quite reasonable visual comparison of the simulated and experimental time histories of the responses and the floodwater accumulation processes, see again Figure 64 and Figure 65, that the survivability predictions are not exactly matching the experiments. As is shown in Table 2, the predicted survival boundary is between Hs=3.50 and 5.50 m, whereas the experimental survivability is clearly established between Hs=4.0 and 4.50m.

Table 2 Relative frequency of capsizing per number of 5 runs (1,800s)

	Experiment	**Numerical**
Hs=3.50m	-	**0**
Hs=3.75m	-	**3**
Hs=4.00m	**0**	**1**
Hs=4.25m	**4**	**3**
Hs=4.50m	**5**	**3**
Hs=4.75m	-	**4**
Hs=5.00m	-	**3**
Hs=5.25m	-	**3**
Hs=5.50m	-	**5**

Notwithstanding the above discrepancies, which naturally prompt for further research, it is hoped that understanding of the damaged ship stability in dynamic mode as well as methods for its modelling have been progressed. The developed tool, however lacking in its composition, can be practically used for guidance purposes.

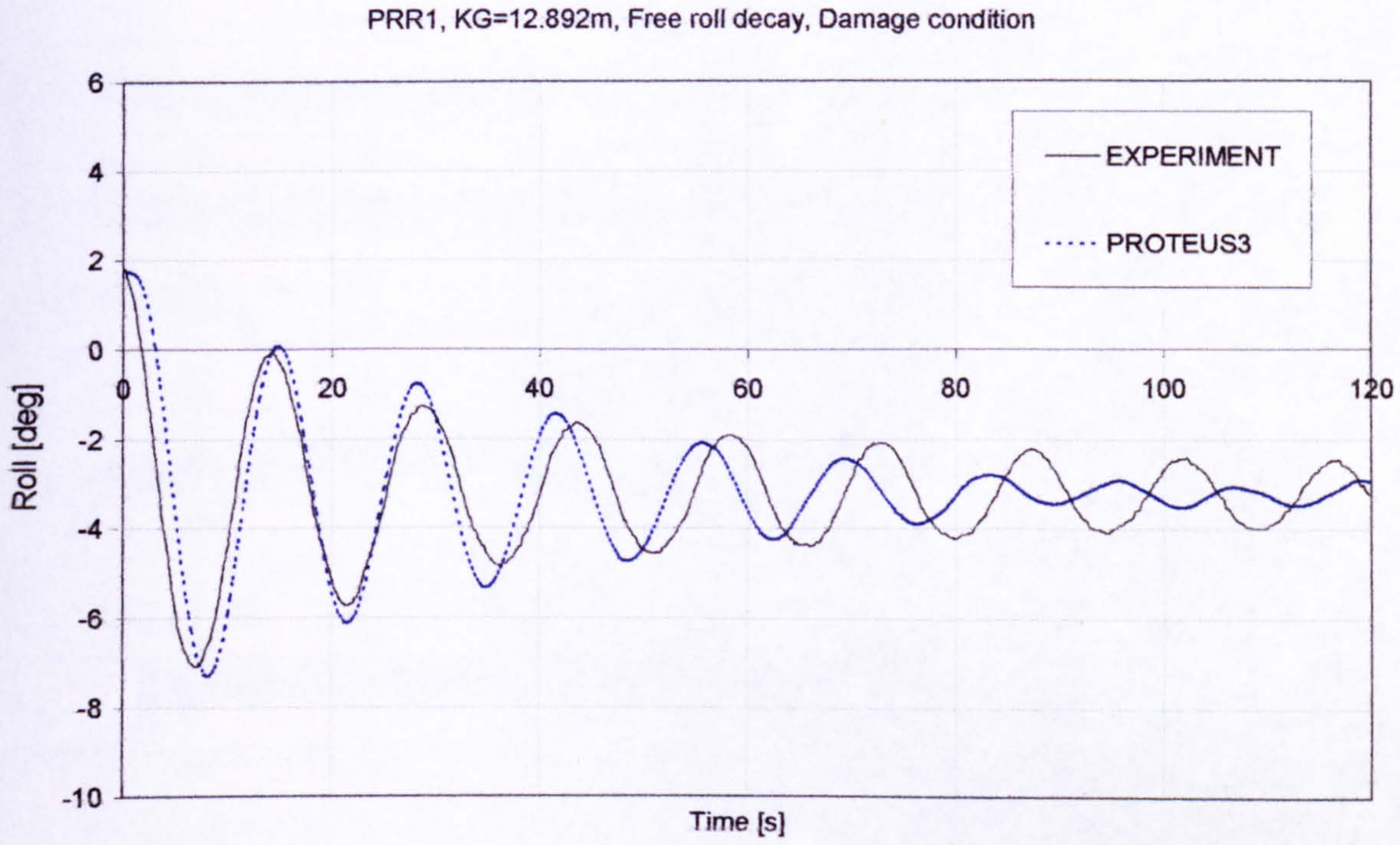

Figure 62 Free roll decay curve for the ship in damaged conditions.

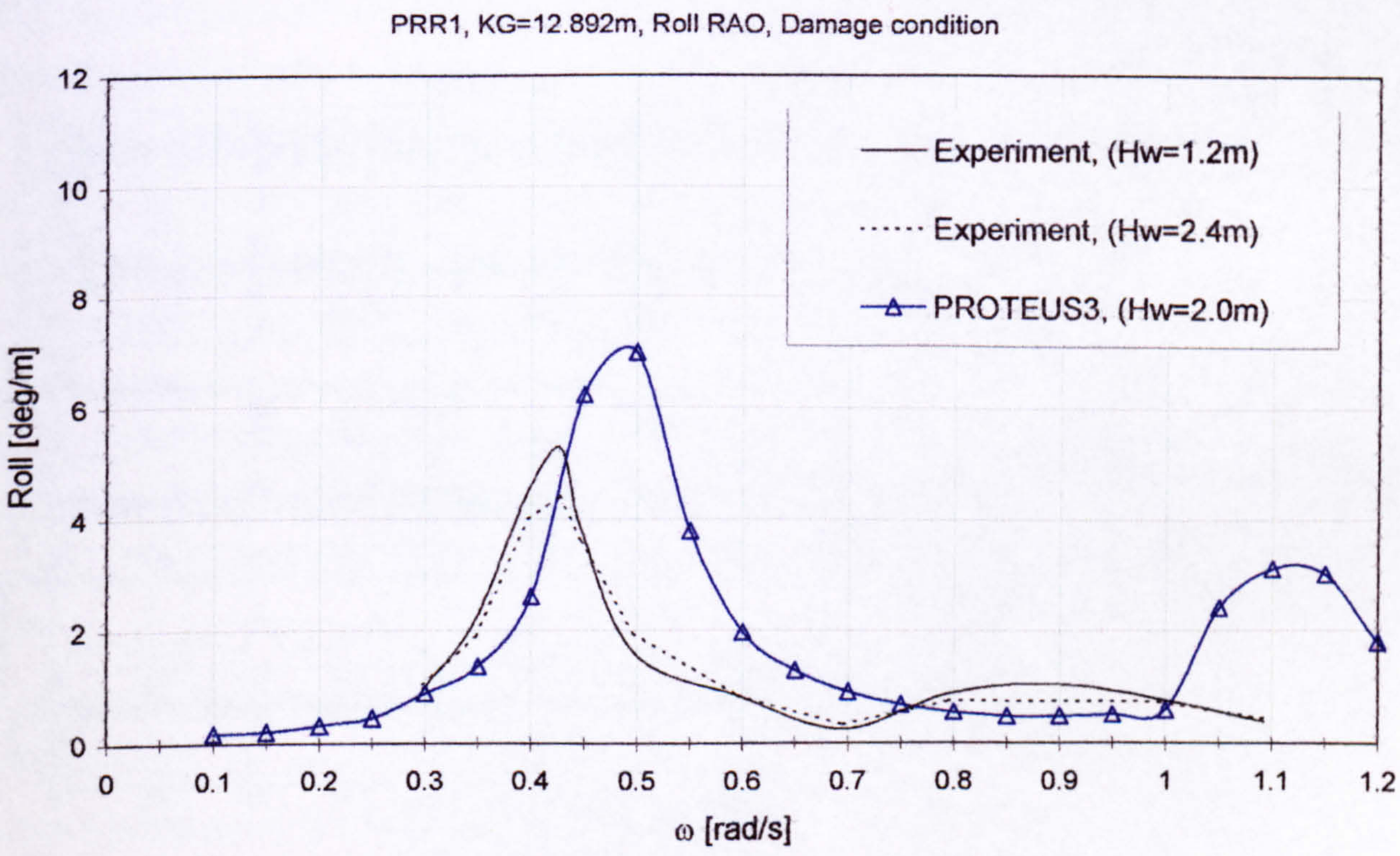

Figure 63 Frequency response curve for the ship in damaged conditions

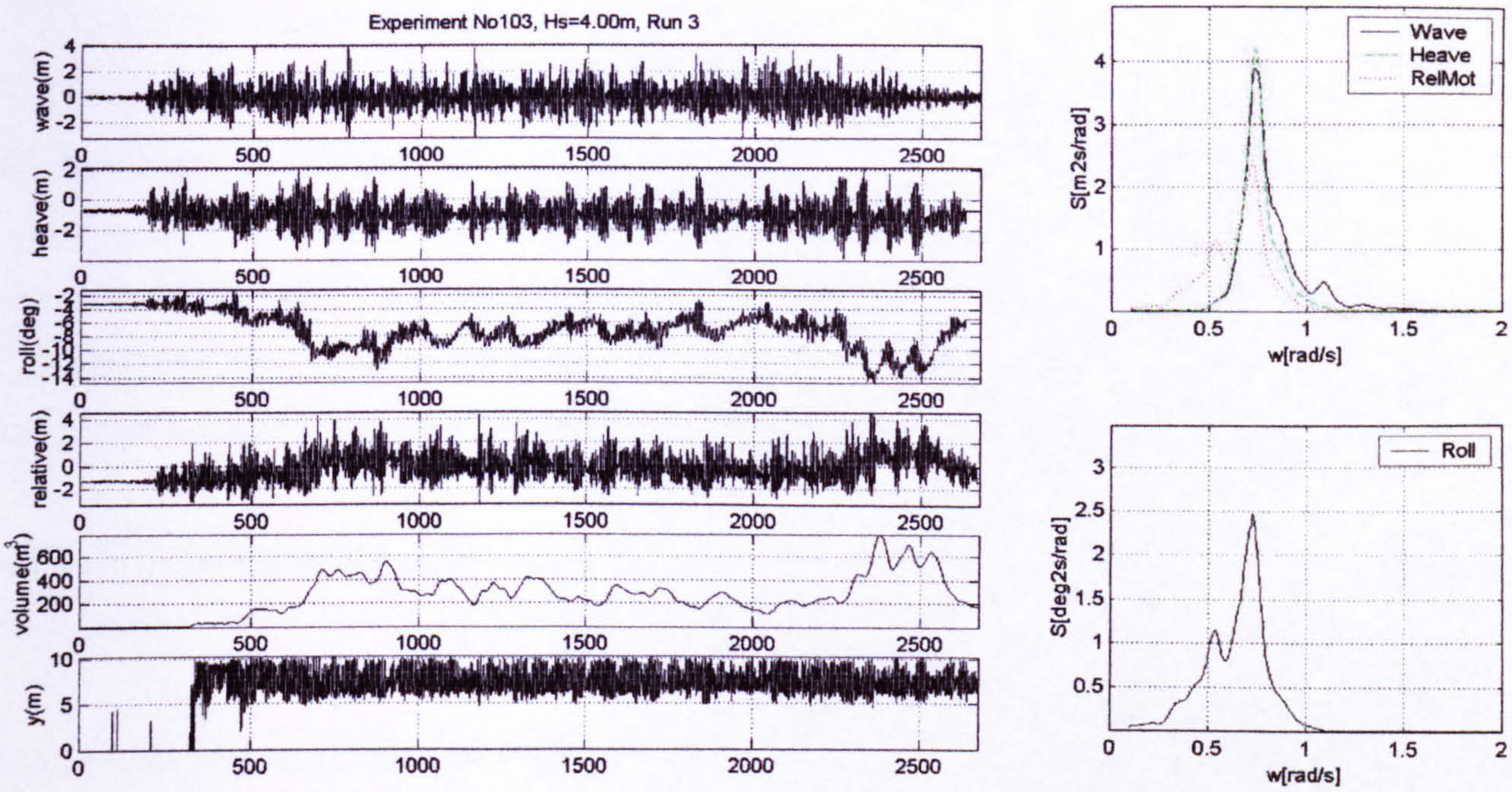

Figure 64 Experiment, damaged ship response in irregular seas, Hs=4.00m

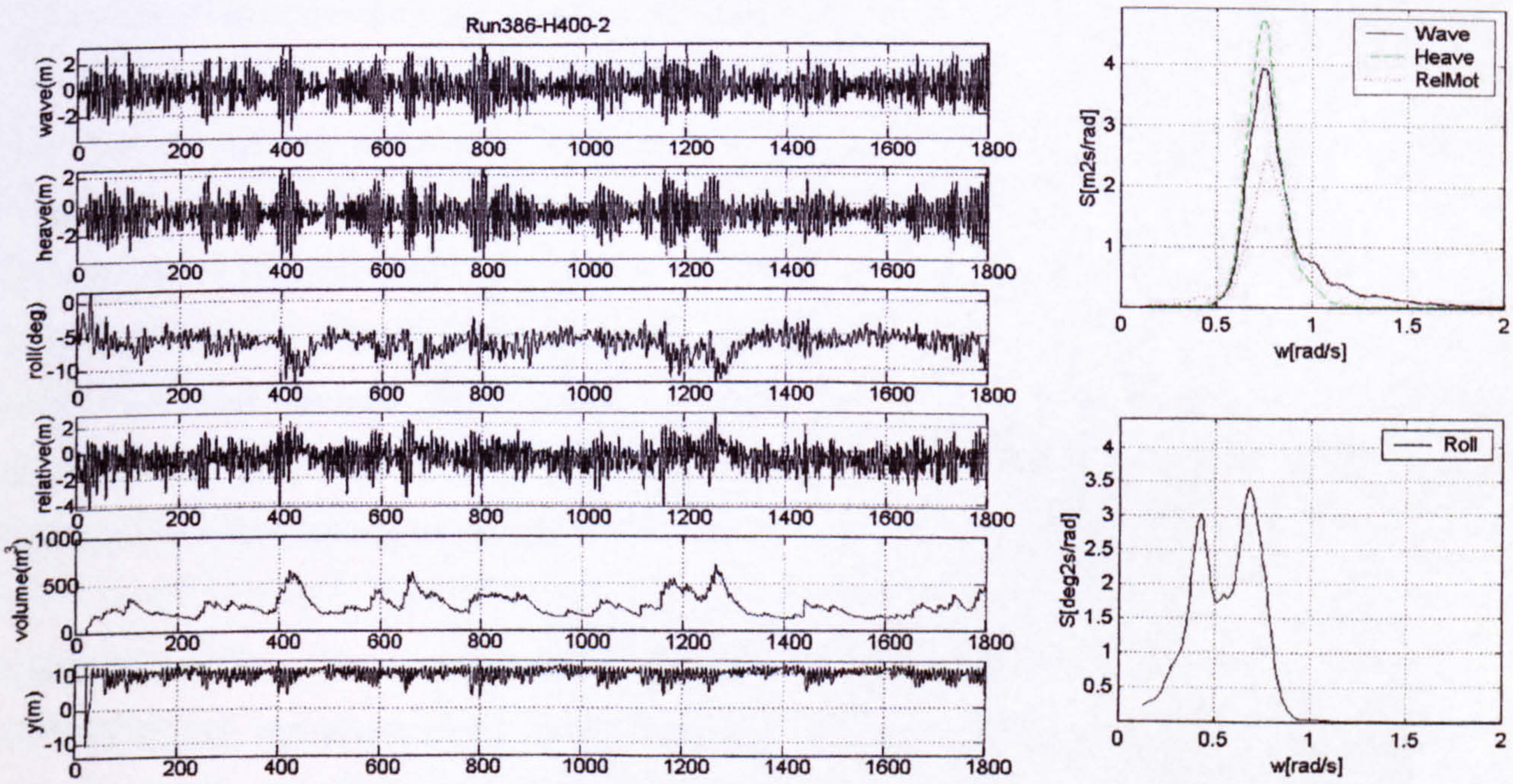

Figure 65 Numerical simulations, damaged ship response in irregular seas, Hs=4.00m

9.5 Practical examples of application of the developed tools

As a general approach the theory summarised in the foregoing is an extension of the previous work concentrating on building of a numerical model that could be used for assessment of the performance of damaged ships. The first version of the code developed some 15 years ago and known as PROTEUS1 have been extensively utilised in "Total Stability Assessment", [217] for upgrading of the existing passenger Ro-Ro fleet in Northern Europe, demonstrating that performance-based approaches to safety can not only be practical but also extremely cost effective.

It is hoped that the model developed in this work, the PROTEUS3, will continue to serve the above purpose.

Furthermore, the whole array of methodological as well as numerical coding developments, such as accounting for speed effects, cargo shifting, more complex geometries, advanced treatment of fluid sloshing, large amplitude motions or sheer code usage, allows for undertaking of as complex researches as reconstruction of ship disasters could be. Such investigations, leading to establishment of the casual factors of the loss, are most likely to have an impact on the legislative proceedings, by which safety issues are addressed and in most cases improved.

Ship loss, in one way or another, is associated with uncontrolled foundering, modes of which can range from straight sinking or capsizing to complex dynamic loss of stability involving all degrees of freedom of ship motions. This process can be a result of almost infinite number of different initiating scenarios, which complexity is the very essence of forensic analysis aiming at establishment of the most likely cause of the loss. Any claim of a particular sequence of events leading to the disaster needs clear substantiation, especially if the matter is disputed and taken for resolution to court, which is most often the case.

It is here, therefore, that the numerical model of ship performance assessment in limiting state, such as PROTEUS3, can prove to be ground breaking in generating understanding of the sequence of events that eventuate in a loss, and therefore can provide with such evidence for consideration and arguments.

Two examples of such research with the use of the PROTEUS3 are discussed next, for further demonstration of capabilities of the developed software as well as for exemplification of the unique and indisputable nature of the results that can be derived from first principles modelling.

9.5.1 Investigation into the loss of MV Derbyshire

The history of the loss and ensuing investigations have been summarised in [218] and detailed in a number of reports [166] - [187], [8] - [16], [18] and [23]. A brief summary pertaining to the subject of this thesis is offered for clarity purposes.

The tragedy and mystery of the Derbyshire began in September 1980 when the vessel disappeared without trace in the Pacific about 350 miles south of Japan. She was an oil/bulk/ore carrier (OBO), in length nearly 300m. All those on board perished – 42 members of crew and two of their wives. She was the largest British ship ever lost at sea.

Under mounting public pressure, an underwater survey have been funded and executed in two phases, in 1997 and 1998 following a survey conducted in 1994 by ITF (International Transport Federation), which located the wreckage on the seabed. Two of the three appointed Assessors concluded on the basis of the photographic evidence (mainly the intact state of the bow section of the ship implying full flooding with seawater prior to commencement of the sinking) that the vessel's loss had been caused by seawater entering the bow section via the improperly fastened hatchways, which caused the vessel to develop a forward trim, thereby exposing its No.1 hatch covers to wave heights great enough to impose loading in excess of their collapse strength. Water then poured into the large empty space above the cargo in the No.1 hold. That put the vessel further down by the bow until No.2 and No.3 hatch covers suffered the same fate sequentially. The vessel would then sink.

This explanation had been challenged and disputed for (a) not providing analytical evidence for its substantiation and (b) implicating of crew negligence as the underlying cause of the loss. Therefore, a full re-opening of the Formal Investigation was announced on 17th December 1998 to be hold in the High Court.

The Ship Stability Research Centre (SSRC) of University of Strathclyde was commissioned by the DETR (Department of Environment, Transport and Regions) to undertake suitable experimental and numerical investigation aiming to test the Assessors theory. PROTEUS3 was the main analytical tool for investigation on the process of the ship loss.

The experimental campaign undertaken by SSRC have provided with ample data concerning frequencies of occurrence of green seas loads and their quantitative estimates for a ship in hove-to position facing oncoming storm of Hs=12.78m with individual waves in excess of 25m in height.

These data were used for calibration of predictions of green seas by PROTEUS3, which phenomenon had by no means been considered in mathematical modelling. The corresponding relative maxima of the undisturbed wave passes over the bow deck, as predicted numerically, had been subject for adjustments after comparison with actual impacts recorded during the experiments. Deriving from this a very tedious task of numerical simulation of water ingress into the spaces forward of the hold No.1 through a series of deck vents and a hatchway while the ship struggled through the typhoon Orchid was performed. This allowed establishing of the time frame, see the summary in Table 3, for the full flooding of the bow spaces in question: Bosun's Store (BS), Ballast Tank (BT) and Deep Fuel Tank (DFT), see Figure 67.

This in conjunction with the statistical analysis of extreme events occurrence, leading to derivation of maximum allowable time of 8.8 hours available for the ship to withstand the storm before hatch breaking occurred with high probability of $p_e = 0.99$, allowed to draw conclusion that within this time substantial flooding could have taken place. The estimated flooding was: BS 100%, BT 39% and DFT 3%, leading to 0.7m freeboard loss, see Figure 66, and this in turn exposing the ship to substantially higher risks and greater loads from green seas, as established by interpolated results from model tests performed in SSRC.

This conclusion supported the scenario derived by the Assessors with the exception, however, that this could have taken place even only via the broken ventilators on the foredeck and, therefore, without requirement of the foredeck hatch to BS left unsecured. The latter, initially somewhat questionable result was fully supported by subsequently undertaken extensive experimental study performed by MARIN, which will be discussed later in this chapter in the quote from the final report by The Honourable Mr Justice Colman.

Table 3 Times to flood spaces within the bow forward of BHD 339 (slow mode bow flooding)

			Ballast Tank (BT)	Deep Fuel Tank (DFT)	Bosun's Store (BS)
A	Total Deck Broken Opening`s Area	m2	0.212	0.025	2.167
B	Manhole's Area	m2	0.223	0.223	-
	Floodable Volume	tonnes of sea water	2939	3185	702
	Time to fully flood through A	hour	**22.8**	**243.3**	**0.6**
	Time to fully flood through A&B	hour	**2.7**	**3.1**	**3.1**

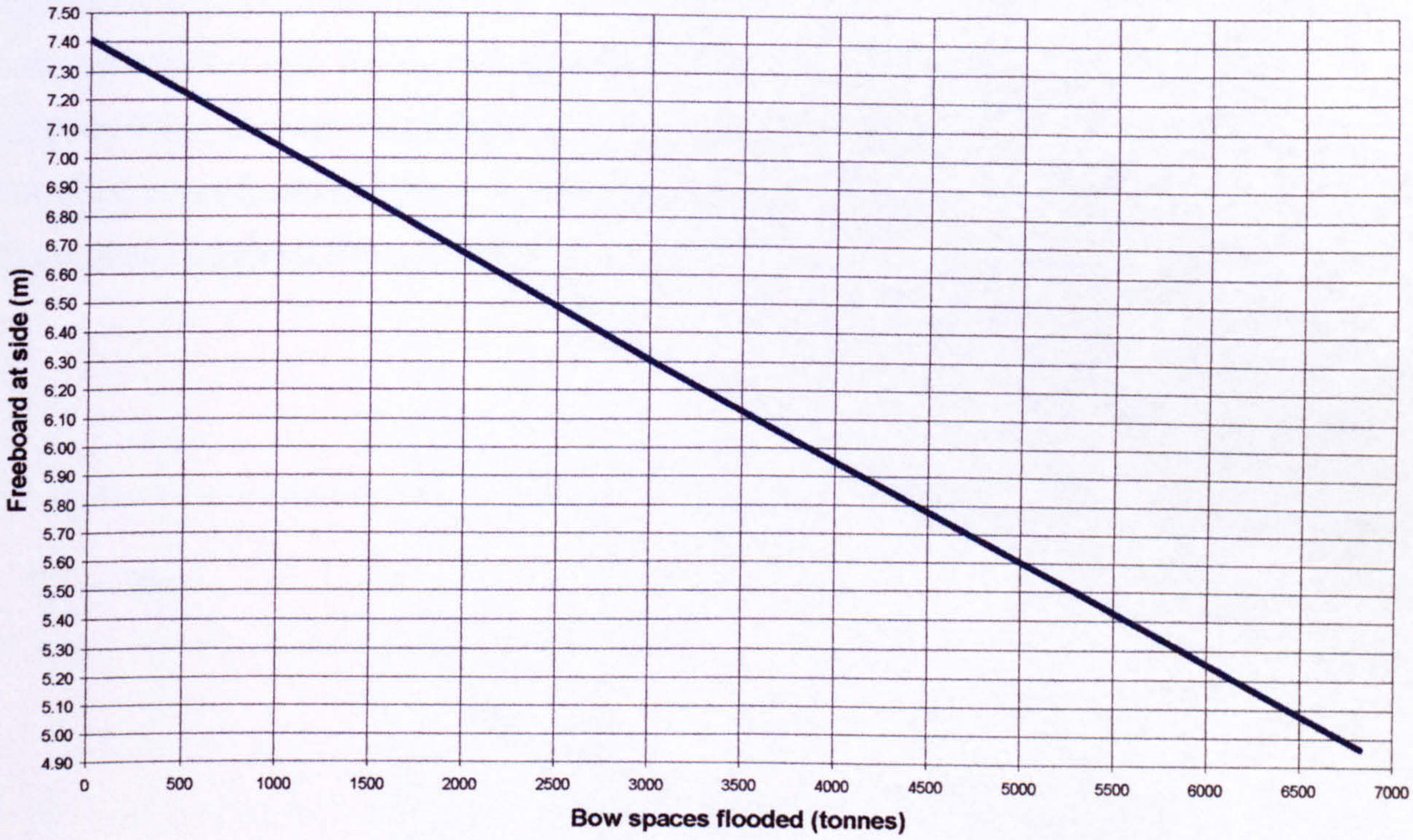

Figure 66 Freeboard loss due to flooding of bow spaces

The above reasoning, however, as much as is consistent, did not constitute a proof that this scenario has indeed taken place. Therefore, further study aiming at negating of this conclusion by considering of the alternative scenario, was undertaken.

The alternative scenario concluded that the loss initiated due to extreme green seas loading event, breaking the hatch of No.1 hold and therefore leading to rapid sinking, during some stage of which the bow spaces fully flooded. This rapid flooding, therefore, accounted for no visible deformations of the bow spaces as found on the wreckage.

A proof, therefore, was required as to the suddenness with which the ship would sink following sequential flooding of the empty holds. PROTEUS3, again, served its purpose, whereby the fast mode sinking, see Figure 68, was simulated while taking into account extreme values of possible drag forces that could be generated by the vessel body piercing through the water. Estimated sinking rate, see Figure 69, allowed subsequently to establish sequence of the ship loss, see Figure 71 and again Figure 68, and resultant bow flooding through consideration of air compression following a reverse adiabatic process with negligible heat transfer effects, see Figure 70. This in conjunction with FEM analyses of the critical loads for the bow structure, see again Figure 67, led to the conclusion that for the weakest element of the bow, the bulkhead 339, not to undergo excessive static pressure differential leading to its collapse, not seen clearly in the wreckage, the amount of onset flooding prior to commencement of sinking had to amount to about **70% in the ballast tank** and about **5% in the deep fuel tank**.

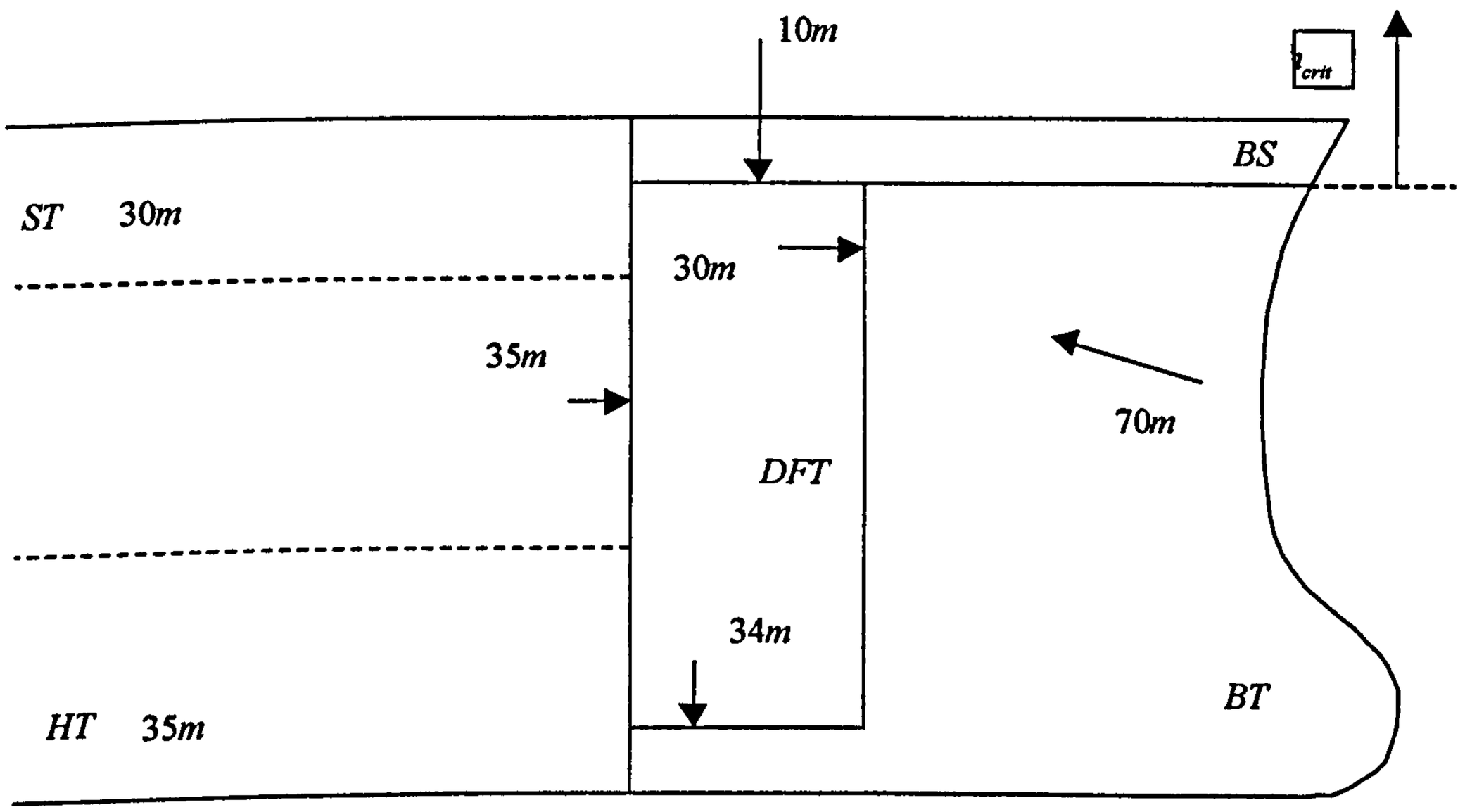

Figure 67 Bow spaces and critical water head pressures (measured from stores deck level). Figure not to scale.

It was established that this amount of flooding could neither have taken place within the time available during the rapid sinking, Figure 69, nor could it happen in the interim time between breach of hatches of No.1 and No.4 holds, estimated through statistical reasoning and experimental data to be of the order of 5-16.5 minutes.

Therefore, the ship must have been undergoing slow flooding of these spaces, possibly through the damaged ventilators, during a period of a number of hours and before breaching of the hatch of No.1 hold.

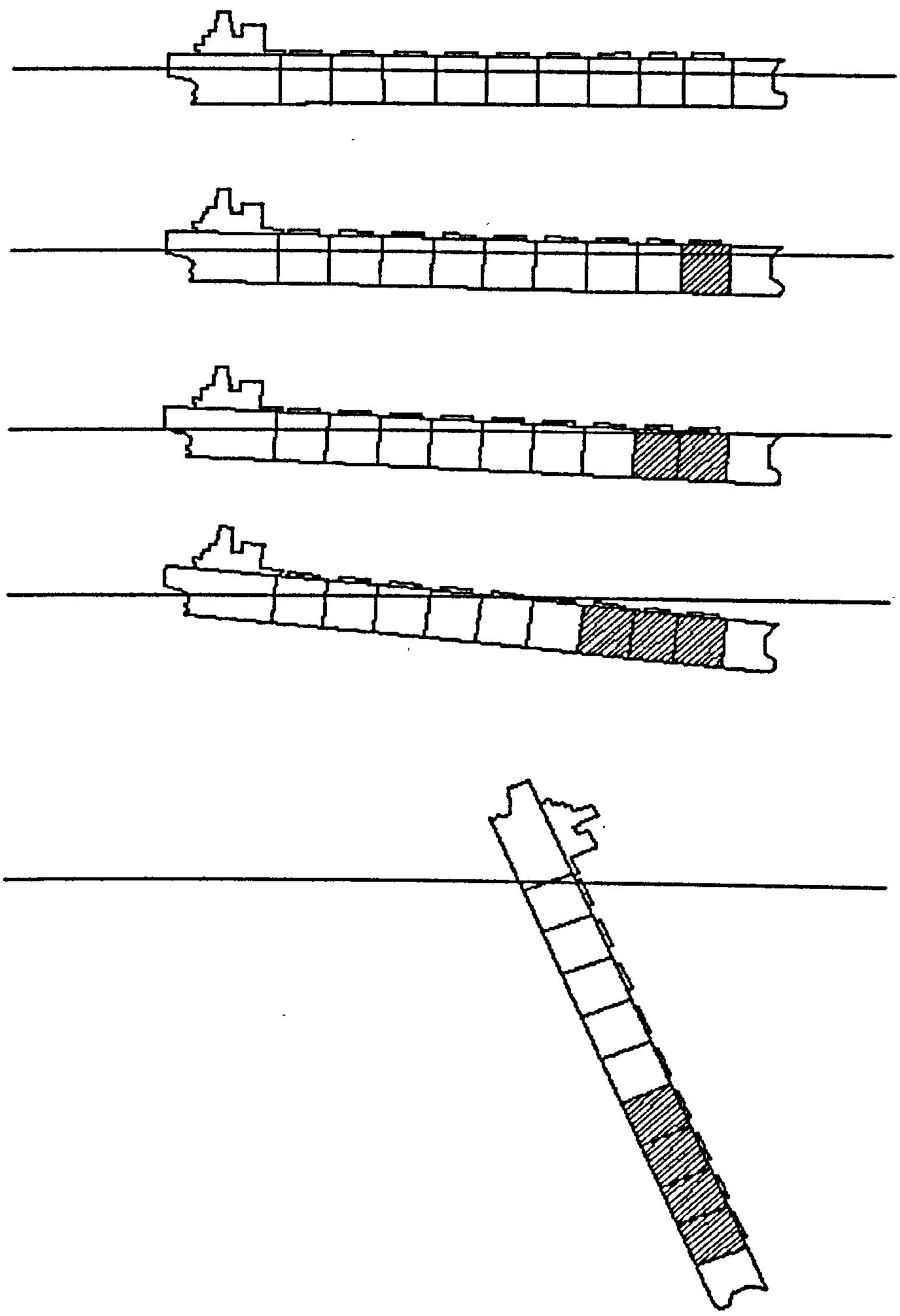

Figure 68 Loss of longitudinal hydrostatic stability and sinking with bow spaces intact.

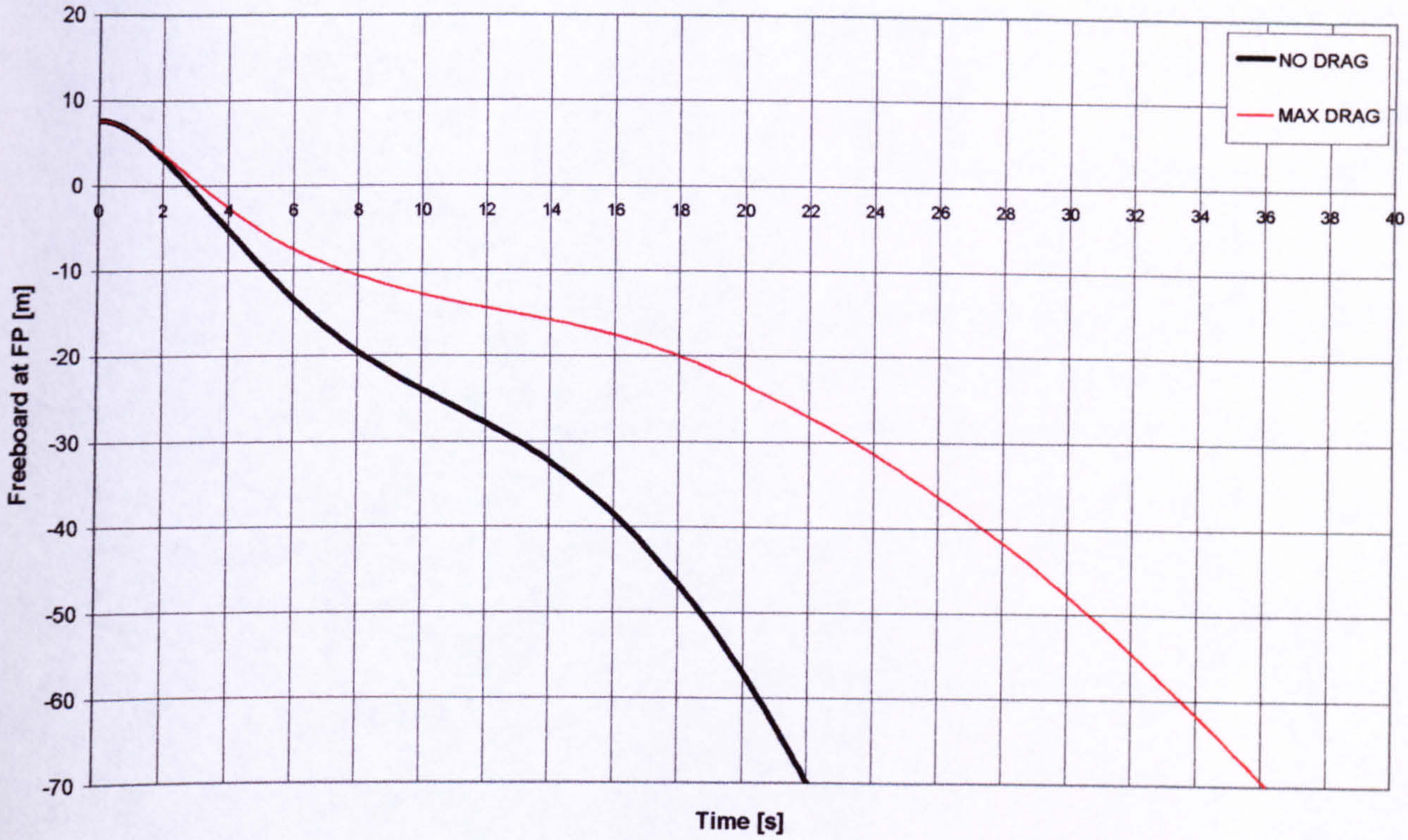

Figure 69 Free sinking of the ship with the bow intact (three holds assumed flooded at initial position)

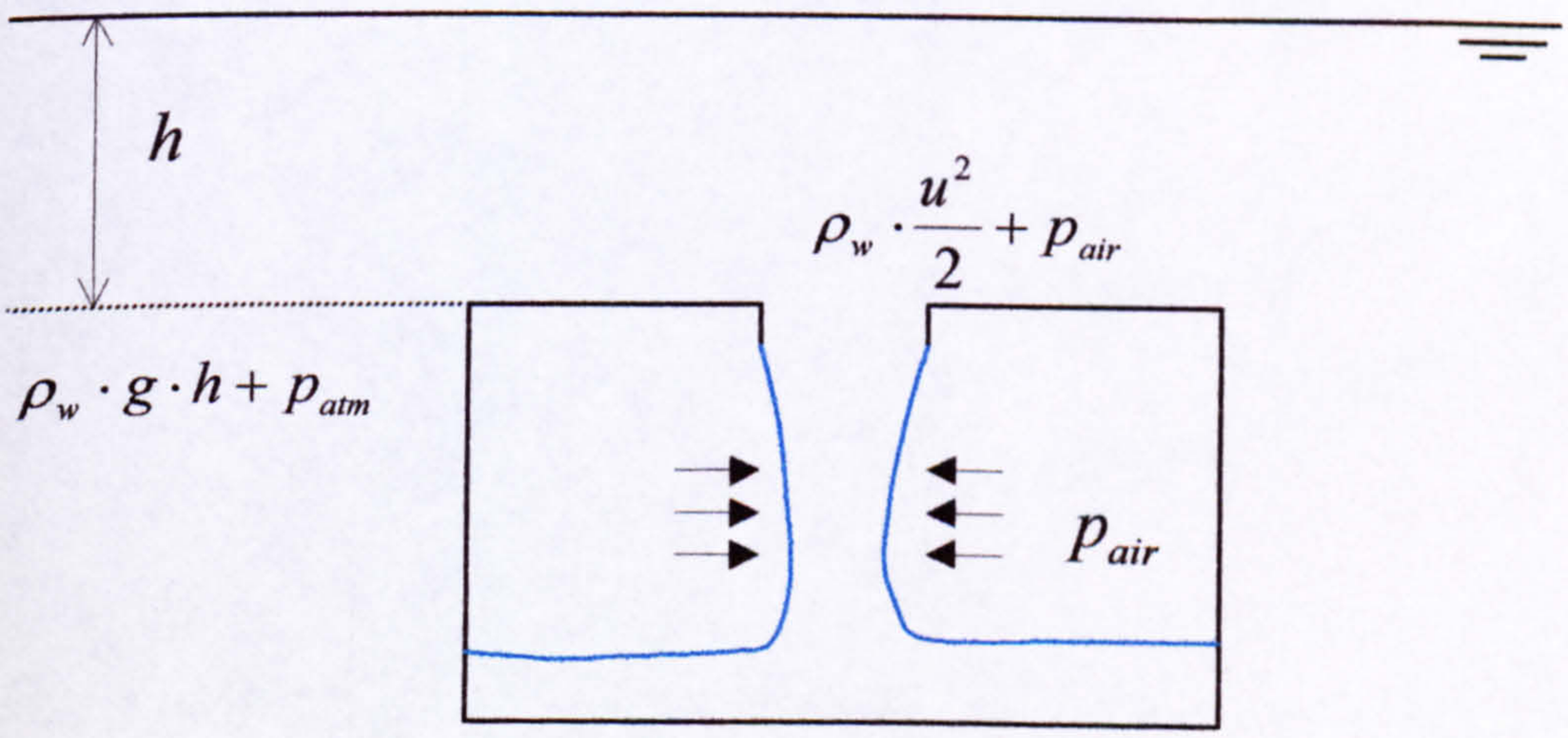

Figure 70 Inflow process

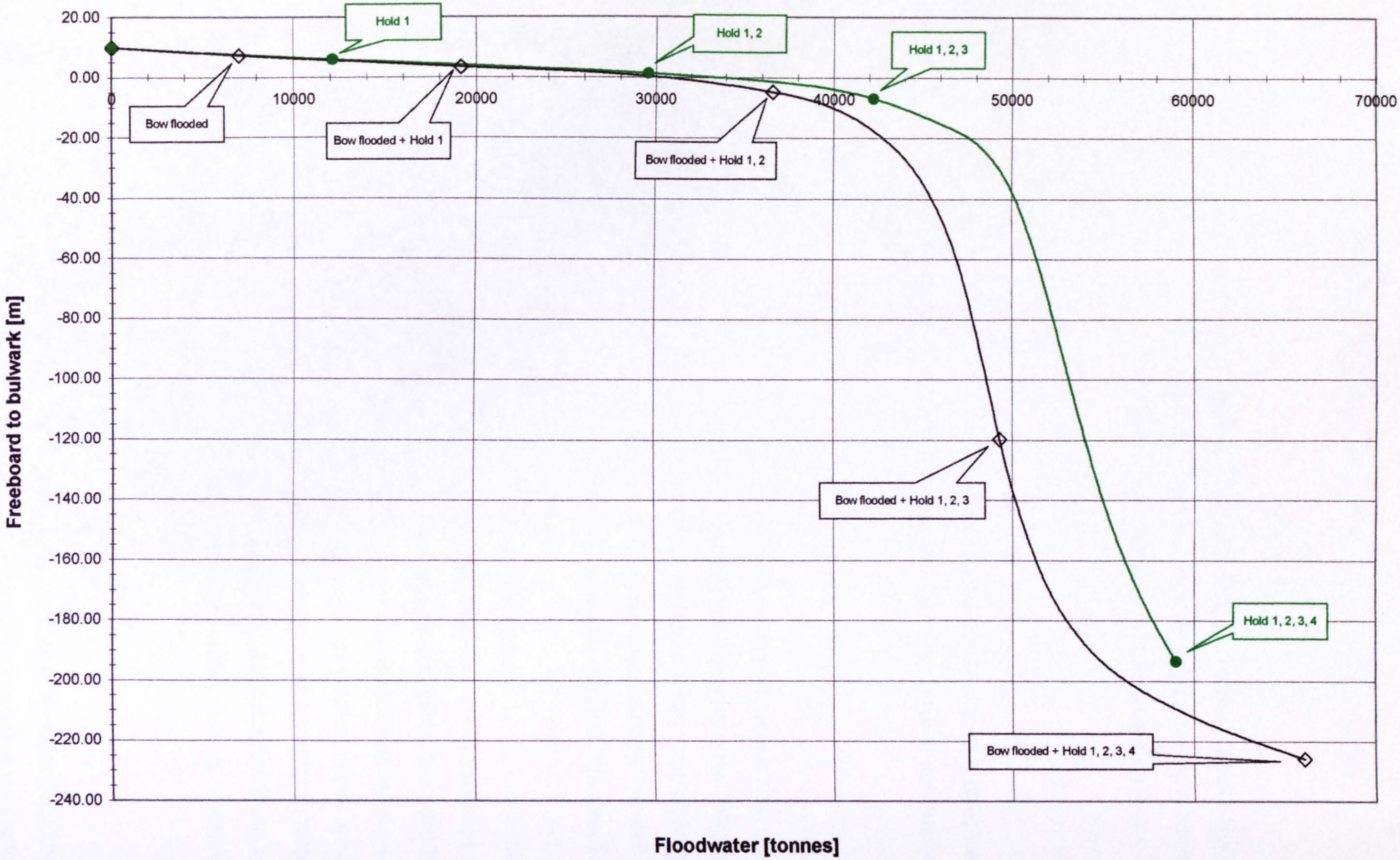

Figure 71 Freeboard loss as a function of progressive flooding of the MV Derbyshire

The investigation undertaken by SSRC delineated above can now be compared to the essential excerpts from the final judgement presented by Honourable Mr Justice Colman in [218]:

...

41 The model tests conducted at the MARIN Research Institute, Wageningen, Netherlands, were designed to measure the magnitude of green water impacts on the No.1 hatch cover in different conditions of trim and at different significant wave heights. The various conditions of trim were designed to ascertain what difference it made to green water loading on the No.1 hatch cover that water had entered the bosun's store and machinery spaces, the forepeak ballast tank and the forepeak fuel tank. They were also directed to ascertaining the rate of seawater entry to those spaces if ventilators and air pipes or their covers had been destroyed.

42 The result of those tests indicated that at speeds of zero or 2 knots, without water ingress, at the peak significant wave height of 10.85 metres, and even at 12.5 metres, the maximum loading on No.1 hatch would be well below the collapse strength. However, in the damaged condition, with the bow flooded, the maximum measured impacts on No.1 hatch at a significant wave height of 10.85 metres exceeded its collapse strength, even at zero speed.

...

45 The evidence derived from the underwater survey of the wreckage and the inferences to be drawn from it can be summarised as follows:

...

(iv) Ventilators and air pipes located on the foredeck and leading into the bosun's store, machinery space, ballast tank and possibly in one case, the fuel tank, were in damaged condition and had sustained that damage prior to the commencement of sinking.

...

(ix) ... This report rejects the Assessor's conclusion that the crew had left the hatch lid inadequately secured prior to the Derbyshire entering the typhoon.

...

(xii) The condition of bulkhead 339 as found in the wreckage does not support the proposition advanced by the UK/EC Assessors that the bow spaces and partially the fuel oil tank ullage space were substantially full of seawater when the vessel began to sink. Rather its condition is consistent with the deep fuel tank and perhaps part of the ballast tank having been substantially empty of water when sinking commenced, but having admitted additional water during sinking.

46 On the basis of the condition of the wreckage and of the data derived from the model tests conducted at MARIN, it can be concluded with reasonable confidence that the initiating cause of the loss was the destruction of some or all of the ventilators and air pipes located on the foredeck by substantial green water loading over many hours in the course of 8th and more probably 9th September 1980. Water was thereby able to enter the bosun's store, machinery spaces and probably the ballast tank in substantial quantities and possibly to a minor extent the fuel tank. The DERBYSHIRE then developed a trim by the bow which, although imperceptible from the bridge, had the effect, as the bow dropped lower and lower, of accentuating green water loading on the No.1 hatch cover as the sea conditions became more severe in the course of that day. By about 1700z those conditions had deteriorated so greatly that there was likely to have been green water loading in excess of the collapse strength of No.1 hatch, very rapidly filling the large ullage space above the cargo and thereby causing the vessel to go still further down by the bow by another 0.7 meters. It is estimated that the filling of No.1 hold might take as little as 5 minutes or as much as 16.5 minutes.

47 This flooding in turn caused the green water loading on No.2 hatch cover progressively and rapidly to increase until it exceeded the collapse strength of that hatch cover and water then entered No.2 hold.

48 No.3 hatch suffered the same fate. At that point the vessel was irretrievably lost.

49 Although it is possible that the No.1 hatch cover collapsed under excessive green water loading before there had been flooding of any of the bow spaces, this is very unlikely indeed.

In view of the findings a series of strong recommendations have been put forward in the above report [218], for considerations by classification societies, IACS and IMO, aiming at increased safety of bulkcarriers. Implementation process is underway.

Summarising, the software developed on the bases of the theory presented in this thesis, the PROTEUS3, even though not at as advanced stage as it has reached by now, has provided the evidence in support of the legal proceedings on disputed loss scenario of the bulkcarrier MV Derbyshire. Generated understanding led to establishment of the most probable cause of the loss and this in turn to improvement of safety.

9.5.2 Investigation into the loss of MV Estonia

The description of the accident and pertaining conclusions and discussions are detailed in references [188] to [198]. Again, a summary have been presented below for clarity purpose.

The ro-ro passenger ferry ESTONIA, 134m in length, sank in the northern Baltic Sea during the early hours of 28 September 1994. Of the 989 people on board, 127 survived. All 95 victims recovered from the sea have been identified and 757 people are still missing.

A "Joint Accident Investigation Commission, (JAIC)" was set up by three countries, Estonia, Finland and Sweden, to carry out the analysis of the accident. In their report the JAIC found that:

- The failure sequence may have started at about 0055 hrs when the AB seaman heard a metallic bang at the bow ramp.
- The locking devices and the hinges of the bow visor failed fully under one or two wave impact loads on the visor shortly after 0100 hrs.

- The visor worked its forward and forced the ramp partly open due to mechanical interference between the visor and the ramp, inherent in the design. Water started entering the car deck at the sides of the partly open ramp.
- The ramp rested for a while within the visor before the visor at about 0115 hrs fell into the sea, pulling the ramp fully open.
- Large amounts of water entered the car deck and in a few minutes a starboard list of more than 15deg developed.
- The vessel drifted with her starboard side towards the waves.
- At about 0125 hrs the list was more than 40deg. By then, windows and a door had broken in the aft part on the starboard side, allowing progressive flooding of the accommodation.
- As the list increased the ESTONIA started to sink stern first. At about 0135 hrs the list was about 80deg.
- The vessel disappeared from the surface at about 0150 hrs.

Therefore the final conclusion reached was as follows:

- The ESTONIA's bow visor locking devices failed due to wave-induced impact loads creating opening moments about the deck hinges.
- The ESTONIA capsized due to large amounts of water entering the deck, loss of stability and subsequent flooding of the accommodation decks.
- The full-width open car deck contributed to the rapid increase in the list. The turn to port – exposing first the open bow and later the listed side to the waves – shortened the time until the first windows and doors broke, which led to progressive flooding and sinking.

This investigation led to the unparalleled scale international actions taken aiming at improvements of stability of passenger Ro-Ro vessels, which becomes impaired when exposed to progressive flooding of the undivided car deck spaces. Notably, the regional agreement have been reached between North-European and Scandinavian countries, known as Stockholm Agreement, which have required stability of Ro-Ro ships to be assessed with prescribed amount of floodwater on the car deck. Therefore safety of these vessels have been greatly increased.

Nevertheless the indisputable improvements that have been achieved in the Ro-Ro ferries safety following the conclusions reached by JAIC, this author claims that the scenario described by the assessors is incomplete and perhaps deficient in correct description of the sinking mechanism.

A series of simulations with the aid of PROTEUS3 have been undertaken aiming at testing of this scenario. Environmental, ship loading as well as operational conditions have been adopted as provided in the final report by JAIC. The prevailing sea conditions were described by JOHNSWAP wave energy spectrum with Hs=4.0m. The ship was heading 150deg into the oncoming waves and progressing with speed of 10 knots. The ship geometrical properties have been modelled with very high level of complexity so as to account in details for the progressive flooding through the accommodation windows, bulkhead doors, stairwells, bow ramp, etc., see Figure 72.

The typical result of the simulation following the loss scenario put forward by JAIC is demonstrated by Figure 73. It has been concluded that the eventual sinking of the ETONIA could not have been a result of the sequence of events as explained by the JAIC and therefore, further investigation should be undertaken aiming at establishment of the sinking process to greater detail. Such investigation should by all means take an advantage of the latest advancements in modelling of damaged ship dynamic stability, such as presented in this thesis.

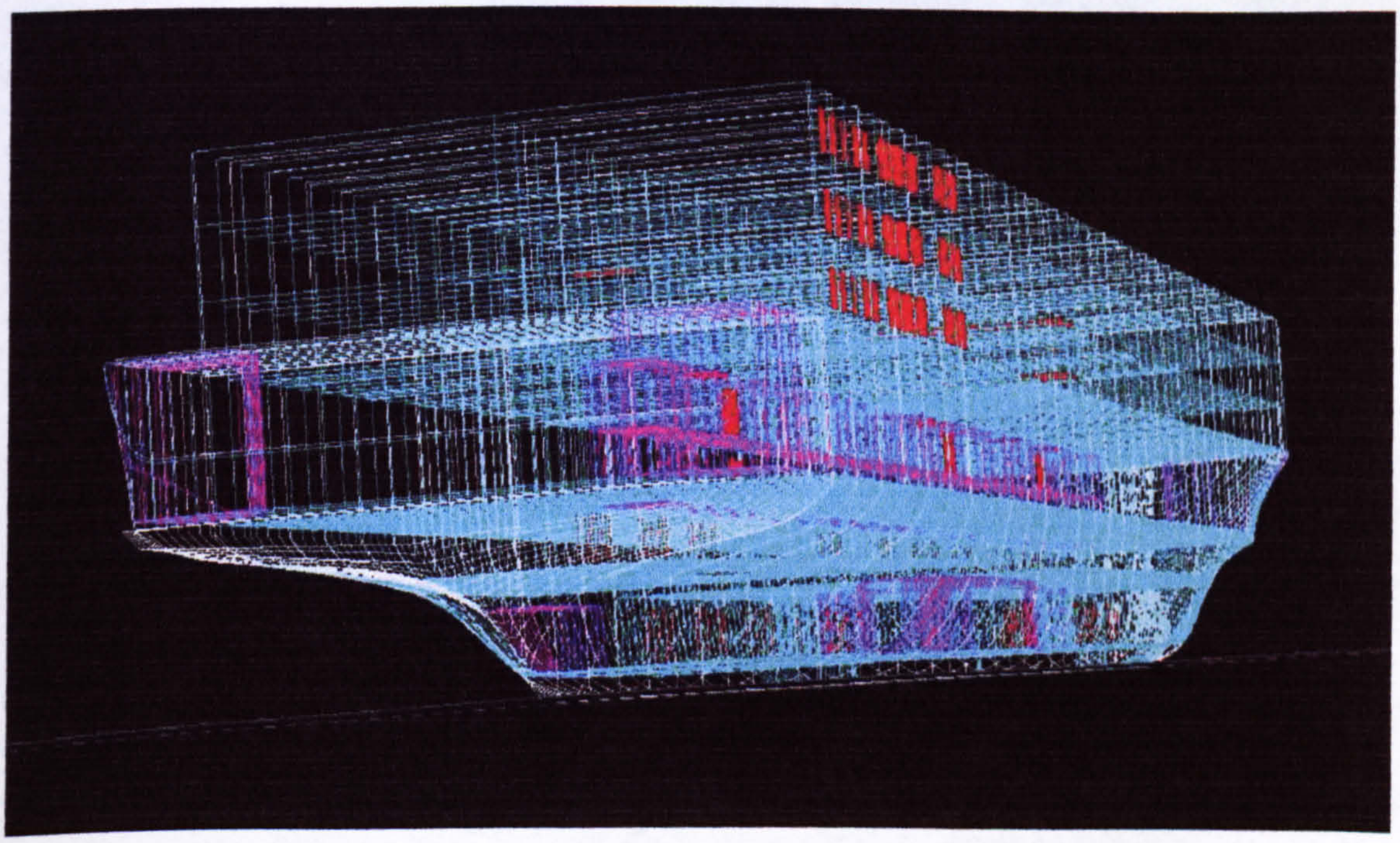

Figure 72 The numerical model of ESTONIA geometry modelled with high level of complexity.

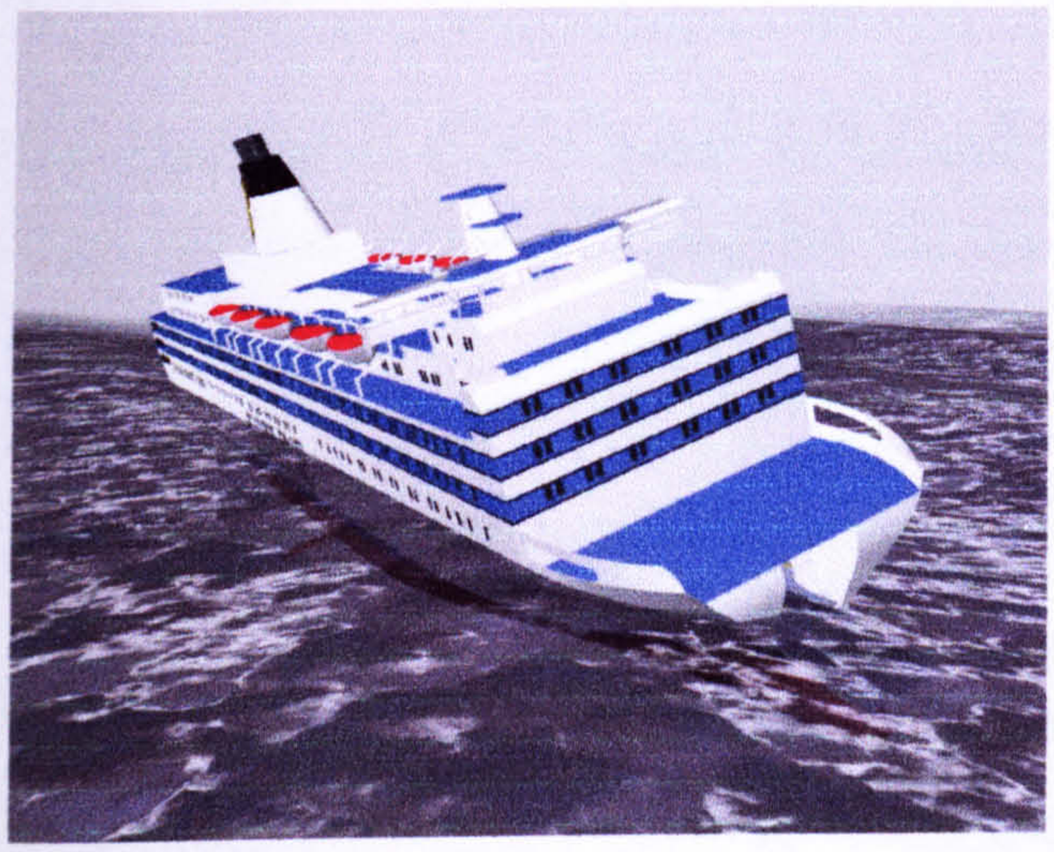

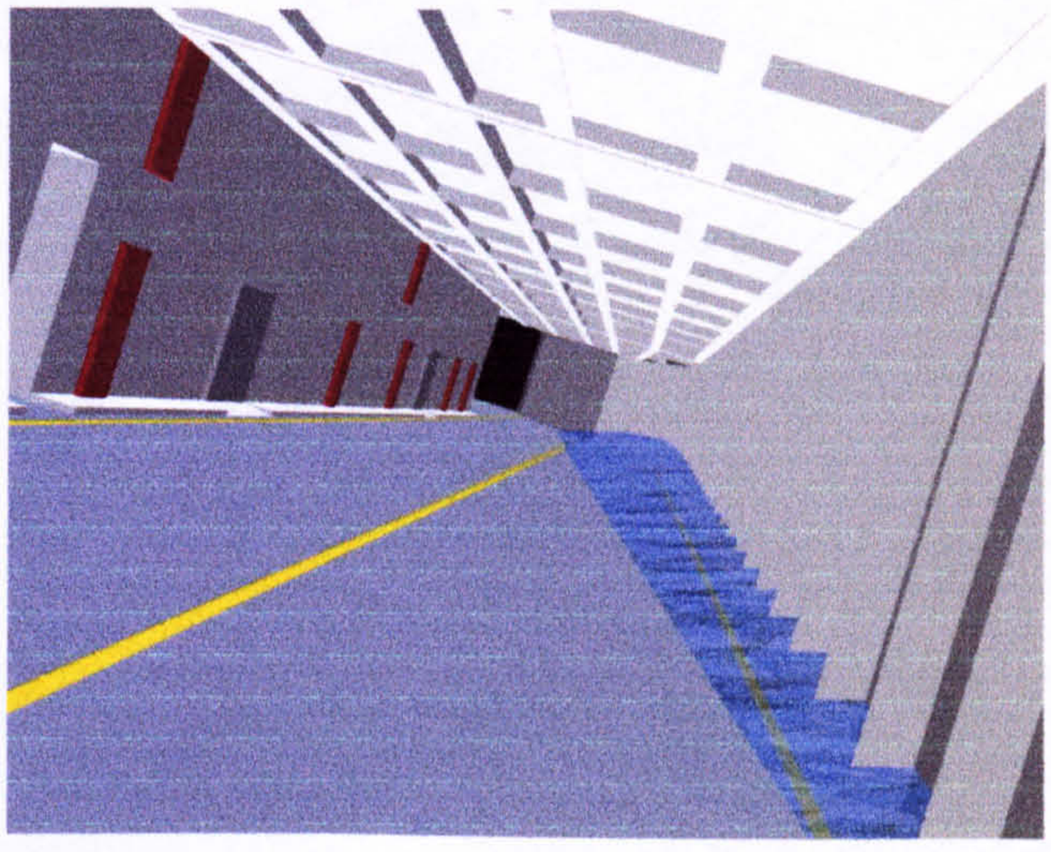

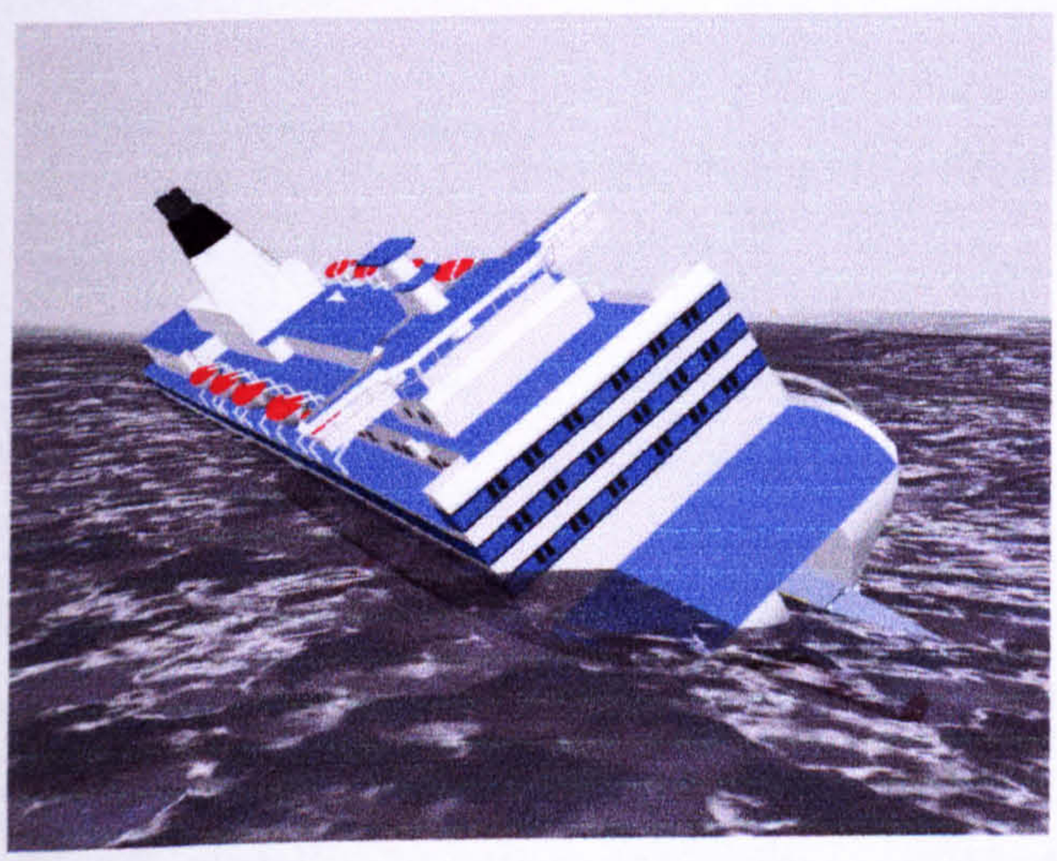

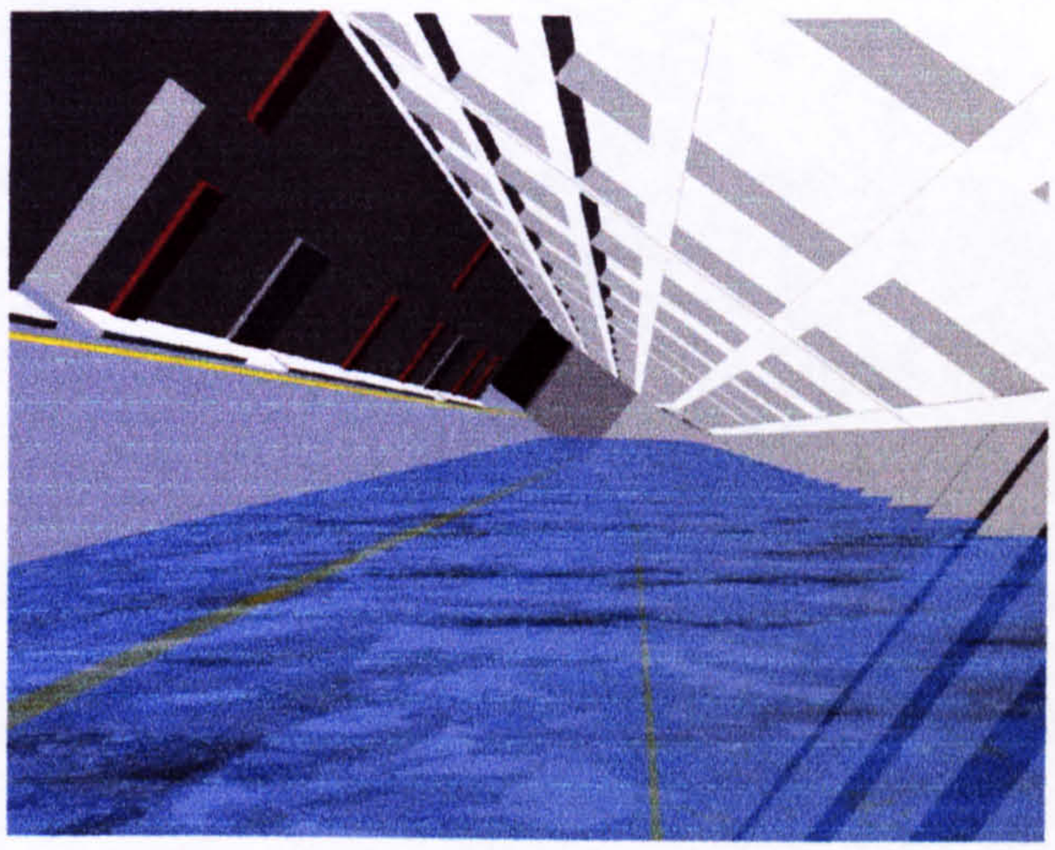

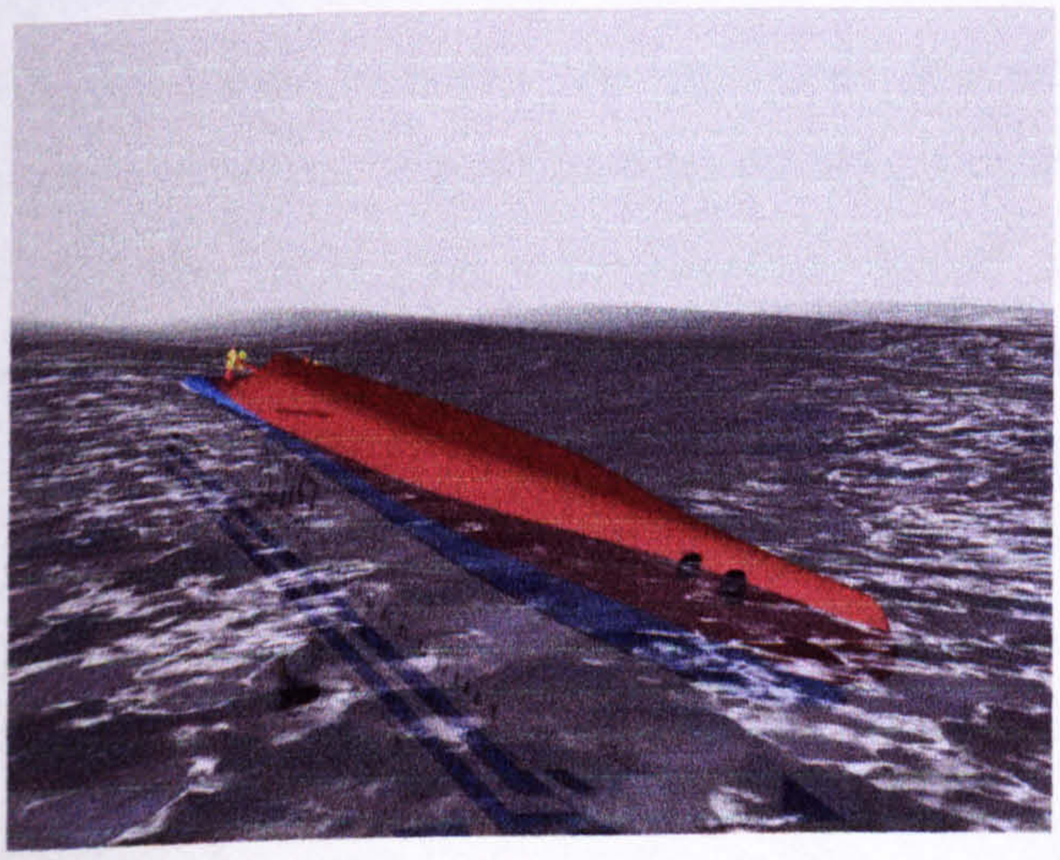

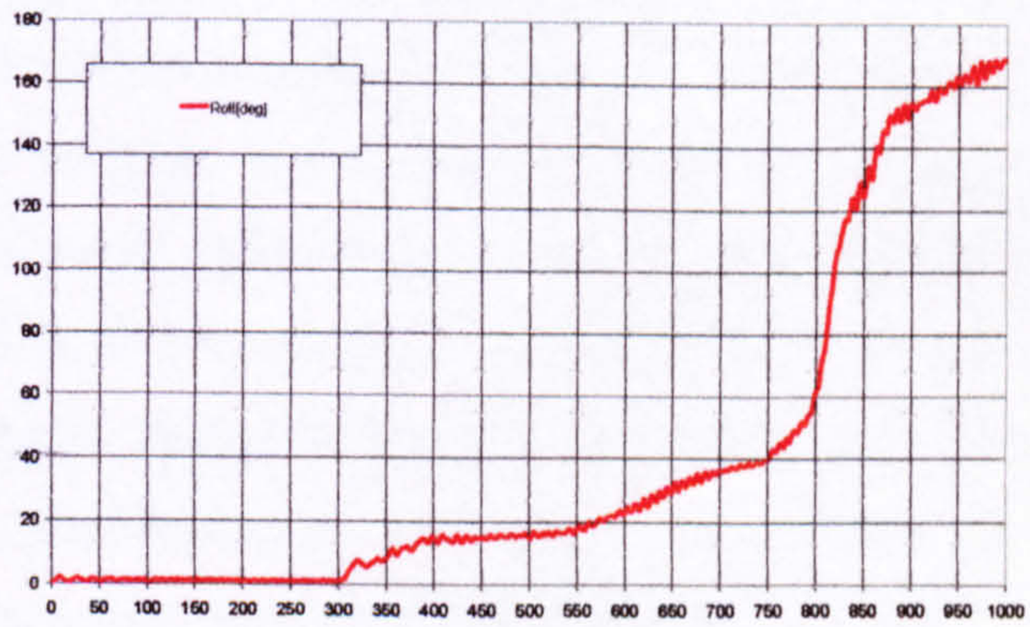

Figure 73 PROTEUS3 simulation of ESTONIA behaviour in the conditions described by JAIC. The ship capsizes immediately but does not sink.

10 Discussion

This chapter gives a brief review of the work undertaken on development of the mathematical model presented in the foregoing and the representative numerical code for ship performance assessment in extreme conditions.

10.1 Choice of the mathematical model

There are three distinctive and elementary, to some extent, models that have been selected to build into the PROTEUS3, which address the following:

- Ship hydrodynamics.
- Ship dynamics.
- Internal dynamics.

The strip theory has been chosen here as an alternative to the more sophisticated panel methods, for its efficiency. As has been discussed in §3.1, the literature documents success of this technique in predicting ship hydrodynamic properties with sufficient engineering accuracy. In this work asymmetric geometry case has been considered by employing basic Rankine source distribution scheme, which proved to be highly reliable and free of commonly present solution irregularities seen in pulsating Green function methods. Thorough validation study in **Appendix 2** and **Appendix 3** allowed identifying some shortcomings of this solution on one hand, and demonstrating its practicality and accuracy in application to asymmetric geometrical cases on the other. The shortcomings refer to under-predictions of diffraction heave forces and hence pitch moments, which in turn can lead to slight over-estimations of both heave and pitch motions. Nevertheless, the time domain simulations of intact ship responses seem to confirm that the modelling applied in this study is sufficiently accurate. Prediction of ship hydrodynamics has been extended to large amplitude motions by direct integration of excitation forces (FK and Restoring) acting on the actual body submerged beneath the exciting waves enabling thereby accounting for geometric non-linearities.

The derived equations (39) and (40), apart from taking into account the effects of dynamics of free mass within the ship, constitute complete angular and linear momentum theorems, respectively,

expressed in non-inertial system of reference. As is commonly known, such full solution is highly non-linear due to inherent coupling between these vectors as well as through the transformation matrix, which must be used to (a) express the right hand side in the same body-fixed coordinate system and, (b) to transform the solution to these equations back to the inertial, earth-fixed system of reference. The adopted Euler angles definitions and ensuing kinematic relations between their derivatives and rotation velocities, allow for precise predictions of large amplitude motions.

The mathematical model for the predictions of motions of free mass within the ship treated as a single point and representing floodwater or the shifting cargo, has been deduced from the mentioned basic theorem on momentum conservation as expressed in body-fixed system of reference. Thus, full non-linear coupling with motions of the ship have been derived, which when superimposed to additional external forces, builds into an independent motion model for each mass point considered. The additional forces refer to the following:

- Gravity force
- Friction force (cargo shifting)
- Reaction force
  - For cargo shifting it is a vertical vector when expressed in body-fixed system of reference, restraining motion to horizontal plane.
  - For floodwater it is a force normal to potential surface of the centre of buoyancy motion.
- Damping force (floodwater)
- Impact force (cargo shifting)

Thus, each free mass represents three or two additional degrees of freedom motion, for floodwater or shifting cargo, respectively.

The choice of these three general models is considered a good balance between required accuracy in representing of given physical phenomenon on one hand, and high efficiency in terms of data-pre-processing, reliability of numerical predictions and computation time, on the other.

10.2 Further work

However advanced progress have been achieved in the modelling of damaged ship dynamic stability, as presented in the foregoing, it would be a fallacy to claim that this model is the ultimate tool for performance assessment in limit state. There are countless improvements that can be implemented, ranging from application of more sophisticated basic integration schemes for better accuracy or speedier solutions, to fundamental changing of the underlying theoretical representation of physics, such as fluid models. In fact the latter seems to be the next envisaged step towards building of a numerical tool that could represent the experimentally observed phenomena in damaged ship behaviour, with higher level of sophistication, and hopefully accuracy.

The proposed further research and developments presented below, aim at outlining the recommendable work for improvements of the modelling pursued in this thesis and deriving from rigid-body theory, as well as expressing authors view as to the future directions in the field of limit state performance predictions.

1. The numerical solutions such as algebraic equation solvers, iteration methods, general integration techniques or integrators of ordinary differential equations, should be improved. This can hopefully increase the speed of the computations and possibly increase the accuracy of predictions.

2. Viscous or other higher order effects, such as current and drift forces should be derived from general first principles reasoning rather than rely on empirical parametric formulations used here. These effects as much as are difficult to model, since their understanding is quite limited, are significantly affecting the predicted ship behaviour and therefore should be improved.

3. Wind excitation should be included in the model as its effect could be significant for high wind-exposed-side-area passenger Ro-Ro vessels. This is probably the easiest of the potential developments to implement.

4. As a first step towards improvements in predictions of ship hydrodynamics, the 3D panel methods seem to be appropriate alternative. The PROTEUS3 have already been made

compatible with available software, however more systematic validation and testing is needed for full implementation.

5. Naturally the process of validation studies is a "never ending story". The model should be constantly confronted with quality experimental studies, so potential shortcomings could be highlighted or more confidence gained. In particular sensitivity of hydrodynamic properties to presence of hull damage and instantaneous water ingress/egress should be understood and methods to deal with it developed. The model should be systematically tested for more operational conditions: headings, speeds, loading conditions, etc.

6. Implementation of model for representing manoeuvring qualities of the ship, such as propulsion systems, rudder effects and its steering pilots, as well as methods for predictions of non-linear hydrodynamic coefficients for planar motions, sway, yaw and surge. This would allow to evolve into a very general model, which when coupled to some virtual reality models cold be used in an interactive manner.

7. RANS methods become widely used in the naval architecture profession for various problems. It seems that these viscous fluid flow models are the most advanced techniques for predictions of interactions between ship and the sloshing fluid on board. As a first step towards implementation some hybrid of the general ship dynamics model presented in this thesis and a RANS or similar fluid momentum solver could be developed, as has already been shown in the literature.

8. The ultimate application of viscous flow techniques for predictions of the fluid sloshing as well as external fluid and the ship interactions is not inconceivable in the near future. Therefore the developments mentioned in the above paragraph seem indispensable.

11 Conclusions

It is believed that the set aims of the work have been accomplished. The tool for assessment of ship performance, when in limiting state, have achieved high level of sophistication, indeed, the mathematical expressions for dynamics phenomenon, the conservation of momentum theory, have been exploited to its limits. This hybrid approach pursued at the University of Strathclyde for more than a decade and found as of high quality and practicality, have been re-built from its fundamentals by development of the new numerical code PROTEUS3.

This software, integrating various modelling techniques of a series of physical phenomena, has allowed achieving a good balance between computation efficiency and accuracy, offering experimentation tool that can be used for a multitude of engineering issues and design practices, as demonstrated in this thesis on practical real life problems.

In summary, the following concluding statements can be made:

1. A robust technique for ship hydrodynamic predictions accounting for hull asymmetries has been developed based on strip theory formulations and fundamental singularity distributions. The non-linearities due to mean attitude variation have been taken into account by database approach. Effects of large amplitude motions in high seas have been approximated by direct integration of the pressure due to the undisturbed wave excitation over the instantaneous geometry under the wave profile.

2. Ship dynamic equations for large amplitude motions and accounting for free mass displacements have been developed.

3. The model of floodwater behaviour has been developed from rigid-body considerations.

4. Planar cargo shifting phenomenon has been modelled.

5. The developed numerical code, PROTEUS3, proved to be effective when applied in real maritime casualty investigations, the loss of MV Derbyshire and disaster of MV Estonia.

12 Bibliography

12.1 Co-publications by the author

[1] Jasionowski, A, Dodworth, K and Vassalos, D: *"Proposal of Passenger Survival-Based Criteria for Ro-Ro Vessels"*, International Shipbuilding Progress, September 1997, 10 pp.

[2] Vassalos, D, Jasionowski, A and Dodworth, K: *"Assessment of Survival Time of Damaged Passenger/RoRo Vessels"*, 2nd International Workshop on the Stability and Operational Safety of Ships, Osaka, Japan, November 1996, 11pp.

[3] Vassalos, D, Jasionowski, A, Dodworth, K, Allan, T, Matthewson, B, Paloyannidis, P: *"Time-Based Survival Criteria For Ro-Ro Vessels"*, RINA Spring Meetings 1998, London, 18pp.

[4] Vassalos, D, Turan, O, Jasionowski, A: *"An Investigation Into The Damage Survivability of High Speed Passenger/Ro-Ro Vessels"*, 6th International Conference on High Speed Marine Vehicles, Copenhagen-Oslo, September 1998, 12 pp.

[5] Vassalos, D, Halvacioglu, I, Jasionowski, A: *"An investigation of the stability and survivability of trimarans"*, 7th International Conference on Stability of Ships and Ocean Vehicles, STAB2000, 7-11 February 2000, Launceston, Tasmania, Australia.

[6] Vassalos, D, Guarin, L, Jasionowski, A, *"Seakeeping and seaworthiness of bulk carriers in extreme weather conditions"*, Japan, September 2000

[7] Vassalos, D, Jasionowski, A and Halvacioglu, I: *"Static And Dynamic Stability of Trimarans – Numerical Simulations, Phase 2"*, Draft Report, MOD contract, The Ship Stability Research Centre, Glasgow, 1997, 128pp.

[8] Vassalos, D, Guarin, L, Jasionowski, A: *"Safety of bulk carriers in extreme seas. Sensitivity of Wetness and Deck Loads to Bow Height and Forward Buoyancy Reserves in Extreme Weather Conditions"*, PHASE I, MSC 70/INF, SSRC-06-99-AJLG-1-ER, June 1998

[9] Vassalos, D, Guarin, L, Jasionowski, A: *"Safety of bulk carriers in extreme seas. Sensitivity of Wetness and Deck Loads to Bow Height and Forward Buoyancy Reserves in*

Extreme Weather Conditions", PHASE I, MSC 70/4, Addition 1 to MSC 70/INF, SSRC-06-99-AJLG-2-ER, June 1999.

[10] Vassalos, D, Guarin, L, Jasionowski, A: *"Safety of bulk carriers in extreme seas. Sensitivity of Wetness and Deck Loads to Bow Height and Forward Buoyancy Reserves in Extreme Weather Conditions"*, PHASE I, Addition 2 to MSC 70/INF, SSRC-06-99-AJLG-3-ER, June 1999.

[11] Vassalos, D, Guarin, L, Jasionowski, A: *"Safety of bulk carriers in extreme seas. Sensitivity of Wetness and Deck Loads to Bow Height and Forward Buoyancy Reserves in Extreme Weather Conditions"*, PHASE I, Comments on MSC 70/INF, SSRC-06-99-AJLG-4-ER, June 1999.

[12] Vassalos, D, Guarin, L, Jasionowski, A: *"Safety of bulk carriers in extreme seas. Sensitivity of Wetness and Deck Loads to Bow Height and Forward Buoyancy Reserves in Extreme Weather Conditions"*, PHASE II, Experimental Test Data, SSRC-06-99-AJLG-5-ER, June 1999.

[13] Vassalos, D, Guarin, L, Jasionowski, A: *"Safety of bulk carriers in extreme seas. Sensitivity of Wetness and Deck Loads to Bow Height and Forward Buoyancy Reserves in Extreme Weather Conditions"*, PHASE II, MSC 71/4, SSRC-06-99-AJLG-6-ER, June 1999.

[14] Jasionowski, A, Guarin, L, Vassalos, D: *"Safety of bulk carriers in extreme seas. Static and dynamic stability"*, SSRC-06-99-AJLG-7-ER, 1999, 20pp.

[15] Jasionowski, A, Vassalos, D: *"Safety of bulk carriers in extreme seas. Correlation studies between independent experiments on the behaviour of MV Derbyshire in extreme seas"*, SSRC-09-99-AJ-8-ER, 1999, 8pp.

[16] Guarin, L, Jasionowski, A, Vassalos, D: *"Safety of bulk carriers in extreme seas. Phasing analysis for M.V. DERYSHIRE"*, SSRC-9-99-AJLG-9-ER 1999, 20pp.

[17] Vassalos, D, Jasionowski, A, Konovessis, D, Tuzcu, C, York, A, Turan, O: *"A realisable concept of a safe haven Ro-Ro"*, the winning design proposal at THE RINA SAFER SHIP COMPETITION, 1999

[18] Vassalos, D, Jasionowski, A: *"Numerical and experimental research on MV Derbyshire"*, SSRC-12-99-AJDV-10-ER, Glasgow, December 1999, 69pp.

[19] Jasionowski, A, Vassalos, D: *"Numerical and experimental research on MV Derbyshire, Sensitivity of the sinking process to initial conditions"*, SSRC-02-00-AJDV-11-ER, Glasgow, February 2000, 96pp.

[20] Vassalos, D, Guarin, L, Jasionowski, A; *"Supplementary report for the DETR-ONI related work and recommendations"*, SSRC-04-00-DVLGAJ-12-ER, Glasgow, April 2000, 18pp.

[21] Jasionowski, A, Vassalos, D: *"Numerical and experimental research on MV Derbyshire, Sensitivity of the sinking process to initial conditions No2"*, SSRC-04-00-AJDV-13-ER, Glasgow, April 2000, 126pp.

[22] Jasionowski, A, Vassalos, D: *"Numerical and experimental research on MV Derbyshire, Sensitivity of the sinking process to initial conditions No3"*, SSRC-05-00-AJDV-14-ER, Glasgow, May 2000, 72pp.

[23] Vassalos, D, Guarin, L, Jasionowski, A, *"Statement On Fast Mode Bow Flooding"*, SSRC-06-00-DVLGAJ-15-ER, Paper Presented in Court, June 2000, 43pp.

[24] Jasionowski, A, *"Advanced mathematical and numerical modelling of ship damage stability and survivability"*, Lecture document, China Ship Scientific Research Centre, Wuxi, November 2000, 80pp.

[25] Jasionowski, A, *"NEREUS, First Principles for Damage Resistance against Capsize"*, 12-months interim report, WP1, December 2000, 25pp.

[26] Jasionowski, A, Vassalos, D, Shu Hong Chai, Samalekos, P, *"Time-based survival criteria for Ro-Ro vessels, Phase II"*, Draft Final Report, January 2001, 765pp.

12.2 Ship hydrodynamics

[27] Beck R. F., Troesch A. W., *"Wave diffraction effects in head seas"*, Contract No N00014-78-C-0109, David W. Taylor Naval Ship Research Centre

[28] Beck Robert F., Liapis Stergios, *"Transient motions of floating bodies at zero forward speed"*, Journal of ship research, Vol. 31, No.3, Sept. 1987, pp. 164-176

[29] Bertram Volker, *"Ship Motions by Rankine Source Method"*, Shiffstechnik Bd. 37 – 1990

[30] Bertram Volker, Laudan Jochen, *"Computation of viscous and inviscid flow around ship hulls"*, Shiffstechnik Bd. 40 – 1993 / Ship technology research Vol. 40 – 1993

[31] Celebi, M., S., Kim, M., H., Beck, R., F.;*"Fully non-linear 3-D numerical wave tank simulation"*, Journal of Ship Research, Vol. 42, No. 1, March 1998, pp. 33-45

[32] Chapman, R, B, *"Large-amplitude transient motion of two-dimensional floating bodies"*, Journal of Ship Research, Vol. 23, No. 1, March 1979, pp. 20-31

[33] Cummins W. E., *"The impulse response function and ship motions"*, Schiffstechnik Bd. 9 - 1962

[34] Faltinsen, O, M; *"Sea loads on ships and offshore structures"*, Cambridge University Press, 1990

[35] Faltinsen O., Zhao R., *"Numerical predictions of ship motions at high speed"*, Phil. Trans. R. Soc. Lond. A, 1991

[36] Frank, W, *"Oscillation of cylinders in or below the free surface of deep fluids"*, DTNSRDC Report 2375, October 1967

[37] Ferrant Pierre, *"Three-dimensional Unsteady Wave-Body Interactions by a Rankine Boundary Element Method"*, Shiffstechnik Bd. 40 – 1993 / Ship Technology Research Vol. 40 – 1993

[38] Grim,"", Hamburg, 1953, Jahrbuch der STG

[39] Ha, Taebum, *"A three dimensional prediction of the seakeeping performance of high speed marine vehicles"*, PhD thesis, University of Strathclyde, SSRC, September 2000.

[40] Hamilton J. Andrew, Yeung Ronald W., *"Shell-Function Solutions for three-dimensional nonlinear body-motion problems"*, Shiffstechnik Bd. 4 – 1997 / Ship Technology Research Vol. 44 – 1997

[41] Hess John L., Smith A. O. M., *"Calculation of nonlifting potential flow about arbitrary three-dimensional bodies"*, Journal of Ship Research, September 1964

[42] Inglis, R, B, Price, W, G, *"A Three Dimensional Ship Motion Theory – Comparison between Theoretical Predictions and Experimental Data of the Hydrodynamic Coefficients with Forward Speed"*, RINA, 1981

[43] Iwashita Hidetsugu, *"The Green Function Method for Ship Motions at Forward Speed"*, Schiffstechnik Bd. 39 – 1992 / Ship Technology Research Vol. 39 - 1992

[44] Iwashita Hidetsugu; *"Numerical Seakeeping calculations based on the 3-D Green function method"*, Ship Technology Research (Shiffstechnik), Vol. 44-1997

[45] Jankowski, J; *"Experimental verification of mathematical models describing the ship moving on the free surface"*, CTO, NO B-063, 1994

[46] Jasionowski, A, *"Series of notes taken during student practice"*, MARINTEK, Trondheim, Norway, June-August 1995

[47] Journee, J, M, J,. *"Experiments and calculations on four Wigley hullforms"*, Ship Hydrodynamic Laboratory, Faculty of mechanical engineering and marine technology, Delft University of Technology, MEMT 21, 1992

[48] Kashiwagi Masashi; *"Numerical Seakeeping calculations based on the slender ship theory"*, Ship Technology Research (Shiffstechnik), Vol. 44-1997

[49] Dodworth, K, *"The application of potential flow theory to damaged hull dynamics"*, PhD thesis, University of Strathclyde, January 2000.

[50] Kim, C, H, Chou, Frank, S, Tien, David; *"Motions and Hydrodynamic Loads of a Ship Advancing in Oblique Waves"*, SNAME Transactions, Vol. 88, 1980, pp.225-256

[51] Larsson Lars, *"CFD in Ship Design – Prospects and Limitations"*, Schiffstechnik Bd. 44 - 1997

[52] Malick Ba, Guilbaud, M; *"A fast method of evaluation for the translating and pulsating Green's function"*, Ship Technology Research (Shiffstechnik), Vol. 42-1995

[53] Nagai Tamotsu, Yoshida Yasushi, *"Estimation of resistance, trim and draft of planing craft"*, Shiffstechnik Bd. 40 – 1993 / Ship Technology Research Vol. 40 – 1993

[54] Newman, J, N; *"Marine Hydrodynamics"*, The Massachusetts Institute of Technology, 7th printing, 1992

[55] Newman John Nicholas, *"The numerical towing tank – fact or fiction ?"*, Shiffstechnik Bd. 36 – 1989

[56] Newman J. N., *"Evaluation of the wave-resistance green function: Part1 – the double integral"*, Journal of Ship Research, Vol. 31, No.2, June 1987, pp.79-90

[57] Nestegard, A, Sclavounos, P, D, *"A numerical solution of two-dimensional deep water wave-body problems"*, Journal of Ship Research, Vol. 28, No 1, March 1984, pp. 48-54

[58] Noblesse F., *"On the fundamental function in the theory of steady motion of ships"*, Journal of Ship Research, December 1978

[59] Noblesse Francis, Hendrix Dane, *"On the theory of potential flow about a ship advancing in waves"*, Journal of Ship Research, Vol. 36, No. 1, March 1992, pp. 17-29

[60] Noblesse F., *"The fundamental solution in the theory of steady motion of a ship"*, Journal of Ship Research, Vol. 21, No.2, June 1977, pp. 82-88

[61] Pawłowski, M; *"Andrzej Jasionowski lecture notes from the MSc course in hydrodynamics"*, Technical University of Gdańsk, 1993

[62] Papanikolau Apostolos D., Schellin Thomas E., *"A three-Dimensional Panel Method for Motions and Loads of Ships with Forward Speed"*, Shiffstchnik Bd. 39 – 1992 / Ship Technology Research Vol. 39 - 1992

[63] Papanikolaou, A, Zaraphonitis, G, *"Computer Program Newdrift Version 6"*, Internal Report, National Technical University of Athens, Novemebr 1989

[64] Raven Hoyte C., *"The nature of nonlinear effects in ship wave making"*, Shiffstechnik Bd. 44 – 1997 / Ship Technology Research Vol. 44 - 1997

[65] Streeter, V, L; *"Fluid dynamics"*, McGraw-Hill Publications in Aeronautical Science, 1948

[66] Salvesen Nils, Tuck, E, O, Odd Faltinsen: *"Ship Motions and Sea Loads"*, SNAME, Vol 78, 1970

[67] Soding Heinrich, *"A Method for Accurate Force Calculations in Potential Flow"*, Schiffstechnik Bd. 40 – 1993 / Ship Technology Research Vol. 40 - 1993

[68] Vugts, Ir, J, H, *"The hydrodynamic coefficients for swaying, heaving and rolling cylinders in a free surface"*, Report 112 S Netherlands Ship Research Centre TNO

[69] Wait R., *"Use of finite elements in multidimensional problems in practice"*, Numerical solutions of integral equations by L.M. Delves and J.Wash

[70] Webster C. William, *"The flow about arbitrary, three-dimensional smooth bodies"*, Journal of Ship Research, Vol. 19, No.4, Dec. 1975, pp. 206-218

[71] Wehausen John. V, *"Use of Lagrangian Coordinates for Ship Wave Resistance (First- and Second-Order Thin-Ship Theory"*, Journal of Ship Research, March 1969

[72] Wu G. X., *"A numerical scheme for calculating the m_j terms in wave-current-body interaction problem"*, Technical Note, Applied Ocean Research, 1991, Vol. 13, No. 6

[73] Wu MingKang, Moan Torgeir, *"Linear and Nonlinear Hydroelastic Analysis of Heigh Speed Vessels"*, Journal of Ship Research, Vol. 40, No. 2, June 1996, pp. 149-163

[74] Yeung Ronald W., *"Sinkage and trim in first-order thin-ship theory"*, Journal of Ship Research, March 1972

[75] Yeung Ronald Wai-Chun, *"A singularity-distribution method for free-surface flow problems with an oscillating body"*, PhD dissertation, University of Berkley, 1973

[76] Yamamoto Y., Fukasawa T., Arai M., Kajita E., *"Nonlinear effects for ship motion in heavy seas"*, Personal collection

[77] Yasukawa Hironori, *"Nonlinear time domain analysis of hydrodynamic forces on a ship advancing in waves"*, 4th Osaka Colloquium on Seakeeping Performance of Ships, October 2000

12.3 Viscous roll damping

[78] Himeno Yoji, *"Prediction of ship roll damping – state of the art"*, Report No 239, University of Michigan, College of Engineering, September 1981

[79] Ikeda Yoshiho, Himeno, Yoji, Tanaka Norio, *"On eddy making component of roll damping force on naked hull"*, Private collection

[80] Ikeda Yoshiho, Himeno Yoji, Tanaka Norio, *"A prediction method for ship roll damping"*, Private collection

[81] Ikeda Yoshiho, Himeno Yoji and Tanaka Norio, *"On roll damping force of ship – effect of friction of hull and normal force of bilge keels"*,Report of Department of Naval Architecture, University of Osaka Prefecture, No 00401, December 1978

[82] Ikeda Yoshiho, Fujiwara Toshihiro, Himeno Yoji and Tanaka Norio, *"Velocity field around ship hull in roll motion"*, Report of Department of Naval Architecture, University of Osaka Prefecture, No 00406, October 1979

[83] Ikeda Yoshiho, Himeno Yoji, Tanaka Norio, *"Components of roll damping of ship at forward speed"*, Private collection

[84] Chaplin John R., Ikeda Yoshiho, *"Viscous forces on offshore structures and their effects on the motion of floating bodies"*, Proceedings of the ninth (1999) International Offshore and Polar Engineering Conference Brest, France, May 30 June 4, 1999

[85] Tanaka Norio, Ikeda Yoshiho, Okada Hidehiko, *"Study on roll characteristics of small fishing vessel, Part 1, Measurement of roll damping"*, in Japanese, Journal of the Kansai Society of Naval Architects, Japan, No 187, 1982

[86] Tanaka Norio, Ikeda Yoshiho, Okada Hidehiko, *"Study on roll characteristics of small fishing vessel, Part 4, Effect of skeg and hard-chine on roll damping"*, in Japanese, Journal of the Kansai Society of Naval Architects, Japan, No 196, 1985

[87] Tanaka Norio, Ikeda Yoshiho, Okada Hidehiko, *"Study on roll characteristics of small fishing vessel, Summary"*, in Japanese, Journal of the Kansai Society of Naval Architects, Japan

[88] Ikeda Yoshiho, Kawahara Yukie, *"Studies on roll characteristics of a high-speed hardchine craft"*,Proceedings of the Second Japan-Korea Joint Workshop on Stability and Marine Hydrodynamics, June 1993

[89] Fujino Masataka, Fuji Iwao, Hamamoto Masami, Ikeda Yoshiho, Ishida Shigesuke, Morita Tomoharu, Tanai Kusuo, Umeda Naoya, *"Examination of roll damping coefficients and effective wave slope coefficient for small passenger craft"*, Vessel Stability Symposium 1993

[90] Ikeda Yoshiho, Fujiwara Toshifumi and Katayama Toru, *"Roll damping of a sharp-cornered barge and roll control by a new-type stabiliser"*, Proceedings of the third (1993) International Offshore and Polar Engineering Conference Singapore, 6-11 June 1993

[91] Ikeda Yoshiho, Katayama Toru, *"Roll motion characteristics of high speed slender vessels"*, Proc. Of Fifth International Conference on Stability of Ship and Ocean Vehicles, Volume 1, Nov. 1994

[92] Ikeda Yoshiho, Umeda Naoya, Tanaka Norio, *"Effect of forward speed on roll damping of a high speed craft"*,in Japanese, Journal of the Kansai Society of Naval Architects, Japan, No 208

[93] Rathje Helge, Schellin Thomas E., *"Viscous effects in seakeeping prediction of twin-hull ships"*, Shiffstechnik Bd. 44 – 1997 / Ship Technology Research Vol. 44 - 1997

12.4 Rigid body dynamics, Ship dynamics, Intact/Damage Stability

[94] Chang Bor-Chau, Blume Peter, *"Survivability of Damaged Ro-Ro Passenger Vessels"*, Proc. 3rd Int. Workshop on Theoretical Advances in Ship Stability and Practical Impact, Crete, October 28-29, 1997

[95] De Kat Jan Otto, *"Numerical Modelling and Simulation of Intact Stability"*, Private Collection

[96] De Kat Jan Otto, *"The Simulation of Ship Motions and Capsizing in Severe Seas"*, SNAME Transactions, Vol. 97, 1989, pp. 139-168

[97] D'Souza, Frank, A; Vijay, K, Garg; *"Advanced Dynamics"*, Prentice-Hall Inc., 1984

[98] Easthope, C, E; *"Three Dimensional Dynamics"*, Second Edition, London, Butterworths, 1964

[99] Gerritsma J., Smith W. E., *"Full-scale Destroyer Motion Measurements"*, Journal of Ship Research, March 1967

[100] Goldstein, H; *"Classical Mechanics"*, 2nd ed., Addison-Wesley Publ. Co., Reading, MA, 1980

[101] Greenwood, Donald, T; *"Principles of Dynamics"*, Prentice-Hall, Inc., Englewood Cliffs, New Jersey, 1965

[102] Katayama Toru, Hinami Takashige, Ikeda Yoshiho, *"Longitudinal motion of a super high-speed planing craft in regular head waves"*, 4th Osaka Colloqium on Seakeeping Performance of Ships, October 2000

[103] Lee B. S., Vassalos D., *"An Investigation Into the Stabilisation Effects of Anti-roll Tanks with Flow Obstructions"*, Int. Shipbuilding Progress, 43, no. 433, 1996, pp. 70-88

[104] Lewandowski Edward M., *"Transverse Dynamics Stability of Planing Craft"*, Marine Technology, April 1997

[105] Marion, Jerry, B; *"Classical Dynamics of Particles and Systems"*, Second Edition, Academic Press, New York and London, 1970

[106] Marwood W. J., Bailey D., *"Transverse Stability of Round-Bottomed High Speed Craft Underway"*,National Physics Laboratory, Ship Division, October 1968

[107] Meriam, J, L, Kraige, L, G; *"Dynamics"*, Vol2, Second Edition

[108] Naoki Isu, Yoneda Shigeo, Hattori Kazuhiko, Koo Jiro, *"The severity of Nauseogenic Effect of Cross-Coupled Rotation is Proportional to Gyroscopic Angular Acceleration"*, Aviation, Space and Environmental Medicine, Vol. 67, No. 4, April 1996

[109] Newton, Isaac; *"Principia"*, Vol.1, *"The motion of bodies"*, University of California Press

[110] Pawłowski, M, *"Równania ruchu i siły działające na statek w symulacjach prowadzących do jego przewrócenia"*, In Polish, Prace badawcze Nr 66/93,Gdańsk, 1993

[111] Pawłowski, M, *"Siły i Momenty Działające na Statek Pdczas Flowania o Wsokich Aplitudach"*, In Polish, Prace badawcze Nr 45/94, Gdańsk 1994

[112] Prescott, John; *"Mechanics of Particles and Rigid Bodies"*, Longmans Green And Co., New York 1923

[113] Roberson, R, E; Schwertassek, R; *"Dynamics of Multibody Systems"*, Springer-Verlag, 1988

[114] Spouge J. R., *"Nonlinear analysis of large amplitude rolling experiments"*, Private Collection

[115] Timoshenko, S, Young, G, H; *"Advanced Dynamics"*, McGraw-Hill Book Company, Inc., 1948

[116] Toxopeus S. L., Keuning J. A., Hooft J. P., *"Dynamic Stability of Planing Ships"*, Private Collection

[117] Turan, O, "*Dynamic Stability Assessment of damaged Ships by Time-Domain Simulation*", PhD Thesis, University of Strathclyde, 1992.

[118] Vassalos, D, "*Capsizal Resistance Prediction of a Damaged Ship in a Random Sea*", Transactions RINA, Vol. 137, 1995.

[119] Letizia, L and Vassalos, D, *"Formulation of a Non-Linear Mathematical Model for a Damaged Ship With Progressive Flooding*", International Symposium on Ship Safety in a Seaway, Kaliningrad, Russia, May 1995.

[120] Letizia, L, "*Damage Survivability of Passenger Ro-Ro Vessels Subjected to Progressive Flooding in a Random Sea*", PhD Thesis, University of Strathclyde, 1997.

[121] Vassalos, D., Letizia, L., Shaw, M., Mac Sherson, C.;*"An investigation on the flooding of damaged Ro-Ro ships"*, RINA 1997

[122] Vassalos, Dracos, *"Damage survivability of passenger/Ro-Ro vessels by numerical and physical model testing"*, WEMT 1998

[123] Hirt, C, W, Nicholas, B, D; *"Volume of fluid (VOF) method for the dynamics of free boundaries"*, Journal of Computational Physics Vol. 39, 1981, p 201-225

[124] Shin, C.;*"Prediction of shipping water on deck of ships"*, 7th International Conference on Stability of Ships and Ocean Vehicles, February 2000, Launceston, Tasmania, Australia

[125] Subramanian, V., Kastner, S.;*"Ship behaviour due to dynamic impact of water on deck"*, 7th International Conference on Stability of Ships and Ocean Vehicles, February 2000, Launceston, Tasmania, Australia

[126] Bass, D., Cumming, D.;*"An experimental and numerical investigation of the effects of water trapped on the deck"*, 7th International Conference on Stability of Ships and Ocean Vehicles, February 2000, Launceston, Tasmania, Australia

[127] Qian, K., Wang, Y. and Wang, D.;*"Calculation of wave load encountered by damaged ships"*, 7th International Conference on Stability of Ships and Ocean Vehicles, February 2000, Launceston, Tasmania, Australia

[128] Ikeda, Y., Ma, Y.;*"An experimental study on large roll motion in intermediate stage of flooding due to sudden ingress of water"*, 7th International Conference on Stability of Ships and Ocean Vehicles, February 2000, Launceston, Tasmania, Australia

[129] R van't Veer, Jan de Kat; *"Experimental and numerical investigation on progressive flooding and sloshing in complex compartment geometries"*, 7th International Conference on Stability of Ships and Ocean Vehicles, February 2000, Launceston, Tasmania, Australia

[130] Zaraphonitis, G., Papanikolau, A, Spanos, D., *"On a 3D Mathematical model of The Damage Stability of Ships in Waves"*, Proc. 6th Int. Conference Stability of Ships and Ocean Structures, STAB'97, Varna, September 1997

[131] Papanikolau Apostolos D., *"Methodology for the evaluation of large amplitude ship motions in waves and of dynamic stability"*, Proc. 3rd Int. Workshop on Theoretical Advances in Ship Stability and Practical Impact, Crete, October 28-29, 1997

[132] Papanikolau, A, Zaraphonitis, G., Spanos, D., Boulougouris, E., Eliopoulou, E.;*"Investigation into the capsizing of damaged Ro-Ro passenger ships in waves"*, 7th International Conference on Stability of Ships and Ocean Vehicles, February 2000, Launceston, Tasmania, Australia

[133] Zhou Z. Q., De Kat J. O., Buchner B., *"A nonlinear 3-D approach to simulate Green Water on Deck"*, 7th International Conference on Numerical Ship Hydrodynamics, Nantes, July 1999

[134] Vassalos, D, *"Capsizal Resistance Prediction of a Damaged Ship in a Random Sea"*, RINA Symposium on Ro-Ro Ships survivability, London, November 1994

[135] Rakhmanin, N, Zhivitsa, S, *"Prediction of Motion of Ships with Flooded Compartments in a Seaway"*, STAB'94, Melbourne, USA, November 1994

[136] Rakhmanin, N, *"Stability of Damaged Ships During Ship Motion in Waves"*, STAB'90 Naples, September 1990

[137] Rakhmanin N. N., Zhivitsa S. G., *"The influence of liquid cargo dynamics on ship stability"*, private collection

[138] Lee, A, Adee, B, *"Numerical Analysis of Vessel's Dynamic Responses with Water Trapped on Deck"*, STAB'94, Melbourne, USA, November 1994

[139] Vermeer, H, *"Mathematical Modelling of Motions and Damage Stability of Ro-Ro in the Intermediate Stages of Flooding"*, STAB'94, Melbourne, USA, November 1994

[140] Petey, F, *"Determination of Capsizing Safety of Damaged Ships by Means of Motion Simulation in Waves"*, STAB'90 Naples, September 1990

[141] Falzarano, J, M, Troesh, A, W, *"Application of Modern Geometric Methods for Dynamical Systems to the Problem of Vessel Capsizing with Water on Deck"*, STAB'90, September 1990

[142] Trincas, G, *"Safety for Damaged Vessels as Probability of Non-Capsizing in Following Seas"*, STAB'90 Naples, September 1990

[143] Dand, I, W, *"Hydrodynamic aspects of the sinking of the ferry Herald of Free Enterprise"*, Transactions RINA, 1988

[144] Pantazopoulos, M, S, *"Three Dimensional Sloshing of Water on Decks"*, Marine Technology, Vol. 25, No 4, pp.253-261, 1988

[145] Murashige Sunao, Aihara Kazuyuki, *"Chaotic Motion of a Flooded Ship in Waves"*, METR 97-01, Janary 1997

[146] Dillingham Jeff, *"Motion Studies of a Vessel with Water on Deck"*, Marine Technology, Vol. 18, No. 1, January 1981, pp. 38-50

[147] Tongue E., Soding H., *"Computing Capsizing Frequencies of Ships in a Seaway"*, private collection

12.5 Sloshing in tanks

[148] Van den Bosh, J, J, Vugts, J, H, "Roll damping by free surface", Report no. 134, Shipbuilding Laboratory, Delft.

[149] Hamlin, N, A, Lou, Y, K, Maclean, W, M, Seibold, F, Chandras, L, M, "Liquid sloshing in slack ship tanks - theory, observations and experiments", SNAME Transactions, Vol. 94, 1986, pp. 159-195

[150] Armenio, V, *"Comportamento dinamico dei liquidi a superficie libera imbarcati a bordo delle navi"*, PhD, Universita di Napoli, Universita di Trieste, Febbraio 1992.

[151] Demirbilek, Zeki, *"Energy dissipation in sloshing waves in a rolling rectangular tank – I. Mathematical theory"*, Ocean Engng, Vol. 10, No5, pp. 347-358, 1983.

[152] Faltinsen, Odd, M, *"A numerical nonlinear method of slosching in tanks with two-dimensional flow"*, Journal of Ship Research, Vol. 22, No. 3, Sept. 1978, pp. 193-202.

[153] E.F.G. van Daalen, K.M.T. Kleefsman, J. Gerrits, H.R. Luth, A.E.P. Veldman, *"Anti-roll tank simulations with a volume of fluid (VOF) based Navier-Stokes Solver"*, 23rd Symposium on Naval Hydrodynamics, 2000, paper issued for discussion

12.6 Cargo shift

[154] Holstad, Elin, *"An investigation into the Cargo Shifting problems of Solid Bulk Cargoes"*, Final year thesis, University of Strathclyde, May 1999

[155] Drobyshevskiy, Y.;*"Stability of a ship under the deformation of cargo"*, 7th International Conference on Stability of Ships and Ocean Vehicles, February 2000, Launceston, Tasmania, Australia

[156] Rakhmanin N., Zhivitsa S., *"The influence of liquid cargo dynamics on ship stability"*, Private Collection

12.7 Waves description

[157] Denis St., M, Pierson, W, J, *"On the motion of Ships in Confused Seas"*, Trans. SNAME, vol. 61, 1953

[158] Urwin Brothers Limited, *"Global wave statistics"*, British Maritime Technologies, 1985

[159] Young, I, R, *"Observation of the Spectra of Hurricane Generated Waves"*, Ocean Engineering, Vol. 25, No. 4-5, page 261-276, 1998

[160] Young, I, R, Burchell, G, P, *"Hurricane Generated Waves as observed by satellite"*, Ocean Engineering, Vol. 23 No. 8, page 761-776, 1996

[161] Young, I, R, *"Parametric Hurricane Wave Prediction Model"*, Journal of Waterway, Port, Coastal and Ocean Engineering, Vol. 114, No. 5, September, 1996

[162] Vincent, J, Cardone, *"M.V. Derbyshire, Results of Rehindcast of Typhoon Orchid"*, October 1999, Oceanweather Inc., Ref. L97/3379D/JPG/A1

[163] Ochi, Michel, K, "On prediction of extreme values", SNAME, March 1973

[164] Ochi, Michael, K, *"Comments on the paper entitled <<Transient Design waves for green water on bilk carriers>> by Drake"*, Fax dated 13/10/99 from The Treasury Solicitor to Prof. Dracos Vassalos

[165] Eilersen, C, Gudmestad, O, T, Ottesen, Hansen, N, E and Jacobsen, *"Freak waves and their effect on Steel Jacket Platforms"*, Report No. 3.12/156 Oil Industries Exploration and Production Forum, Paris, 1989

12.8 Investigation into the loss of MV Derbyshire

[166] *"M.V. Derbyshire Surveys"*, UK/EC Assessors' Main Report

[167] *"M.V. Derbyshire Surveys"*, UK/EC Assessors' Report - A Summary

[168] "Bulk Carrier - Seakeeping Tests", DMI 85266, Carried out for: Burness, Corlett & Partners (IOM), Ltd., England, Volume I, November 1985

[169] "Appendix to Preliminary Report on the total loss of M.V. Derbyshire", , Burness, Corlett & Partners (IOM), Ltd., England, Volume 2 Appendices IX to XI, BCL/J/4025, August 1987

[170] Faulkner, D, *"An analytical assessment of the sinking of the M.V. Derbyshire"*, RINA, W218 (1999), Paper issued for written discussion

[171] Prescott, A, Williams, B, J, *"FE analyses of a hatch cover from M.V. Derbyshire"*, EATEC, Report No ER2280, November 1999

[172] Baltrop, N, Burke, A, Jones, J, Ward, I, Ward, R, Gould, L, Knowles, N, C, *"M.V. Derbyshire, Finite Element Study, Damage to bulkhead 339"*, WSA Report No. AM3974-R1, May 1999

[173] Jones, J, Burke, A, Gould, L, Knowles, N, C, *"M.V. Derbyshire, Fuel Tank Integrity"*, WSA Report No. AM3974-R2, August 1999

[174] Stagg, P, R, Williams, B, J, *"Finite element analysis of bulkhead 339 from MV Derbyshire"*, EATEC Report No ER2253/A, June 1999

[175] Hutton, R, Williams, B, J, *"A static finite element analysis of a section of the bow of MV Derbyshire"*, EATEC Report No ER2253/B, June 1999

[176] Stagg, P, R, Williams, B, J, *"Finite element analysis of the Fuel Deep Tank from MV Derbyshire"*, EATEC Report No ER 2259, July 1999

[177] Antill, M, Williams, B, J, *"Collapse of the M.V. Derbyshire saddle tanks"*, EATEC, Report No ER2286/1, November 1999

[178] Stagg, P, R, Williams, B, J, *"A further finite element analysis of the bow section around Web4"*, EATEC, Report No ER2278, November 1999

[179] Stagg, P, R, Williams, B, J, *"A finite analyses of Web5 and the chain locker with surrounding structure"*, EATEC, Report No ER2277, November 1999

[180] Prescott, A, Williams, B, J, *"FE analyses of sections of the M.V. Derbyshire stores deck"*, EATEC, Report No ER2281, November 1999

[181] Stagg, P, R, Williams, B, J, *"A FE analyses of a section of bulkhead 339 from M.V. Derbyshire"*, EATEC, Report No ER2279, November 1999

[182] Gilchrist, A, *"The MV Derbyshire: Bow Tank Flooding During Sinking, Analysis and Simulation of the Variation of Hull Pressure Differential with Time/Depth"*, Department of Mechanical Engineering, University of Starthclyde, October 1999

[183] *"Trim and Stability Manuals"*, Hull Design Office, Swan Hunter Shipbuilders, October 1976

[184] *"MV Liverpool Bridge, general arrangement"*, Swan Hunter Shipbuilders Ltd.

[185] *"Lines Plan (Forward End)t"*, Swan Hunter Shipbuilders Ltd.

[186] Faulkner, D, Corlet, B, J, Romeling, J, U, *"Design of hatch covers and coamings for abnormal waves"*, RINA Proceedings, November 1996

[187] Kim, H, S, *"Virtual Model of MV Derbyshire"*, University of Strathclyde, December 1999

12.9 Investigation into the loss of MV Estonia

[188] *"Final Report on the capsizing on 28 September 1994 in the Baltic Sea of the Ro-Ro Passenger Vessel MV Estonia"*, The Joint Accident Investigation Comission of Estonia, Finland and Sweden, December 1997

[189] *"Supplement to Final Report on the capsizing on 28 September 1994 in the Baltic Sea of the Ro-Ro Passenger Vessel MV Estonia, Part II"*, Preliminary Version, The Joint Accident Investigation Comission of Estonia, Finland and Sweden, December 1997

[190] Bjorkman Anders, *"Lies And Truths About The M/V Estonia"*, Edition EGC, ISBN 2-911469-09-7, January 1998

[191] Asard Per-Erik, *"The JAIC report – unverified and contradictory conclusions. A critical examination of the Joint Accident Investigation Commission final report regarding MV Estonia"*, International MV Estonia Seminar, Stockholm, 29-30 May 2000

[192] Bemis Gregg Jr., *"Marine forensics for Naval Architects and Marine Engineers"*, International MV Estonia Seminar, Stockholm, 29-30 May 2000

[193] De Kat Jan Otto, *"Estonia Ship Stability ... and Sinking"*, International MV Estonia Seminar, Stockholm, 29-30 May 2000

[194] Fellows Michael G, *"A Second Opinion on the Explosion Damage Report On the Car/Passenger Ferry Estonia"*, International MV Estonia Seminar, Stockholm, 29-30 May 2000

[195] Ridderstolpe Johan, *"Non-evaluated damages and misleading conclusions"*, International MV Estonia Seminar, Stockholm, 29-30 May 2000

[196] Rutgersson Olle, *"Consequences for the Safety Culture within Authorities and Shipping Companies. The Estonia Accident – a wake-up call for improved safety"*, International MV Estonia Seminar, Stockholm, 29-30 May 2000

[197] Stenberg Bjorn, *"An Impossible Visor Scenario"*, International MV Estonia Seminar, Stockholm, 29-30 May 2000

[198] Ulfvarson Anders, *"Investigation methodologies – conclusions of an event tree analysis"*, International MV Estonia Seminar, Stockholm, 29-30 May 2000

12.10 Safety related

[199] Terry, G, J, *"Engineering System Safety"*, Mechanical Engineering Publications Limited, London, 1991

[200] Hazards Forum, *"Safety-related systems, Guidance for engineers"*, March 1995

[201] Hignett, K, C, *"Practical safety and reliability assessment"*, E&FN SPON, 1996

[202] Kuhlmann, A, *"Introduction to Safety Science"*, Spring-Verlag, New York, 1986

[203] Redmill, Felix, Anderson, Tom, *"Safety-critical Systems"*, Chapman & Hall, 1993

[204] Hunter, A, Thomas, *"Engineering Design For Safety"*, McGraw-Hill, Inc, 1992

[205] Gloss, David, S, Wardle, Miriam, Gayle,*"Introduction to Safety Engineering"*, John Wiley & Sons, 1984

[206] Ferry, Ted, S., *"Modern Accident Investigation and Analysis"*, John Wiley & Sons, 1987

[207] Vassalos, D, Oestvik, I, Konovessis, D, *"Design for safety: Development And Application of a Formalised Methodology"*, The Ship Stability Research Centre, Paper distributed to participants of EU project NEREUS, 19 June 2000.

[208] Vassalos, D, *"Shaping Ship Safety: The Face of The Future"*, Inaugural Lecture, University of Strathclyde, Glasgow, 5 March 1998.

[209] Konovessis, D, Vassalos, D, *"Development of a Procedure for Integration of Damage Stability and Survivability in the Ship Design Process"*, Draft working document, ROROPROB, 16 Nov 2000.

[210] Leaflet, Department of Transport, Marine Accident Investigation Branch

[211] Green, A, E, "Safety Systems Reliability", John Wiley & Sons, A Wiley-Interscience Publication, © 1983

[212] Heinrich, H, W, *"Industrial accident prevention"*, Forth Edition, McGraw-Hill Book Company, Inc., 1959.

12.11 Other

[213] Payne, Peter, R, *"Design of High Speed Boats - Planing"*, 1988

[214] Lloyd, A. R. J. M., *"Seakeeping: Ship Behaviour in Rough Weather"*, Ellis Horwood Limited, 1989

[215] Letizia, Luca, personal discussions, October 2000.

[216] Nabergoj, R, Obreja, D,C, Trincas, G, Crudu, L, Stoicescu, L, *"Dynamic transverse stability in longitudinal waves: theoretical and experimental researches"*, STAB'97

[217] Vassalos, D, *"An anatomy of the Stockholm Agreement"*, 7th STAB'2000, 7-11 February 2000, Launceston, Tasmania, Australia.

[218] The Honourable Mr Justice Colman, *"Report of the re-opened formal investigation into the loss of the M/V Derbyshire"*, In The High Court of Justice (Admiralty Court), 2000.

[219] Francescutto, A, Contento, G, *"An experimental study of the coupling between roll motion and sloshing in a compartment"*, ISOPE'94, Osaka, 10-15 April 1994, Paper N. 94-YI1-4.

[220] Hilsberg M., Kolmiński J., *"Poradnik fizyczny"*, Wydawnictwa Naukowo-Techniczne Warszawa 1965, str 80-95.

Appendix 1

Parameterisation of rigid body motion

1.1 Preamble

The position of a body with respect to any reference frame is known, [113, p.59], if the locations of all the points of the body in this frame are known. If the body is rigid the reference can be assumed embedded in the body, and hence all points of the body have constant and known in this system coordinates. Furthermore, the location of all the points of the body with respect to the global/inertial reference frame can be determined when the position of the body-fixed frame is known with respect to the inertial one. This relative position can be considered to be composed of the location of the origin of the body-fixed with respect to the origin of the inertial system of reference and their orientation with respect to each other.

Parameters characterising the relative location (translation) and orientation (rotation) of the two frames as a function of time describe the most general motions of the rigid body in space.

The translation will not be contemplated further, as it is perceived as a universally recognised description of rectilinear motion. Rotations, however, are sensitive to their adopted definition and hence require careful interpretation.

1.2 Eulerian theorem on rotation

Before the middle of the 18th Century, Euler showed that rotation is a motion with three degrees of freedom, so it requires only three independent variables to describe it, [113, p.68]. The most widely used parameters for this purpose are angle variables, which follow from Euler's theorem on rotation about a fixed point, [113, p.61]. It states that any motion of a body about a fixed point is equivalent to a rotation of the body with an axis (spin axis) through that point (two parameters being needed to describe the direction of such an axis: precession and nutation angles) and an angle of rotation about that axis (spin angle), see Figure 74.

The spin angle is then an angle of rotation about an arbitrarily chosen and fixed to the body spin axis. The precession angle, describing orientation of spin axis on the horizontal plane, is a rotation around an axis normal to the horizontal plane. Nutation is a rotation around the so-called nodal axis, resulting from the intersection of two planes, horizontal and normal to spin axis, and describes orientation of the spin axis in the vertical plane.

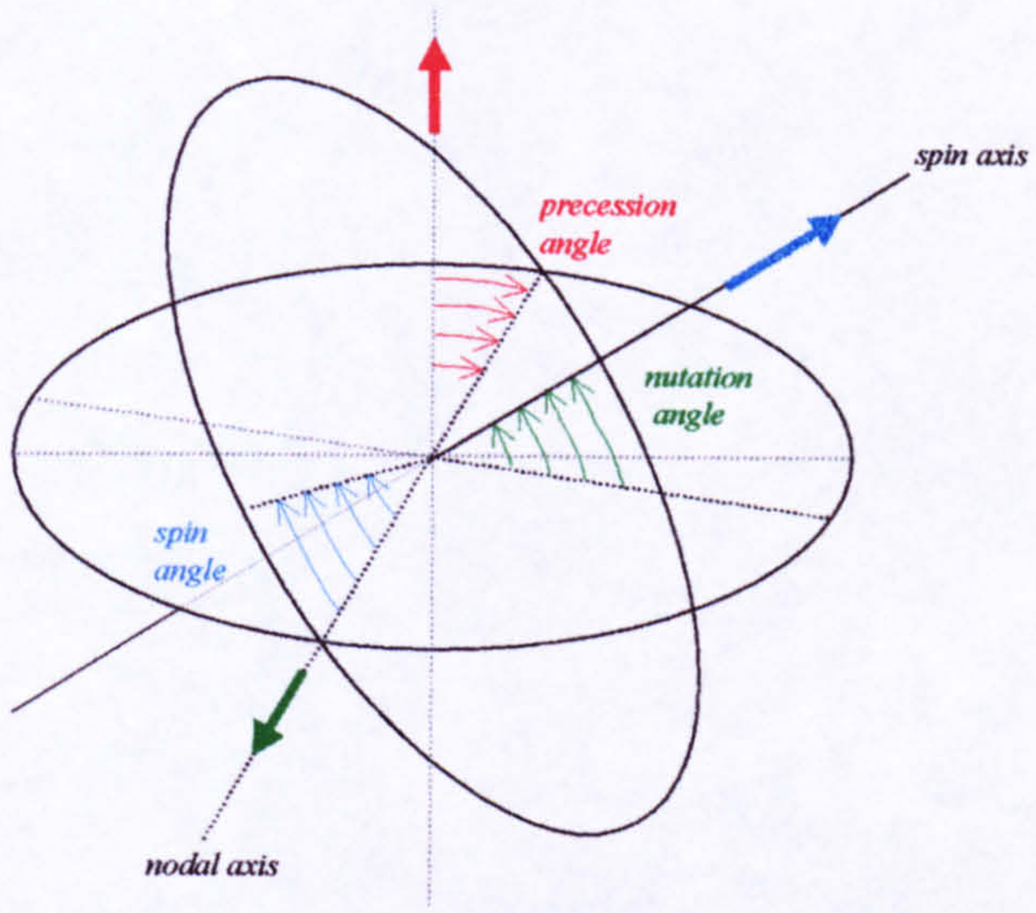

Figure 74 Definition of Euler's angles

Note that the spin axis is not the actual, instantaneous axis of rotation i.e. the axis around which rotation takes place. The spin axis is a judiciously chosen line fixed to the body and is used as a reference to describe its orientation in space. The time varying instantaneous axis of rotation, the unit vector along the direction of which is called the unit eigenvector of rotation, [113, p.64], is a resultant of all the rotations. This is explained in detail later.

1.3 Ship motion angles

In common naval architecture practise the angles describing ship orientation; pitch, roll and yaw have the following, intuitive definition:

- **Pitch** is the angle between the ship longitudinal axis and the horizontal plane
- **Roll** is the angle between the ship transverse axis and the horizontal plane
- **Yaw** is the angle of rotation around the normal axis to the horizontal plane

As a first step to mathematically define the above angles, a spin axis has to be chosen. Since the first two "intuitive" definitions, pitch and roll, refer to the angles measured from the horizontal plane, an axis fixed to the body and parallel to the horizontal plane will be taken. Hence, the precession angle can be measured on the horizontal plane and this corresponds directly to the above defined **yaw** angle. The remaining two angles, however, will not be represented by Euler's

description of rotation exactly, because the spin angle is measured on a plane the orientation of which depends on a nutation angle and hence the plane is not always vertical. Only if this plane stays close to the vertical one i.e. nutation angle approaches zero value the two definitions would converge. It is rather natural to expect the pitch angle to be of smaller magnitude than roll, and hence the **pitch** will be designated as the nutation angle. Deriving from this, the spin axis will be chosen to be normal to the transverse plane of the vessel and hence the spin angle, not always measured on a vertical plane, see Figure 74, will represent the **roll** angle of the vessel.

Note that there is no inherent sequence of rotations to be followed in order to achieve the orientation of the body in space as given by the three angles, again analyse carefully Figure 74.

1.4 Transformation tensor

As mentioned at the beginning of this chapter, to describe most efficiently motion and particularly rotation of the rigid body in space, relation between inertial and body-fixed reference frames is required. So a second step in defining rotations mathematically is to utilise coordinate systems to describe the just-adopted angles.

Let then consider two Cartesian sets of axis OXYZ and Gx'y'z', see Figure 8 and Figure 12, described by a set of unit vectors $\vec{i},\vec{j},\vec{k}$ and $\vec{i}',\vec{j}',\vec{k}'$ respectively, where the later can rotate with respect to the former considered as inertial, i.e. the unit vectors of which are constant.

It seems that the easiest way to define a relation between the two systems of reference is by resolving of a free vector in both of them, [110]. Let then vector $\vec{r} = x\cdot\vec{i} + y\cdot\vec{j} + z\cdot\vec{k}$ be expressed in OXYZ system. It may be resolved in Gx'y'z' by employing basic law of projection of a vector $\vec{r}$ onto a given direction $\vec{e}$, $r_e = \vec{e}\cdot\vec{r}$.

The three coordinates of vector $\vec{r}$, expressed in Gx'y'z' system can be found as:

$$x' = \vec{i}'\cdot\vec{r} = \vec{i}'\cdot\vec{i}\cdot x + \vec{i}'\cdot\vec{j}\cdot y + \vec{i}'\cdot\vec{k}\cdot z$$

$$y' = \vec{j}'\cdot\vec{r} = \vec{j}'\cdot\vec{i}\cdot x + \vec{j}'\cdot\vec{j}\cdot y + \vec{j}'\cdot\vec{k}\cdot z$$

$$z' = \vec{k}'\cdot\vec{r} = \vec{k}'\cdot\vec{i}\cdot x + \vec{k}'\cdot\vec{j}\cdot y + \vec{k}'\cdot\vec{k}\cdot z$$

When rewriting the above in matrix form, the following is obtained:

$$\begin{bmatrix} x' \\ y' \\ z' \end{bmatrix} = D \cdot \begin{bmatrix} x \\ y \\ z \end{bmatrix} \qquad (227)$$

Where:

$$D = \begin{bmatrix} \vec{i}'\cdot\vec{i} & \vec{i}'\cdot\vec{j} & \vec{i}'\cdot\vec{k} \\ \vec{j}'\cdot\vec{i} & \vec{j}'\cdot\vec{j} & \vec{j}'\cdot\vec{k} \\ \vec{k}'\cdot\vec{i} & \vec{k}'\cdot\vec{j} & \vec{k}'\cdot\vec{k} \end{bmatrix} \qquad (228)$$

Equation (227) shows how coordinates of one vector expressed in one of the reference systems can be expressed in another one rotated with respect to the first, provided the nine direction cosines, (228), between their axes are known. Now, since it has already been shown above that there are only three independent variables sufficient to fully describe the rotation, the above matrix will be a function of only these three parameters. For efficient parameterisation, however, some basic relation between rotation and its tensor representation must be quoted. Firstly it is worth pondering a rotation of two coordinate systems with respect to each other, the eigenvector of which is parallel to any of axes of these systems. Such rotation called then elementary or canonical, [113, p.68], allows for easy definition of the matrix D:

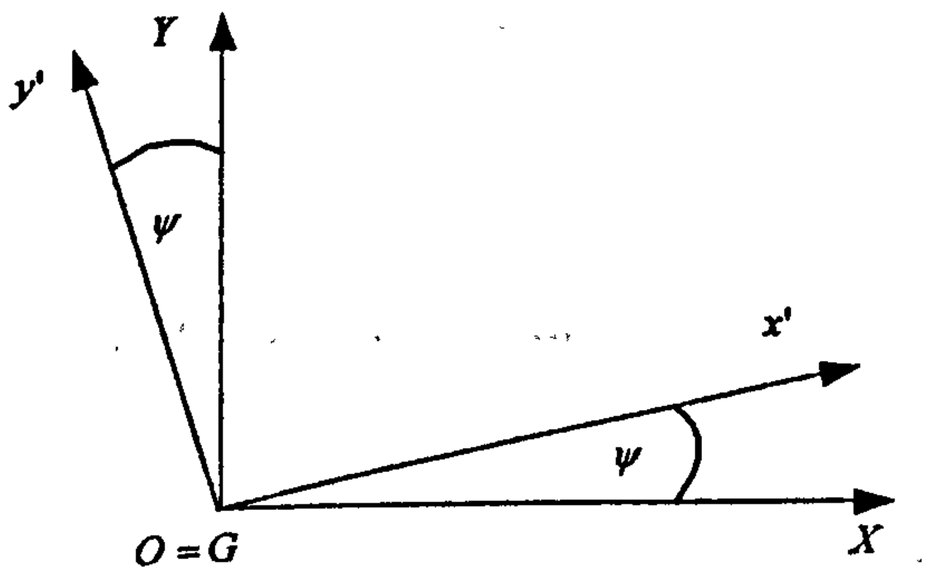

Eigenvector parallel to OZ or Gz'

$$\begin{bmatrix} x' \\ y' \\ z' \end{bmatrix} = [\Psi] \cdot \begin{bmatrix} x \\ y \\ z \end{bmatrix}$$

$$[\Psi] = \begin{bmatrix} \cos(\psi) & \sin(\psi) & 0 \\ -\sin(\psi) & \cos(\psi) & 0 \\ 0 & 0 & 1 \end{bmatrix}$$

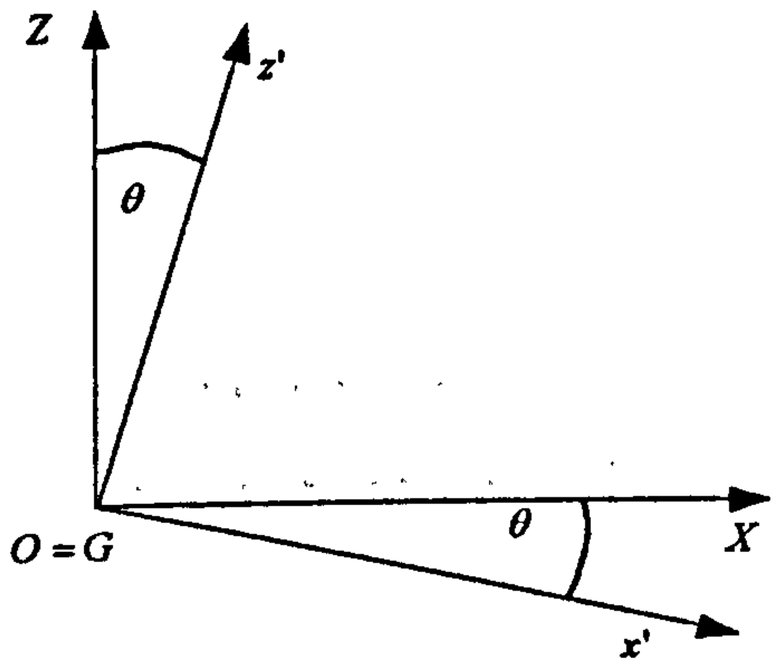

Eigenvector parallel to OY or Gy'

$$\begin{bmatrix} x' \\ y' \\ z' \end{bmatrix} = [\Theta] \cdot \begin{bmatrix} x \\ y \\ z \end{bmatrix}$$

$$[\Theta] = \begin{bmatrix} \cos(\theta) & 0 & -\sin(\theta) \\ 0 & 1 & 0 \\ \sin(\theta) & 0 & \cos(\theta) \end{bmatrix}$$

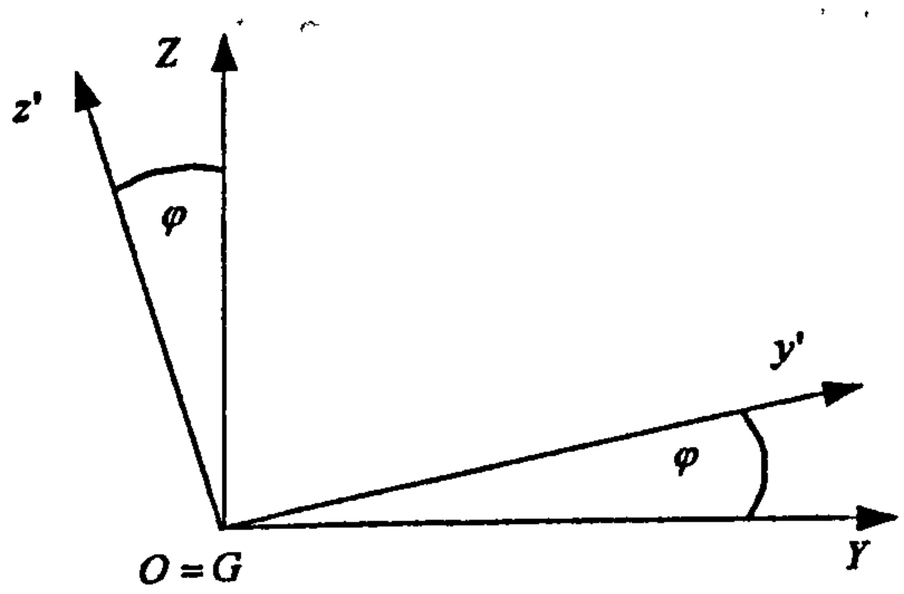

Eigenvector parallel to OX or Gx'

$$\begin{bmatrix} x' \\ y' \\ z' \end{bmatrix} = [\Phi] \cdot \begin{bmatrix} x \\ y \\ z \end{bmatrix}$$

$$[\Phi] = \begin{bmatrix} 1 & 0 & 0 \\ 0 & \cos(\varphi) & \sin(\varphi) \\ 0 & -\sin(\varphi) & \cos(\varphi) \end{bmatrix}$$

Secondly, a rotation and its tensor representation can be composed of a number of rotations, i.e. if

$$\begin{bmatrix} x'_1 \\ y'_1 \\ z'_1 \end{bmatrix} = [D_1] \cdot \begin{bmatrix} x \\ y \\ z \end{bmatrix} \text{ and } \begin{bmatrix} x'_2 \\ y'_2 \\ z'_2 \end{bmatrix} = [D_2] \cdot \begin{bmatrix} x'_1 \\ y'_1 \\ z'_1 \end{bmatrix}, \text{ then } \begin{bmatrix} x'_2 \\ y'_2 \\ z'_2 \end{bmatrix} = [D_2] \cdot [D_1] \cdot \begin{bmatrix} x \\ y \\ z \end{bmatrix}, \text{ and so on.}$$

This means that the matrix D can be composed, for great simplicity, from the canonical rotation matrixes, $[\Psi]$, $[\Theta]$ and $[\Phi]$. There is, however, a sequence of the elementary rotations and hence matrix multiplication to be followed in order to adhere to Euler's angles as described above, see Figure 74:

First rotation around axis normal to horizontal plane, OZ or Gz', has to take place, which rotates spin axis (parallel to Gx') with yaw/precession angle ψ. The matrix representation will be:

$$\begin{bmatrix} x'_1 \\ y'_1 \\ z'_1 \end{bmatrix} = [\Psi] \cdot \begin{bmatrix} x \\ y \\ z \end{bmatrix}$$

Second rotation with the pitch/nutation angle θ, takes place around nodal axis Gy' i.e. the axis resultant from intersection between planes: horizontal and normal to spin axis, and defines orientation of spin axis in vertical plane: $\begin{bmatrix} x'_2 \\ y'_2 \\ z'_2 \end{bmatrix} = [\Theta] \cdot [\Psi] \cdot \begin{bmatrix} x \\ y \\ z \end{bmatrix}$

The third rotation takes place around spin axis Gx' with roll/spin angle φ,

$$\begin{bmatrix} x'_3 \\ y'_3 \\ z'_3 \end{bmatrix} = [\Phi] \cdot [\Theta] \cdot [\Psi] \cdot \begin{bmatrix} x \\ y \\ z \end{bmatrix}$$

See Figure 75. This implies that the relation between body-fixed and inertial coordinate systems and based on Euler's angles has the following matrix representation:

$$D = [\Phi] \cdot [\Theta] \cdot [\Psi]$$

And after multiplication:

$$D = \begin{bmatrix} \cos(\theta)\cdot\cos(\psi) & \cos(\theta)\cdot\sin(\psi) & -\sin(\theta) \\ \sin(\varphi)\cdot\sin(\theta)\cdot\cos(\psi) - \cos(\varphi)\cdot\sin(\psi) & \sin(\varphi)\cdot\sin(\theta)\cdot\sin(\psi) + \cos(\varphi)\cdot\cos(\psi) & \sin(\varphi)\cdot\cos(\theta) \\ \cos(\varphi)\cdot\sin(\theta)\cdot\cos(\psi) + \sin(\varphi)\cdot\sin(\psi) & \cos(\varphi)\cdot\sin(\theta)\cdot\sin(\psi) - \sin(\varphi)\cdot\cos(\psi) & \cos(\varphi)\cdot\cos(\theta) \end{bmatrix} \quad (229)$$

Note that the different sequence of elementary rotations considered, when defining rotation matrix, would not correspond to Euler's angles as defined by Figure 74.

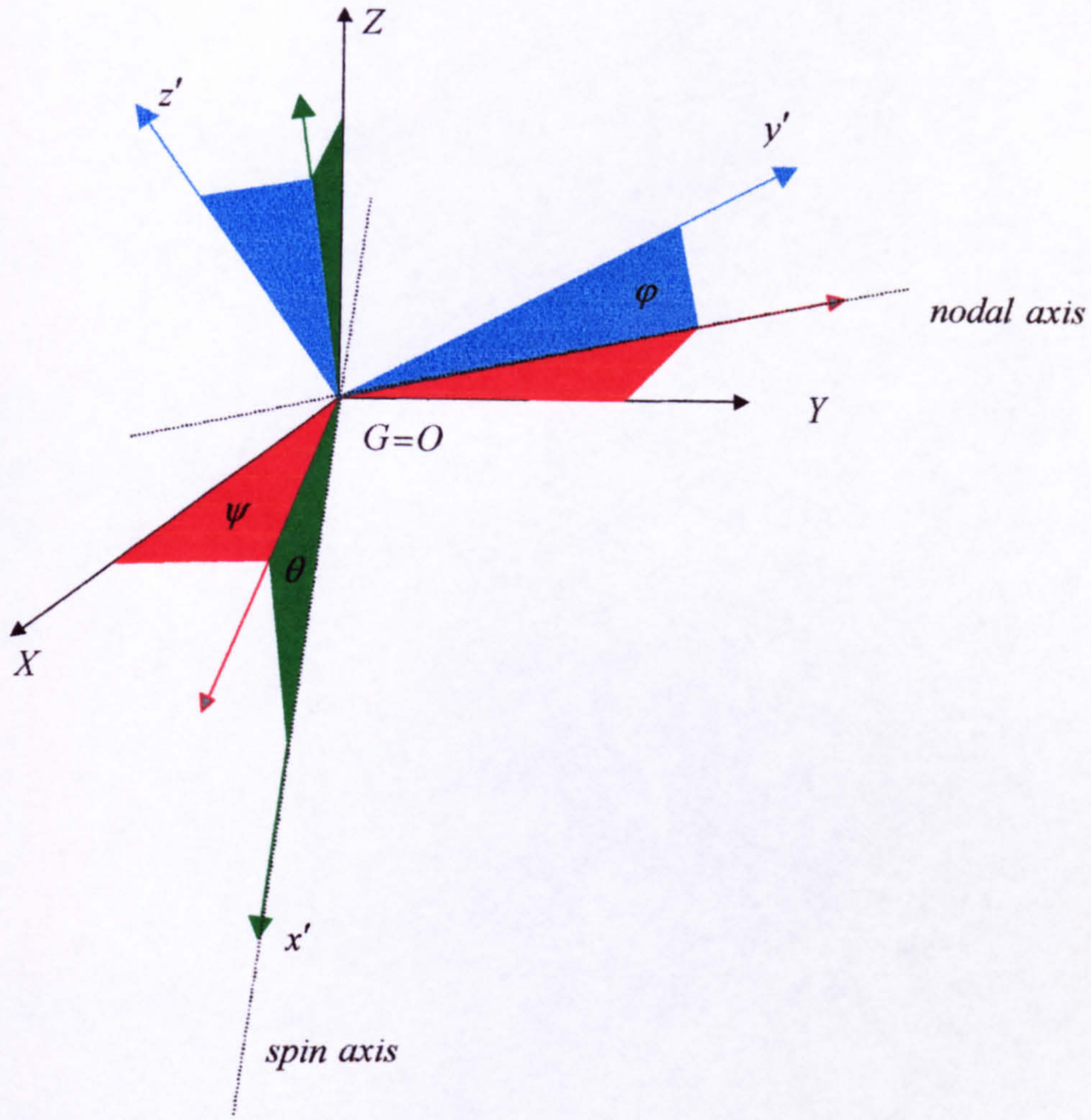

Figure 75 Definition of relation between inertial and body-fixed coordinate systems

1.5 Angular velocities

Having defined the mathematical expression defining orientation of two coordinate systems with respect to each other, a practical question now arises as to how to express the ratio of change in this orientation and deriving from that how to determine the Euler angular parameters. This chapter aims at answering these questions.

Generally, the angular velocity can be expressed in the following vector form:

$$\dot{\vec{\chi}} = \dot{\varphi} \cdot \vec{e}_1 + \dot{\theta} \cdot \vec{e}_2 + \dot{\psi} \cdot \vec{e}_3 \qquad (230)$$

Where:

$$\dot{\varphi}\cdot\vec{e}_1 \equiv \dot{\vec{\varphi}}$$
$$\dot{\theta}\cdot\vec{e}_2 \equiv \dot{\vec{\theta}} \qquad (231)$$
$$\dot{\psi}\cdot\vec{e}_3 \equiv \dot{\vec{\psi}}$$

$\vec{e}_1, \vec{e}_2, \vec{e}_3$ Time dependent unit vectors defining axes around which the rotations take place. Note that the unit vectors can be resolved in either body-fixed or inertial coordinate systems. (232)

Furthermore:

$$\dot{\varphi} = \lim_{\Delta t \to 0} \frac{\Delta\varphi}{\Delta t} \qquad \dot{\theta} = \lim_{\Delta t \to 0} \frac{\Delta\theta}{\Delta t} \qquad \dot{\psi} = \lim_{\Delta t \to 0} \frac{\Delta\psi}{\Delta t} \qquad (233)$$

1.5.1 Infinitesimal rotations

Let us consider a rotation, defined by matrix (229) and taking place within infinitesimal interval of time Δt when the angles of rotation approach zero, $\Delta\varphi, \Delta\theta, \Delta\psi \to 0$, see expression (235). In this case square and higher powers of a rotation angles can be neglected and their trigonometric functions can be approximated as $\cos(\Delta\chi) = 1$ and $\sin(\Delta\chi) = \Delta\chi$. The rotation matrix (229) can then be expressed as (234):

$$D_{\Delta\varphi,\Delta\theta,\Delta\psi\to 0} = \begin{bmatrix} 1 & \Delta\psi & -\Delta\theta \\ -\Delta\psi & 1 & \Delta\varphi \\ \Delta\theta & -\Delta\varphi & 1 \end{bmatrix} \qquad (234)$$

$$\begin{bmatrix} \vec{i}'(t+\Delta t) \\ \vec{j}'(t+\Delta t) \\ \vec{k}'(t+\Delta t) \end{bmatrix} = D_{\Delta\varphi,\Delta\theta,\Delta\psi\to 0} \cdot \begin{bmatrix} \vec{i}'(t) \\ \vec{j}'(t) \\ \vec{k}'(t) \end{bmatrix} \qquad (235)$$

An assumption of infinitesimal rotations, leading subsequently to commutative rotation matrix given by (234), allows to reason that the vectors (232) around which the rotation take place correspond to axes of the rotated coordinate system, that is:

$$\begin{aligned} \vec{e}_1 &\rightarrow \vec{i}' \\ \vec{e}_2 &\rightarrow \vec{j}' \\ \vec{e}_3 &\rightarrow \vec{k}' \end{aligned} \qquad (236)$$

Denoting now the angular velocities around each of the respective axes as (237), leads to the definition derived from (230) of the well known instantaneous rotational velocity vector (238), ref. [97, p.24].

$$\dot{\varphi} \equiv \omega'_x \qquad \dot{\theta} \equiv \omega'_y \qquad \dot{\psi} \equiv \omega'_z \qquad (237)$$

Note that the components (237) in vector (238) define the instantaneous axis of rotation expressed in body-fixed coordinate system.

$$\dot{\vec{\chi}}_{\Delta\varphi,\Delta\theta,\Delta\psi\rightarrow 0} \rightarrow \vec{\omega} \qquad (238)$$

$$\vec{\omega} = \omega'_x \cdot \vec{i}' + \omega'_y \cdot \vec{j}' + \omega'_z \cdot \vec{k}'$$

1.5.2 Ratio change in orientation

The ratio of change in the orientation of rotating coordinate system can be defined as:

$$\begin{bmatrix} \frac{\Delta}{\Delta t}\vec{i}' \\ \frac{\Delta}{\Delta t}\vec{j}' \\ \frac{\Delta}{\Delta t}\vec{k}' \end{bmatrix} \equiv \begin{bmatrix} \frac{\vec{i}'(t+\Delta t)-\vec{i}'(t)}{\Delta t} \\ \frac{\vec{j}'(t+\Delta t)-\vec{j}'(t)}{\Delta t} \\ \frac{\vec{k}'(t+\Delta t)-\vec{k}'(t)}{\Delta t} \end{bmatrix} \qquad (239)$$

Following from (235) and (234) allows to express definition (239) as:

$$\begin{bmatrix} \frac{\Delta}{\Delta t}\vec{i}' \\ \frac{\Delta}{\Delta t}\vec{j}' \\ \frac{\Delta}{\Delta t}\vec{k}' \end{bmatrix} = \frac{D_{\Delta\varphi,\Delta\theta,\Delta\psi\to 0} - I}{\Delta t} \cdot \begin{bmatrix} \vec{i}' \\ \vec{j}' \\ \vec{k}' \end{bmatrix} \qquad (240)$$

After rearrangement, (240) can be further rewritten as follows:

$$\begin{bmatrix} \frac{\Delta}{\Delta t}\vec{i}' \\ \frac{\Delta}{\Delta t}\vec{j}' \\ \frac{\Delta}{\Delta t}\vec{k}' \end{bmatrix} = \begin{bmatrix} 0 & \frac{\Delta\psi}{\Delta t} & \frac{-\Delta\theta}{\Delta t} \\ \frac{-\Delta\psi}{\Delta t} & 0 & \frac{\Delta\varphi}{\Delta t} \\ \frac{\Delta\theta}{\Delta t} & \frac{-\Delta\varphi}{\Delta t} & 0 \end{bmatrix} \cdot \begin{bmatrix} \vec{i}' \\ \vec{j}' \\ \vec{k}' \end{bmatrix} \qquad (241)$$

Deriving finally from (233) and (237) and replacing finite difference notations by differentials leads to the following expression for (241):

$$\begin{bmatrix} \frac{d}{dt}\vec{i}' \\ \frac{d}{dt}\vec{j}' \\ \frac{d}{dt}\vec{k}' \end{bmatrix} = \begin{bmatrix} 0 & \omega'_z & -\omega'_y \\ -\omega'_z & 0 & \omega'_x \\ \omega'_y & -\omega'_x & 0 \end{bmatrix} \cdot \begin{bmatrix} \vec{i}' \\ \vec{j}' \\ \vec{k}' \end{bmatrix} \qquad (242)$$

Which can be alternatively expressed in the following form:

$$\frac{d}{dt}\vec{i}' = \vec{\omega} \times \vec{i}' \qquad \frac{d}{dt}\vec{j}' = \vec{\omega} \times \vec{j}' \qquad \frac{d}{dt}\vec{k}' = \vec{\omega} \times \vec{k}' \qquad (243)$$

1.5.3 Finite rotations

It was shown above that when infinitesimal rotations are considered the angular velocity vector, (230) could be directly expressed using Cartesian coordinate axes, (238). However, when the

rotation angles have finite values it is easily noticeable that axes (232) around which Euler's angles are measured, are not parallel to either inertial or body-fixed reference frame axes, see Figure 76. Therefore it is not possible to determine ships orientation by direct differentiation of this vector. It is practicable, however, to derive a relation between the instantaneous angular velocity vector and rates of change of Euler angles, which after differentiation will allow to predict vessel orientation in space using matrix (229).

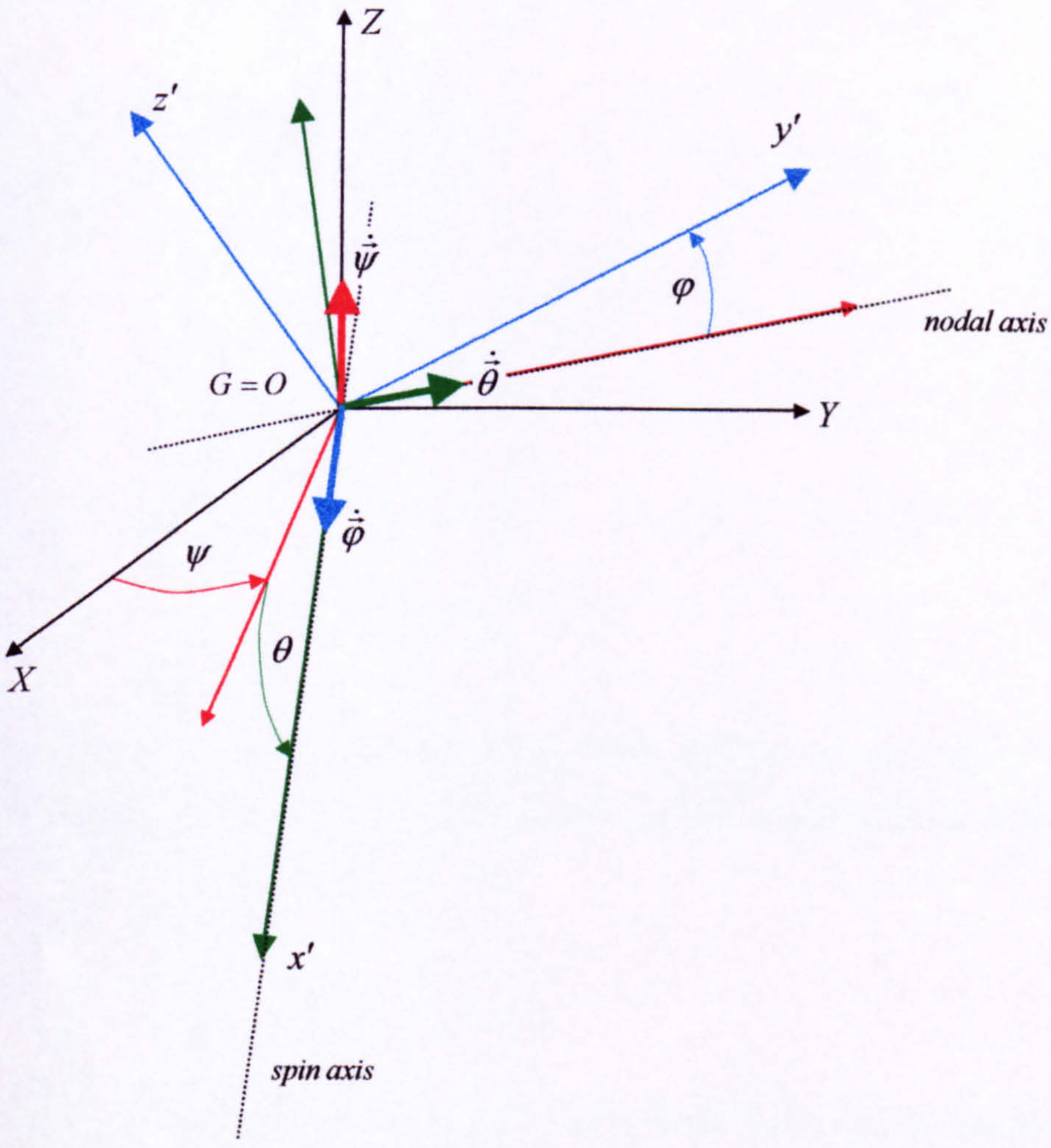

Figure 76 Kinematic relation between Euler and Cartesian angular velocities

For finite rotations, the unit vectors (232), about which rotations take place, when resolved in inertial coordinate system OXYZ as shown in Figure 76, will take the form:

$$\begin{aligned}\vec{e}_1 &= \cos(\theta)\cdot\cos(\psi)\cdot\vec{i} + \cos(\theta)\cdot\sin(\psi)\cdot\vec{j} - \sin(\theta)\cdot\vec{k}\\ \vec{e}_2 &= -\sin(\psi)\cdot\vec{i} + \cos(\psi)\cdot\vec{j}\\ \vec{e}_3 &= \vec{k}\end{aligned} \qquad (244)$$

Formulae (244) is sometimes referred to as "Euler's geometrical relation", [98, p.196]. Note again that these vectors are resolved in "earth" coordinate system.

Applying (244) in (231) and (230), allows to express the angular velocity vector as coordinates in the (inertial) Cartesian system of reference (written here, for simplicity, in the matrix form):

$$\begin{bmatrix}\omega_X\\ \omega_Y\\ \omega_Z\end{bmatrix} = \begin{bmatrix}\cos(\theta)\cdot\cos(\psi) & -\sin(\psi) & 0\\ \cos(\theta)\cdot\sin(\psi) & \cos(\psi) & 0\\ -\sin(\theta) & 0 & 1\end{bmatrix}\cdot\begin{bmatrix}\dot{\varphi}\\ \dot{\theta}\\ \dot{\psi}\end{bmatrix} \qquad (245)$$

Or for clarity:

$$\vec{\omega} = [\beta]\cdot\begin{bmatrix}\dot{\varphi}\\ \dot{\theta}\\ \dot{\psi}\end{bmatrix} \qquad (246)$$

Note the difference between (238) and (246). When the rotational velocity vector $\vec{\omega}'$ is known in body-fixed coordinate system, it can be expressed in earth one by using relations (227) and (229):

$$\vec{\omega} = D^{-1}\cdot\vec{\omega}' \qquad (247)$$

So finally, the relation between rates of change of Euler's angles and rotation velocities about axes of Cartesian body-fixed coordinate system are given as:

$$\begin{bmatrix}\dot{\varphi}\\ \dot{\theta}\\ \dot{\psi}\end{bmatrix} = [\beta]^{-1}\cdot D^{-1}\cdot\vec{\omega}' \qquad (248)$$

Appendix 2

Validation studies on numerical predictions of intact ship hydrodynamics

1 Summary

As presented in the thesis, the key part of any numerical modelling of ship motions establishes around the accuracy of predicting the hydrodynamic properties of the hull. Mathematical models of the fluid flow accounting for the presence of a free surface are overly complex and therefore simplifications must be adopted, as discussed in detail in §6. The major assumptions allowing for derivation of vessel hydrodynamics in this thesis are that of potential character of fluid flow and the slender body shape. The hydrodynamic coefficients and forces (in form of added mass, damping and diffraction forces following preposition of oscillatory character of motions) for a ship are derived from integration of 2D section (strip) fluid forces, §6.6.

This Appendix contains study into validity of numerical code developed on the bases of mathematical model adopted and presented in §6.5 and §6.6. The derived coefficients for 2D cylinders are compared with experimental data found in open literature,. The hydrodynamic coefficients and forces for two 3D monohull forms, Wigley1 and Series60, CB=0.7, are compared with results derived from experiments e.g. Journee [47] as well as available advanced 3D-panel methods, Taebum Ha [39] and Papanikolaou [63]. Note that all of the coefficients are derived for point of rotation assumed at the calm water plane level.

The study for a series of 2D sections and different modes of motions are shown in Figure 1 to Figure 20. Except for roll mode of motion, there is generally good agreement between results derived by means of experiments or different numerical schemes for section shapes varying from rectangle, circle to triangle. As has been documented in the literature, e.g. by Ikeda at al, the predictions of fluid forces based on potential flow approximation fail for the roll mode where the flow often displays highly vorticular and hence non-linear character. The order of these discrepancies is demonstrated in Figure 13, Figure 14, Figure 19 and Figure 20.

Figure 23 to Figure 30 display the investigation on the radiation coefficients for the mentioned typical example of slender hull geometry, the Wigly1 form, in heading seas at Fn=0.2. As can be seen, the agreement between the strip theory applied and coded in this work and the experimental values is acceptable. Some noted discrepancies especially for cross-coupling coefficients (pitch-heave) show consistent trends as any other strip theory. Generally the 3D techniques show closer agreement to the experiment, but some numerical problems are noticeable in irregularities in the frequency curves.

In Figure 33 to Figure 47, study has been performed on the excitation forces and moments, based on the fairly representative of real ship hull form, the Series 60, for beam and heading seas at zero speed. As can be seen, the trends in curves are clearly distinguishable, and allow assessing consistency of strip theory predictions. Some differences between the two methods can be noted in case of predictions of the excitation forces and moments amplitudes as is demonstrated by the slight disagreement in heave (and hence in pitch) mode of motion, Figure 40. The disagreement is a clear result of under-predictions of the heave diffraction forces, which problem has not been resolved at this stage but seem insignificant for heave mode of motion. Perhaps, care must be taken when applying this strip theory code for simulations of motions in conditions leading to significant pitch oscillations (i.e. heading other than beam seas).

It is not quite clear, which of the methods approximate better the experimental hydrodynamic coefficients available for the case of heading seas and Fn=0.2, Figure 48 to Figure 64. It seems, for instance that the sway & heave damping coefficients, Figure 49 or Figure 51, are better approximated by the strip theory. Quite substantial discrepancy between the two 3D methods can be seen for the roll damping coefficient, Figure 55, where the experimental coefficients are approximated closest by the 3D NEWDRIFT code. Clearly, also the sway added mass, Figure 48, is best approximated by the NEWDRIFT. Consistency between the two 3D codes as well as their somewhat better than 2D-theory accuracy can be seen in predictions of heave-pitch cross-coupling coefficients, Figure 52 or Figure 64. However, in case of the yaw coefficients, Figure 60 and Figure 61, only the HA code proves accurate. Such overall inconsistencies between the different software calculations are emphasised by predictions of heave damping coefficient, Figure 51, where the NEWDRIFT is the least accurate code, or the pitch damping coefficient, Figure 59, where in turn the 3D HA code is the least accurate. It is rather rare that the results from the three codes converge to the degree that can be seen in predictions of heave added mass, Figure 50. Poor match of the experimental roll-into-sway damping coefficient shown in Figure 57 by all three codes, or lack of convergence in their predictions seen for instance in Figure 54, Figure 56, Figure 62 or Figure 63, adds to some level of uncertainty as regards predictions of ship hydrodynamics by the available tools.

Therefore, in view of the above discussion addressing the degree of coherence in the derived results, it can be considered that the methods for treatment of the physical phenomenon of ship hydrodynamic response are in need of further research considering both the mathematical formulation of the problem as well as their numerical solutions.

However, as the experience of the last few decades shows, the type of the methods used in this exercise is very successful in resolving many engineering issues involving ship motion problems. Therefore it can be concluded that such techniques, including strip theory applied in this thesis, are sufficiently accurate for predicting ship hydrodynamic properties, even if some inconsistencies can be identified. This assertion will be put to ultimate test in studies addressing ship motion as well as survivability predictions.

2 Comparative study

2.1 Hydrodynamic coefficients in two dimensions

For convenience all of the 2D coefficients are non-dimensionalised in the following manner:

Table 1 Non-dimensional form of 2D hydrodynamic coefficients

$$\omega[-]=\frac{\left(\omega\left[\frac{rad}{s}\right]\right)^2\cdot R[m]}{g\left[\frac{m}{s^2}\right]} \qquad R\rightarrow\begin{cases} radius\ for\ circle \\ beam\ for\ other\ shapes \end{cases}$$ sway & heave

$$\omega[-]=\omega\left[\frac{rad}{s}\right]\cdot\sqrt{\frac{B[m]}{2\cdot g\left[\frac{m}{s^2}\right]}}$$ roll & sway-roll

$$a_{22},a_{33}[-]=\frac{a_{22},a_{33}\left[\frac{kg}{m}\right]}{\rho\left[\frac{kg}{m^3}\right]\cdot area[m^2]} \qquad b_{22},b_{33}[-]=\frac{b_{22},b_{33}\left[\frac{kg}{m\cdot s}\right]}{\omega\left[\frac{rad}{s}\right]\cdot\rho\left[\frac{kg}{m^3}\right]\cdot area[m^2]}$$

$$a_{44}[-]=\frac{a_{44}\left[\frac{kg\cdot m^2}{m}\right]}{\rho\left[\frac{kg}{m^3}\right]\cdot area[m^2]\cdot(B[m])} \qquad b_{44}[-]=\frac{b_{44}\left[\frac{kg\cdot m^2}{m\cdot s}\right]}{\rho\left[\frac{kg}{m^3}\right]\cdot area[m^2]\cdot(B[m])^2\cdot\sqrt{\frac{2\cdot g\left[\frac{m}{s^2}\right]}{B[m]}}}$$

$$a_{24}[-]=\frac{a_{24}\left[\frac{kg\cdot m}{m}\right]}{\rho\left[\frac{kg}{m^3}\right]\cdot area[m^2]\cdot B[m]} \qquad b_{24}[-]=\frac{b_{24}\left[\frac{kg\cdot m}{m\cdot s}\right]}{\rho\left[\frac{kg}{m^3}\right]\cdot area[m^2]\cdot B[m]\cdot\sqrt{\frac{2\cdot g\left[\frac{m}{s^2}\right]}{B[m]}}}$$

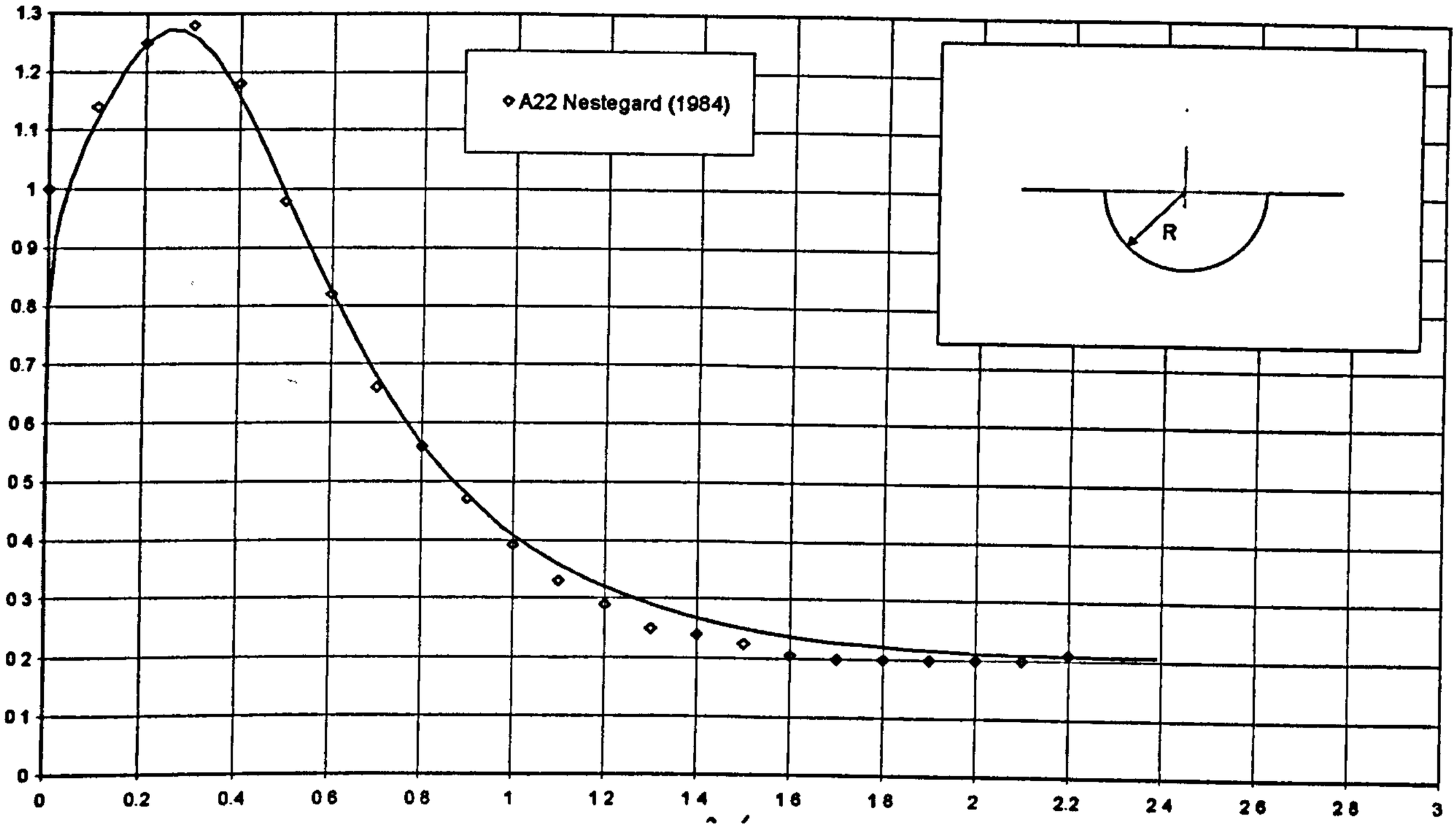

Figure 1 Dimensionless added mass in sway for 2D half-cylindrical hull form, comparison between predictions by 2D method and experiments. Solid line is derived by means of PROTEUS3.

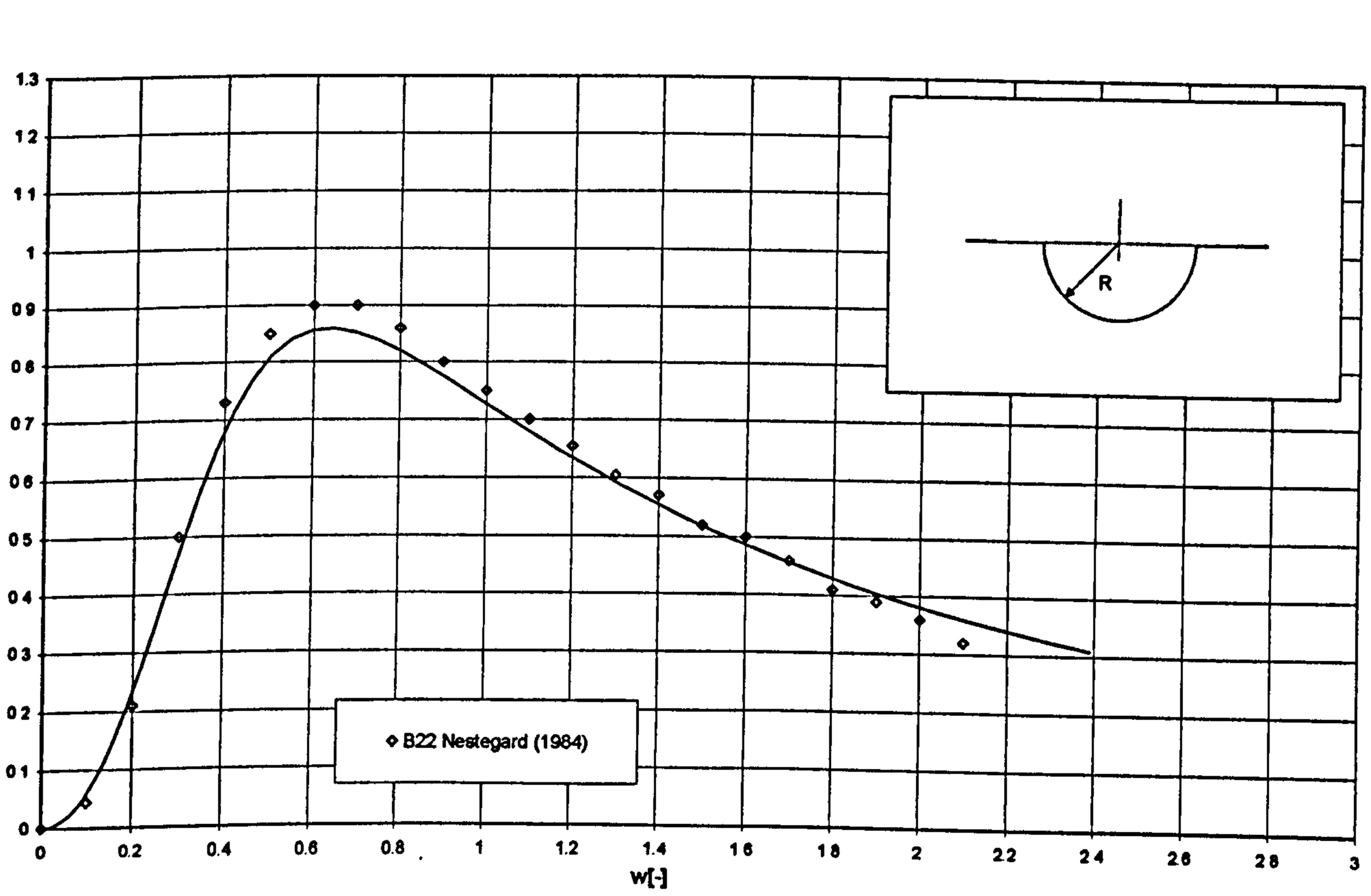

Figure 2 Dimensionless potential damping in sway for 2D half-cylindrical hull form, comparison between predictions by 2D method and experiments. Solid line is derived by means of PROTEUS3.

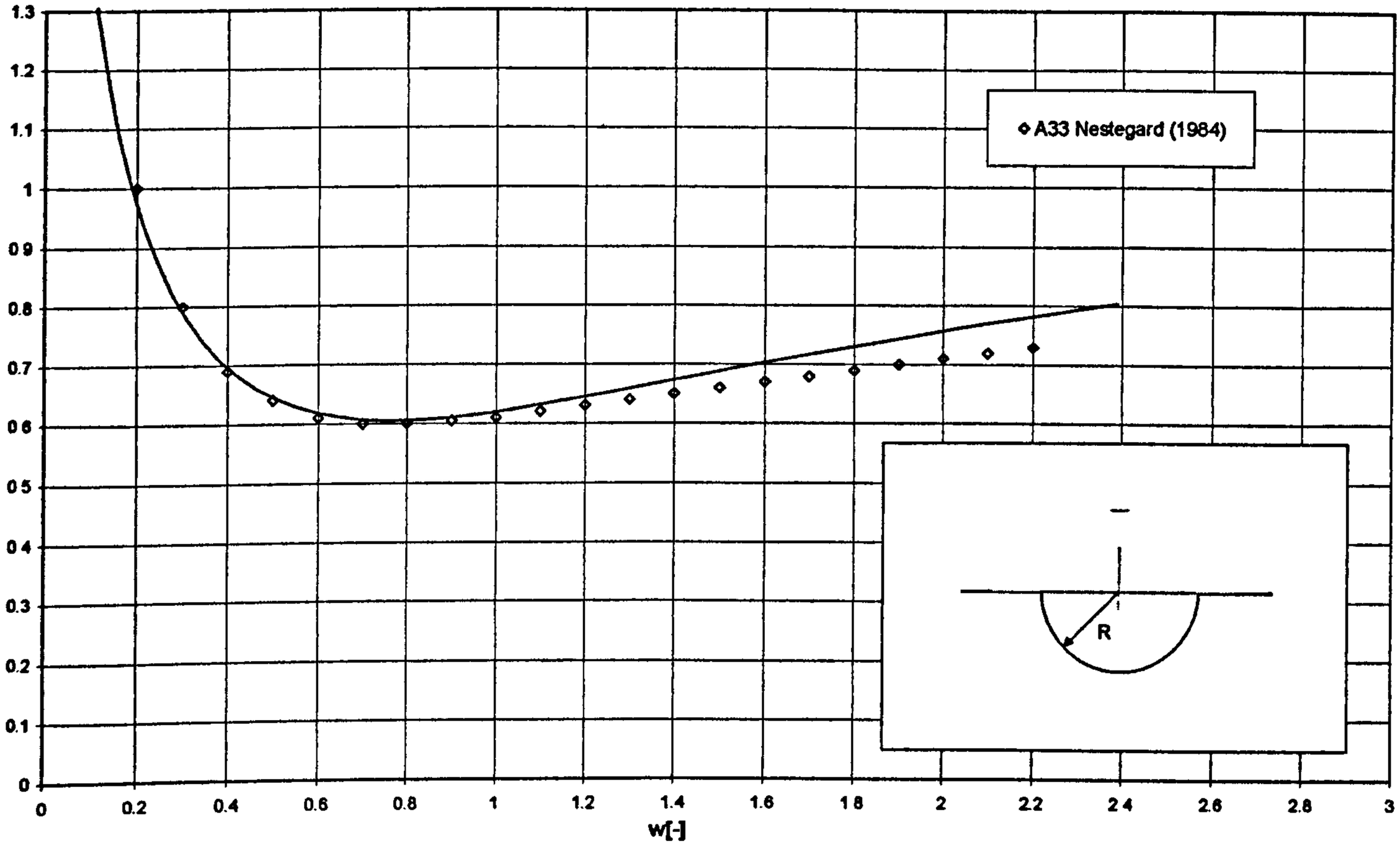

Figure 3 Dimensionless added mass in heave for 2D half-cylindrical hull form, comparison between predictions by 2D method and experiments. Solid line is derived by means of PROTEUS3.

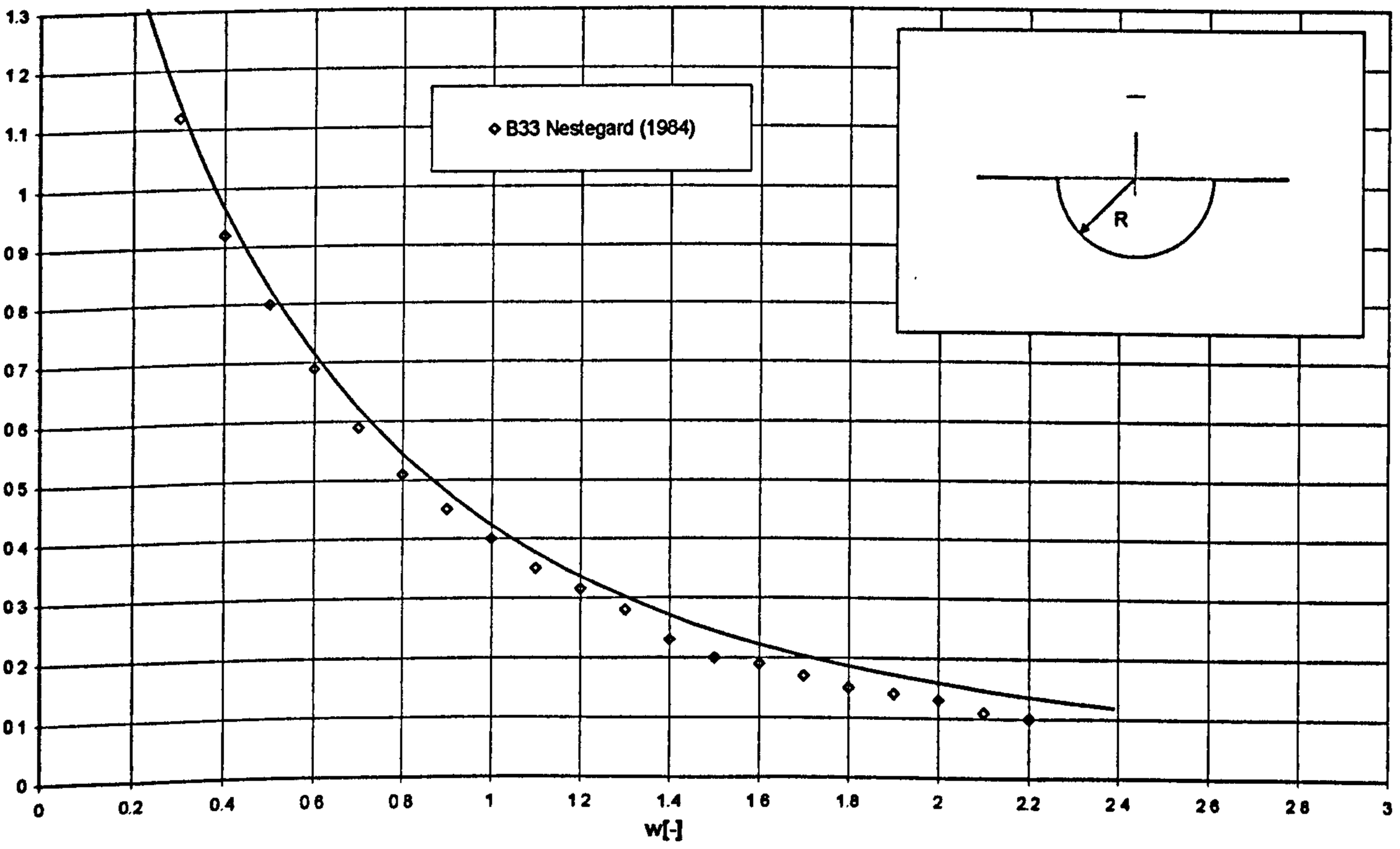

Figure 4 Dimensionless potential damping in heave for 2D half-cylindrical hull form, comparison between predictions by 2D method and experiments. Solid line is derived by means of PROTEUS3.

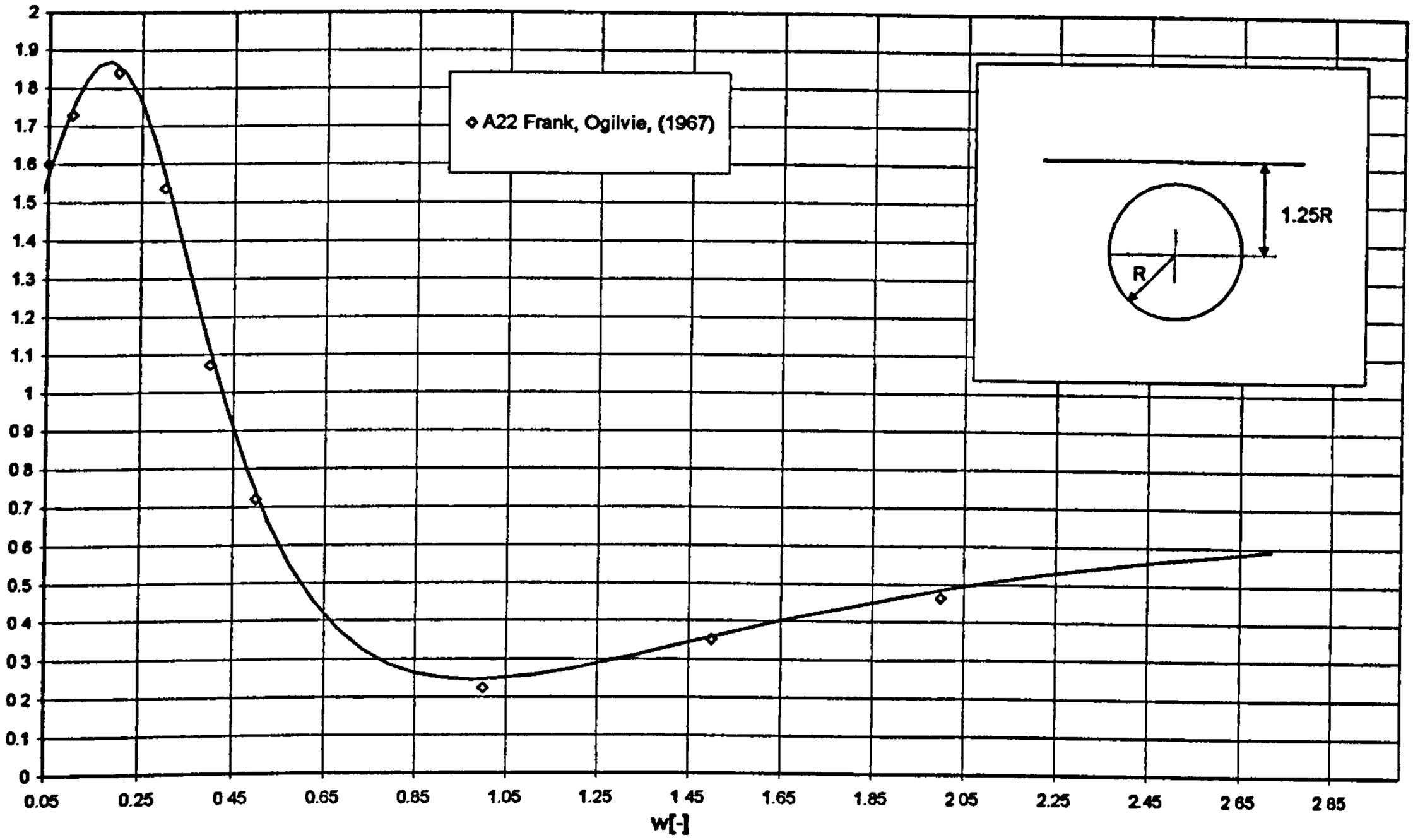

Figure 5 Dimensionless added mass in sway for fully submerged 2D cylindrical hull form, comparison between predictions by 2D method and experiments. Solid line is derived by means of PROTEUS3.

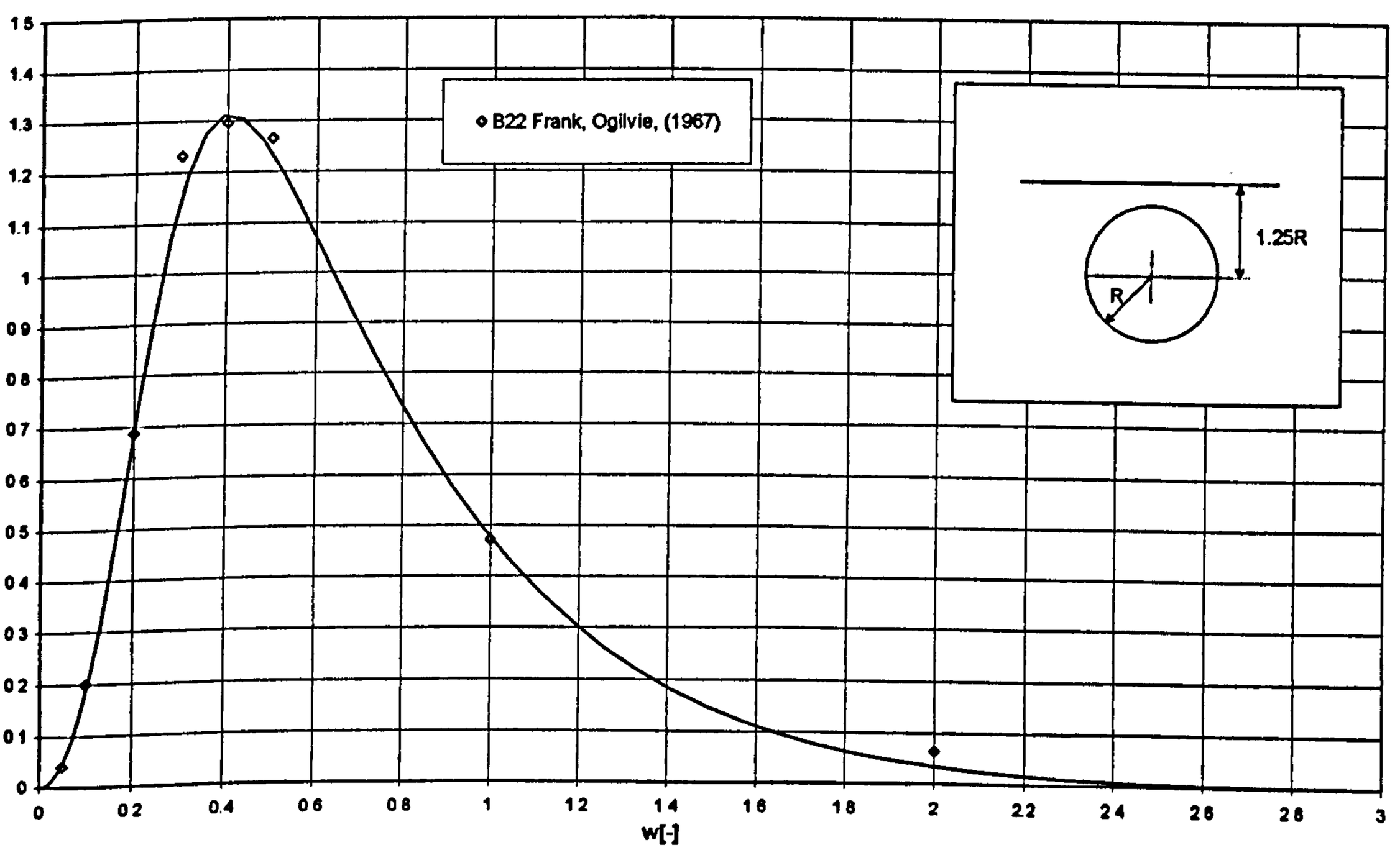

Figure 6 Dimensionless potential damping in sway for fully submerged 2D cylindrical hull form, comparison between predictions by 2D method and experiments. Solid line is derived by means of PROTEUS3.

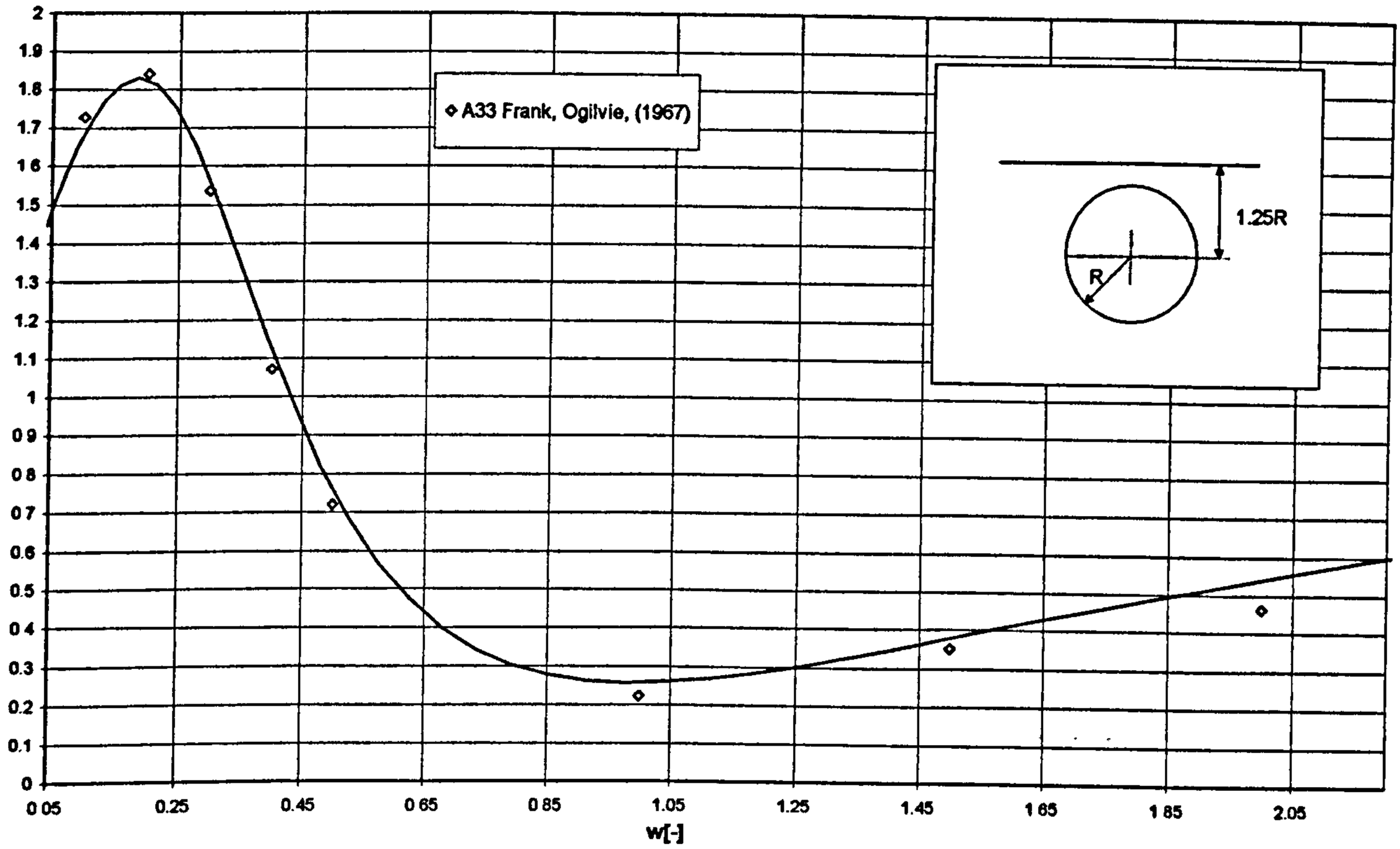

Figure 7 Dimensionless added mass in heave for fully submerged 2D cylindrical hull form, comparison between predictions by 2D method and experiments. Solid line is derived by means of PROTEUS3.

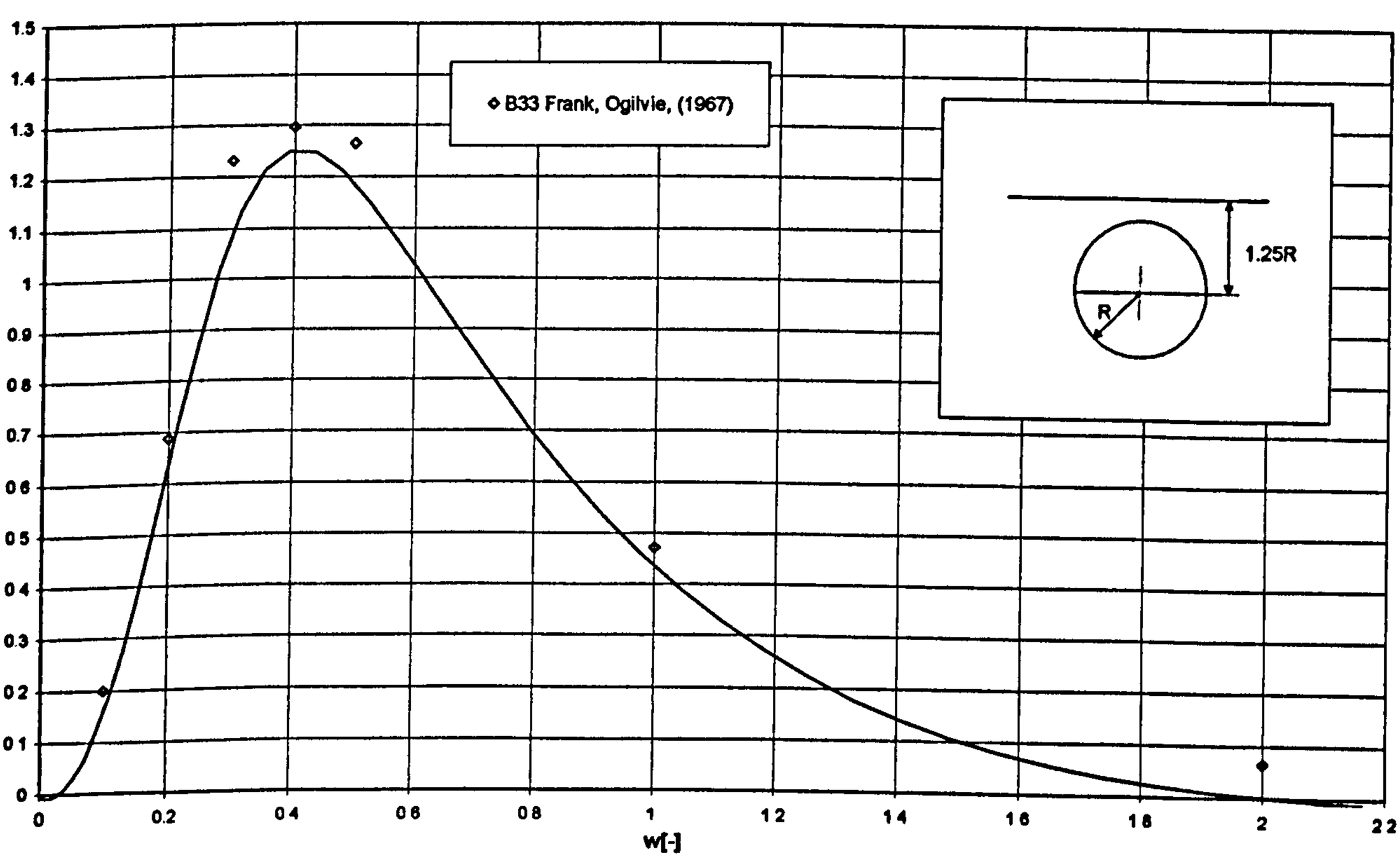

Figure 8 Dimensionless potential damping in heave for fully submerged 2D cylindrical hull form, comparison between predictions by 2D method and experiments. Solid line is derived by means of PROTEUS3.

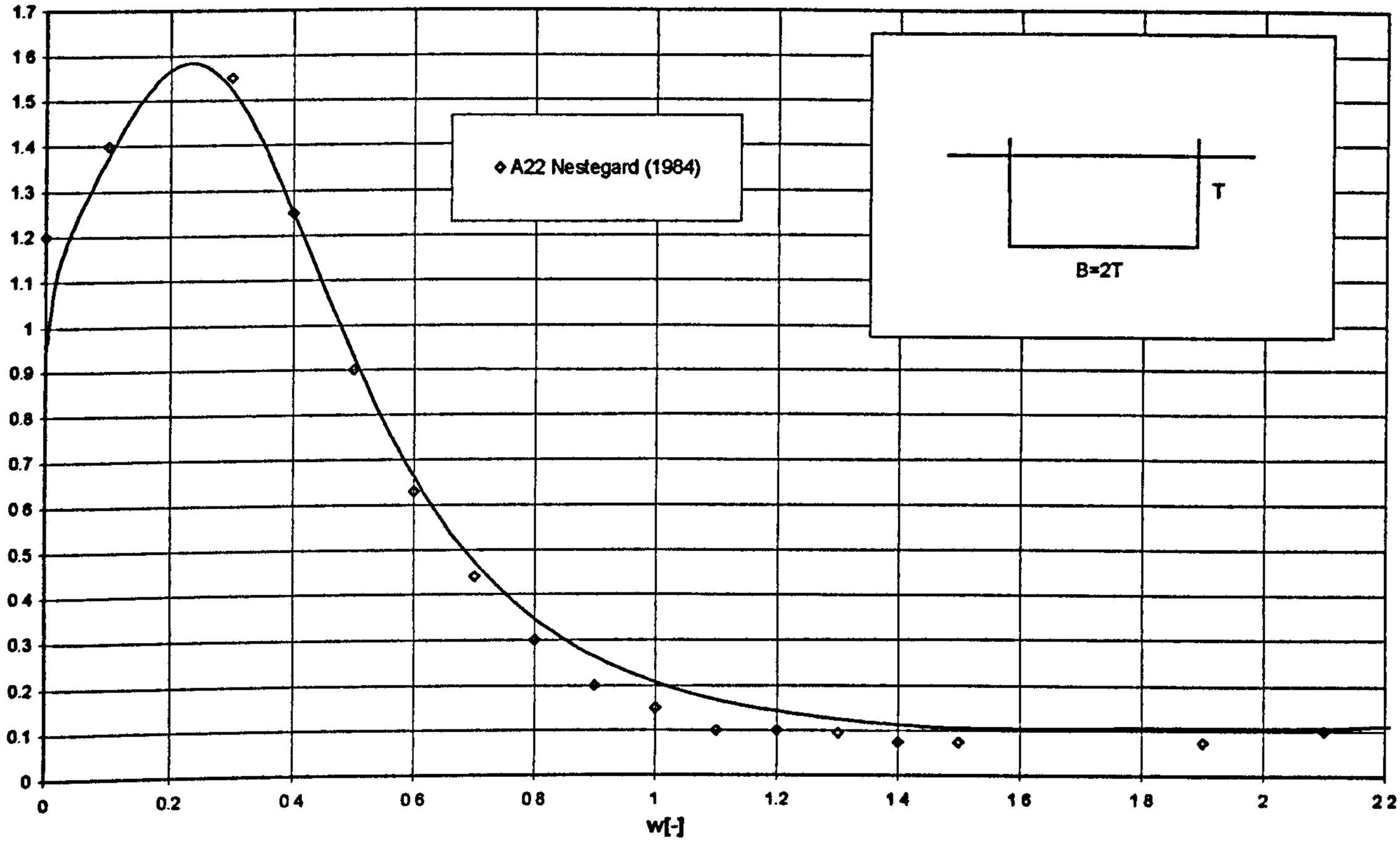

Figure 9 Dimensionless added mass in sway for 2D rectangular hull form, comparison between predictions by 2D method and experiments. Solid line is derived by means of PROTEUS3.

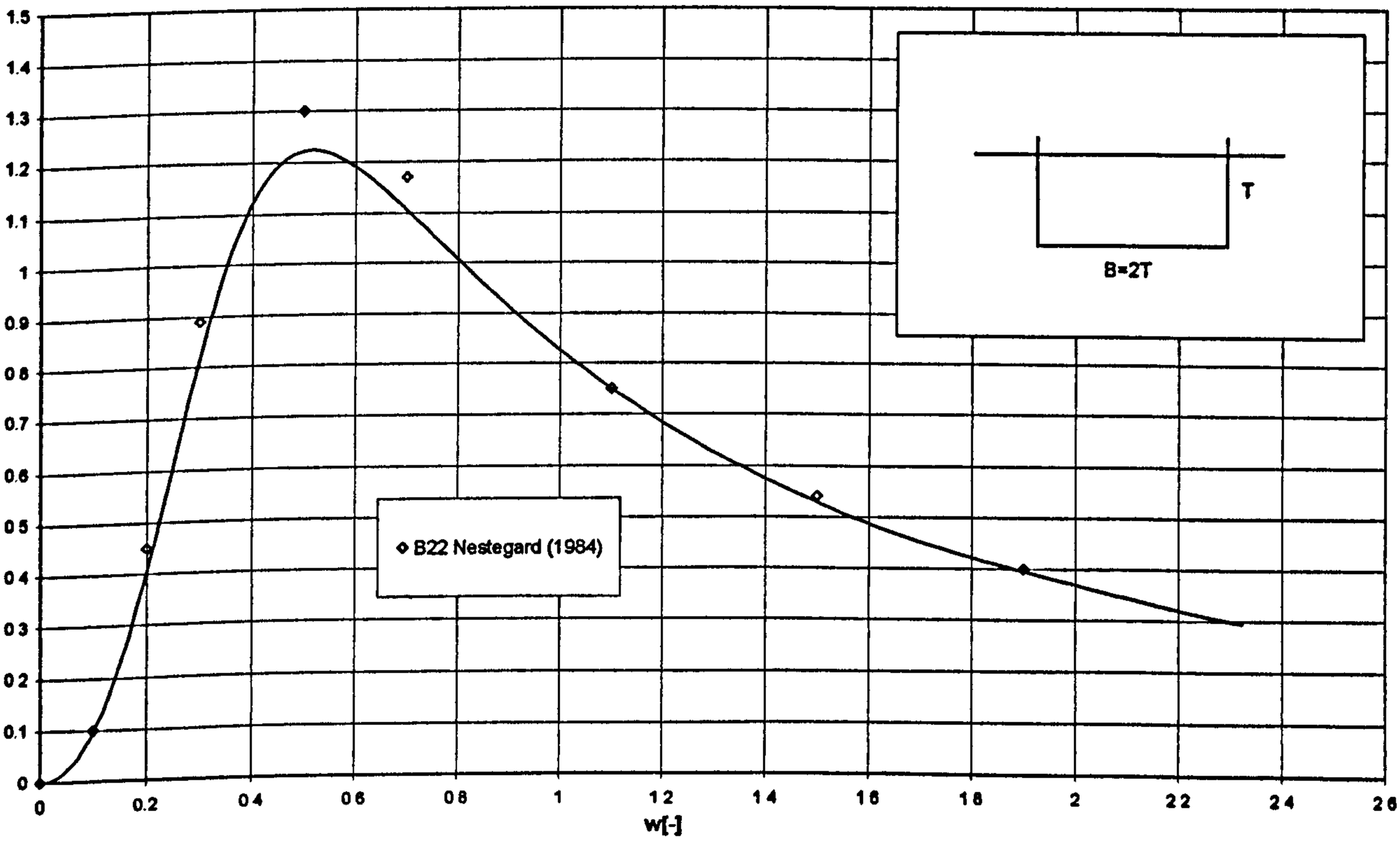

Figure 10 Dimensionless potential damping in sway for 2D rectangular hull form, comparison between predictions by 2D method and experiments. Solid line is derived by means of PROTEUS3.

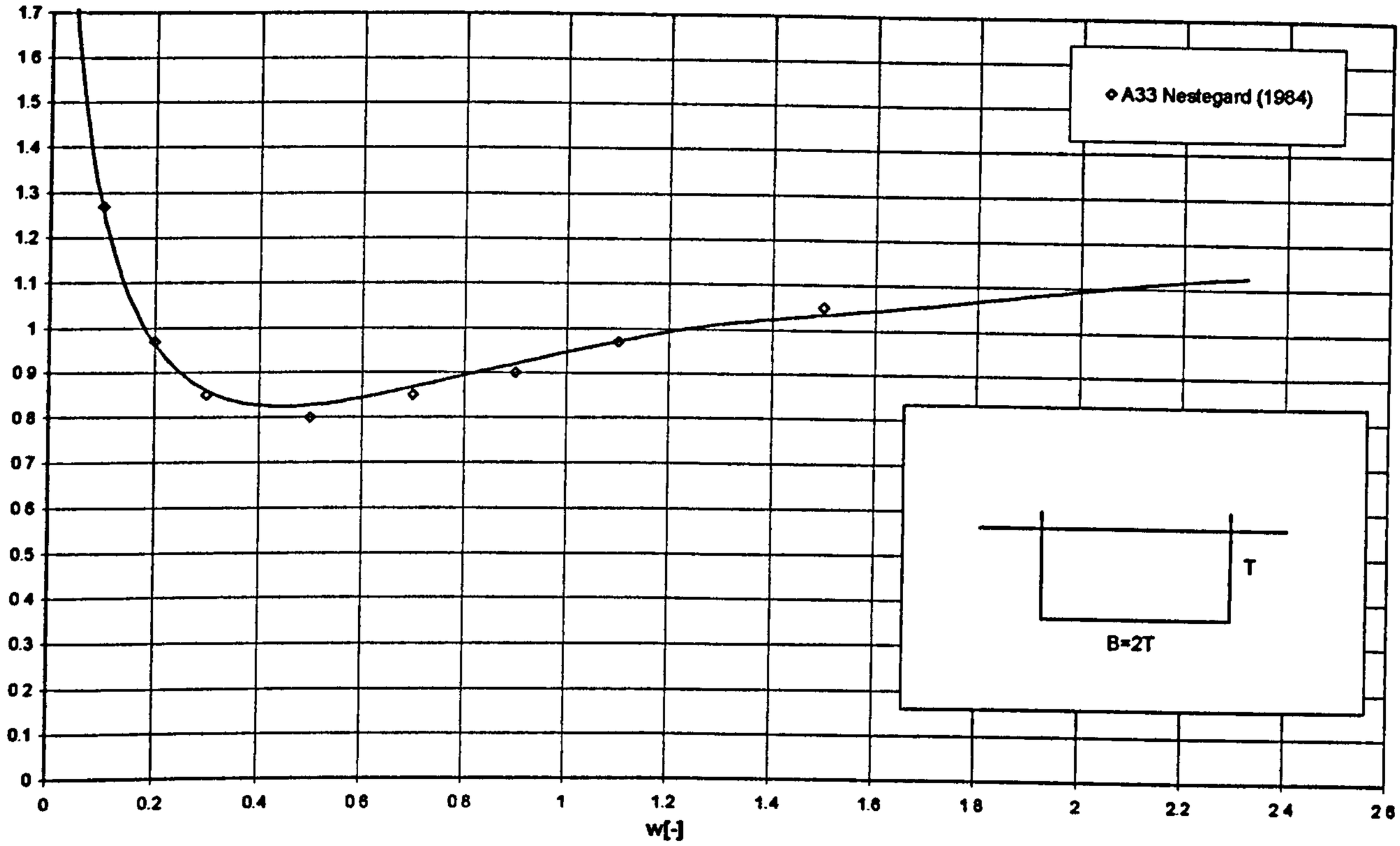

Figure 11 Dimensionless added mass in heave for 2D rectangular hull form, comparison between predictions by 2D method and experiments. Solid line is derived by means of PROTEUS3.

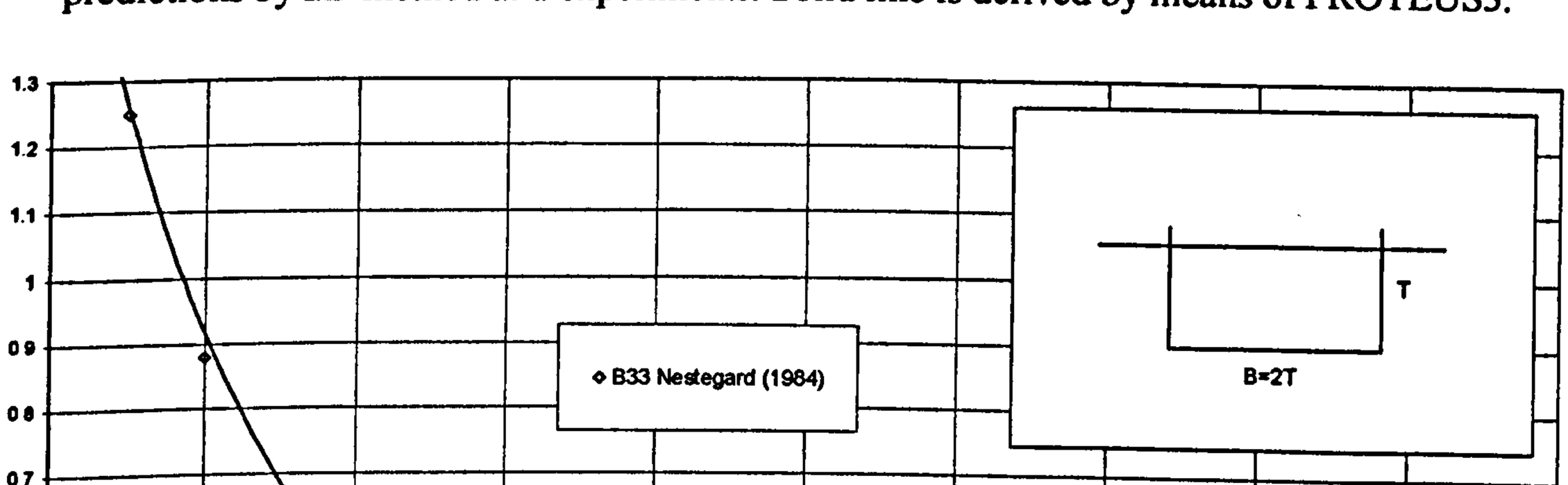

Figure 12 Dimensionless potential damping in heave for 2D rectangular hull form, comparison between predictions by 2D method and experiments. Solid line is derived by means of PROTEUS3.

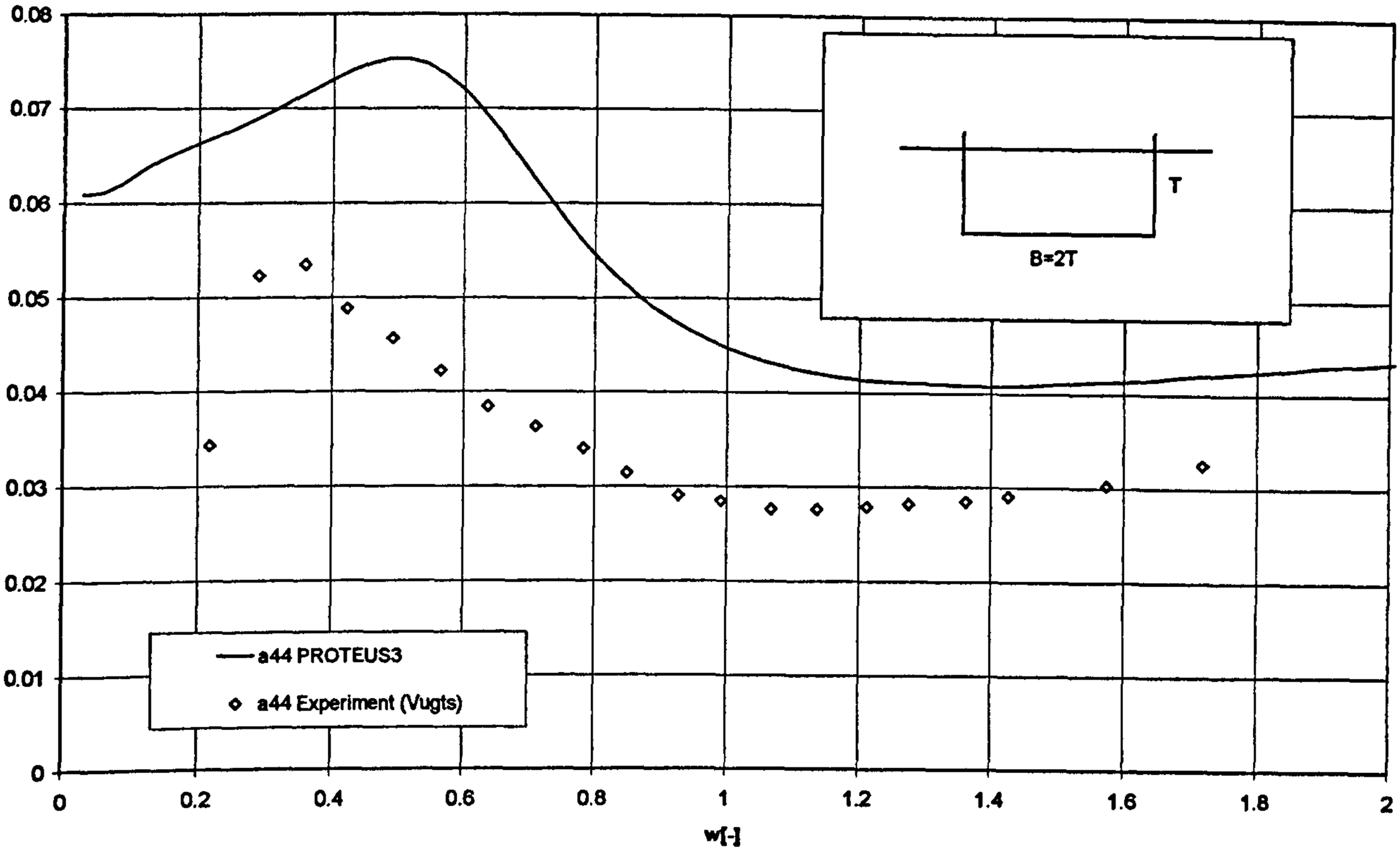

Figure 13 Dimensionless added moment of inertia in roll for 2D rectangular hull form, comparison between predictions by 2D method and experiments. Solid line is derived by means of PROTEUS3.

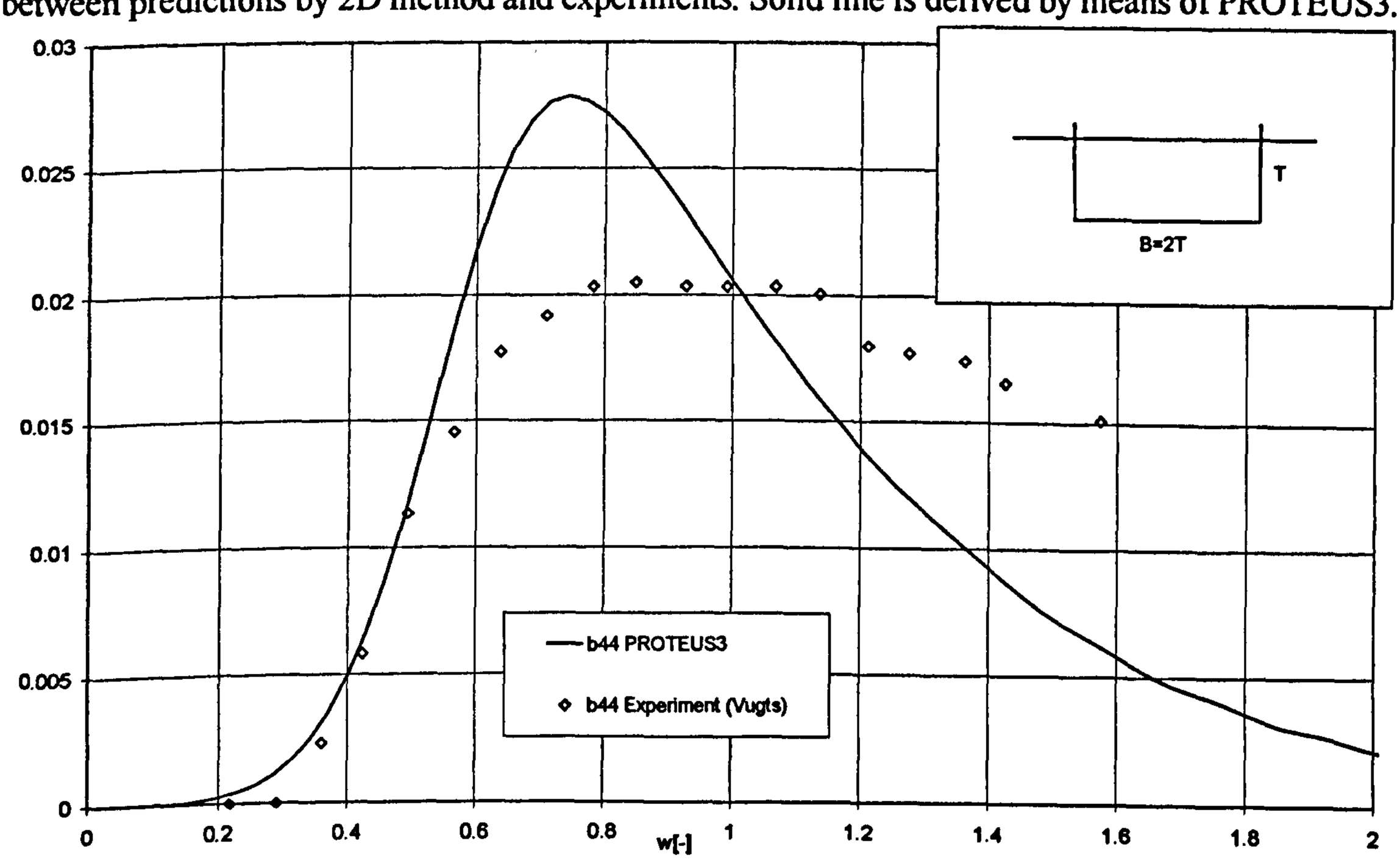

Figure 14 Dimensionless potential damping in roll for 2D rectangular hull form, comparison between predictions by 2D method and experiments. Solid line is derived by means of PROTEUS3.

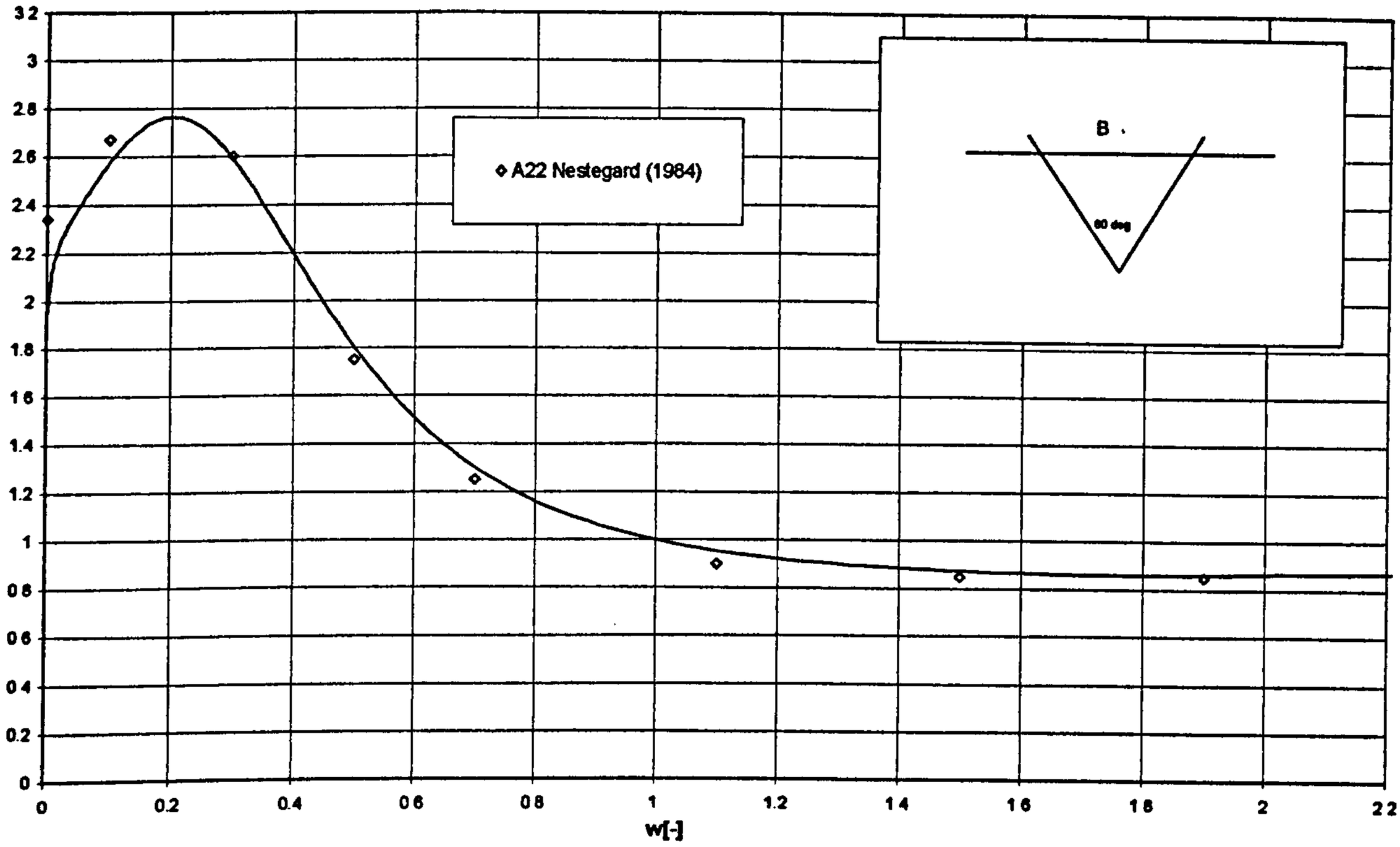

Figure 15 Dimensionless added mass in sway for 2D triangular hull form, comparison between predictions by 2D method and experiments. Solid line is derived by means of PROTEUS3.

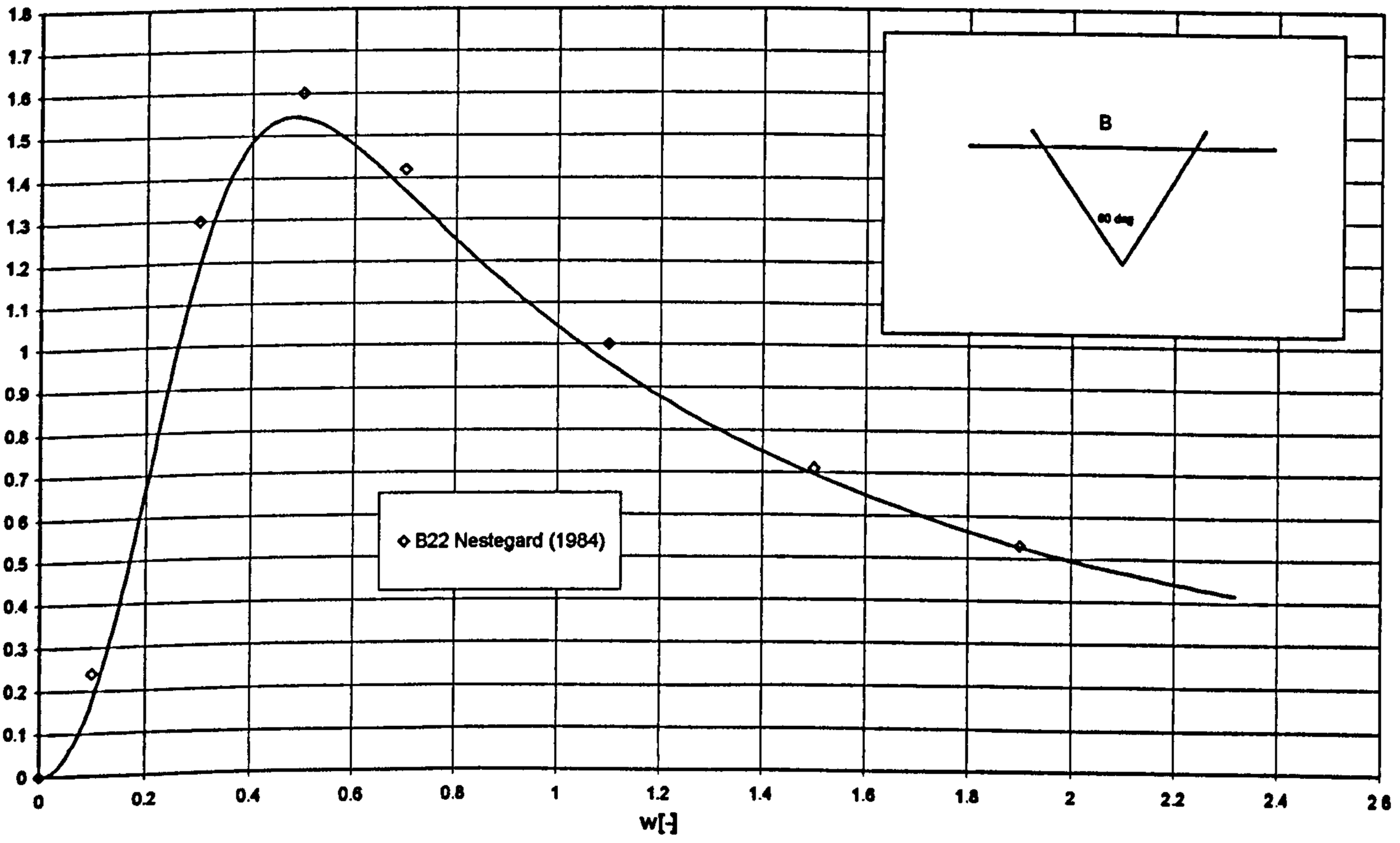

Figure 16 Dimensionless potential damping in sway for 2D triangular hull form, comparison between predictions by 2D method and experiments. Solid line is derived by means of PROTEUS3.

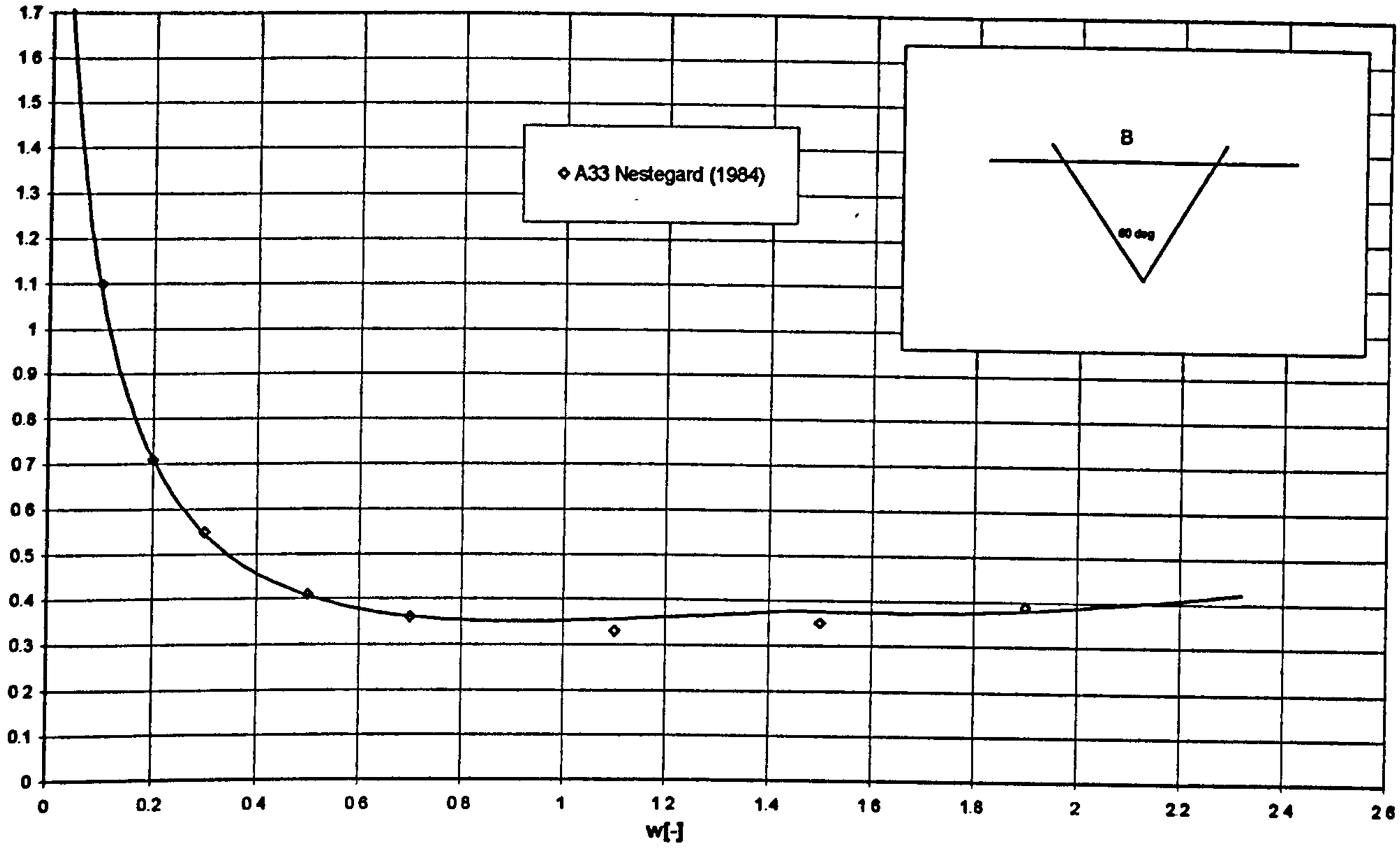

Figure 17 Dimensionless added mass in heave for 2D triangular hull form, comparison between predictions by 2D method and experiments. Solid line is derived by means of PROTEUS3.

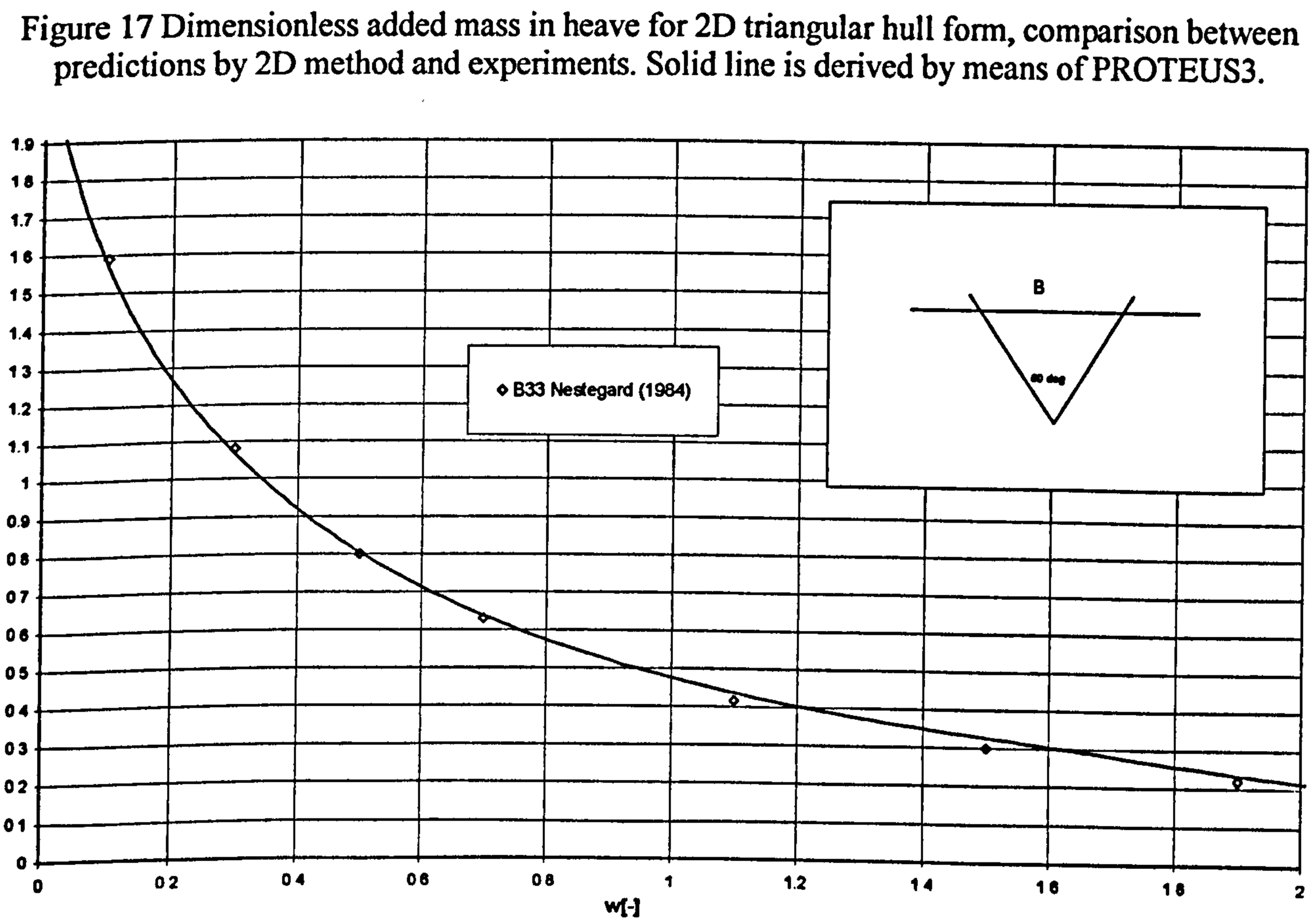

Figure 18 Dimensionless potential damping in sway for 2D triangular hull form, comparison between predictions by 2D method and experiments. Solid line is derived by means of PROTEUS3.

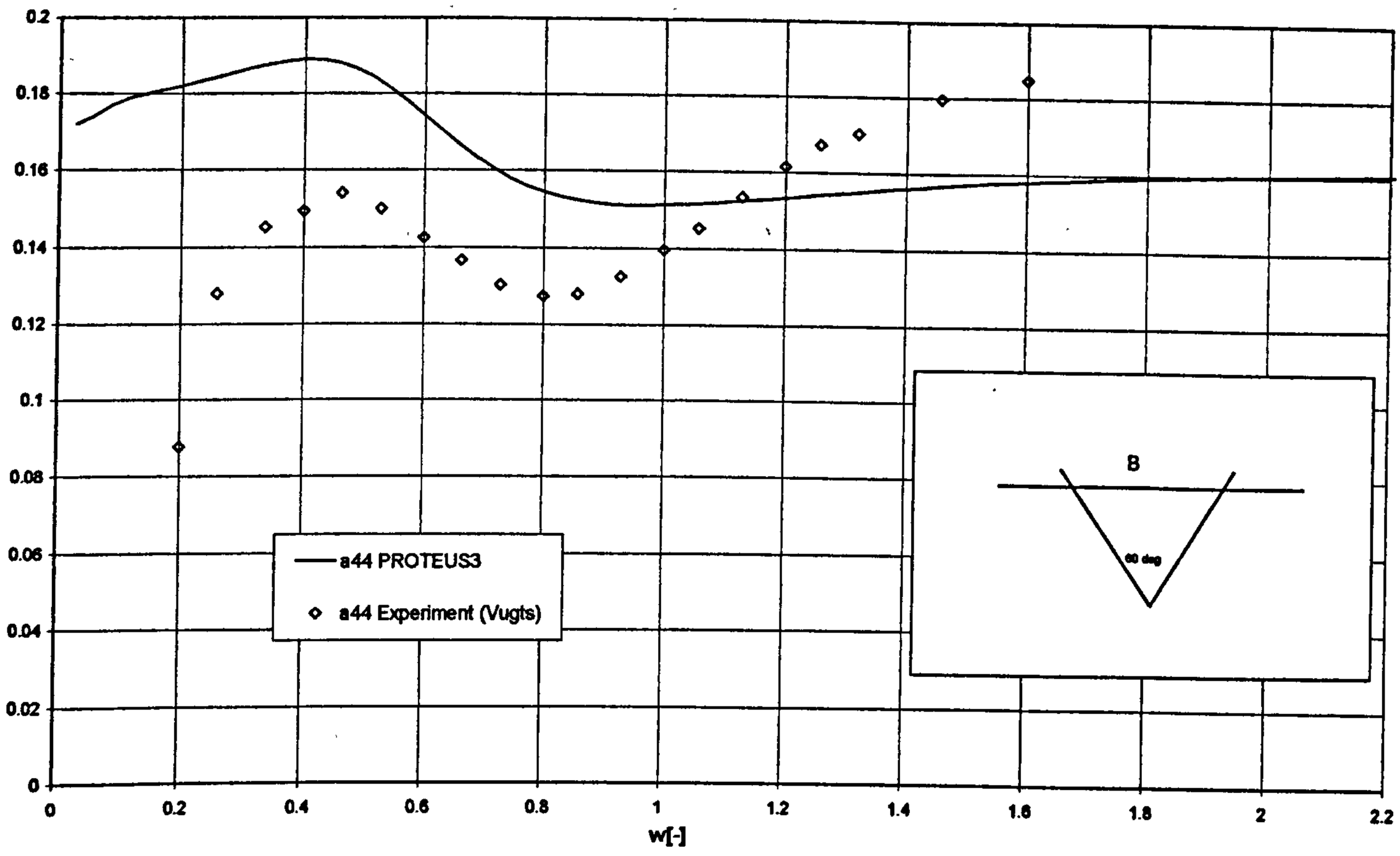

Figure 19 Dimensionless added moment in roll for 2D triangular hull form, comparison between predictions by 2D method and experiments. Solid line is derived by means of PROTEUS3.

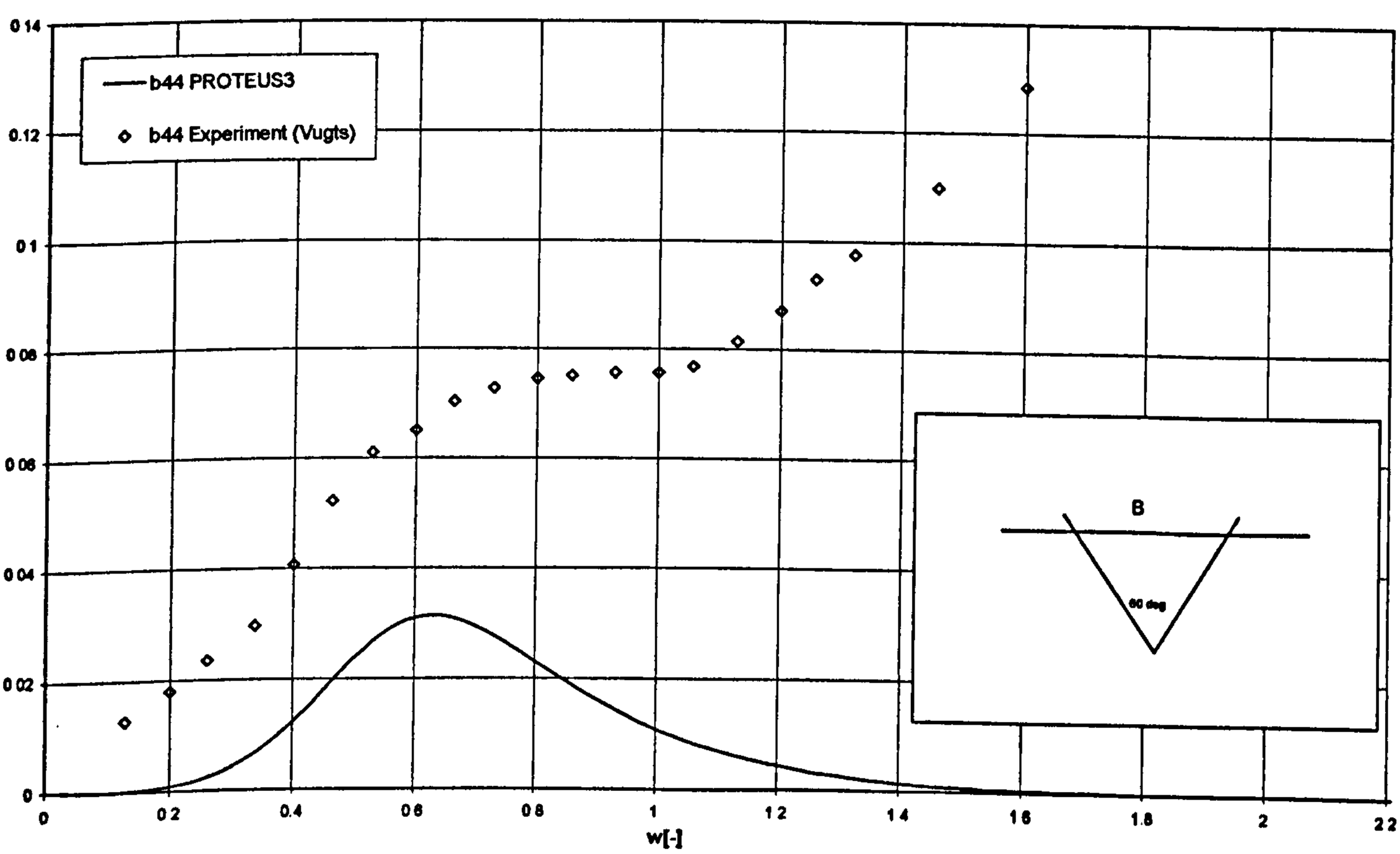

Figure 20 Dimensionless potential damping in roll for 2D triangular hull form, comparison between predictions by 2D method and experiments. Solid line is derived by means of PROTEUS3.

2.2 Hydrodynamic coefficients in three dimensions

All of the three dimensional coefficients are presented in dimensionless form as is summarised in Table 2 below.

Table 2 Non-dimensional form of 3D hydrodynamic coefficients

$$\omega_L[-]=\frac{\omega_E\left[\frac{rad}{s}\right]}{\sqrt{\frac{g\left[\frac{m}{s^2}\right]}{L[m]}}}$$

sway, heave, pitch, yaw, heave-pitch

$$\omega_B[-]=\omega_E\left[\frac{rad}{s}\right]\cdot\sqrt{\frac{B[m]}{2\cdot g\left[\frac{m}{s^2}\right]}}$$

roll, roll-yaw, sway-roll, sway-yaw

$$A_{22},A_{33}[-]=\frac{A_{22},A_{33}[kg]}{\rho\left[\frac{kg}{m^3}\right]\cdot\nabla[m^3]}$$

$$B_{22},B_{33}[-]=\frac{B_{22},B_{33}\left[\frac{kg}{s}\right]}{\rho\left[\frac{kg}{m^3}\right]\cdot\nabla[m^3]\cdot\sqrt{\frac{g\left[\frac{m}{s^2}\right]}{L[m]}}}$$

$$A_{55},A_{66}[-]=\frac{A_{55},A_{66}[kg\cdot m^2]}{\rho\left[\frac{kg}{m^3}\right]\cdot\nabla[m^3]\cdot(L[m])^2}$$

$$B_{55},B_{66}[-]=\frac{B_{55},B_{66}\left[\frac{kg\cdot m^2}{s}\right]}{\rho\left[\frac{kg}{m^3}\right]\cdot\nabla[m^3]\cdot(L[m])^2\cdot\sqrt{\frac{g\left[\frac{m}{s^2}\right]}{L[m]}}}$$

$$A_{35}[-]=\frac{A_{35}[kg\cdot m]}{\rho\left[\frac{kg}{m^3}\right]\cdot\nabla[m^3]\cdot L[m]}$$

$$B_{35}[-]=\frac{B_{35}\left[\frac{kg\cdot m}{s}\right]}{\rho\left[\frac{kg}{m^3}\right]\cdot\nabla[m^3]\cdot L[m]\cdot\sqrt{\frac{g\left[\frac{m}{s^2}\right]}{L[m]}}}$$

$$A_{44},A_{46}[-]=\frac{A_{44},A_{46}[kg\cdot m^2]}{\rho\left[\frac{kg}{m^3}\right]\cdot\nabla[m^3]\cdot(B[m])^2}$$

$$B_{44},B_{46}[-]=\frac{B_{44},B_{46}\left[\frac{kg\cdot m^2}{s}\right]}{\rho\left[\frac{kg}{m^3}\right]\cdot\nabla[m^3]\cdot(B[m])^2\cdot\sqrt{\frac{2\cdot g\left[\frac{m}{s^2}\right]}{B[m]}}}$$

$$A_{24},A_{34},A_{26}[-]=\frac{A_{24},A_{34},A_{26}[kg\cdot m]}{\rho\left[\frac{kg}{m^3}\right]\cdot\nabla[m^3]\cdot B[m]}$$

$$B_{24},B_{34},B_{26}[-]=\frac{B_{24},B_{34},B_{26}\left[\frac{kg\cdot m}{s}\right]}{\rho\left[\frac{kg}{m^3}\right]\cdot\nabla[m^3]\cdot B[m]\cdot\sqrt{\frac{2\cdot g\left[\frac{m}{s^2}\right]}{B[m]}}}$$

2.2.1 Wigley1 hull form

The definition of this mathematical hull form can be found in [50] together with experimental results of a systematic series of tests on seakeeping properties of the vessel. Her main particulars are presented in Table 3 below.

Table 3 Main particulars of Wigley1 vessel

Lpp [m]	120.0
B [m]	12.0
Draught [m]	7.5
Displ [m^3]	6030.0

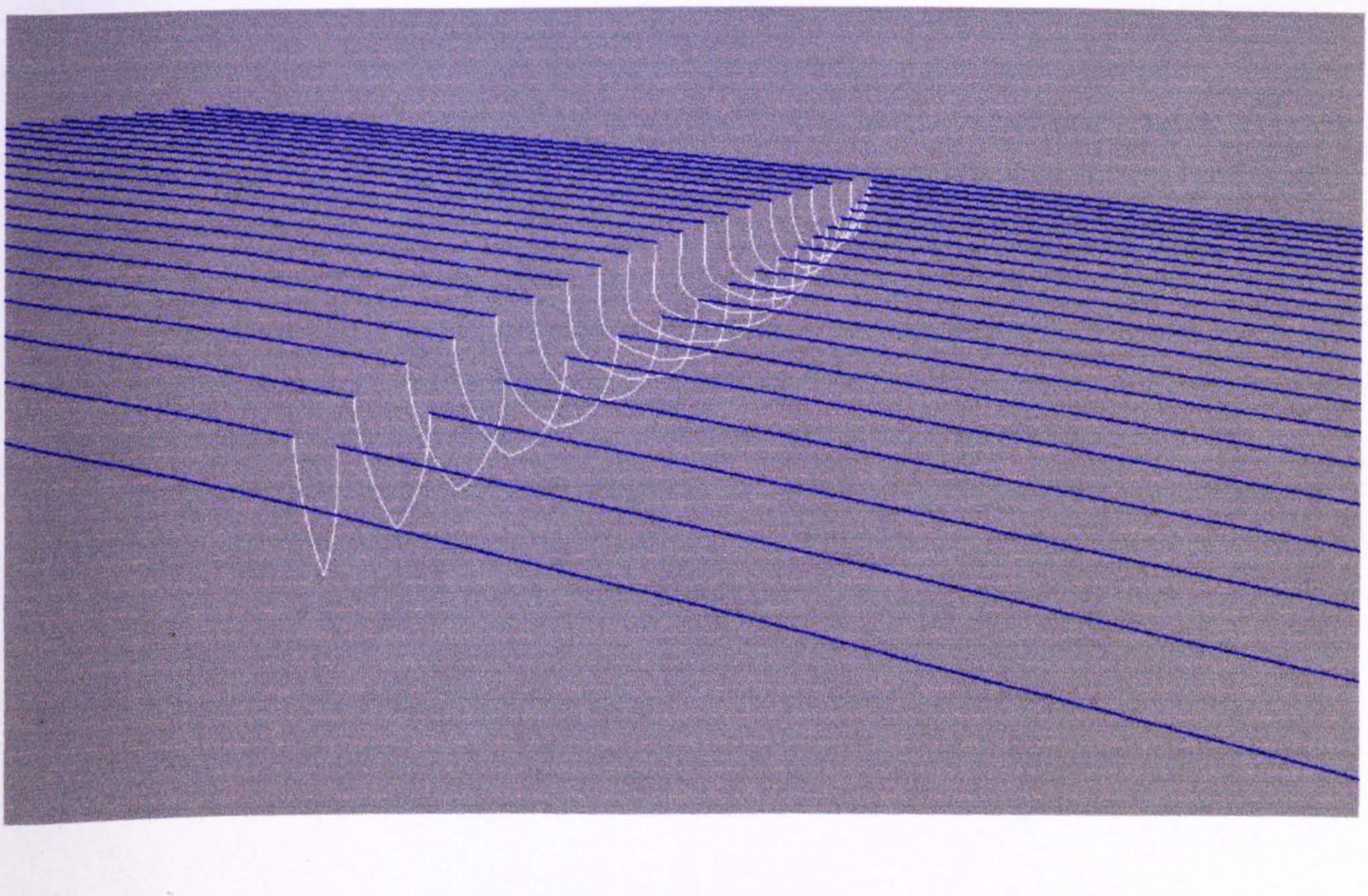

Figure 21 Section-wise (strip) representation of the geometry of the Wigley1 hull

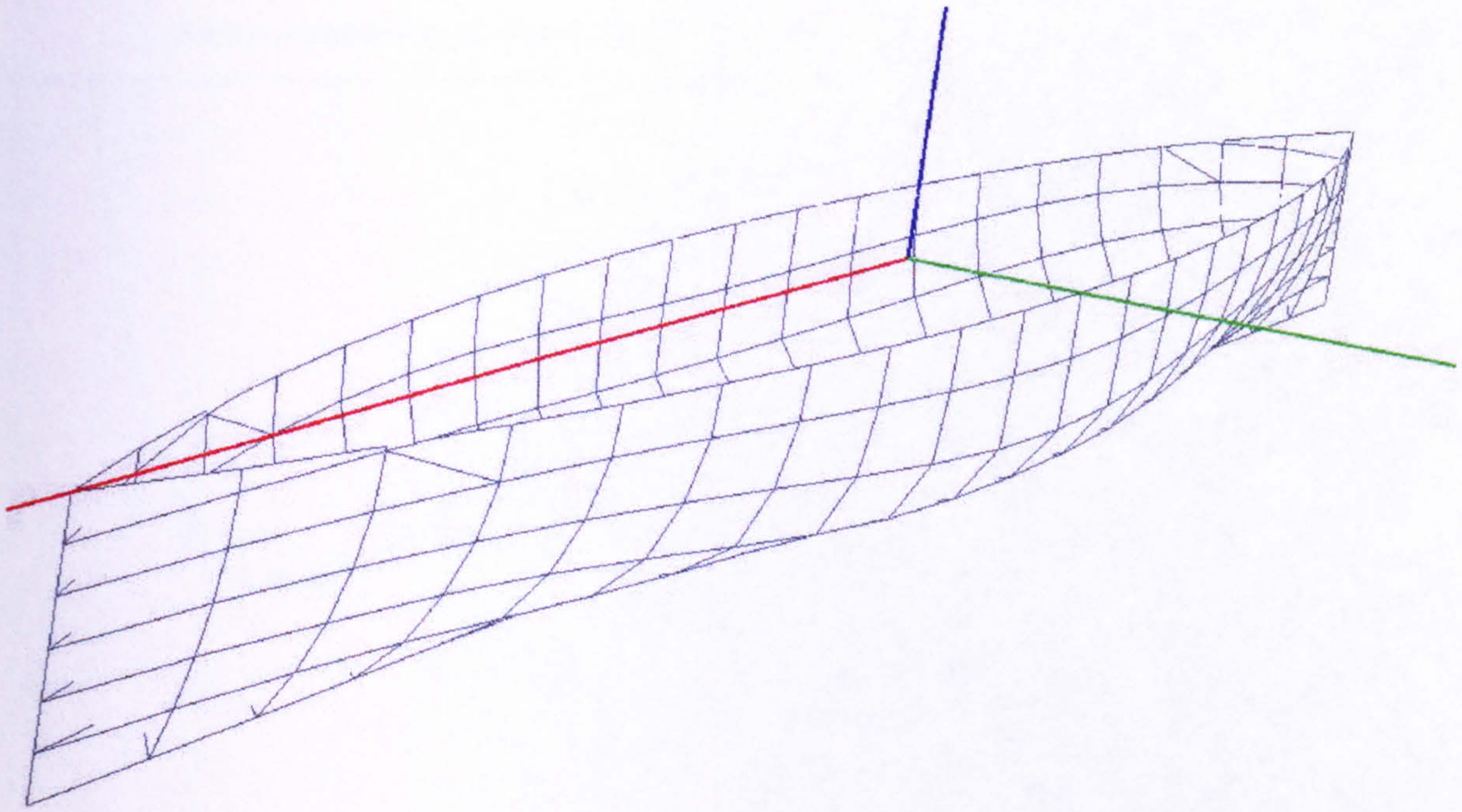

Figure 22 Panel-wise representation of the geometry of the Wigley1 hull, 212 panels

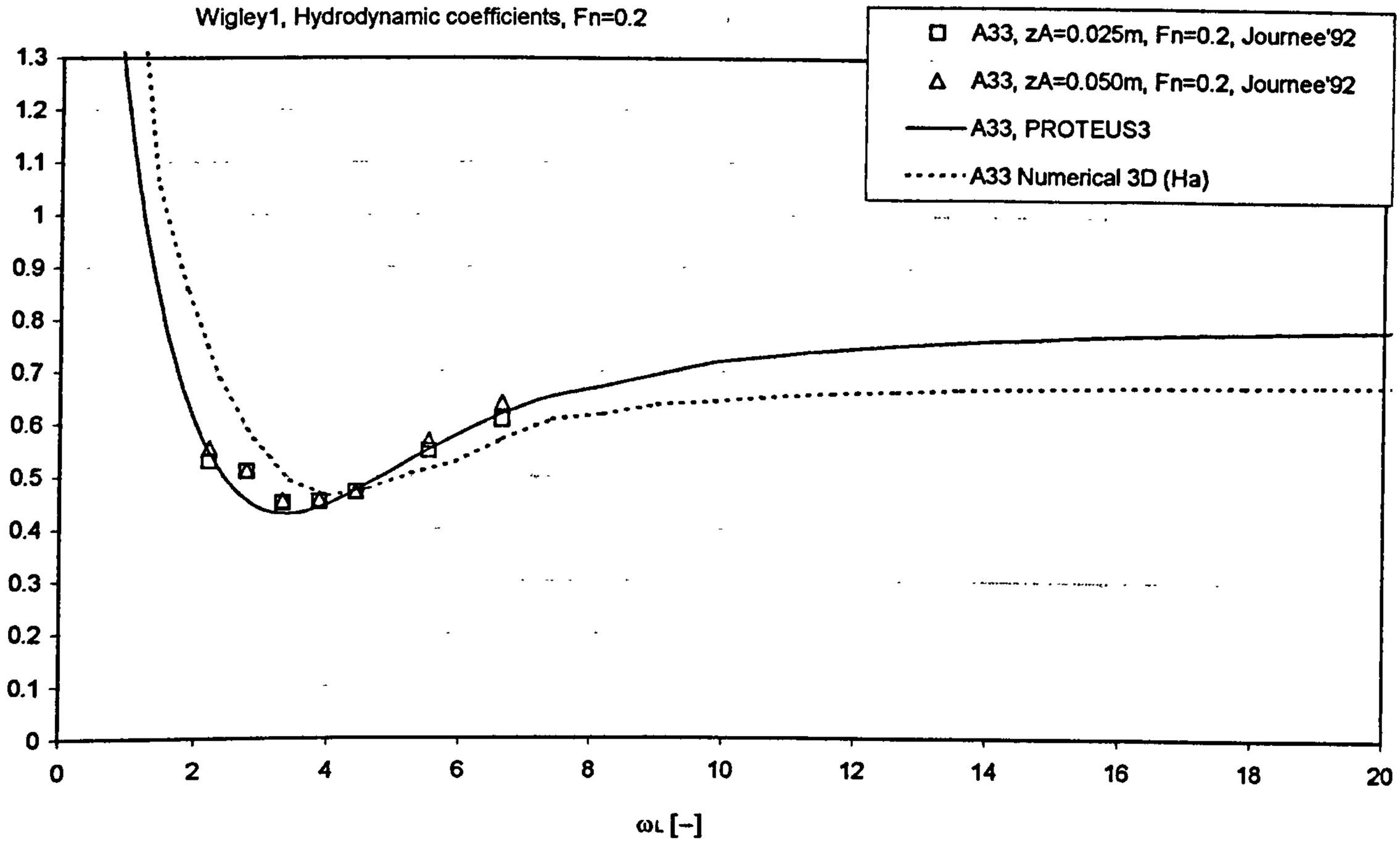

Figure 23 Dimensionless added mass in heave for 3D Wigley hull form, comparison between predictions by strip theory and 3D Green function methods and experiments

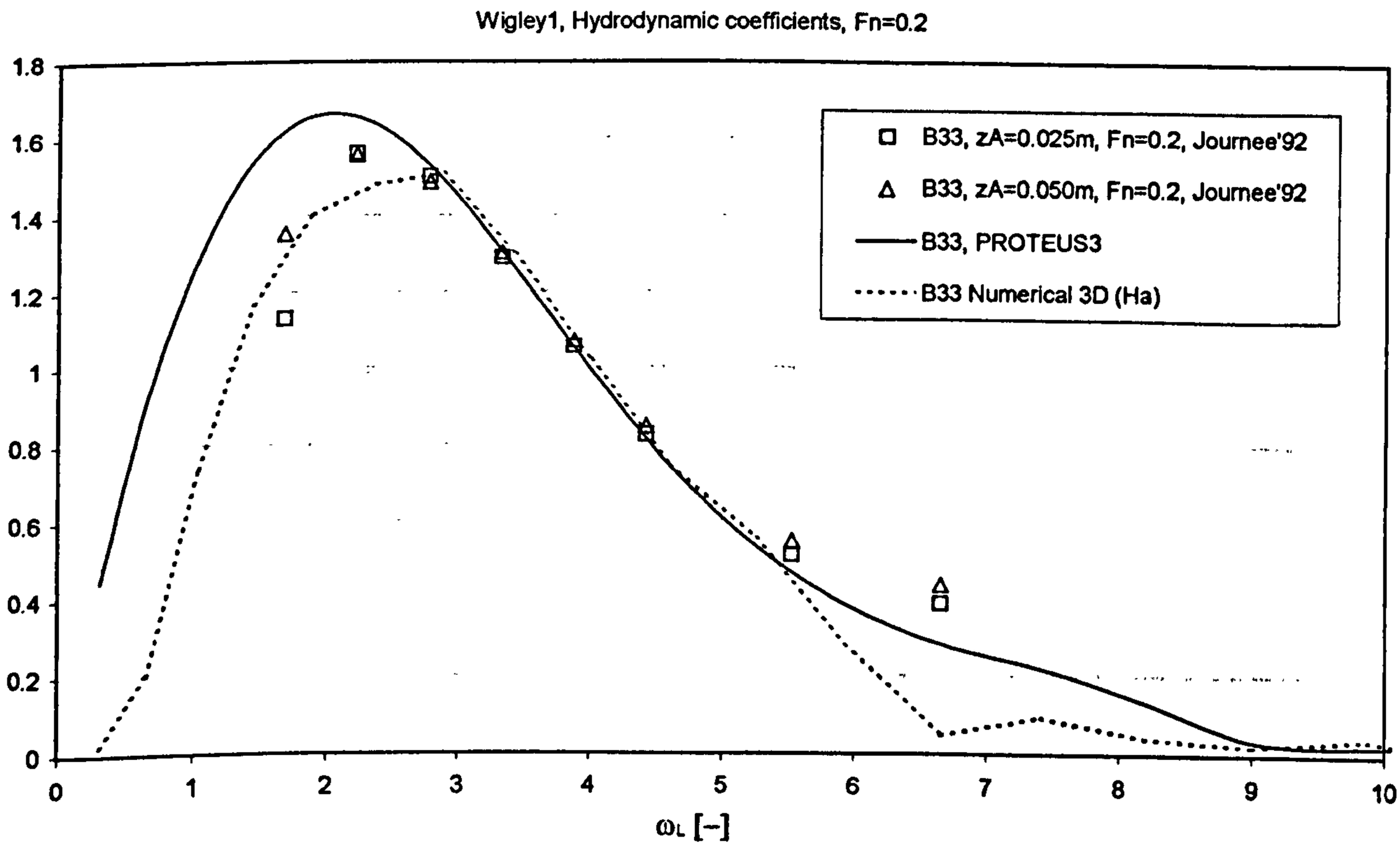

Figure 24 Dimensionless potential damping in heave for 3D Wigley hull form, comparison between predictions by strip theory and 3D Green function methods and experiments

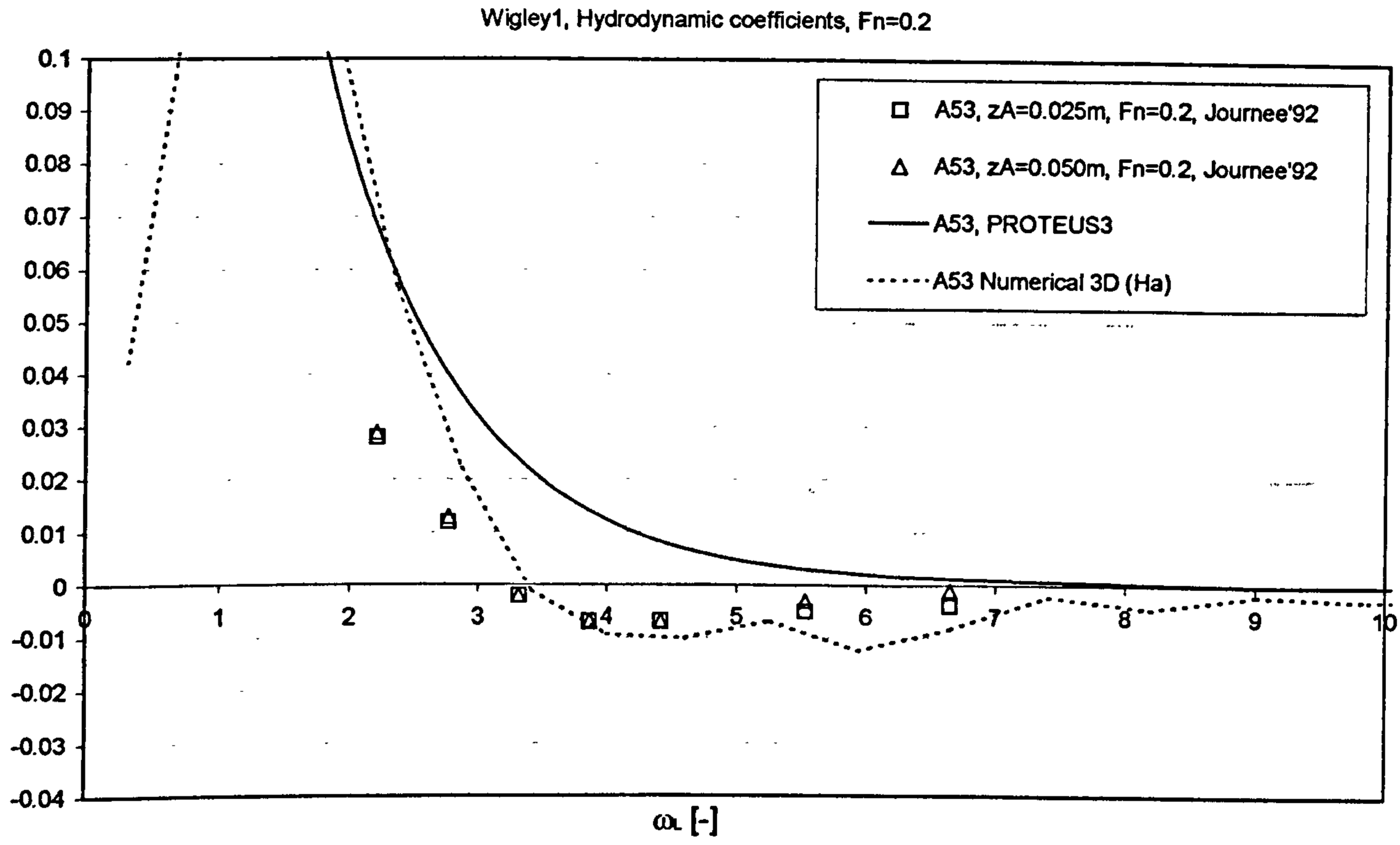

Figure 25 Dimensionless added mass of cross coupling between pitch and heave for 3D Wigley hull form, comparison between predictions by strip theory and 3D Green function methods and experiments

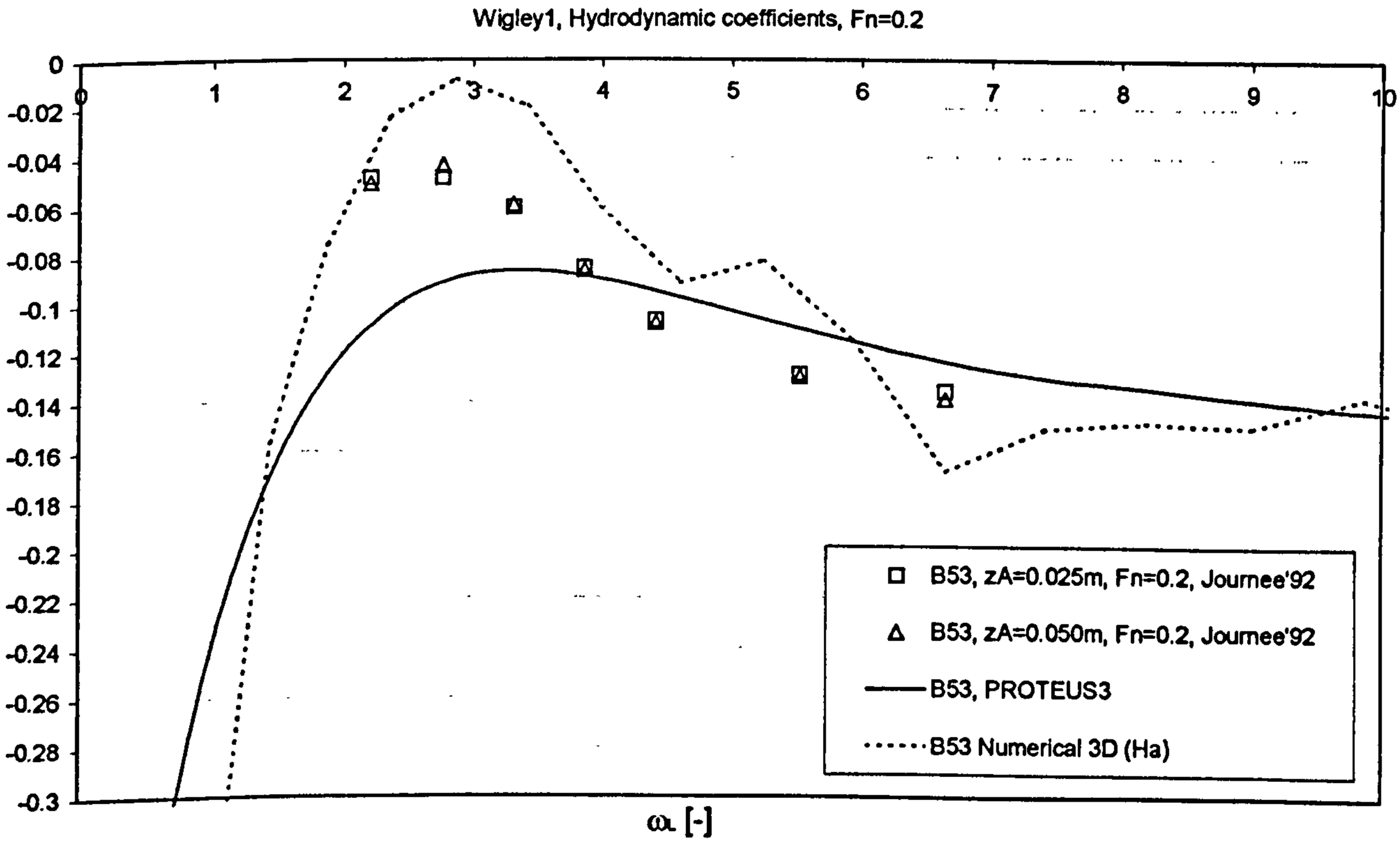

Figure 26 Dimensionless potential damping of cross coupling between pitch and heave for 3D Wigley hull form, comparison between predictions by strip theory and 3D Green function methods and experiments

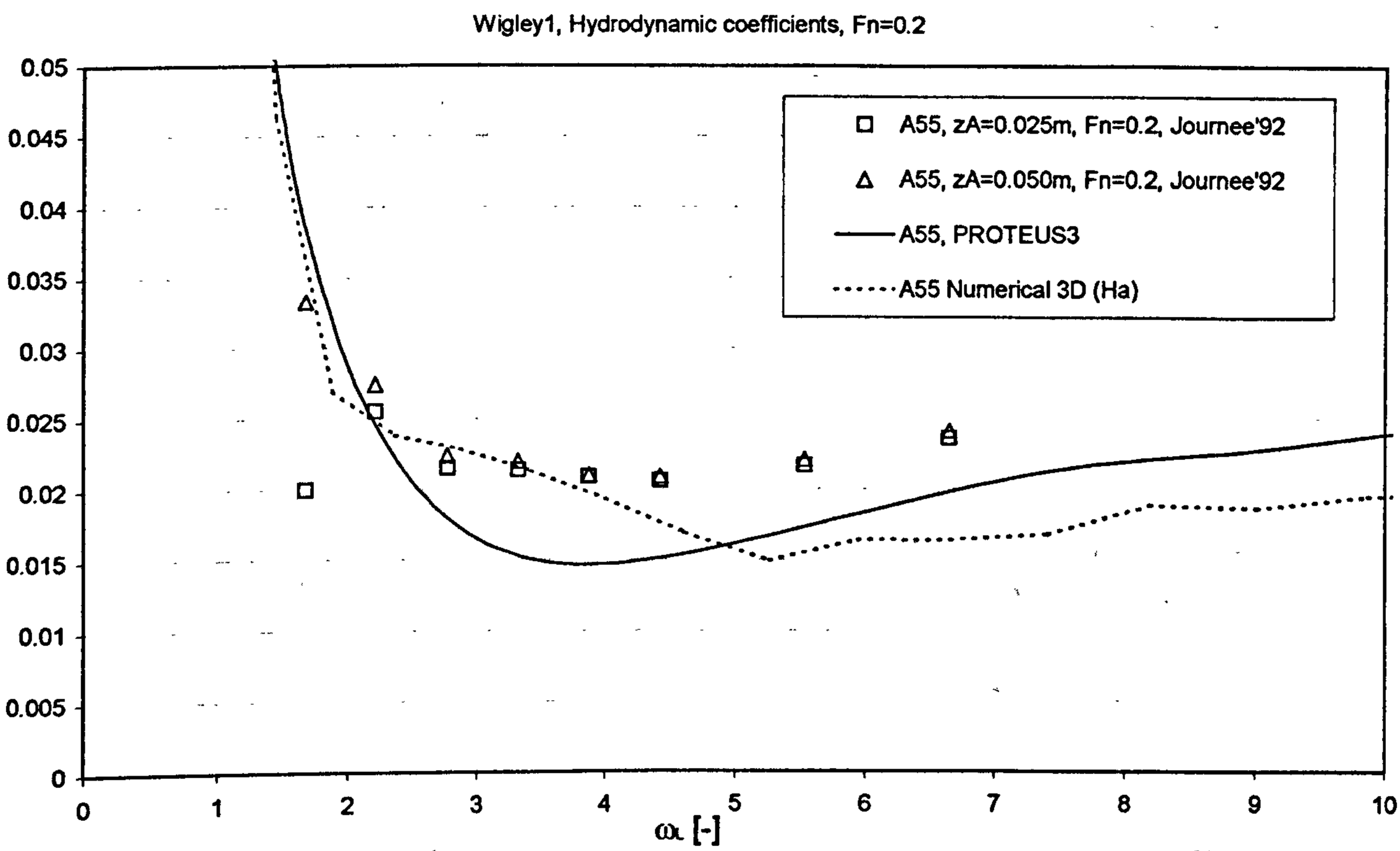

Figure 27 Dimensionless added mass in pitch for 3D Wigley hull form, comparison between predictions by strip theory and 3D Green function methods and experiments

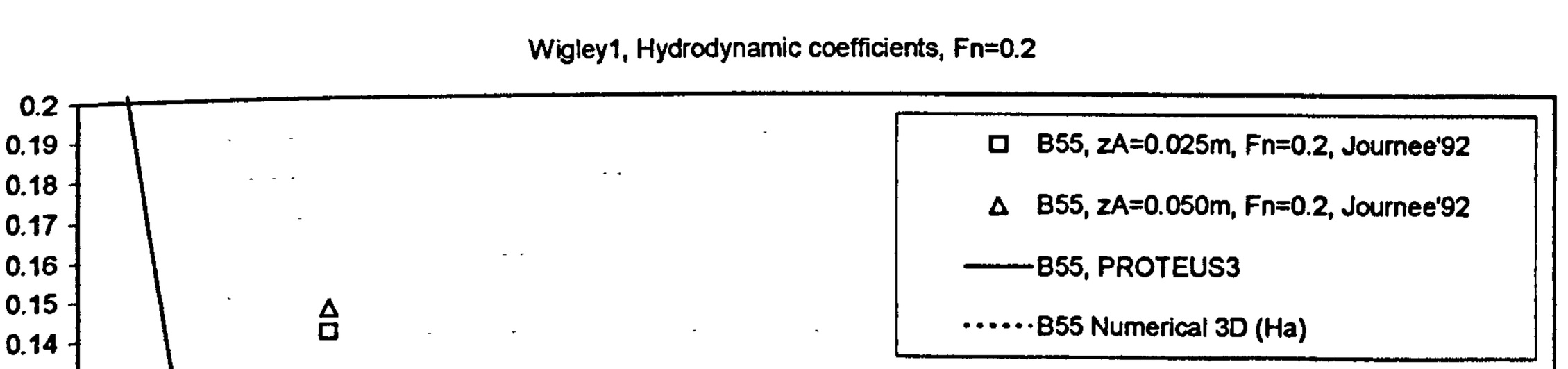

Figure 28 Dimensionless potential damping in pitch for 3D Wigley hull form, comparison between predictions by strip theory and 3D Green function methods and experiments

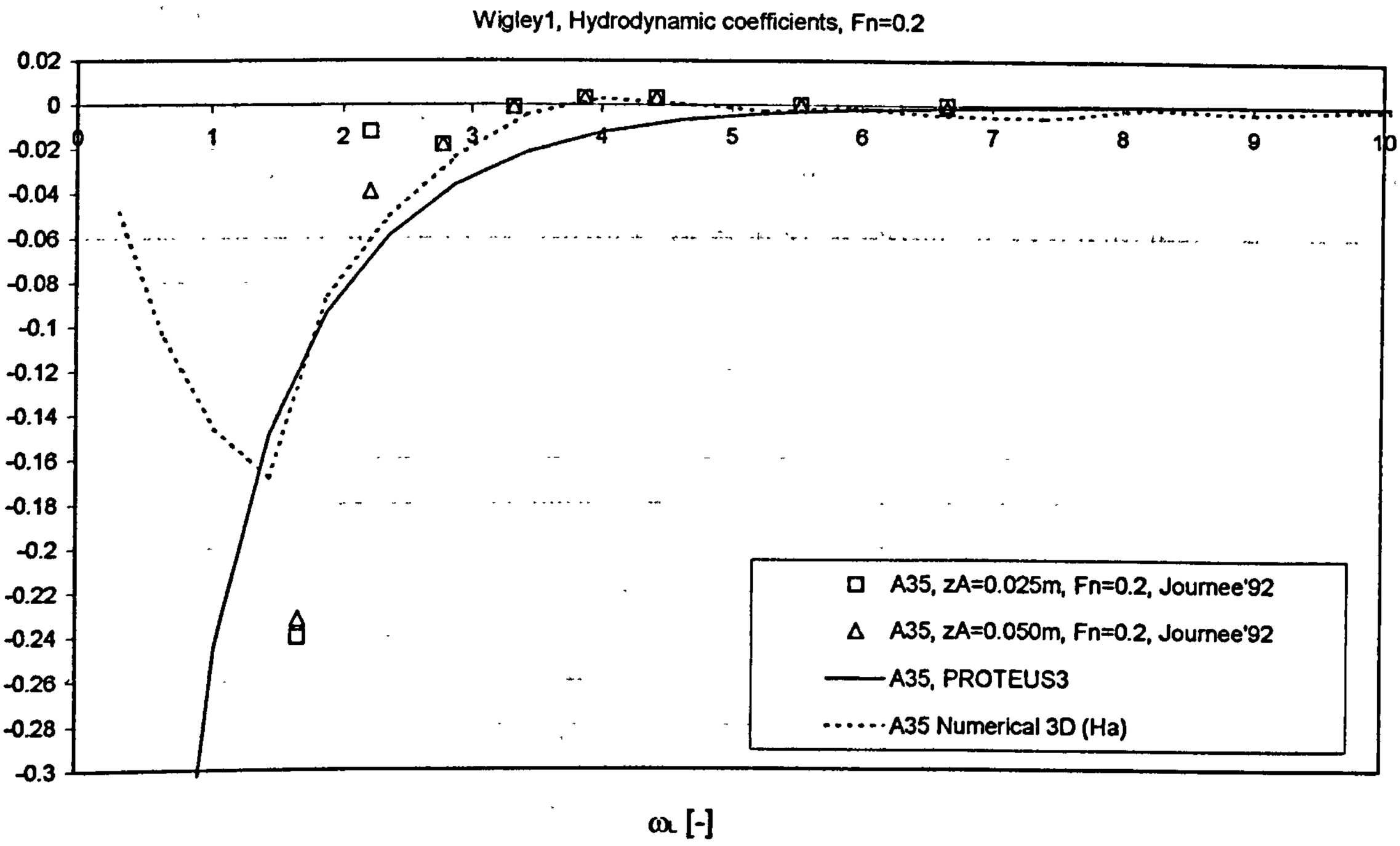

Figure 29 Dimensionless added mass of cross coupling between heave and pitch for 3D Wigley hull form, comparison between predictions by strip theory and 3D Green function methods and experiments

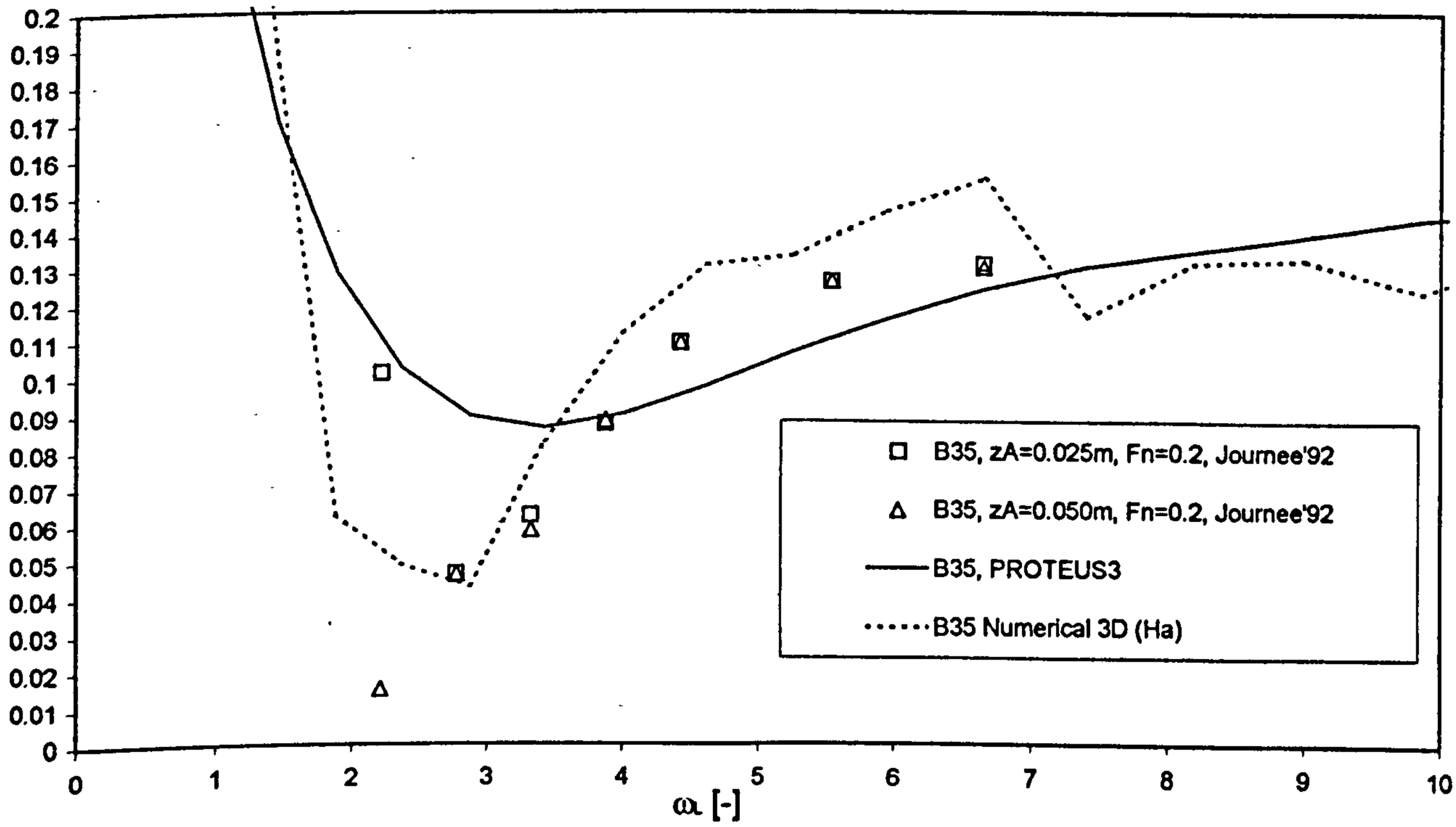

Figure 30 Dimensionless potential damping of cross coupling between heave and pitch for 3D Wigley hull form, comparison between predictions by strip theory and 3D Green function methods and experiments

2.2.2 Series 60 hull form

Series 60 hull form is fairly representative shape of typical cargo vessels and have the most substantial database of experimental results on seakeeping qualities generated, providing therefore, a reliable and extensive source of information for numerical testing. A ship with main particulars as given in Table 4 have been used in this study.

Table 4 Main particulars of Series 60, CB=0.7 vessel

Lpp [m]	140.0
B [m]	20.0
Draught [m]	8.0
Displ [m^3]	15680.0

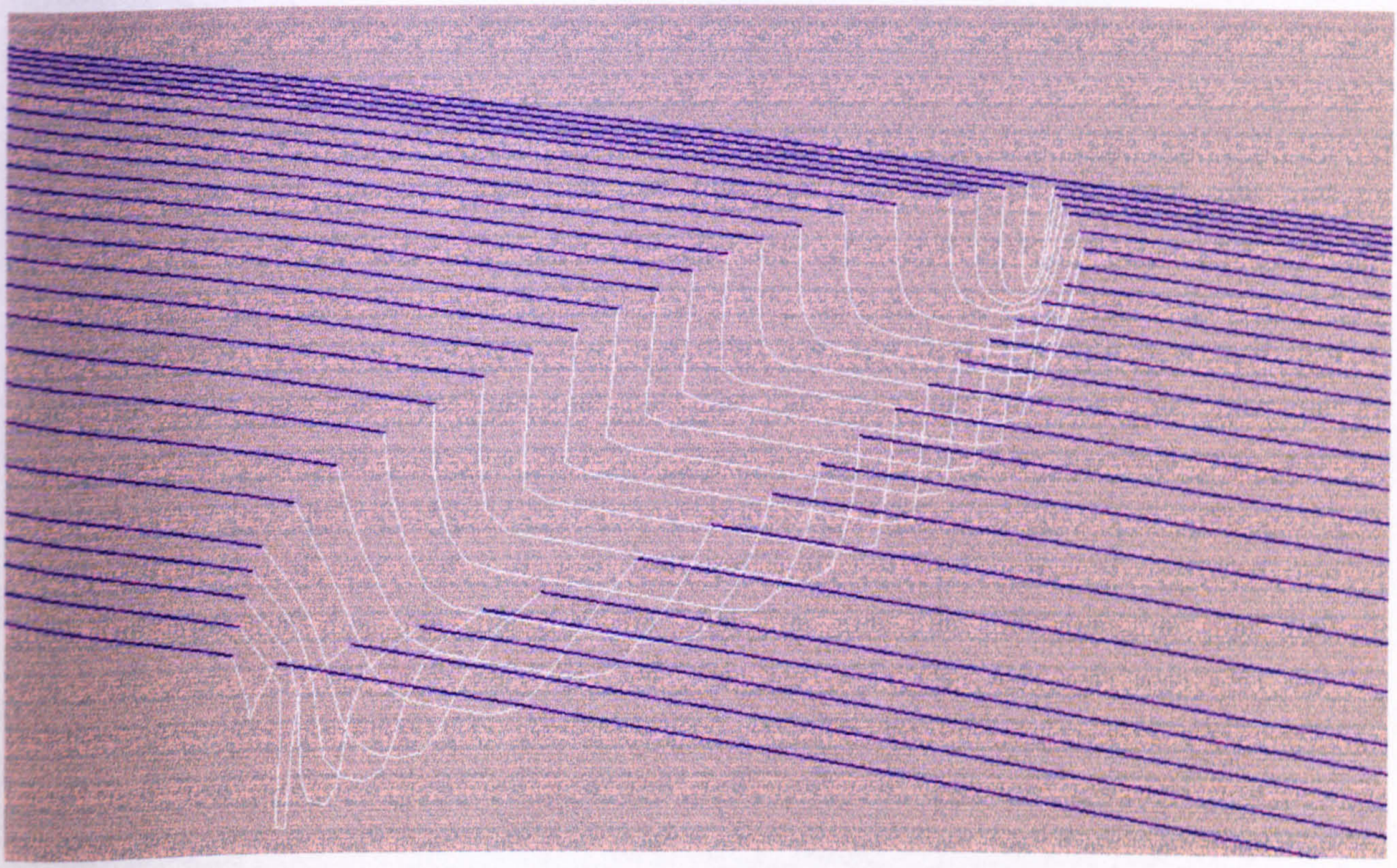

Figure 31 Section-wise (strip) representation of the geometry of the Series 60, CB=0.7 hull

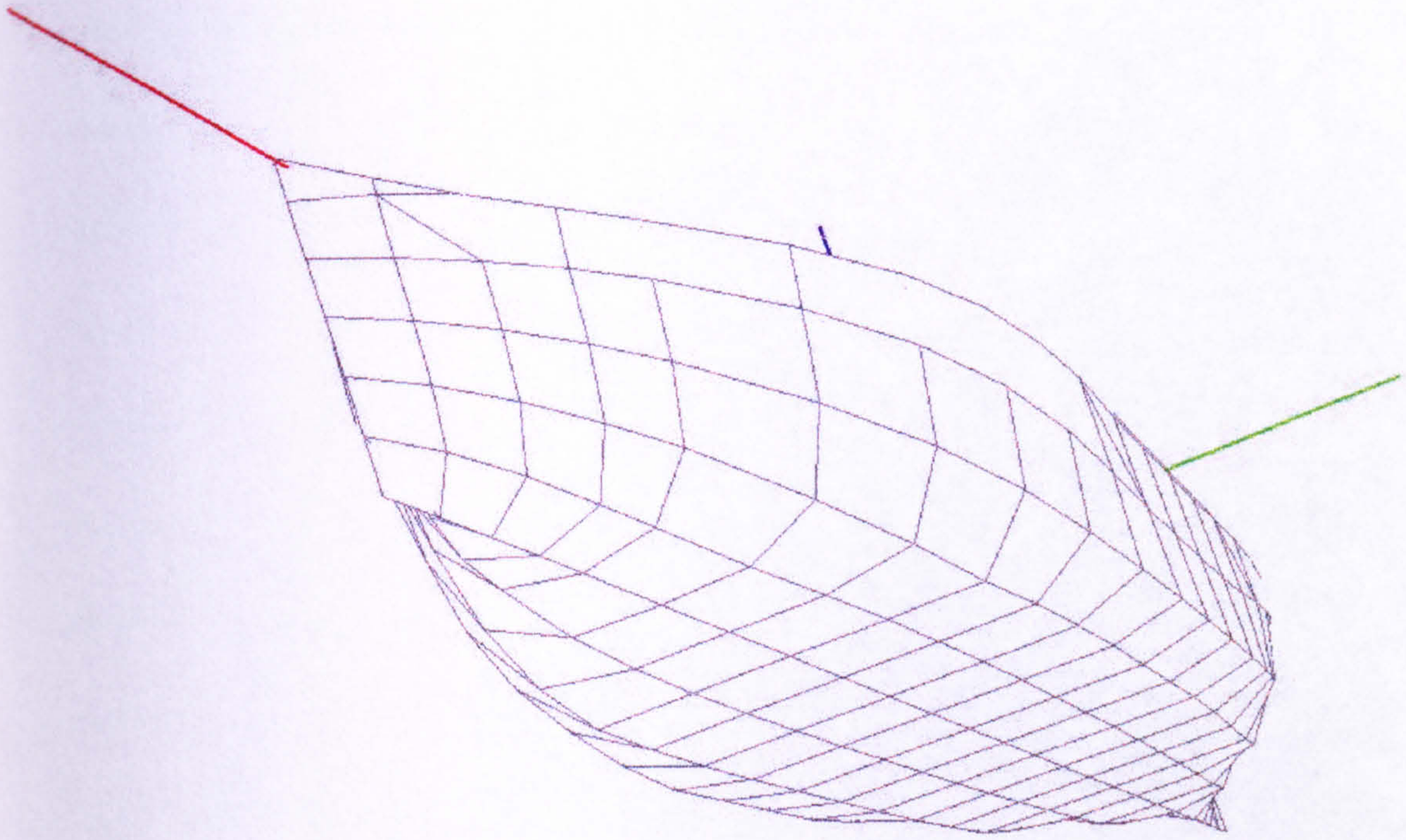

Figure 32 Panels of the geometry of the Series 60, CB=0.7 hull, 254 panels on the whole body used by HA code, and 123 used by NEWDRIFT on half the body.

*Hydrodynamic forces and moments for **zero speed** case*

Comparison between strip theory and 3D panel methods

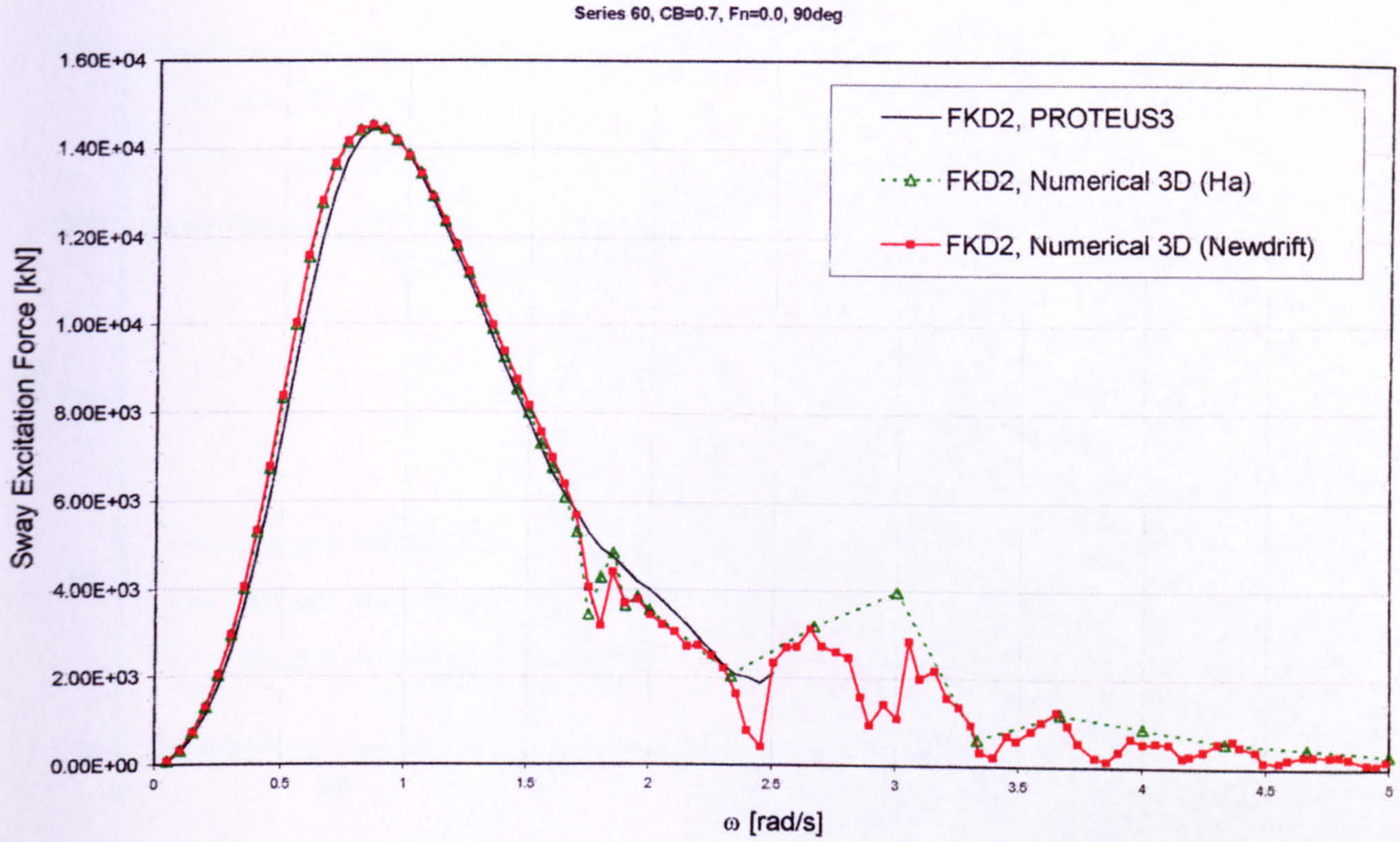

Figure 33 Excitation force in sway mode for 3D Series 60, CB=0.7 hull form, comparison between predictions by strip theory and 3D panel methods, Fn=0.0, Heading 90deg

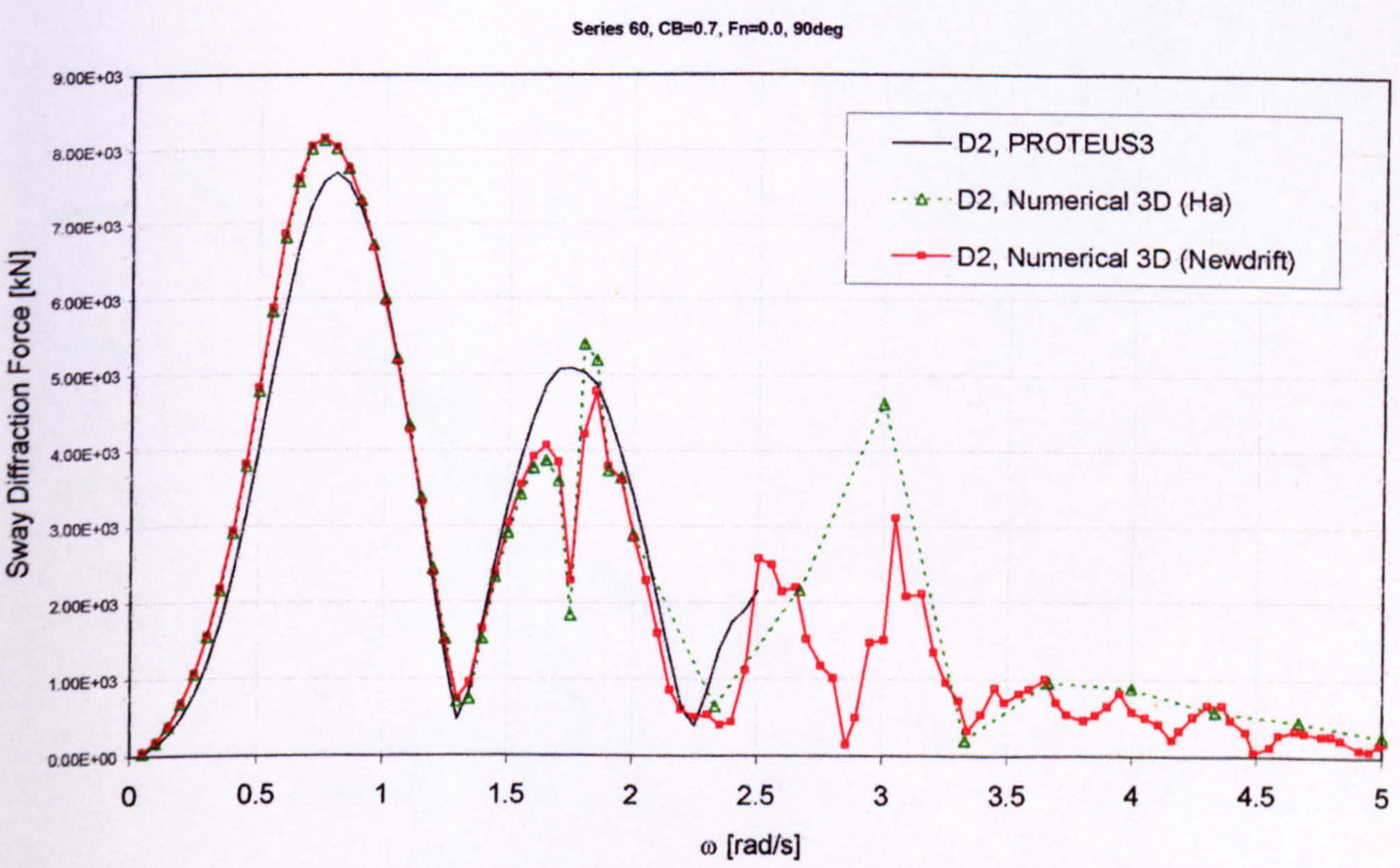

Figure 34 Diffraction force in sway mode for 3D Series 60, CB=0.7 hull form, comparison between predictions by strip theory and 3D panel methods, Fn=0.0, Heading 90deg

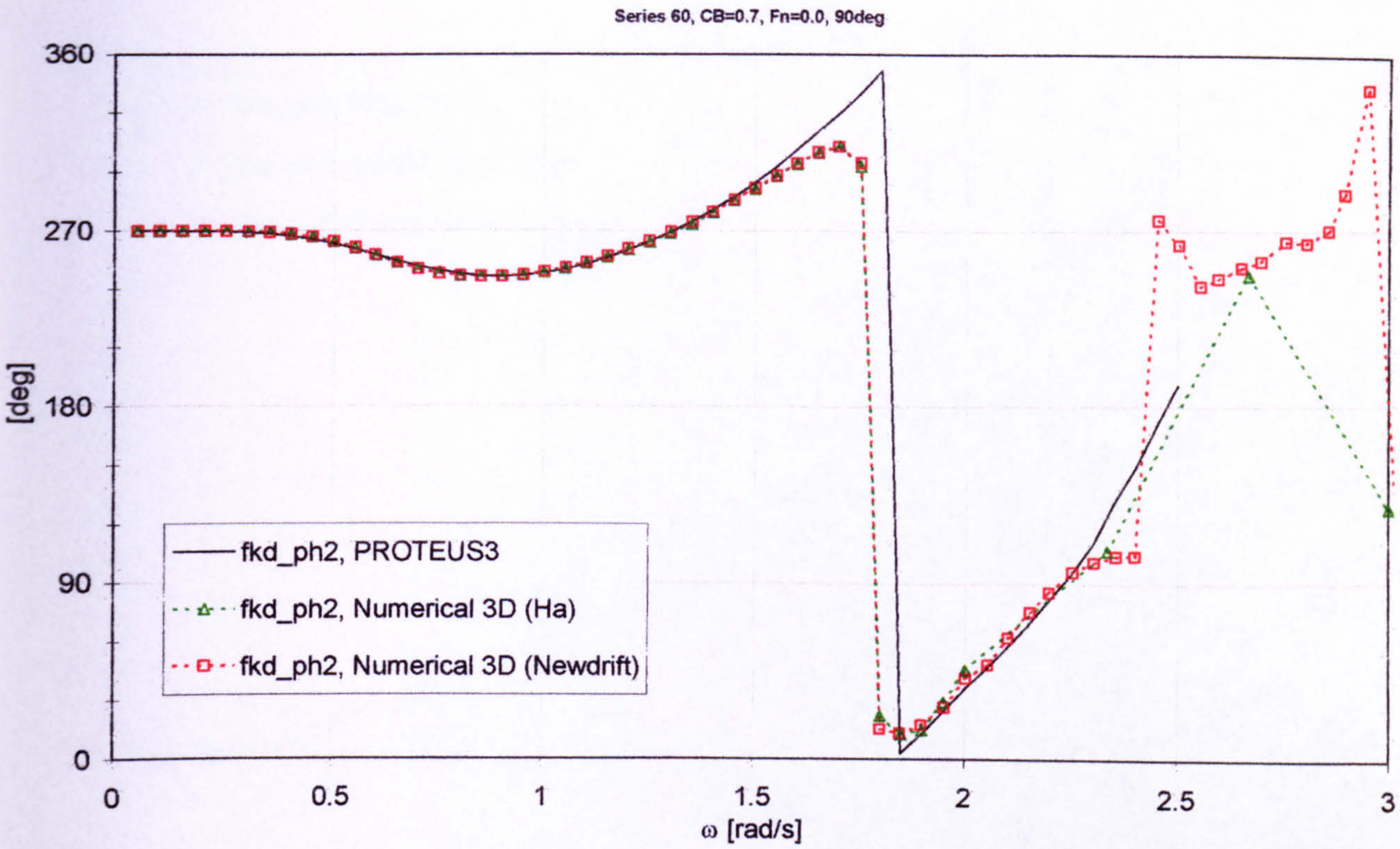

Figure 35 Excitation force phase angle in sway mode for 3D Series 60, CB=0.7 hull form, comparison between predictions by strip theory and 3D panel methods, Fn=0.0, Heading 90deg

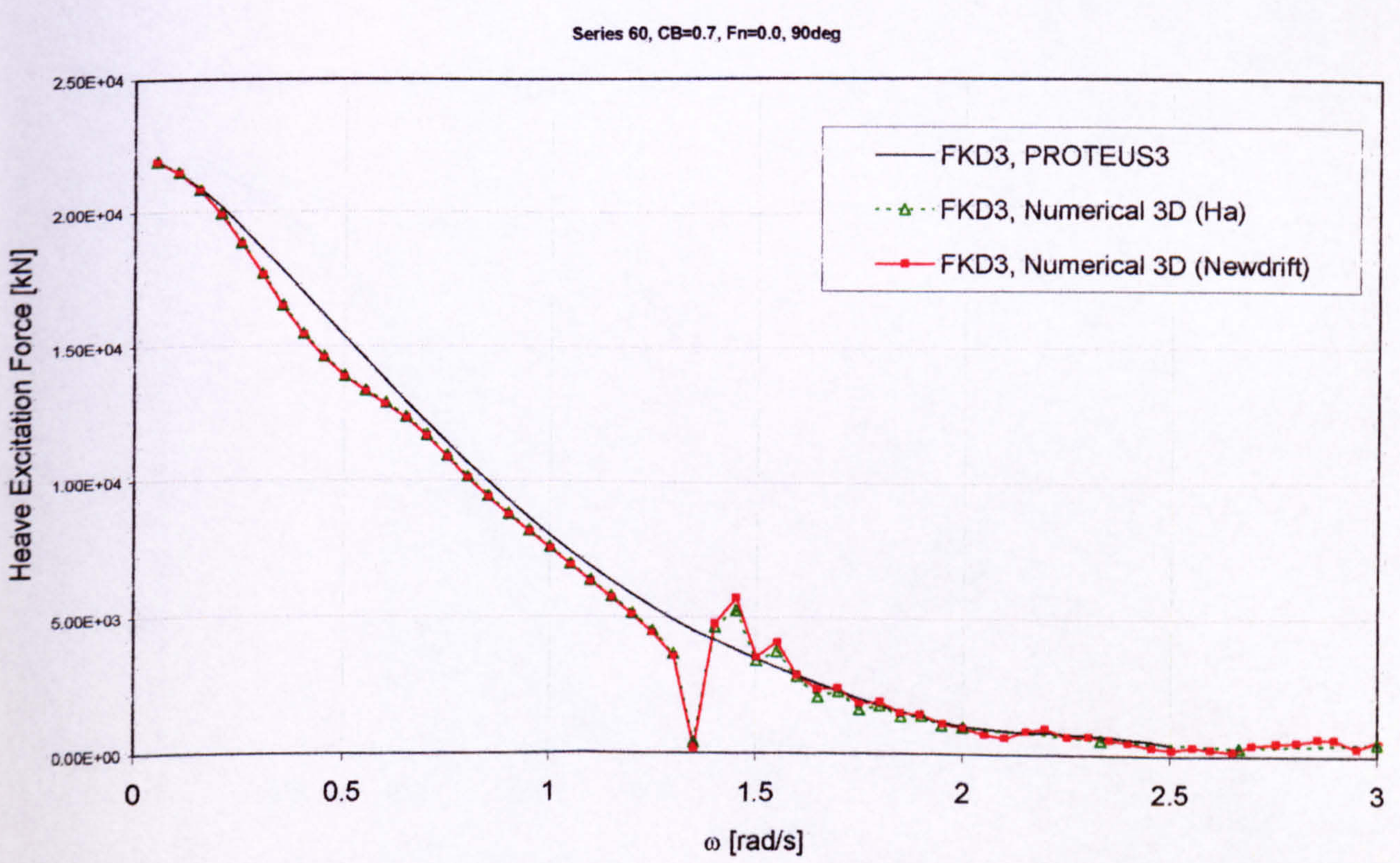

Figure 36 Excitation force in heave mode for 3D Series 60, CB=0.7 hull form, comparison between predictions by strip theory and 3D panel methods, Fn=0.0, Heading 90deg

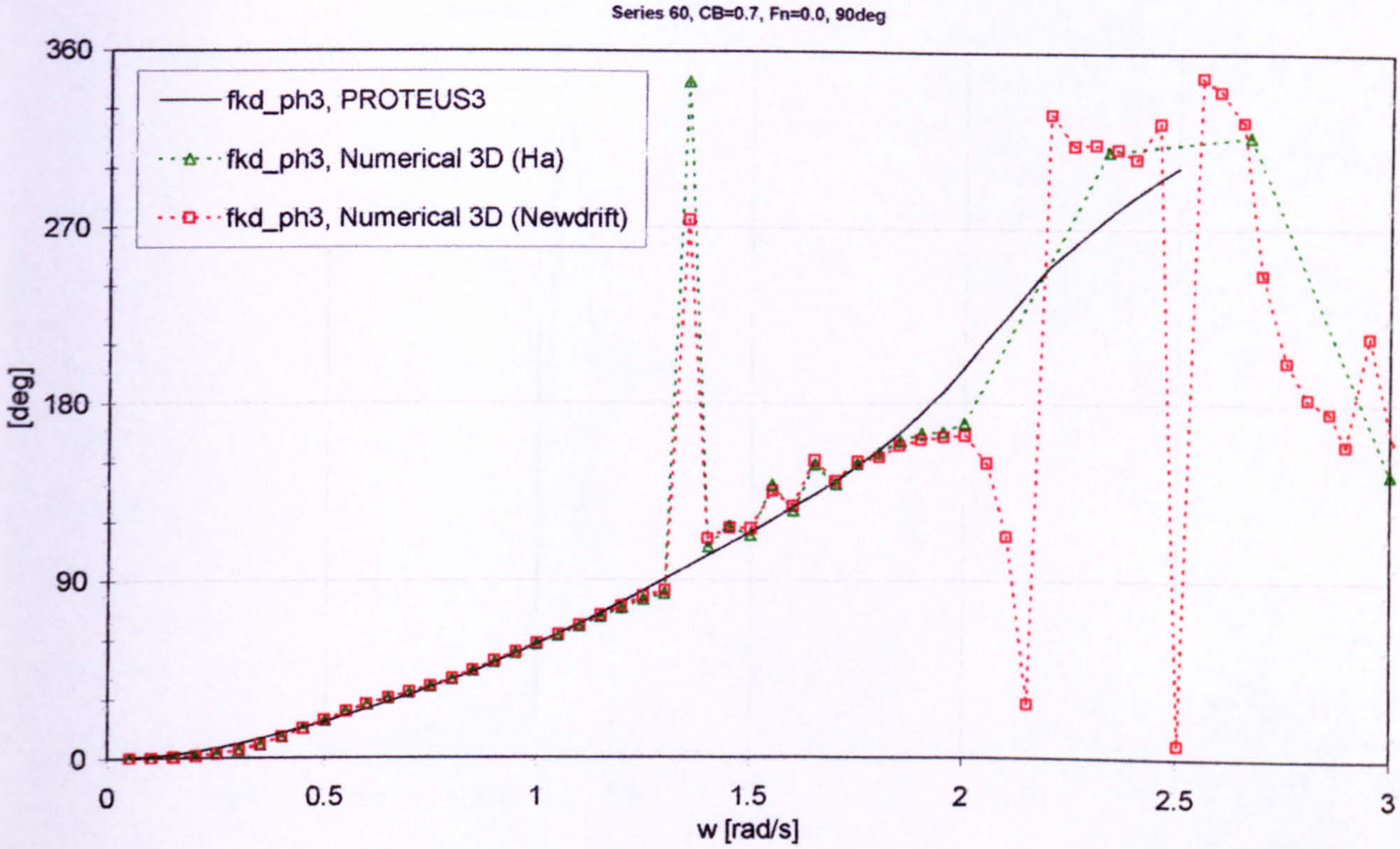

Figure 37 Excitation force phase angle in heave mode for 3D Series 60, CB=0.7 hull form, comparison between predictions by strip theory and 3D panel methods, Fn=0.0, Heading 90deg

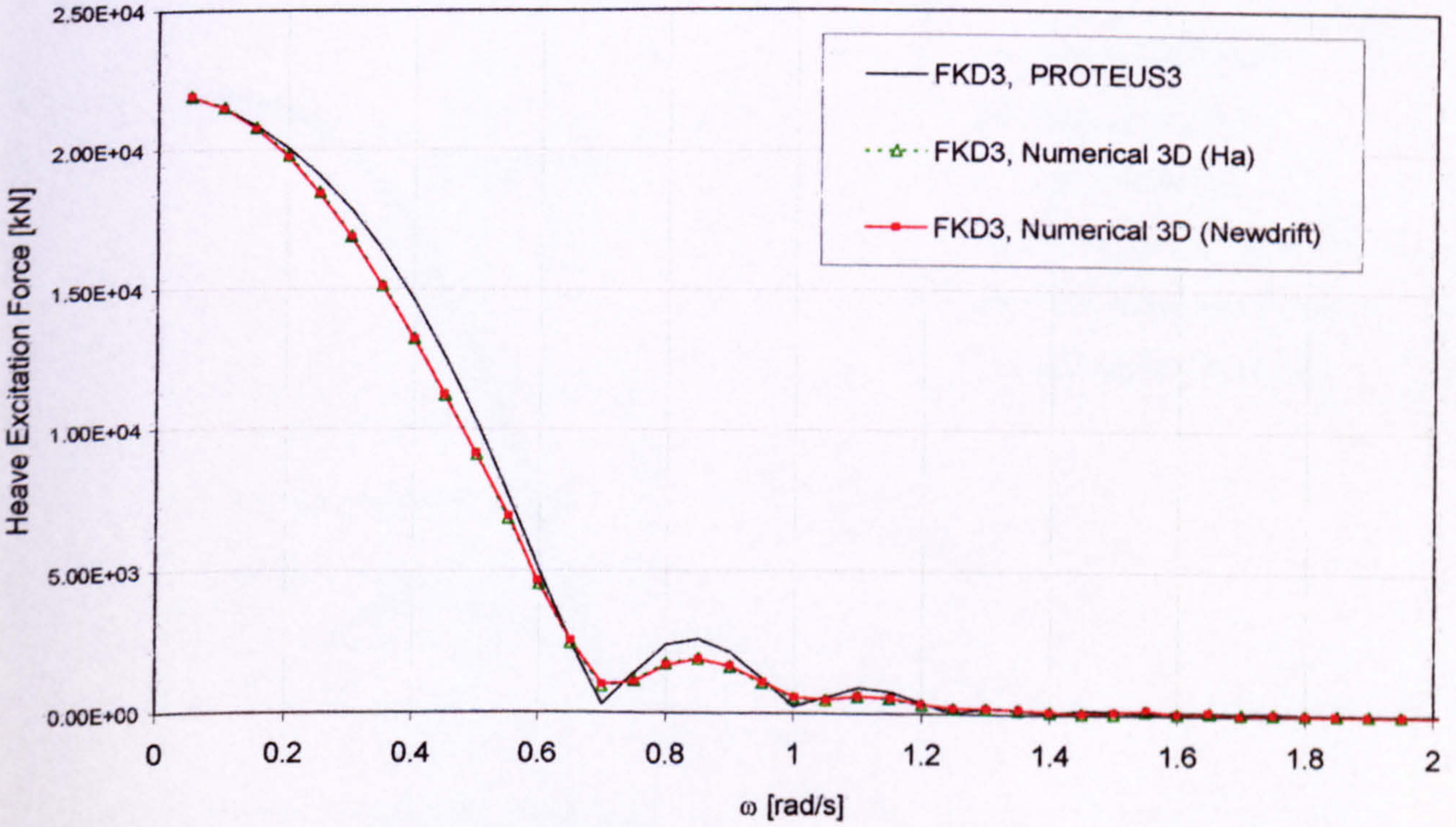

Figure 38 Excitation force in heave mode for 3D Series 60, CB=0.7 hull form, comparison between predictions by strip theory and 3D panel methods, Fn=0.0, Heading 180deg

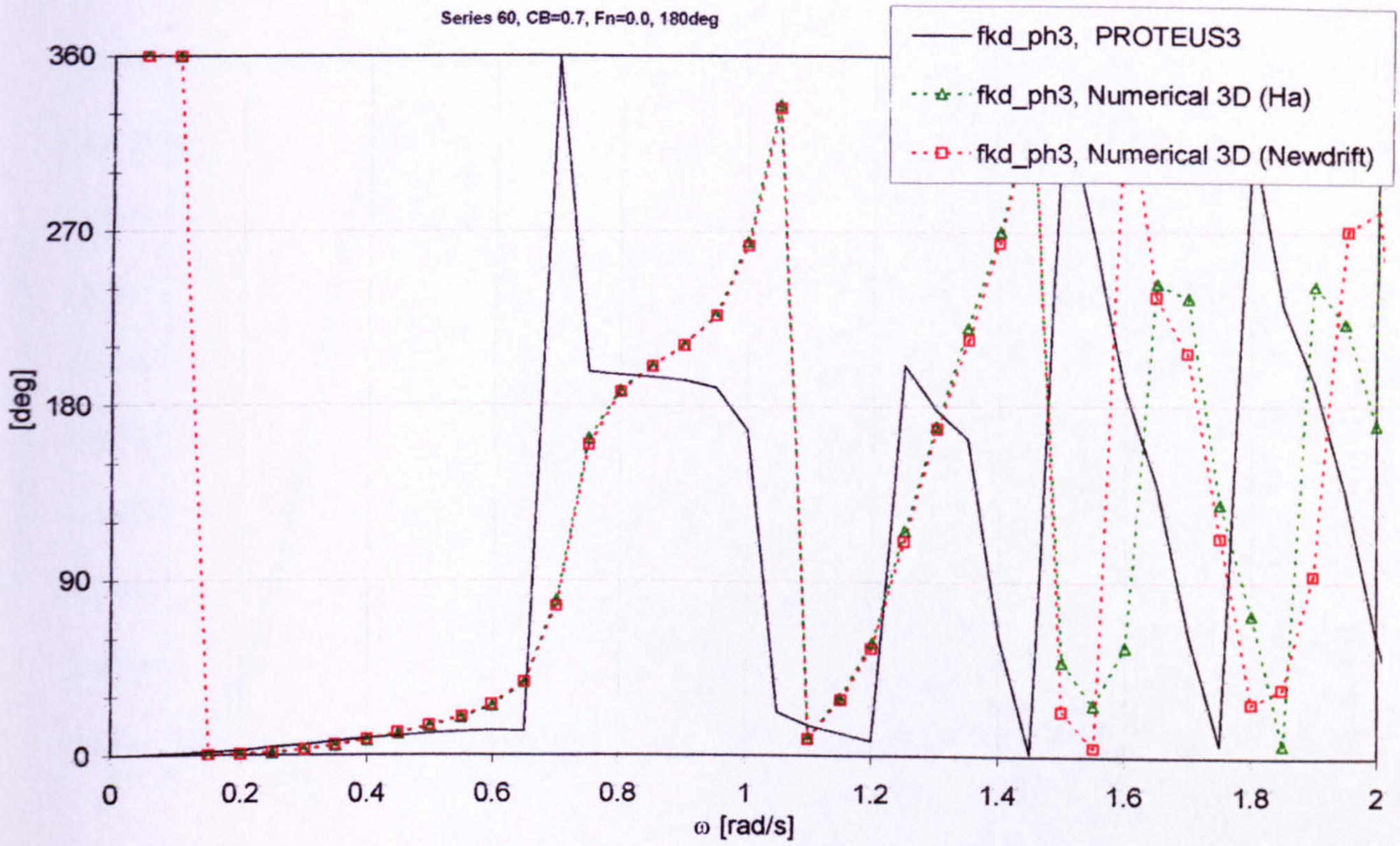

Figure 39 Excitation force phase angle in heave mode for 3D Series 60, CB=0.7 hull form, comparison between predictions by strip theory and 3D panel methods, Fn=0.0, Heading 180deg

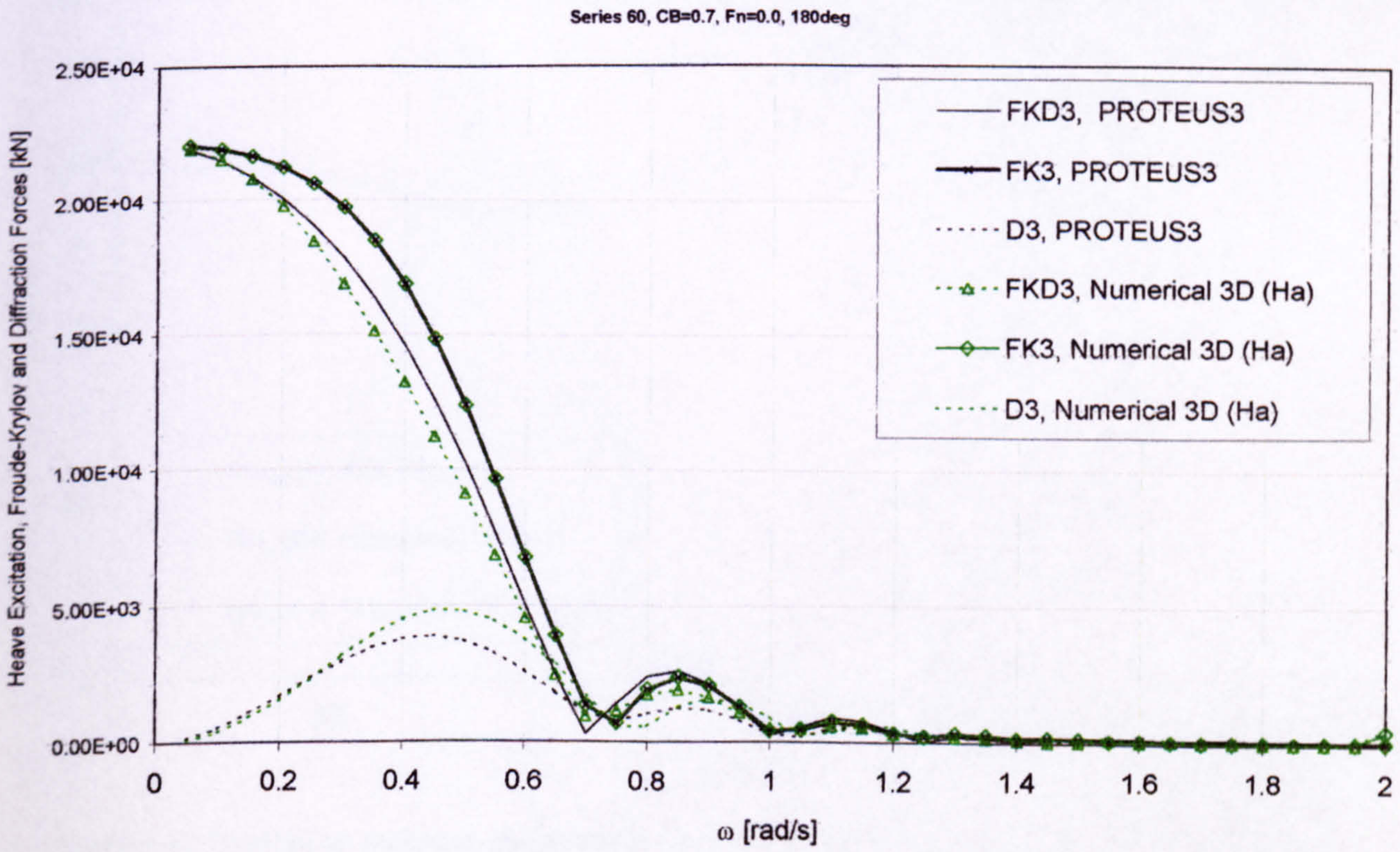

Figure 40 Excitation, Froude-Krylov and Diffraction forces in heave mode for 3D Series 60, CB=0.7 hull form, predictions by strip theory and 3D panel methods, Fn=0.0, Heading 180deg

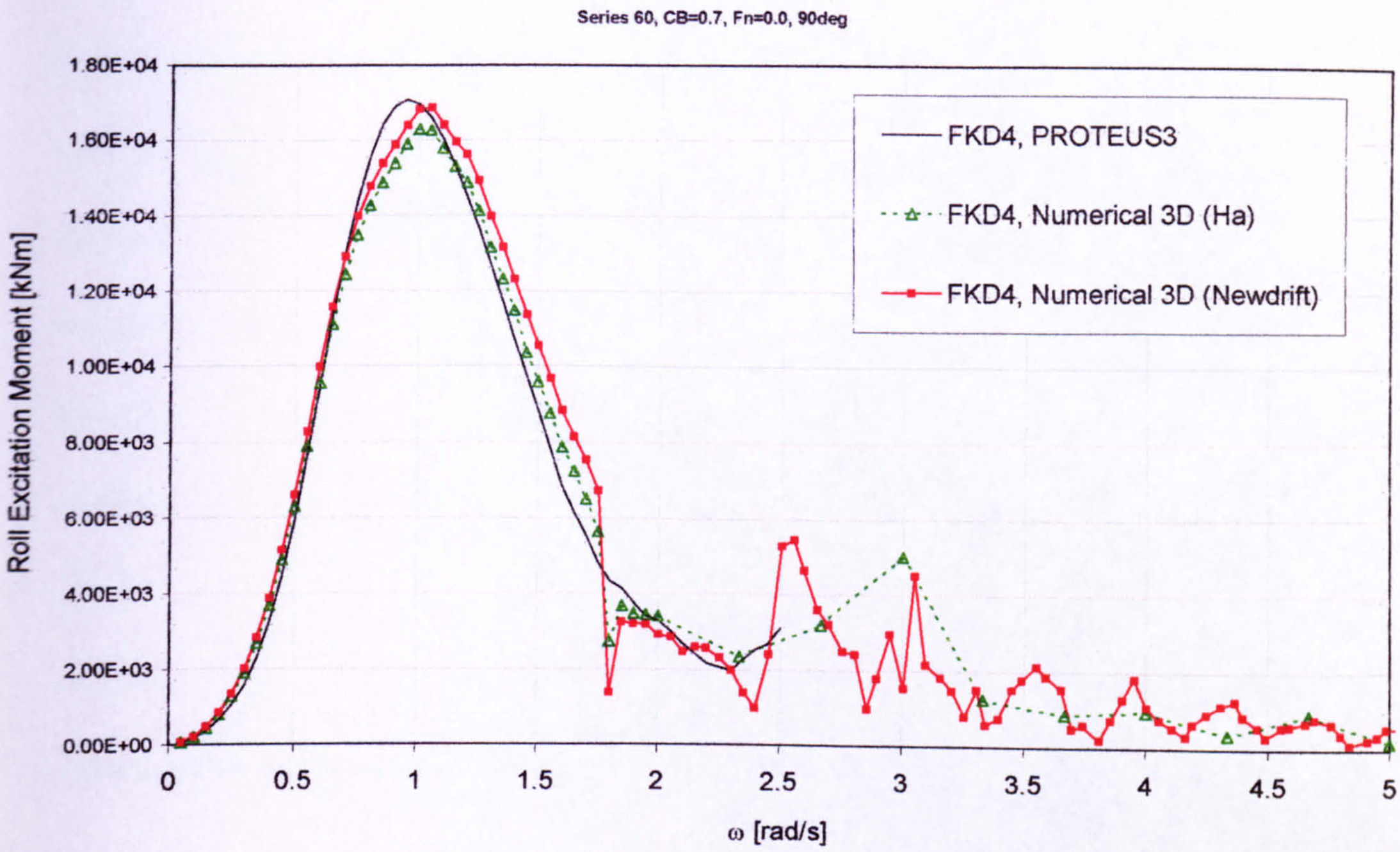

Figure 41 Excitation moment in roll mode for 3D Series 60, CB=0.7 hull form, comparison between predictions by strip theory and 3D panel methods, Fn=0.0, Heading 90deg

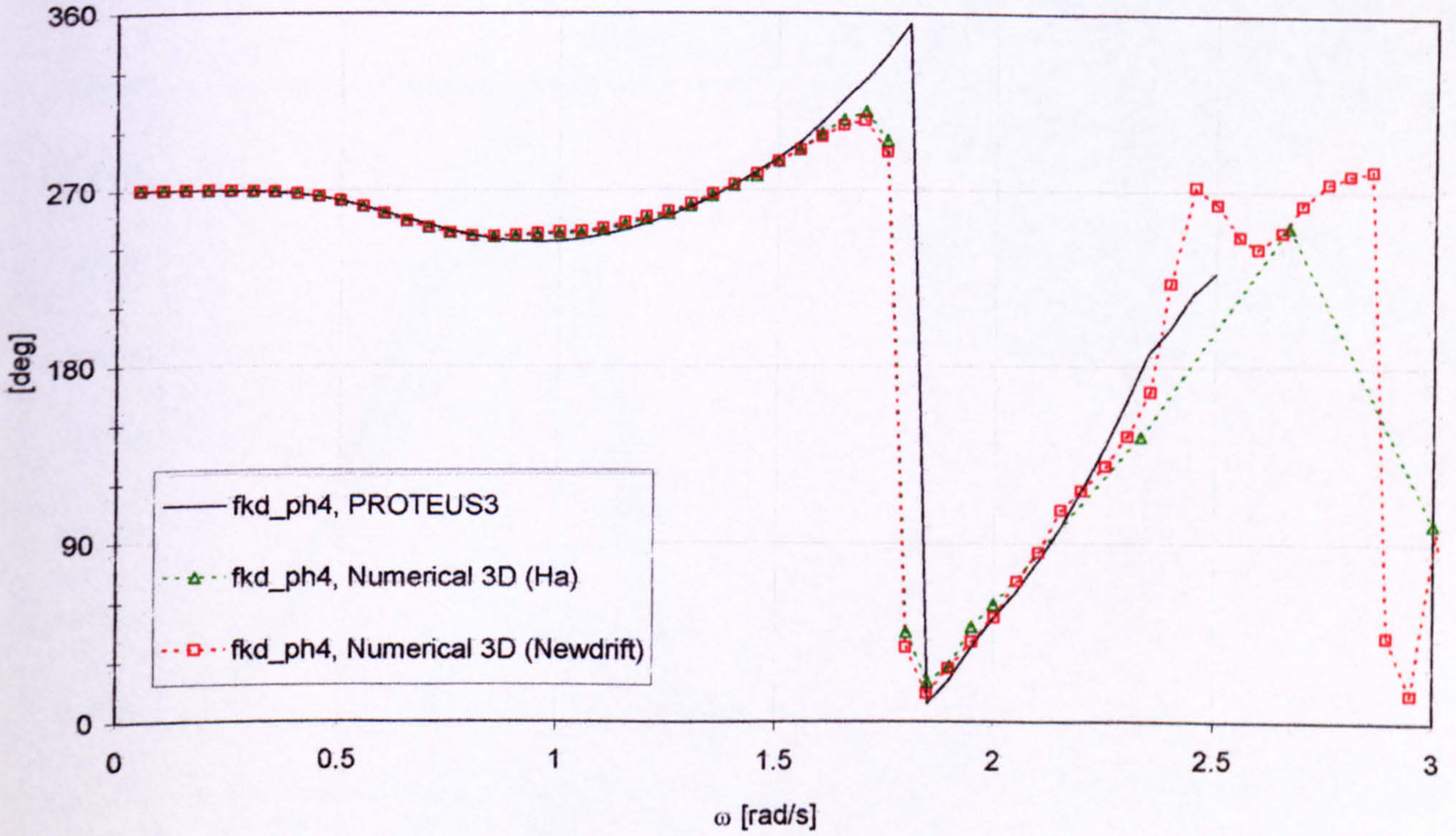

Figure 42 Excitation moment phase angle in roll mode for 3D Series 60, CB=0.7 hull form, comparison between predictions by strip theory and 3D panel methods, Fn=0.0, Heading 90deg

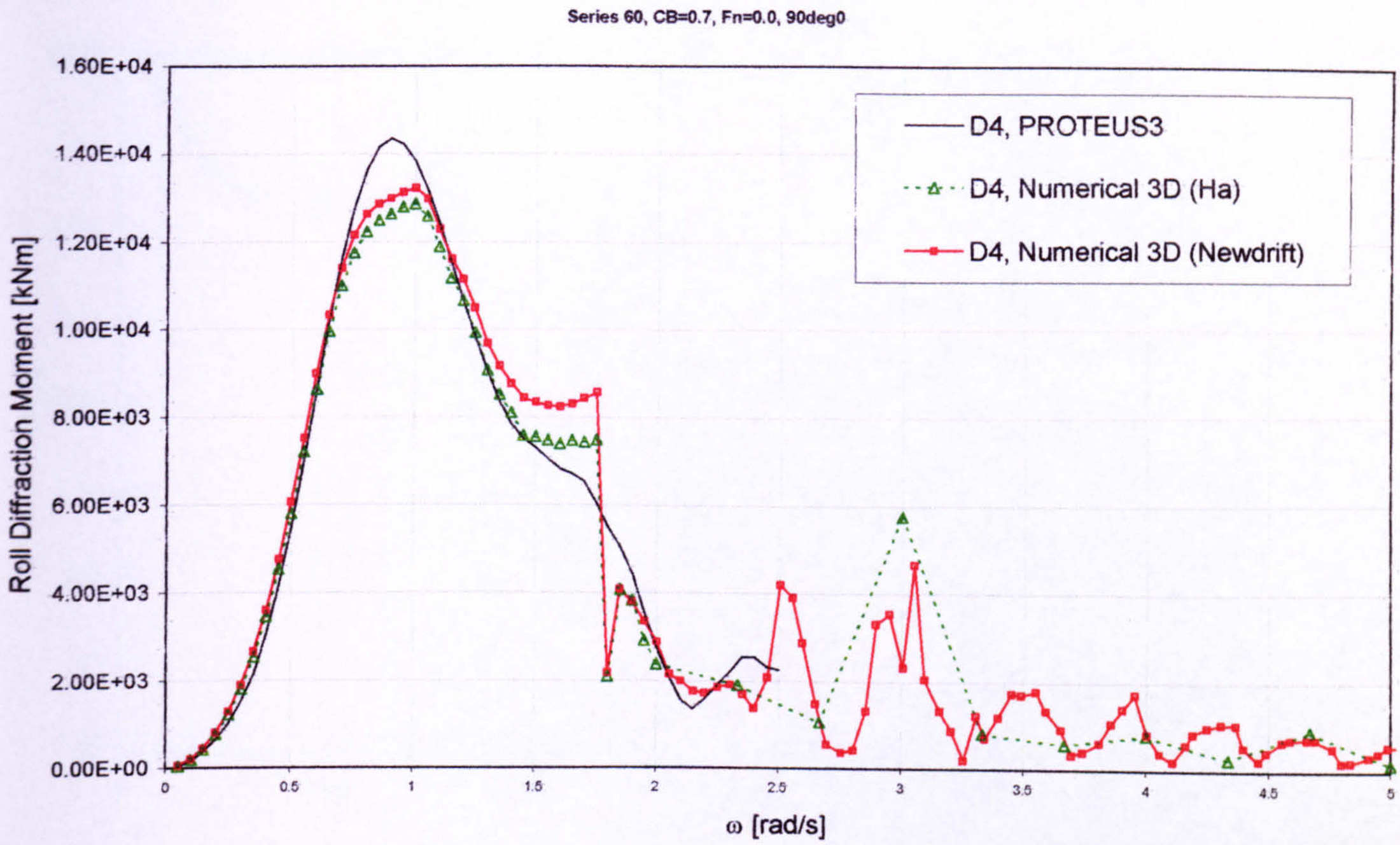

Figure 43 Diffraction moment in roll mode for 3D Series 60, CB=0.7 hull form, comparison between predictions by strip theory and 3D panel methods, Fn=0.0, Heading 90deg

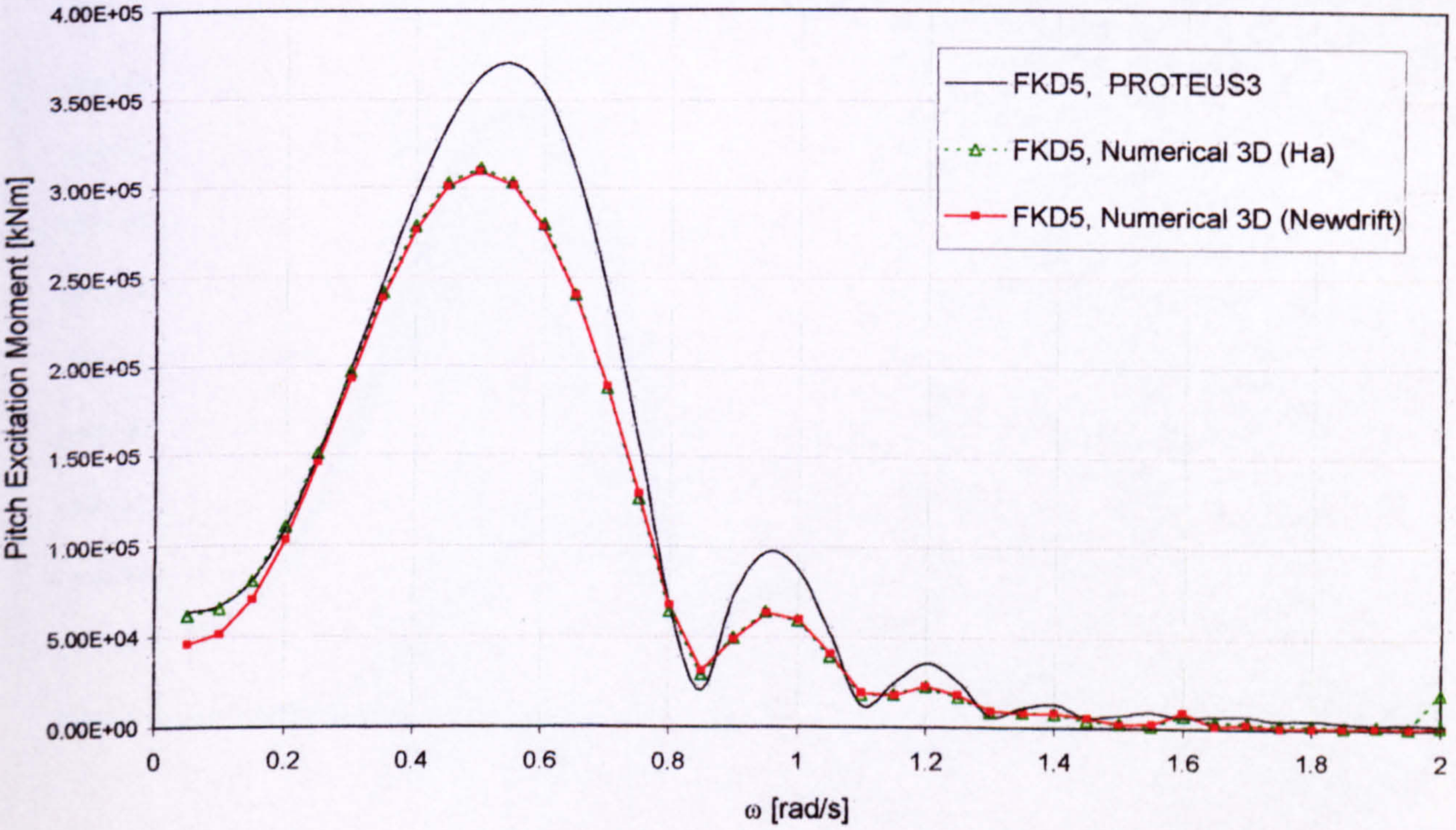

Figure 44 Excitation moment in pitch mode for 3D Series 60, CB=0.7 hull form, comparison between predictions by strip theory and 3D panel methods, Fn=0.0, Heading 180deg

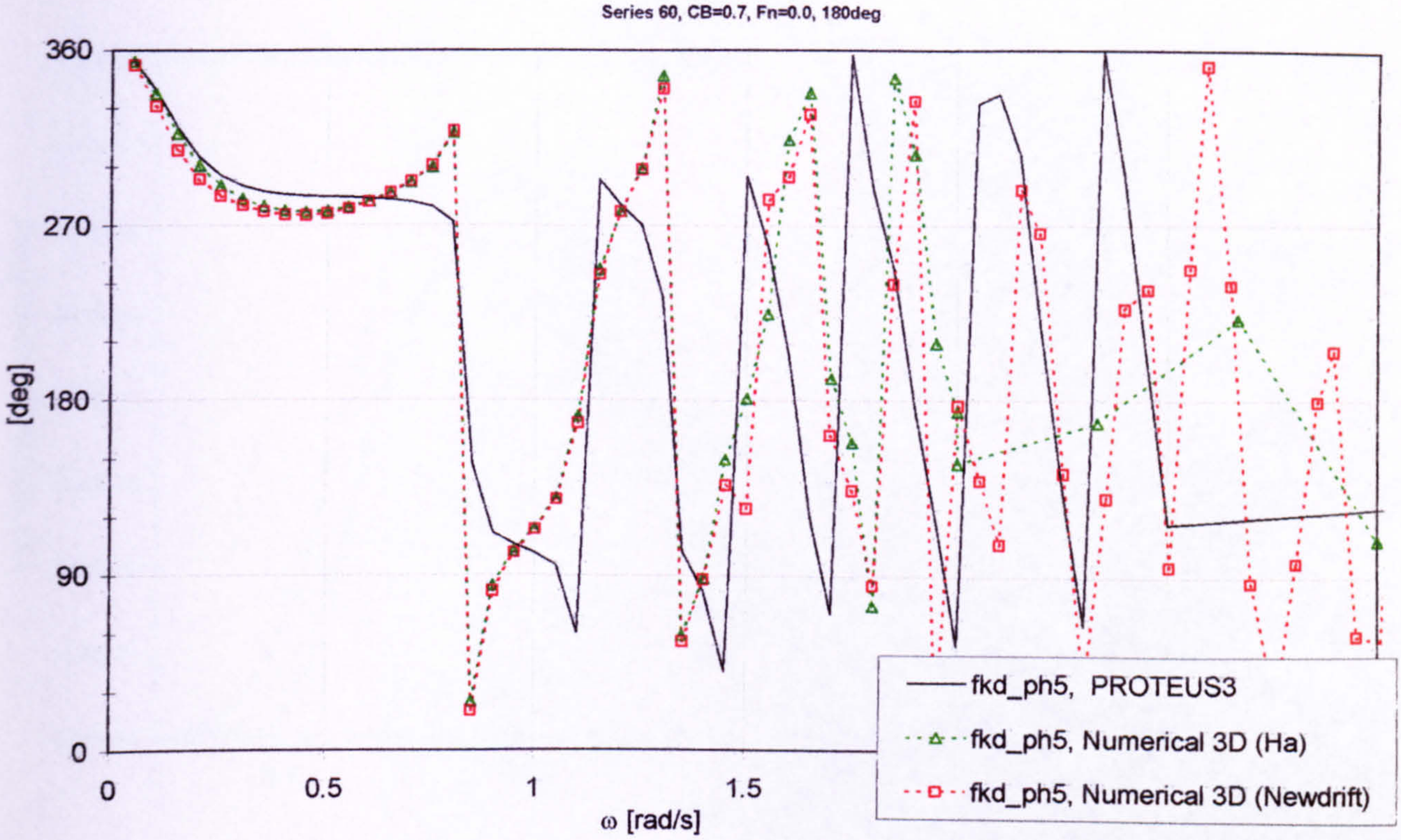

Figure 45 Excitation moment phase angle in pitch mode for 3D Series 60, CB=0.7 hull form, comparison between predictions by strip theory and 3D panel methods, Fn=0.0, Heading 180deg

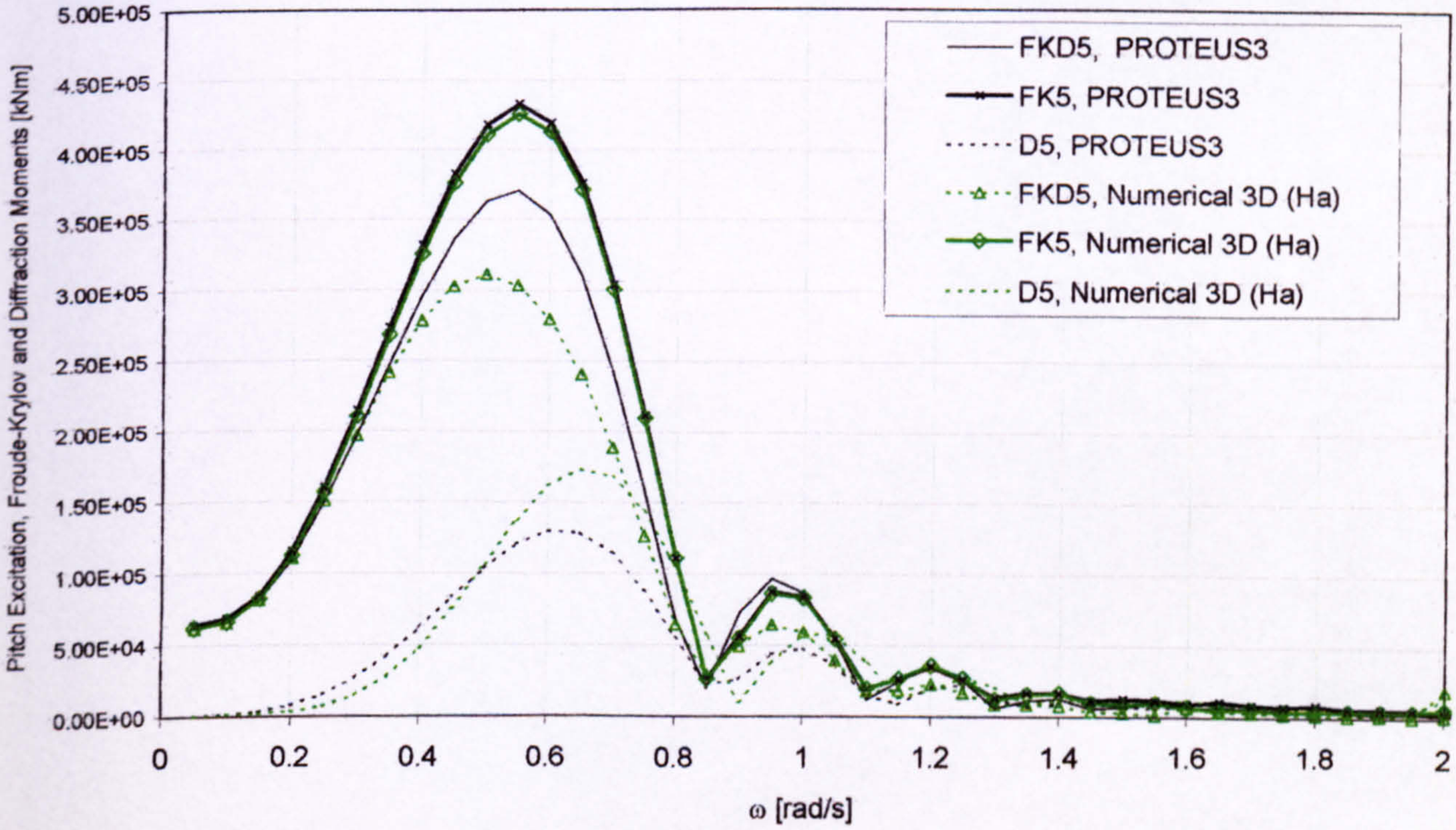

Figure 46 Excitation, Froude-Krylov and Diffraction moment in pitch mode for 3D Series 60, CB=0.7 hull form, predictions by strip theory and 3D panel methods, Fn=0.0, Heading 180deg

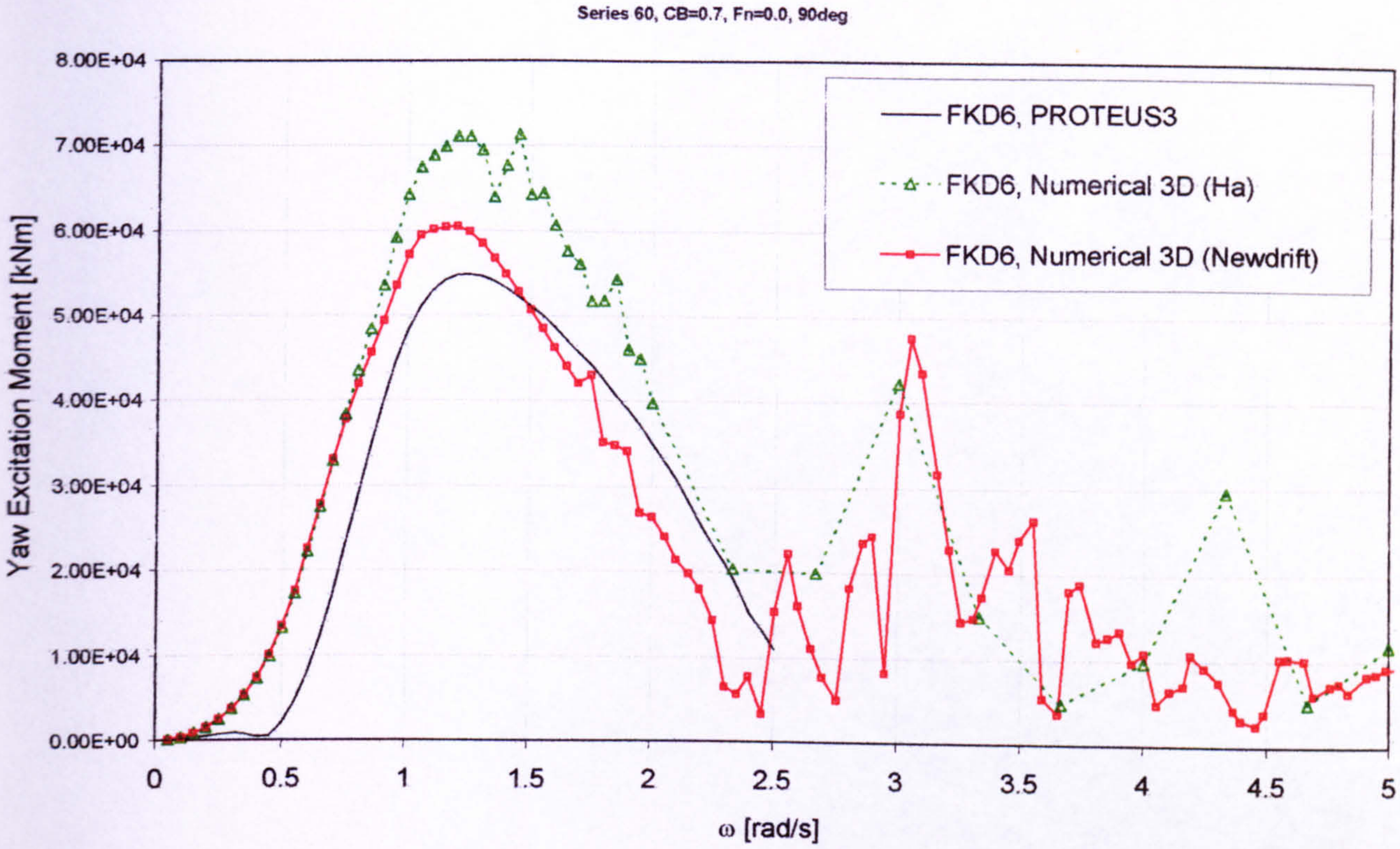

Figure 47 Excitation moment in yaw mode for 3D Series 60, CB=0.7 hull form, comparison between predictions by strip theory and 3D panel methods, Fn=0.0, Heading 90deg

Hydrodynamic coefficients for Fn=0.2

Comparison between strip theory, 3D panel methods and experimental data

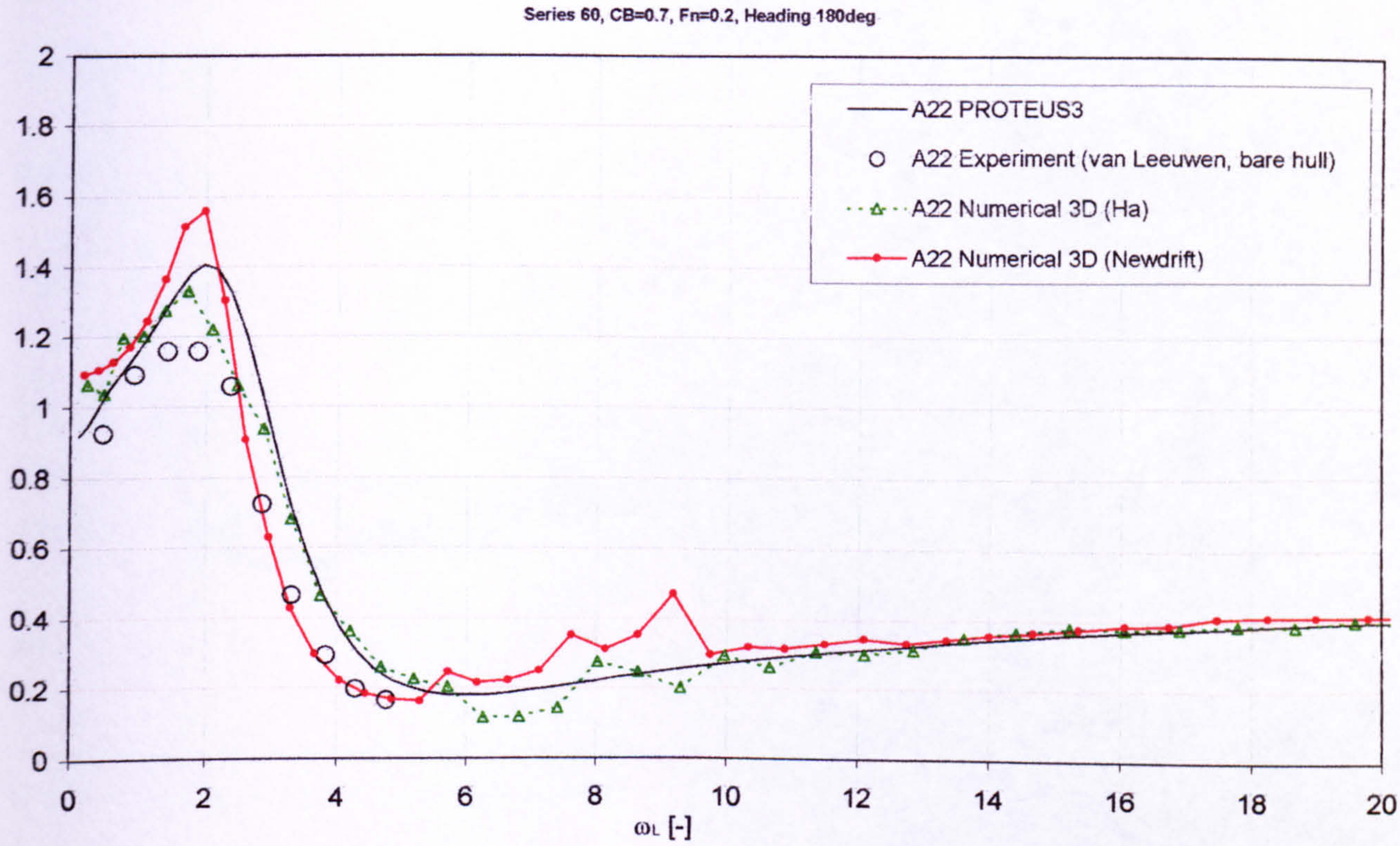

Figure 48 Dimensionless added mass in sway mode for 3D Series 60, CB=0.7 hull form, comparison between predictions by strip theory, 3D panel methods and experiments, Fn=0.2

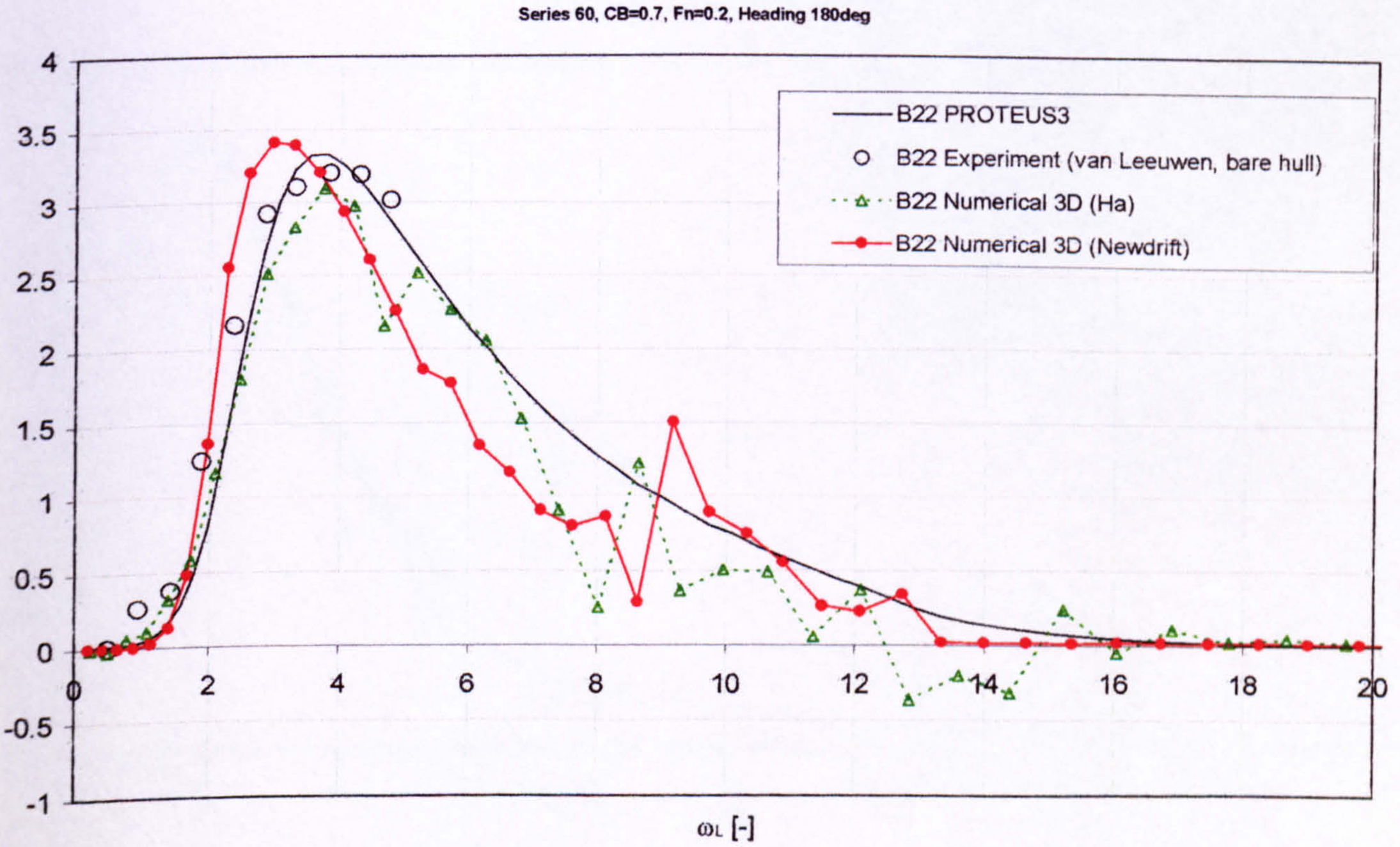

Figure 49 Dimensionless potential damping in sway mode for 3D Series 60, CB=0.7 hull form, comparison between predictions by strip theory, 3D panel methods and experiments, Fn=0.2

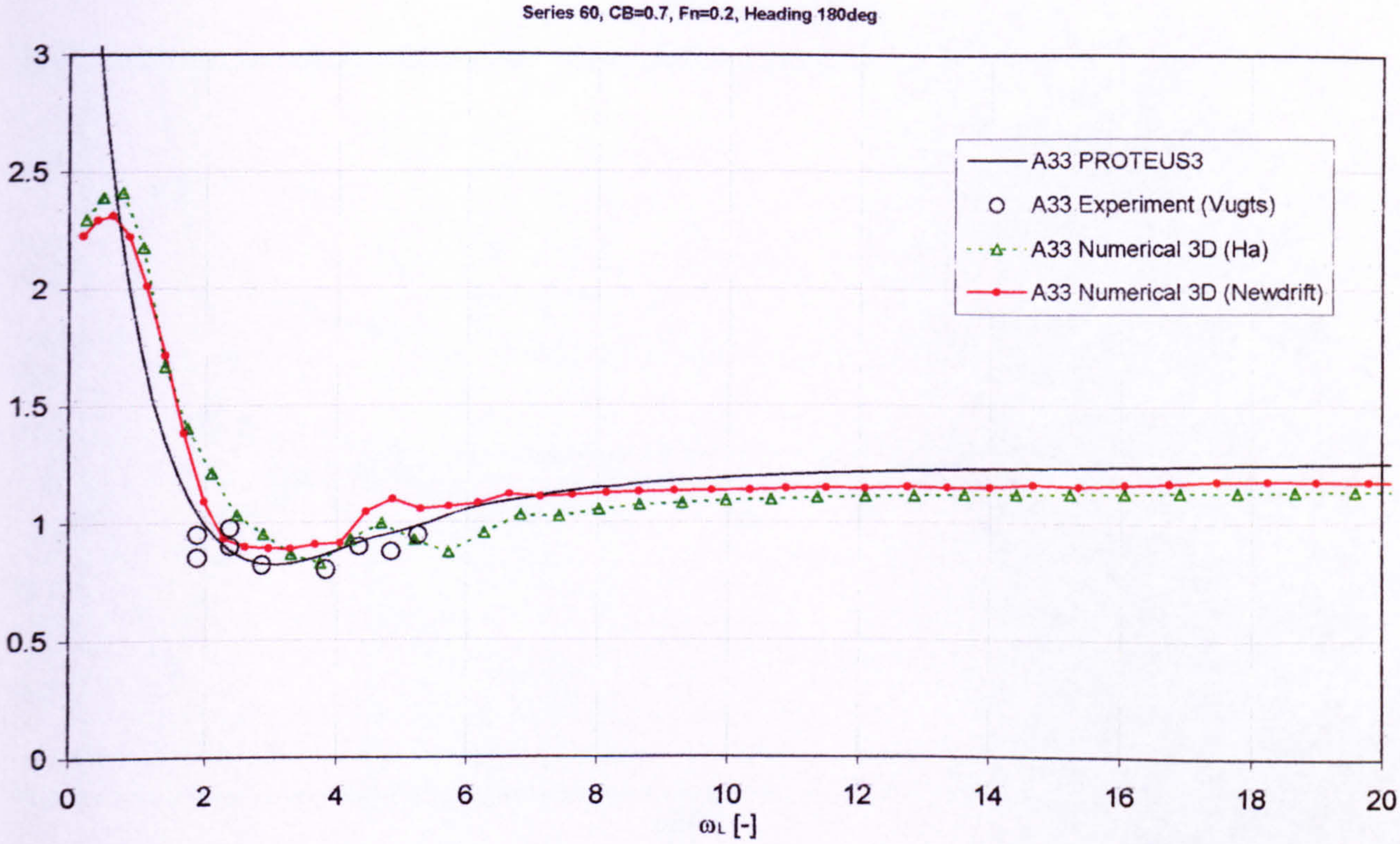

Figure 50 Dimensionless added mass in heave mode for 3D Series 60, CB=0.7 hull form, comparison between predictions by strip theory, 3D panel methods and experiments, Fn=0.2

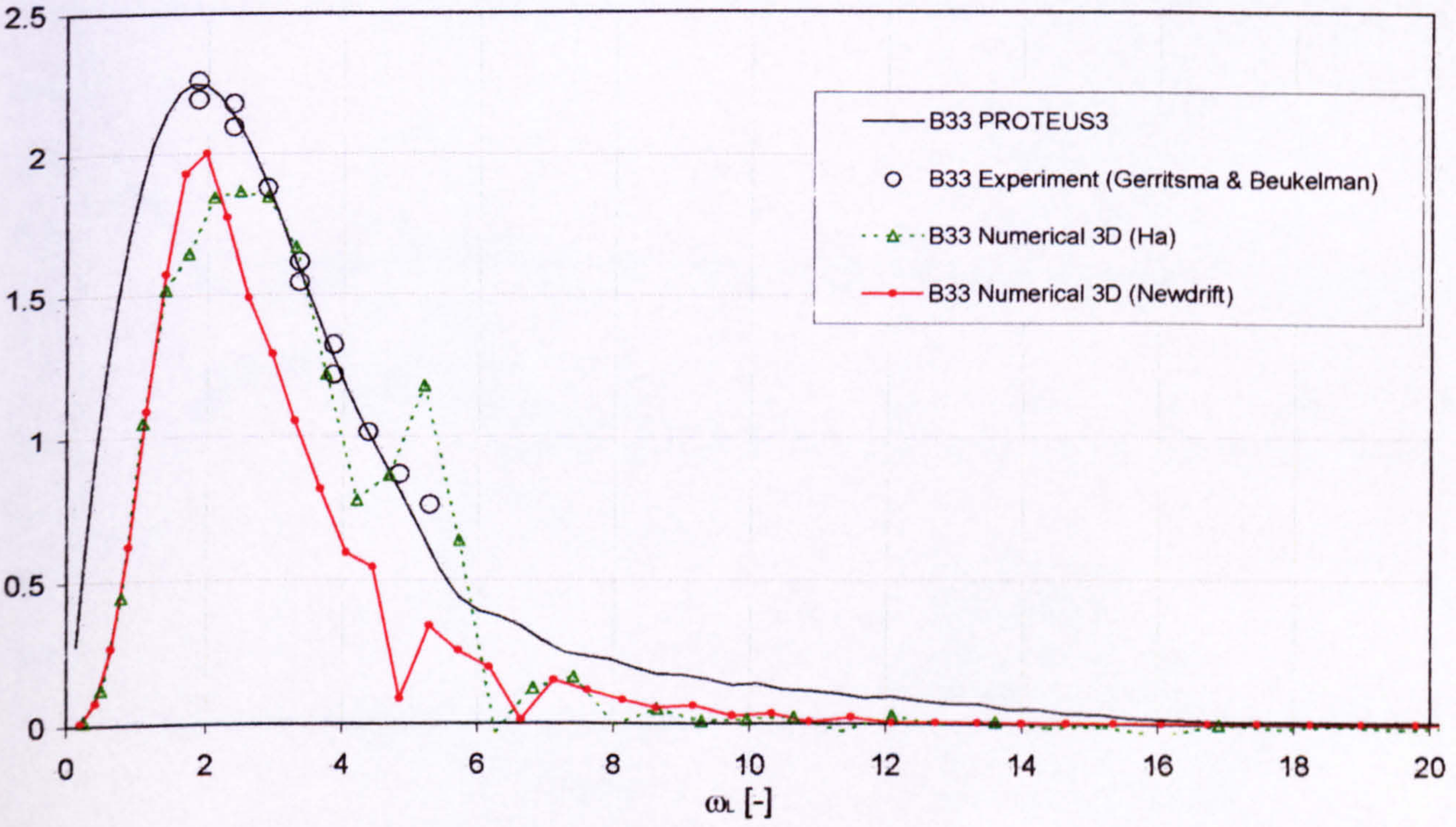

Figure 51 Dimensionless potential damping in heave mode for 3D Series 60, CB=0.7 hull form, comparison between predictions by strip theory, 3D panel methods and experiments, Fn=0.2

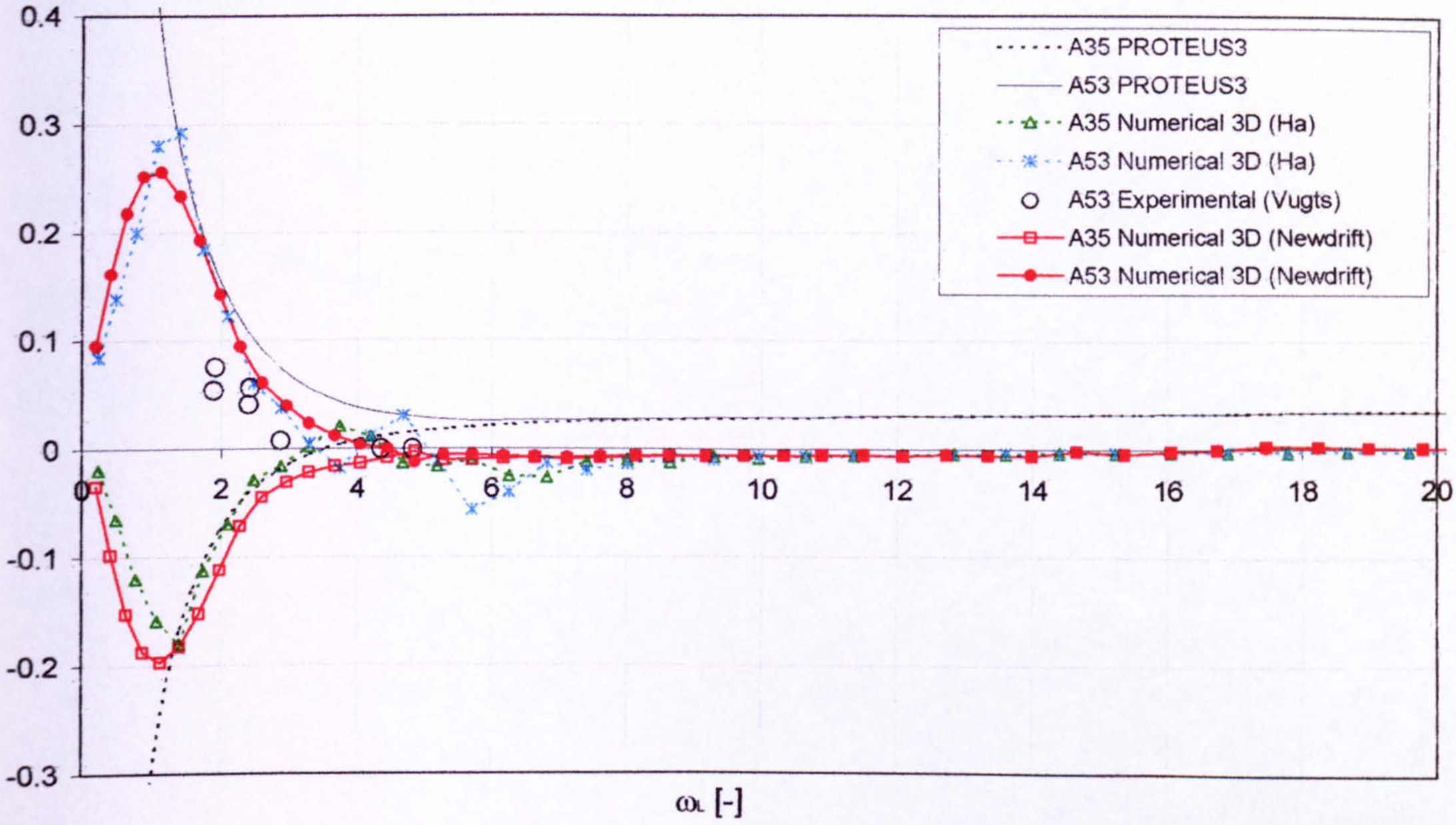

Figure 52 Dimensionless added mass in heave-into-pitch mode for 3D Series 60, CB=0.7 hull form, comparison between predictions by strip theory, 3D panel methods and experiments, Fn=0.2

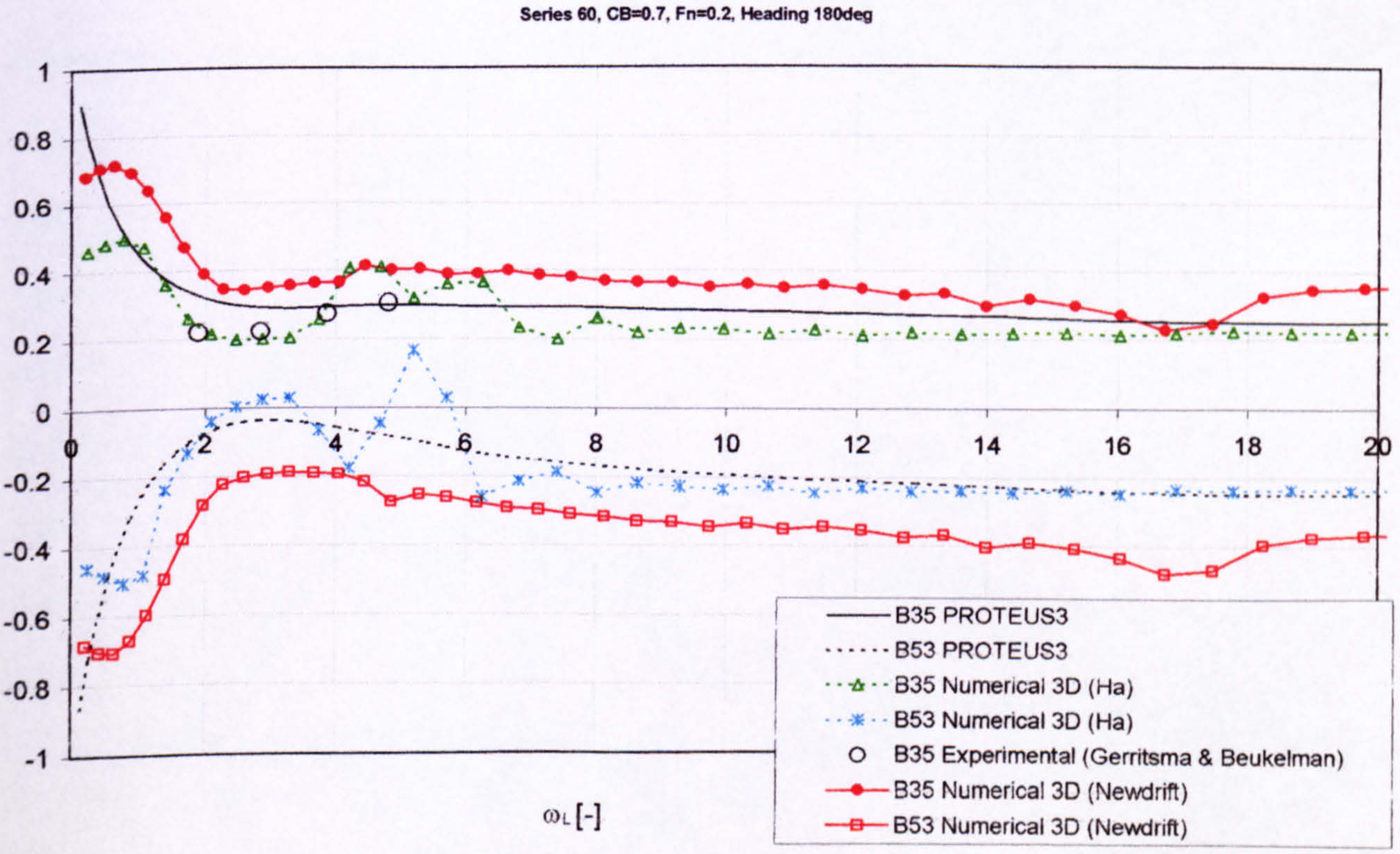

Figure 53 Dimensionless potential damping in heave-into-pitch mode for 3D Series 60, CB=0.7 hull form, comparison between predictions by strip theory, 3D panel methods and experiments, Fn=0.2

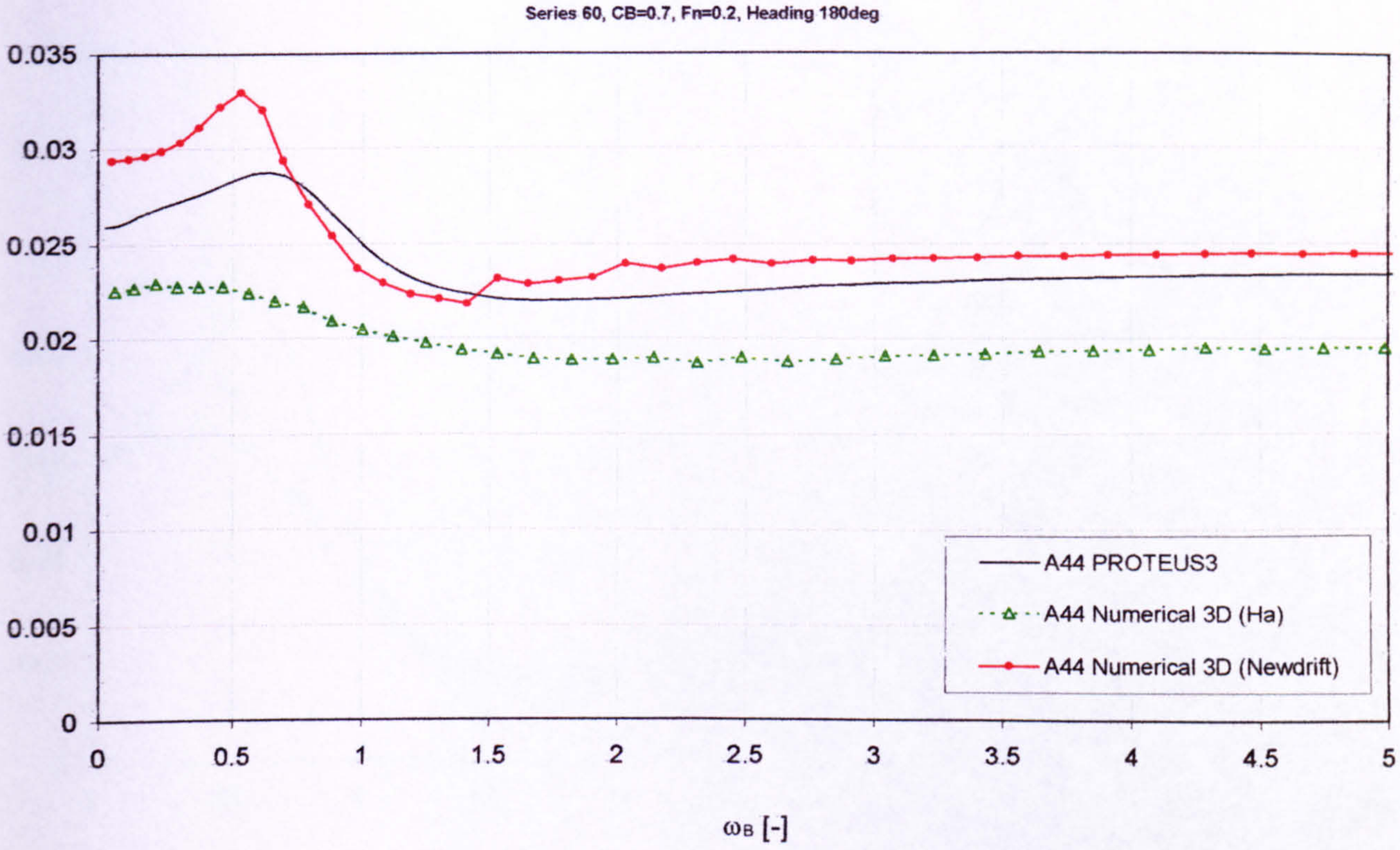

Figure 54 Dimensionless added mass moment of inertia in roll mode for 3D Series 60, CB=0.7 hull form, comparison between predictions by strip theory, 3D panel methods, Fn=0.2

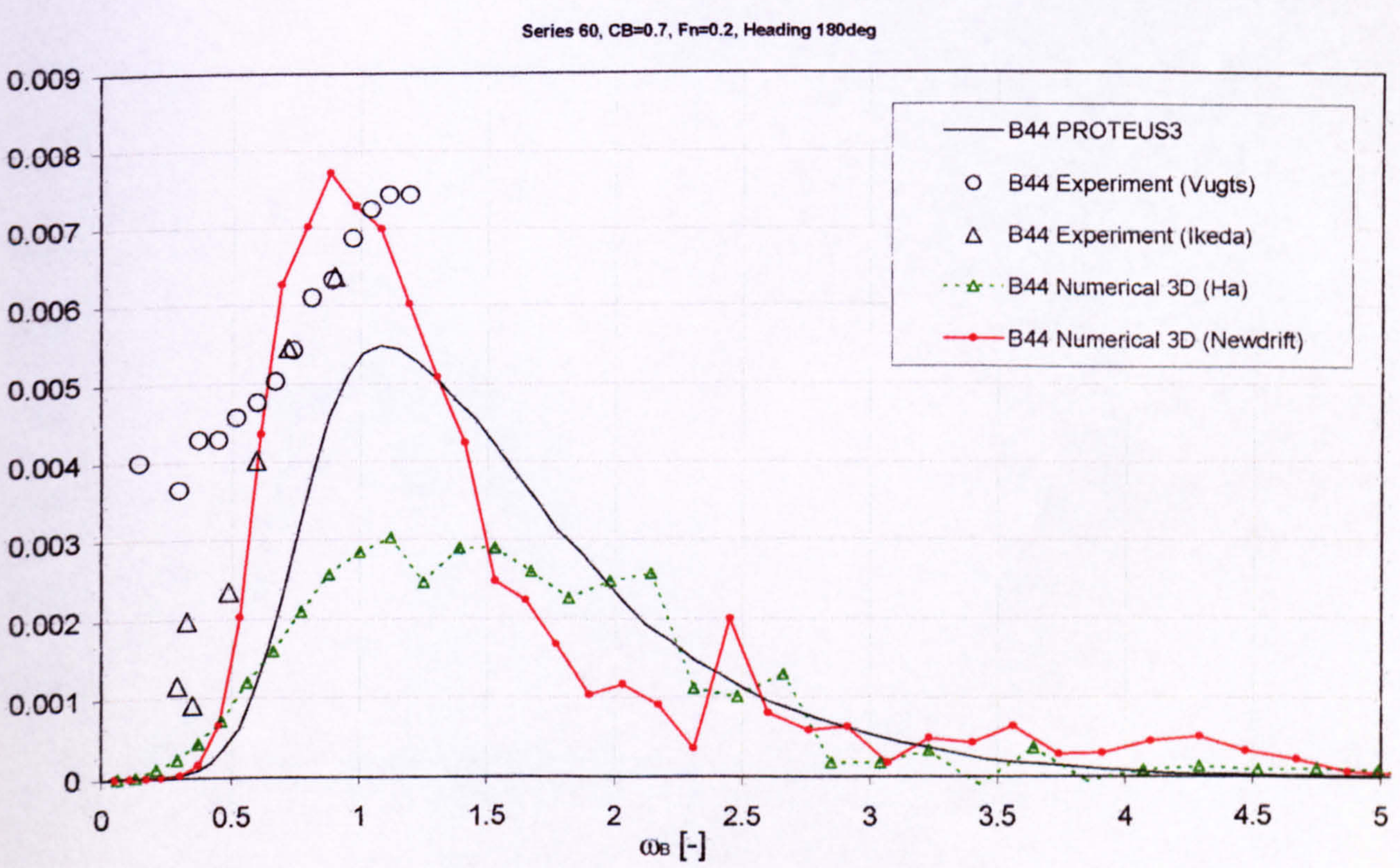

Figure 55 Dimensionless potential damping in roll mode for 3D Series 60, CB=0.7 hull form, comparison between predictions by strip theory, 3D panel methods and experiments, Fn=0.2

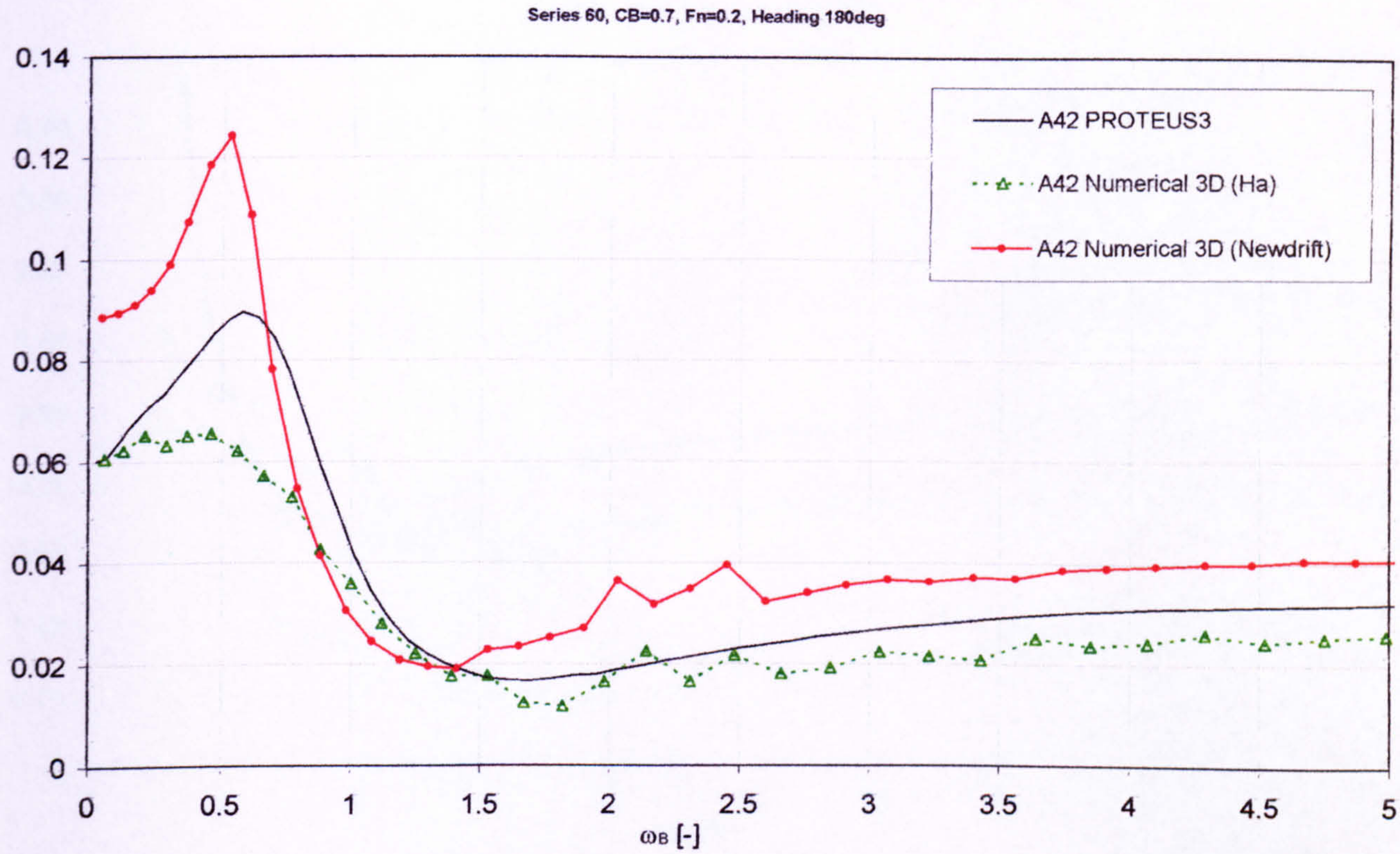

Figure 56 Dimensionless added mass in roll-into-sway mode for 3D Series 60, CB=0.7 hull form, comparison between predictions by strip theory and 3D panel methods, Fn=0.2

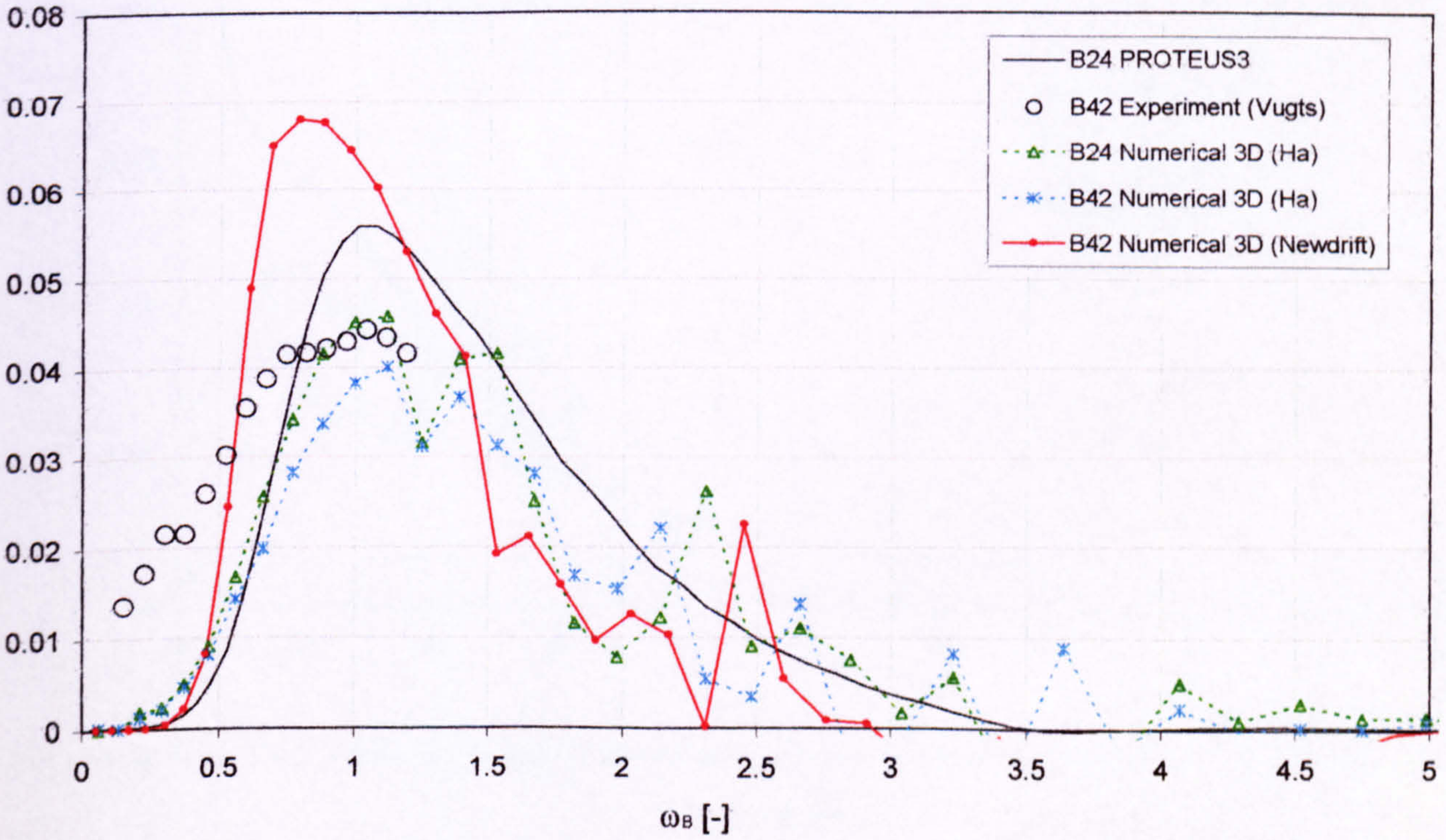

Figure 57 Dimensionless potential damping in roll-into-sway mode for 3D Series 60, CB=0.7 hull form, comparison between predictions by strip theory, 3D panel methods and experiments, Fn=0.2

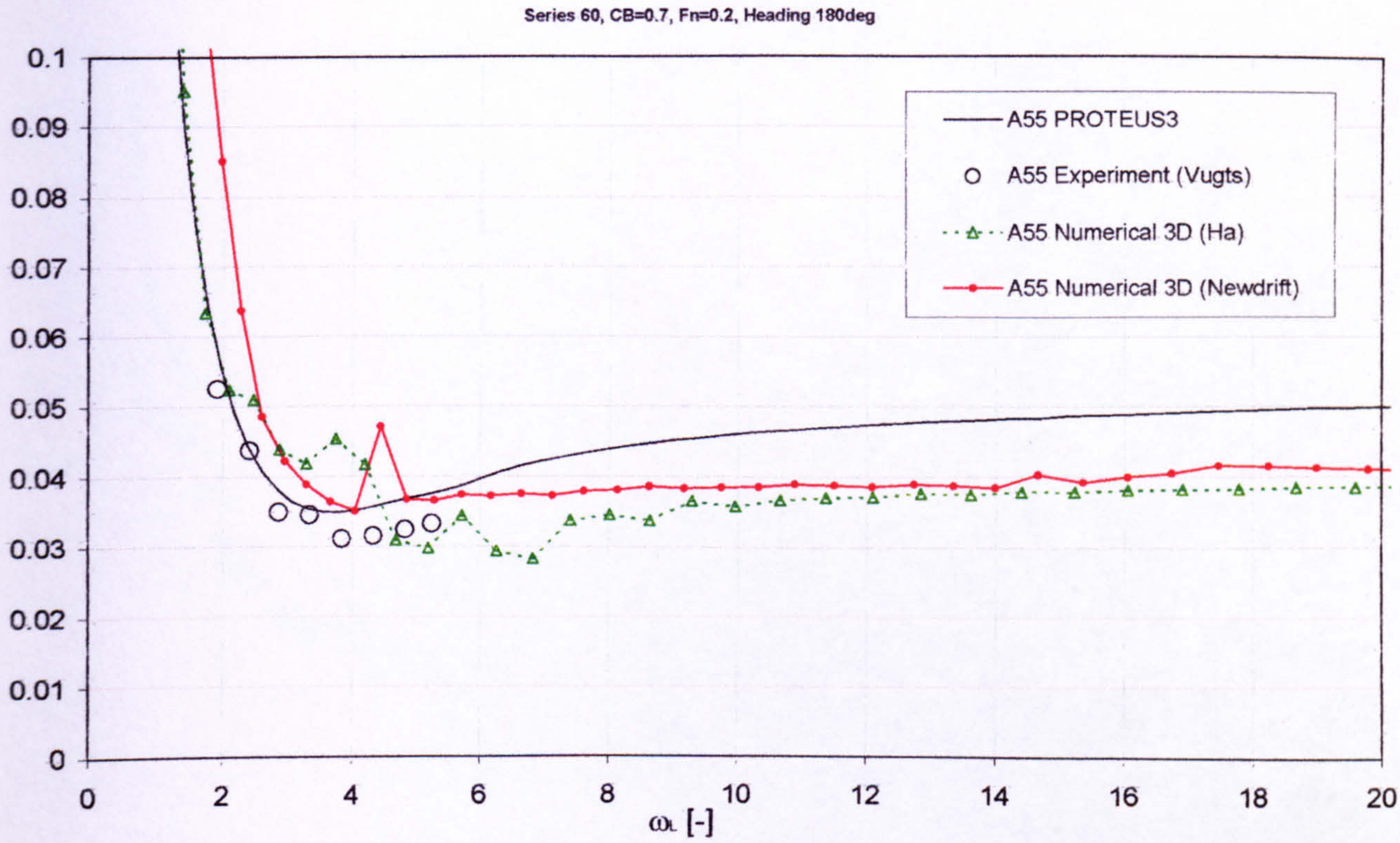

Figure 58 Dimensionless added mass moment of inertia in pitch mode for 3D S60, CB=0.7 hull form, comparison between predictions by strip theory, 3D panel methods and experiments, Fn=0.2

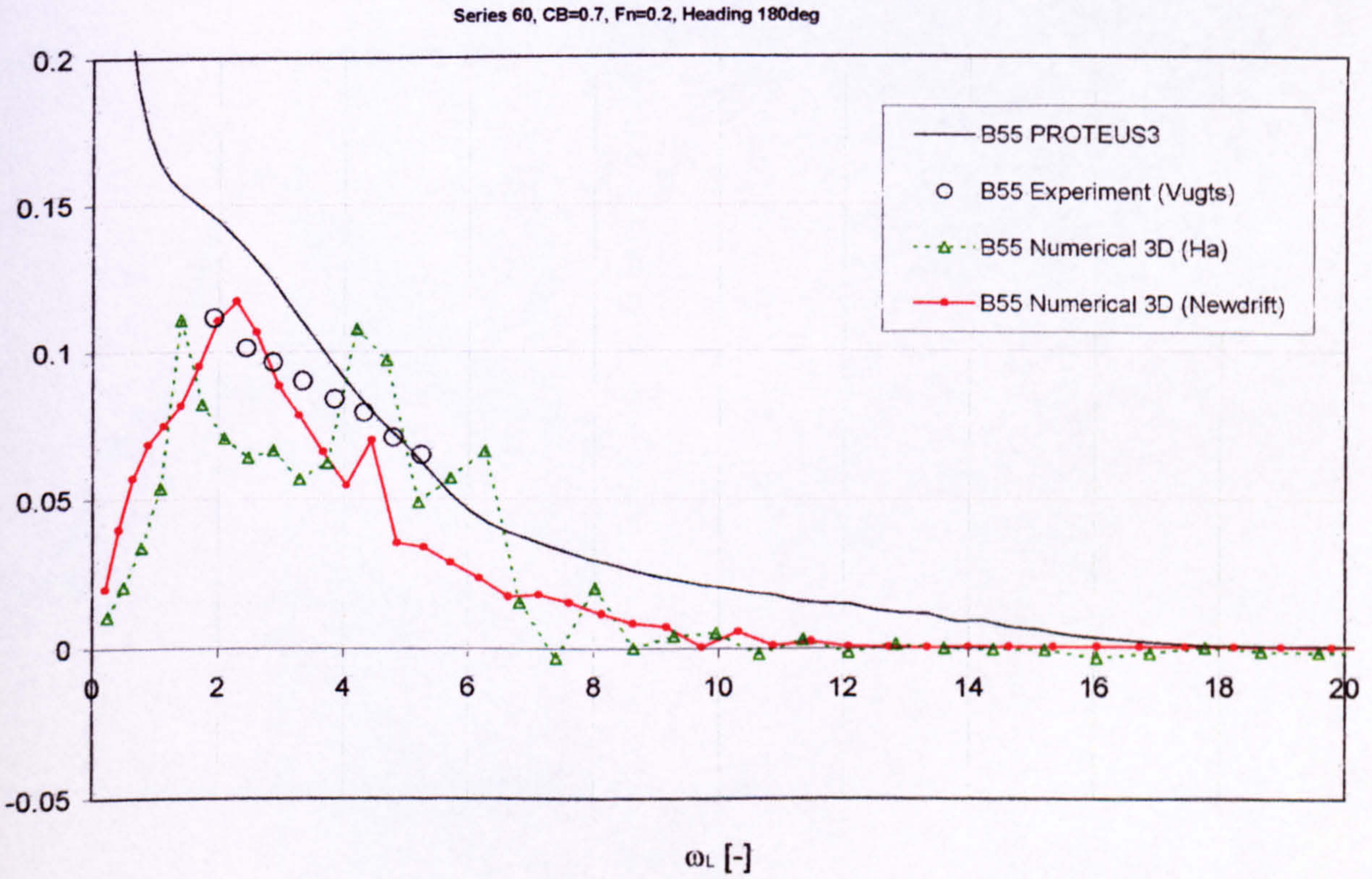

Figure 59 Dimensionless potential damping in pitch mode for 3D Series 60, CB=0.7 hull form, comparison between predictions by strip theory, 3D panel methods and experiments, Fn=0.2

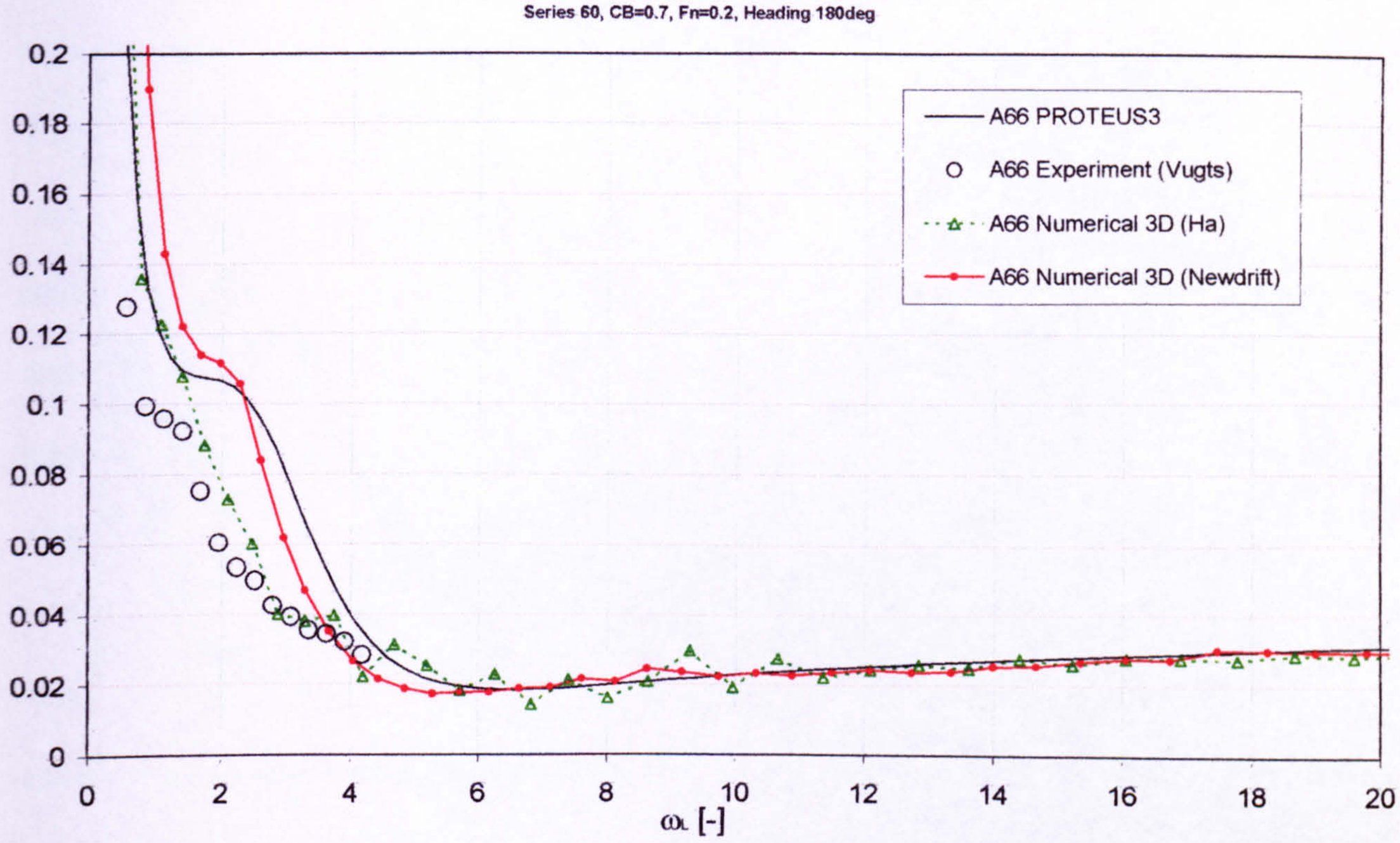

Figure 60 Dimensionless added mass moment of inertia in yaw mode for 3D Series 60, CB=0.7 hull form, comparison between predictions by strip theory, 3D panel methods and experiments, Fn=0.2

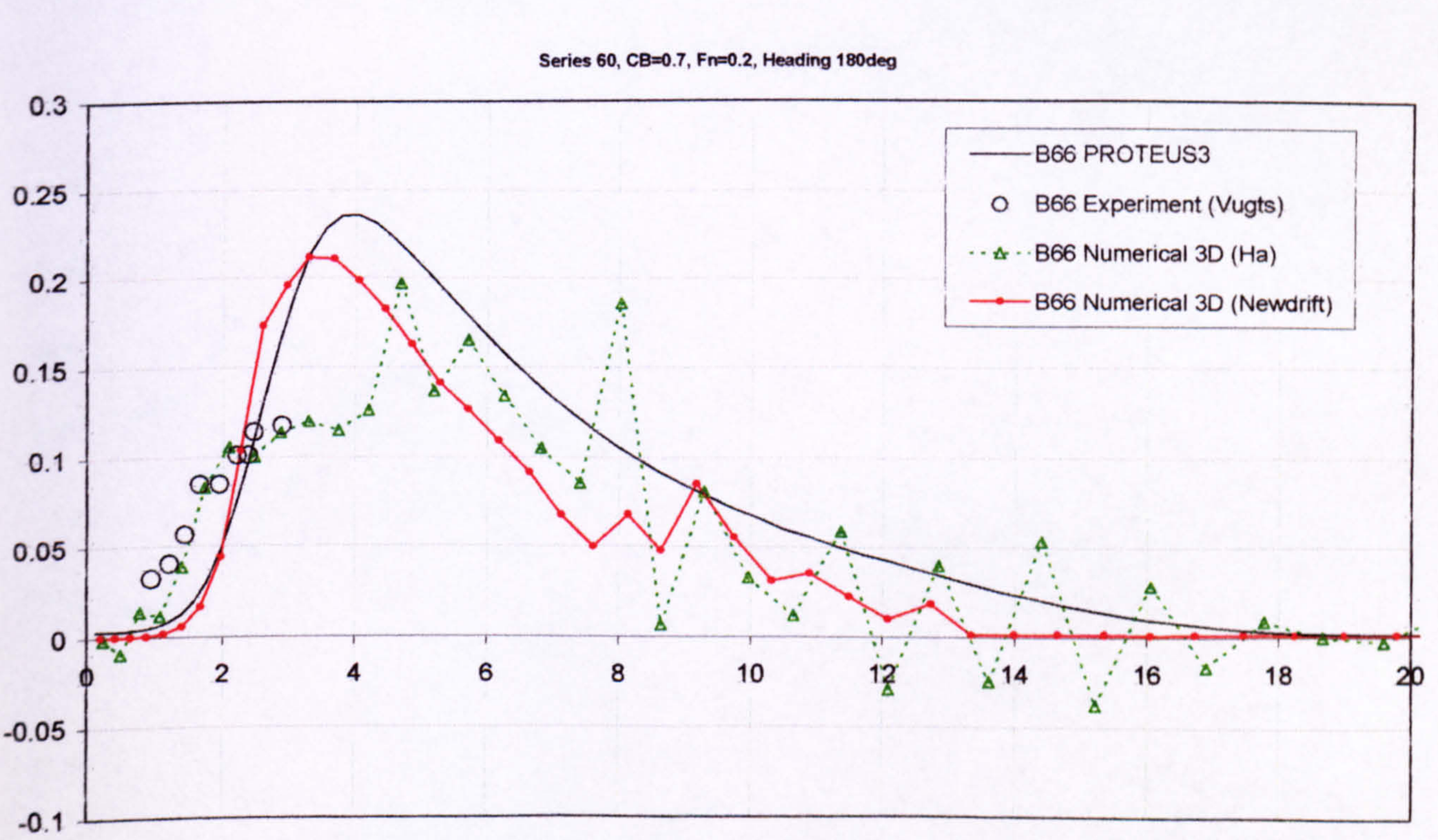

Figure 61 Dimensionless potential damping in yaw mode for 3D Series 60, CB=0.7 hull form, comparison between predictions by strip theory, 3D panel methods and experiments, Fn=0.2

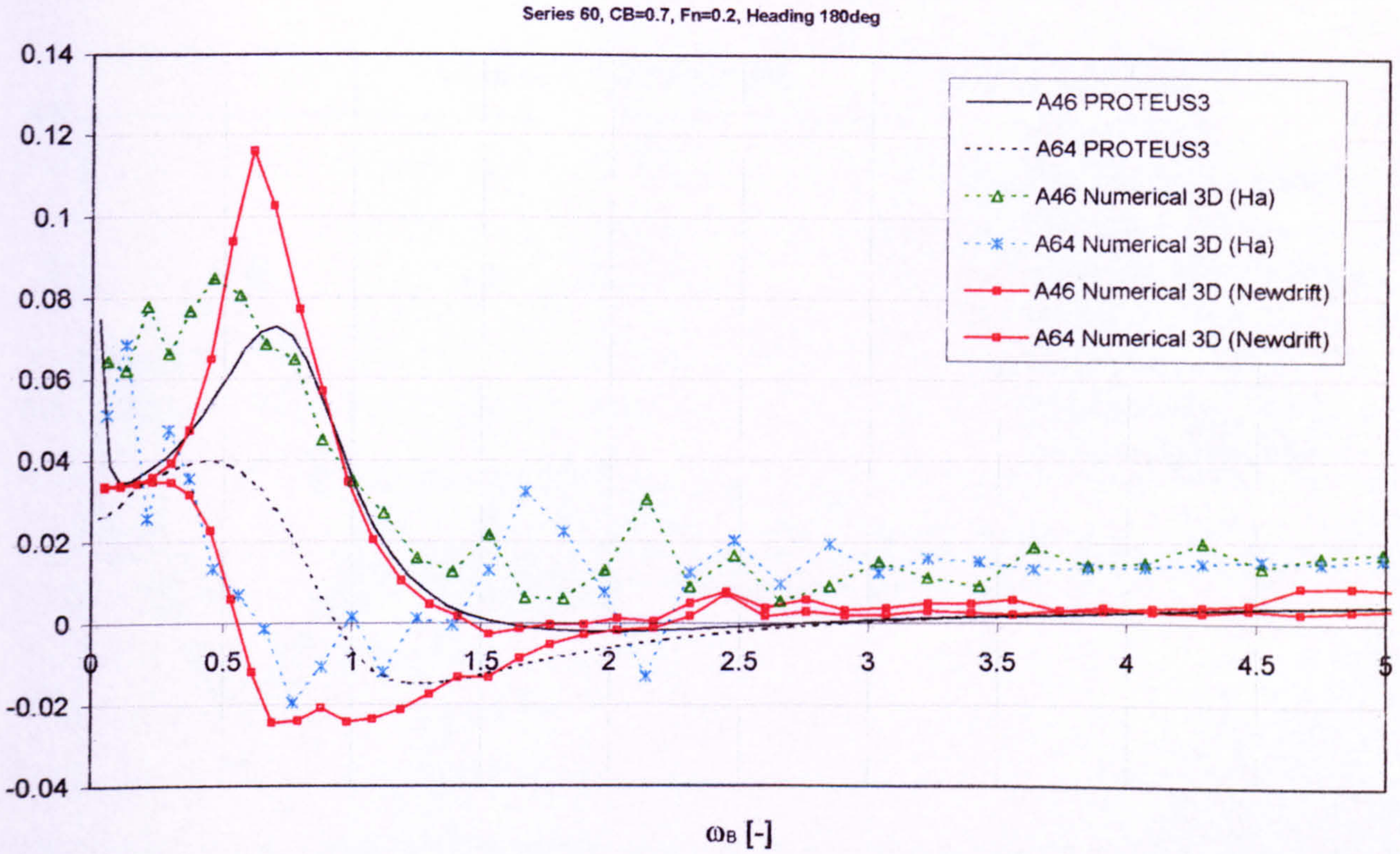

Figure 62 Dimensionless added mass in roll-into-yaw mode for 3D Series 60, CB=0.7 hull form, comparison between predictions by strip theory and 3D panel methods, Fn=0.2

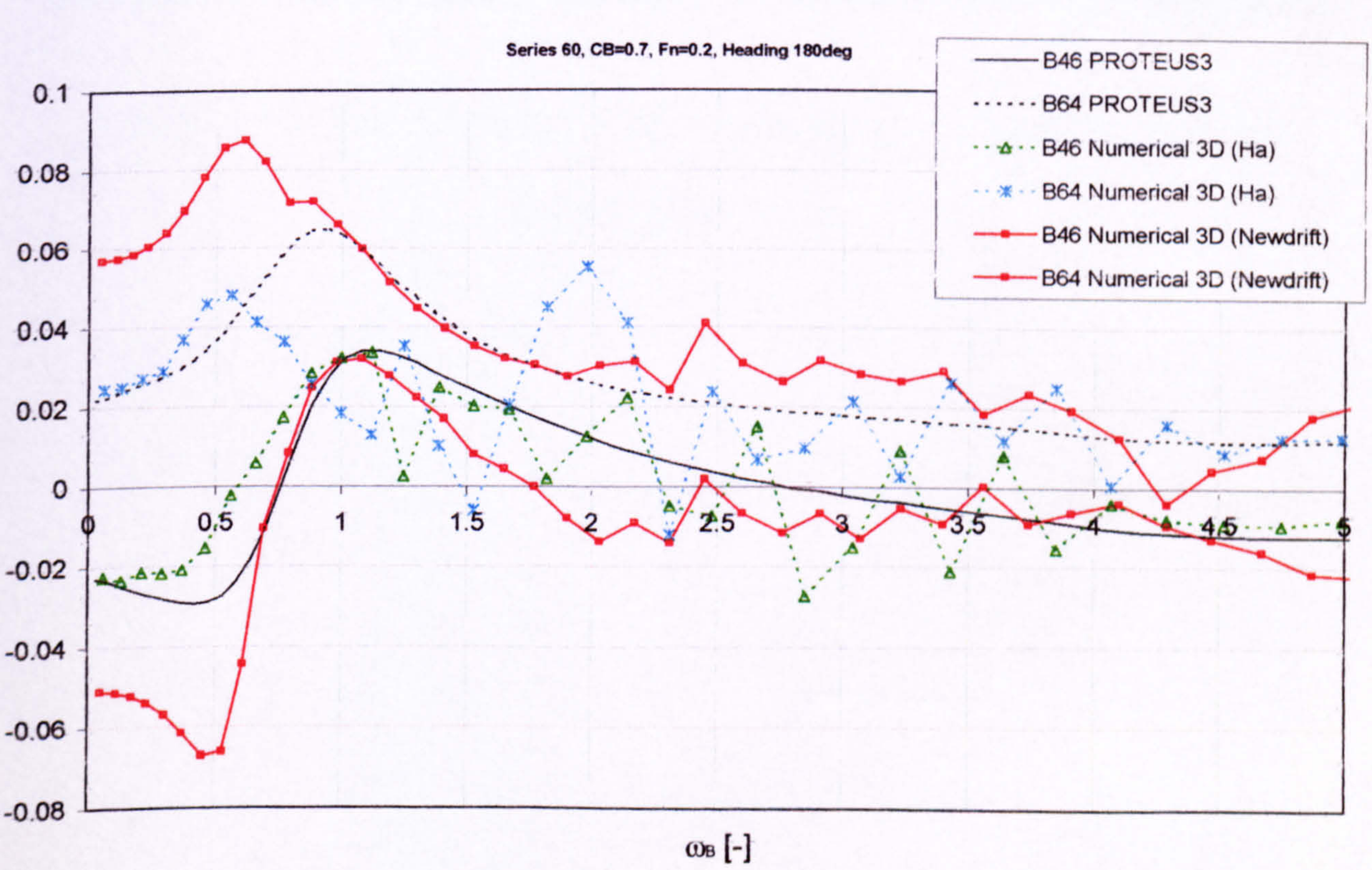

Figure 63 Dimensionless potential damping in roll-into-yaw mode for 3D Series 60, CB=0.7 hull form, comparison between predictions by strip theory and 3D panel methods, Fn=0.2

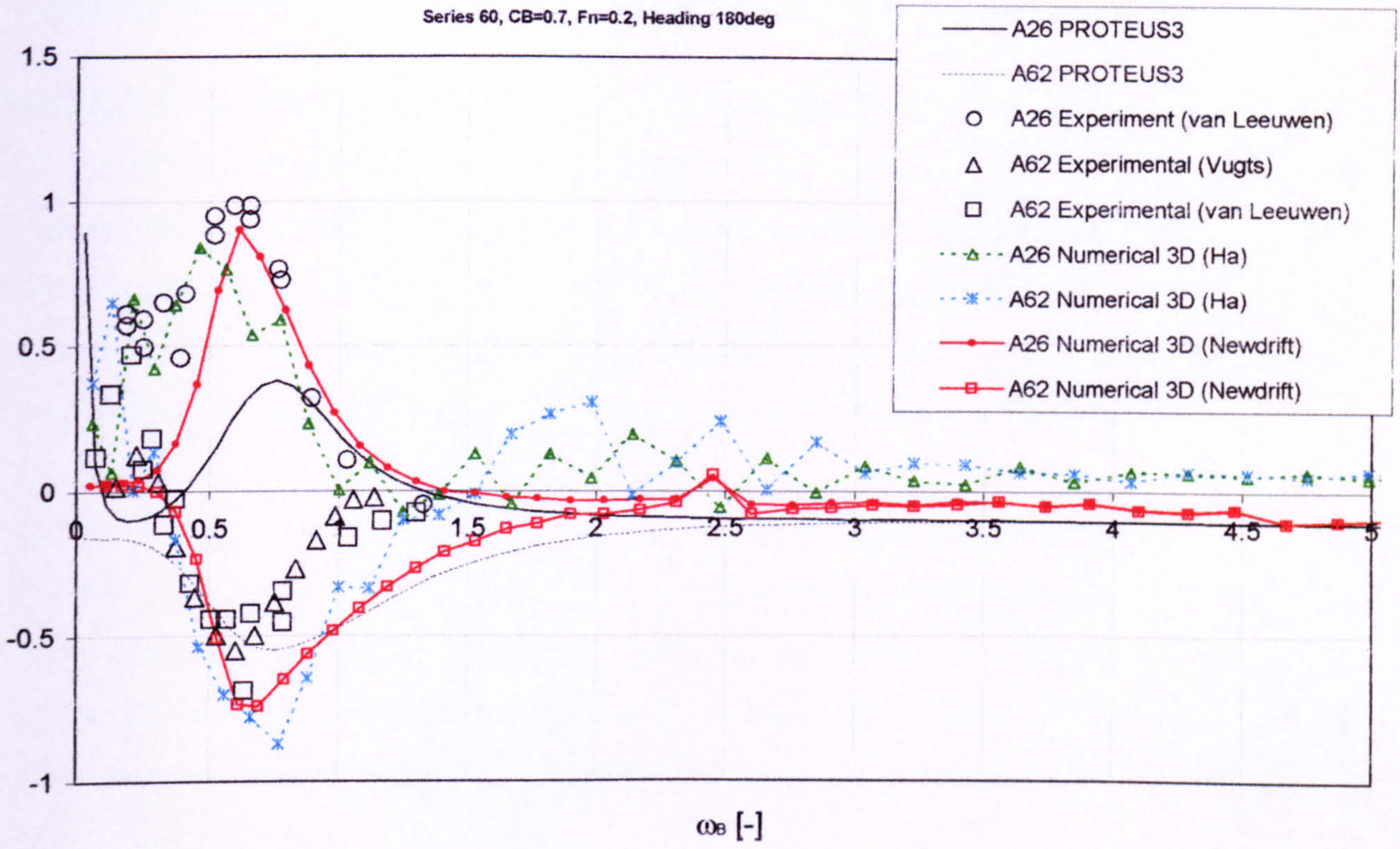

Figure 64 Dimensionless added mass in sway-into-yaw mode for 3D Series 60, CB=0.7 hull form, comparison between predictions by strip theory, 3D panel methods and experiments, Fn=0.2

Appendix 3

Study into the accuracy of modelling of damage vessel hydrodynamics

1 Study into the accuracy of modelling of damage vessel dynamics

This appendix aims at thorough testing of essential elements of the numerical code developed based on the ship motion model presented in the main body of this thesis. After introducing of the particulars and static properties of the study vessel in intact and damaged conditions, consideration is given to predictions of ship hydrodynamics using strip theory approach. This methodology is put to test by comparison with available 3D panel methods-based solutions, [39], aiming at establishing of suitability of 2D approach for investigations of damaged ship behaviour in a seaway.

Note that the terms "intact" and "damaged" conditions in context of predictions of hydrodynamic properties of the ship are used to denote and differentiate between up-right-no-sinkage vessel attitude while in intact condition and "final" attitude after anticipated extent of flooding took place in damaged conditions. This approach ignores any effect of the collision opening and ensuing water ingress/egress on the flow around the ship, significance of which assumption have not been verified as yet.

Note that all coefficients and forces are expressed in inertial coordinate system, e.g. in case of heel attitude the heave direction is to be understood "perpendicular to calm water level"!

As discussed in this appendix, the hydrodynamic generalised forces and coefficients derived by means of strip theory methods compare satisfactorily with much more sophisticated approaches based on 3D formulations, this concerning ship in either intact or damaged conditions. Furthermore, the study showed that the hydrodynamic properties show quite considerable dependency on the mean vessel attitude, which finding prompts inclusion of this effects in time domain solution, as has been suggested and initiated in earlier works.

1.1 General particulars

A representative large passenger Ro-Ro ship has been designated as a study case in this research. All the essential details of this vessel, denoted as PRR1, are given in Table 1 to Table 3 and representative Figure 1 to Figure 5.

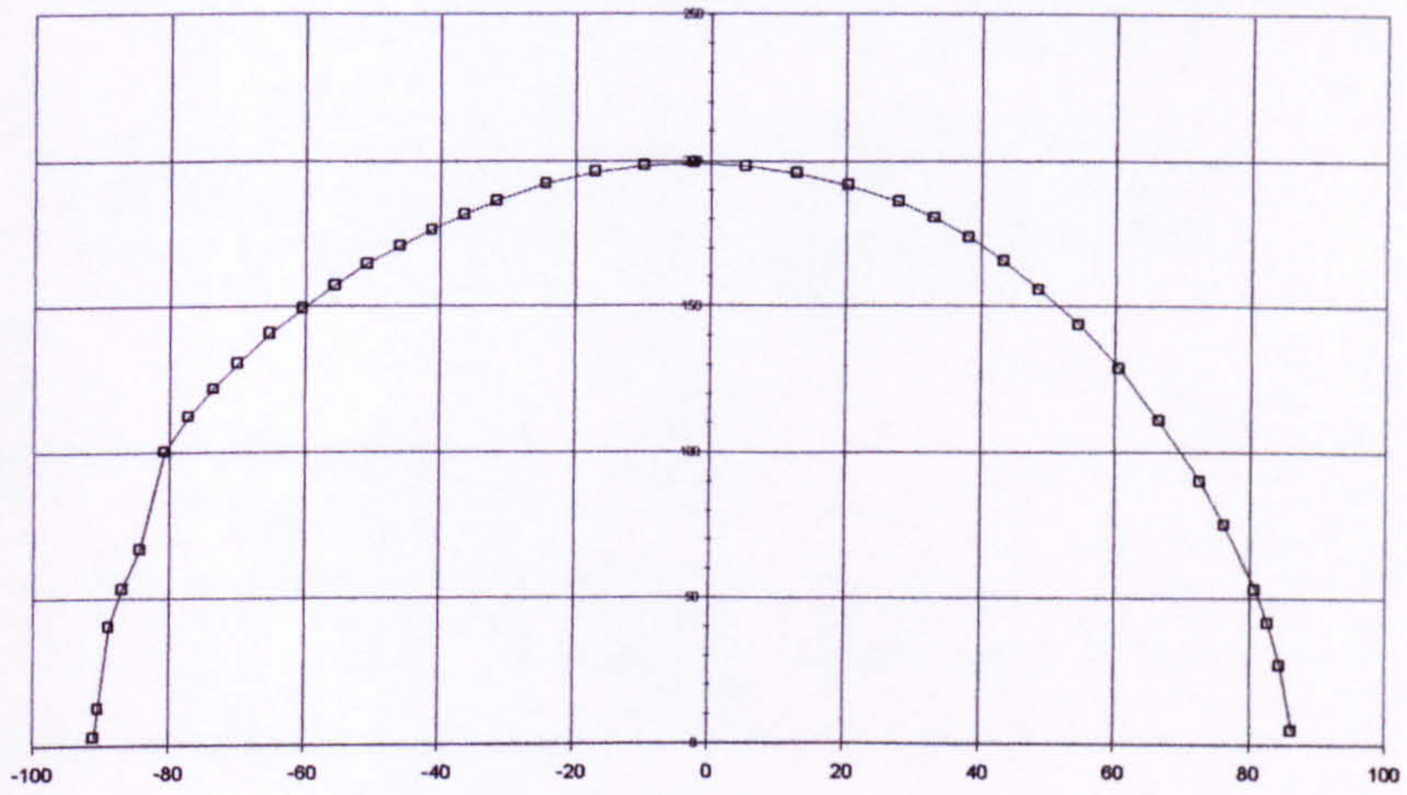

Figure 1 The sectional area distribution, integrated up to a depth of 14.85m

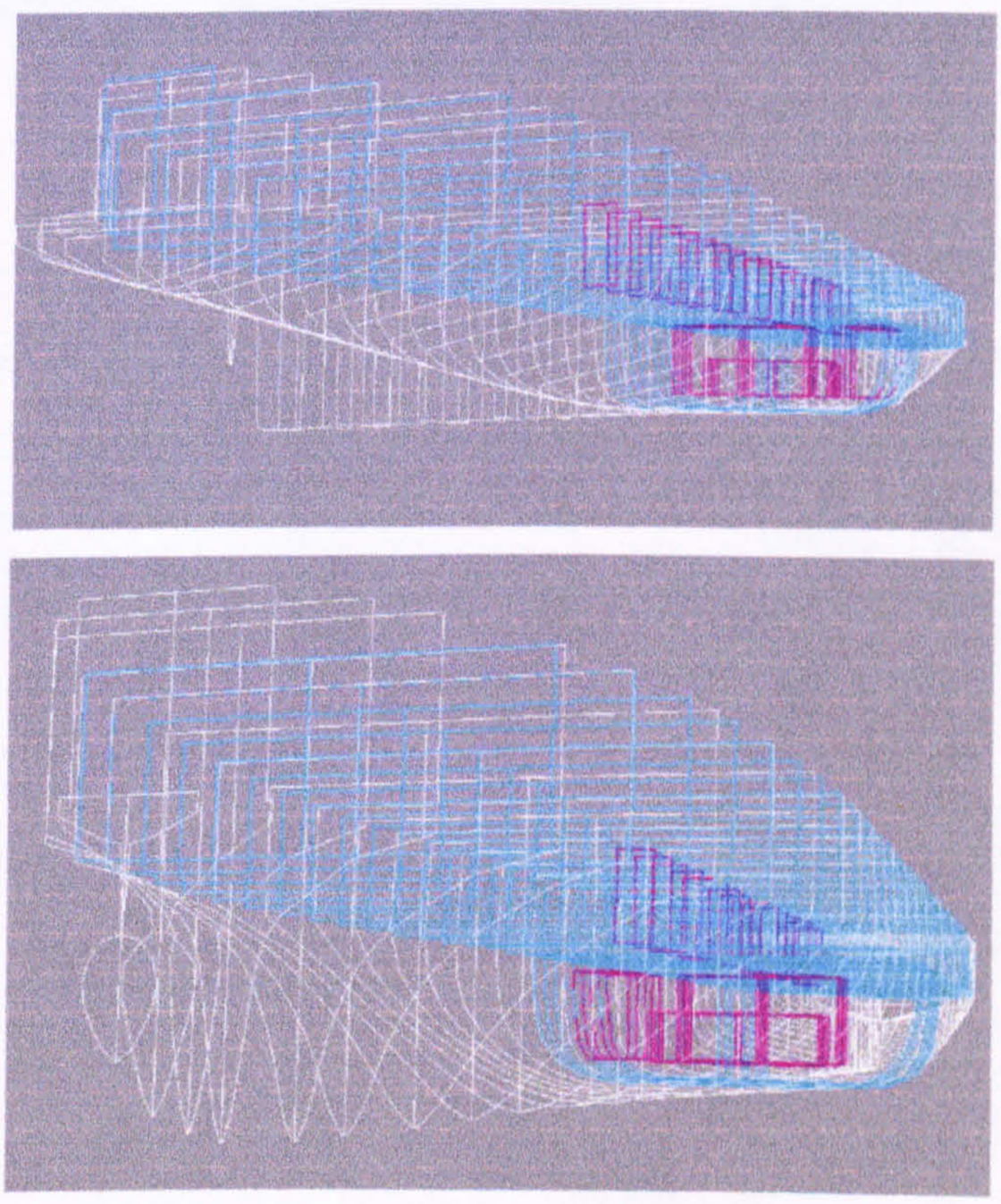

Figure 2 3D view of the external/internal geometry modelling for the test vessel PRR1

1.2 Static Stability

1.2.1 Intact Condition

Table 1 Hydrostatic properties in intact conditions derived by PROTEUS3

```
2D Hydrostatic Calculations (Geometry file prr1.sus').
 Ship's name    PRR1 INTACT

Kxyz
 Lpp.............   170.000 [m]
 Breadth.........    27.800 [m]
 Draught.........     6.250 [m]
 Mass........... 17321.900 [t]
 CGs.............    -2.609   0.000000     12.892 [m]

 Intact Ship

Oxyz
 Up-right/No-sinkage condition:
 GMT.............     2.588 [m]
 GML.............   383.873 [m]
 WPA.............  3791.319 [m2]
 Displ........... 17123.832 [t]
 CB..............    -2.566   0.000000     -2.642 [m]

 After Equilibrium Reached condition:
 GMT.............     2.564 [m]
 GML.............   384.311 [m]
 WPA.............  3809.037 [m2]
 CB..............    -2.609   0.000000     -2.662 [m]
 Trim............ equilibrium sought
 Heel............ equilibrium sought

Sinkage[m]   Trim[deg]   Heel[deg]        GZ[m]        TA[m]        TF[m]     Displ[t]
    -0.051       0.001       0.000    0.000000        6.299        6.302    17321.900
```

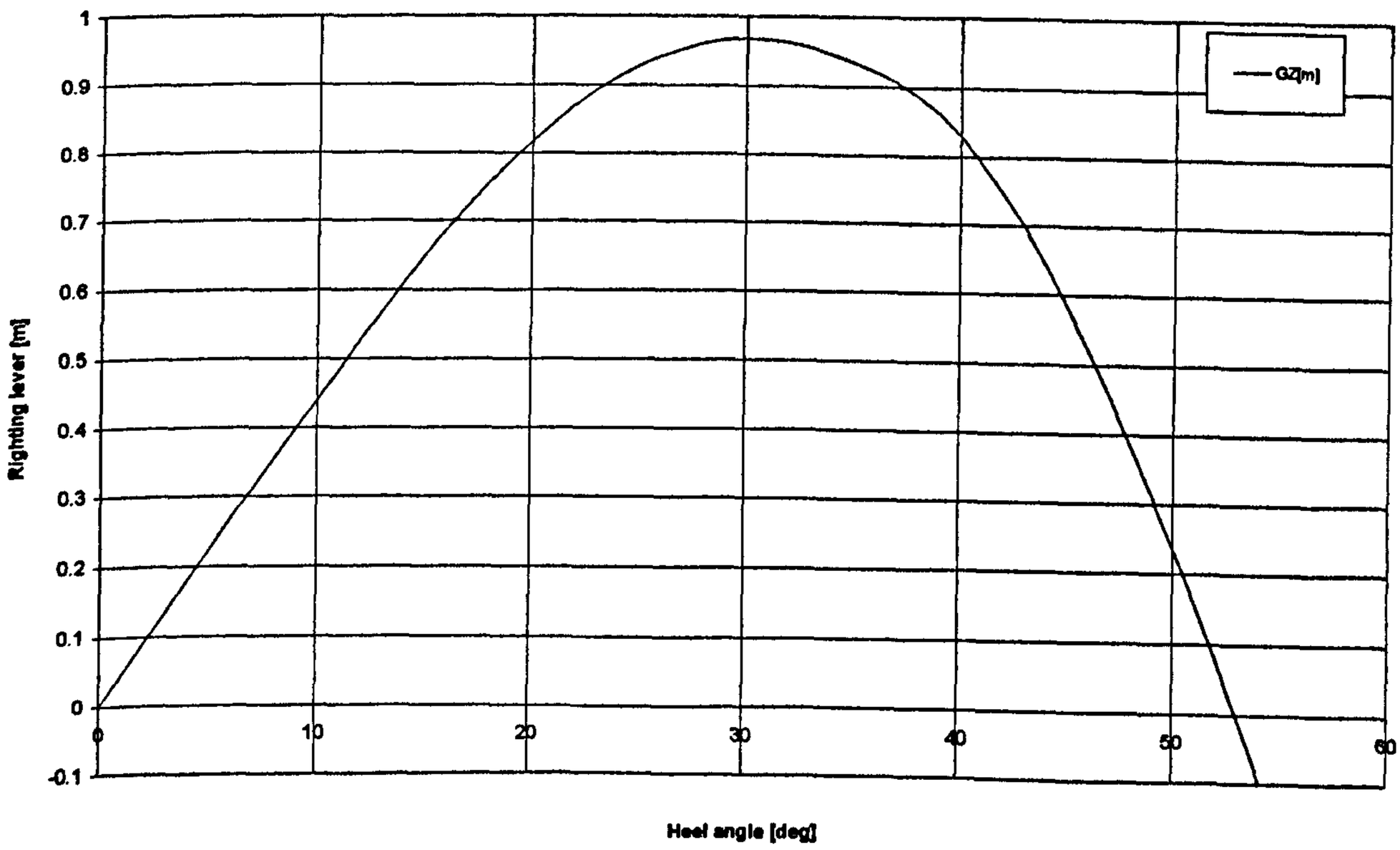

Figure 3 GZ curve for intact conditions

1.2.2 Damaged Condition

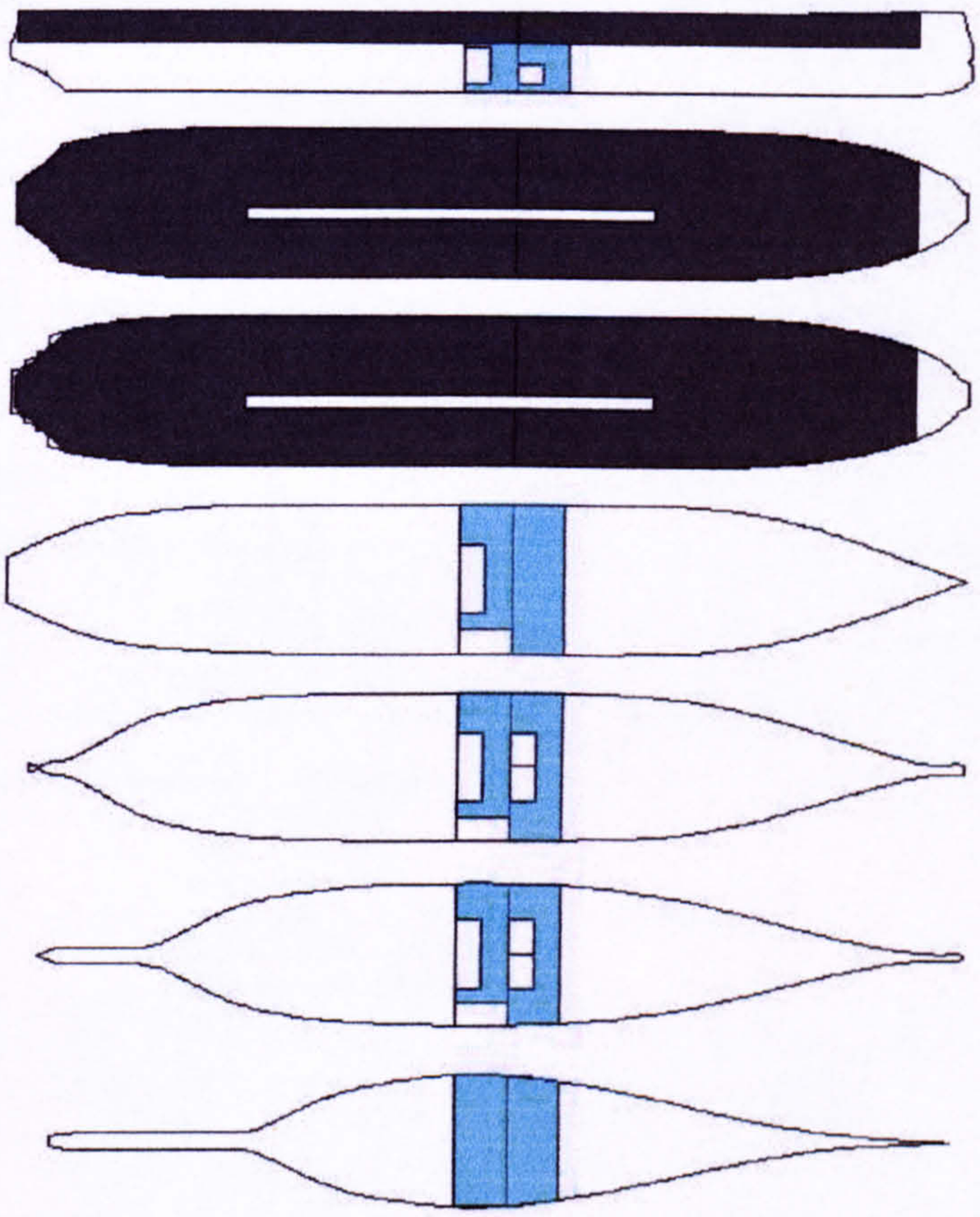

Figure 4 Permeability plot of the PRR1, see Table 2

Table 2 Details of the modelled compartments of PRR1

DAM sections of 'd901.dam' file

No	V[m3]/*A[m2]	x[m]	y[m]	z[m]	Perm[-]	Sym[-]	Vol*Perm*Sym[m3]
1	1123.091	7.381	6.548	4.682	0.950	2	2133.873
2	1137.425	-2.201	6.611	4.639	0.950	2	2161.107
3	277.701	-2.202	-11.339	5.039	-0.950	1	-263.816
4	110.592	5.000	3.200	3.300	-0.950	1	-105.062
5	110.592	5.000	-3.200	3.300	-0.950	1	-105.062
6	208.896	-4.600	3.200	4.900	-0.950	2	-396.902
7	6911.824	-40.640	6.595	11.918	0.980	2	13547.176
8	5681.704	38.215	6.524	11.972	0.980	2	11136.139
9	1055.808	-9.400	-2.000	11.925	-0.980	1	-1034.692
10*	84.864	0.000	11.882	5.101		SEA & Below	(0.000) <>
11*	47.445	0.000	13.802	12.934		SEA & CarDeck	(0.000) <>
GROUPS							
1	Below	3.606	0.874	4.687			3424.137
2	CarDeck	-4.874	0.088	11.944			23648.623

Table 3 Hydrostatic properties in damaged conditions derived by PROTEUS3

```
2D Hydrostatic Calculations (Geometry file 'prr1.sus').
 Ship's name    PRR1 INTACT

Kxyz
 Lpp..............   170.000 [m]
 Breadth..........    27.800 [m]
 Draught..........     6.250 [m]
 Mass.............. 17132.900 [t]
 CGs..............    -2.566   0.000000     12.892 [m]

 Ship Damaged (Damage file 'd901.dam')
 Damage name          D901
 Dam Comp       9
 DMass.............  2612.875 [t]
 DCG...............     3.549   0.942963     -3.467 [m]

Oxyz
 Up-right/No-sinkage condition:
 GMT...............     2.588 [m]
 GML...............   383.912 [m]
 WPA...............  3791.319 [m2]
 Displ............. 17123.832 [t]
 CB................    -2.566   0.000000     -2.642 [m]

 After Equilibrium Reached condition:
 GMT...............     2.422 [m]
 GML...............   441.685 [m]
 WPA...............  3579.548 [m2]
 CB................    -2.566   0.000000     -2.839 [m]
 Trim.............. equilibrium sought
 Heel.............. equilibrium sought
```

Sinkage[m]	Trim[deg]	Heel[deg]	GZ[m]	TA[m]	TF[m]	Displ[t]
-0.671	0.217	-3.234	0.000000	6.599	7.242	17132.900

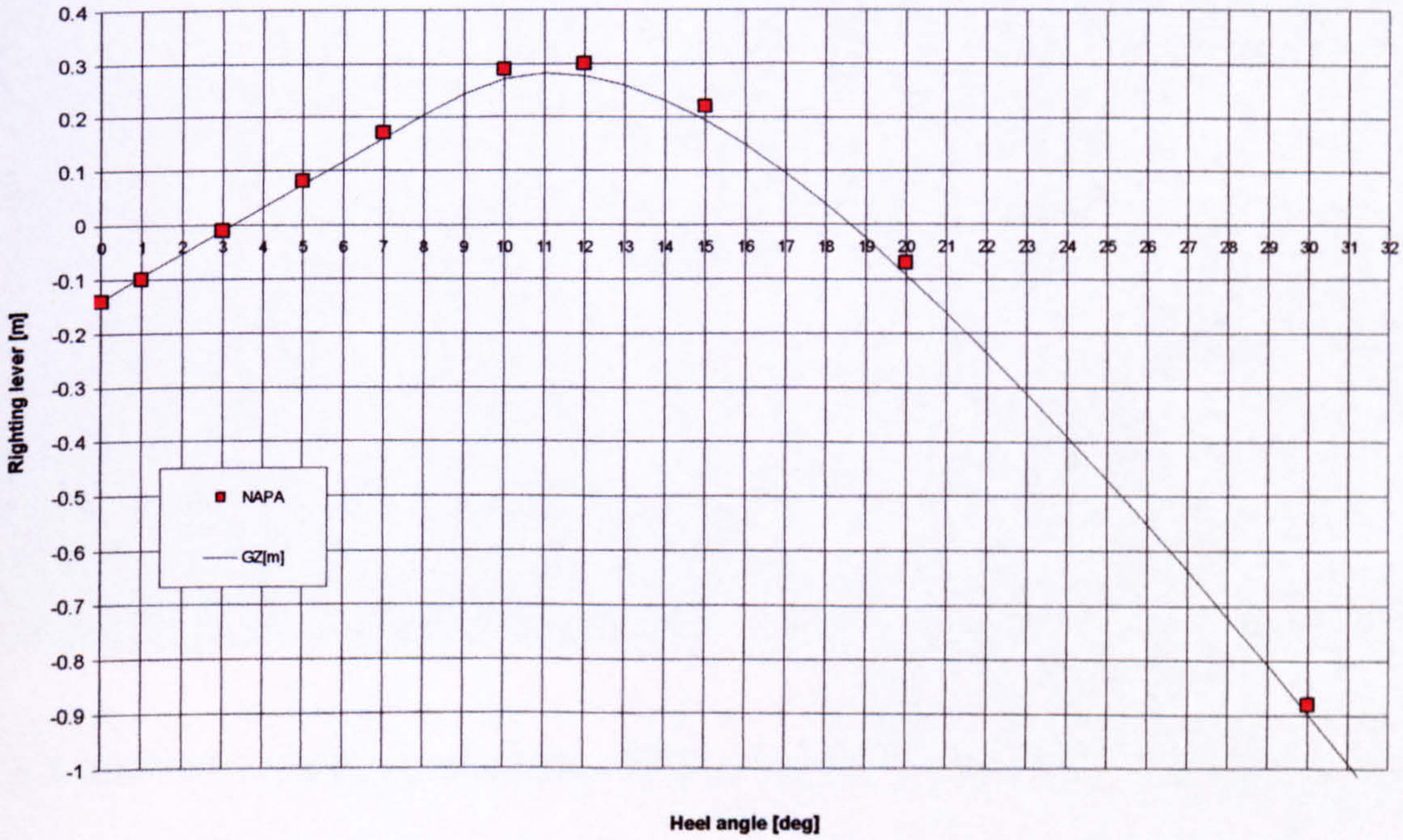

Figure 5 GZ curve for damaged conditions

1.3 Hydrodynamic coefficients

As has been mentioned in the introductory part of this appendix, a set of hydrodynamic coefficients as well as excitation and diffraction forces and moments will be presented and discussed. The hydrodynamic properties will be derived by means of strip theory approach with Rankine source technique employed for section-wise velocity potential predictions. See Figure 6 for strip-wise definition of ship hull and the adjacent free surface. Furthermore, a more sophisticated 3D formulation with translating/pulsating source distribution for potential flow predictions will be used for comparison purposes, [39], see Figure 8, the aim being that of establishing suitability of strip theory for predictions of hydrodynamics of asymmetrical underwater geometry. The study described below addresses intact ship properties first, followed by predictions of hydrodynamics for various combinations of ship sinkage, trim and heel, so effects of varying geometry can be straightforwardly assessed.

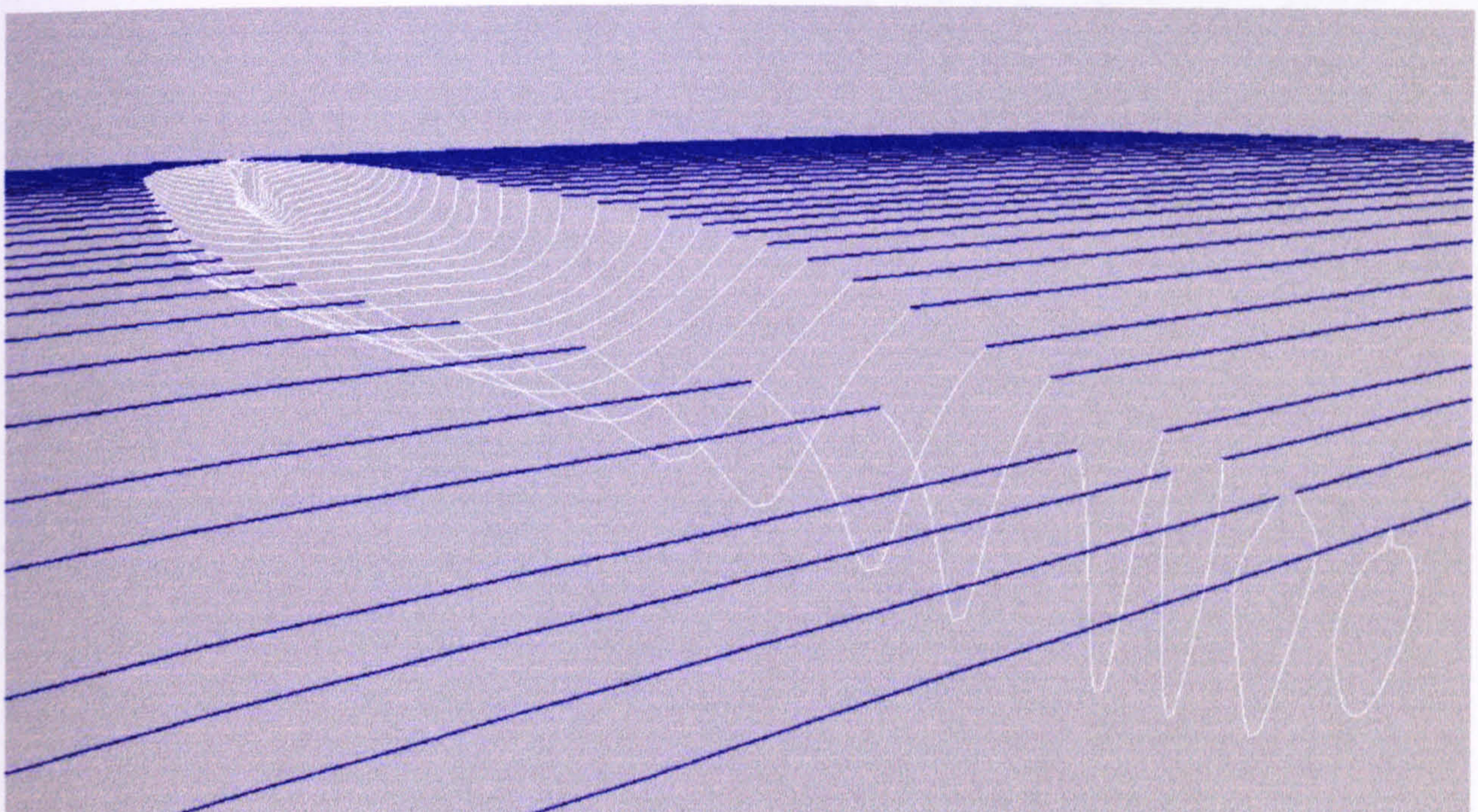

Figure 6 Section-wise (strip) representation of the geometry of the PRR1 hull in up-right condition

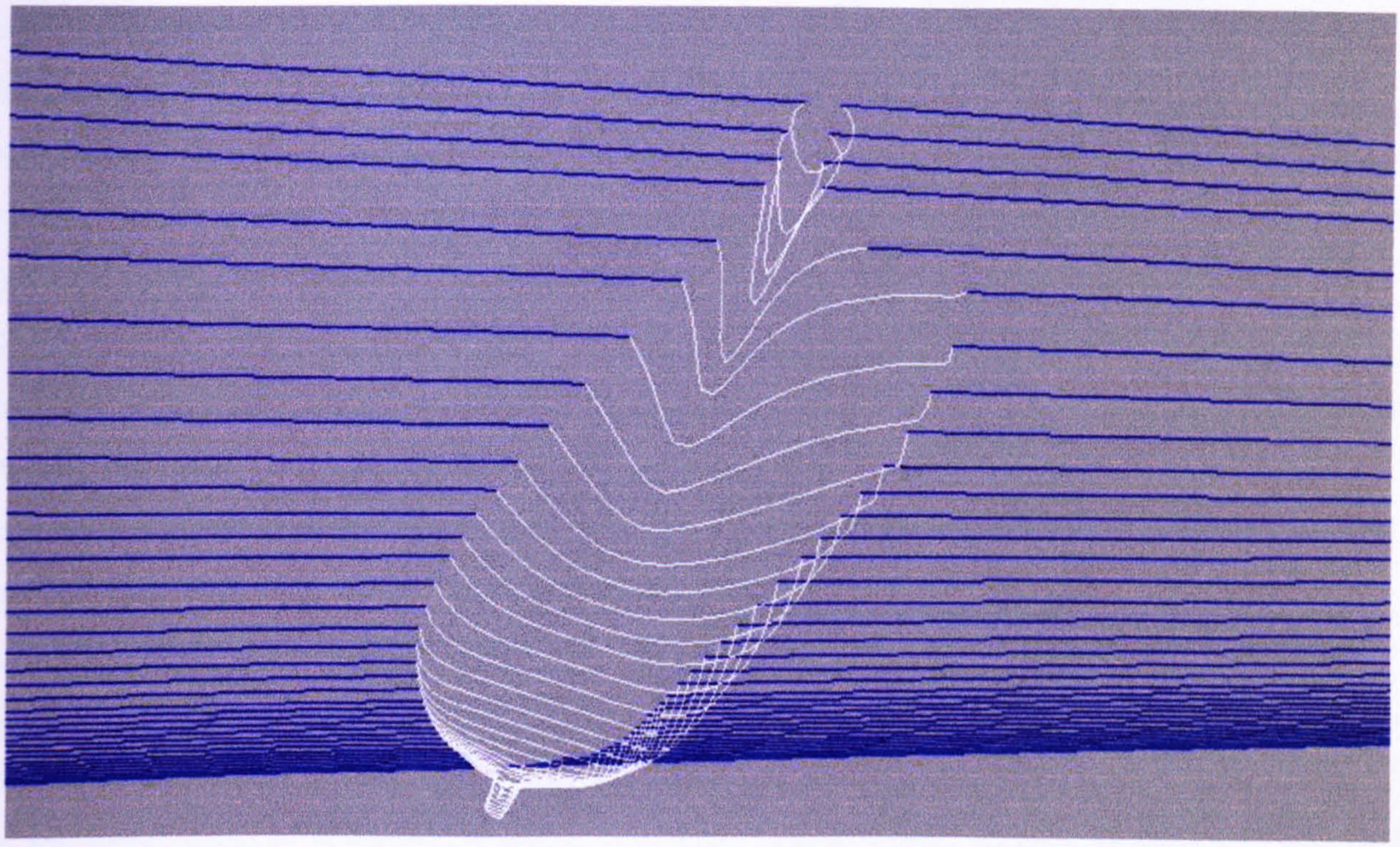

Figure 7 Section-wise representation of asymmetric case of vessel underwater geometry, -1m sinkage, -1deg trim, -20deg heel

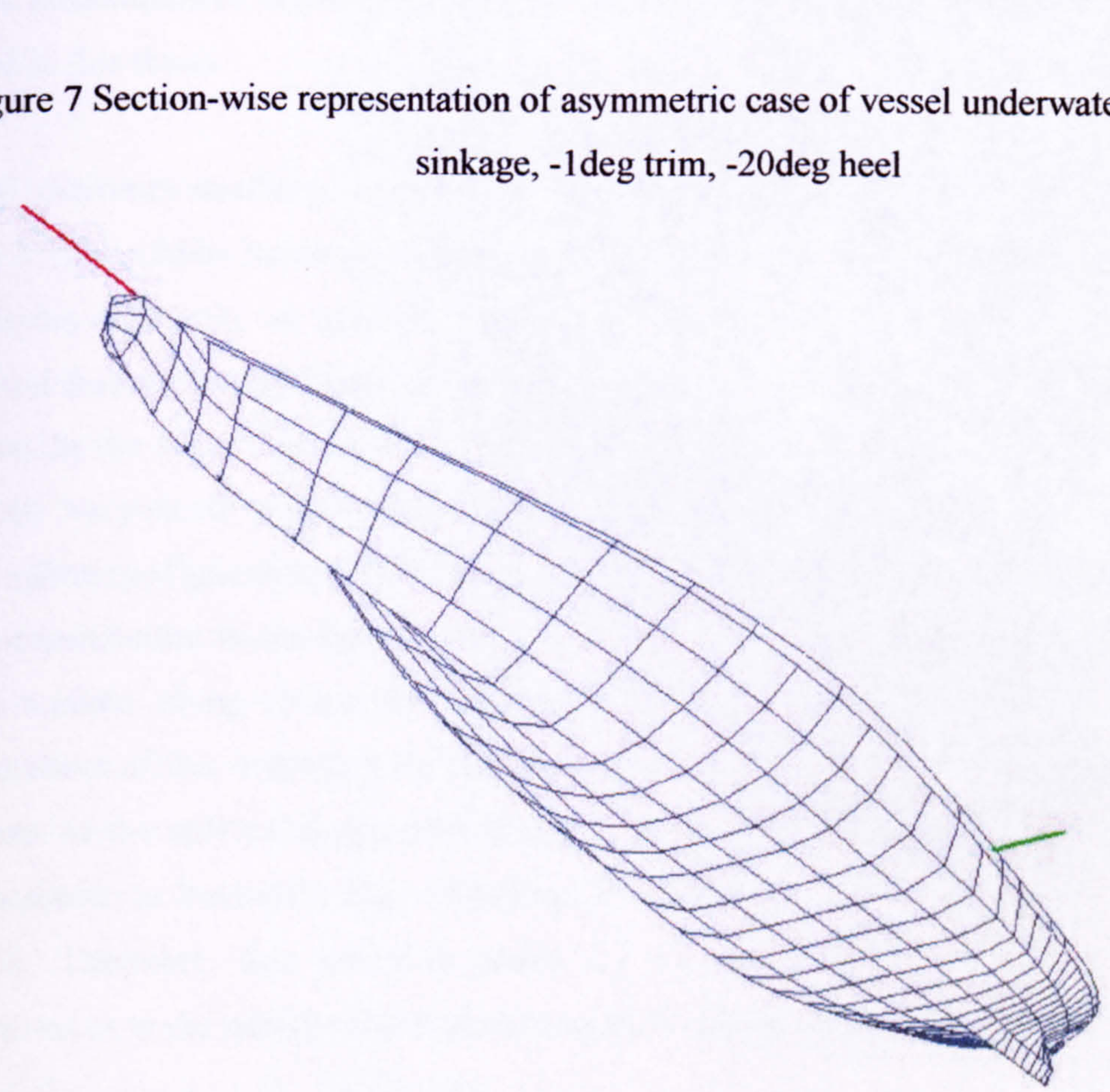

Figure 8 Panel-wise representation of the geometry of the PRR1 hull, 360 panels

Quite thorough testing of the ship hydrodynamics in intact conditions is reported in **Appendix 2,** where numerically derived hydrodynamic forces, moments and coefficients were compared with experiments. Referring to this study it should be noted that both of the 3D methods employed displayed some higher or lesser degree of irregularities. It is known that these result either from "natural" irregular frequencies inherent in the formulae due to use of pulsating or pulsating/translating source fulfilling free surface condition in the domain also contained by the ship; due to some inherent irregularities of numerical procedures adopted; or perhaps due to the geometrical input (panels) not being fine enough. However, for the sake of setting a reference it will be assumed here, that the 3D techniques, are of high reliability this deriving from far more sophisticated treatment of the 3D geometrical effects, neglected in strip theory formulation. Therefore the obvious "irregularities" appearing in 3D-based results will not be commented upon on the assumption that some smoothing procedures would be applied before further use of the predicted coefficients, forces and moments. Only the method of Taebum Ha, [39] will be used to test the predictions of ship hydrodynamics in damaged conditions by the strip theory formulation applied in this thesis.

Typical geometry resulting from submergence of a ship in flooding conditions is demonstrated in Figure 7. It should be borne in mind that such geometry, here represented either by a set of strips or by a series of panels, as used for predictions of hydrodynamic properties of the ship based on linearised free surface and body boundary conditions, violates the underlying assumptions of little variation in the mean control surfaces due to vessel oscillatory motions. It is clear from Figure 7 that even "very small" ship motion amplitudes will significantly affect both the free surface and the vessel submerged geometry. This, unlike the case of up-right ship attitude, is due to lack of wall sides perpendicular to the calm water level, which condition implies little variation of the hull-wetted surface, along almost the whole length of the ship. However, it is difficult to assess consequences of this modelling on the accuracy of predictions of overall hydrodynamic forces and moments, as the only valid approach here is time domain solution to BVP accounting for at least non-linearities in kinematic ship wetted surface conditions, which study is beyond scope of this research. Therefore, this potential source of inaccuracy, although kept in mind in drawing conclusions as to the quality of the whole numerical model, will not be addressed in this study.

Notwithstanding possible problems with the mentioned inconsistencies between the underlying assumptions of the model and the specific nature of the application, a study has been performed on the effects that variation of the mean underwater geometry during ship progressive flooding, have

on the hydrodynamic excitation and reaction forces and moments. Additionally applied strip theory formulation is confronted with the 3D panel methods.

In summary, the outcome of this investigation has been much of a surprise as regards the validity of 2D approach for predictions of hydrodynamics in damaged conditions. All the predicted values of hydrodynamic coefficients, forces and moments as derived by either of the methods, unlike expected, showed exactly the same trends dependent on the ship mean attitude, study Figure 9 to Figure 78.

Starting with the sway mode, it has been found that the most influential of attitude variations is sinkage and heel, with trim having only minor effects, see Figure 9 to Figure 16, and Figure 39 to Figure 46. The compound result of parallel sinkage, trim and heel is sort of a superposition of all of the separate effects. Worth noting is, that the heel has the most influence on the phasing between the wave passage and the exerted force in sway mode, see Figure 40, Figure 42, Figure 44 and Figure 46.

Change in the attitude has very little influence on the coefficients and forces in the heave mode of motion, Figure 17 to Figure 24 and Figure 48 to Figure 54. Heel mode, again, proves to affect the phasing the most.

Surprisingly enough, the radiation coefficients for roll mode of motion (both added mass and *damping*) do not show much of a change with attitude, Figure 25 to Figure 32, with the trim affecting the coefficients the least. However, the excitation moments show quite noticeable increase in amplitudes due to sinkage, and even more pronounced due to heel, with almost negligible influence of the trim, see Figure 55 to Figure 62. Quite conspicuous is the 90deg phase shift for low frequencies due to heel, Figure 58. Again noticeable is superposition of all the separate effects of sinkage, heel and trim, in case of attitude resulting from simultaneous variation in each of these modes of motion, Figure 30, Figure 31, Figure 61 and Figure 62.

The cross-coupling coefficients also show quite high dependency on the vessel attitude, see for example the roll-into-sway coefficients in Figure 33 and Figure 34.

The sway-into-heave or heave-into-roll are the cross-coupling terms that are zero for geometry with ZY symmetry plane. In case of the attitude with heel this symmetry disappears and these terms must

be taken into account. Therefore, the strip theory formulation has been extended and the coefficients for asymmetrical geometry have been included. As shown in Figure 35 to Figure 38, the extended strip theory formulation predicts "almost" identical values as the 3D panel methods.

The excitation moments for pitch mode, although small at beam-to heading, Figure 63 to Figure 70, show that concerning the amplitudes the trim is as influential attitude variation as sinkage and heel. However, the heel, again, affects the phasing most.

The excitation moments in yaw mode show the most peculiar dependency on heel and trim, with sinkage having very marginal effect, Figure 71 to Figure 78. Both, the heel and trim, lead to 180deg shift in the phasing between the wave passage and the exerted moment, Figure 76 and Figure 74.

Concluding the study it must be stressed that it came as a surprise to find such a profound effect of the heel attitude on all the quantitative values of hydrodynamic properties of the monohull geometry. Also as a surprise it has been found that the trim of as much as ~3m (6.25m draught!) has considerably little influence on the hydrodynamics of the damaged ship. Disregarding the latter, it is recommendable, that demonstrated non-linearity of hydrodynamic properties of the damaged ship deriving from variation of mean attitude due to progressive flooding, be included in the time domain solution of equations of motions. Such effects can be accounted for, most efficiently, by DATABASE approach, where these properties are predicted for a series of anticipated attitudes, and the relevant values interpolated.

All of the figures referred to above are shown next.

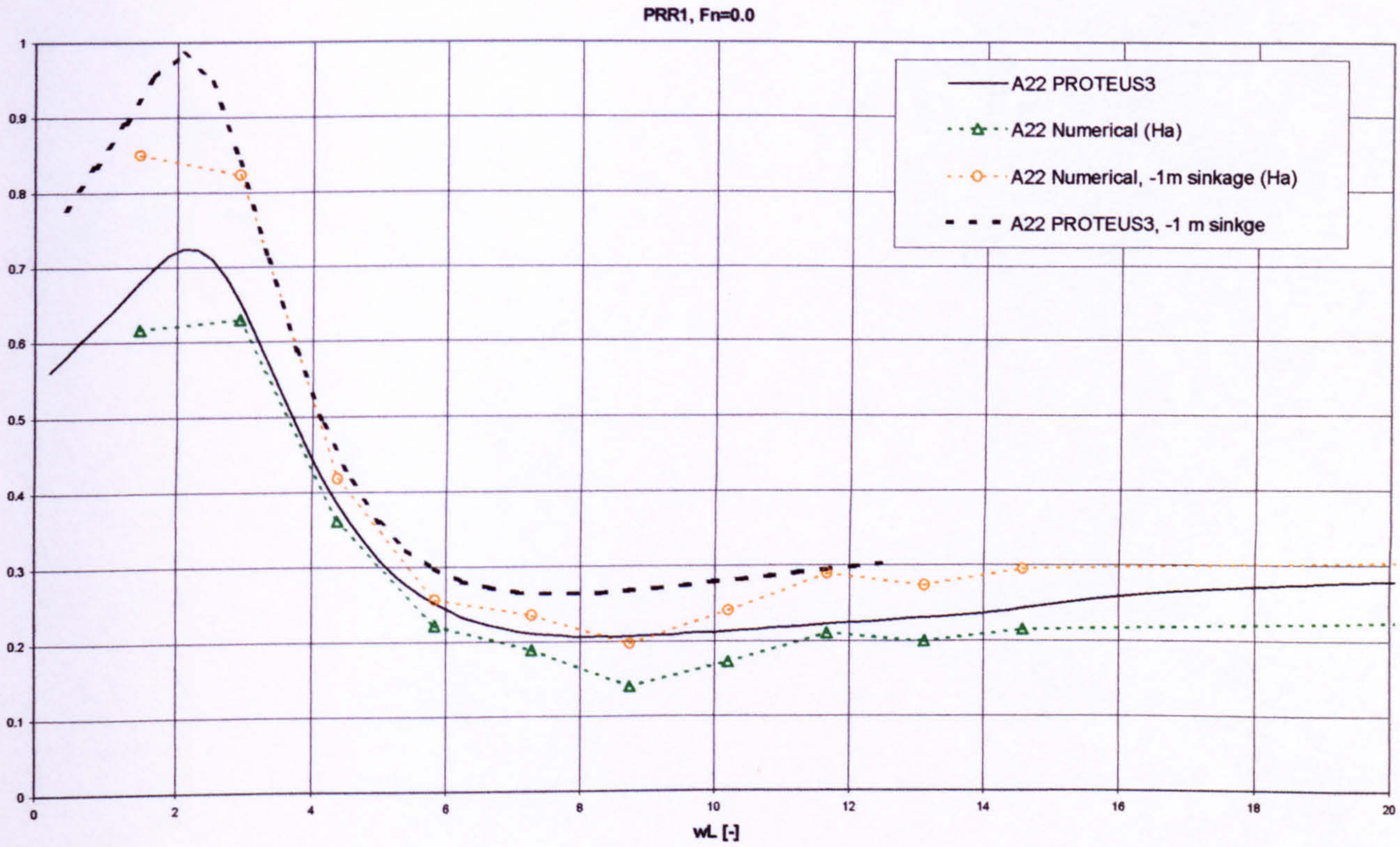

Figure 9 Dimensionless added mass in sway mode for 3D PRR1 hull form, effect of –1m sinkage, comparison between predictions by strip theory and 3D panel methods, Fn=0.0

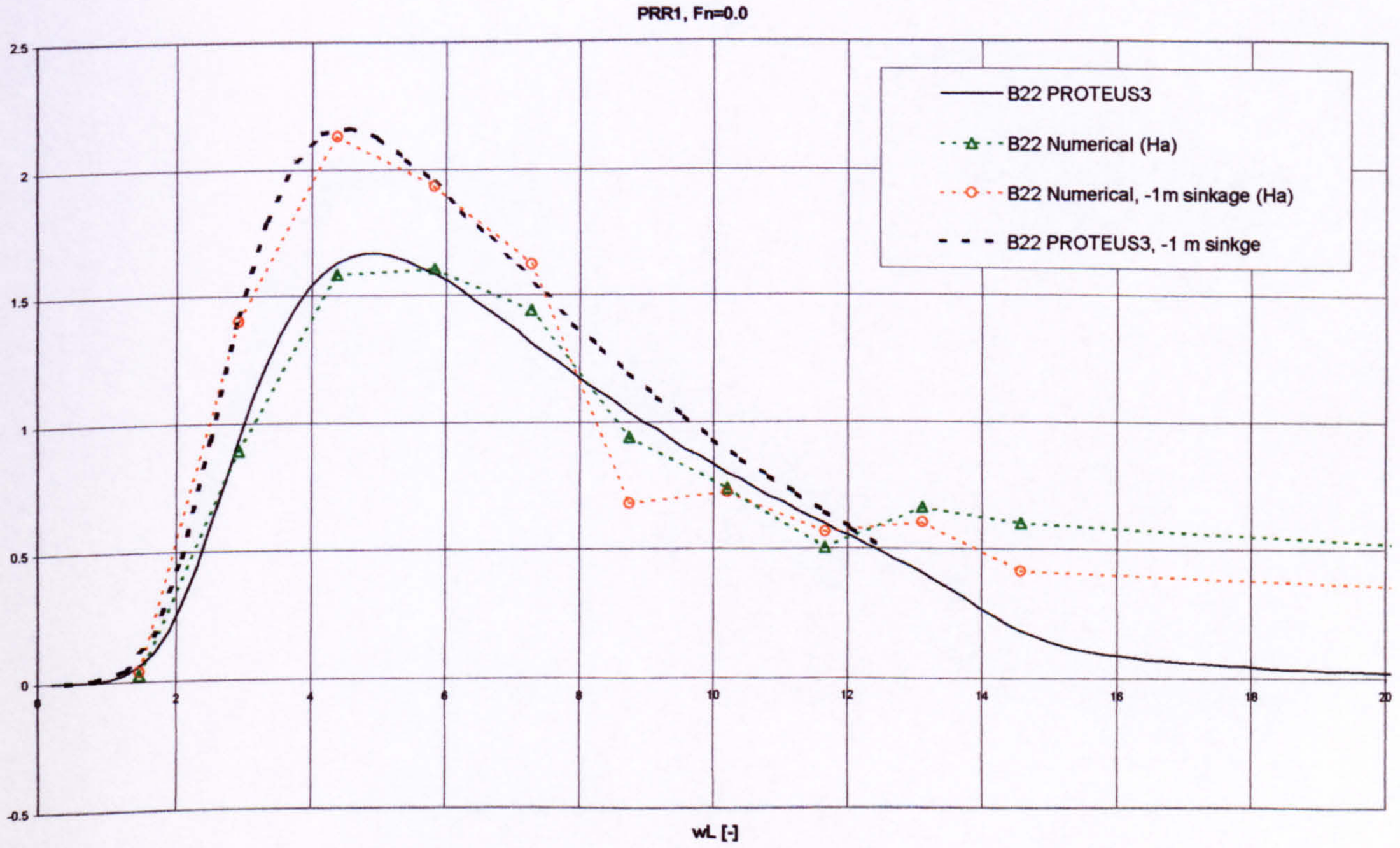

Figure 10 Dimensionless damping in sway mode for 3D PRR1 hull form, effect of -1m sinkage, comparison between predictions by strip theory and 3D panel methods, Fn=0.0

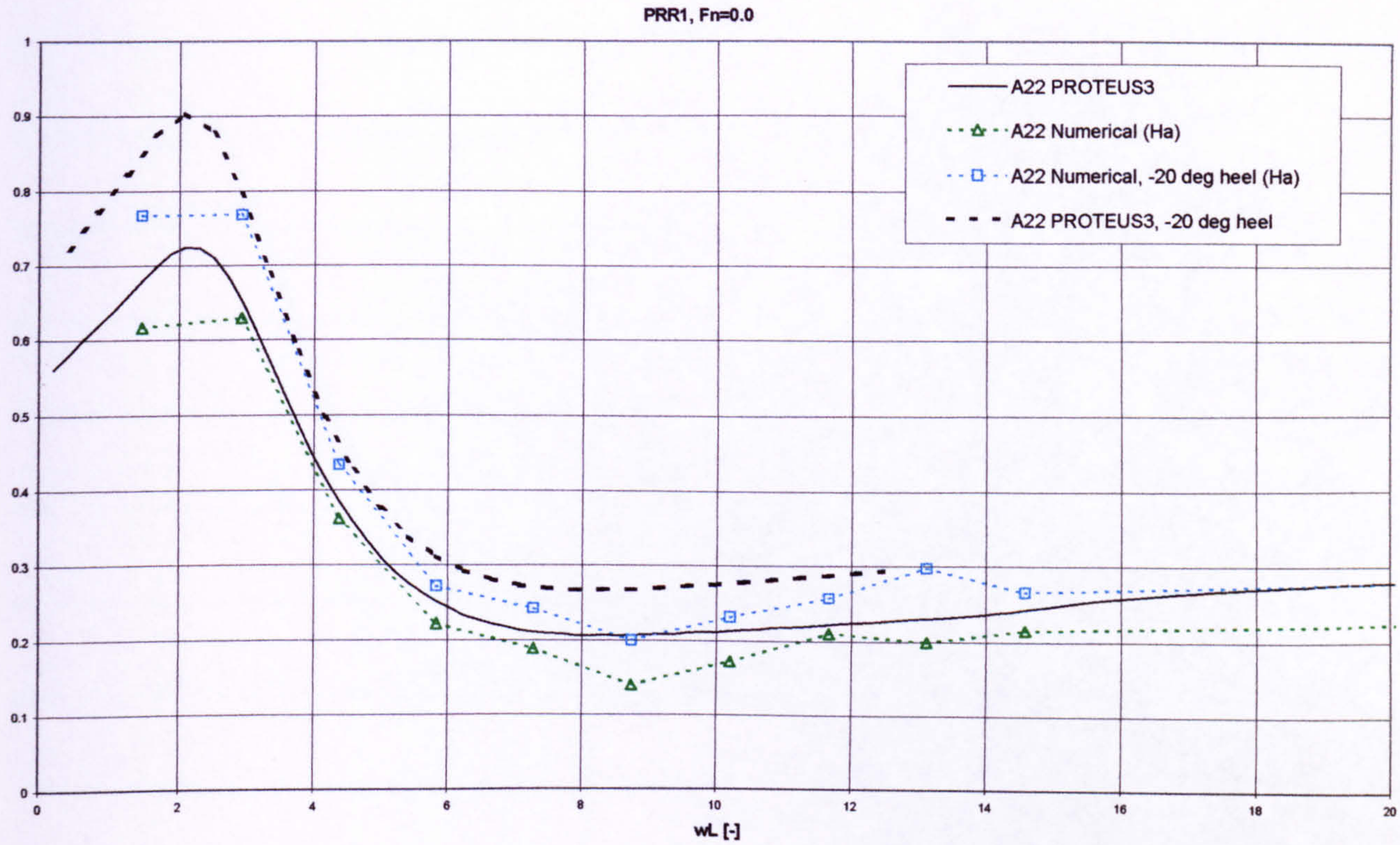

Figure 11 Dimensionless added mass in sway mode for 3D PRR1 hull form, effect of –20deg (port) heel, comparison between predictions by strip theory and 3D panel methods, Fn=0.0

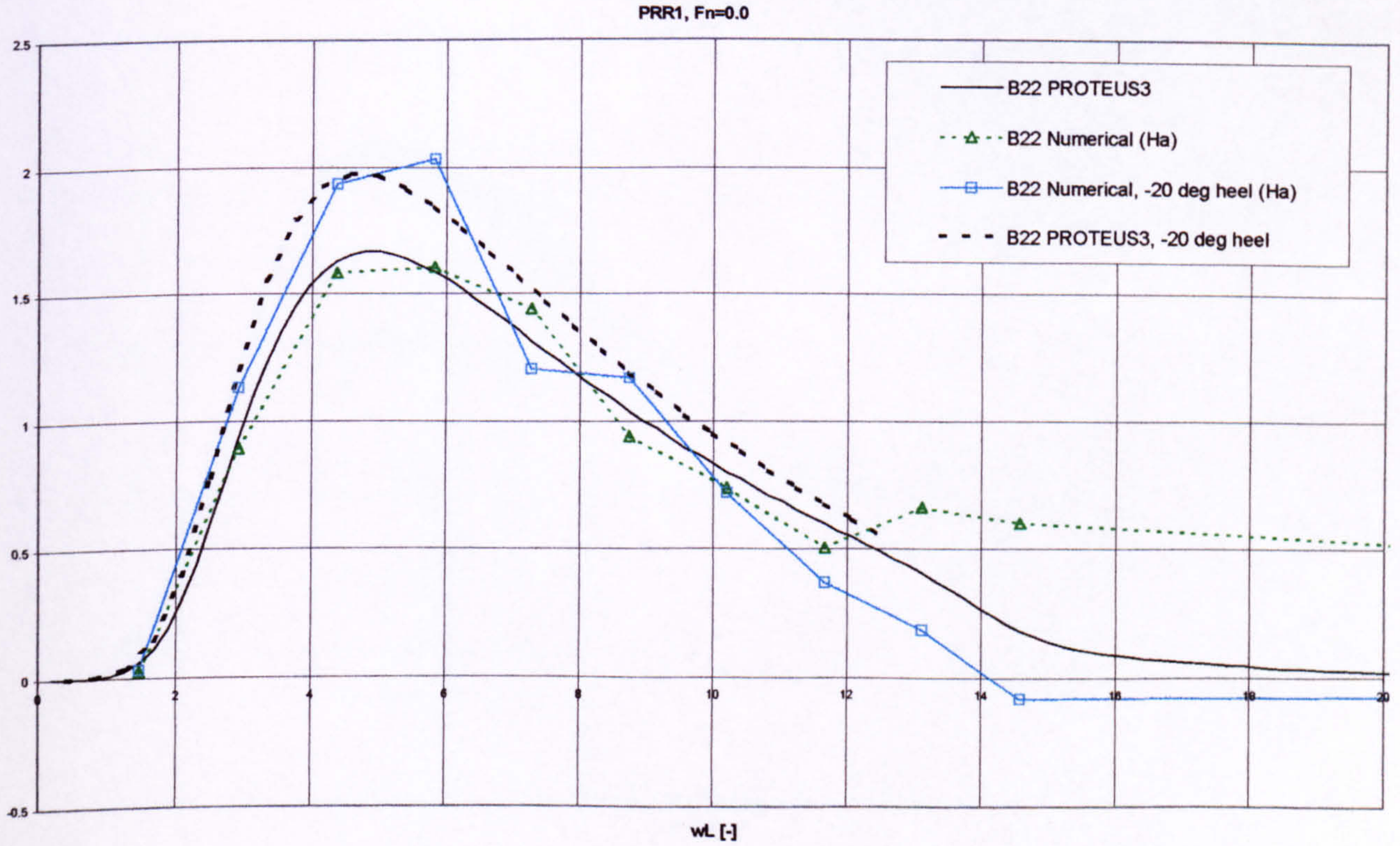

Figure 12 Dimensionless damping in sway mode for 3D PRR1 hull form, effect of –20deg (port) heel, comparison between predictions by strip theory and 3D panel methods, Fn=0.0

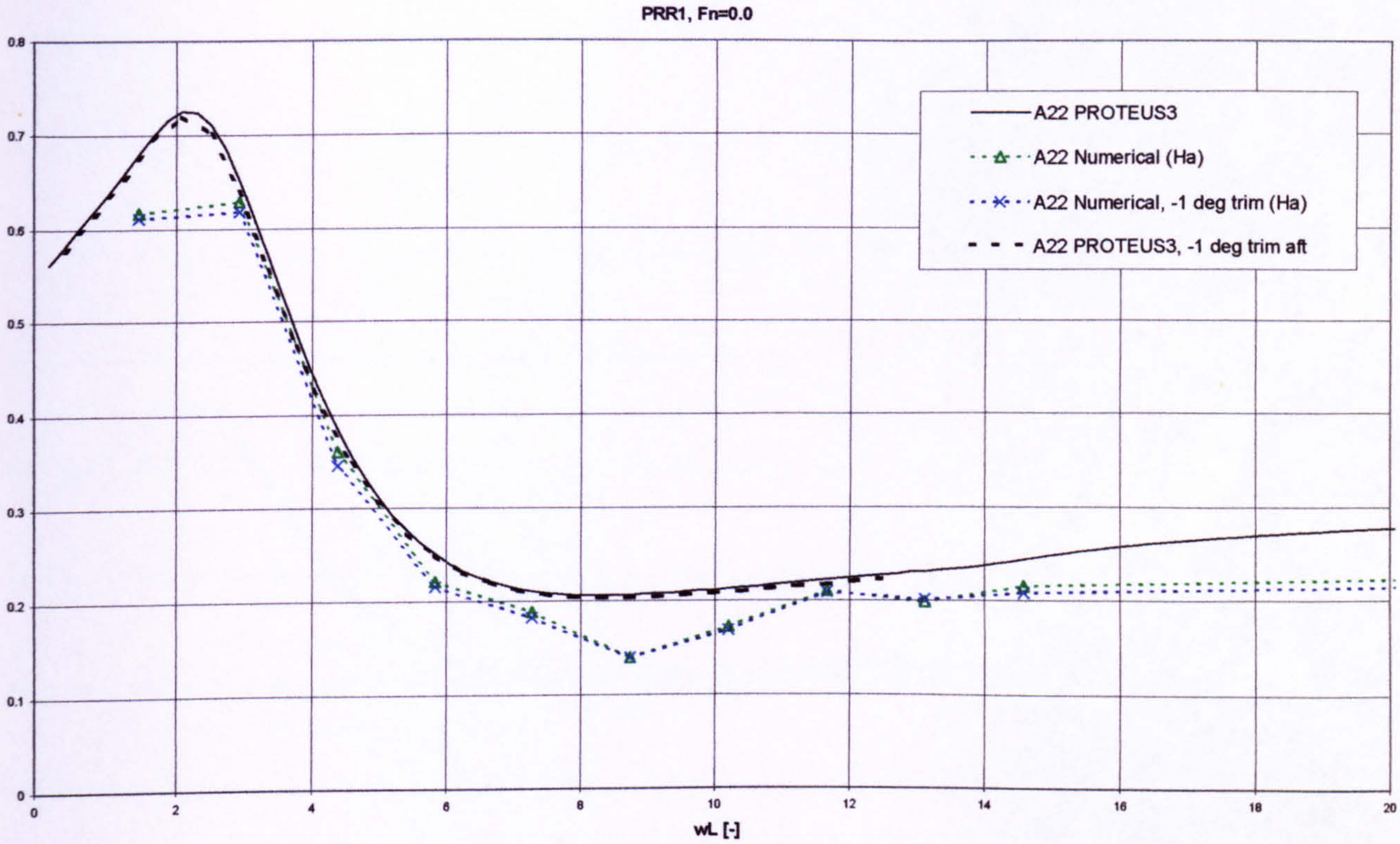

Figure 13 Dimensionless added mass in sway mode for 3D PRR1 hull form, effect of –1deg (aft) trim, comparison between predictions by strip theory and 3D panel methods, Fn=0.0

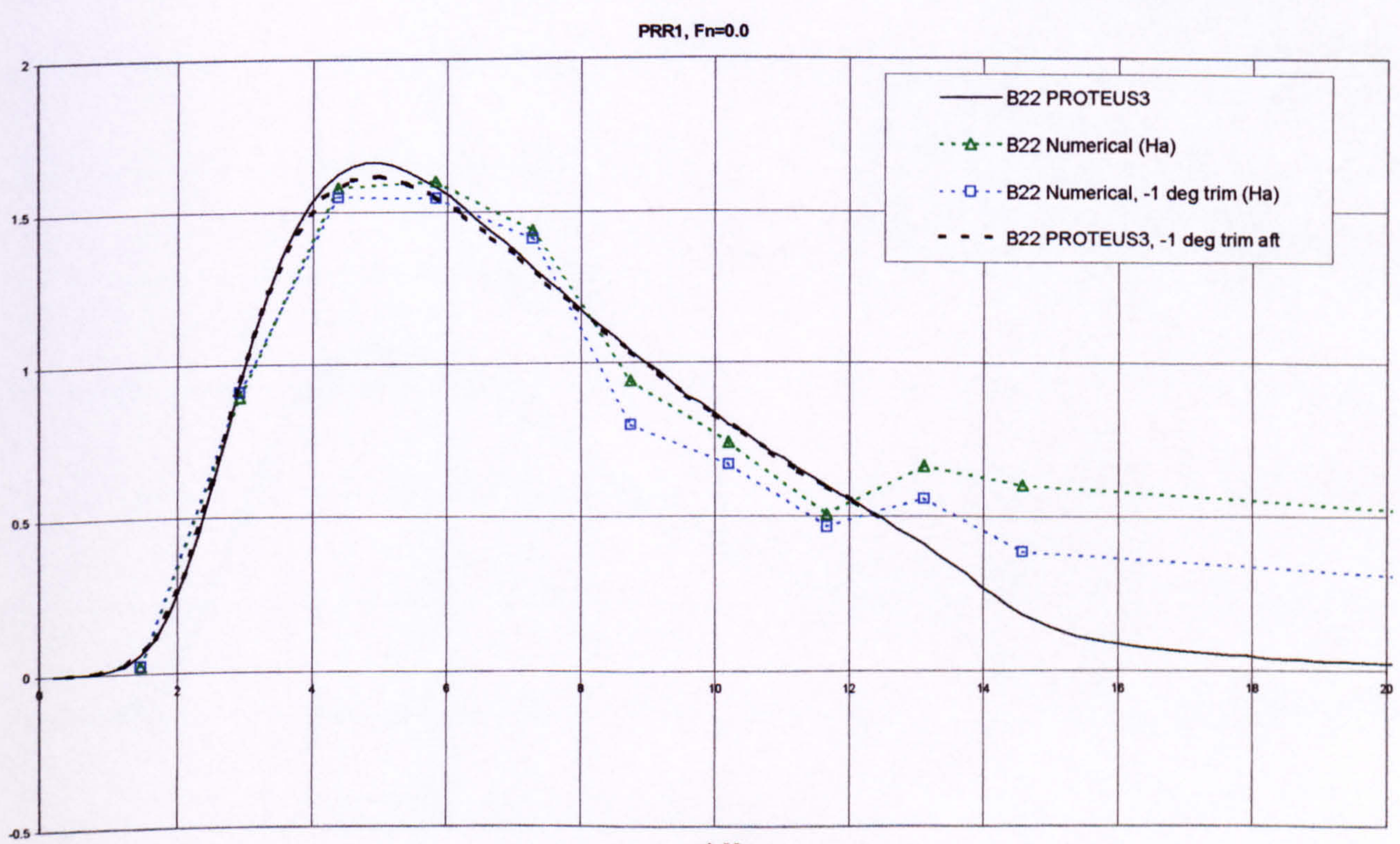

Figure 14 Dimensionless damping in sway mode for 3D PRR1 hull form, effect of –1deg (aft) trim, comparison between predictions by strip theory and 3D panel methods, Fn=0.0

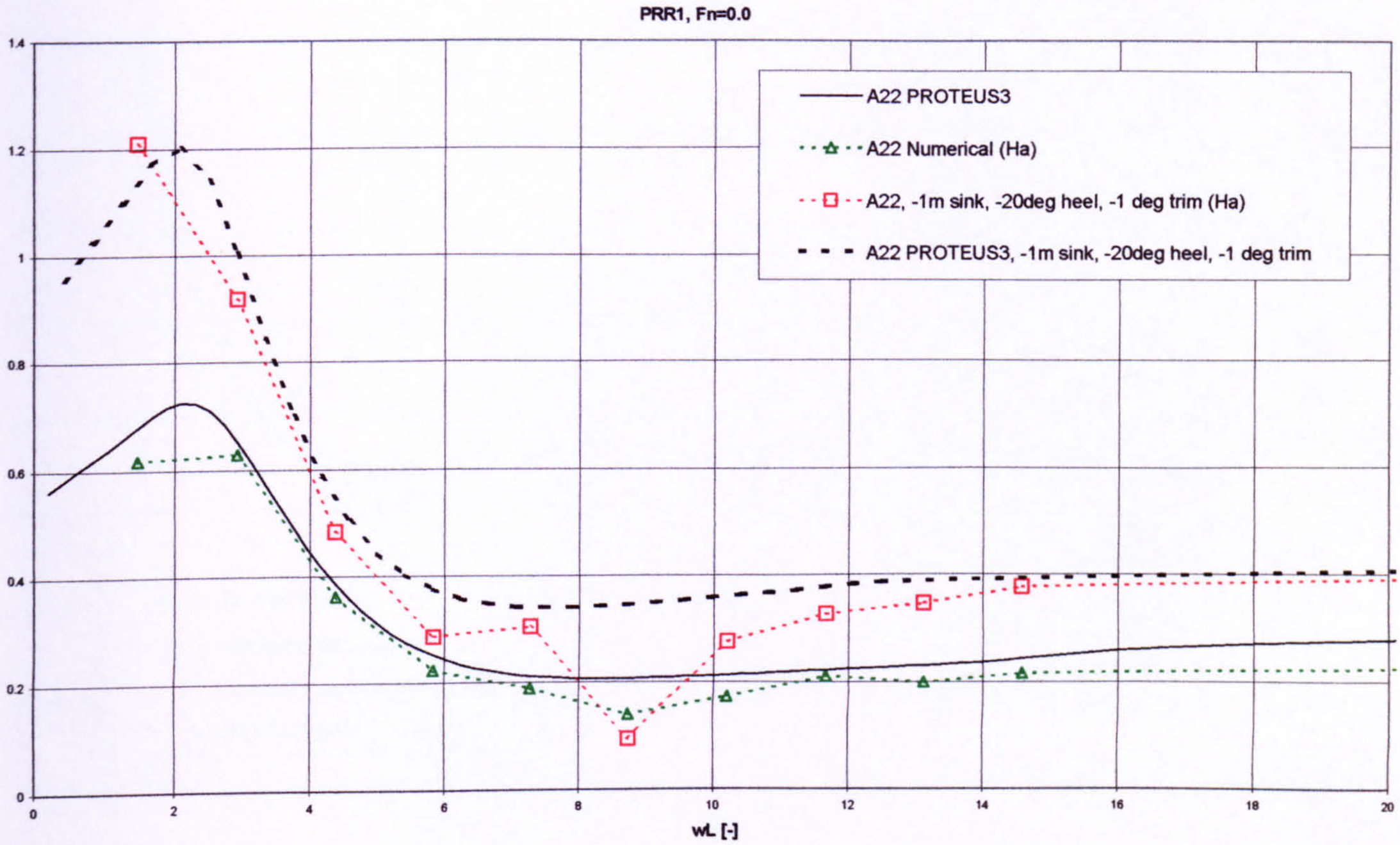

Figure 15 Dimensionless added mass in sway mode for 3D PRR1 hull form, effect of –1m sinkage, -20deg heel and –1deg (aft) trim, derived by strip theory and 3D panel methods, Fn=0.0

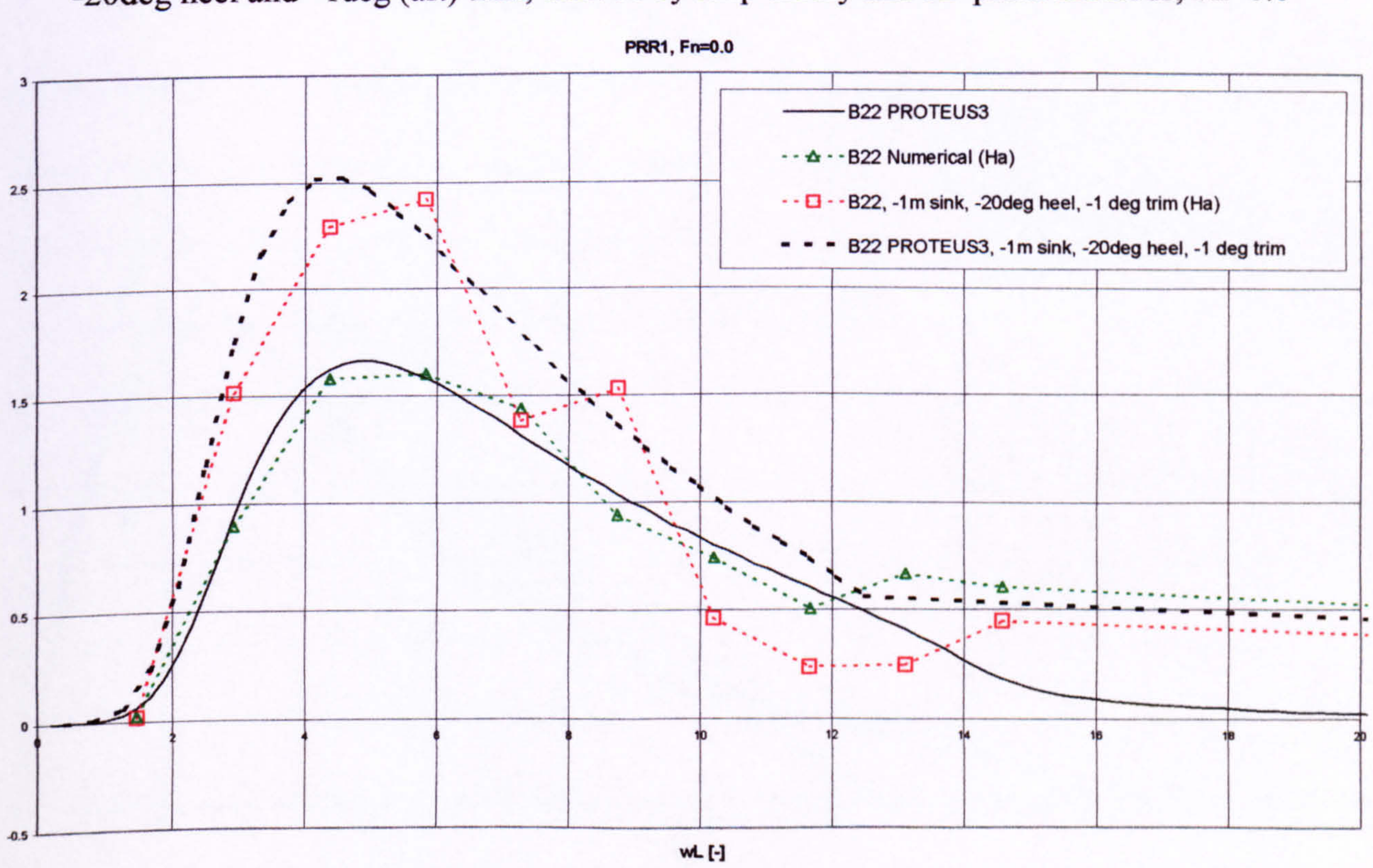

Figure 16 Dimensionless damping in sway mode for 3D PRR1 hull form, effect of –1m sinkage, -20deg heel and –1deg (aft) trim, derived by strip theory and 3D panel methods, Fn=0.0

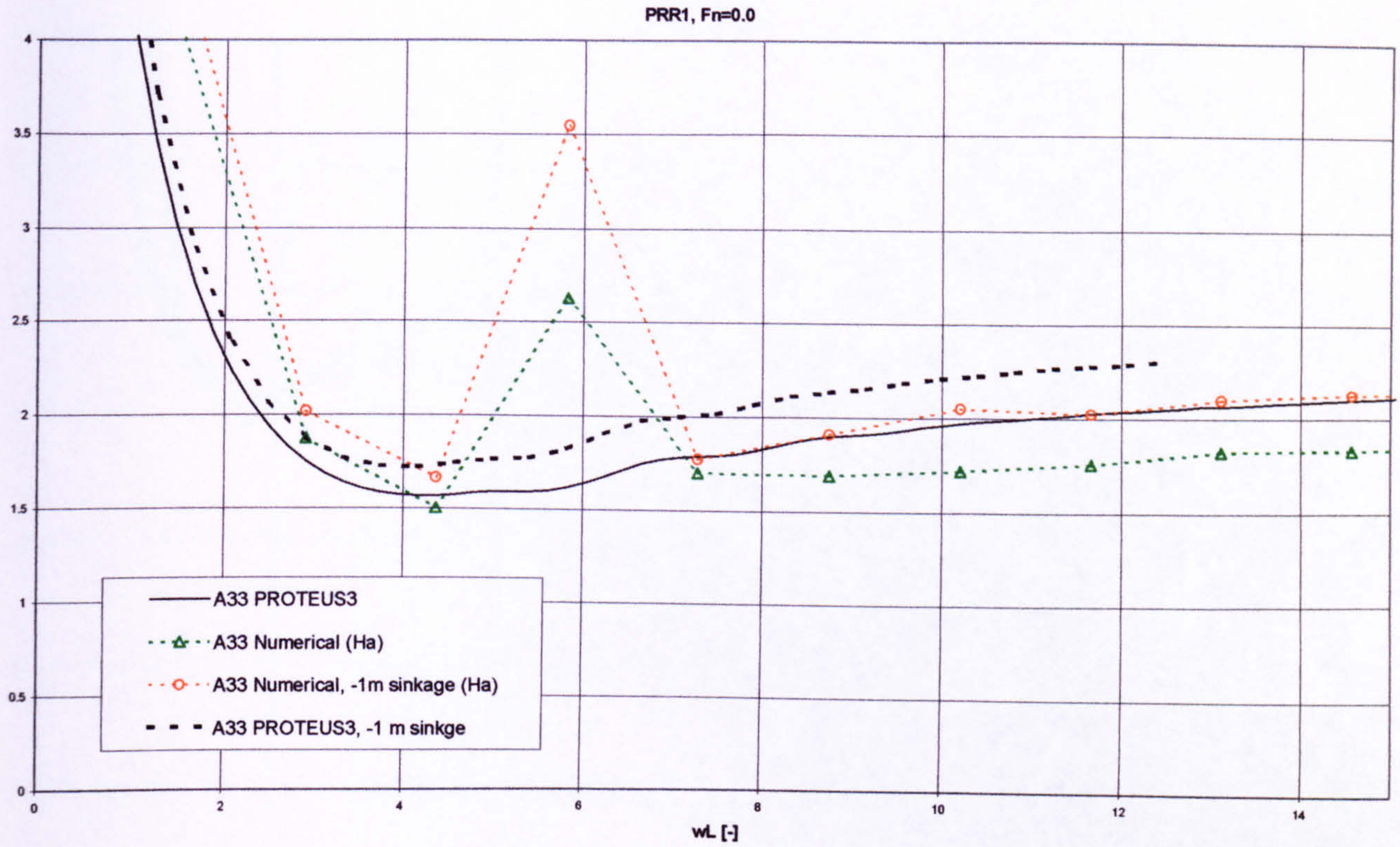

Figure 17 Dimensionless added mass in heave mode for 3D PRR1 hull form, effect of –1m sinkage, comparison between predictions by strip theory and 3D panel methods, Fn=0.0

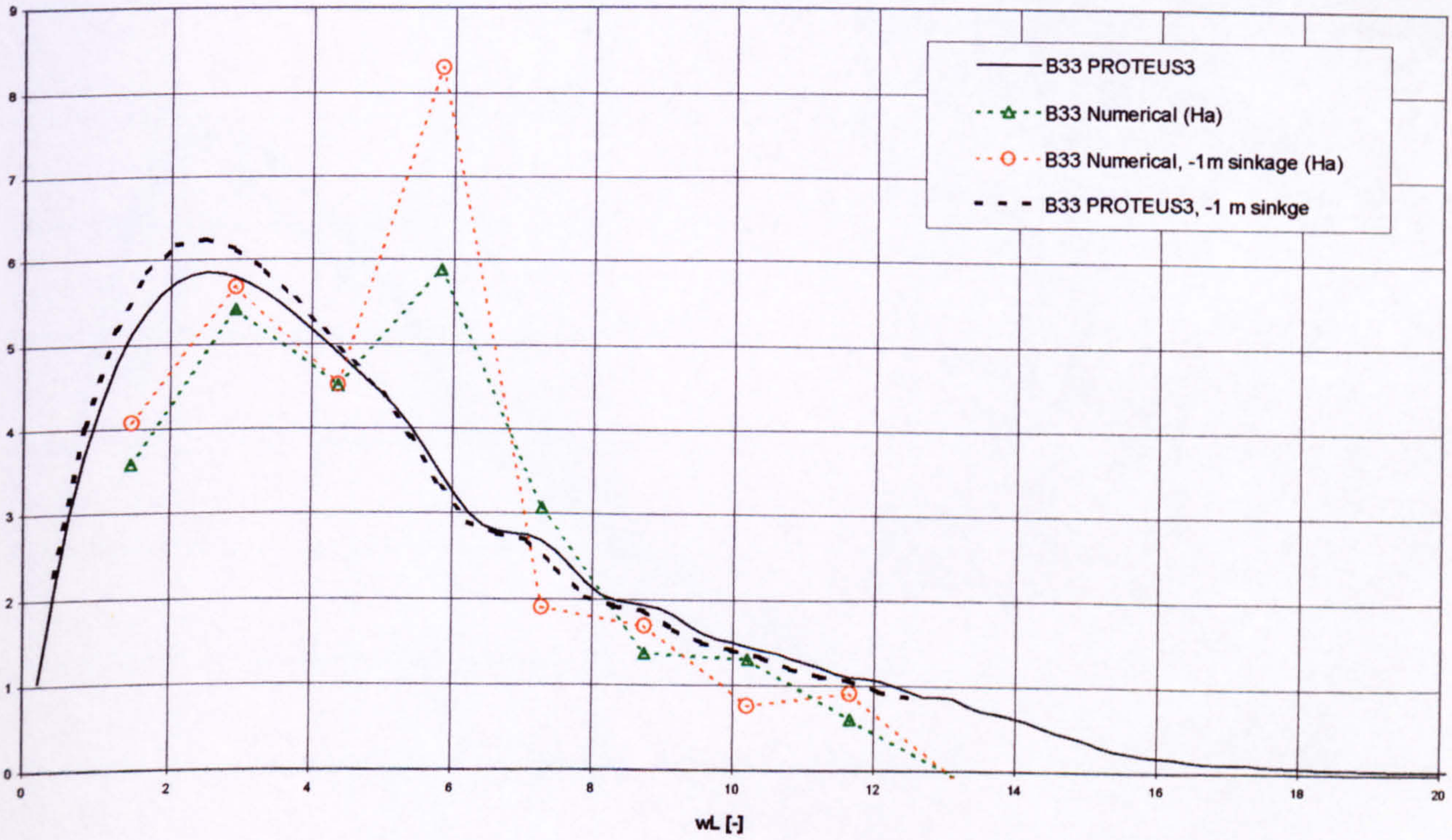

Figure 18 Dimensionless damping in heave mode for 3D PRR1 hull form, effect of –1m sinkage, comparison between predictions by strip theory and 3D panel methods, Fn=0.0

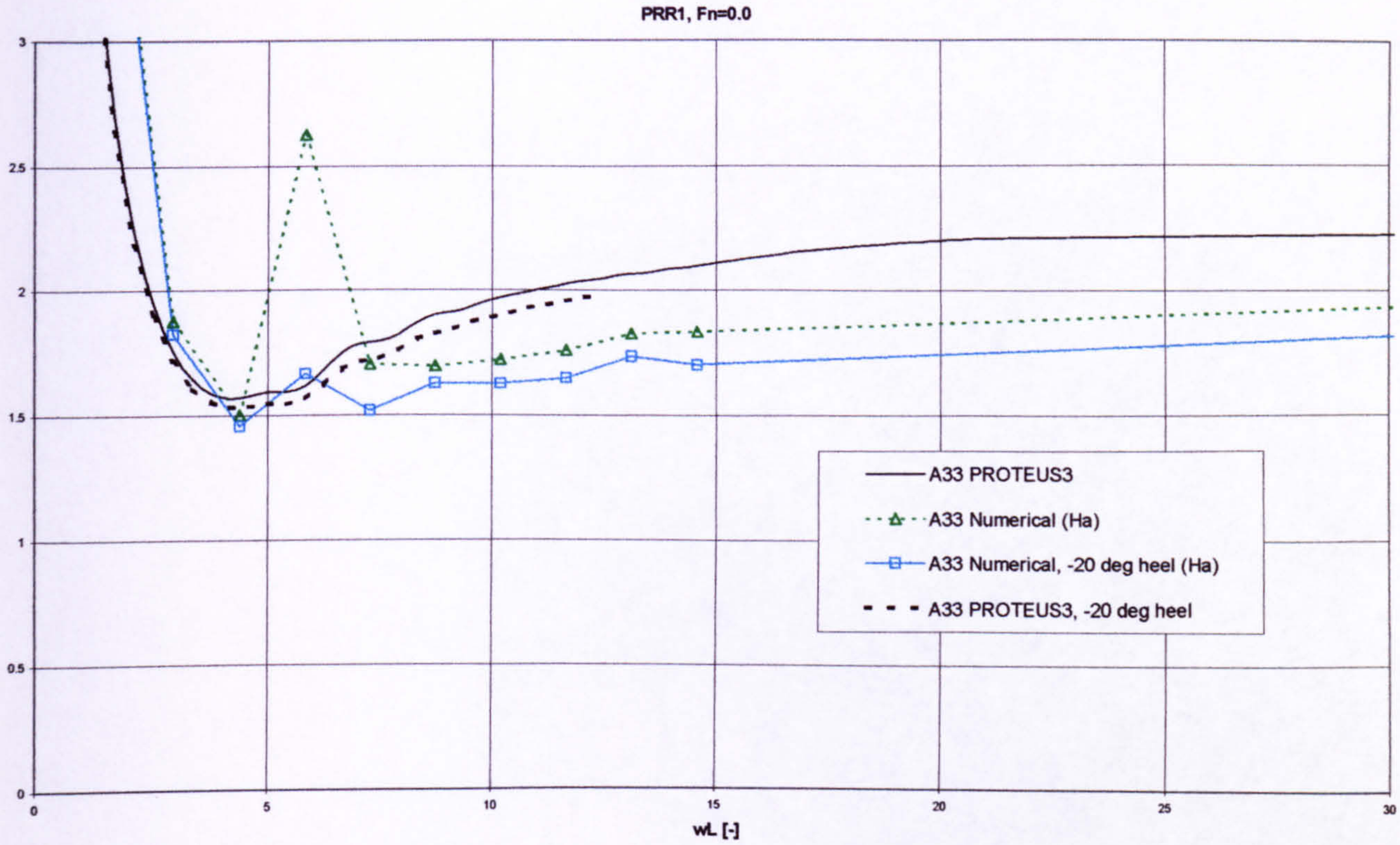

Figure 19 Dimensionless added mass in heave mode for 3D PRR1 hull form, effect of –20deg (port) heel, comparison between predictions by strip theory and 3D panel methods, Fn=0.0

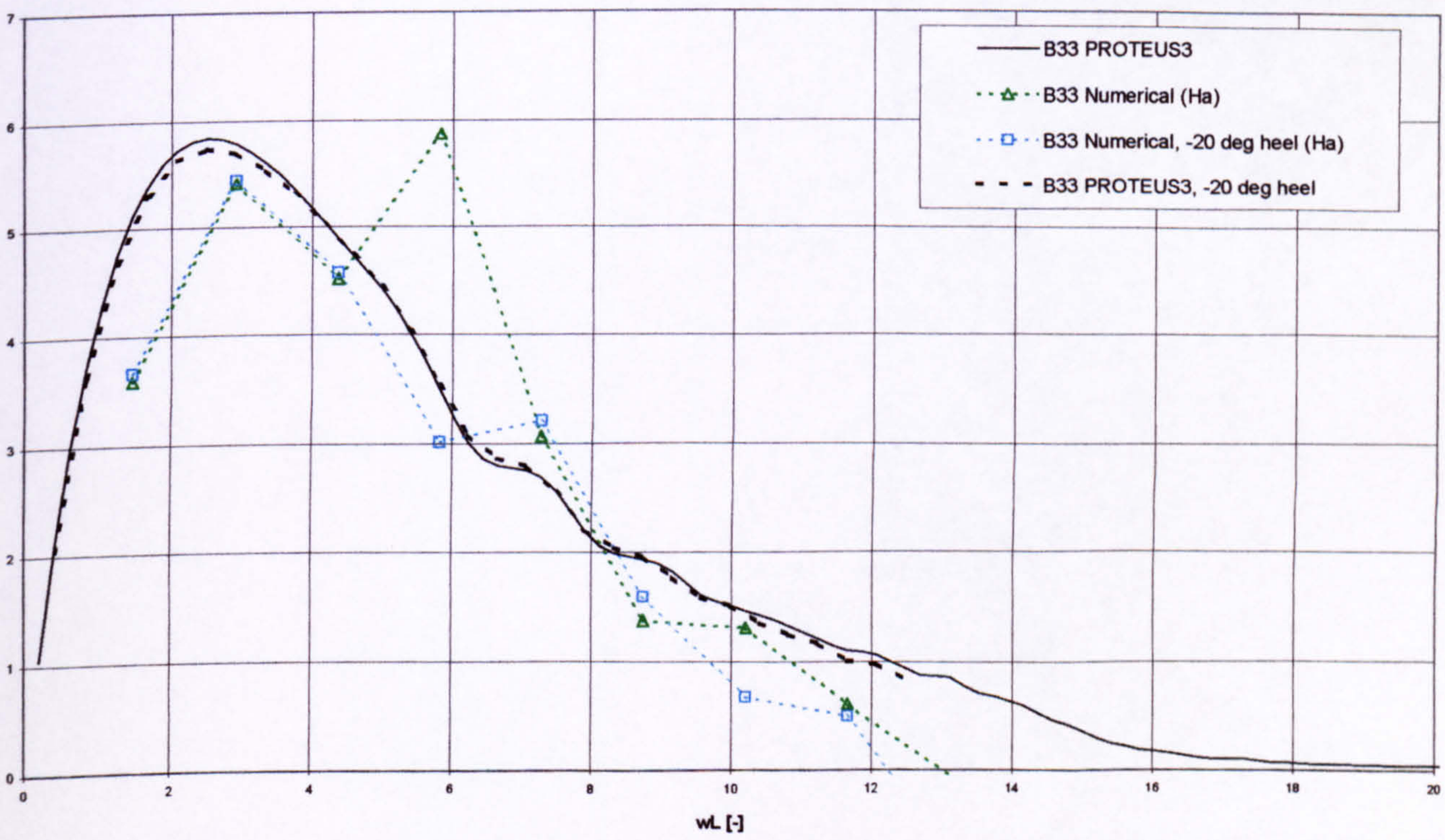

Figure 20 Dimensionless damping in heave mode for 3D PRR1 hull form, effect of –20deg (port) heel, comparison between predictions by strip theory and 3D panel methods, Fn=0.0

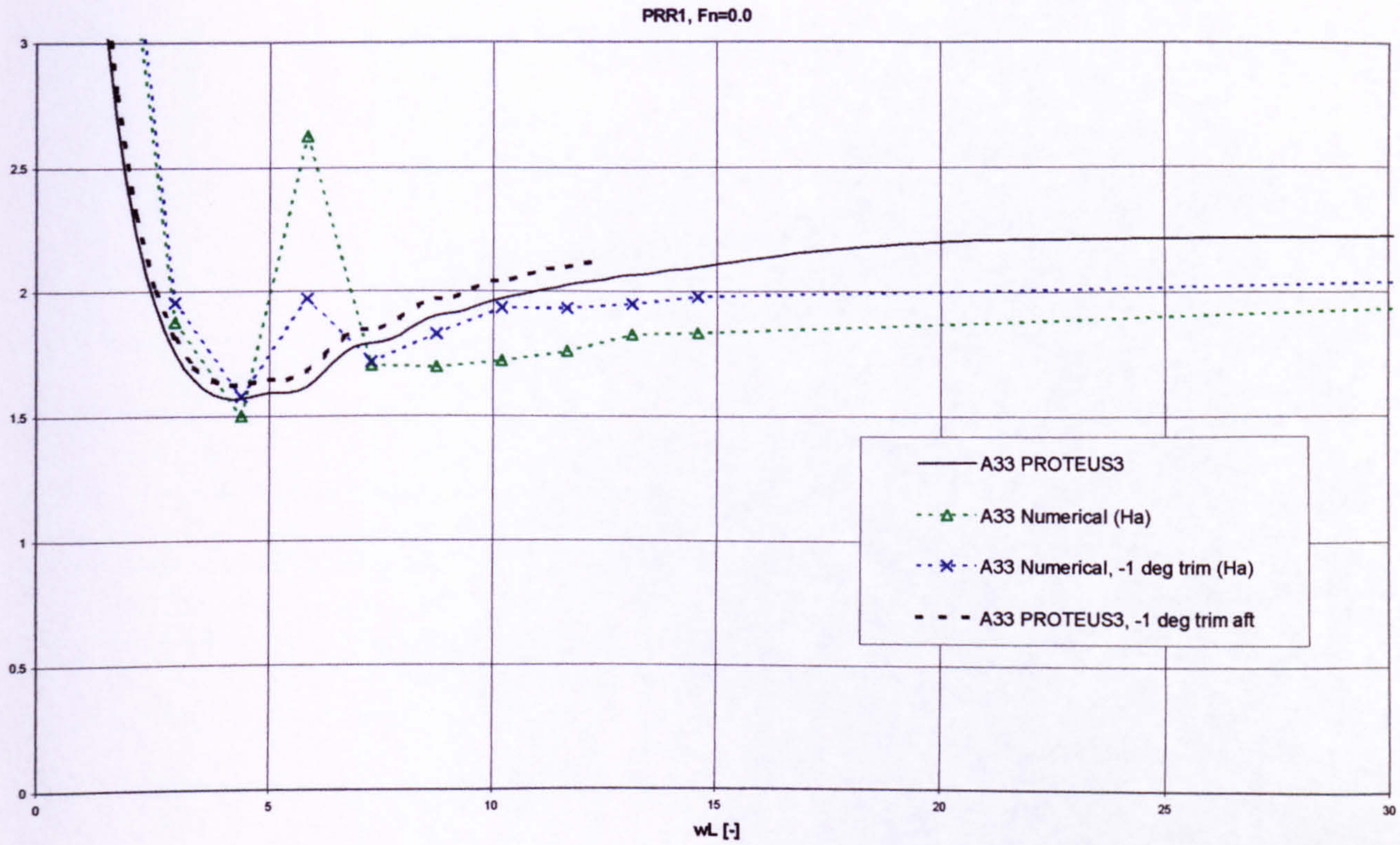

Figure 21 Dimensionless added mass in heave mode for 3D PRR1 hull form, effect of –1deg (aft) trim, comparison between predictions by strip theory and 3D panel methods, Fn=0.0

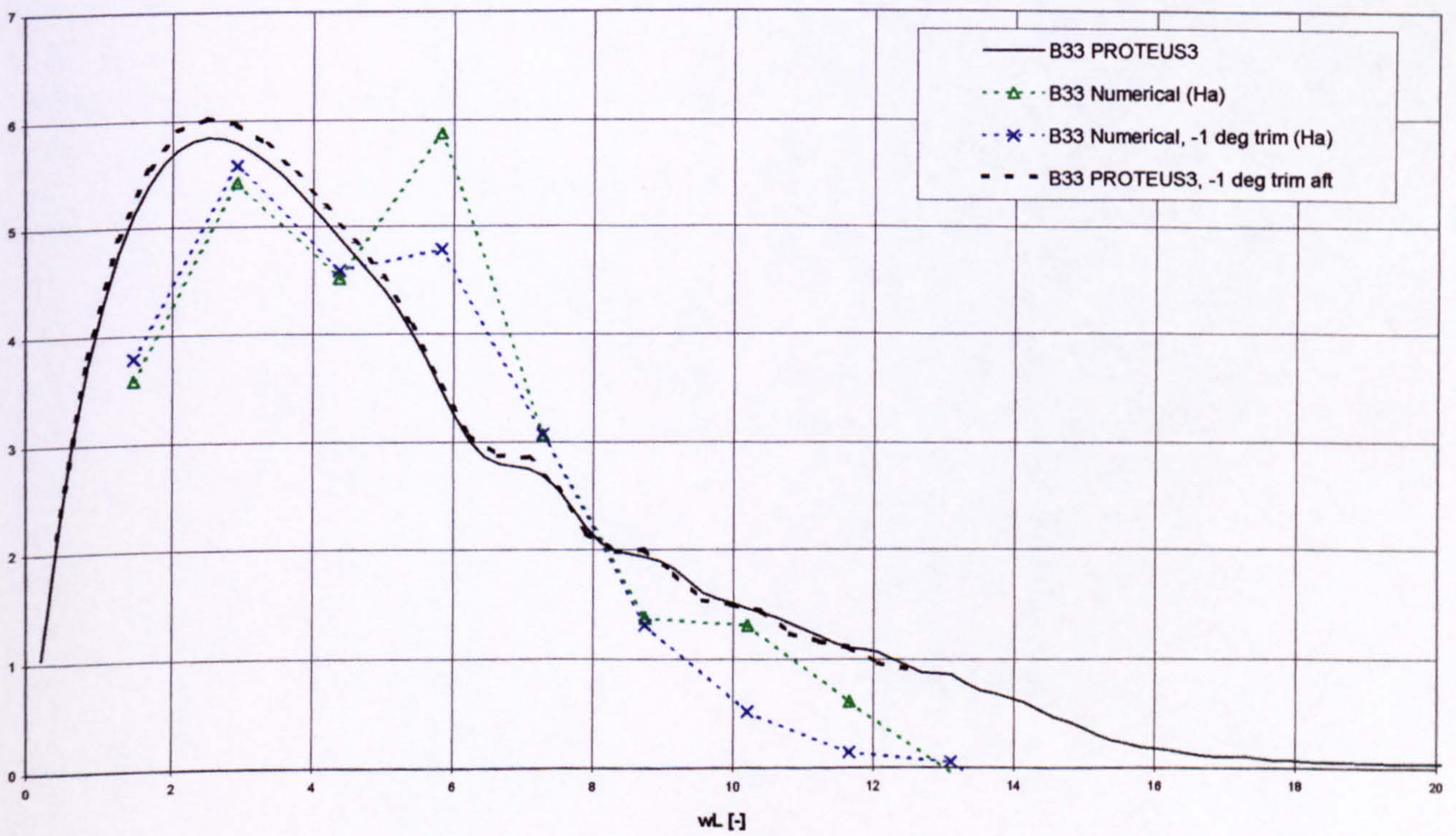

Figure 22 Dimensionless damping in heave mode for 3D PRR1 hull form, effect of –1deg (aft) trim, comparison between predictions by strip theory and 3D panel methods, Fn=0.0

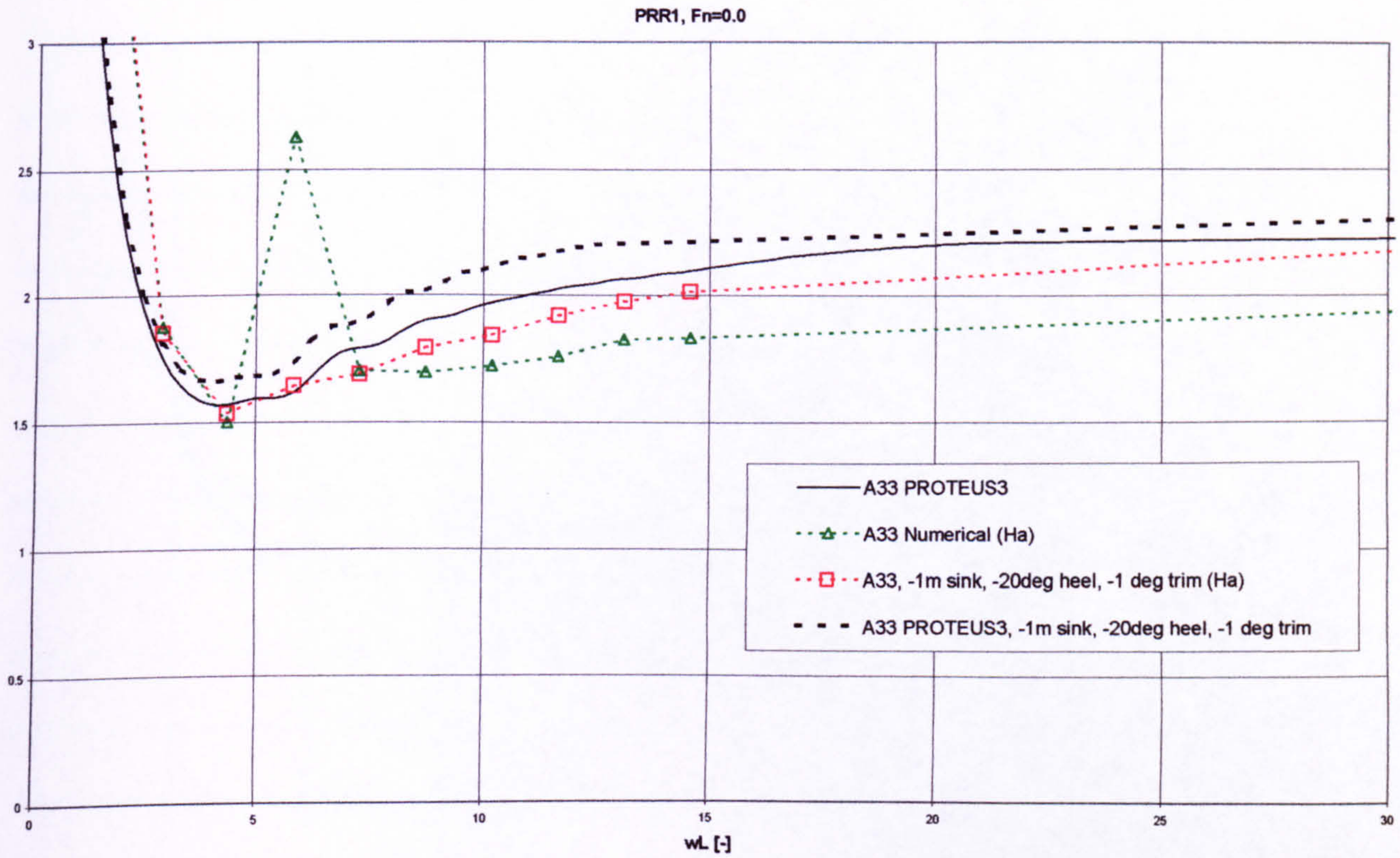

Figure 23 Dimensionless added mass in heave mode for 3D PRR1 hull form, effect of –1m sinkage, -20deg heel and –1deg (aft) trim, derived by strip theory and 3D panel methods, Fn=0.0

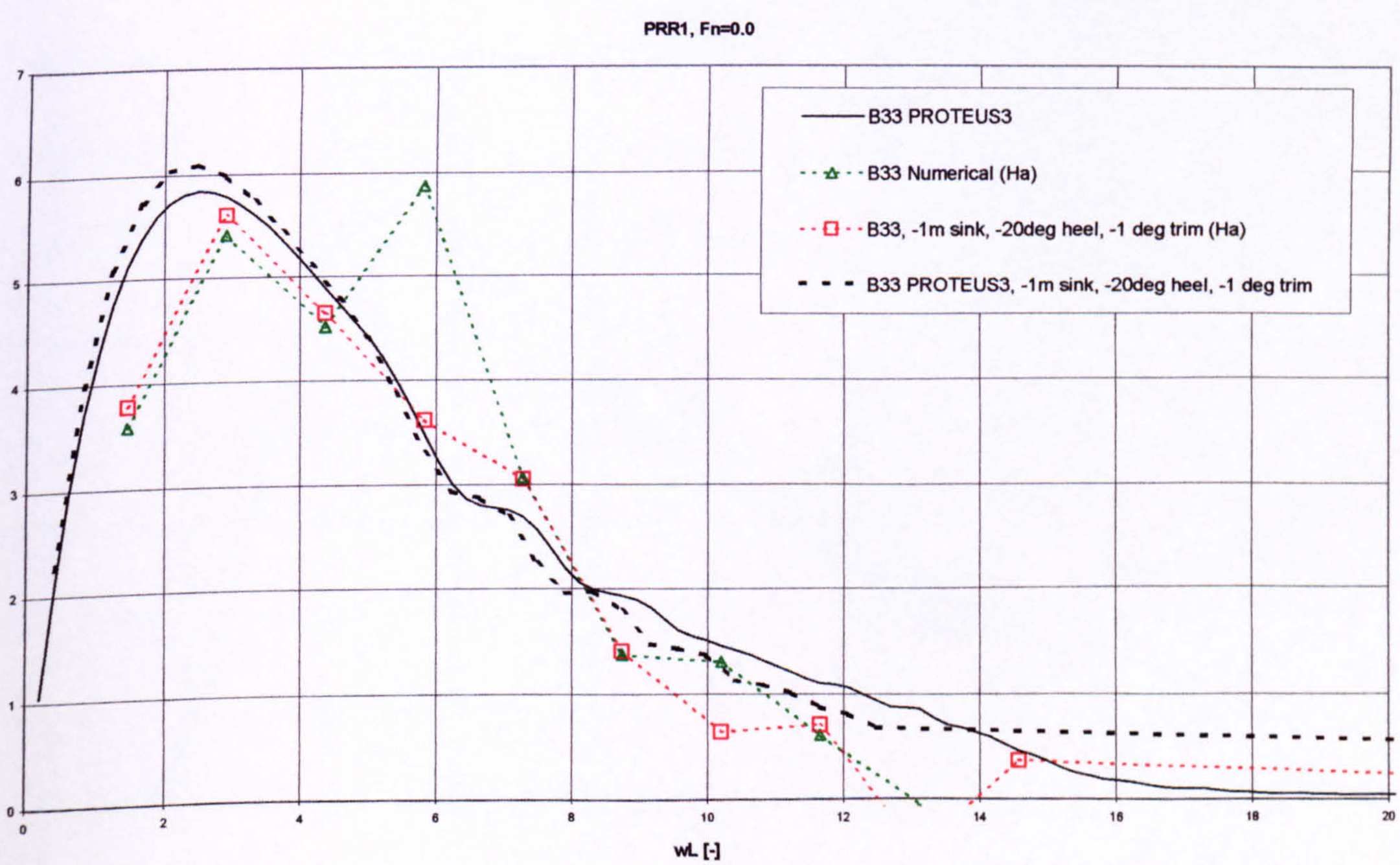

Figure 24 Dimensionless damping in heave mode for 3D PRR1 hull form, effect of –1m sinkage, -20deg heel and –1deg (aft) trim, derived by strip theory and 3D panel methods, Fn=0.0

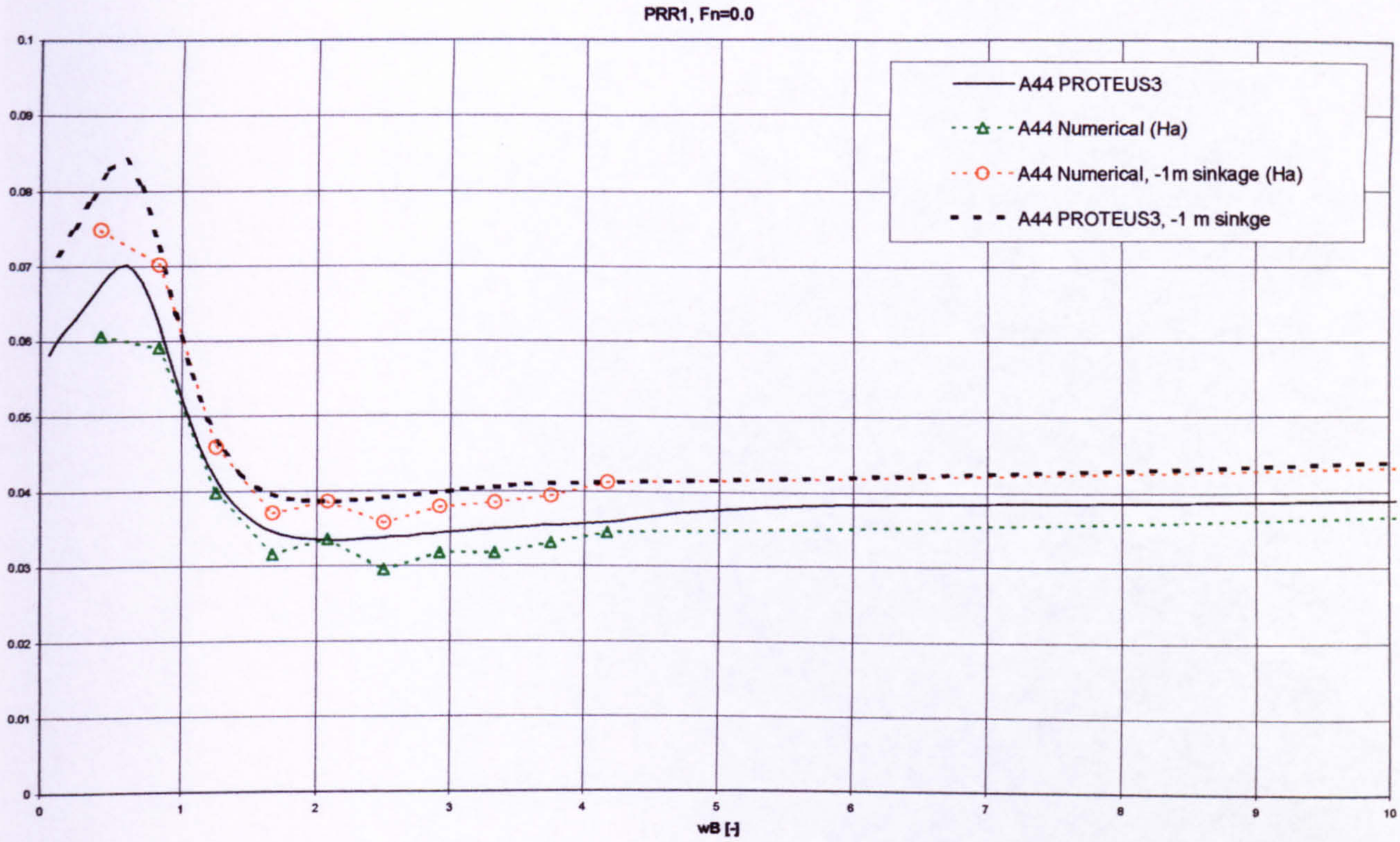

Figure 25 Dimensionless added mass in roll mode for 3D PRR1 hull form, effect of –1m sinkage, comparison between predictions by strip theory and 3D panel methods, Fn=0.0

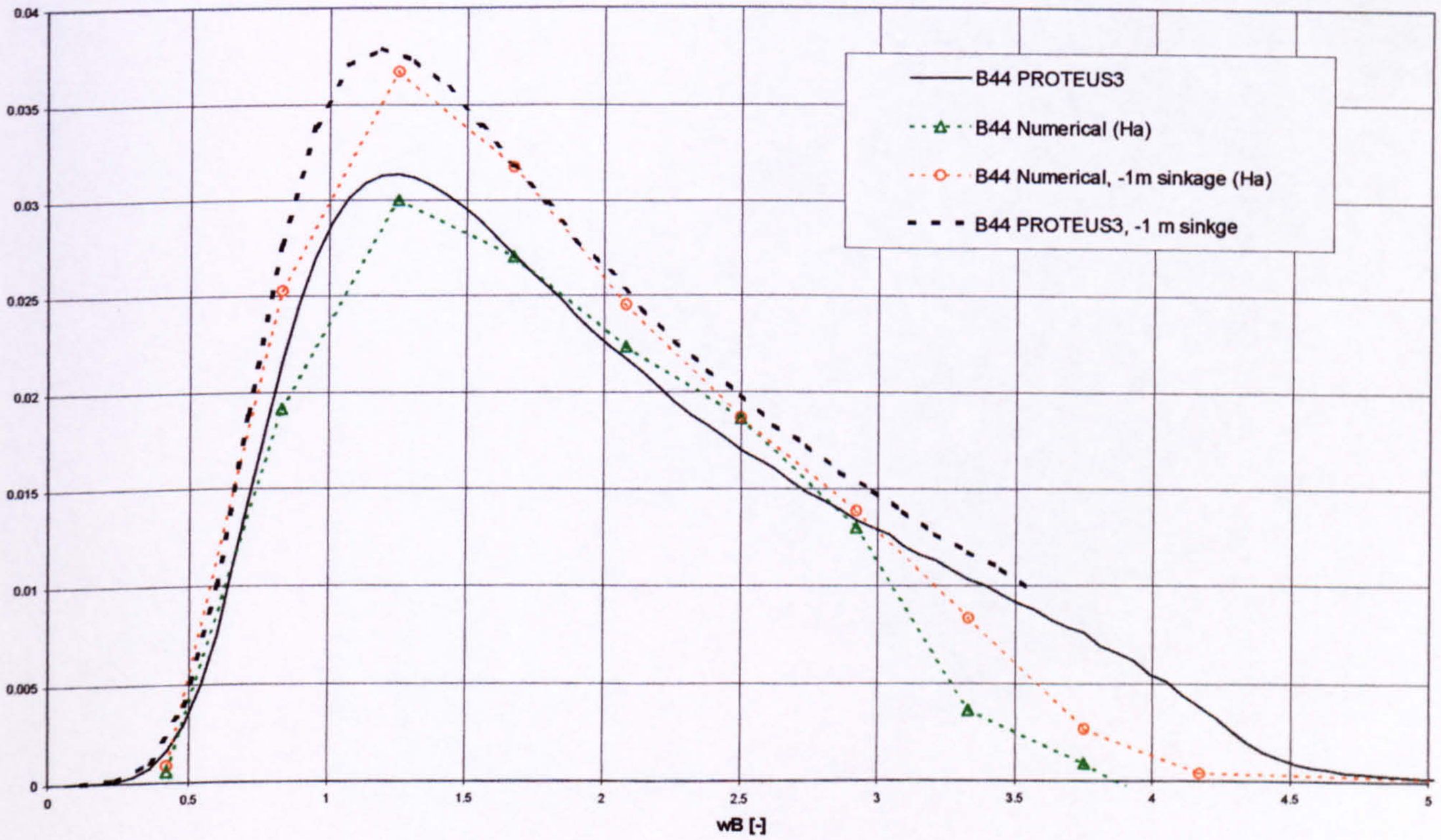

Figure 26 Dimensionless damping in roll mode for 3D PRR1 hull form, effect of –1m sinkage, comparison between predictions by strip theory and 3D panel methods, Fn=0.0

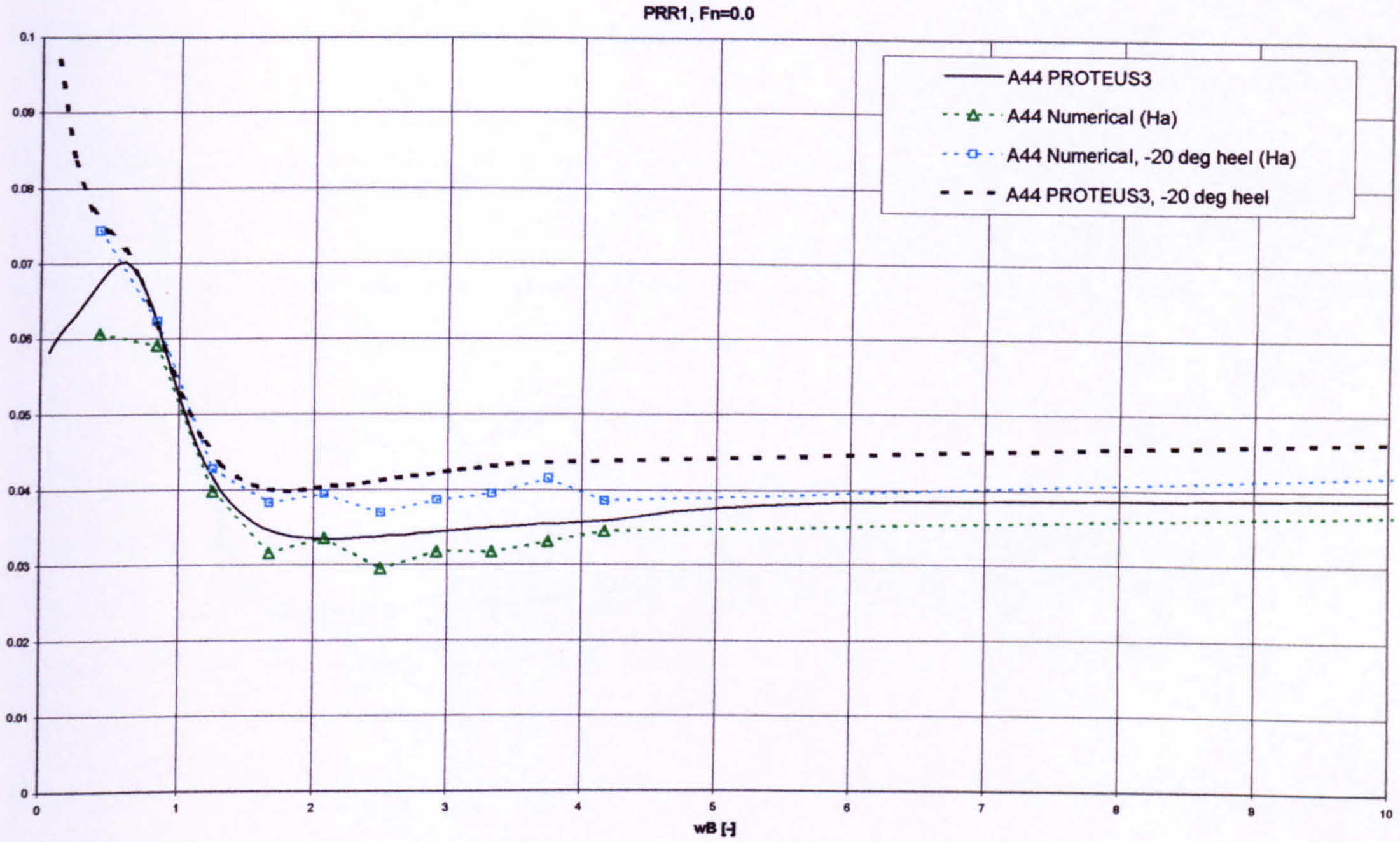

Figure 27 Dimensionless added mass in roll mode for 3D PRR1 hull form, effect of –20deg (port) heel, comparison between predictions by strip theory and 3D panel methods, Fn=0.0

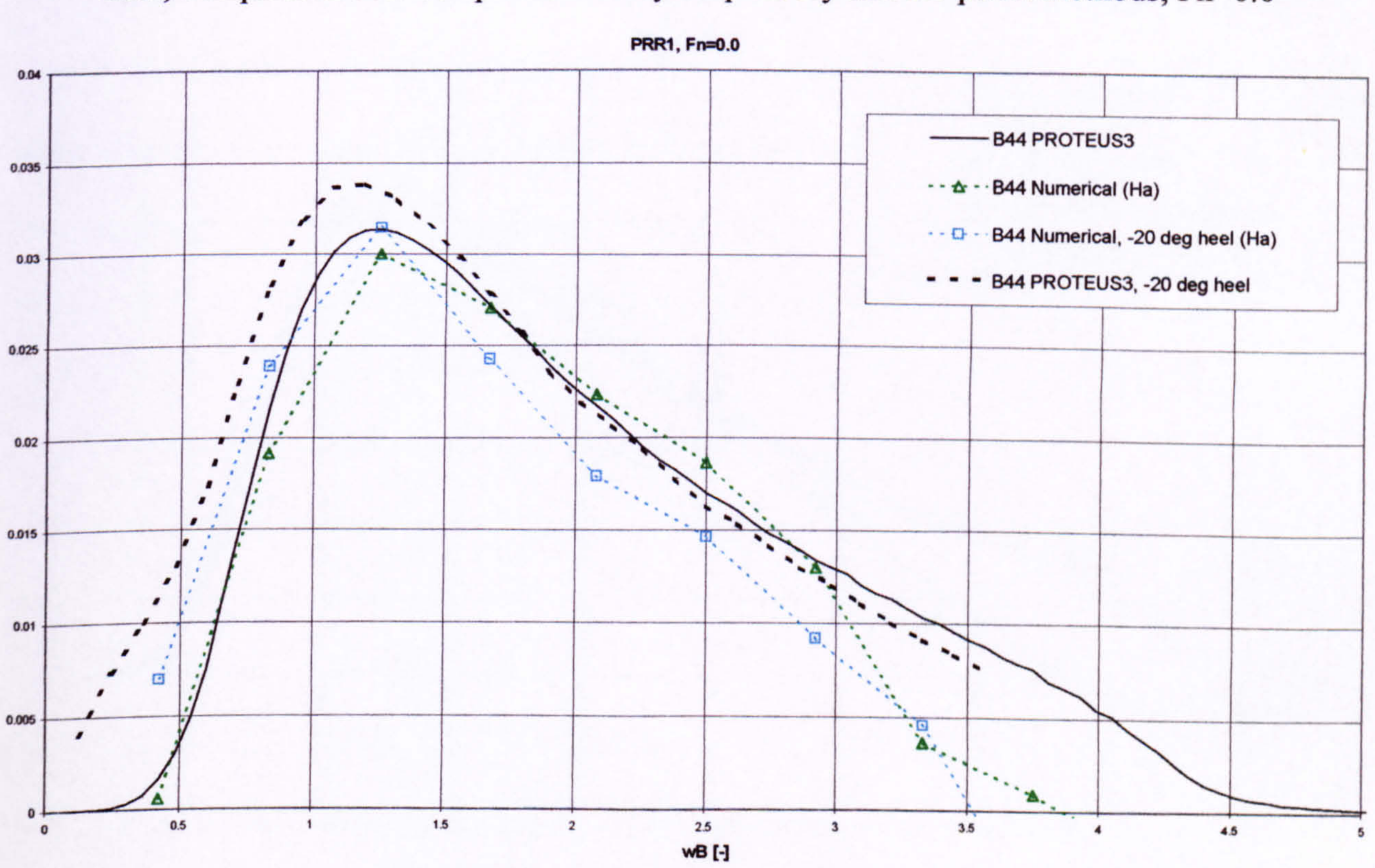

Figure 28 Dimensionless damping in roll mode for 3D PRR1 hull form, effect of –20deg (port) heel, comparison between predictions by strip theory and 3D panel methods, Fn=0.0

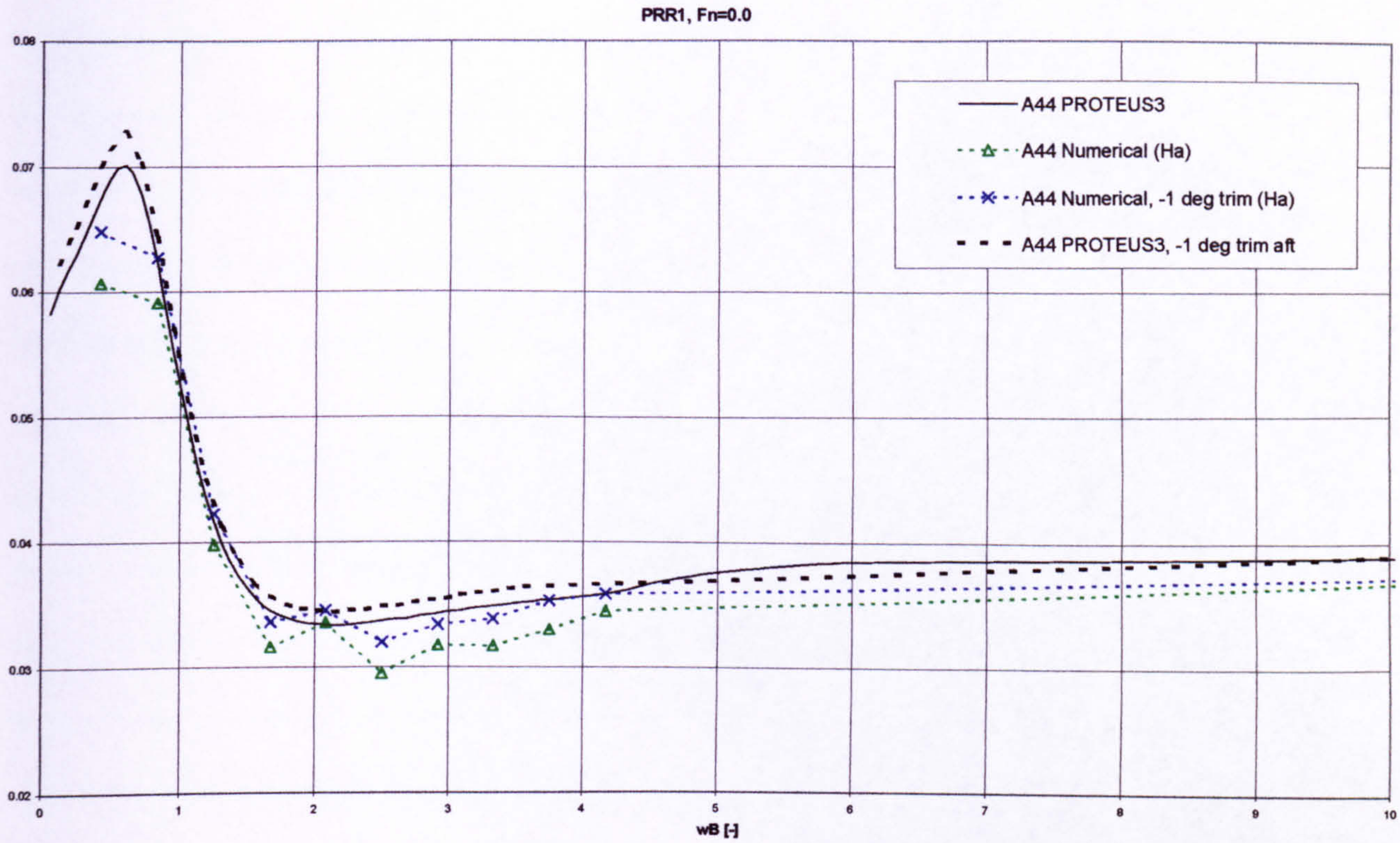

Figure 29 Dimensionless added mass in roll mode for 3D PRR1 hull form, effect of –1deg trim (aft), comparison between predictions by strip theory and 3D panel methods, Fn=0.0

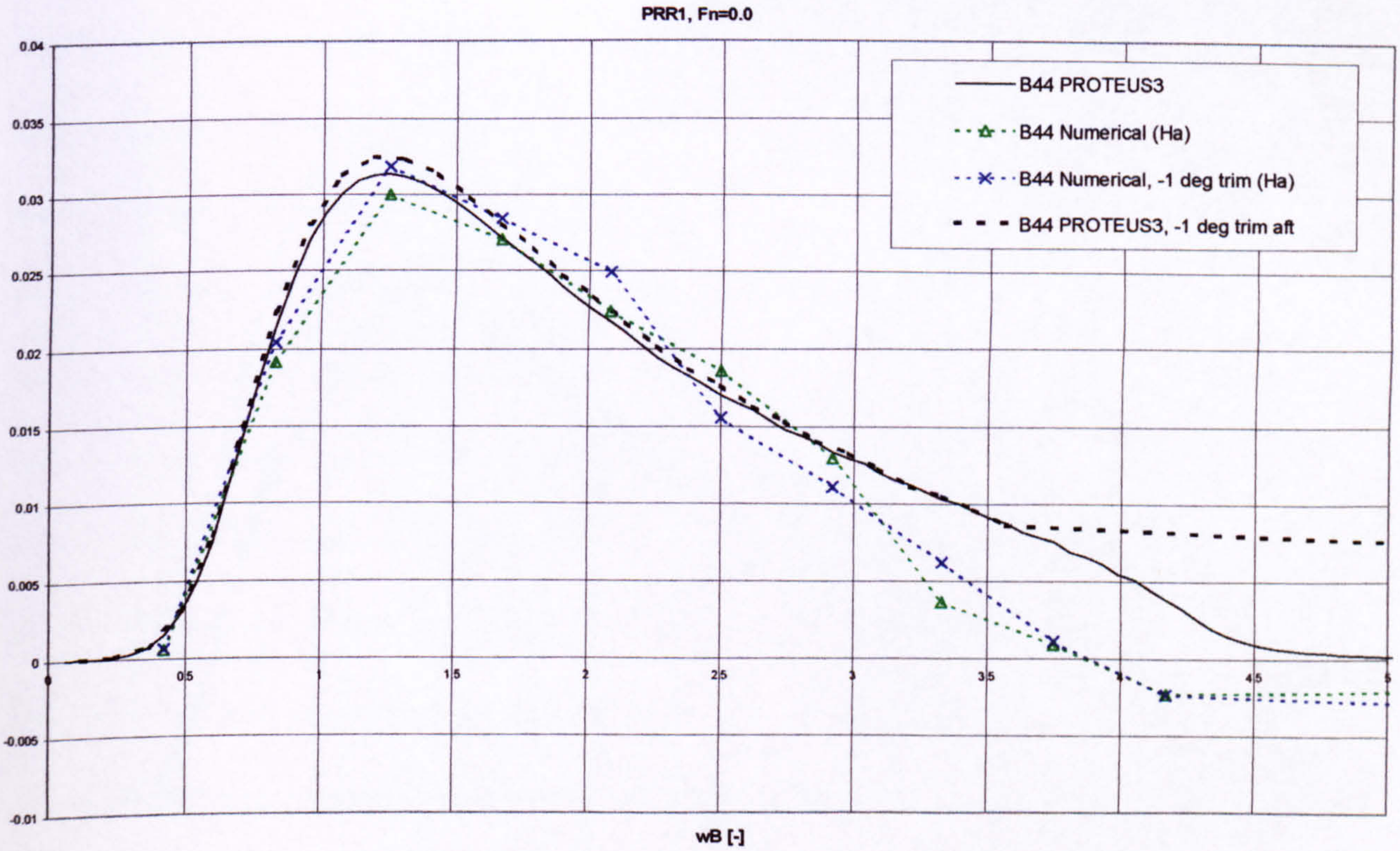

Figure 30 Dimensionless damping in roll mode for 3D PRR1 hull form, effect of –1deg trim (aft), comparison between predictions by strip theory and 3D panel methods, Fn=0.0

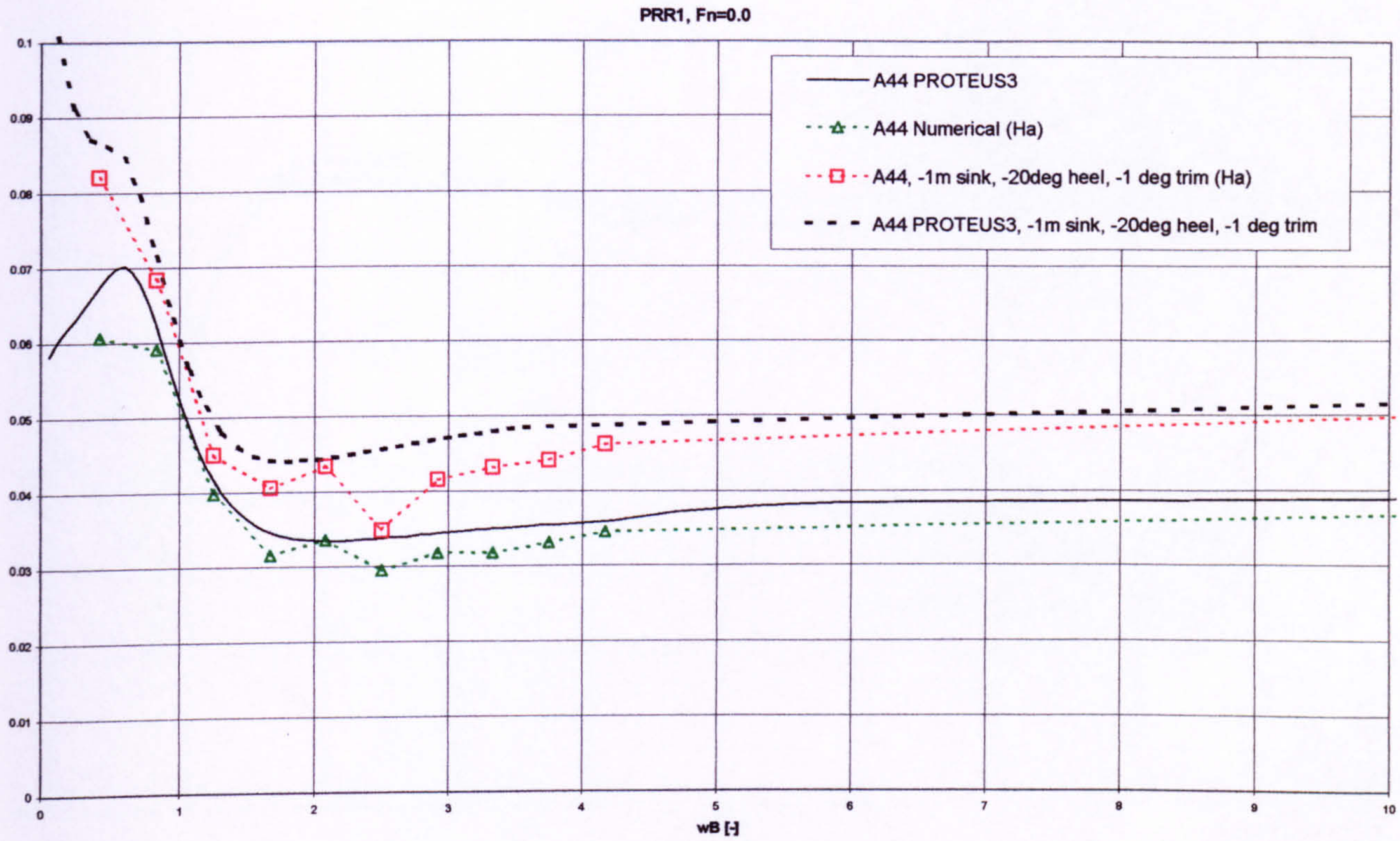

Figure 31 Dimensionless added mass in roll mode for 3D PRR1 hull form, effect of –1m sinkage, -20deg heel and –1deg (aft) trim, derived by strip theory and 3D panel methods, Fn=0.0

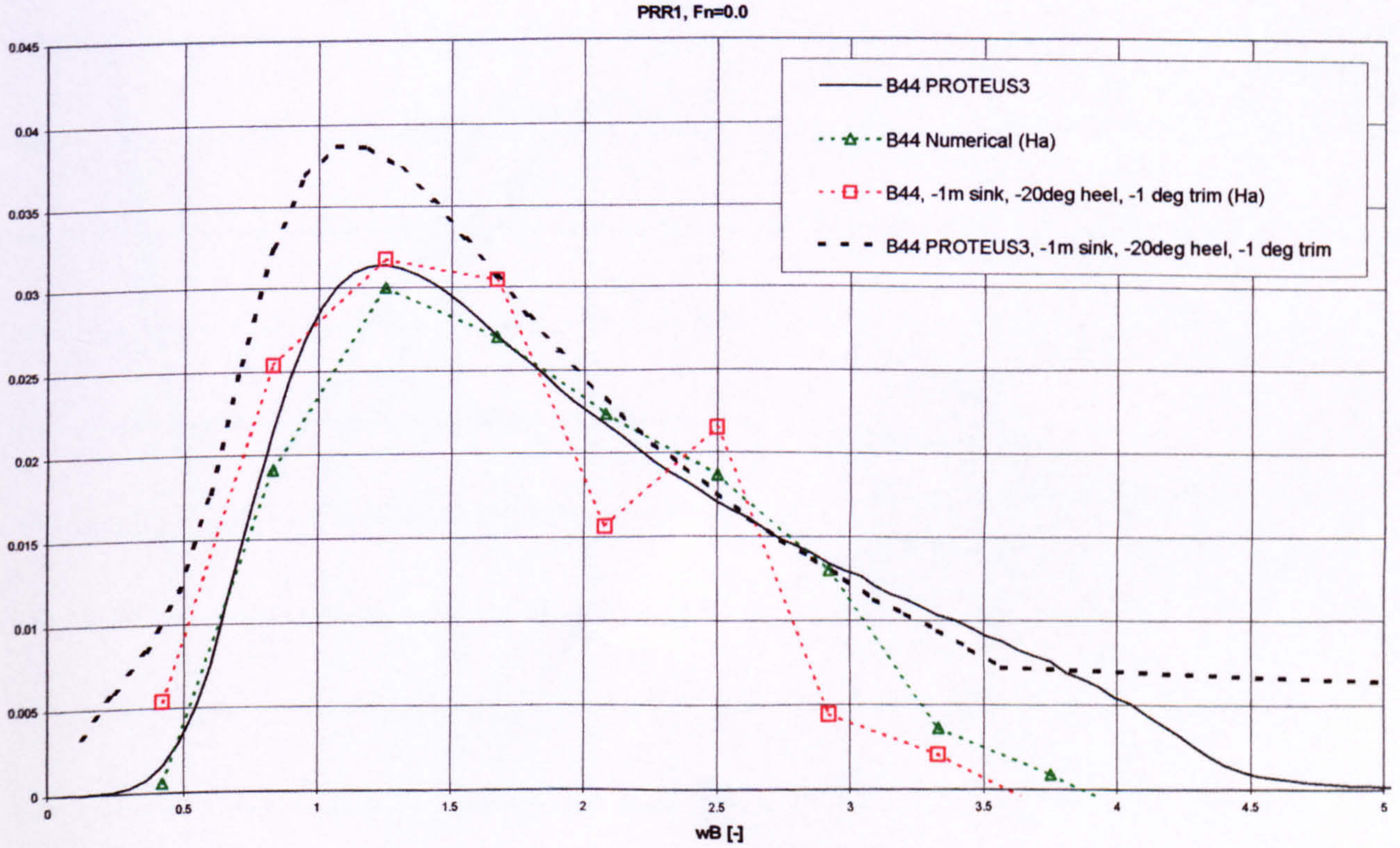

Figure 32 Dimensionless damping in roll mode for 3D PRR1 hull form, effect of –1m sinkage, -20deg heel and –1deg (aft) trim, derived by strip theory and 3D panel methods, Fn=0.0

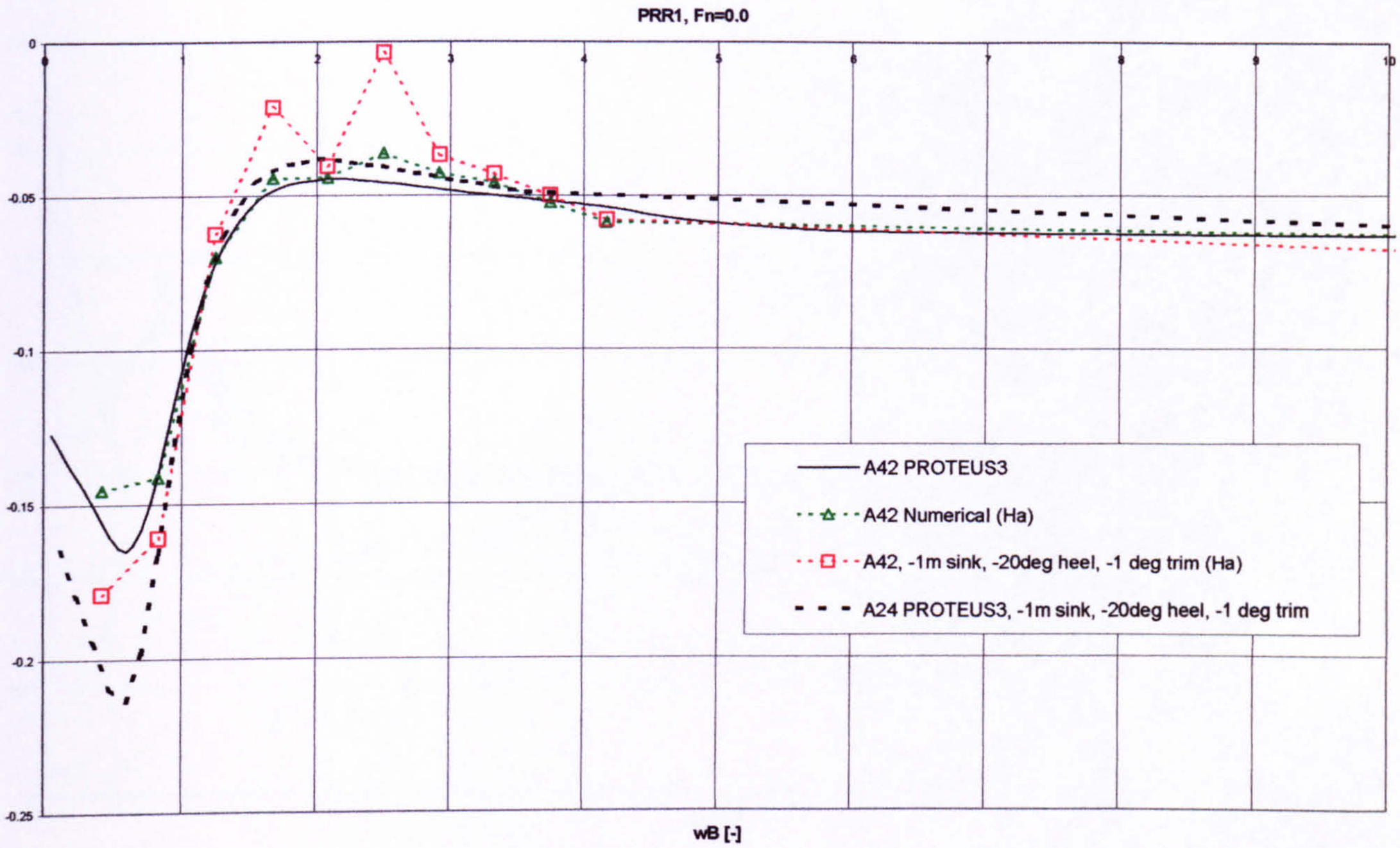

Figure 33 Dimensionless added mass in sway-into-roll mode for 3D PRR1 hull form, effect of –1m sinkage, -20deg heel and –1deg (aft) trim, derived by strip theory and 3D panel methods, Fn=0.0

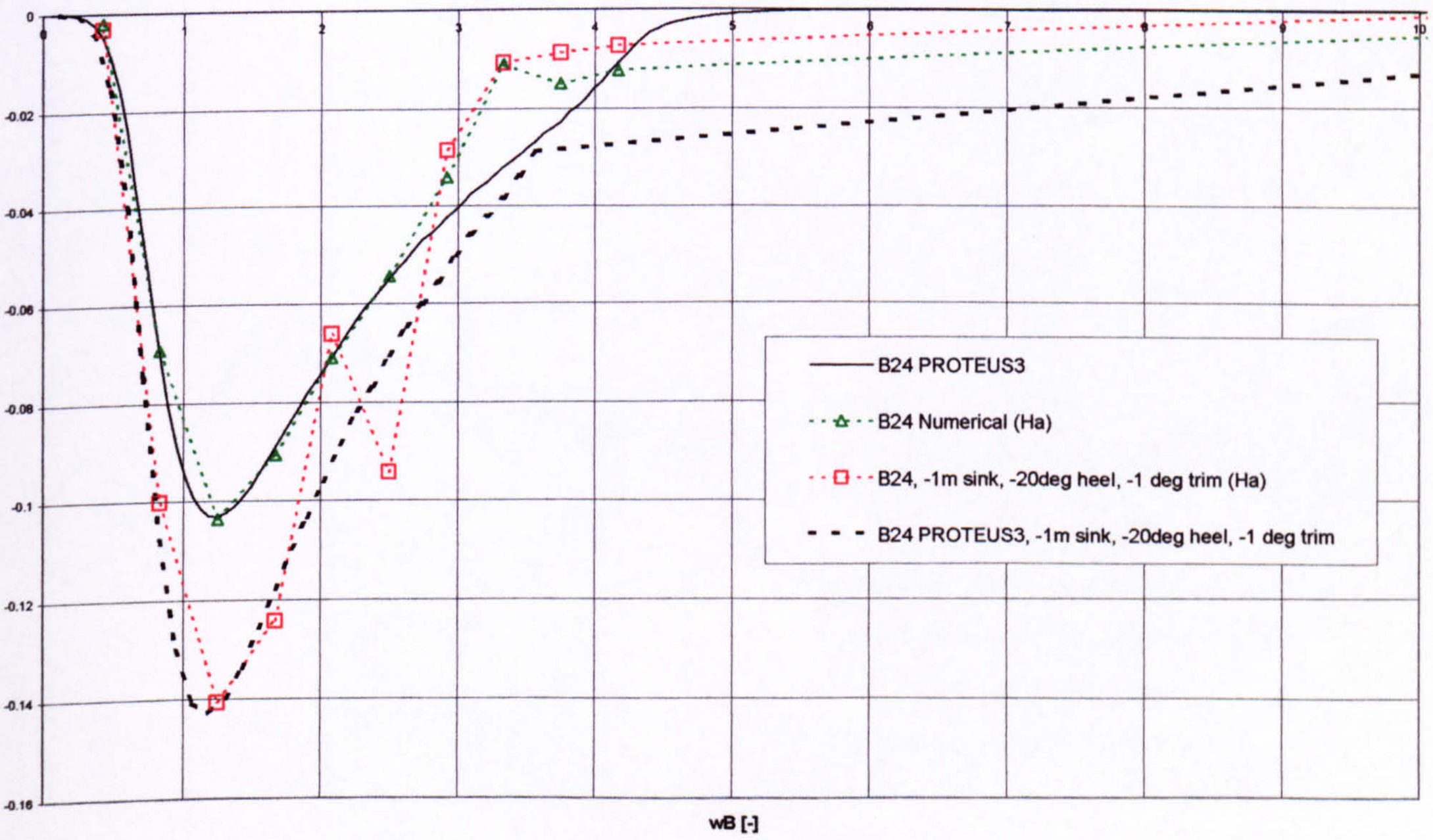

Figure 34 Dimensionless damping in sway-into-roll mode for 3D PRR1 hull form, effect of –1m sinkage, -20deg heel and –1deg (aft) trim, derived by strip theory and 3D panel methods, Fn=0.0

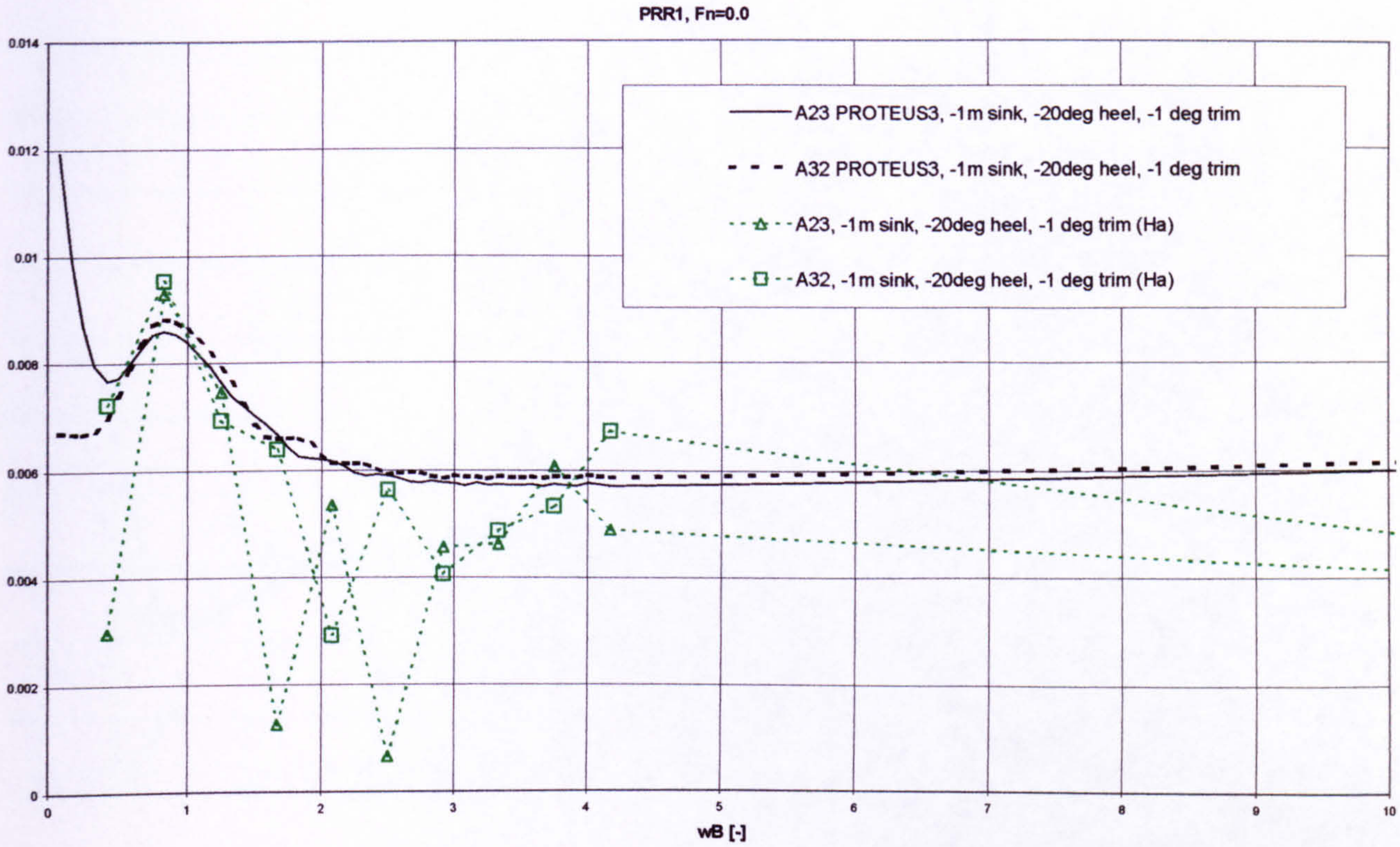

Figure 35 Dimensionless added mass in sway-into-heave mode for 3D PRR1 hull form, effect of –1m sinkage, -20deg heel, –1deg (aft) trim, derived by strip theory and 3D panel methods, Fn=0.0

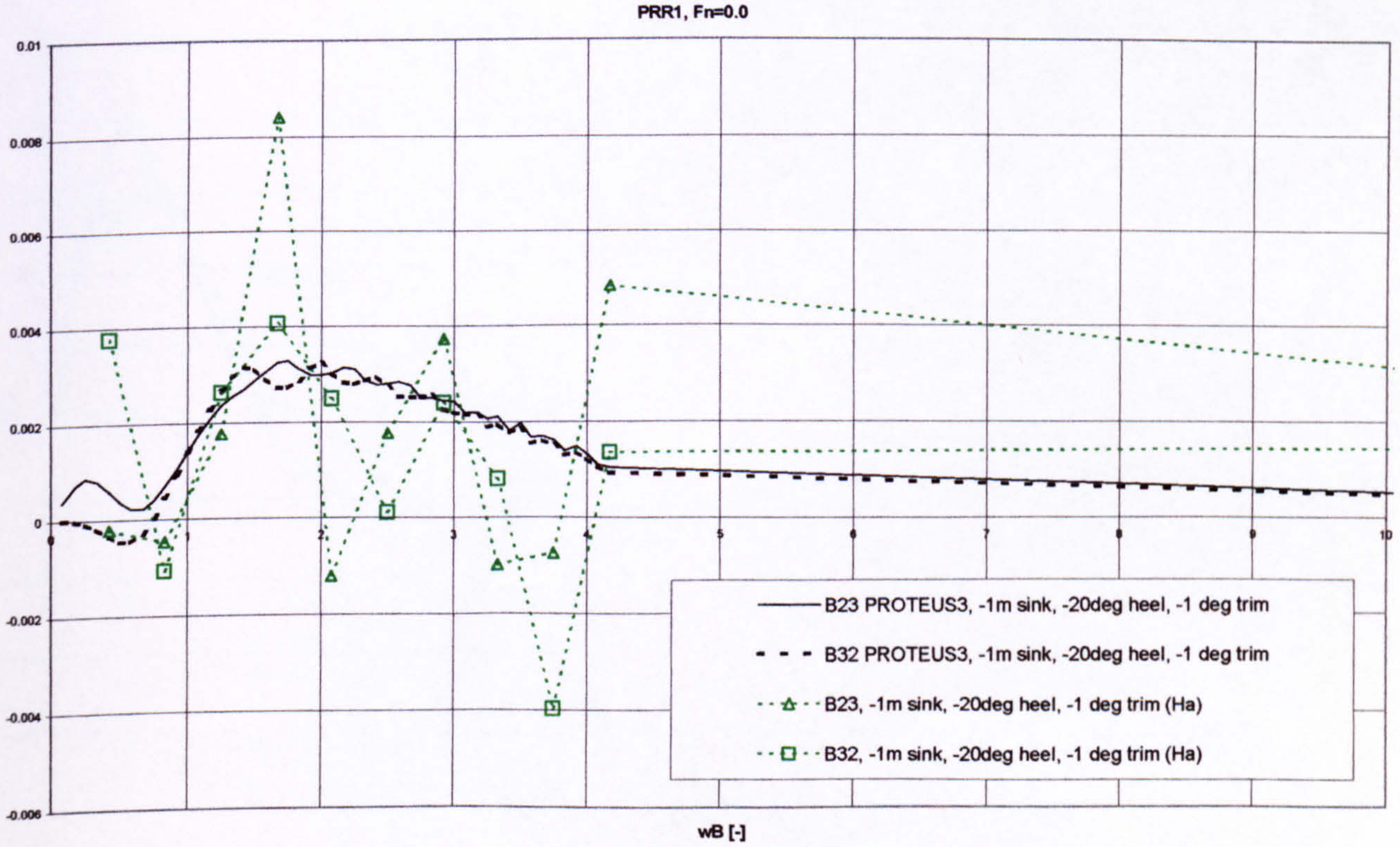

Figure 36 Dimensionless damping in sway-into-heave mode for 3D PRR1 hull form, effect of –1m sinkage, -20deg heel and –1deg (aft) trim, derived by strip theory and 3D panel methods, Fn=0.0

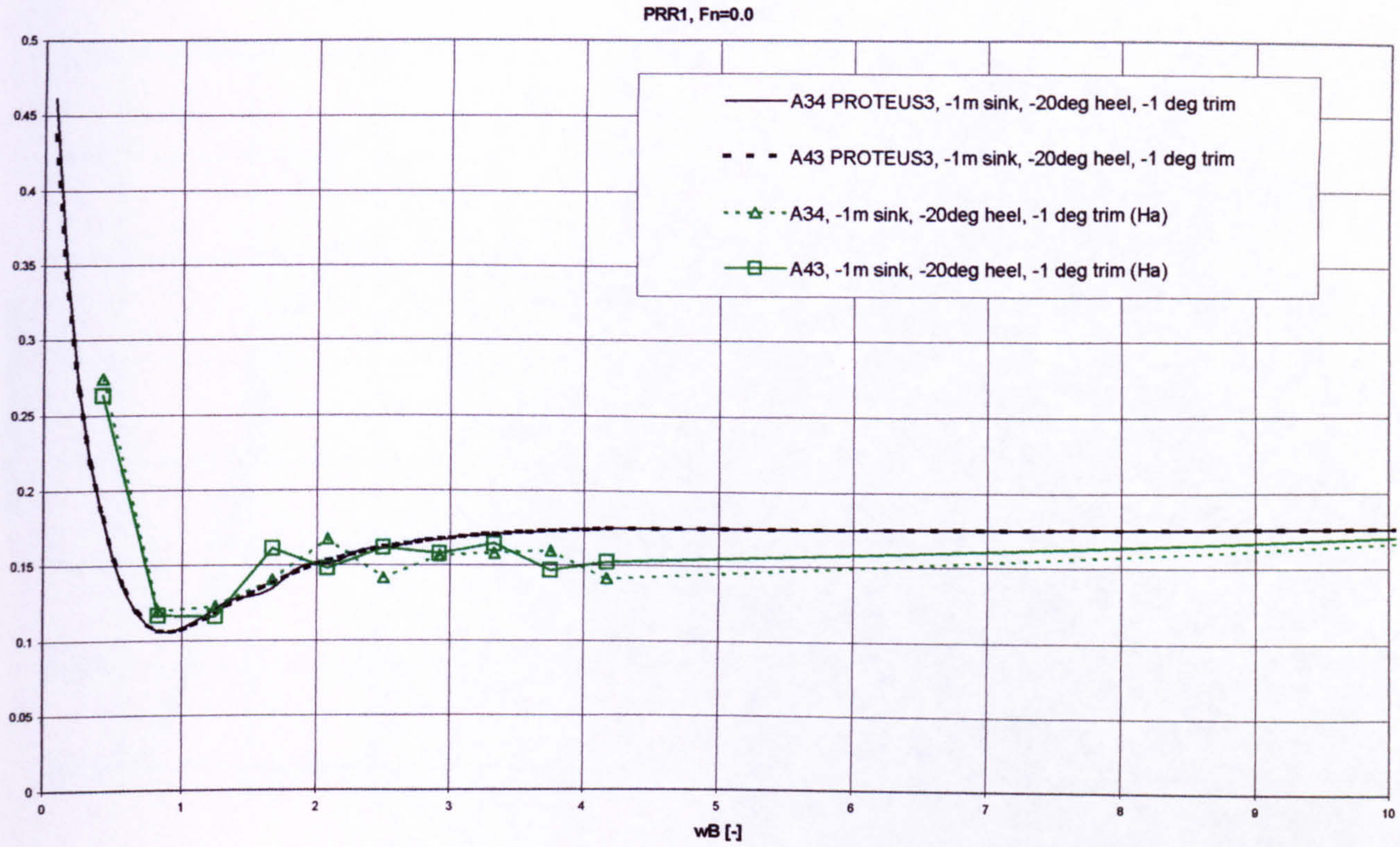

Figure 37 Dimensionless added mass in heave-into-roll mode for 3D PRR1 hull form, effect of –1m sinkage, -20deg heel and –1deg (aft) trim, derived by strip theory and 3D panel methods, Fn=0.0

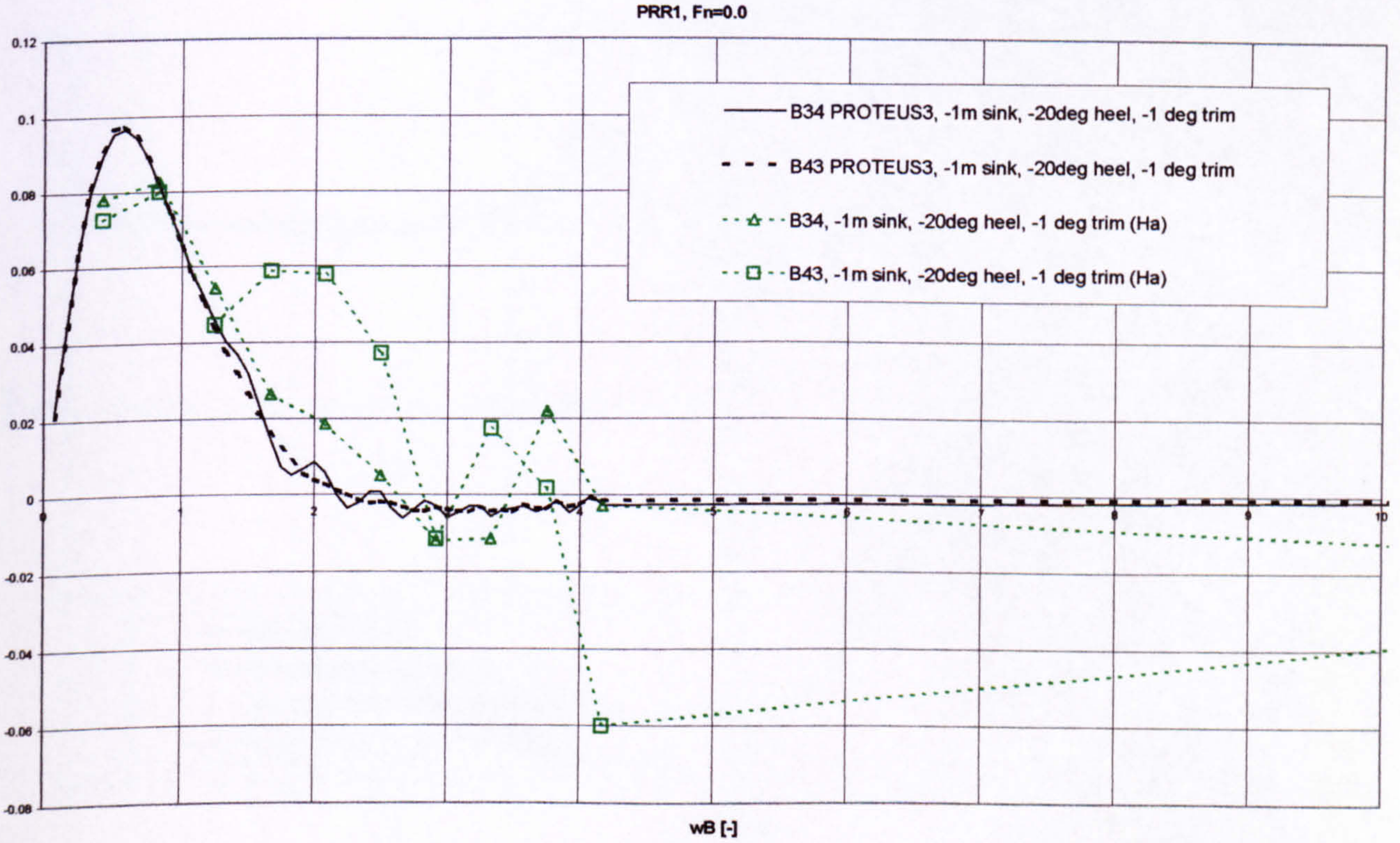

Figure 38 Dimensionless damping in heave-into-roll mode for 3D PRR1 hull form, effect of –1m sinkage, -20deg heel and –1deg (aft) trim, derived by strip theory and 3D panel methods, Fn=0.0

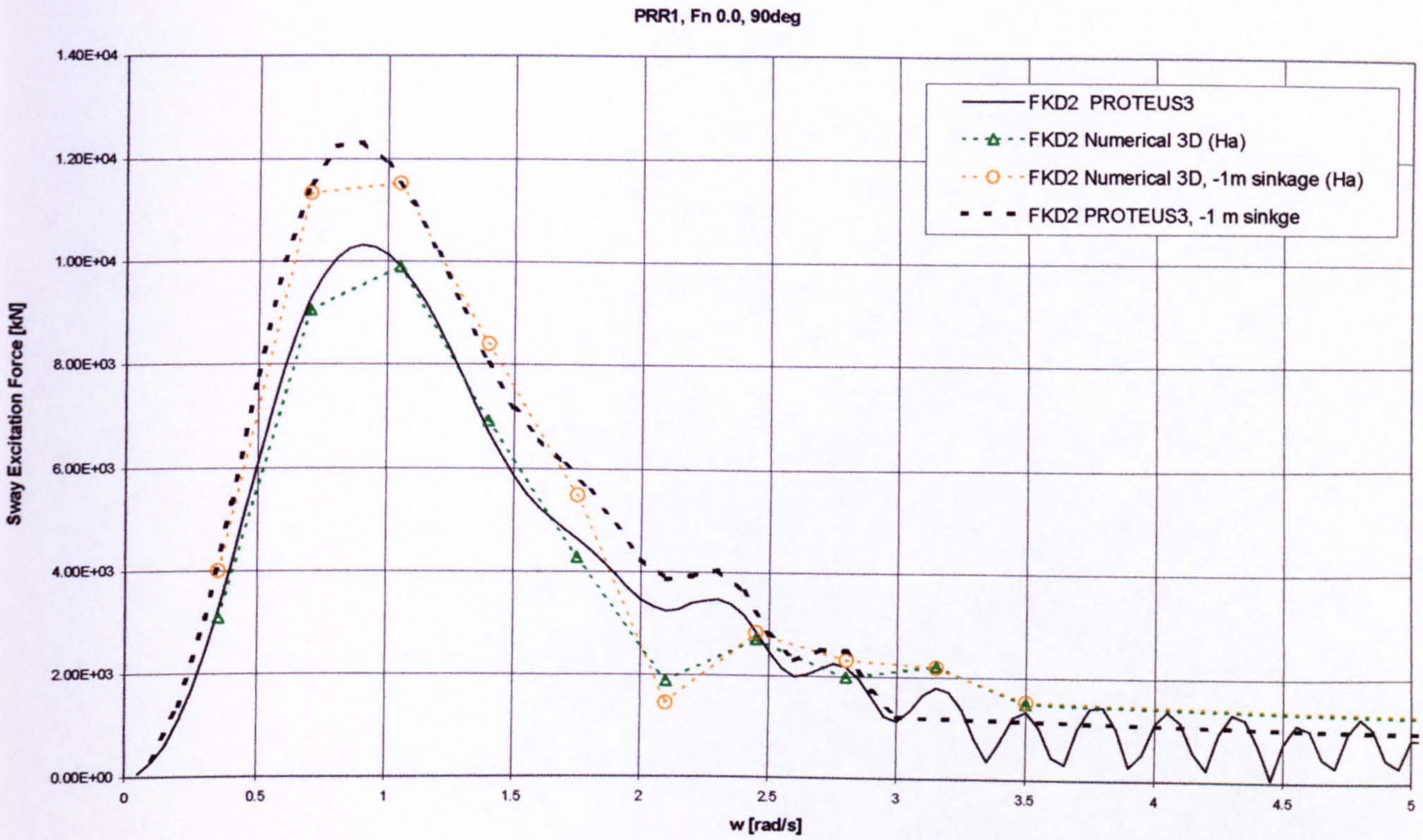

Figure 39 Excitation forces in sway mode for 3D PRR1 hull form, predictions by strip theory and 3D panel methods, Fn=0.0, Heading 90deg, effect of –1m sinkage

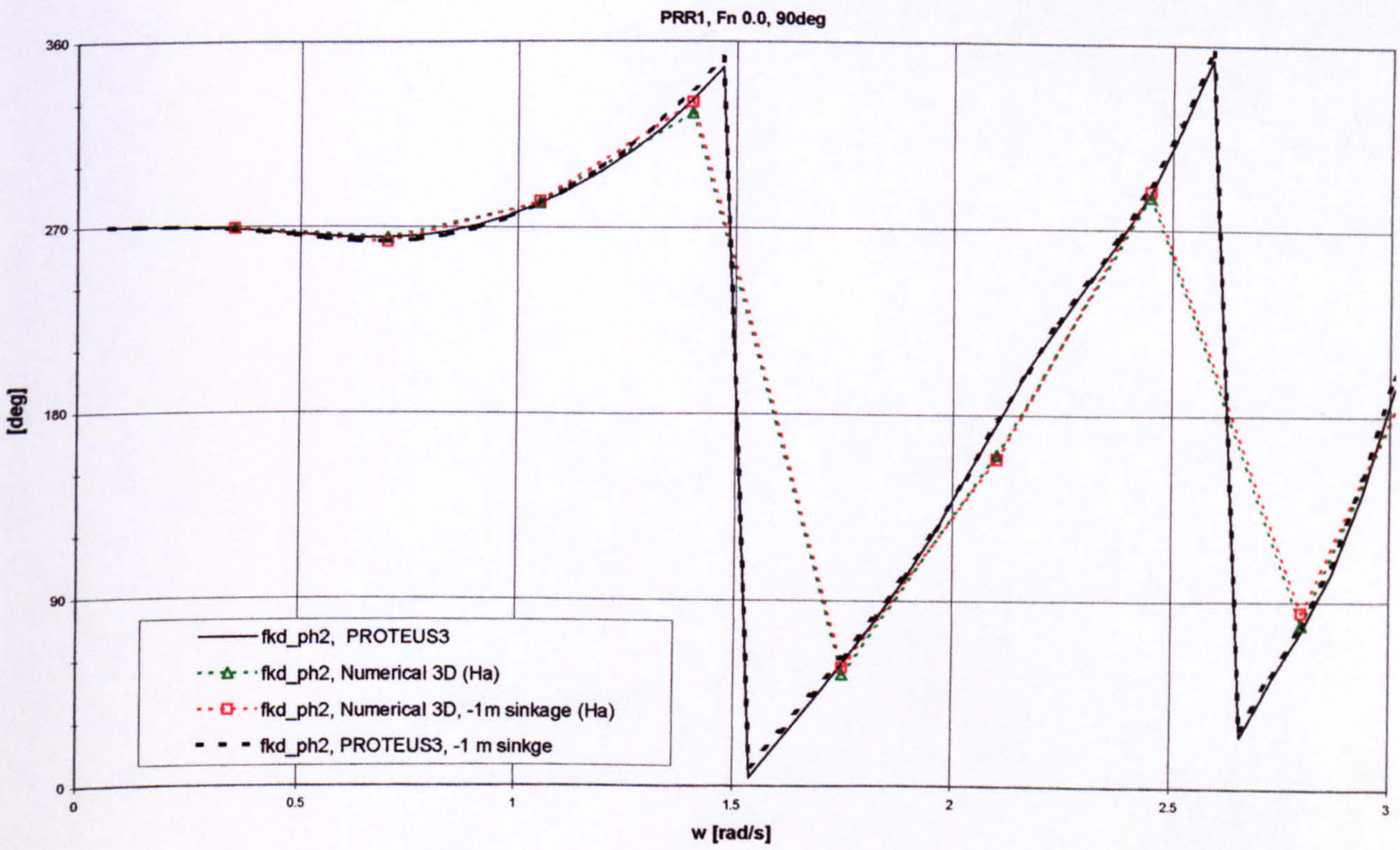

Figure 40 Excitation forces phase angle in sway mode for 3D PRR1 hull form, predictions by strip theory and 3D panel methods, Fn=0.0, Heading 90deg, effect of –1m sinkage

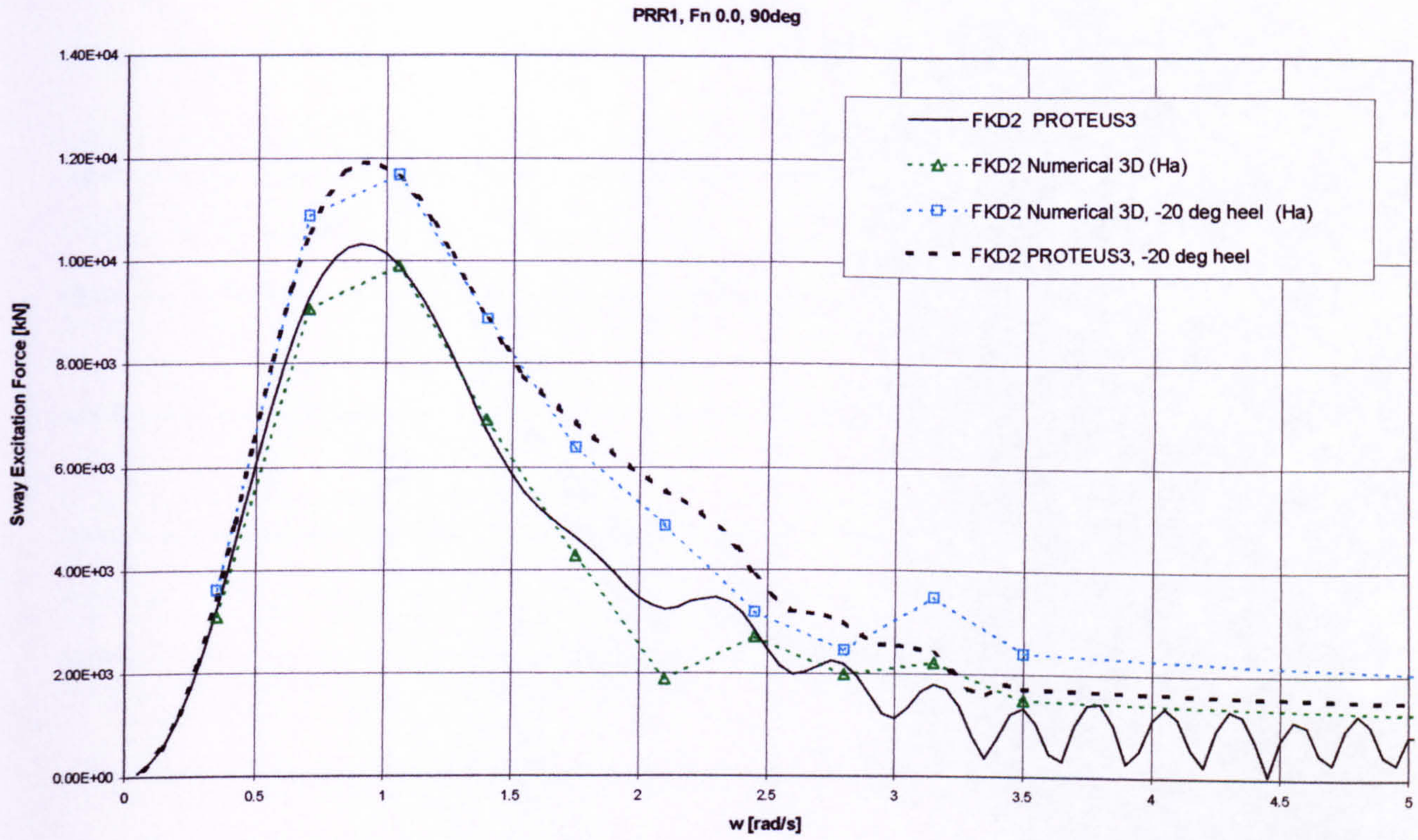

Figure 41 Excitation forces in sway mode for 3D PRR1 hull form, predictions by strip theory and 3D panel methods, Fn=0.0, Heading 90deg, effect of –20deg heel

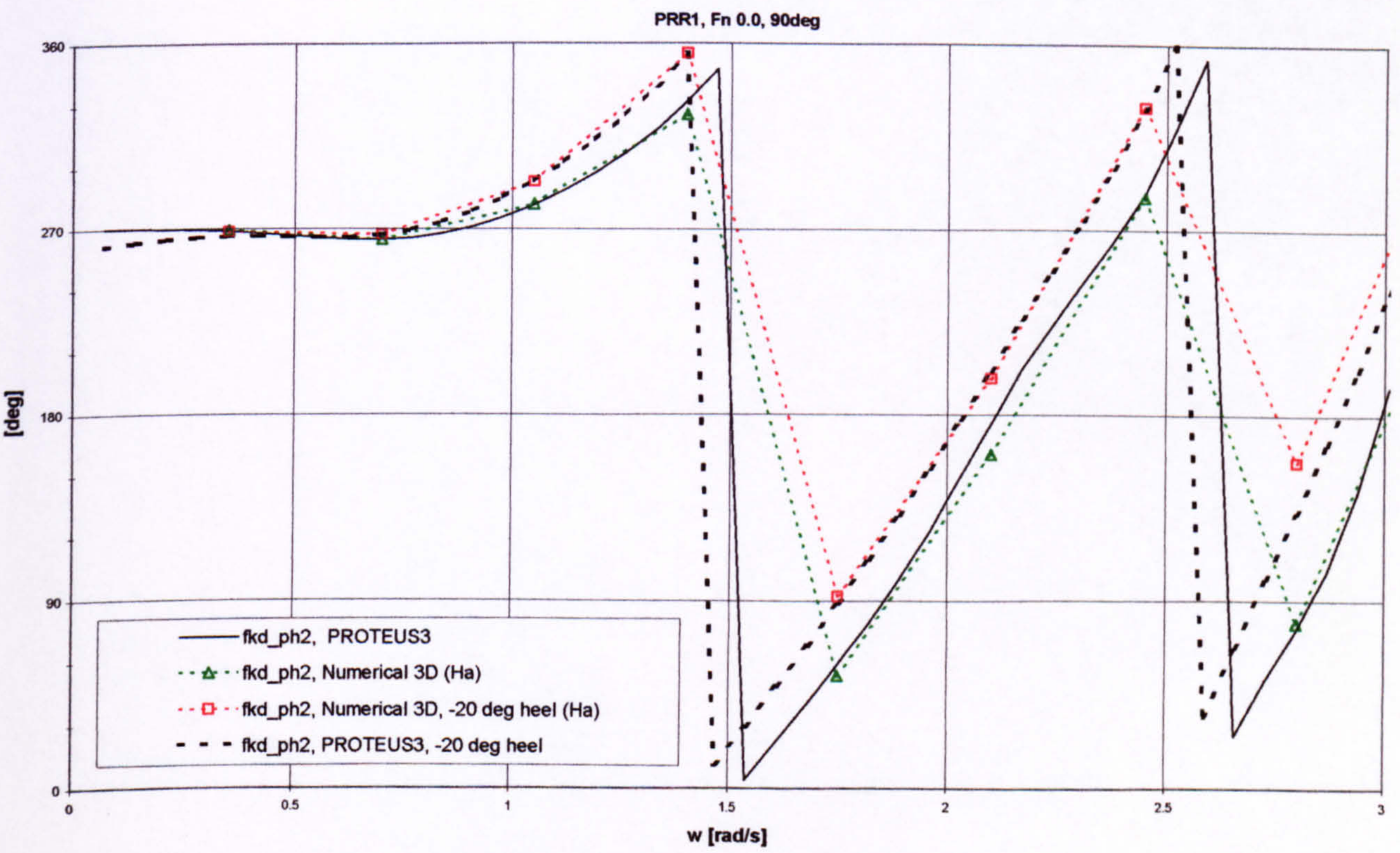

Figure 42 Excitation forces phase angle in sway mode for 3D PRR1 hull form, predictions by strip theory and 3D panel methods, Fn=0.0, Heading 90deg, effect of –20deg heel

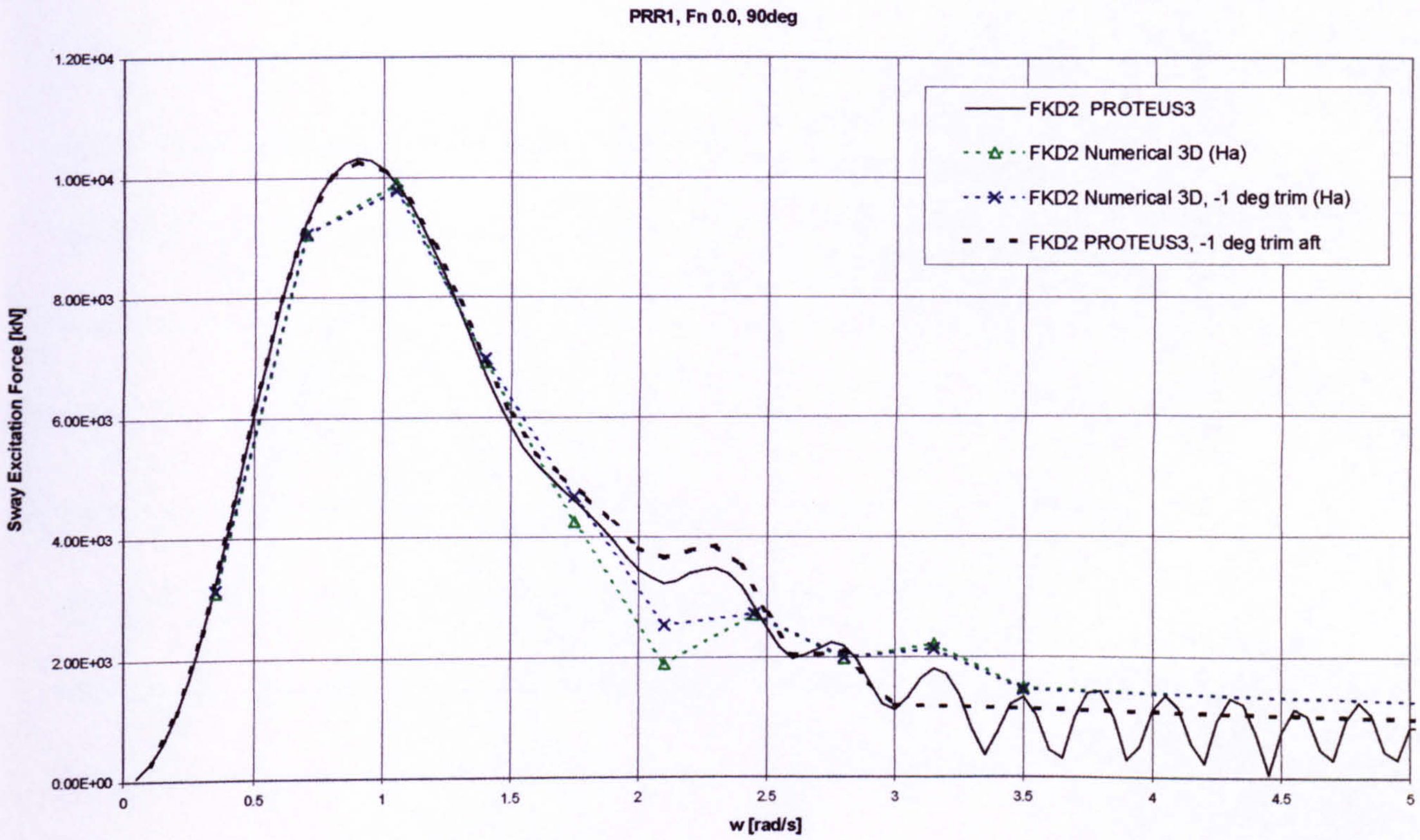

Figure 43 Excitation forces in sway mode for 3D PRR1 hull form, predictions by strip theory and 3D panel methods, Fn=0.0, Heading 90deg, effect of –1 deg trim (aft)

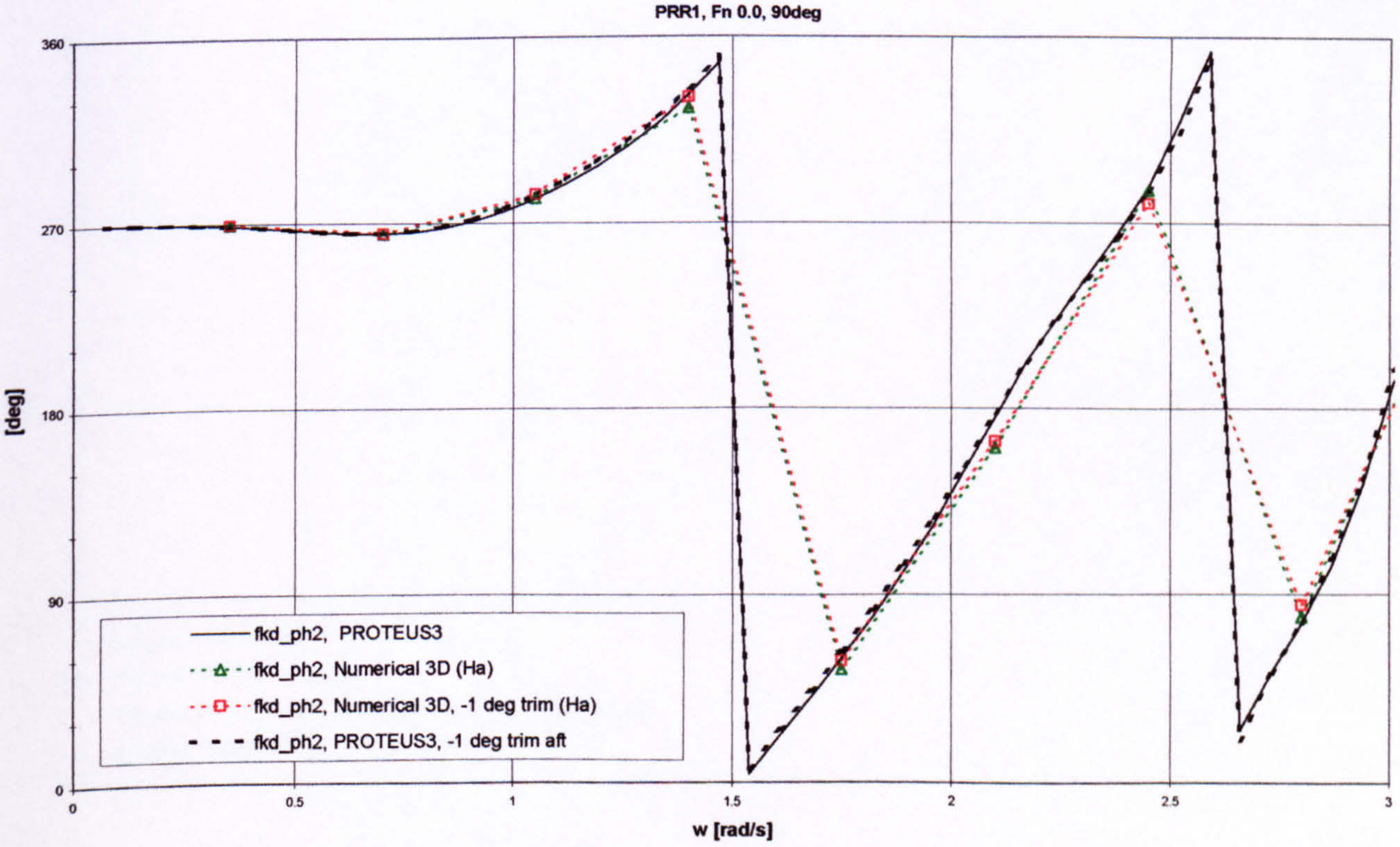

Figure 44 Excitation forces phase angle in sway mode for 3D PRR1 hull form, predictions by strip theory and 3D panel methods, Fn=0.0, Heading 90deg, effect of –1 deg trim aft

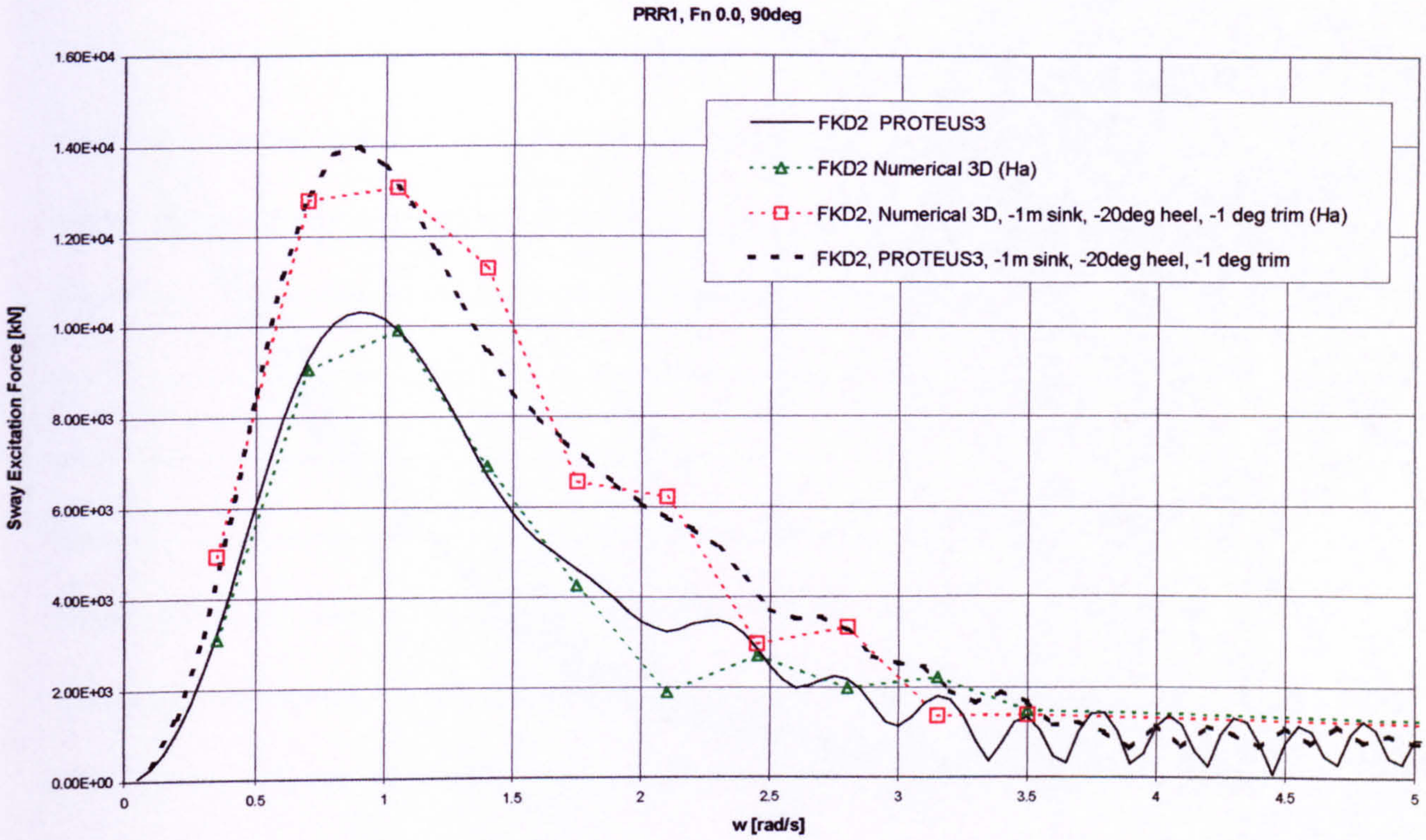

Figure 45 Excitation forces in sway mode for 3D PRR1 hull form, strip theory and 3D panel methods, Fn=0.0, Heading 90deg, effect of –1m sinkage, –20deg heel and –1 deg trim

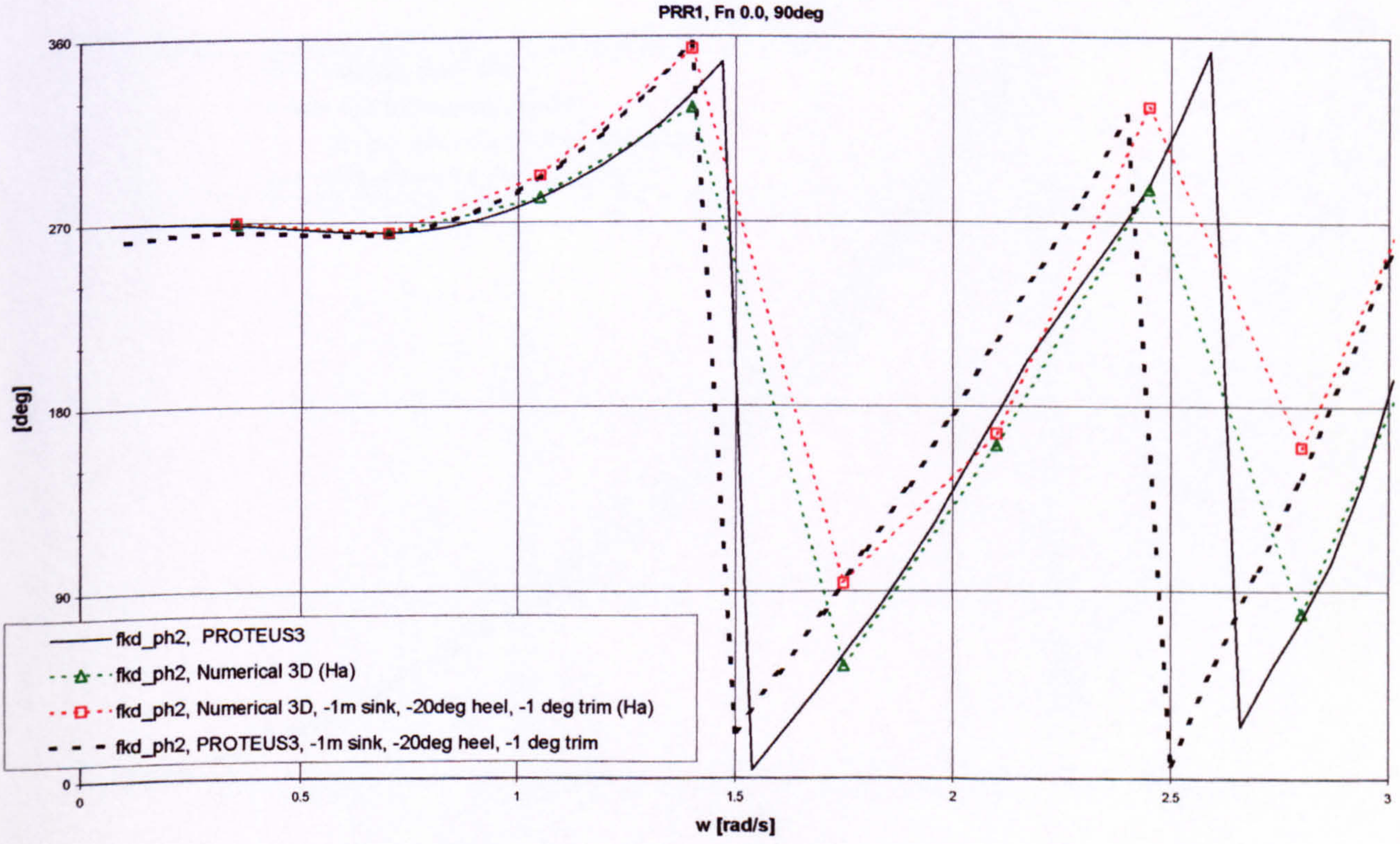

Figure 46 Excitation forces phase angle in sway mode for 3D PRR1 hull form, strip theory and 3D panel methods, Fn=0.0, Heading 90deg, effect of –1m sinkage, –20deg heel and –1 deg trim

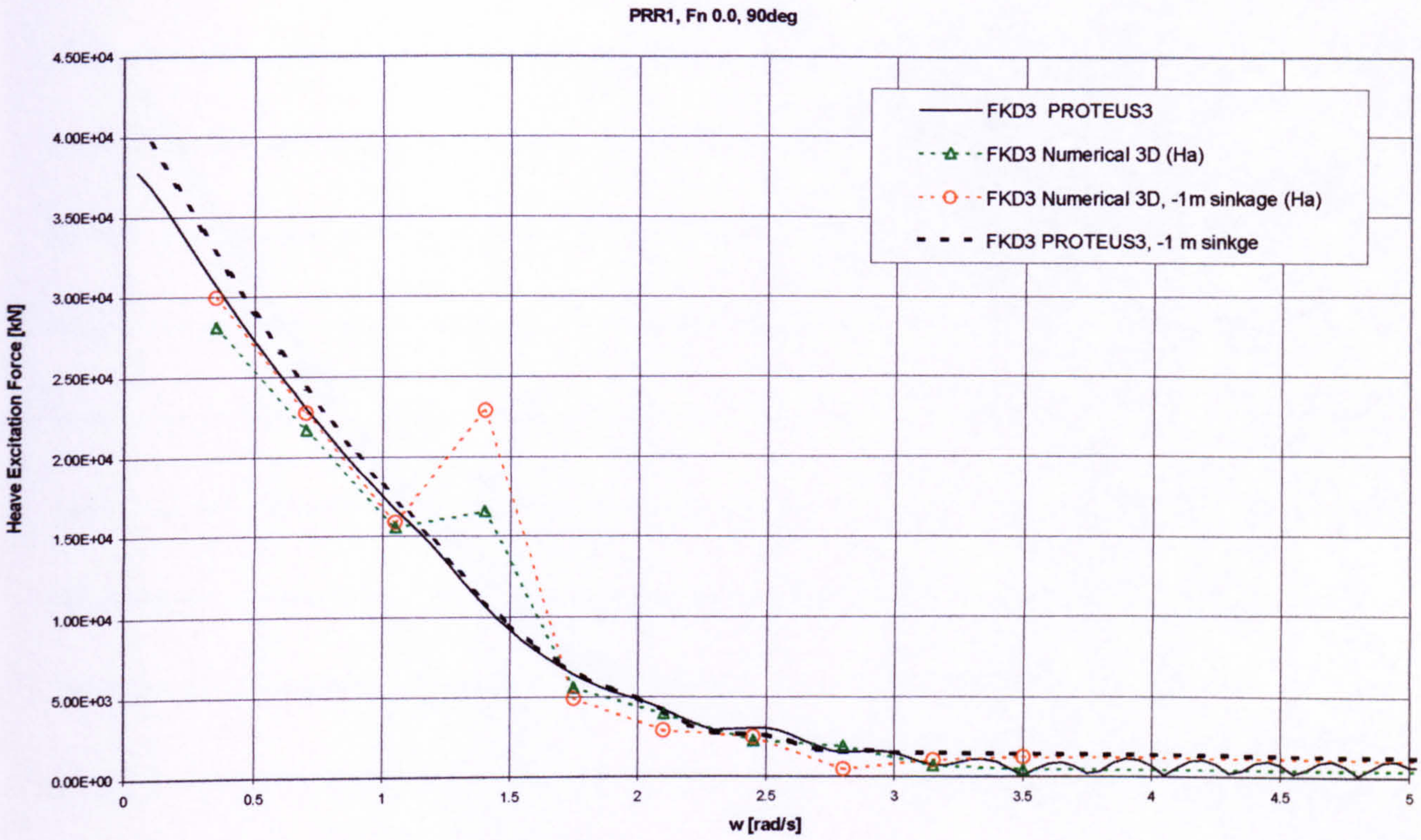

Figure 47 Excitation forces in heave mode for 3D PRR1 hull form, predictions by strip theory and 3D panel methods, Fn=0.0, Heading 90deg, effect of –1m sinkage

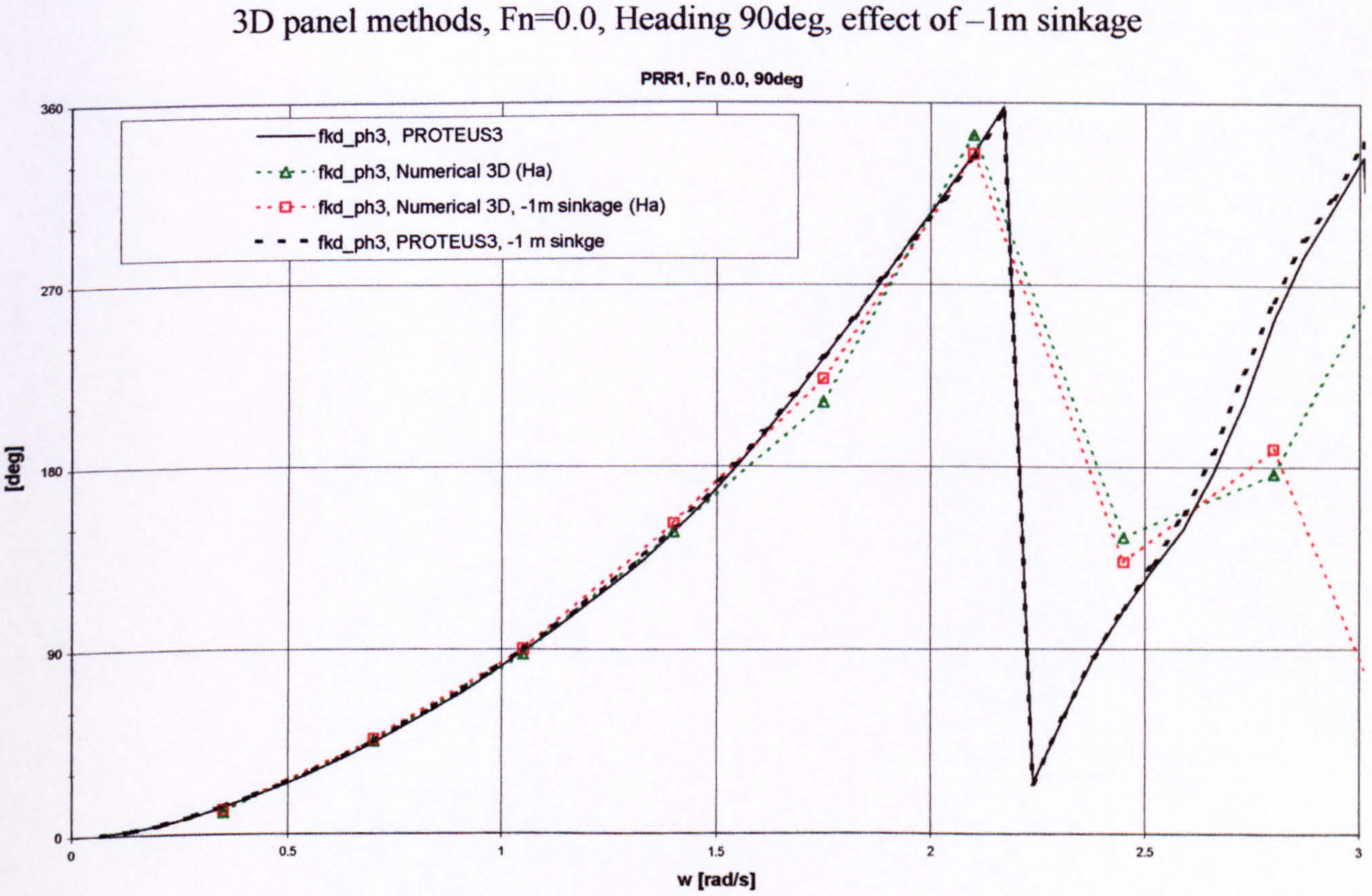

Figure 48 Excitation forces phase angles in heave mode for 3D PRR1 hull form, predictions by strip theory and 3D panel methods, Fn=0.0, Heading 90deg, effect of –1m sinkage

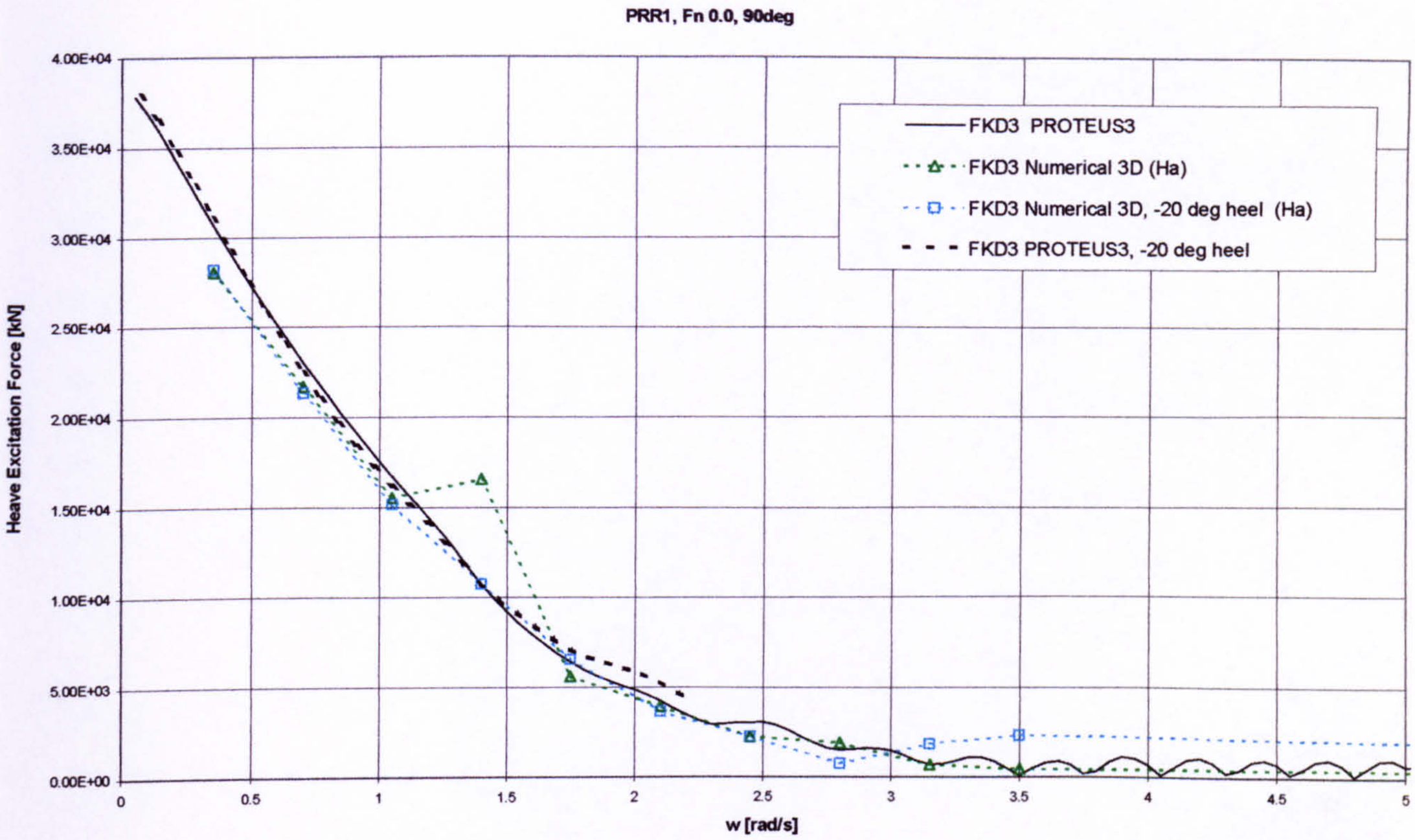

Figure 49 Excitation forces in heave mode for 3D PRR1 hull form, predictions by strip theory and 3D panel methods, Fn=0.0, Heading 90deg, effect of –20 deg heel

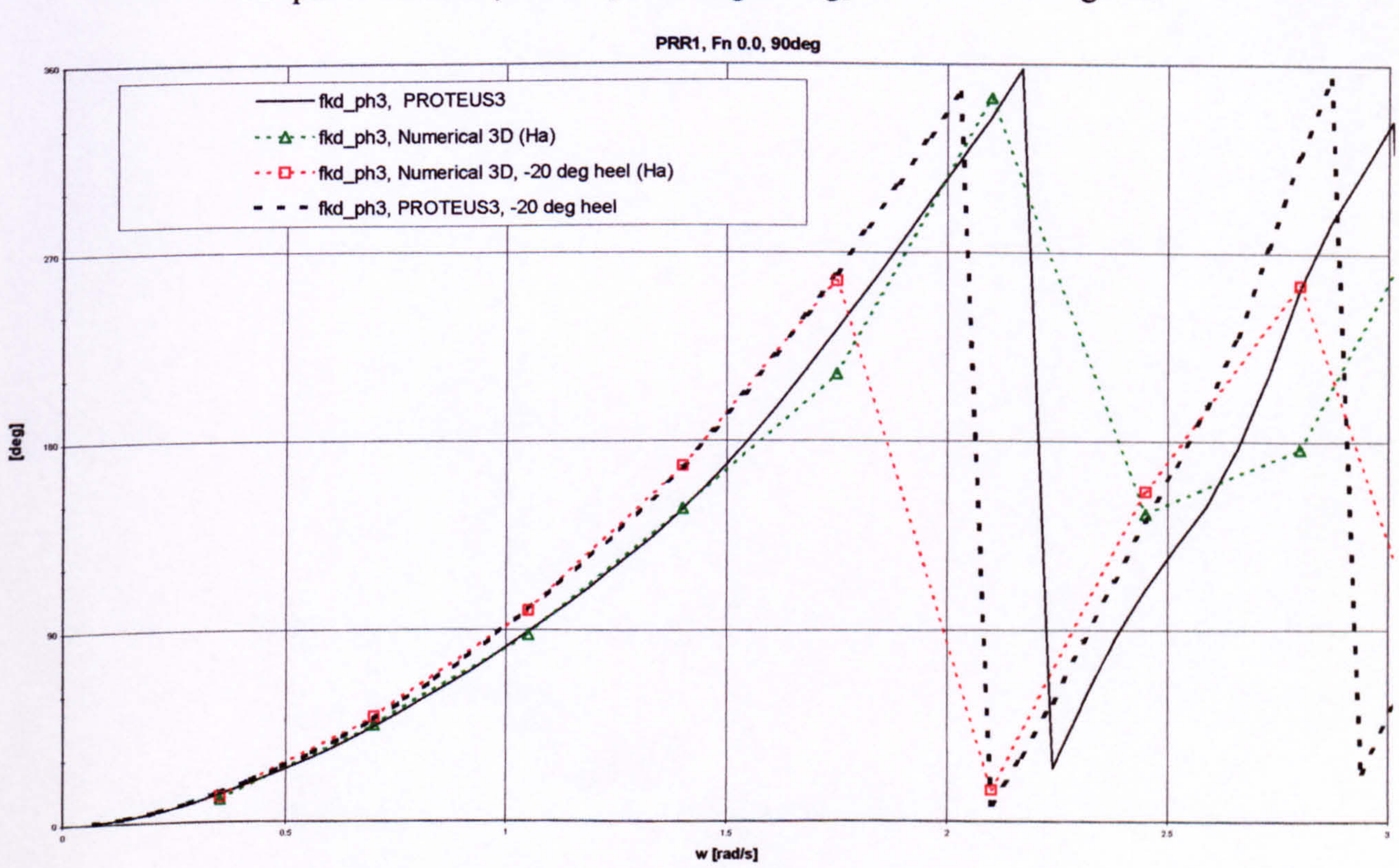

Figure 50 Excitation forces phase angles in heave mode for 3D PRR1 hull form, predictions by strip theory and 3D panel methods, Fn=0.0, Heading 90deg, effect of –20 deg heel

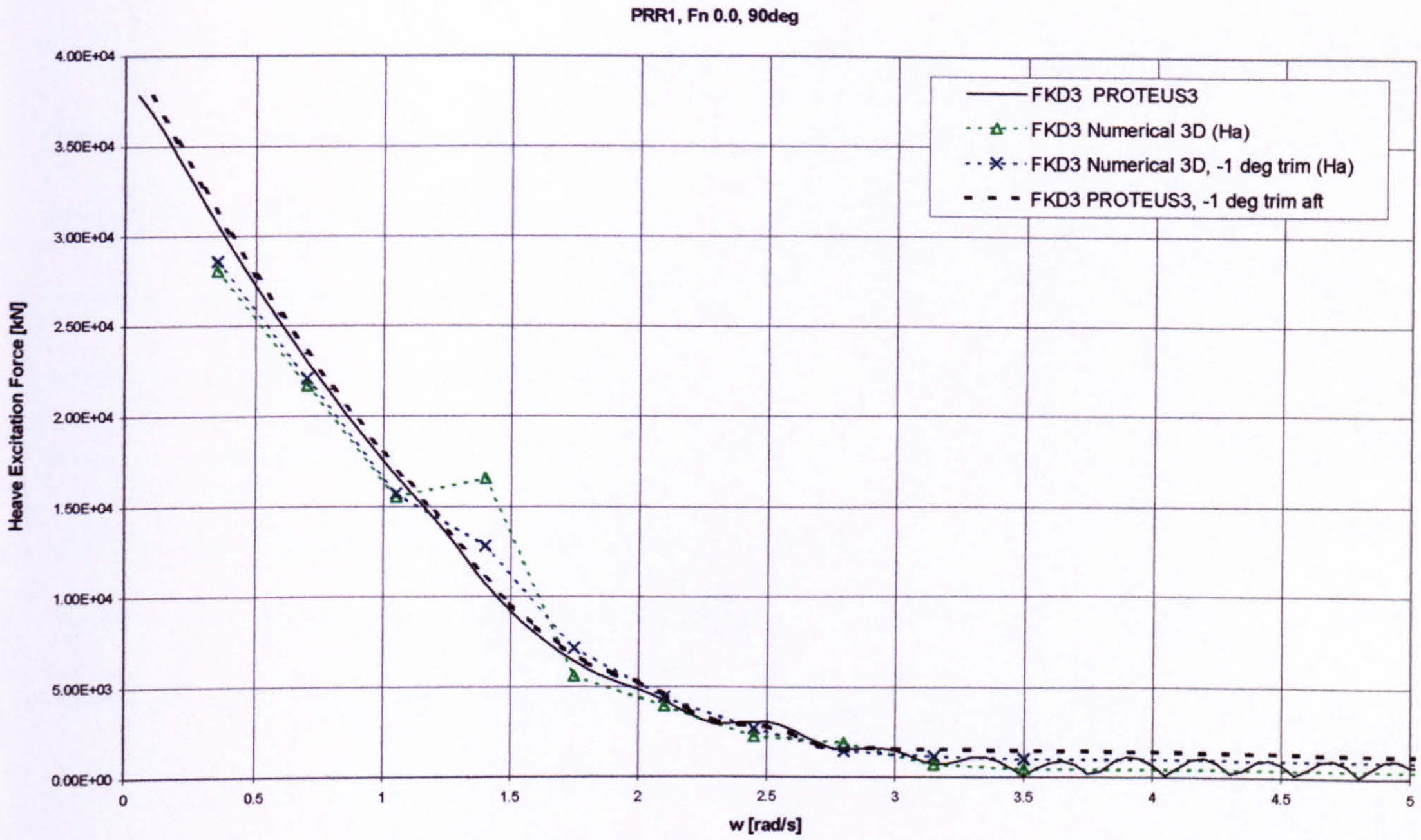

Figure 51 Excitation forces in heave mode for 3D PRR1 hull form, predictions by strip theory and 3D panel methods, Fn=0.0, Heading 90deg, effect of –1 deg trim aft

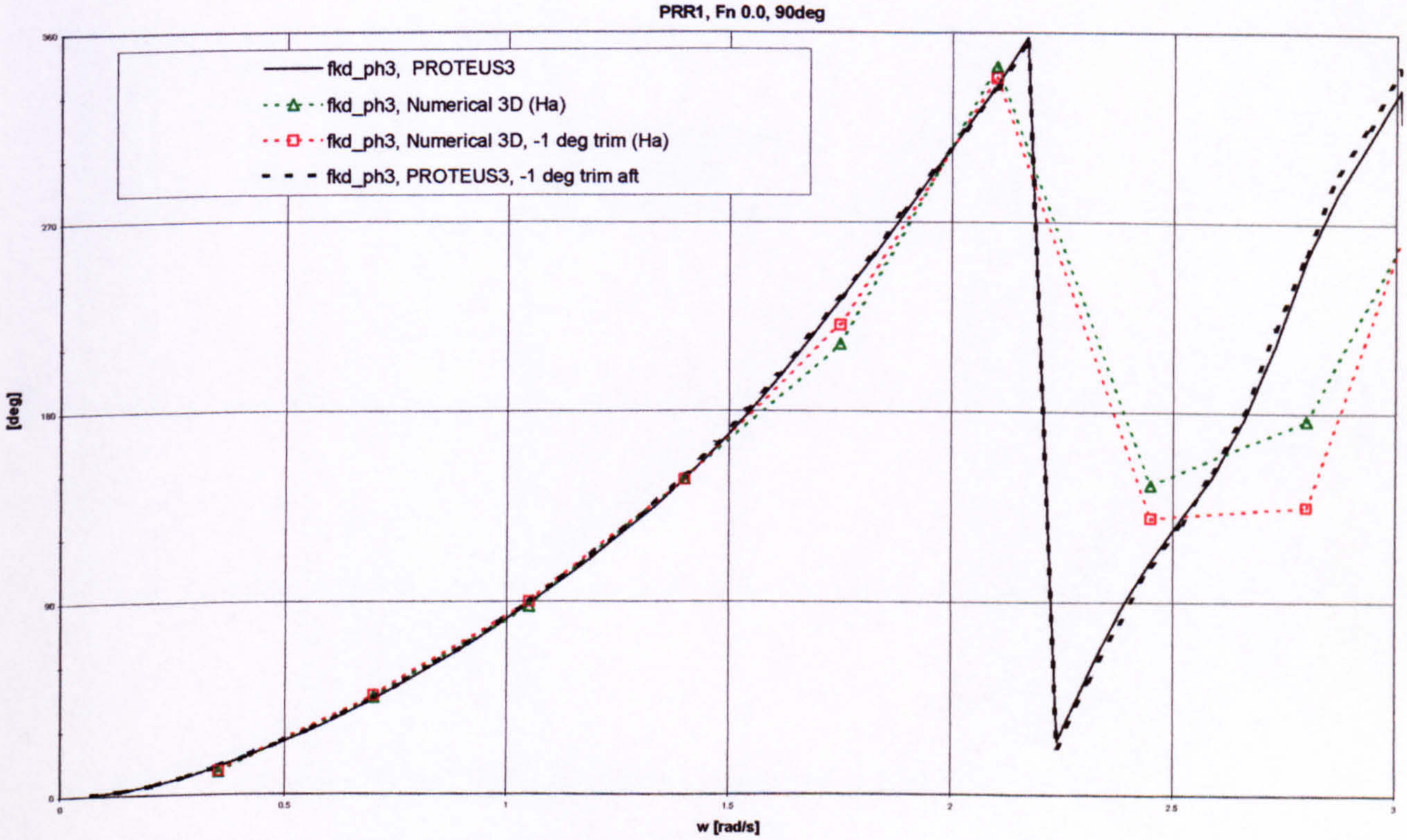

Figure 52 Excitation forces phase angles in heave mode for 3D PRR1 hull form, predictions by strip theory and 3D panel methods, Fn=0.0, Heading 90deg, effect of –1 deg trim aft

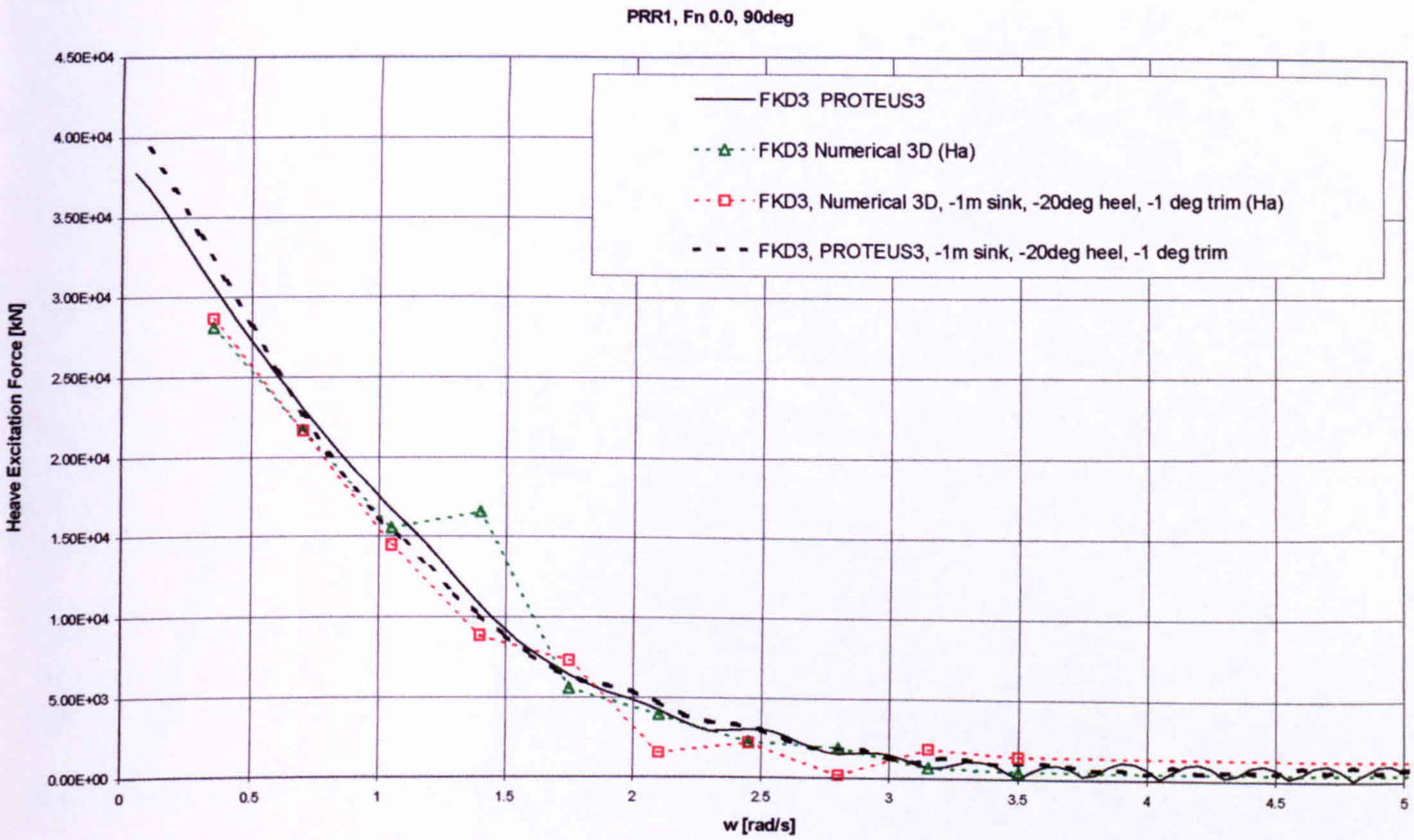

Figure 53 Excitation forces in heave mode for 3D PRR1 hull form, strip theory and 3D panel methods, Fn=0.0, Heading 90deg, effect of –1m sinkage, –20deg heel and –1 deg trim

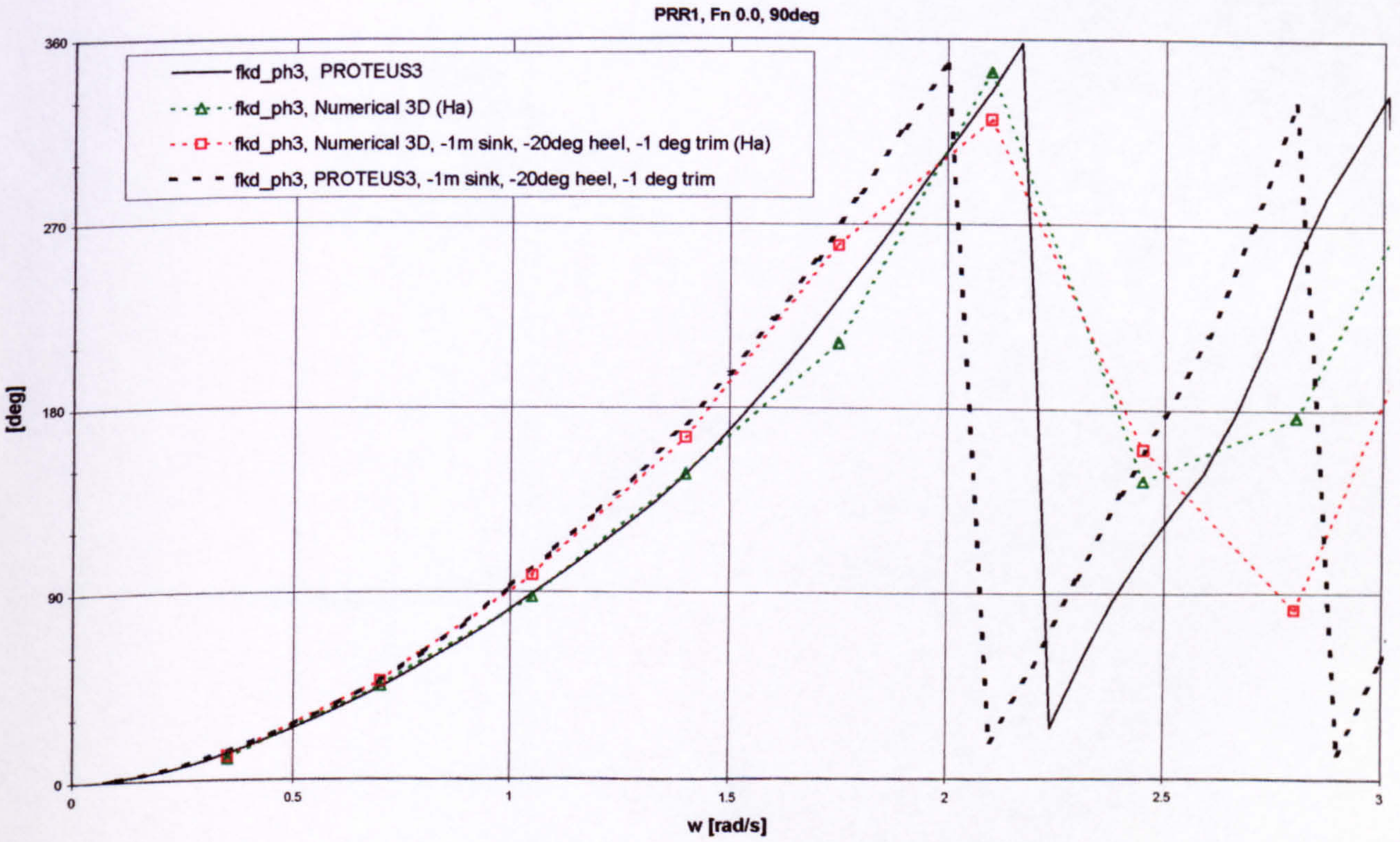

Figure 54 Excitation forces phase angles in heave mode for 3D PRR1 hull form, strip theory and 3D panel methods, Fn=0.0, Heading 90deg, effect of –1m sinkage, –20deg heel and –1 deg trim

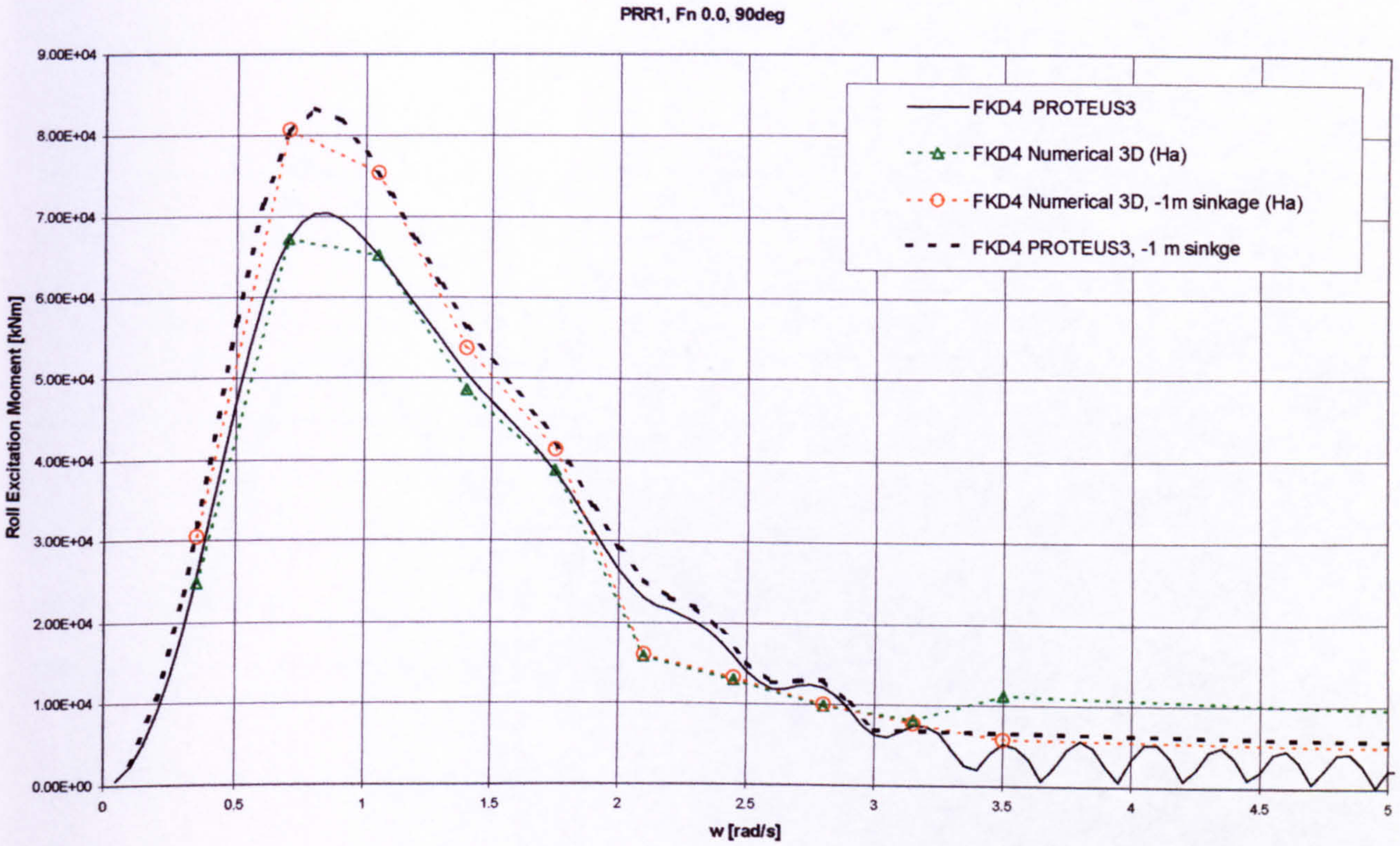

Figure 55 Excitation moments in roll mode for 3D PRR1 hull form, predictions by strip theory and 3D panel methods, Fn=0.0, Heading 90deg, effect of –1m sinkage

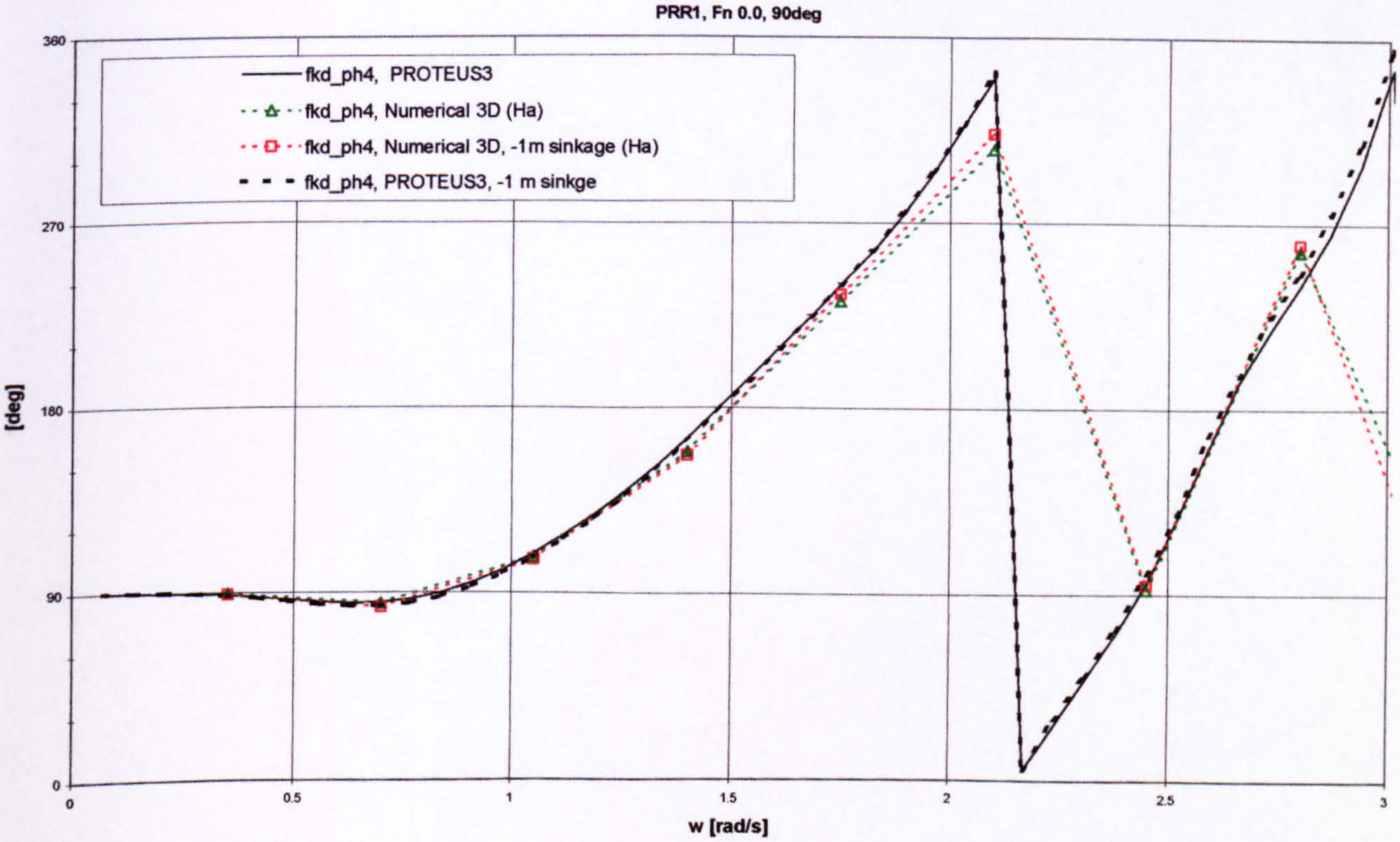

Figure 56 Excitation moments phase angles in roll mode for 3D PRR1 hull form, predictions by strip theory and 3D panel methods, Fn=0.0, Heading 90deg, effect of –1m

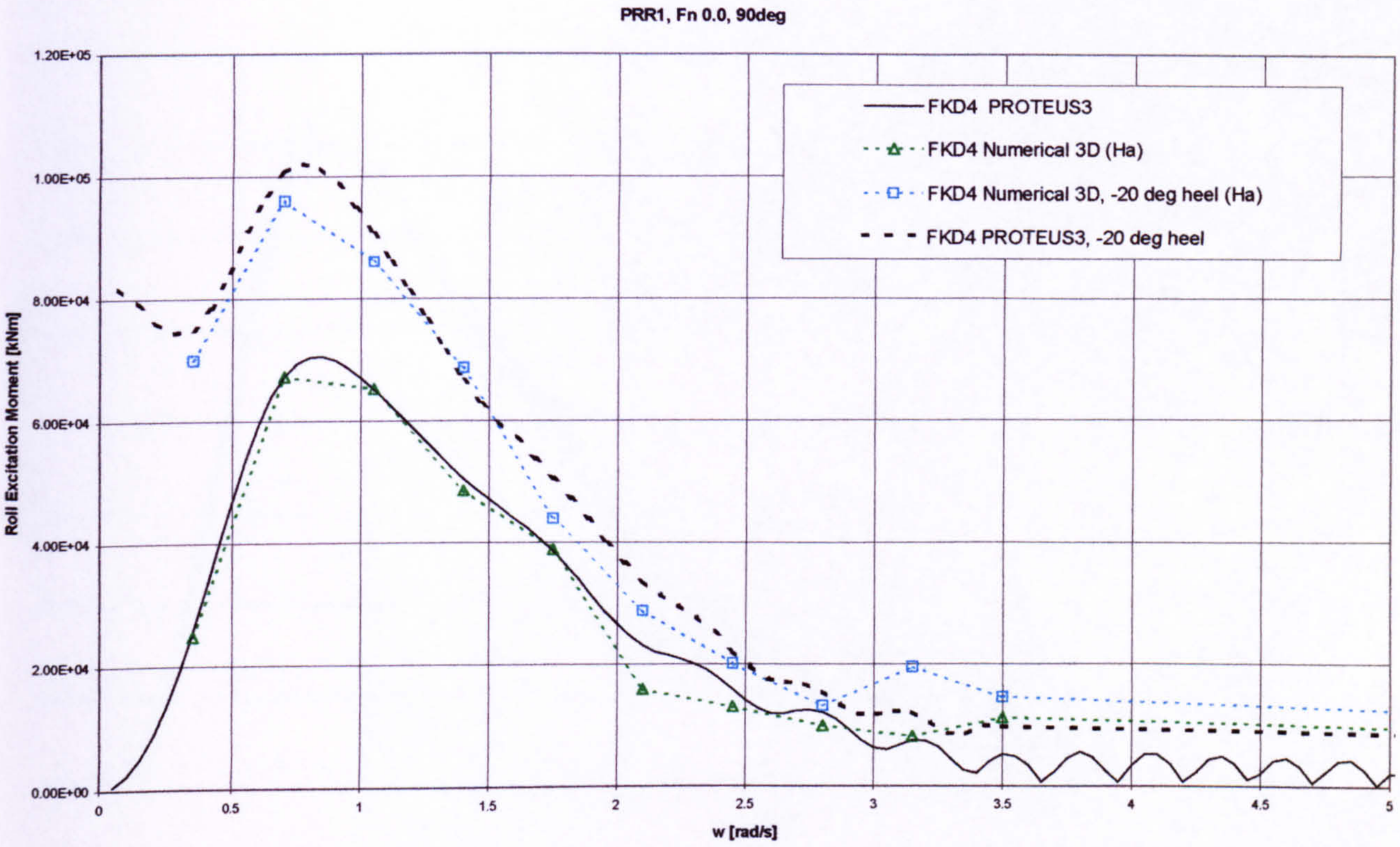

Figure 57 Excitation moments in roll mode for 3D PRR1 hull form, predictions by strip theory and 3D panel methods, Fn=0.0, Heading 90deg, effect of –20deg heel

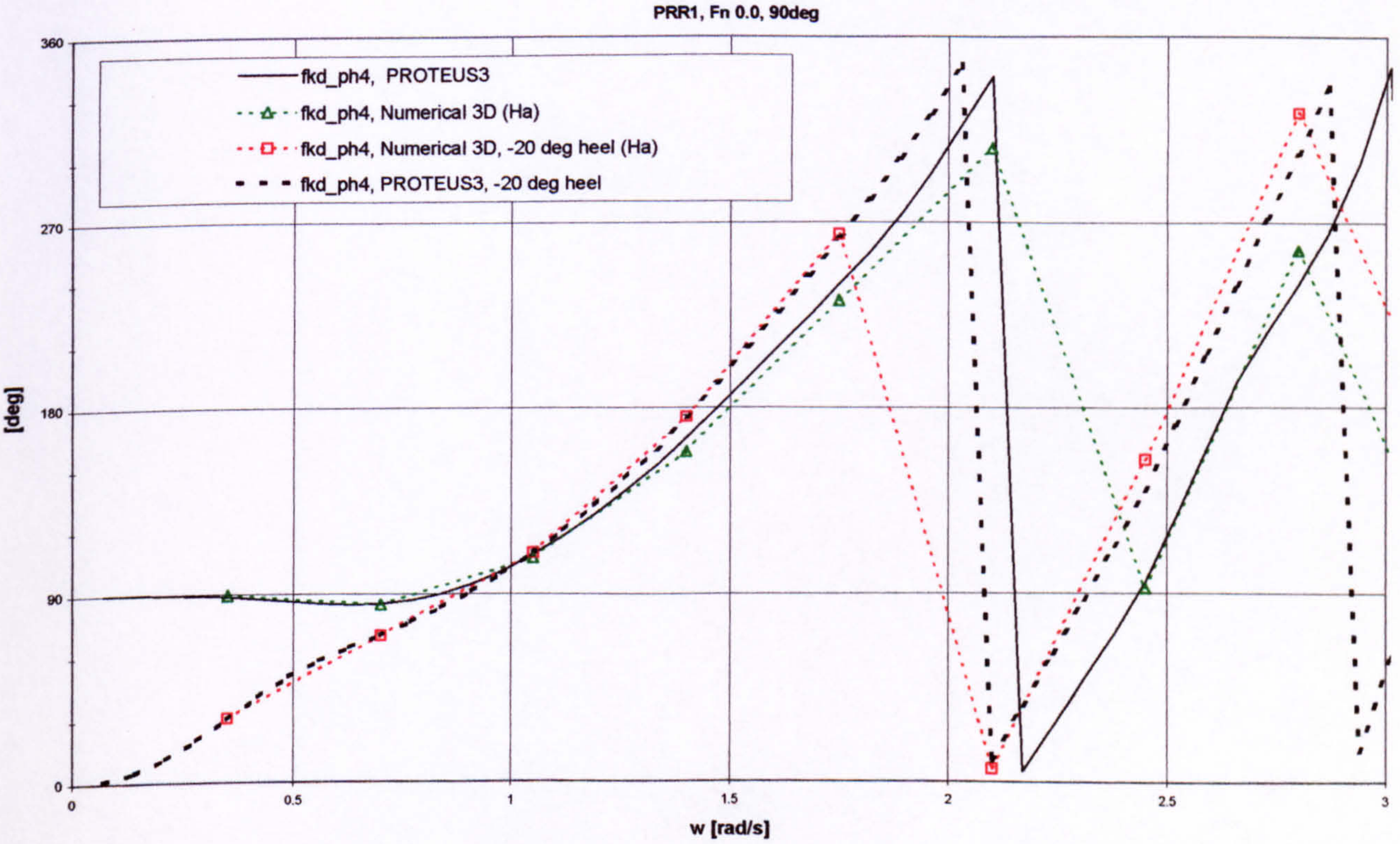

Figure 58 Excitation moments phase angles in roll mode for 3D PRR1 hull form, predictions by strip theory and 3D panel methods, Fn=0.0, Heading 90deg, effect of –20 deg heel

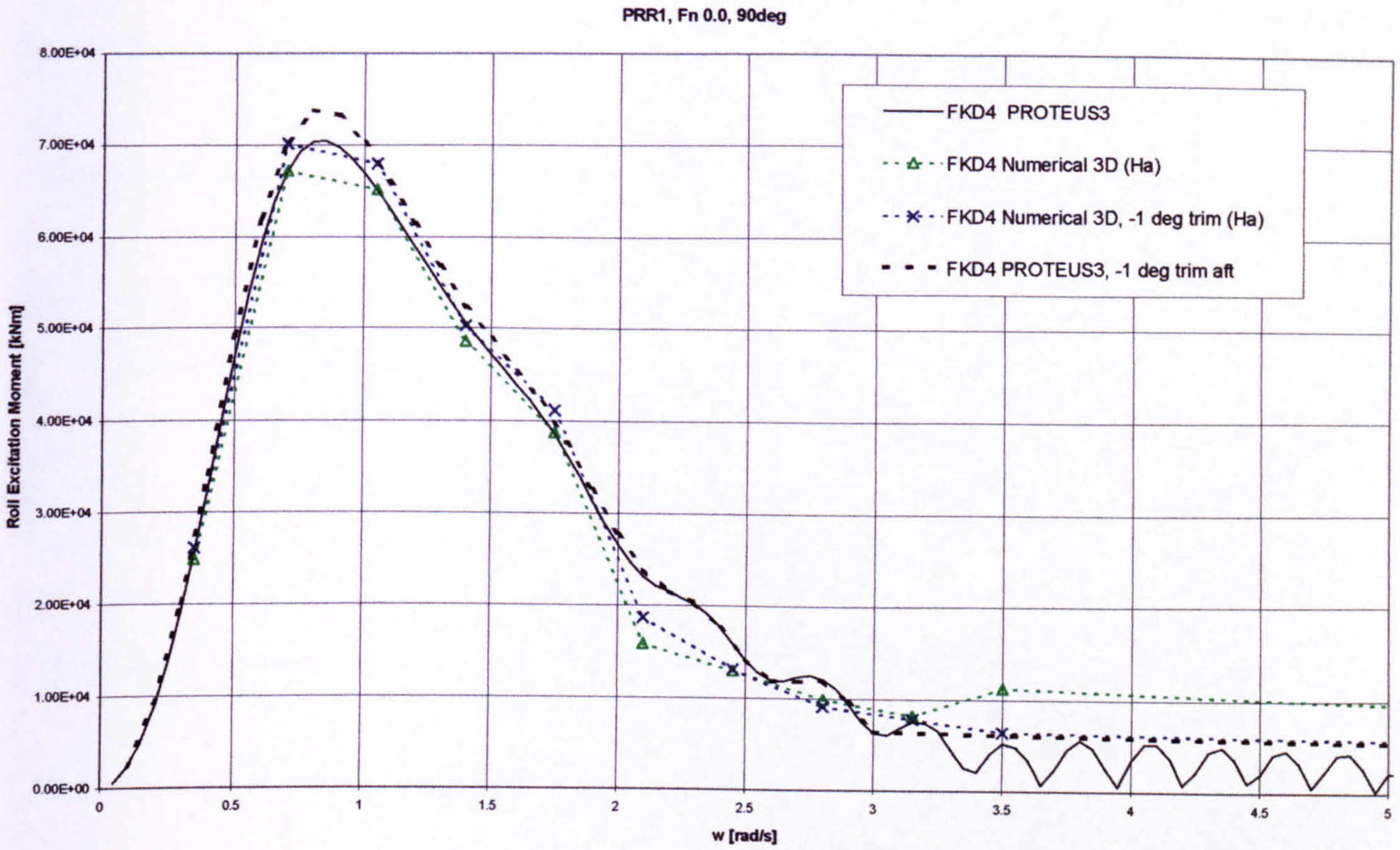

Figure 59 Excitation moments in roll mode for 3D PRR1 hull form, predictions by strip theory and 3D panel methods, Fn=0.0, Heading 90deg, effect of –1m sinkage –1 deg trim

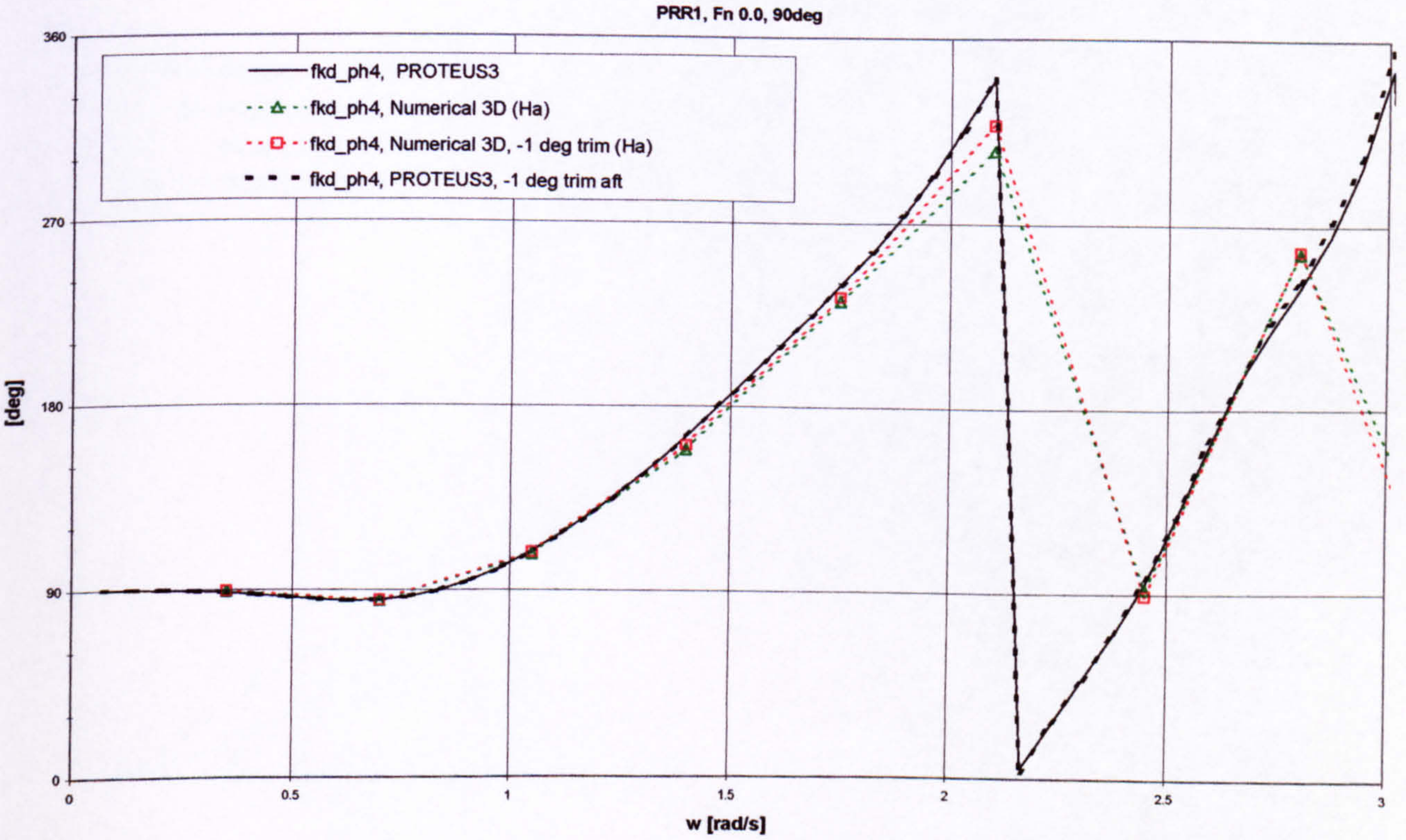

Figure 60 Excitation moments phase angles in roll mode for 3D PRR1 hull form, predictions by strip theory and 3D panel methods, Fn=0.0, Heading 90deg, effect –1 deg trim

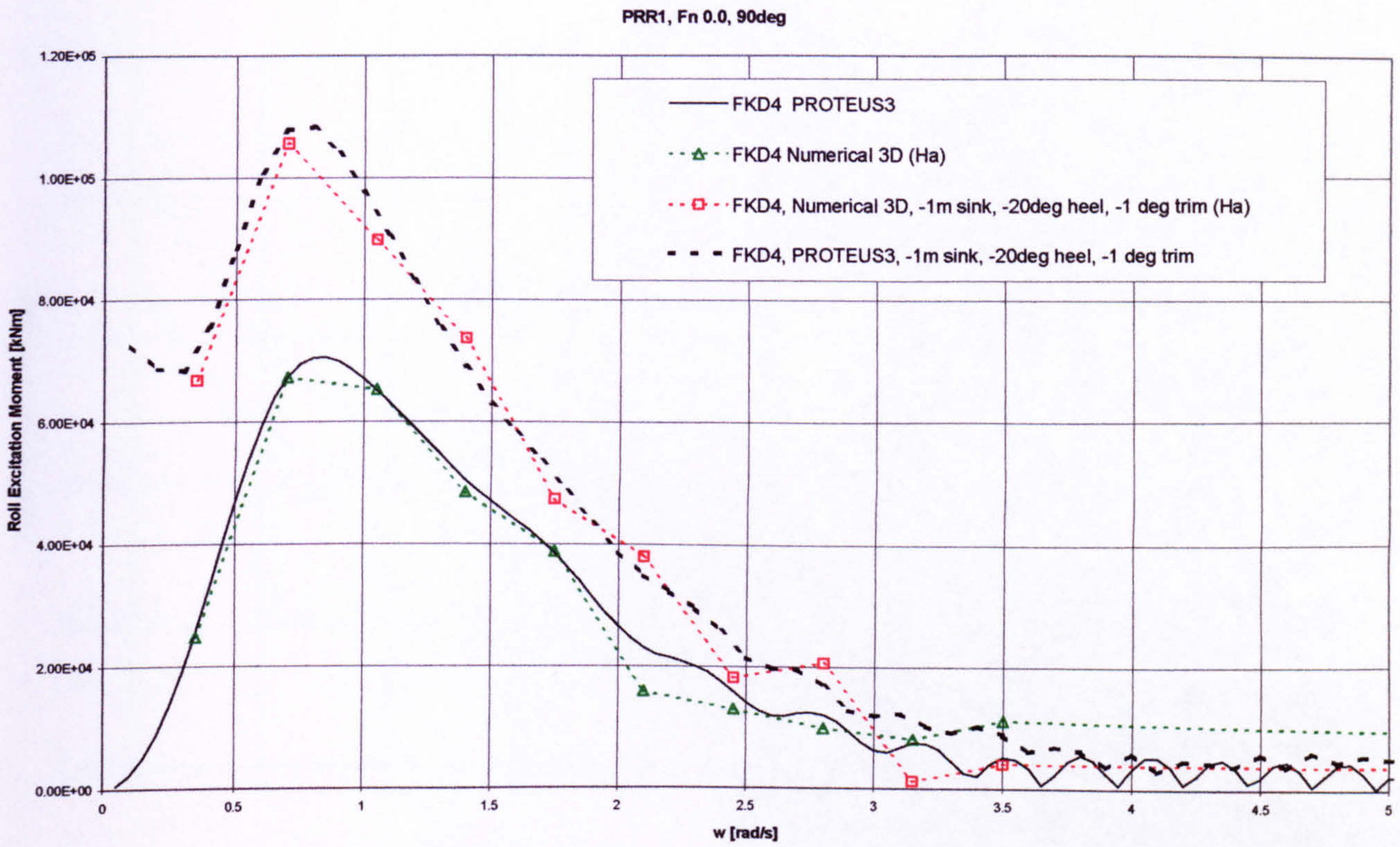

Figure 61 Excitation moments in roll mode for 3D PRR1 hull form, predictions by strip theory and 3D panel methods, Fn=0.0, Heading 90deg, effect of –1m sinkage, –20deg heel and –1 deg trim

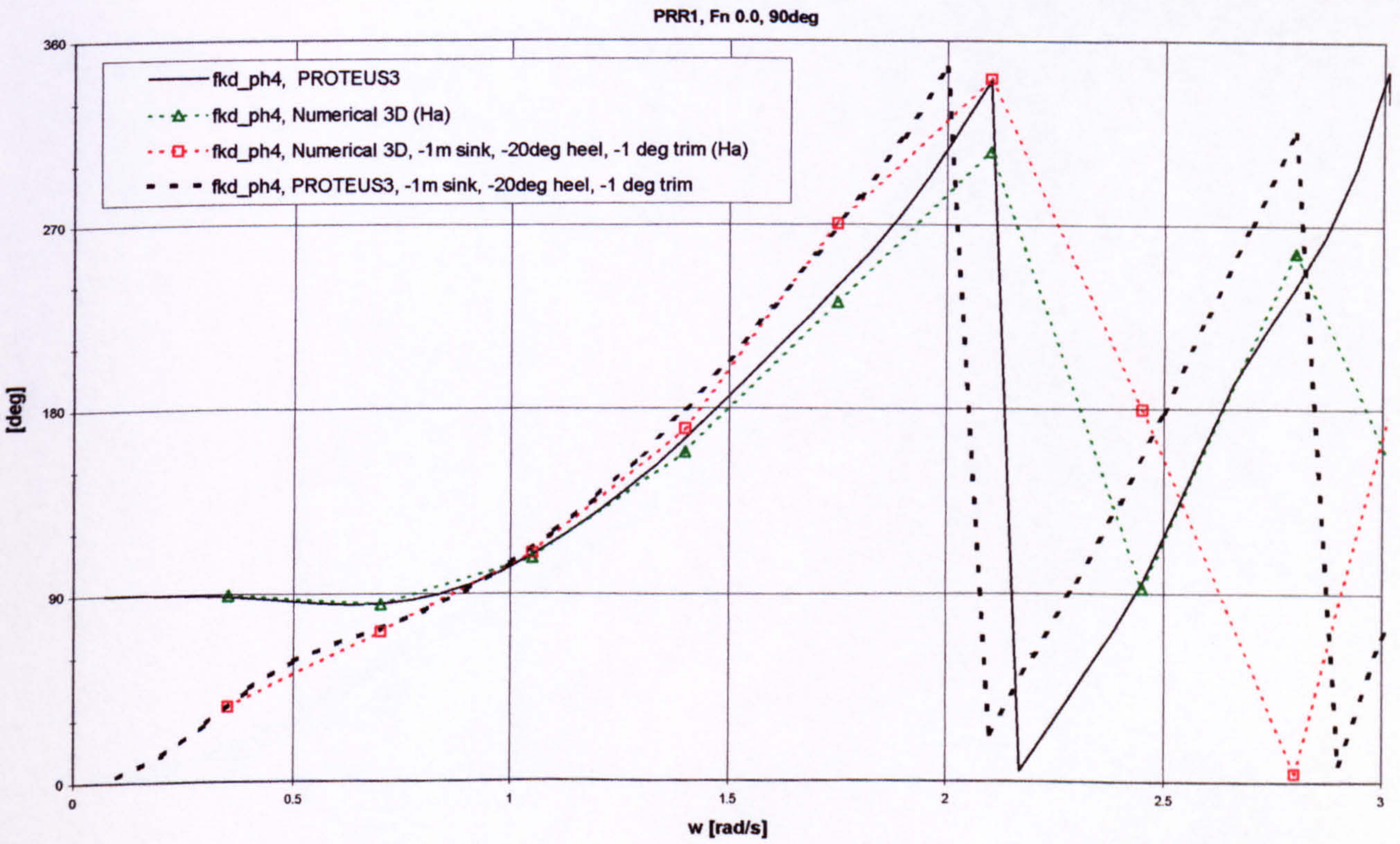

Figure 62 Excitation moments phase angles in roll mode for 3D PRR1 hull form, strip theory and 3D panel methods, Fn=0.0, Heading 90deg, effect of –1m sinkage, –20deg heel and –1 deg trim

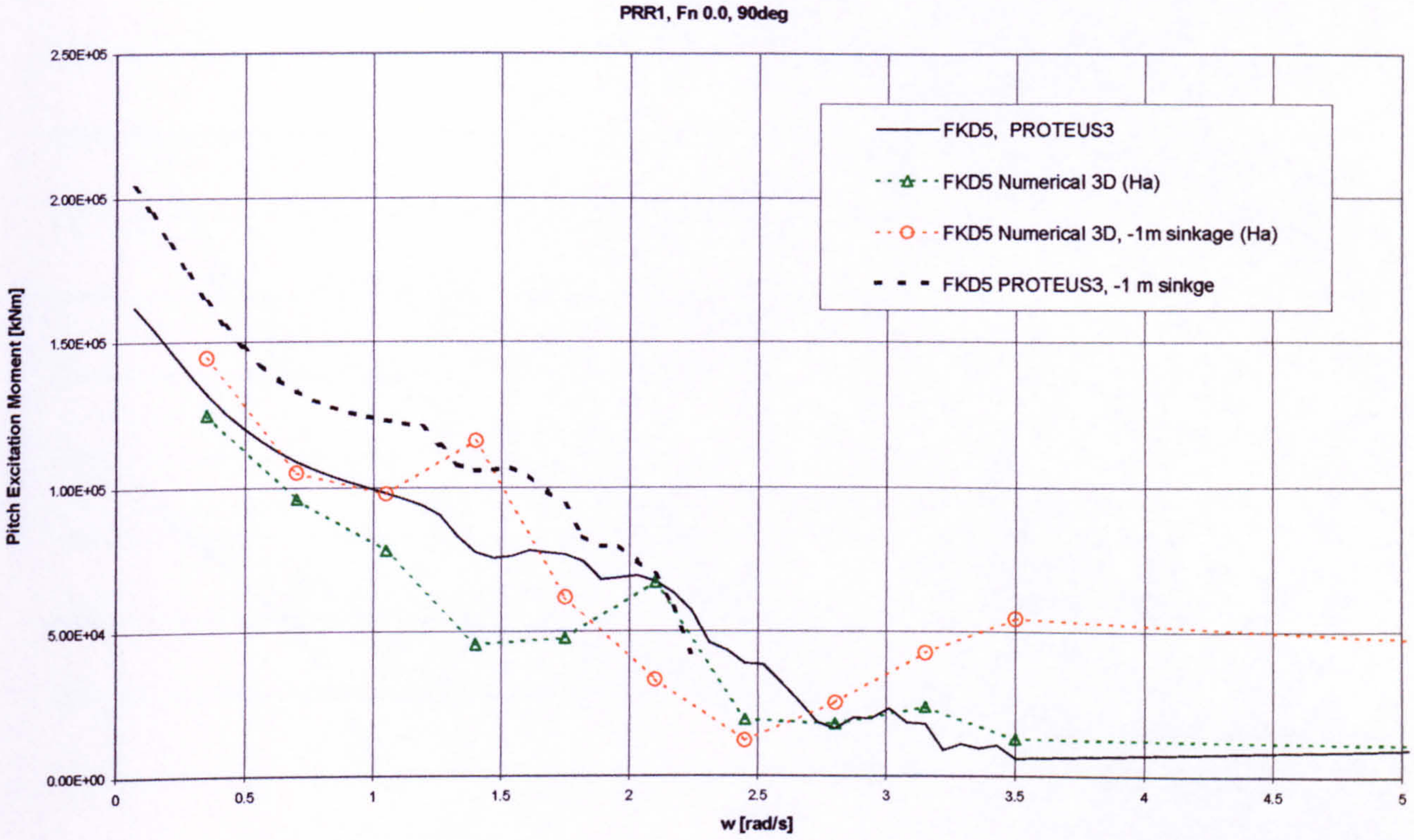

Figure 63 Excitation moments in pitch mode for 3D PRR1 hull form, predictions by strip theory and 3D panel methods, Fn=0.0, Heading 90deg, effect of –1m sinkage

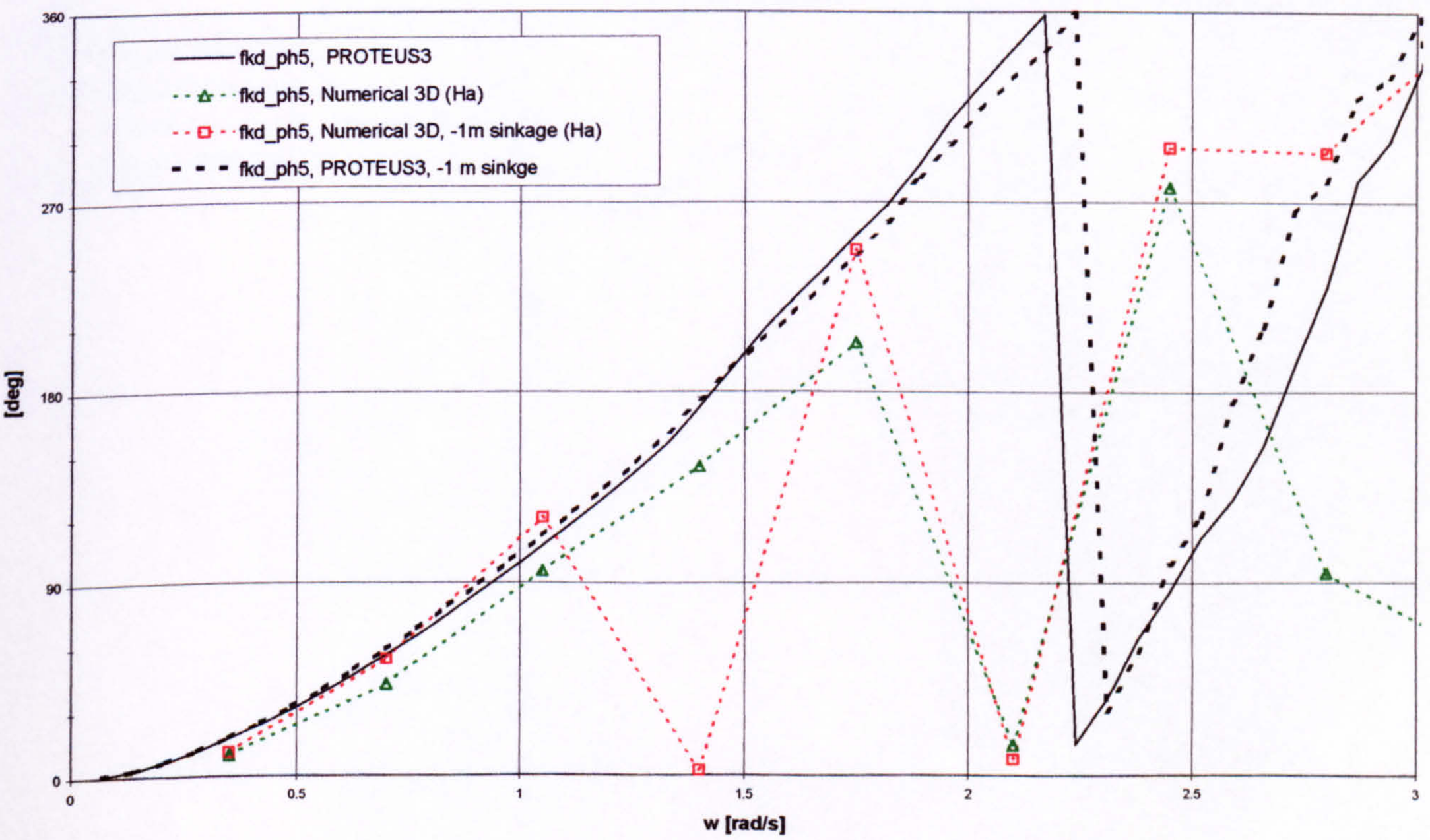

Figure 64 Excitation moments phase angles in pitch mode for 3D PRR1 hull form, predictions by strip theory and 3D panel methods, Fn=0.0, Heading 90deg, effect of –1m sinkage

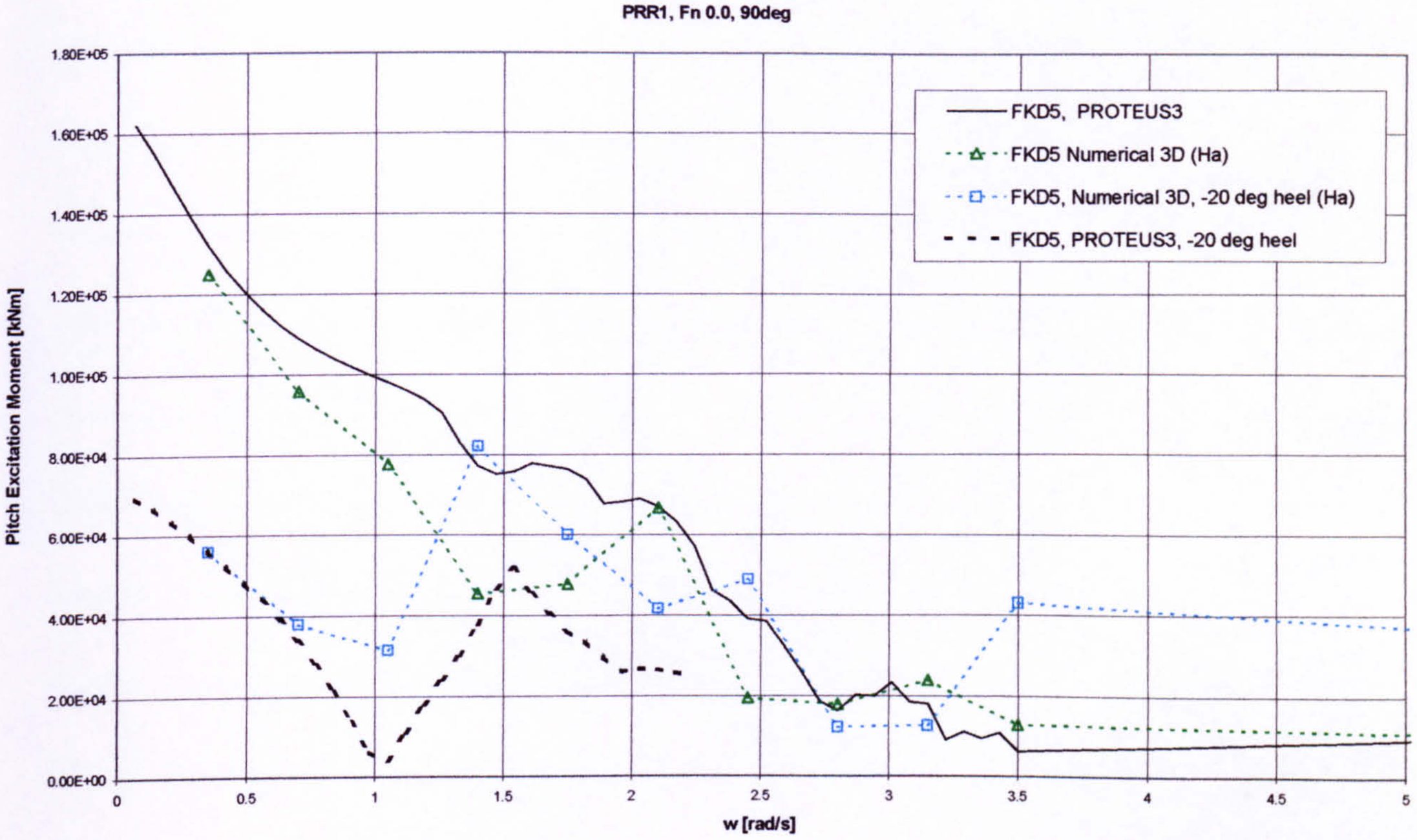

Figure 65 Excitation moments in pitch mode for 3D PRR1 hull form, predictions by strip theory and 3D panel methods, Fn=0.0, Heading 90deg, effect of –20deg heel

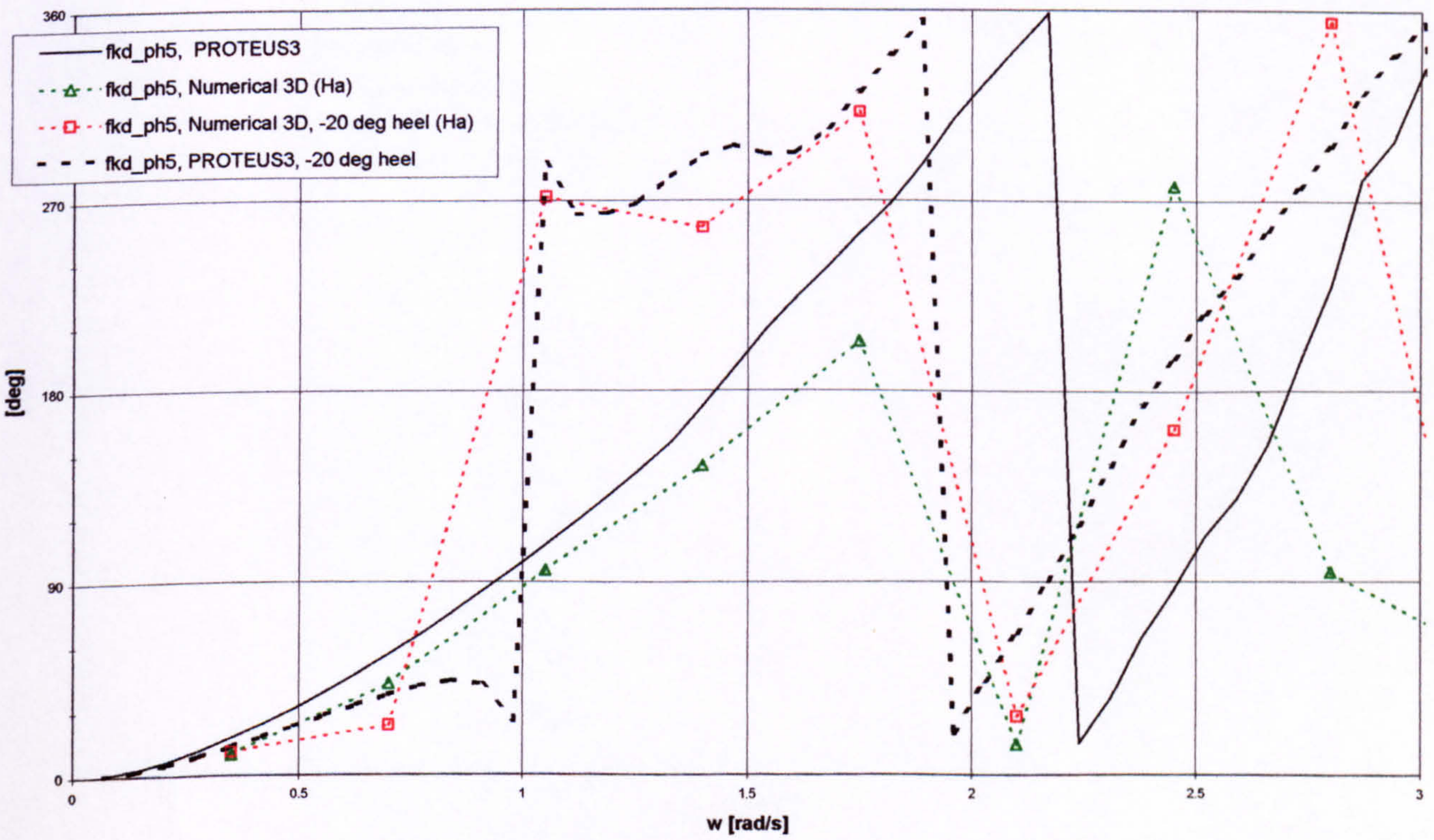

Figure 66 Excitation moments phase angles in pitch mode for 3D PRR1 hull form, predictions by strip theory and 3D panel methods, Fn=0.0, Heading 90deg, effect of –20deg heel

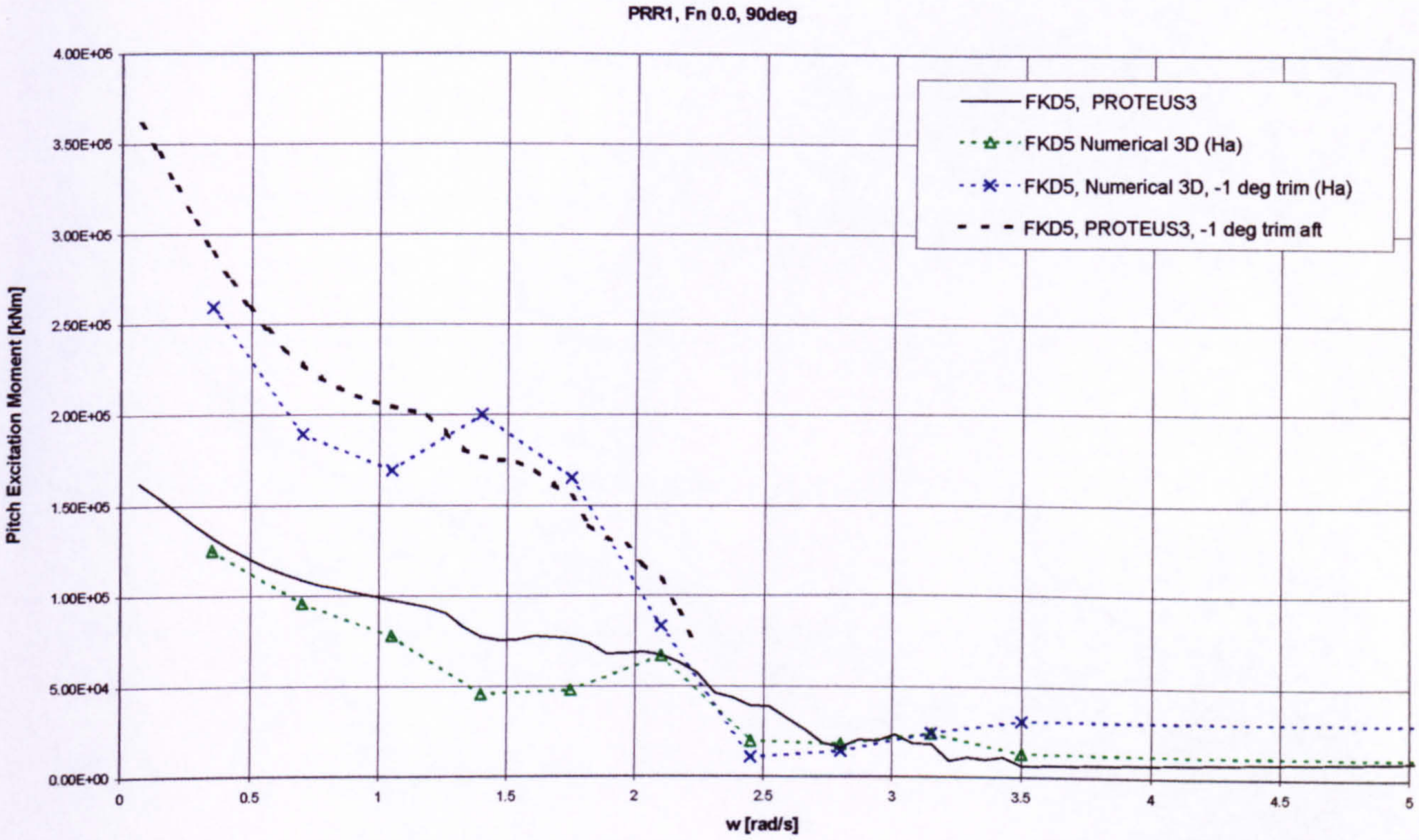

Figure 67 Excitation moments in pitch mode for 3D PRR1 hull form, predictions by strip theory and 3D panel methods, Fn=0.0, Heading 90deg, effect of –1 deg trim

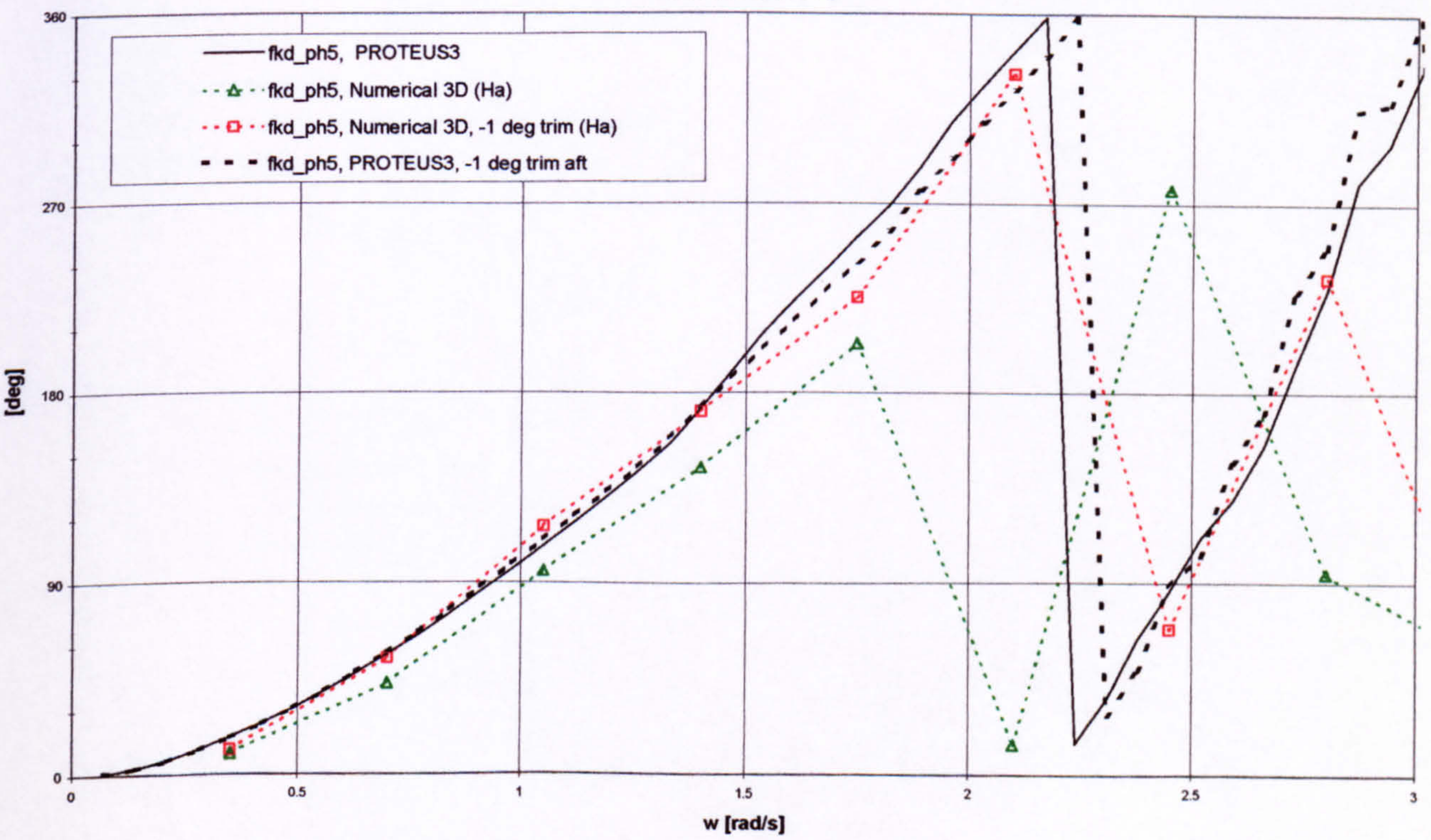

Figure 68 Excitation moments phase angles in pitch mode for 3D PRR1 hull form, predictions by strip theory and 3D panel methods, Fn=0.0, Heading 90deg, effect of –1 deg trim

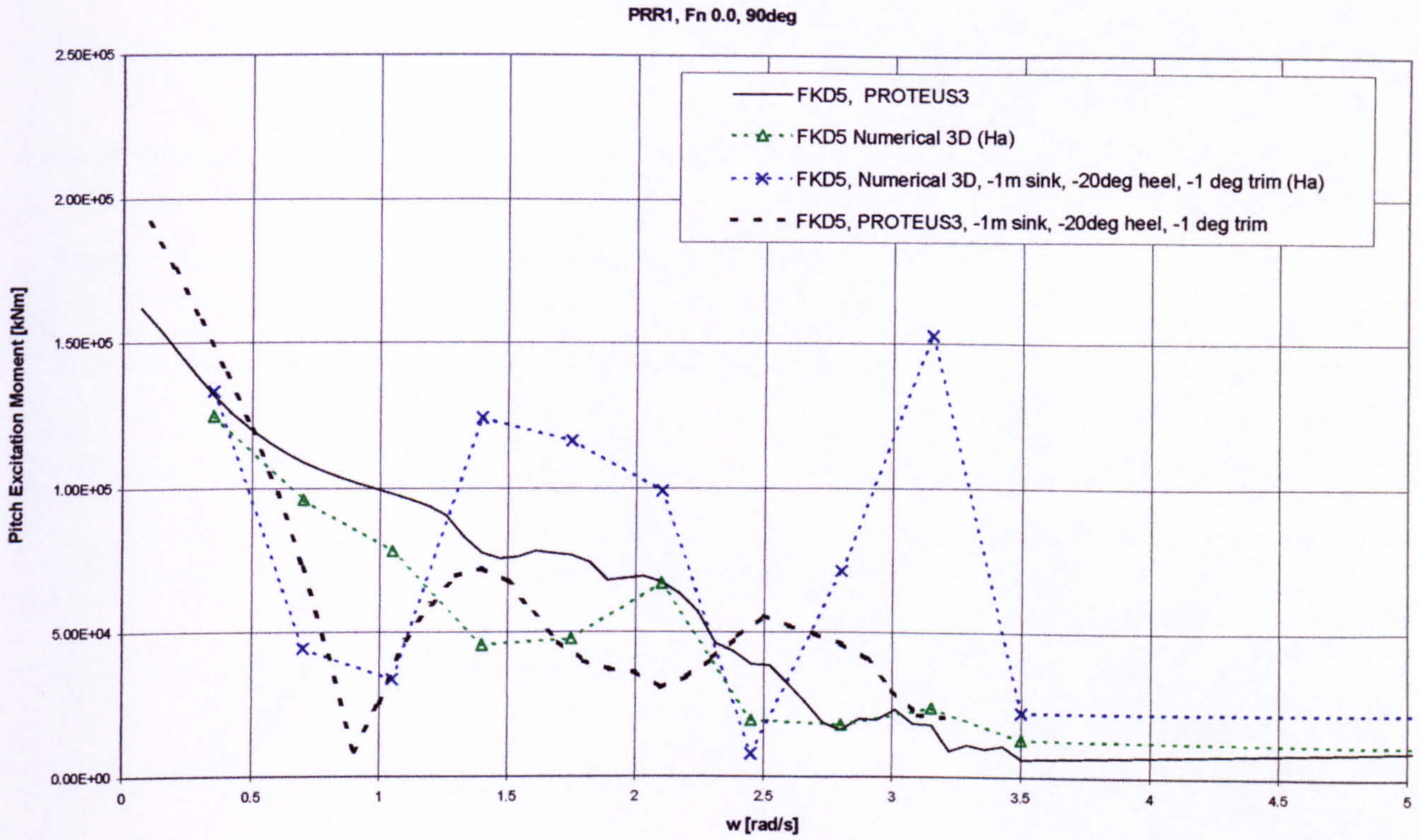

Figure 69 Excitation moments in pitch mode for 3D PRR1 hull form, predictions by strip theory and 3D panel methods, Fn=0.0, Heading 90deg, effect of –1m sinkage, –20deg heel and –1 deg trim

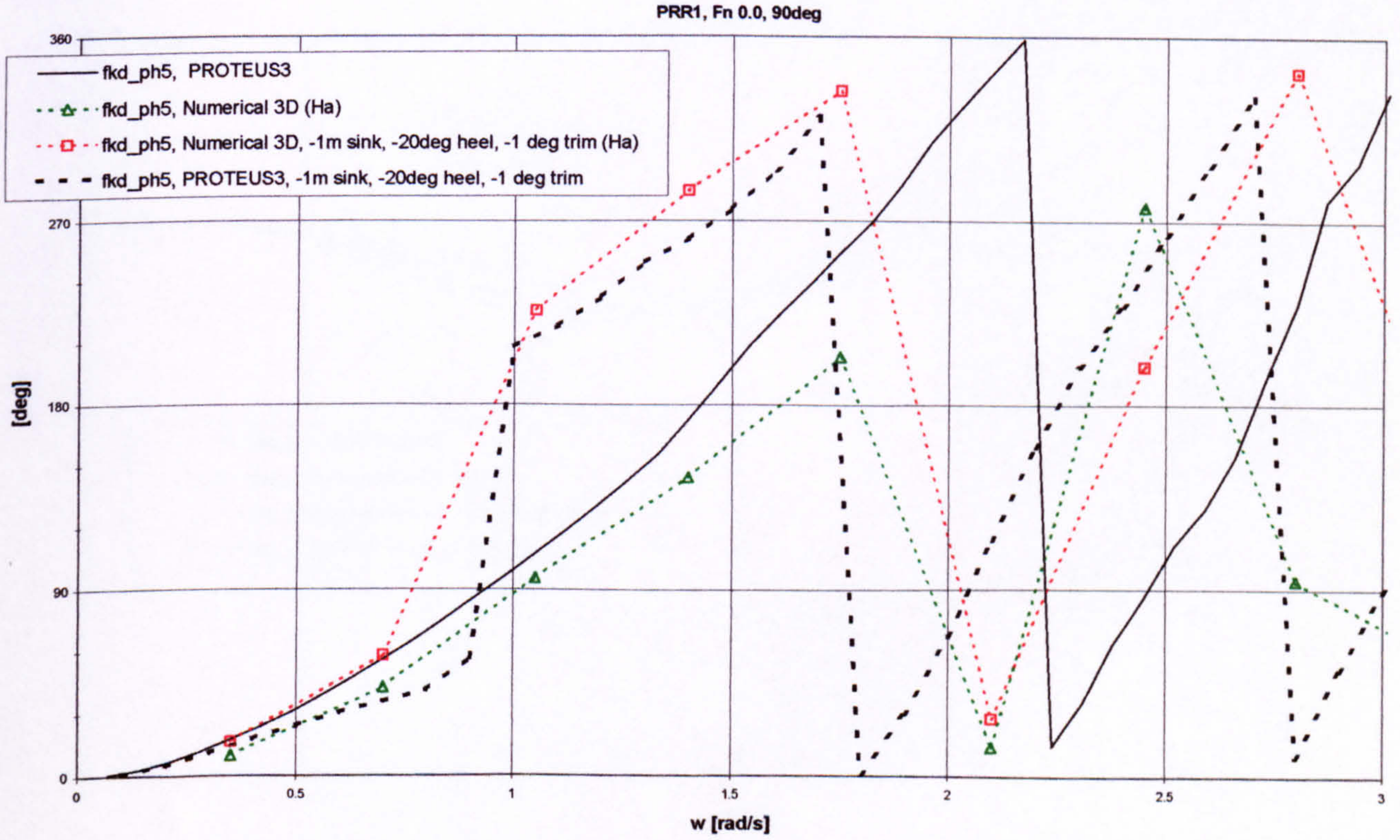

Figure 70 Excitation moments phase angles in pitch mode for 3D PRR1 hull form, strip theory and 3D panel methods, Fn=0.0, Heading 90deg, effect of –1m sinkage, –20deg heel and –1 deg trim

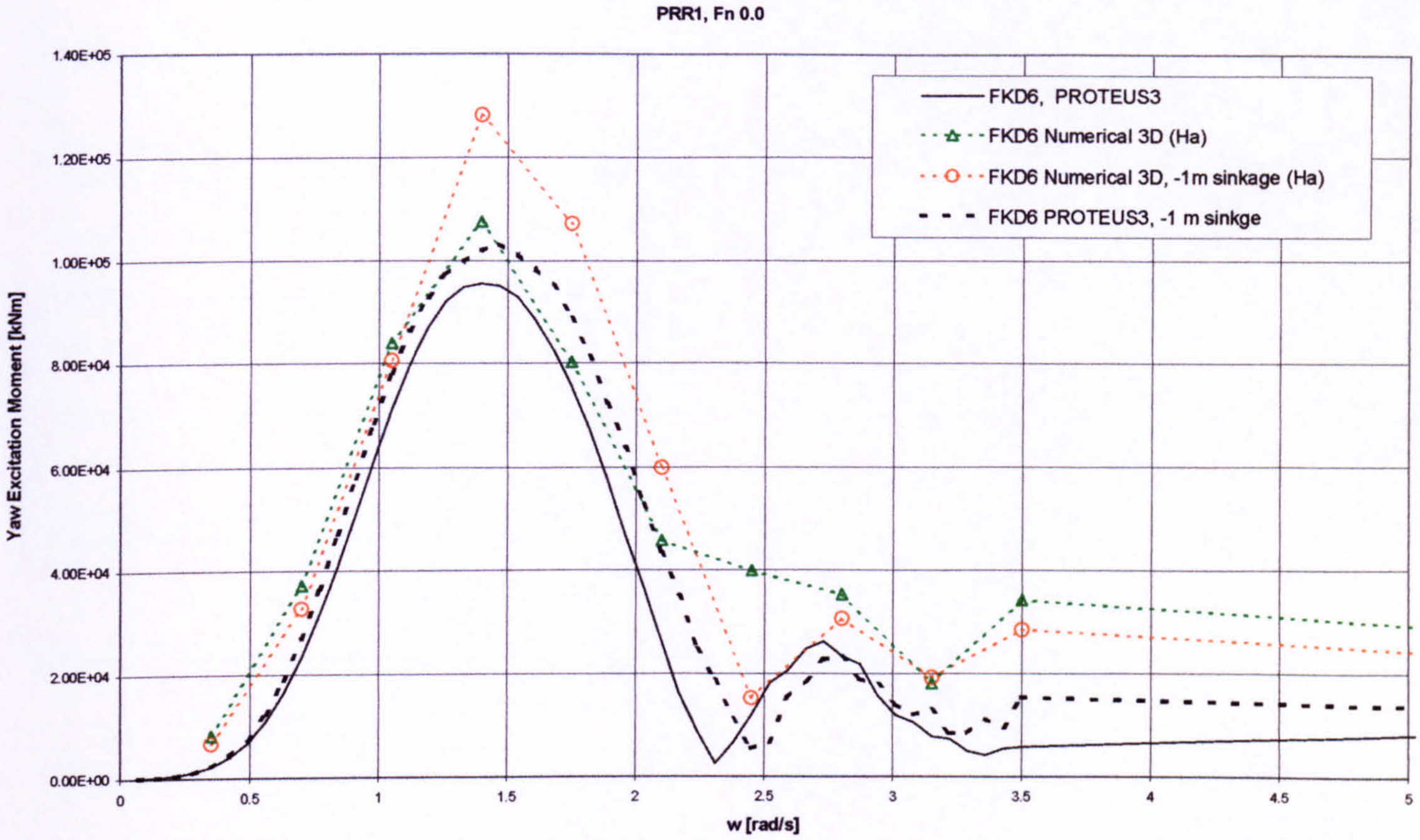

Figure 71 Excitation moments in yaw mode for 3D PRR1 hull form, predictions by strip theory and 3D panel methods, Fn=0.0, Heading 90deg, effect of –1m sinkage

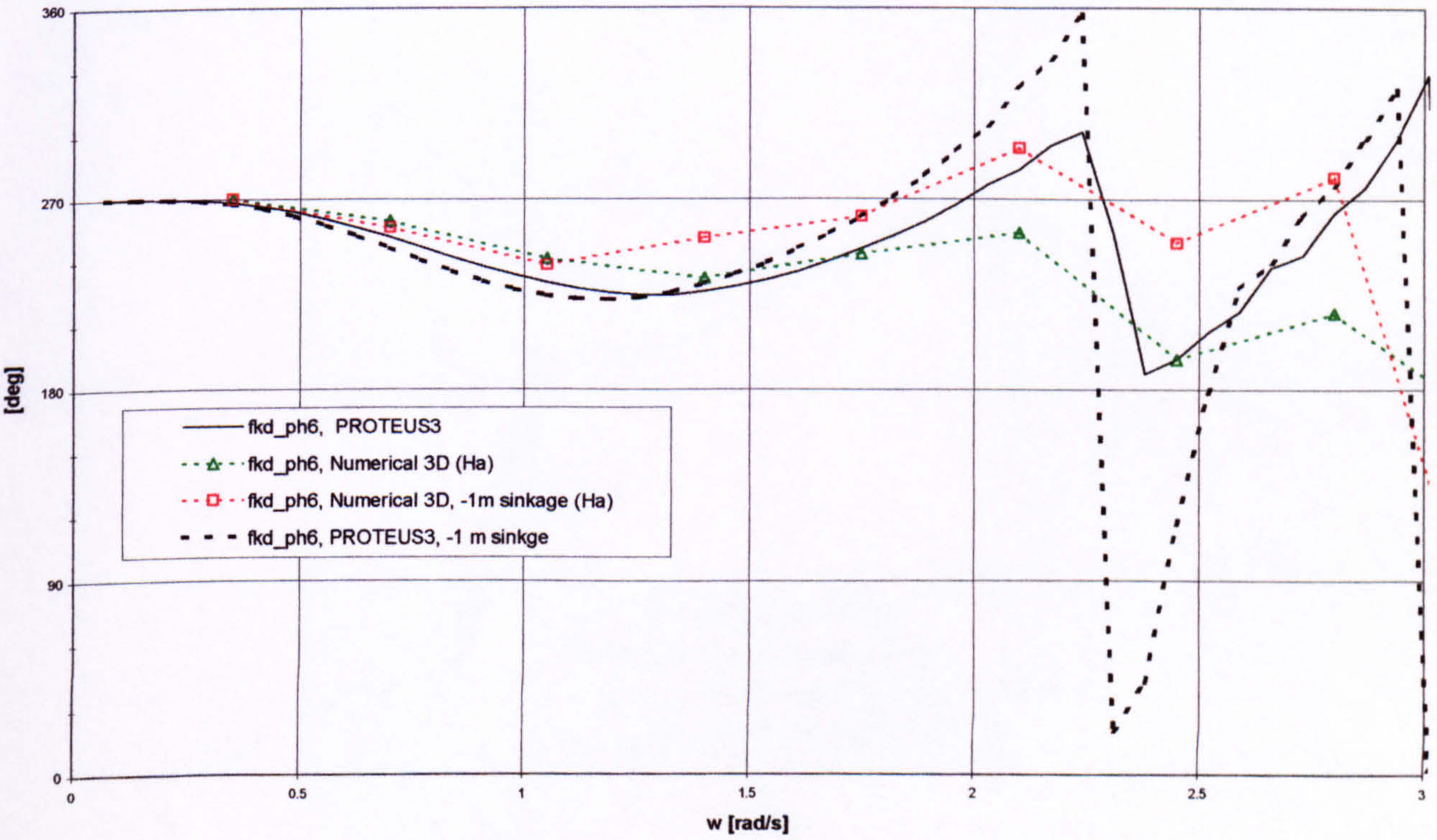

Figure 72 Excitation moments phase angles in yaw mode for 3D PRR1 hull form, predictions by strip theory and 3D panel methods, Fn=0.0, Heading 90deg, effect of –1m sinkage

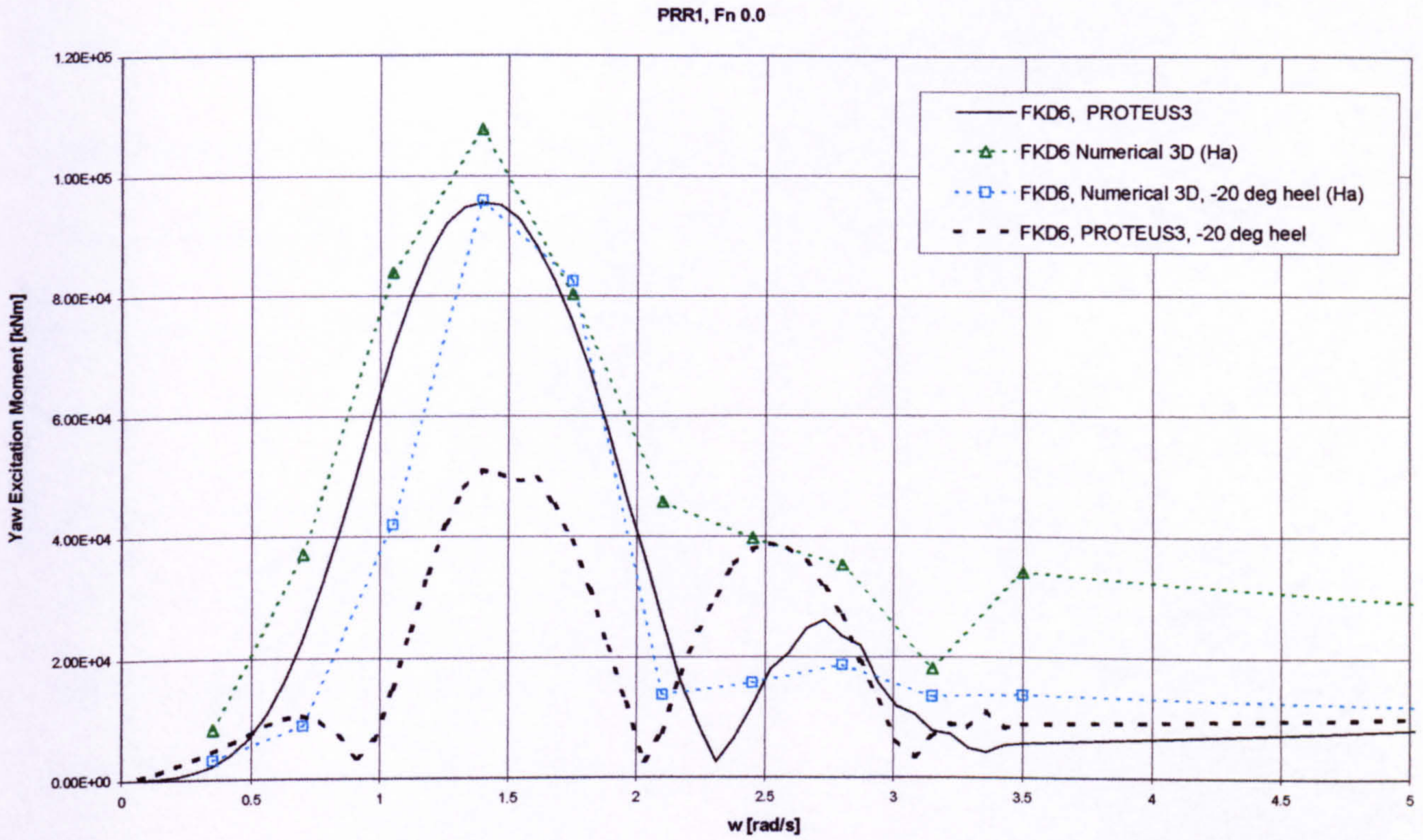

Figure 73 Excitation moments in yaw mode for 3D PRR1 hull form, predictions by strip theory and 3D panel methods, Fn=0.0, Heading 90deg, effect of –20deg heel

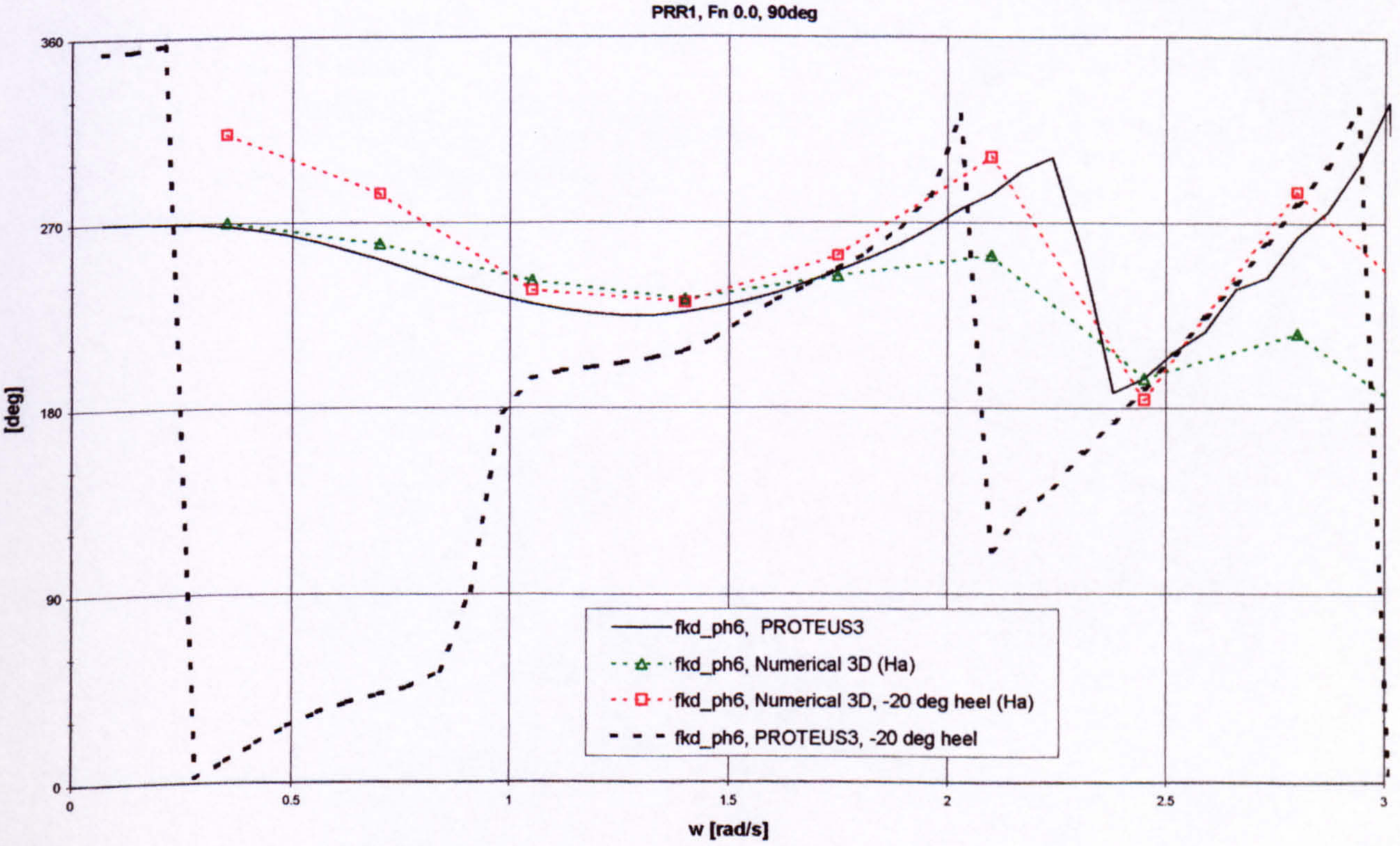

Figure 74 Excitation moments phase angles in yaw mode for 3D PRR1 hull form, predictions by strip theory and 3D panel methods, Fn=0.0, Heading 90deg, effect of –20deg heel

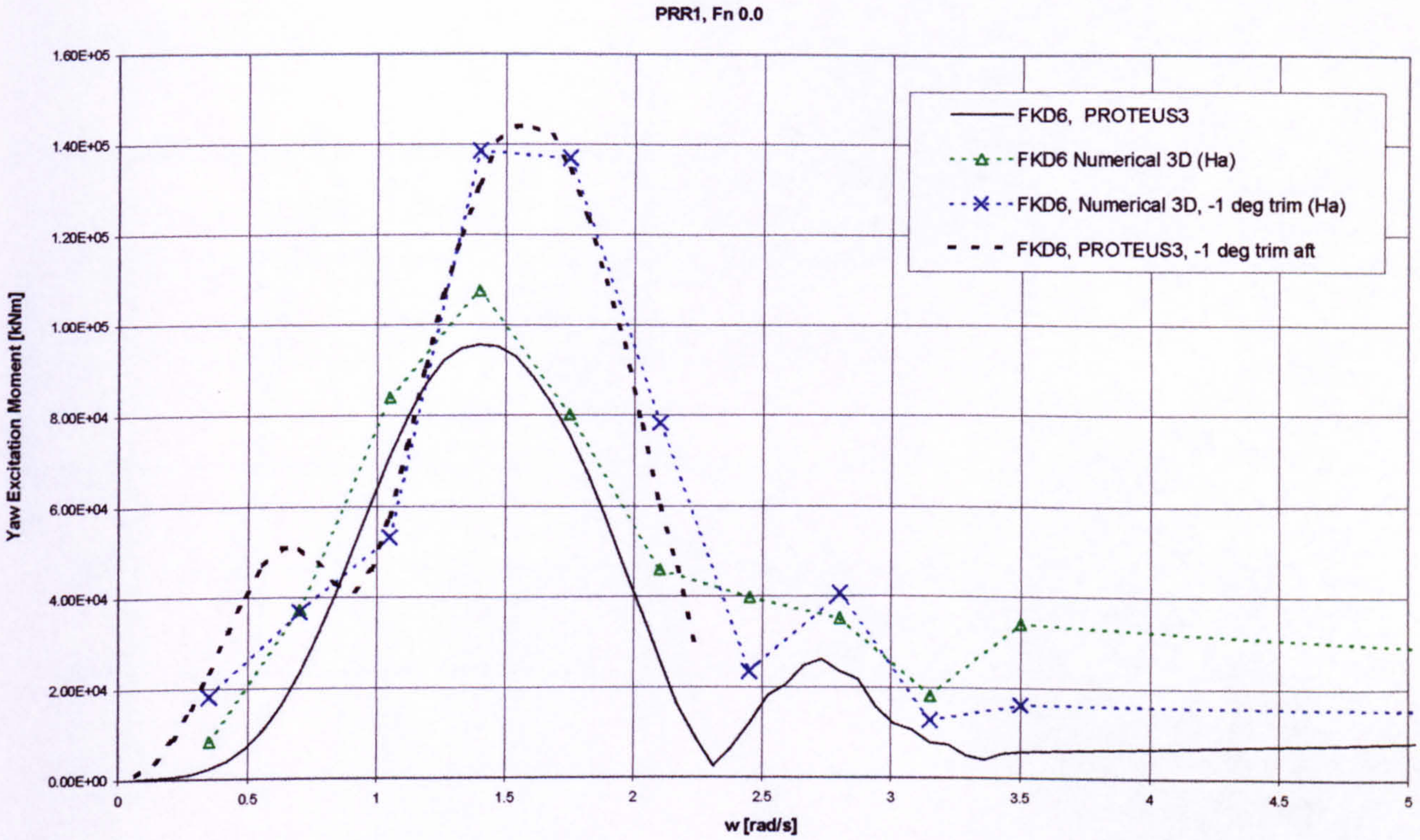

Figure 75 Excitation moments in yaw mode for 3D PRR1 hull form, predictions by strip theory and 3D panel methods, Fn=0.0, Heading 90deg, effect of –1 deg trim

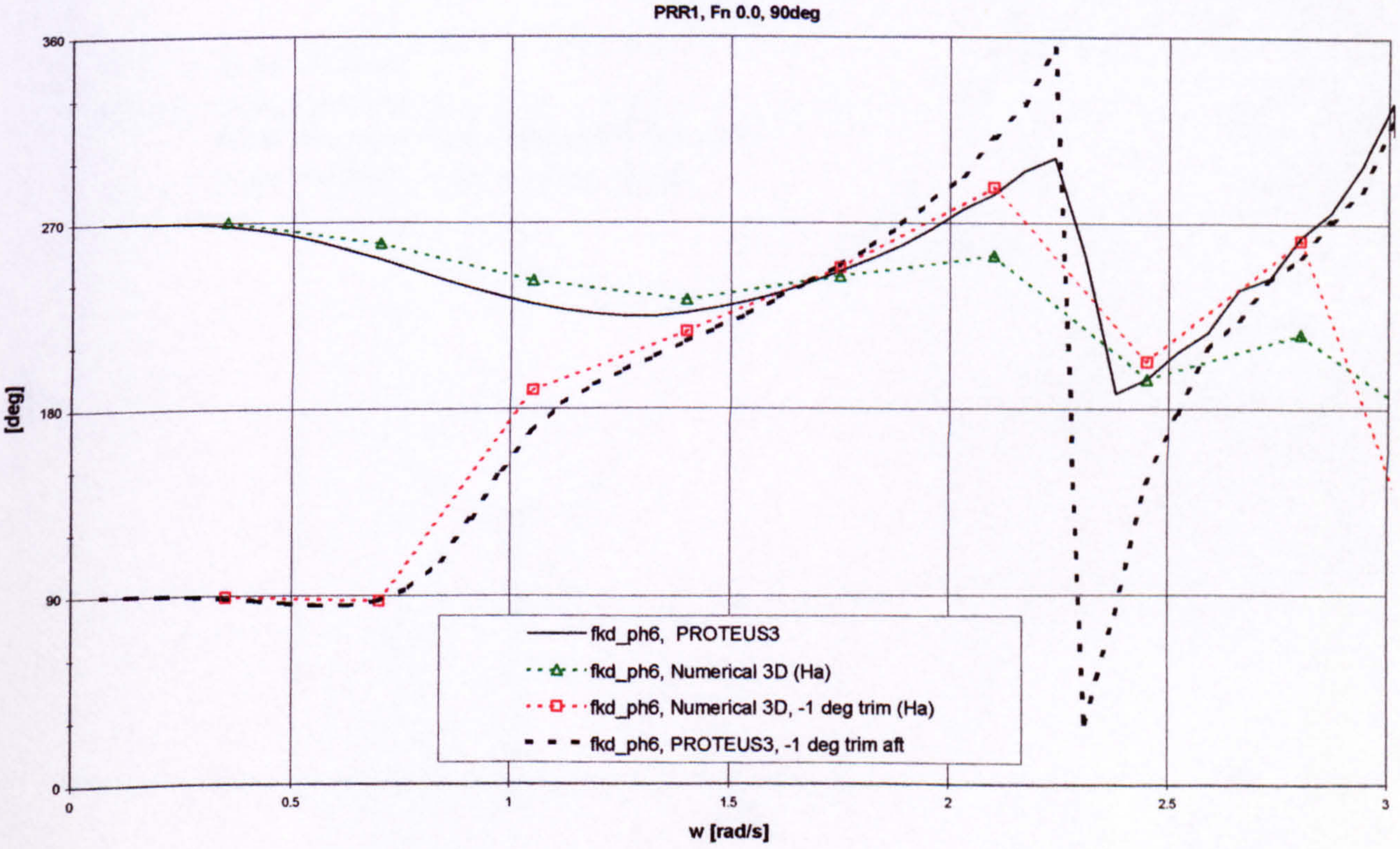

Figure 76 Excitation moments phase angles in yaw mode for 3D PRR1 hull form, predictions by strip theory and 3D panel methods, Fn=0.0, Heading 90deg, effect of –1 deg trim

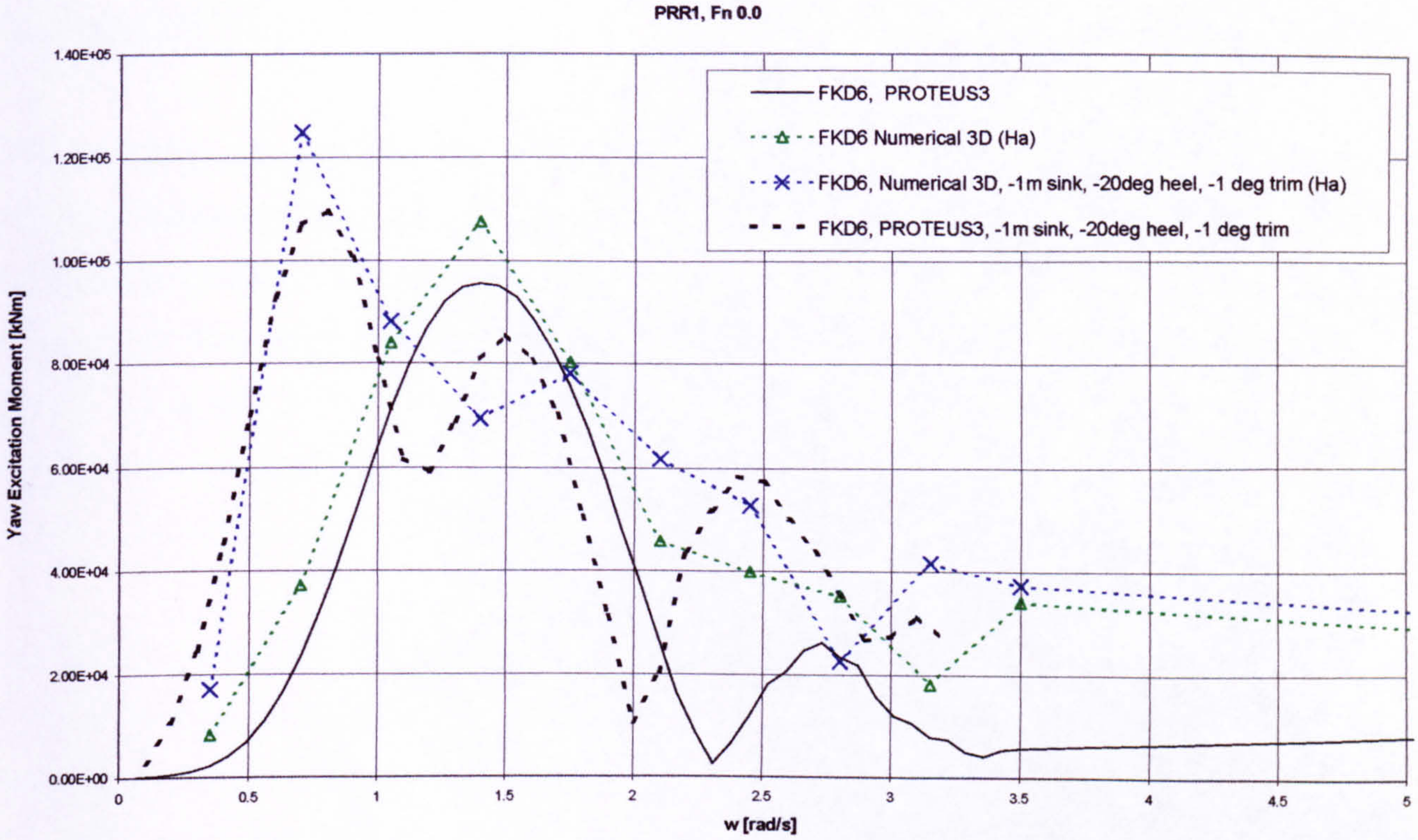

Figure 77 Excitation moments in yaw mode for 3D PRR1 hull form, predictions by strip theory and 3D panel methods, Fn=0.0, Heading 90deg, effect of –1m sinkage, –20deg heel and –1 deg trim

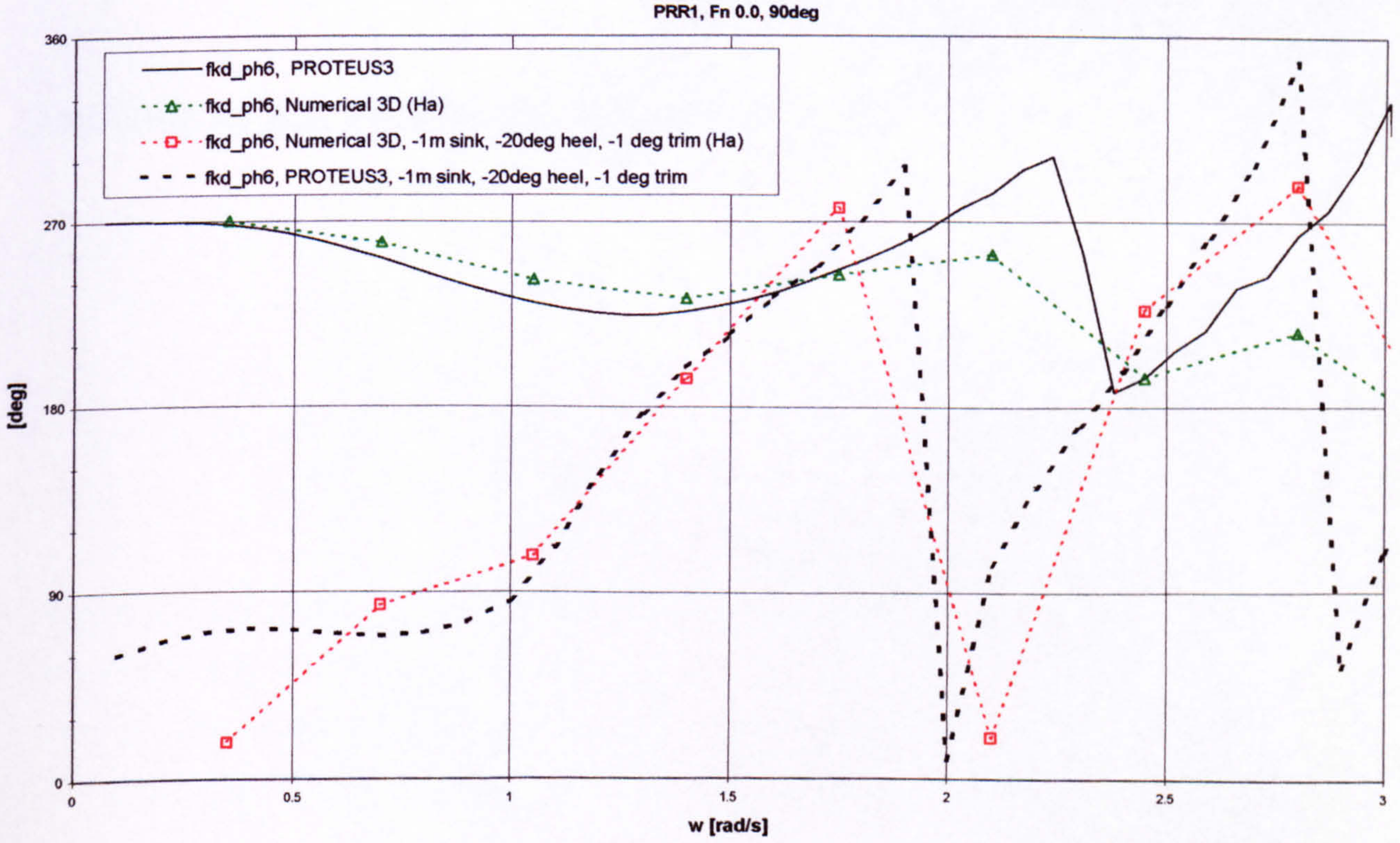

Figure 78 Excitation moments phase angles in yaw mode for 3D PRR1 hull form, strip theory and 3D panel methods, Fn=0.0, Heading 90deg, effect of –1m sinkage, –20deg heel and –1 deg trim

Appendix 4

Testing of survivability of the Passenger Ro-Ro vessel PRR1

Summary

This appendix provides with the time series of the relevant quantities derived during physical experimentation and the corresponding numerical simulations of the behaviour of ship undergoing progressive flooding, with the aim to providing data for comparative studies. Details of the experiments are given. Fourier analysis of all the motion time series is also provided.

1 Model Experiments

For the validation purposes a set of 15 out of 627 tests on a 1:40 scale GRP model of Passenger Ro-Ro PRR1 have been used. General experimentation set-up as well as the pertinent outcome has been summarised below.

During the experiment the model was equipped with 14 wave probes (Wp1-14) on the car deck and another two wave probes (W15 and W16) in front of the opening to measure the amount of ingress water on the car deck. Only the bilge keels were mounted as external appendages.

The model tests were performed at Denny Tank, the University of Strathclyde model testing facility in Dumbarton. The Denny Tank is a conventional towing tank used also successfully for the seakeeping model tests, which measures 100×7×2.7 metres in length, width and water depth, respectively. The Denny Tank is fitted with a new high speed 10m/s manned/unmanned carriage and a flap-type wave maker capable of accurately generating irregular waves of a given spectral description with significant wave height up to 0.5m. The tank is equipped with the latest computer systems for data acquisition and analysis and a range of sophisticated instrumentation including the resistance type wave probes, a six-degrees-of-freedom non-contact infrared photogrammetry motion measurement system Vicon 140.

The excitation sea conditions were modelled by the JOHNSWAP wave energy spectrum as given in §9.3 in the main body of the thesis. A range of sea states of Hs=1.0 – 6.25 [m], each of which represented by at least 5 different time realisations, have been pre-tested to ensure modelling of the environment with high accuracy ($\pm 1mm$ model scale in Hs). The model was removed from the tank and the wave measured by a fixed wave probe.

In summary, the following quantities were measured during the experiments: amount of floodwater on the car deck by WP1-14, relative wave elevation by WP15 and WP16, absolute wave elevation by travelling and tank-fixed wave probes, 6dof of ship motions by photogrammetry instrumentation and velocity of the carriage. All of these signals were recorded at frequency of 30Hz.

The established survivability per individual experiment is summarised in Table 1, with all records from these runs presented next in graphical form, Figure 1 to Figure 16. Summary of survivability

from all of the 627 experiments, together with performed numerical simulations is given in Table 2 for the purpose of providing convenient reference.

The complementary Fourier analyses of the motions records, attached with all the figures, were performed after high-pass filtering ($\omega > 0.2$ rad/s) and for time duration as achieved. Therefore, caution should be exercised when examining test cases terminated by capsize events, as the record duration affects the analyses.

Table 1 Experimental testing of survivability of PRR1

Case	Run No.	Wave File	Target Wave Height Hs(m)	Wave Steepness	Comments
2	Run101	W4001	4.0	1/25	Passed
2	Run102	W4002	4.0	1/25	Passed
2	Run103	W4003	4.0	1/25	Passed
2	Run104	W4004	4.0	1/25	Passed
2	Run105	W4005	4.0	1/25	Passed
2	Run106	W4251	4.25	1/25	Passed
2	Run107	W4252	4.25	1/25	**Capsized**
2	Run108	W4253	4.25	1/25	**Capsized**
2	Run109	W4254	4.25	1/25	**Capsized**
2	Run110	W4255	4.25	1/25	**Capsized**
2	Run111	W4251	4.25	1/25	Passed
2	Run112	W4501	4.5	1/25	**Capsized**
2	Run113	W4502	4.5	1/25	**Capsized**
2	Run114	W4503	4.5	1/25	**Capsized**
2	Run115	W4504	4.5	1/25	**Capsized**
2	Run116	W4505	4.5	1/25	**Capsized**

Table 2 PRR1 Survival Boundary derived by different methods against initial conditions.

Case No	Permeability	Initial draught	Initial trim [deg]	KG	PROTEUS1, 1/25		PROTEUS3.12, 1/25		EXPERIMENT 1/20		EXPERIMENT 1/25	
					0% C	100% C	0% C	100% C	0% C	100% C	0% C	100% C
1	0.95	6.25	0.000	***12.200***	4.50	6.00	6.75	-	>4.75		4.75	
2	0.95	6.25	0.000	***12.892***	3.75	5.00	3.75	4.75	4.00	4.50	4	4.5
3	0.95	6.25	0.000	***13.456***	3.50	4.25	2.75	3.5	2.75	3.25	2.5	3.25
4	0.95	6.25	0.000	***14.114***	2.00	2.75	0.75	1				2
5	0.95	6.25	***-1.000***	12.200	3.25	4.00					4	4.75
6	0.95	6.25	***-1.000***	12.892	2.50	3.25					3	3.75
7	0.95	6.25	***-1.000***	13.456	1.75	2.00					2.5	3
8	0.95	6.25	***-1.000***	14.114	0.50	1.00						
9	0.95	6.25	***1.000***	12.200	4.25	5.00					3.5	4.25
10	0.95	6.25	***1.000***	12.892	3.50	4.50						
11	0.95	6.25	***1.000***	13.456	2.75	3.50						
12	0.95	6.25	***1.000***	14.114	1.50	2.00						
13	0.95	***5.75***	0.000	12.200	5.50	6.75						
14	0.95	***5.75***	0.000	12.892	4.75	6.75					6.25	
15	0.95	***5.75***	0.000	13.456	4.25	5.50					5	6.25
16	0.95	***5.75***	0.000	14.114	3.75	4.50					3.25	4.25
17	0.95	***6.75***	0.000	12.200	3.50	4.00					3	3.75
18	0.95	***6.75***	0.000	12.892	2.75	3.75					2	2.75
19	0.95	***6.75***	0.000	13.456	2.00	2.75					1.5	1.75
20	0.95	***6.75***	0.000	14.114	0.50	1.00						
22	***0.70***	6.25	0.000	12.200	4.50	6.00						
23	***0.70***	6.25	0.000	12.892	4.00	5.00					4.75	5.75
24	***0.70***	6.25	0.000	13.456	3.50	4.25					4	4.75
25	***0.70***	6.25	0.000	14.114	2.00	2.75					2.5	3
26	0.7	6.250	-1.000	**12.200**							4.5	5.75
27	0.7	6.250	-1.000	**12.892**							4	4.5
28	0.7	6.250	-1.000	**13.456**								
29	0.7	6.250	-1.000	**14.114**								

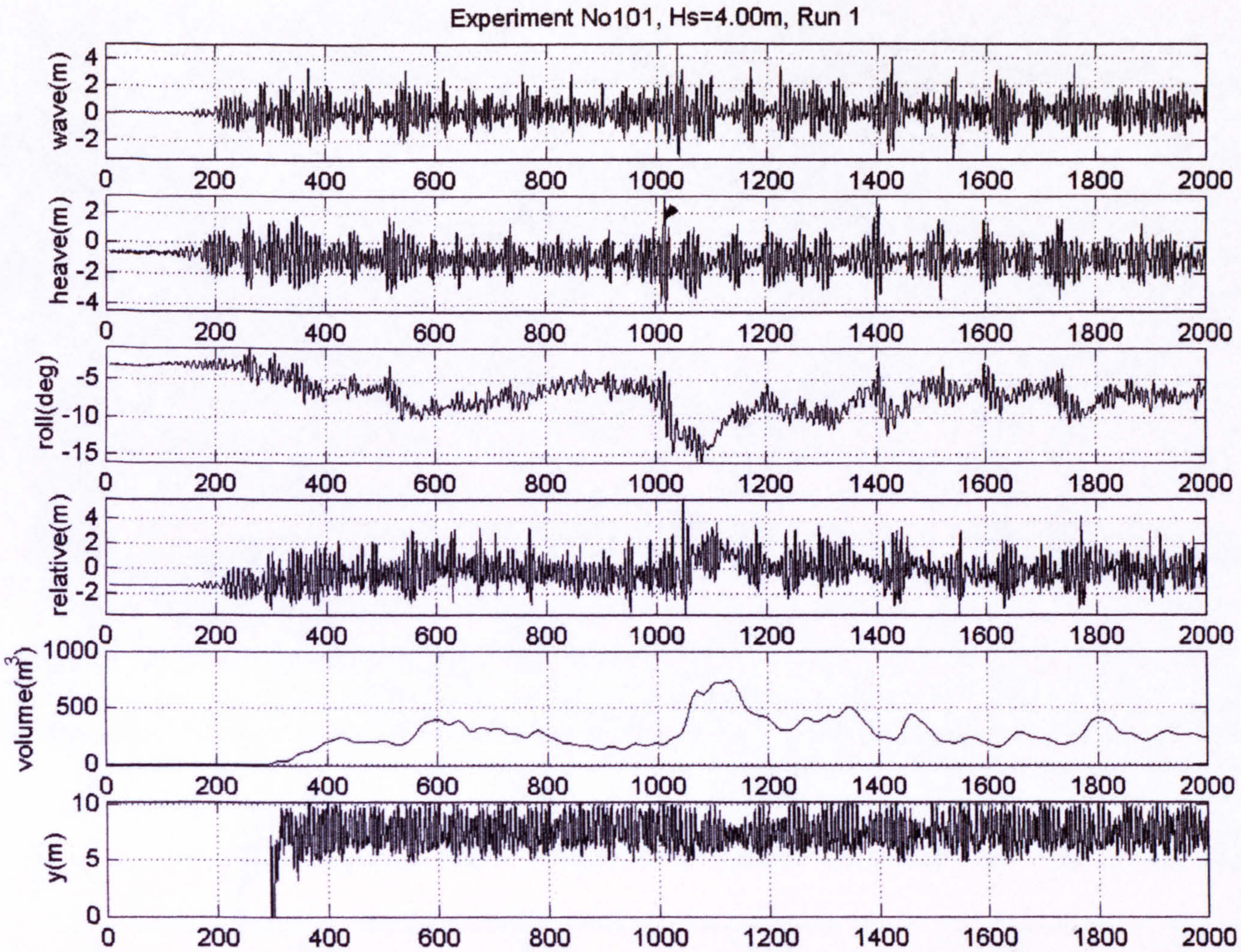

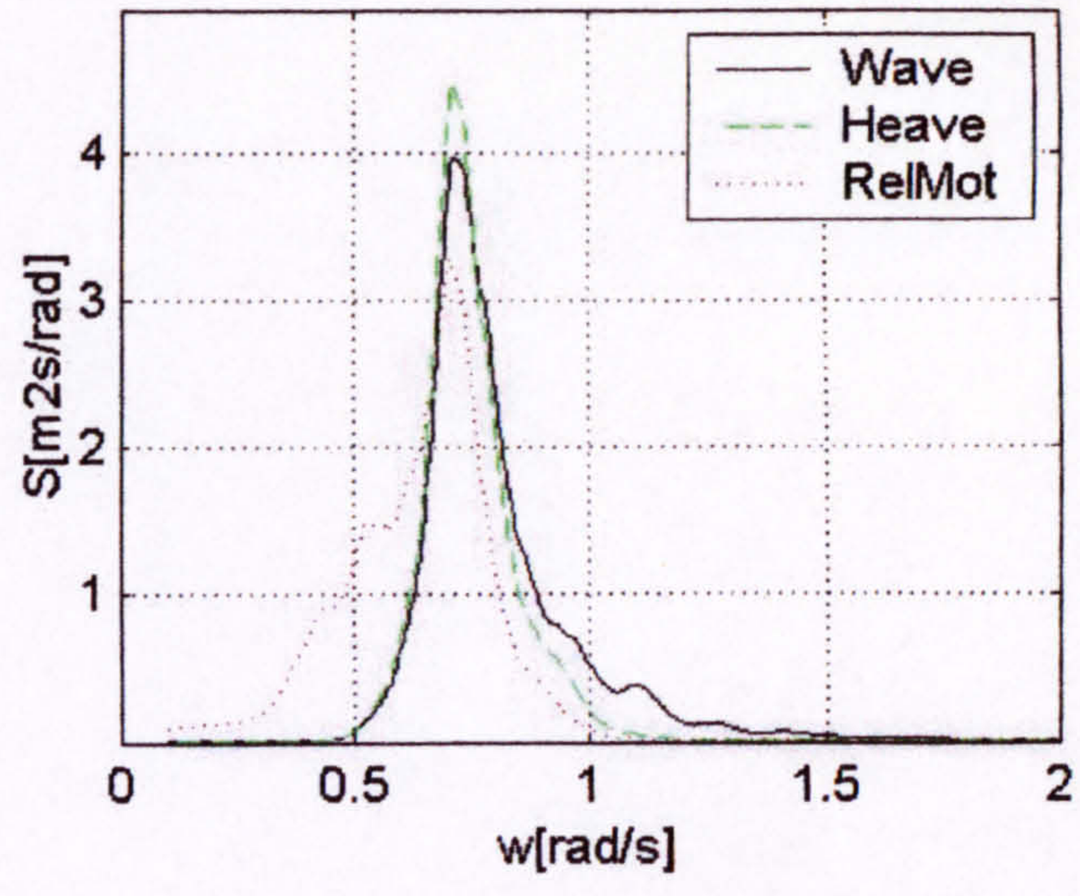

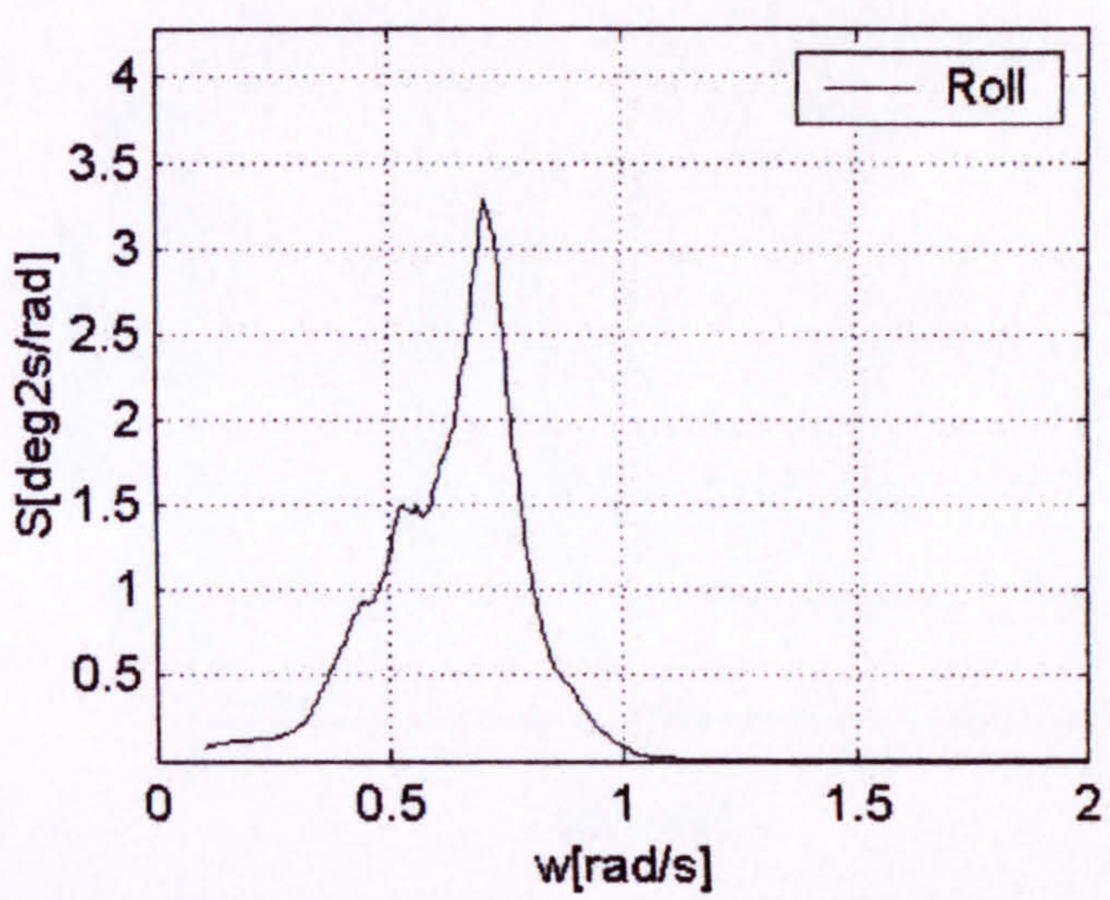

Figure 1 Experiment, Hs=4.00m

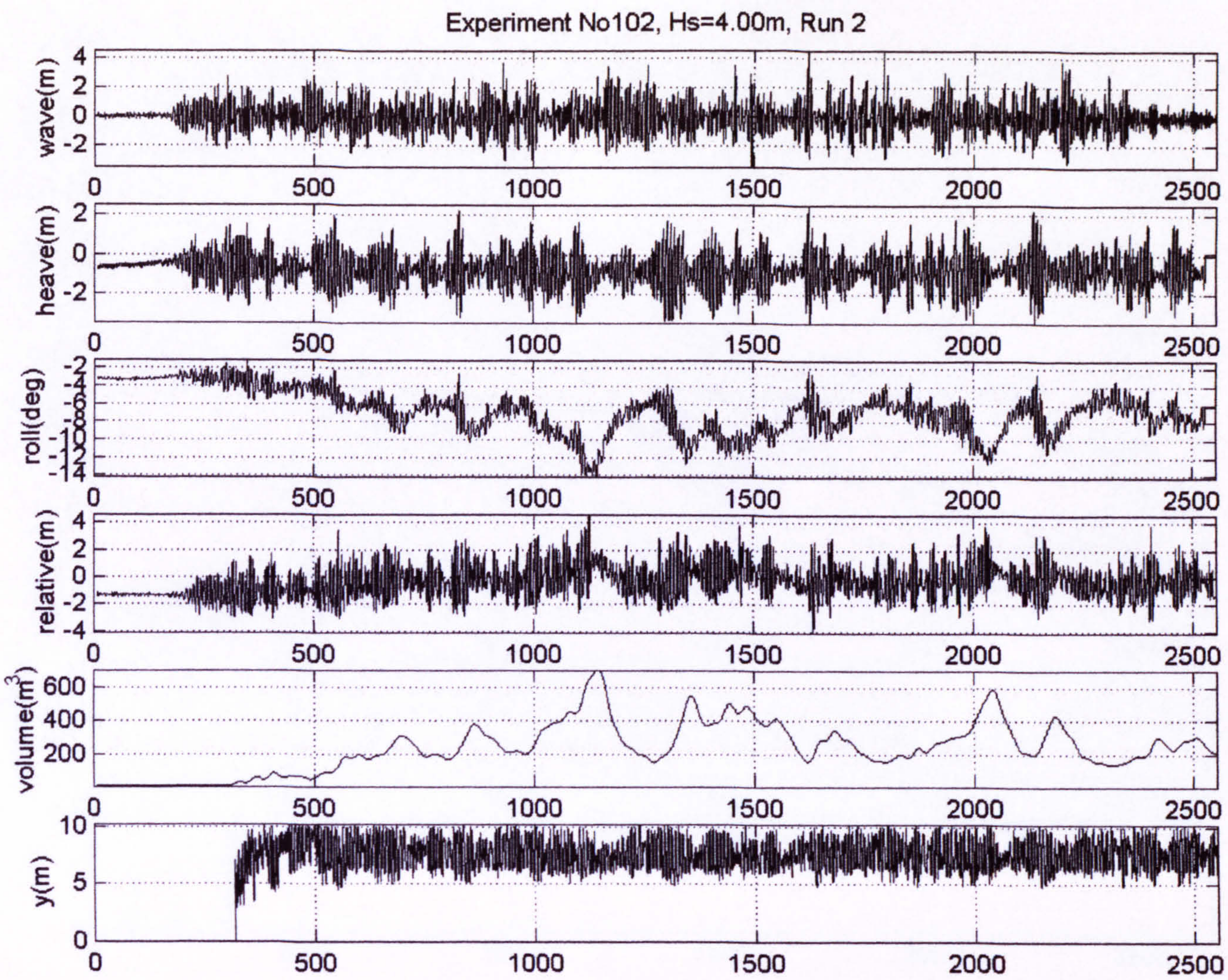

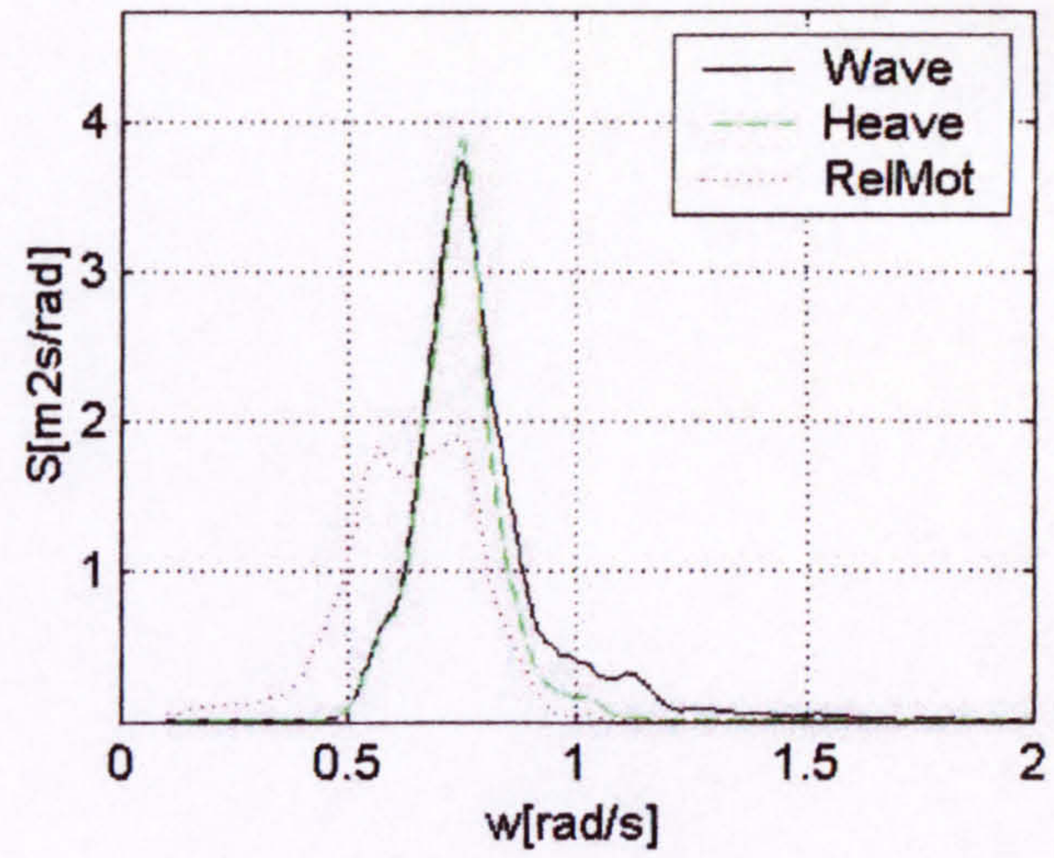

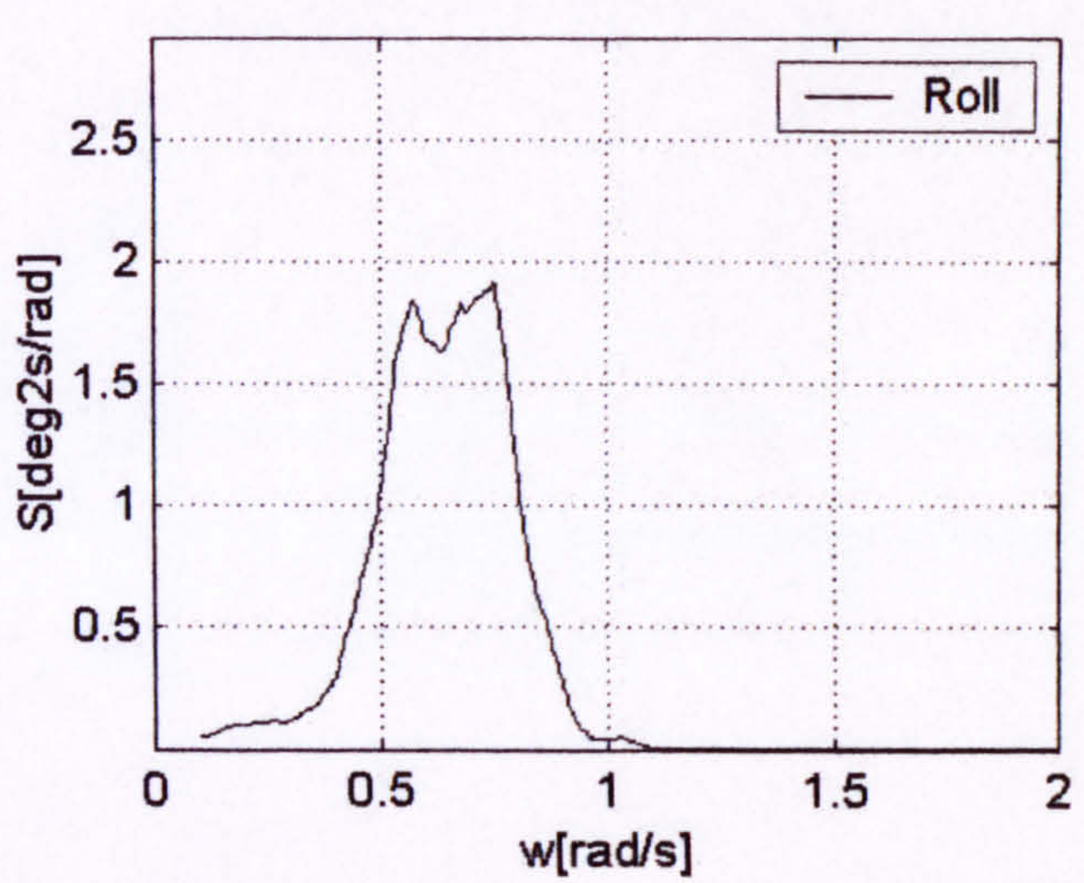

Figure 2 Experiment, Hs=4.00m

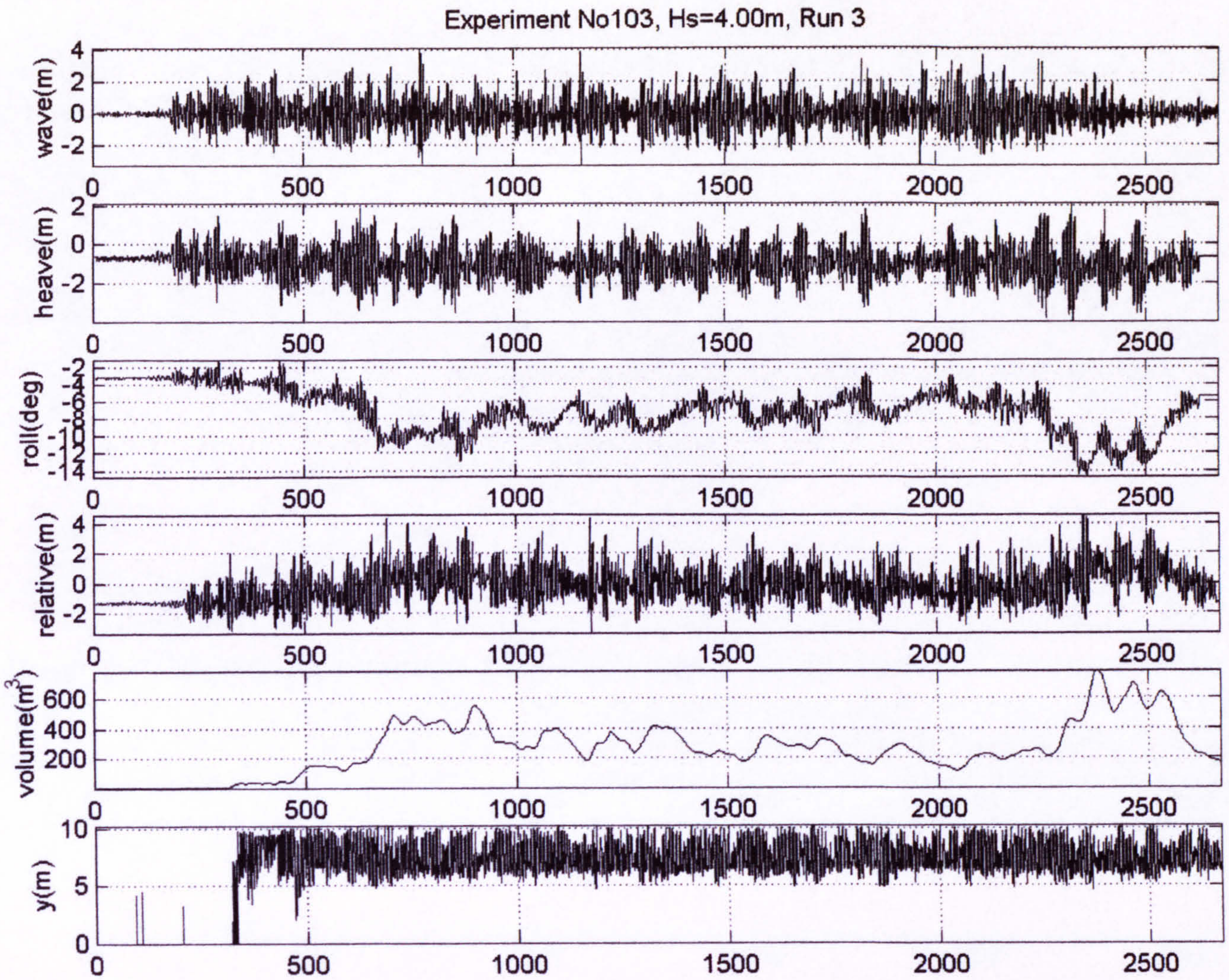

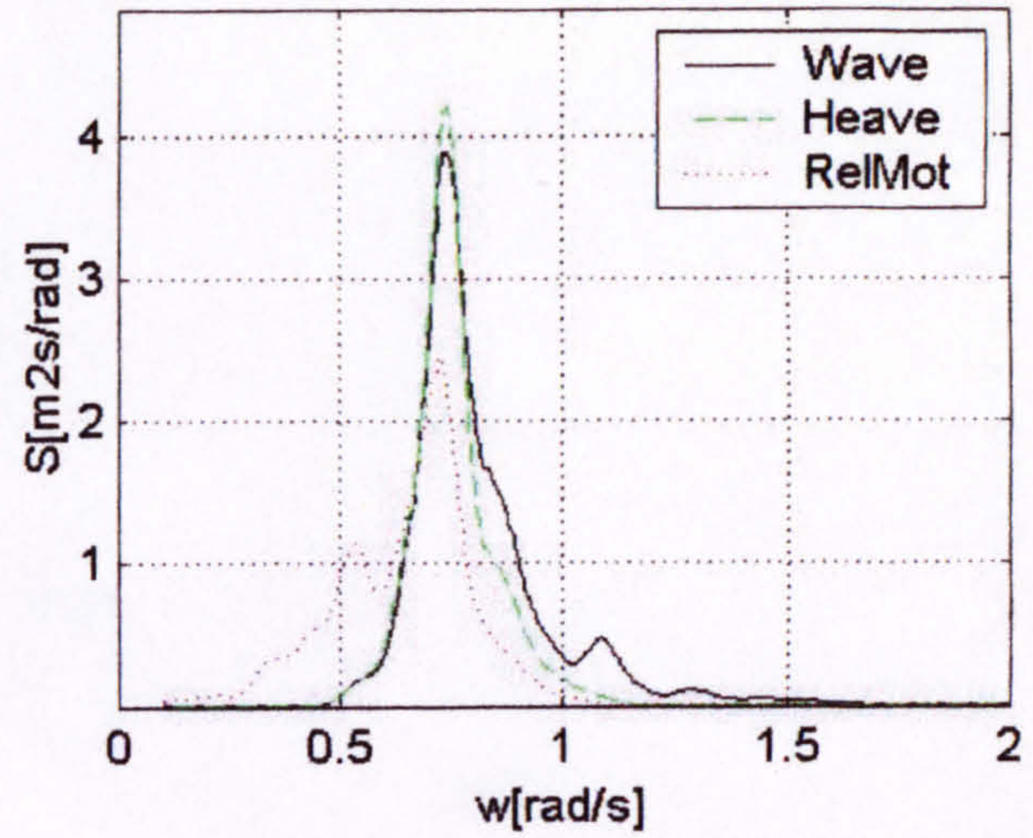

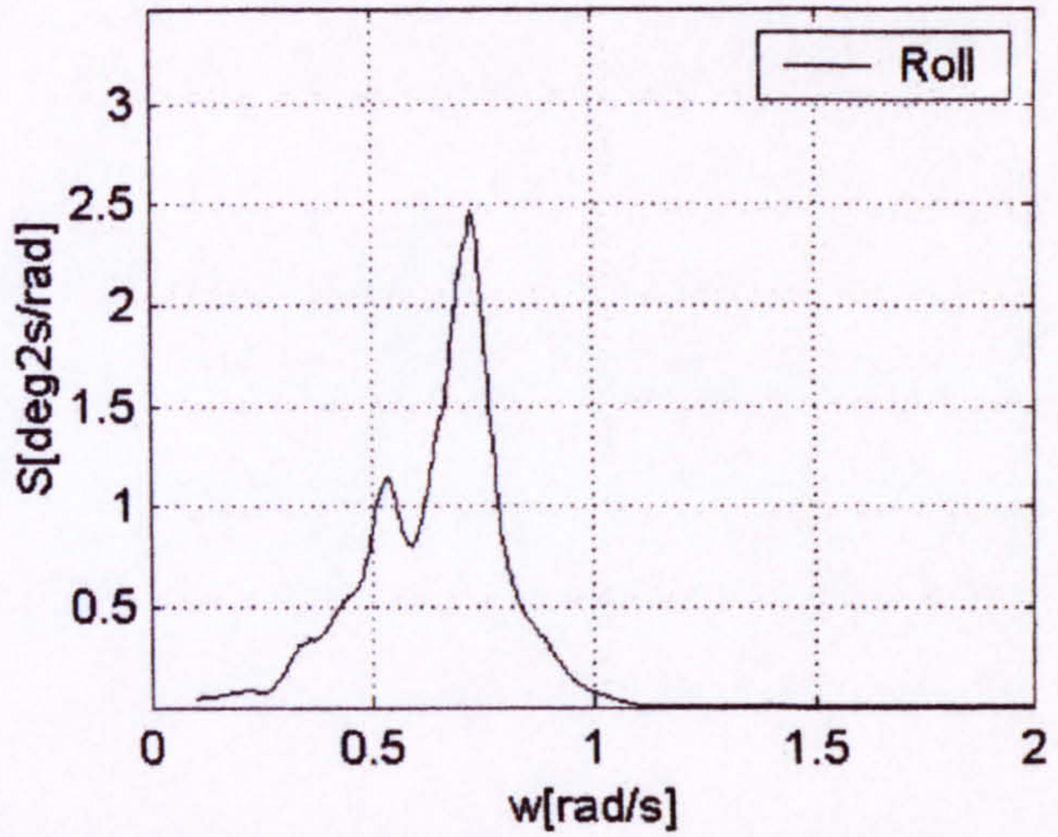

Figure 3 Experiment, Hs=4.00m

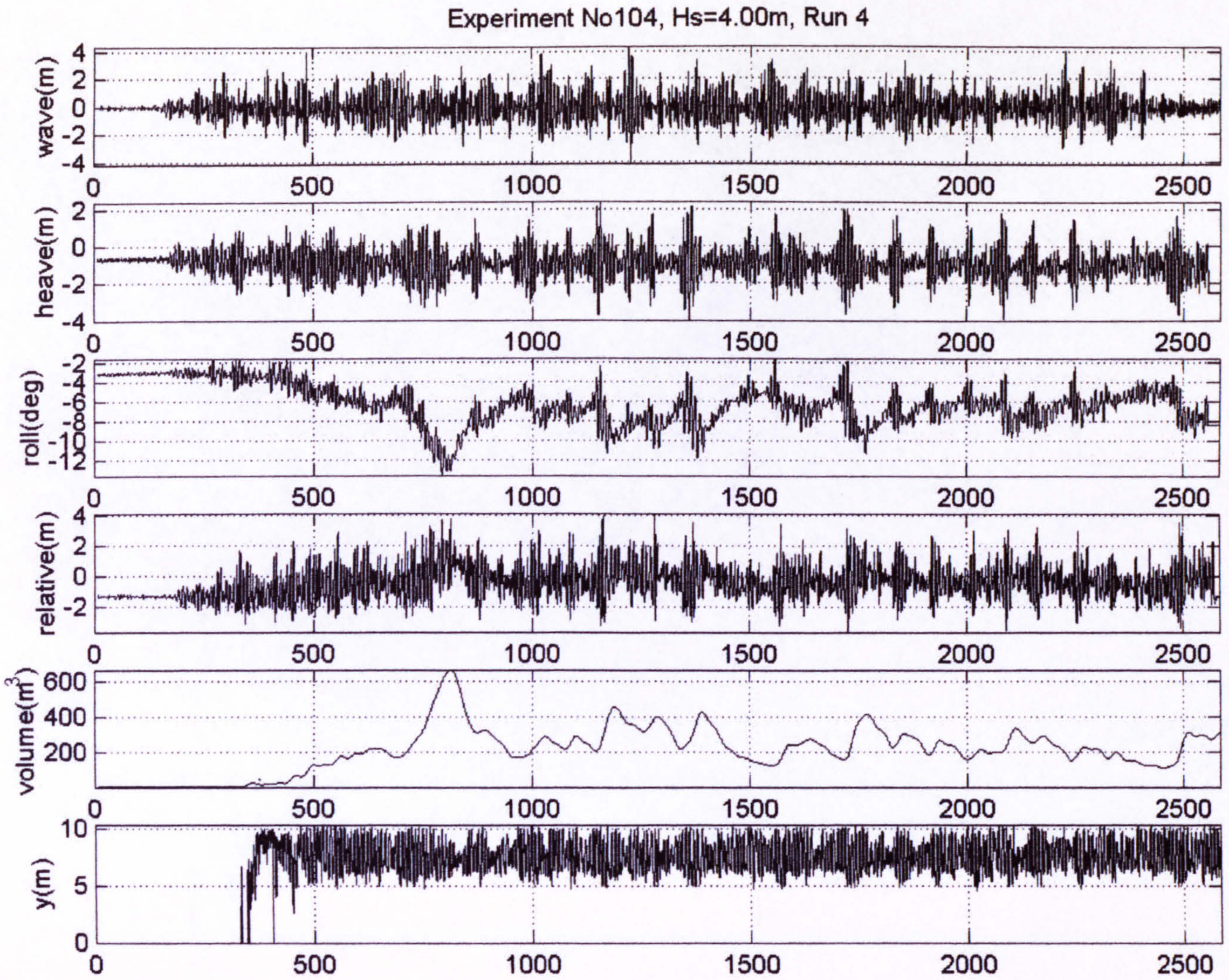

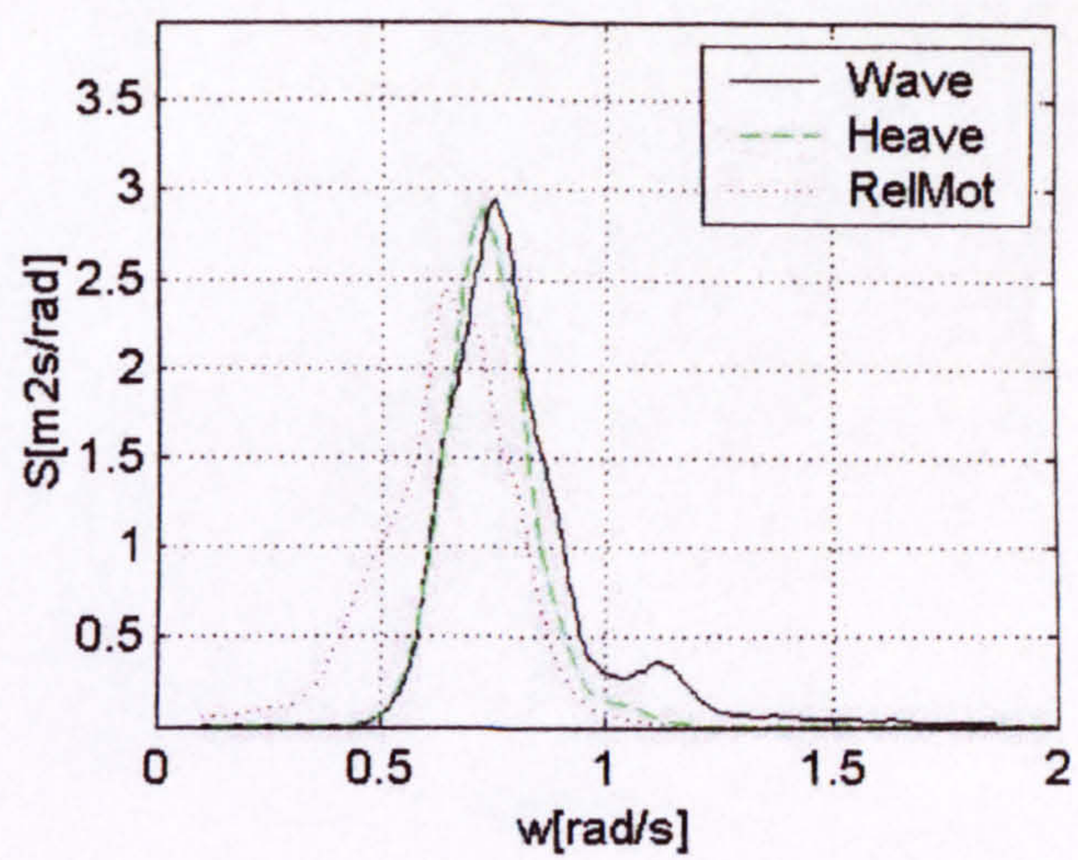

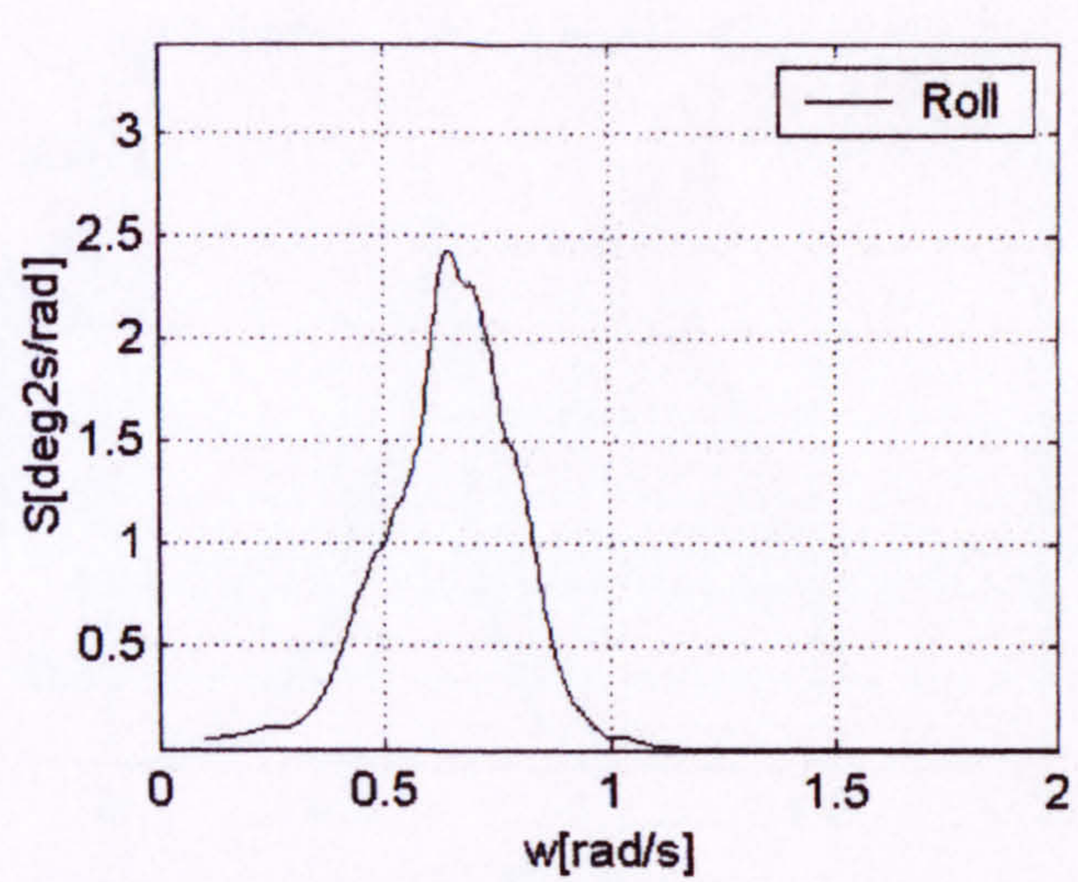

Figure 4 Experiment, Hs=4.00m

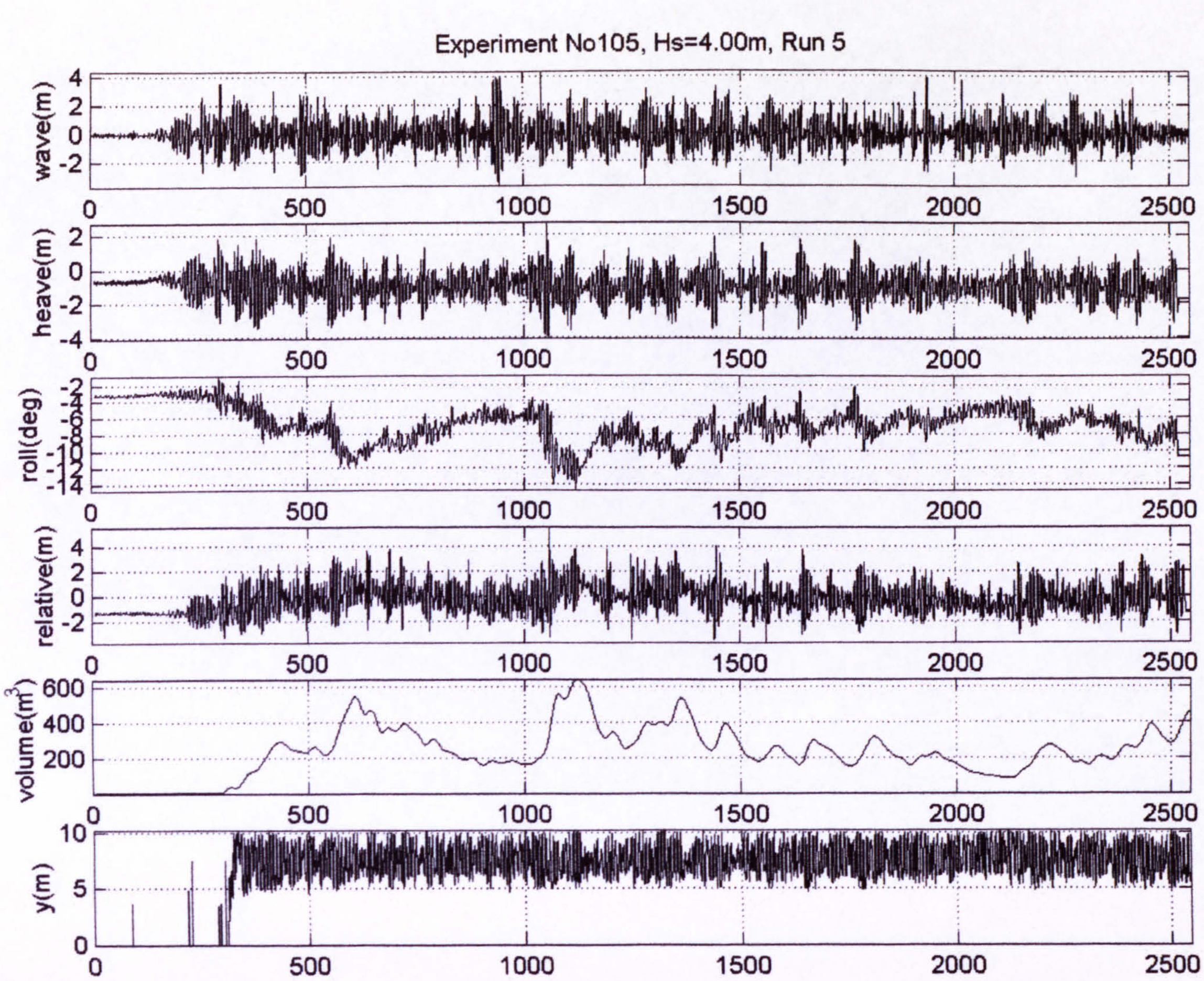

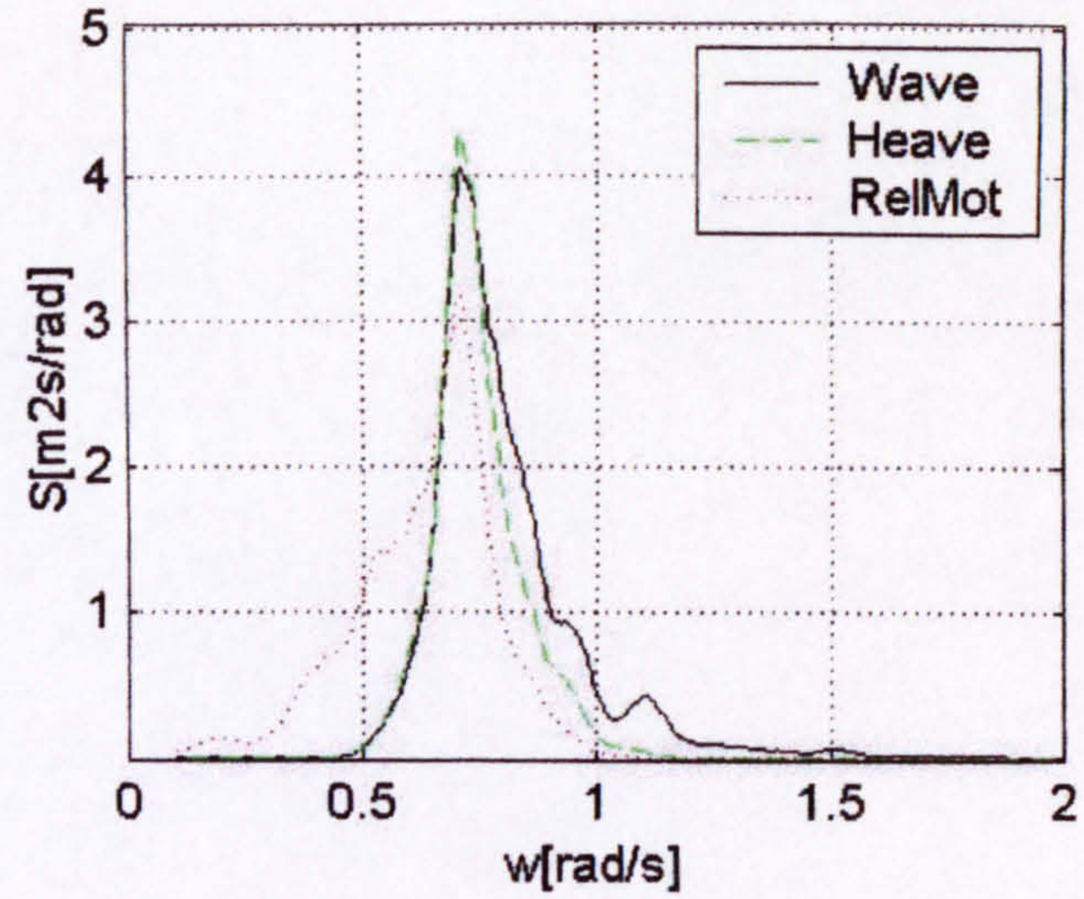

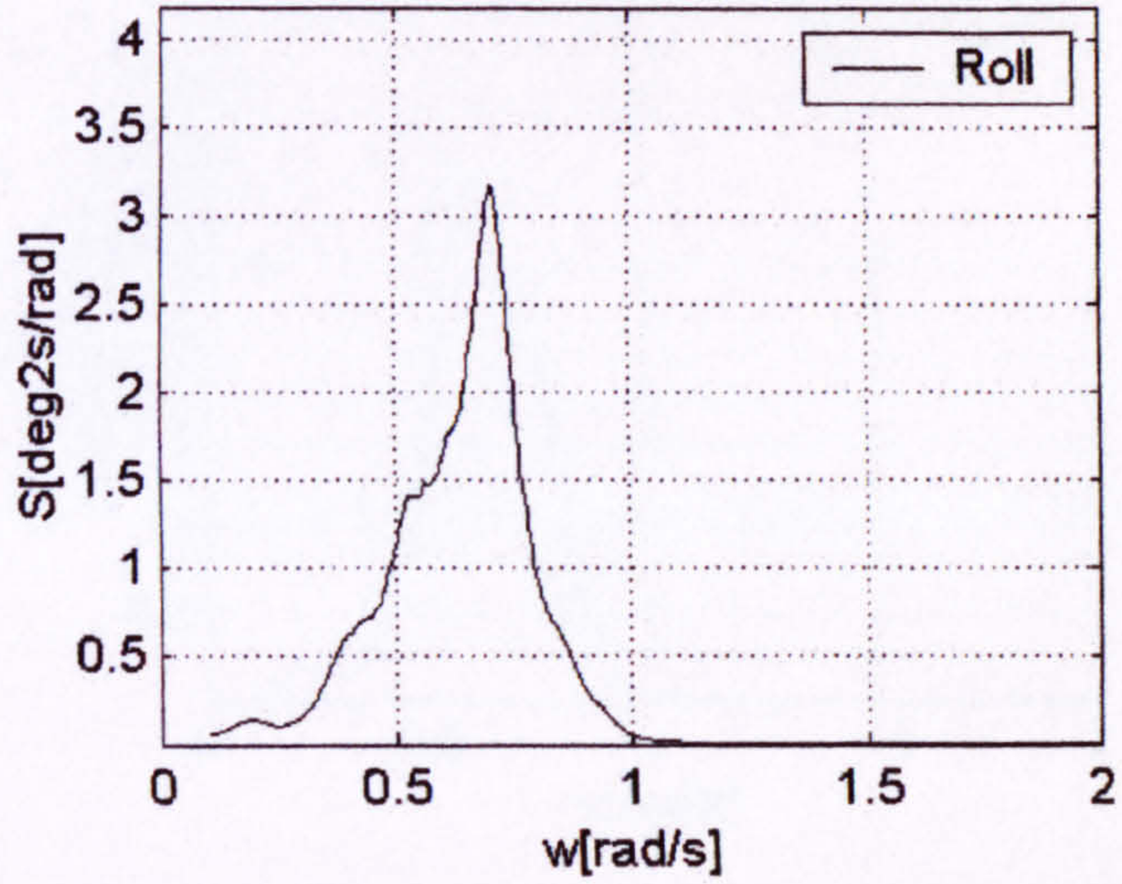

Figure 5 Experiment, Hs=4.00m

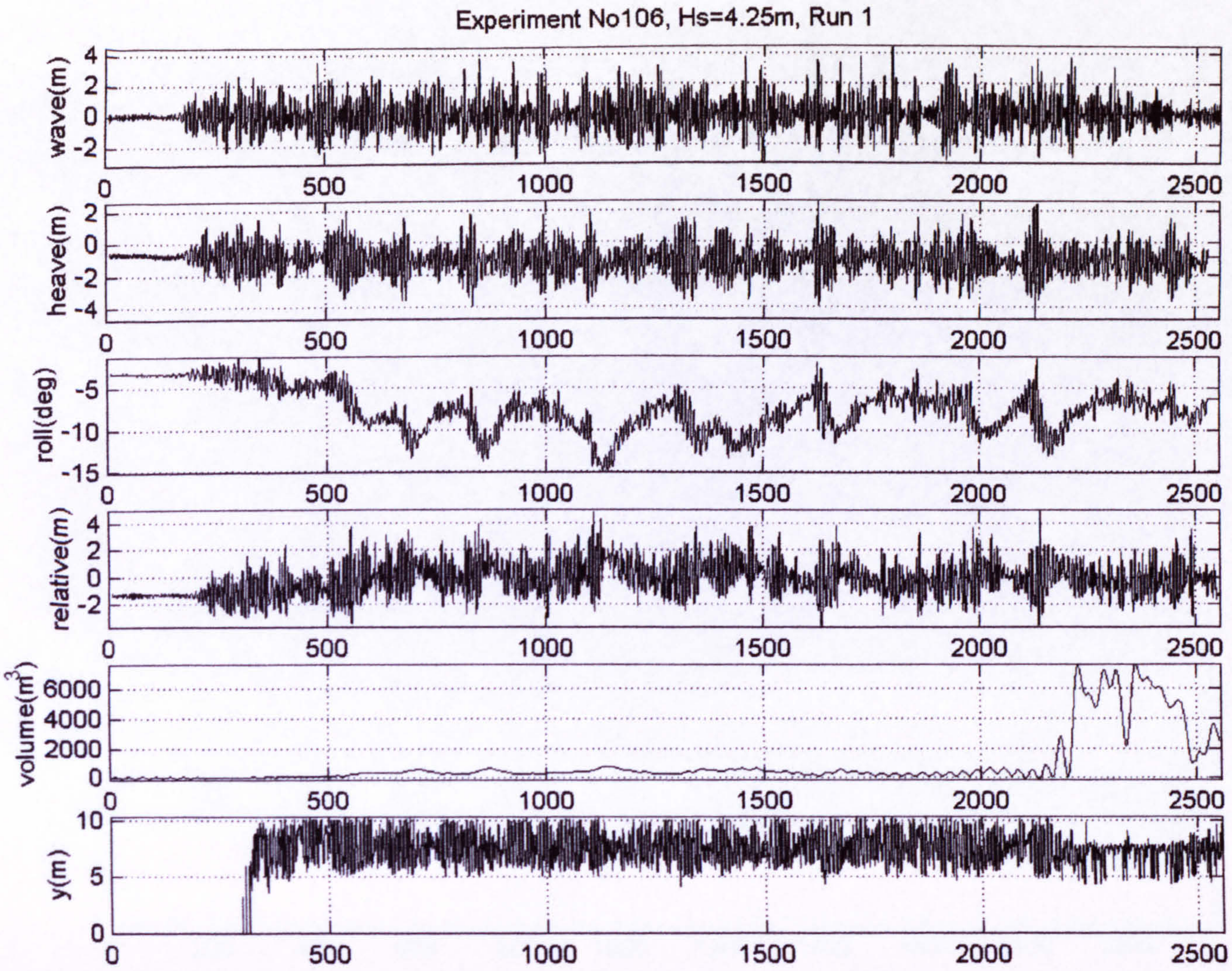

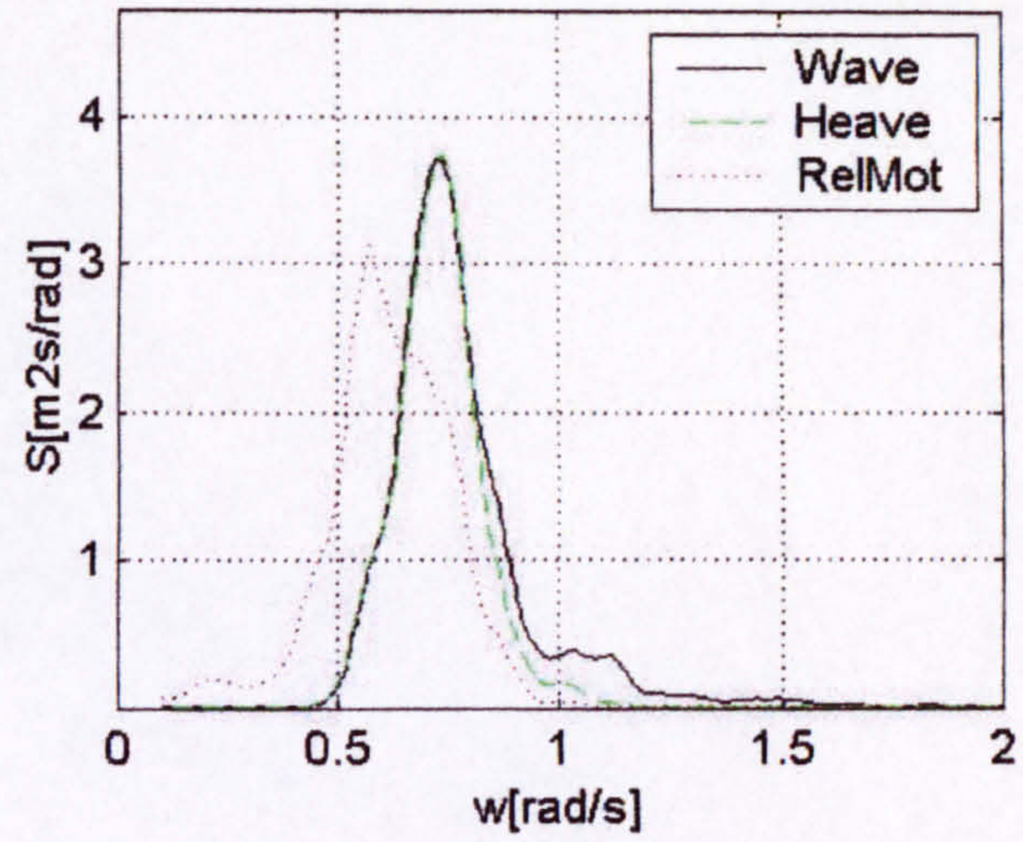

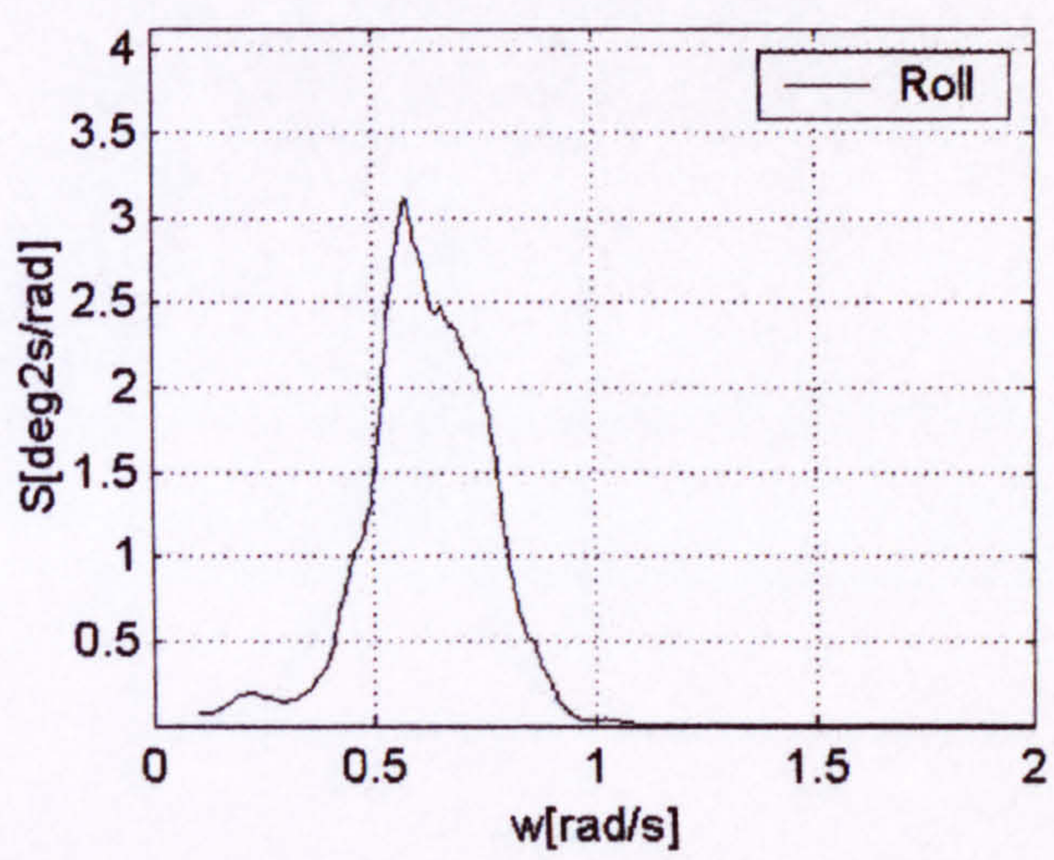

Figure 6 Experiment, Hs=4.25m

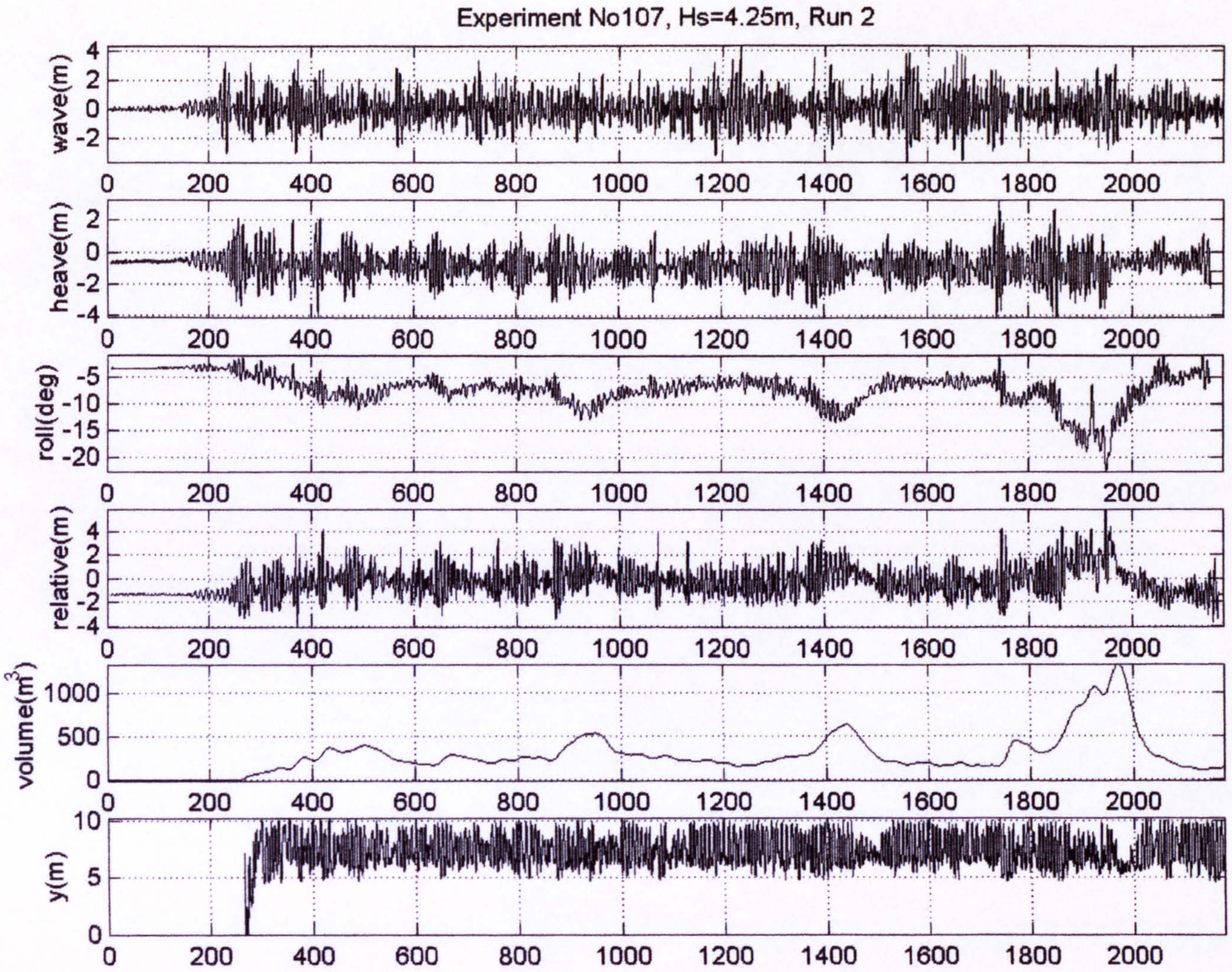

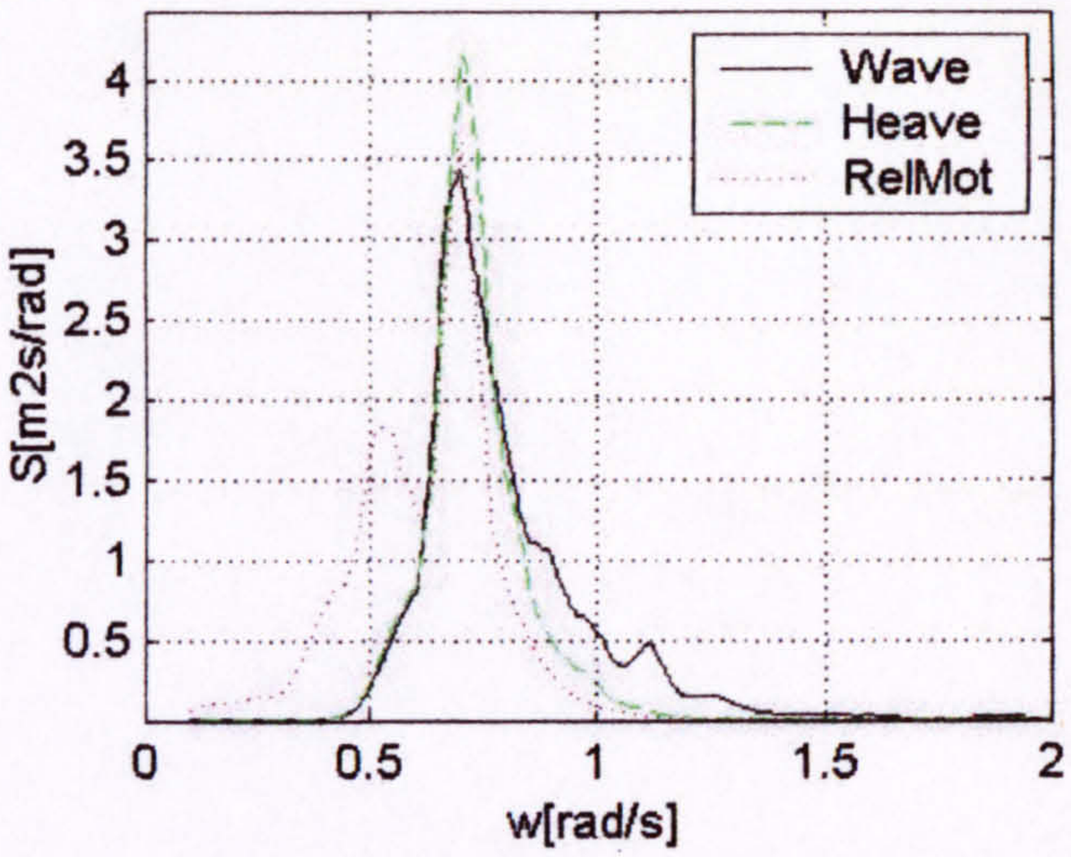

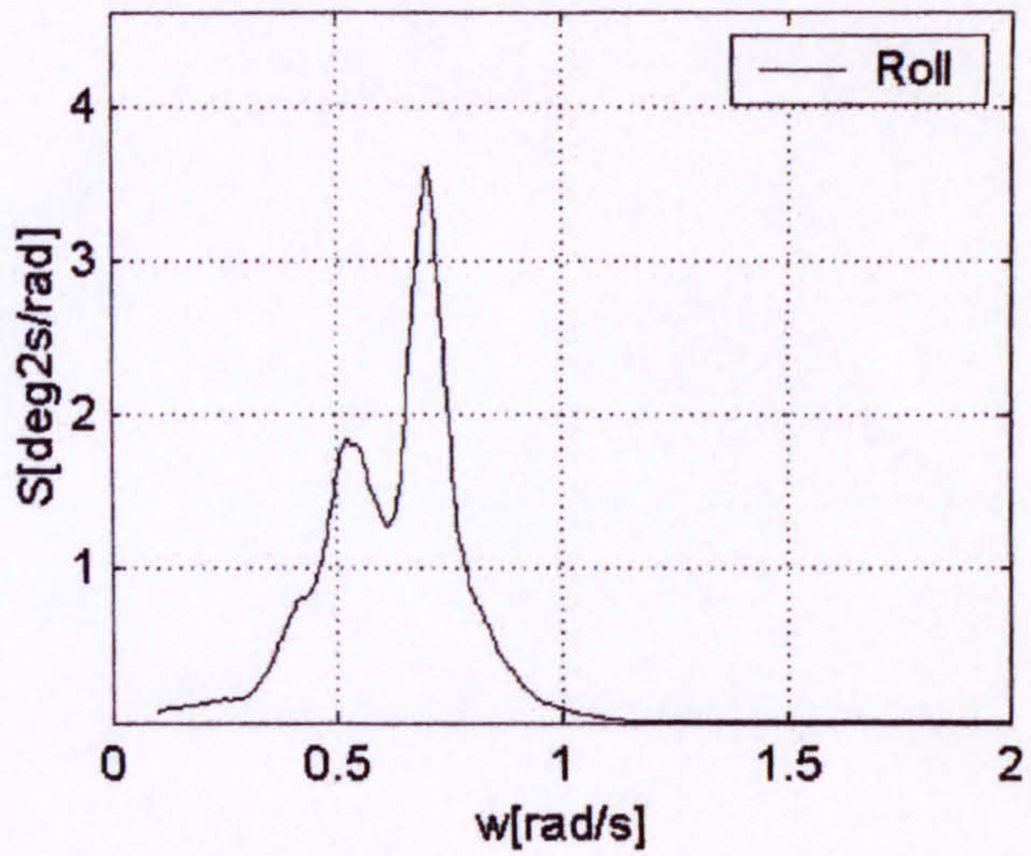

Figure 7 Experiment, Hs=4.25m

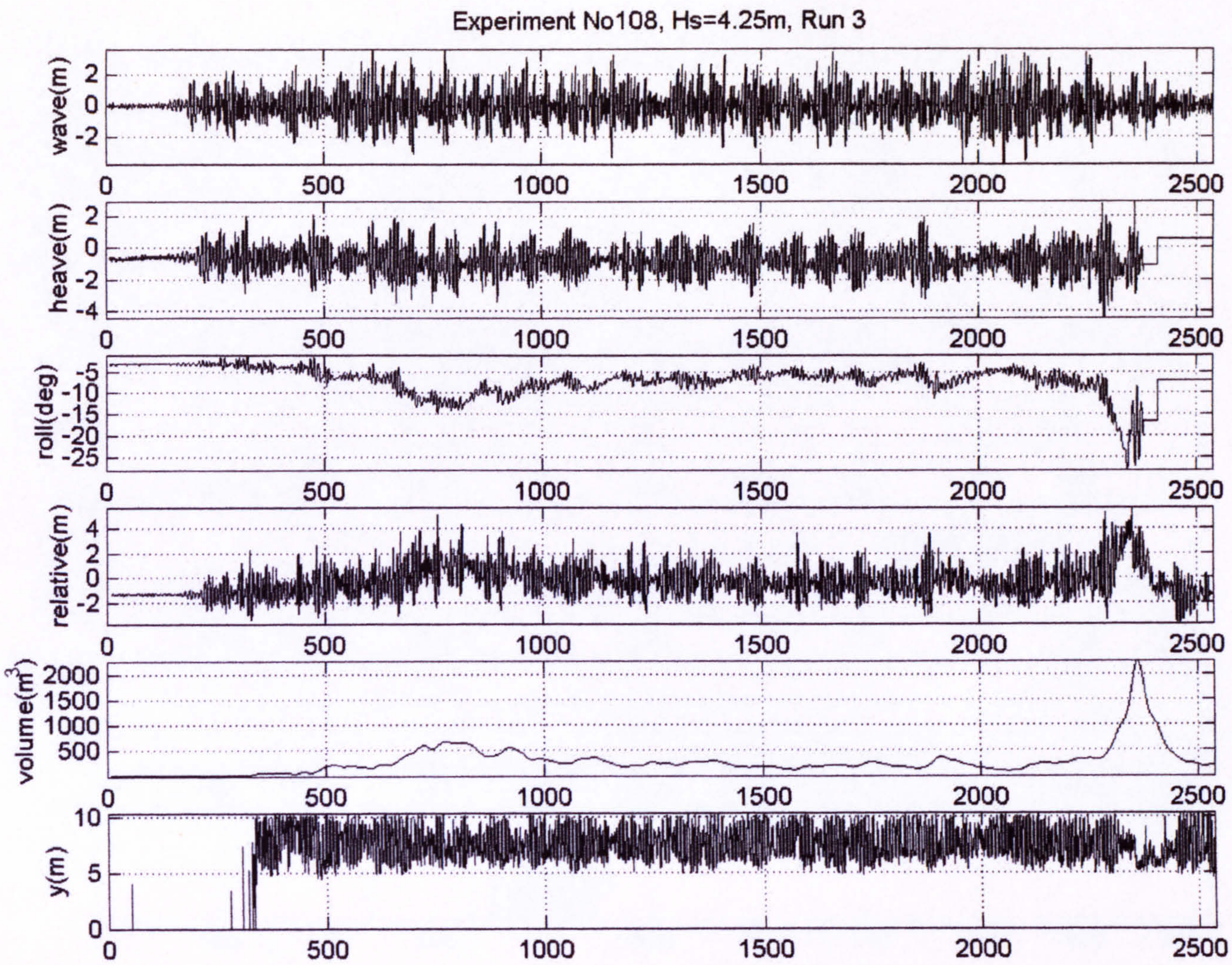

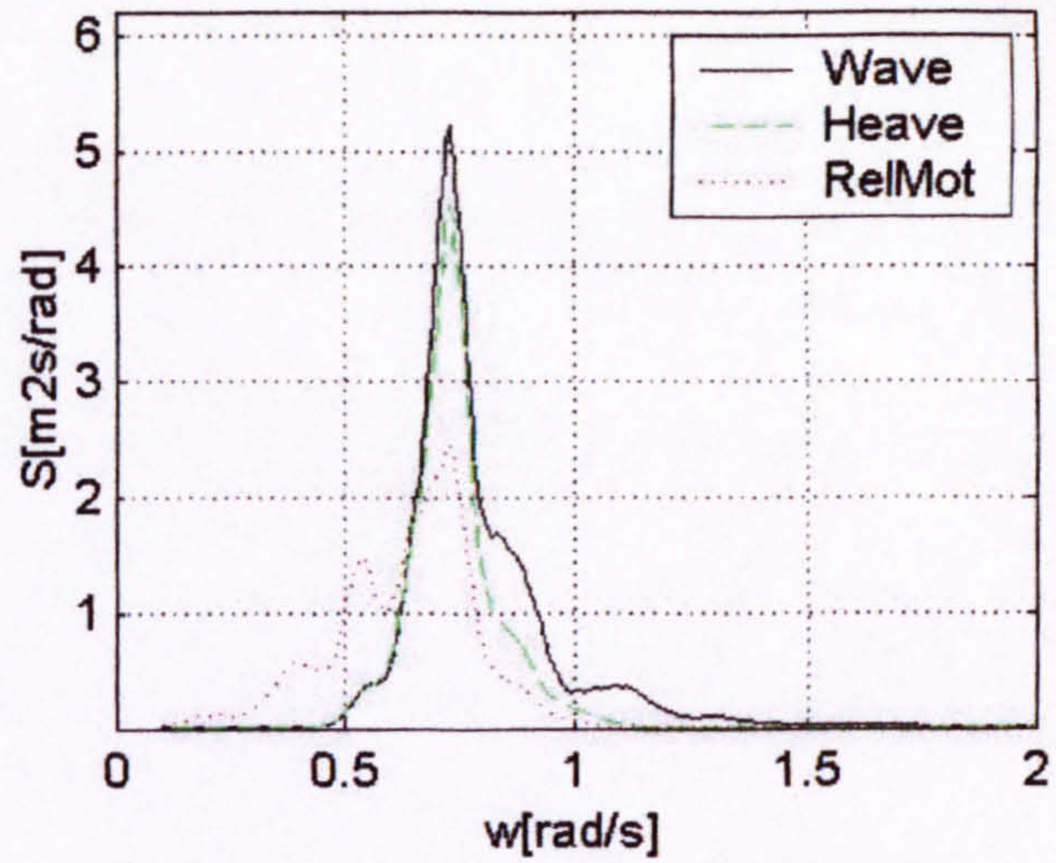

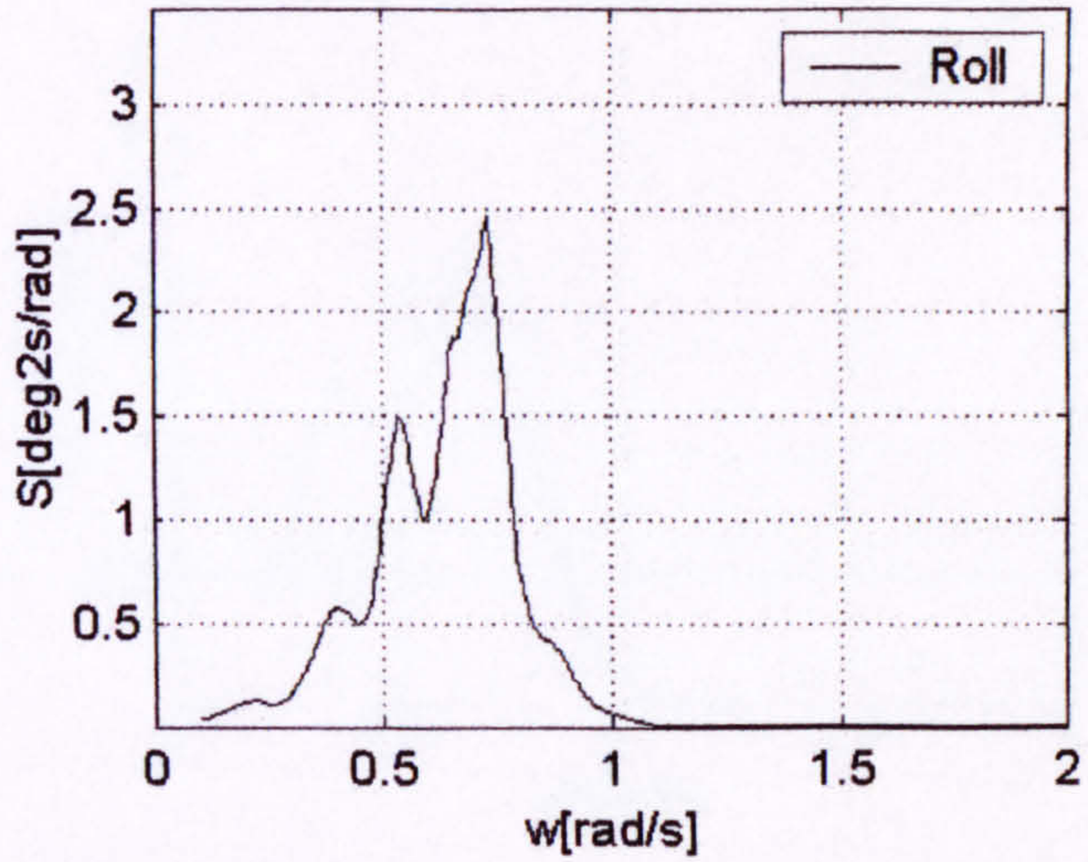

Figure 8 Experiment, Hs=4.25m

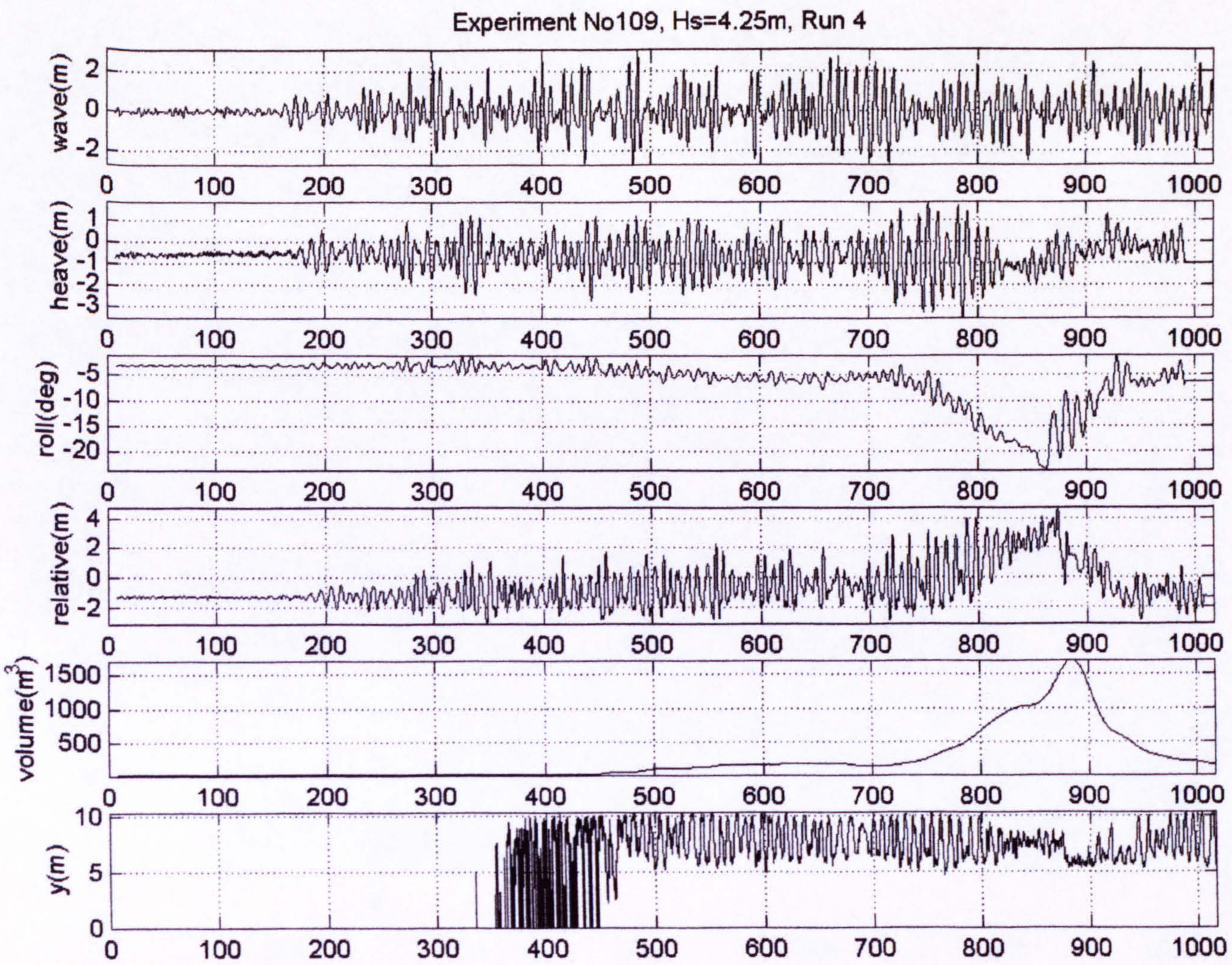

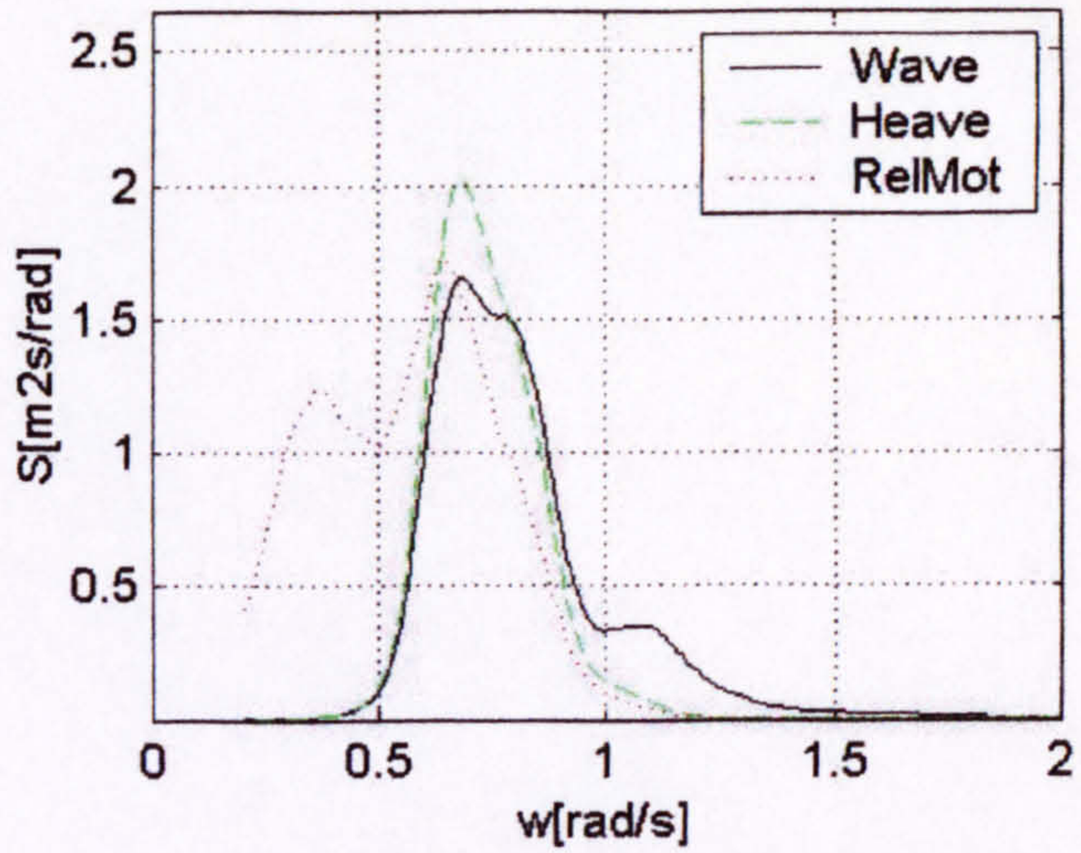

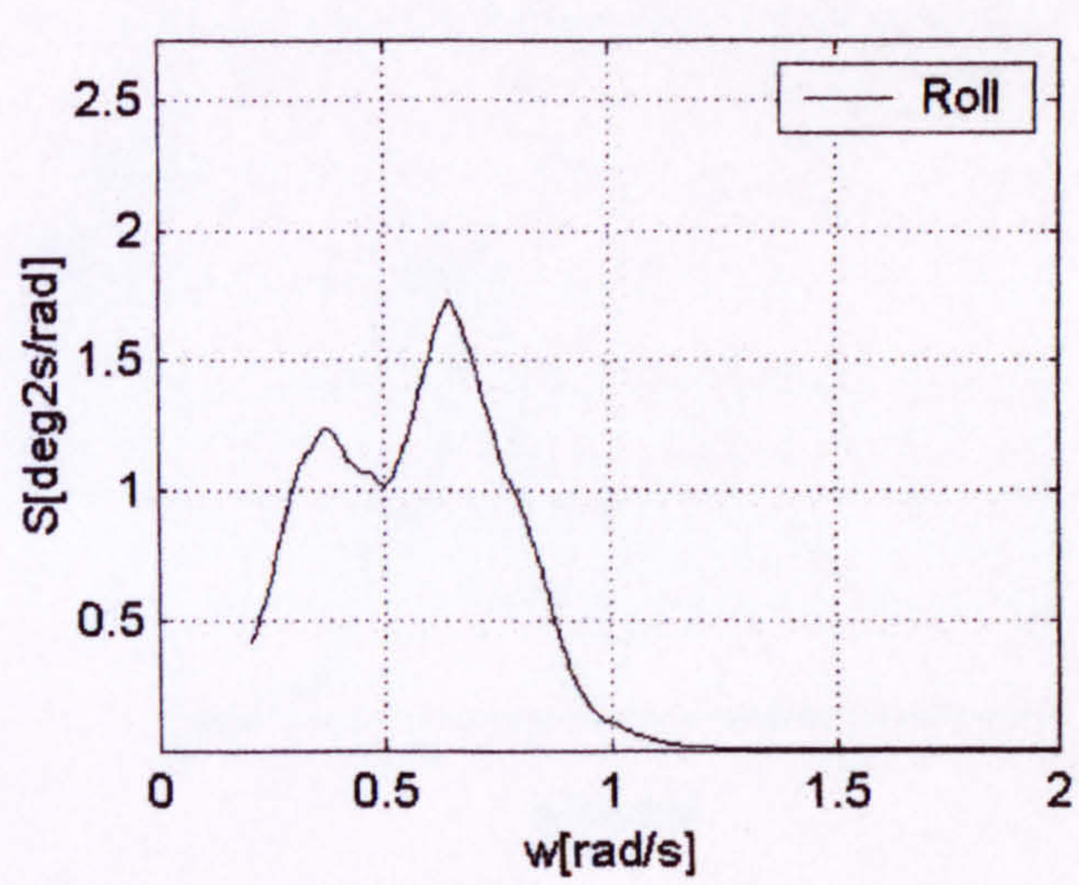

Figure 9 Experiment, Hs=4.25m

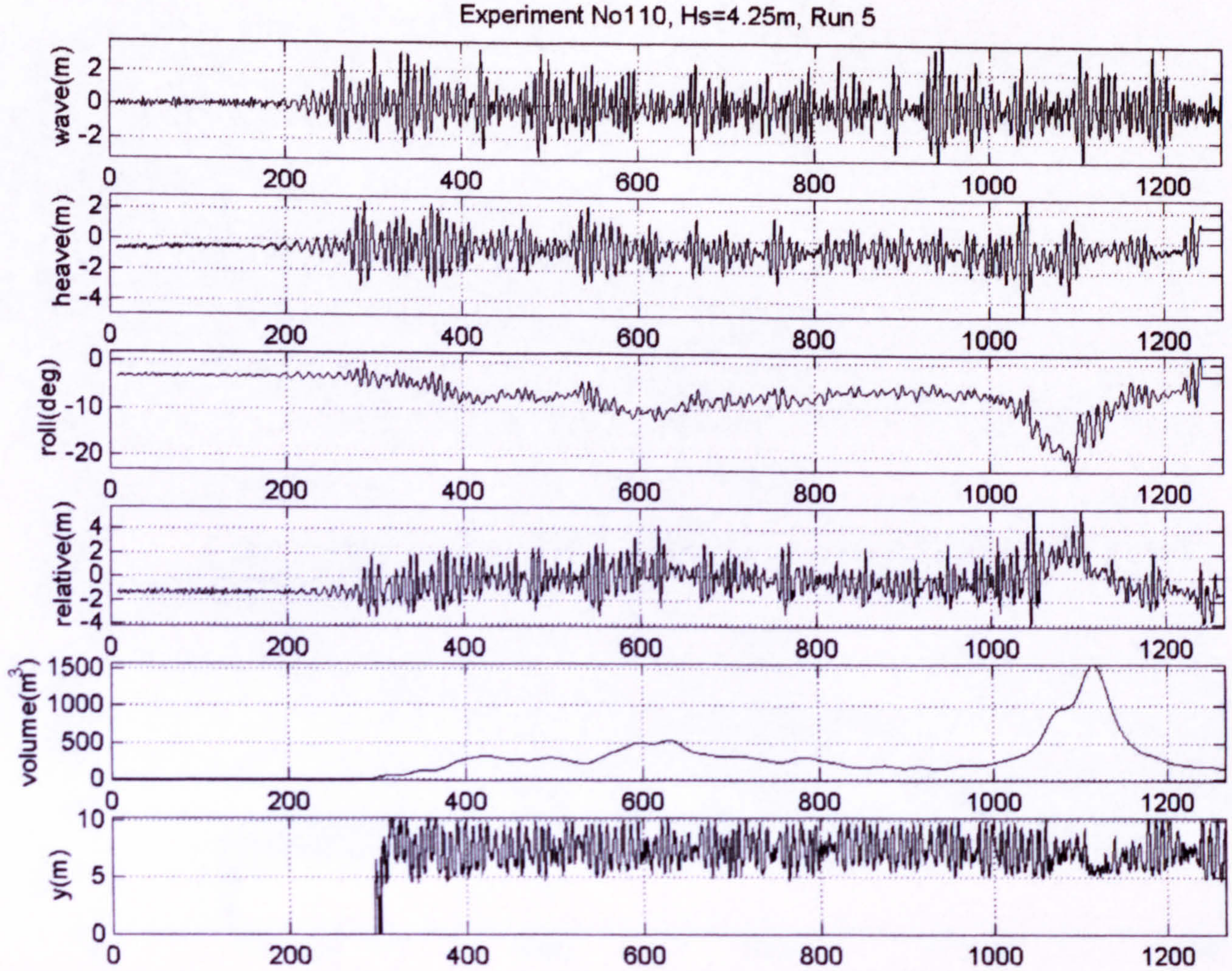

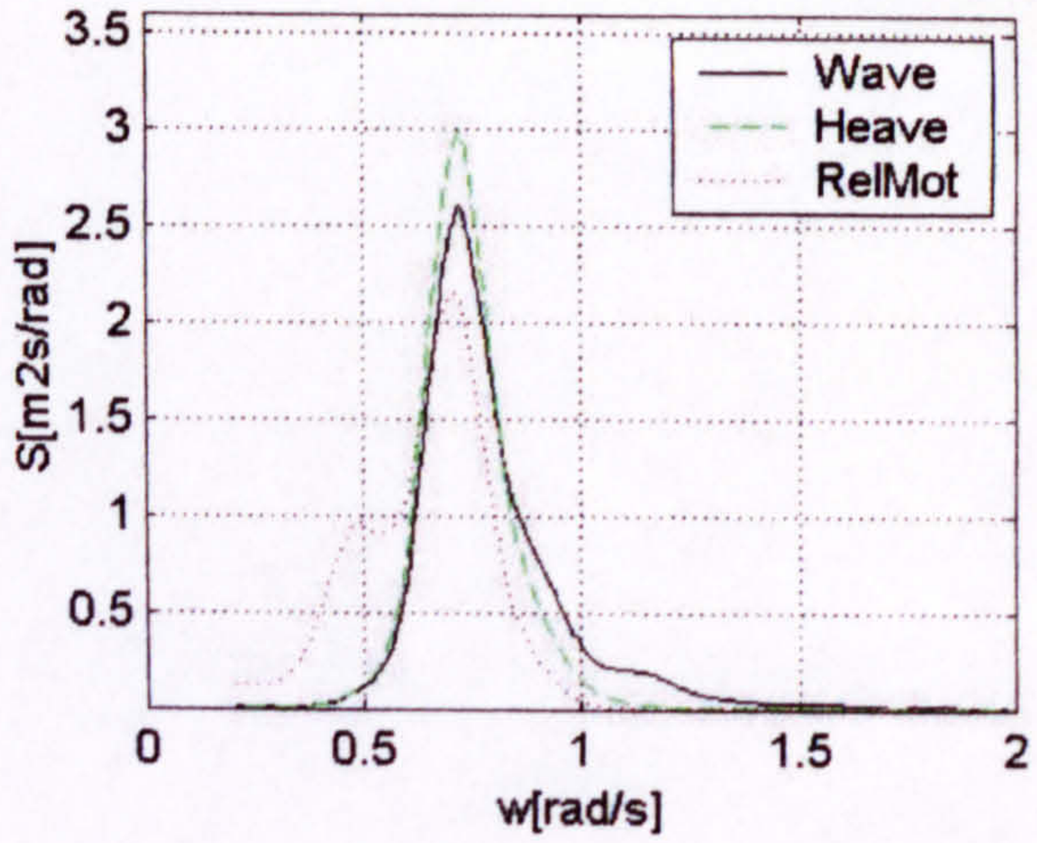

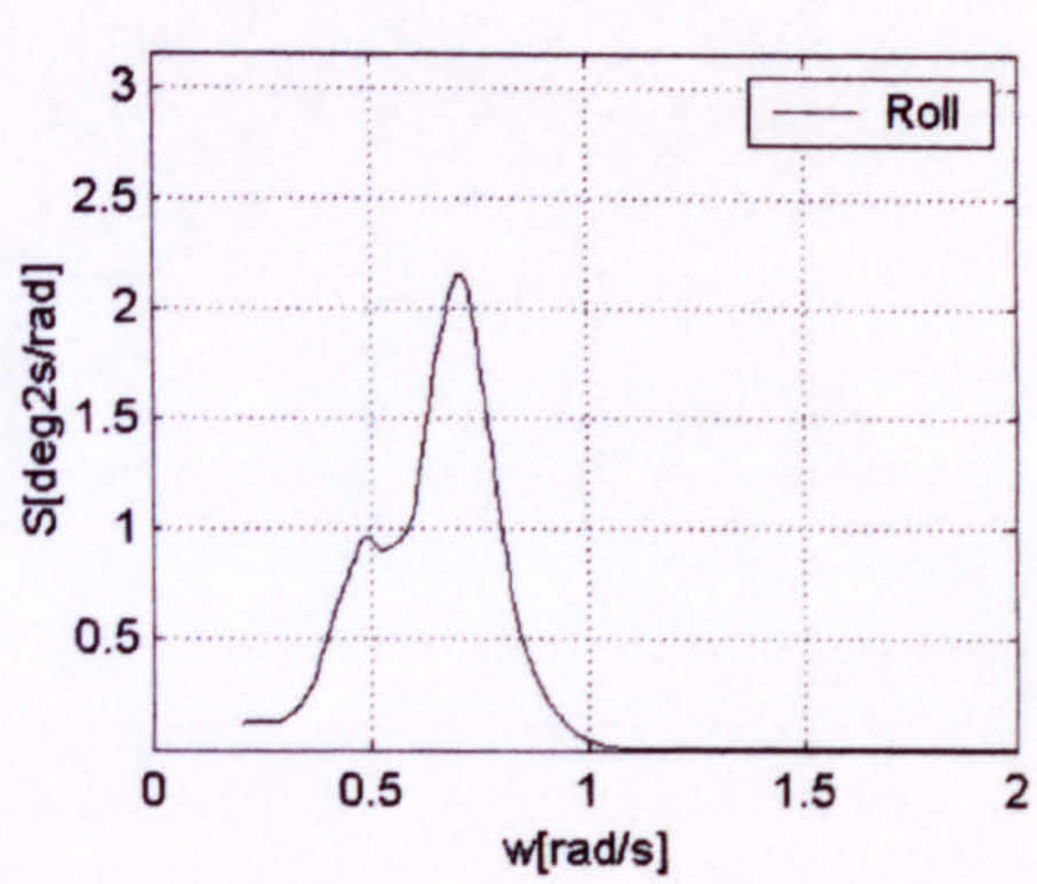

Figure 10 Experiment, Hs=4.25m

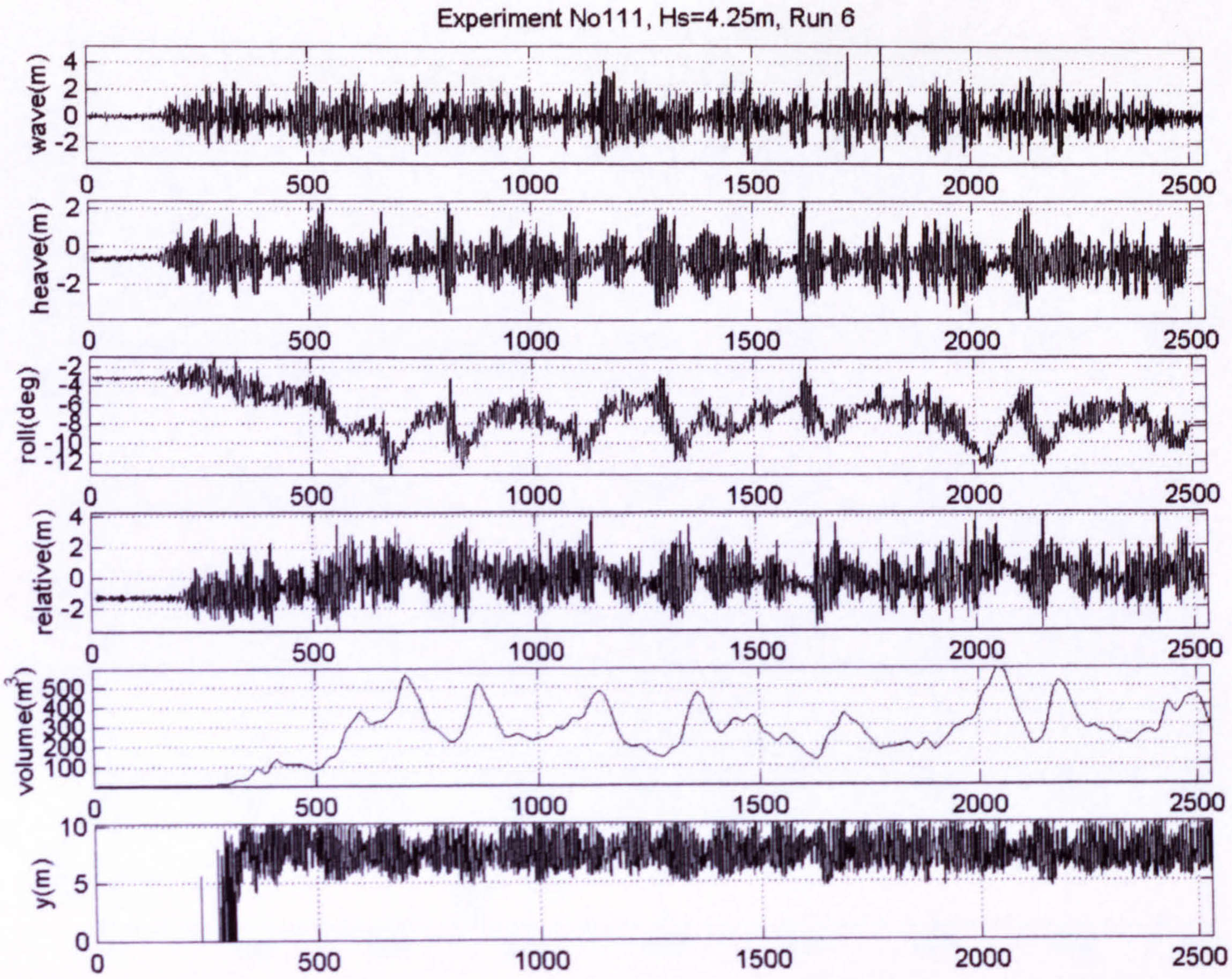

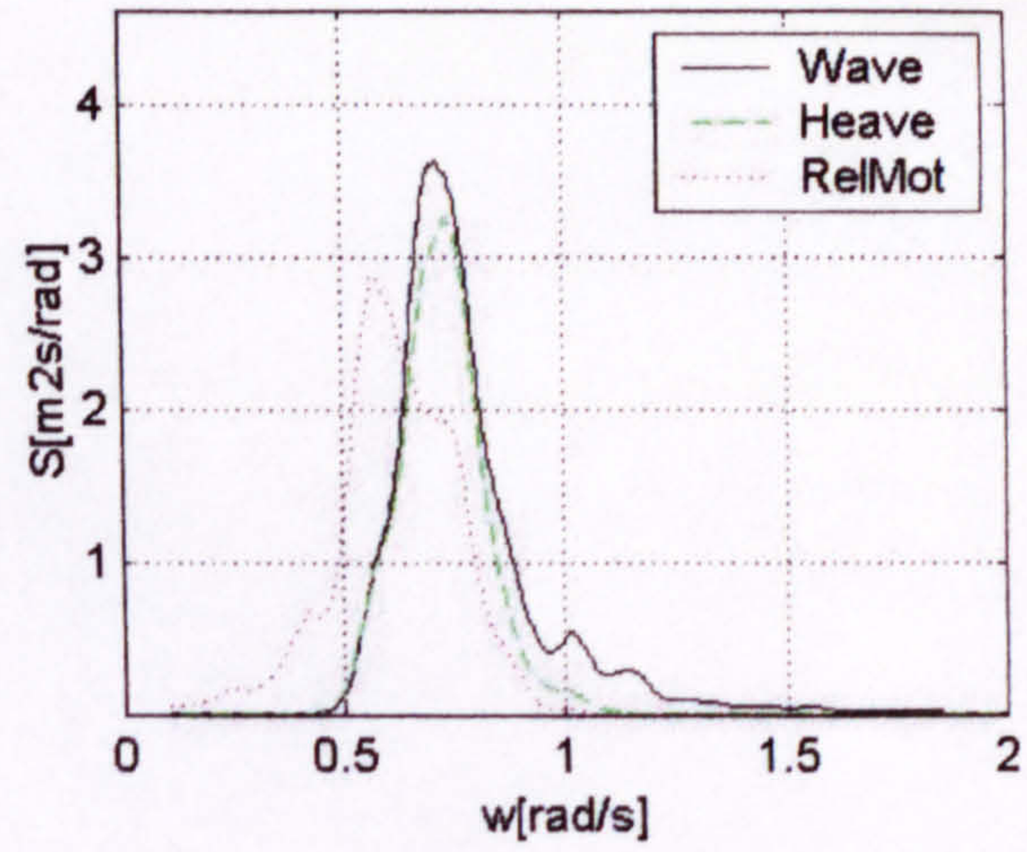

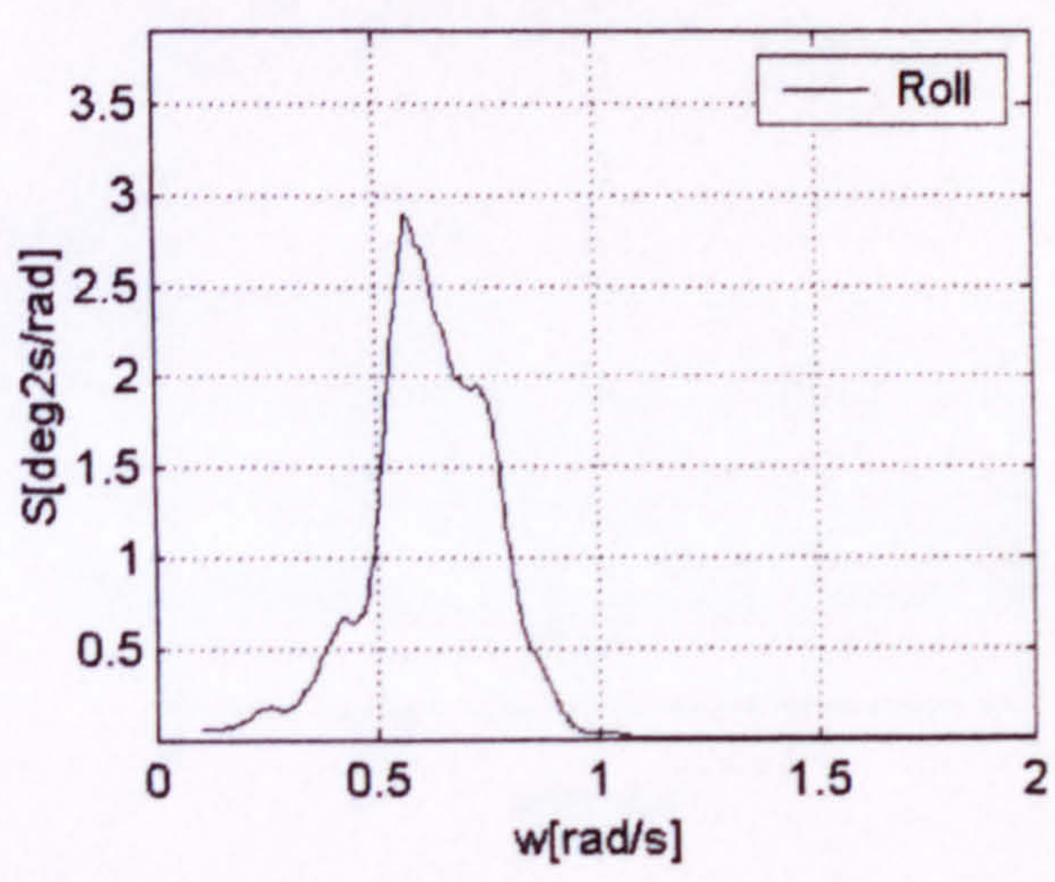

Figure 11 Experiment, Hs=4.25m

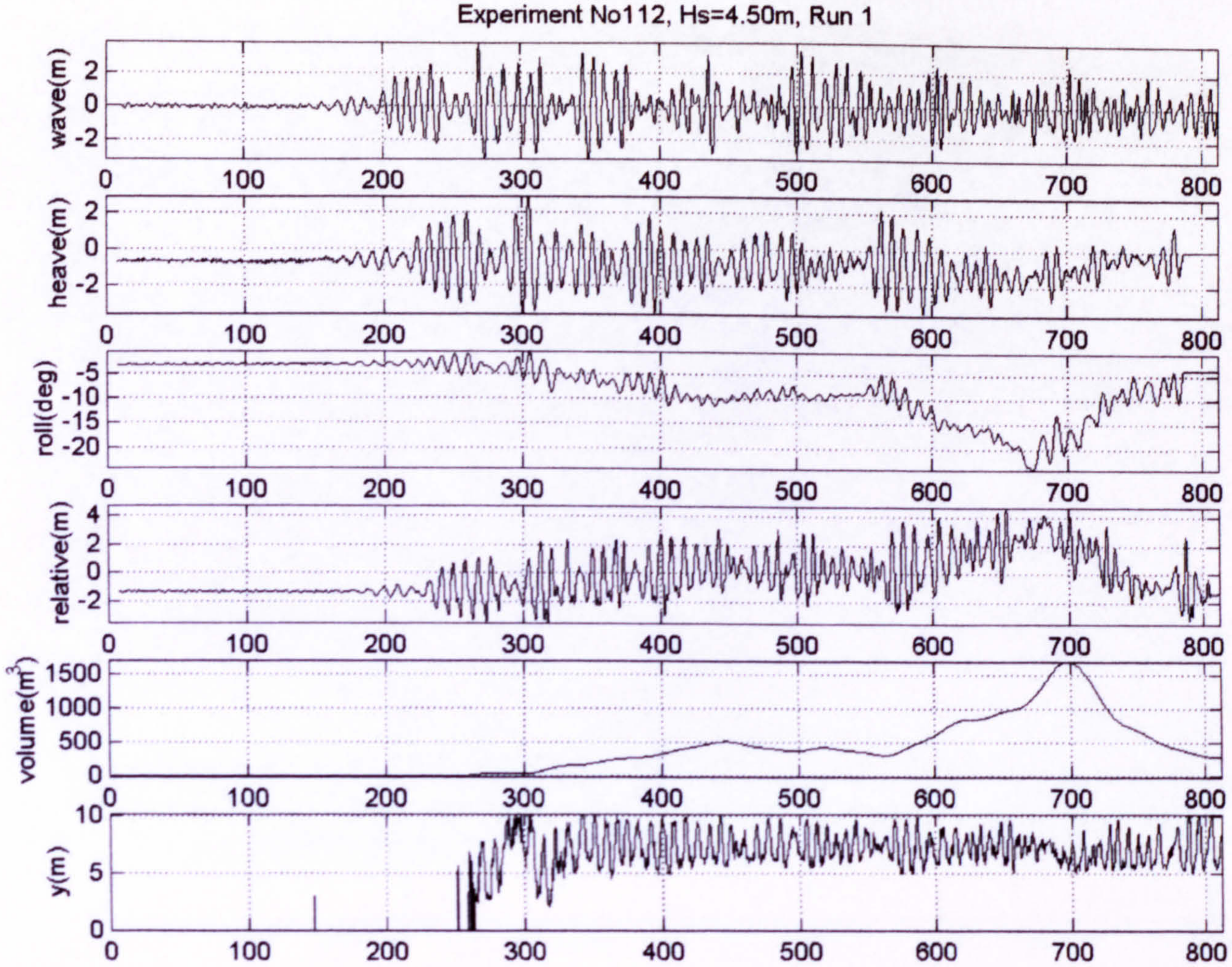

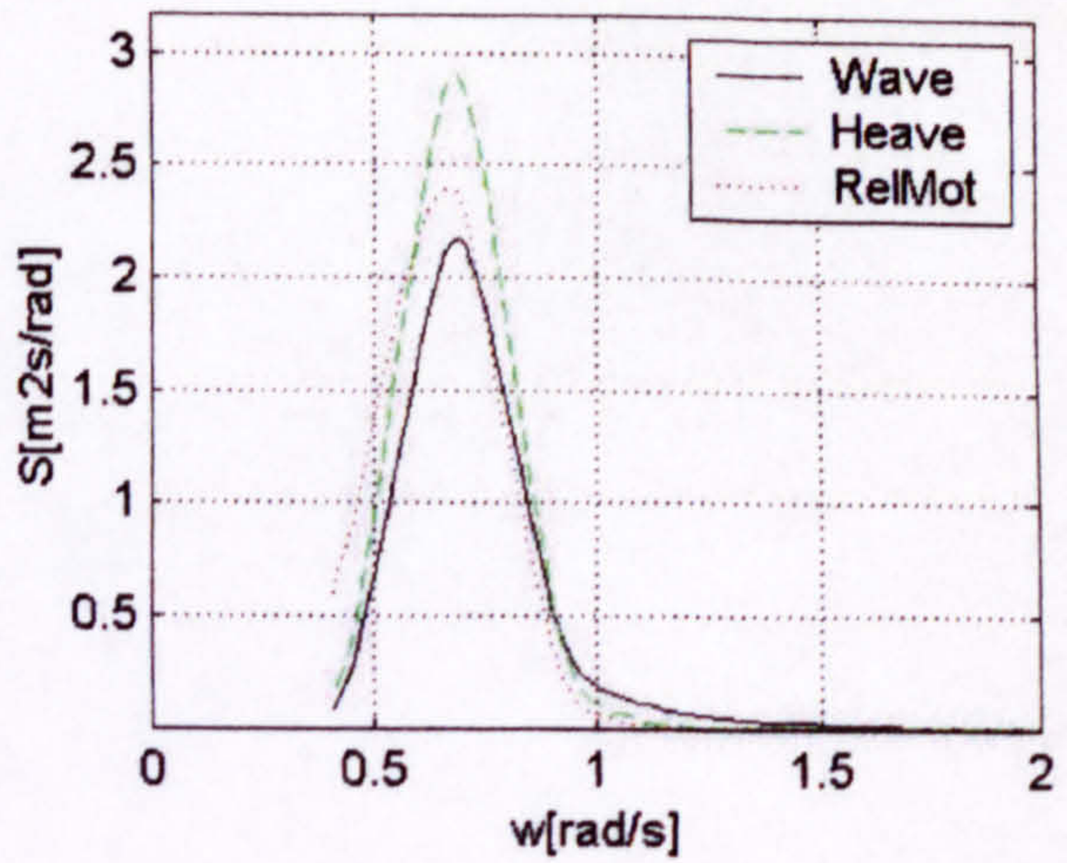

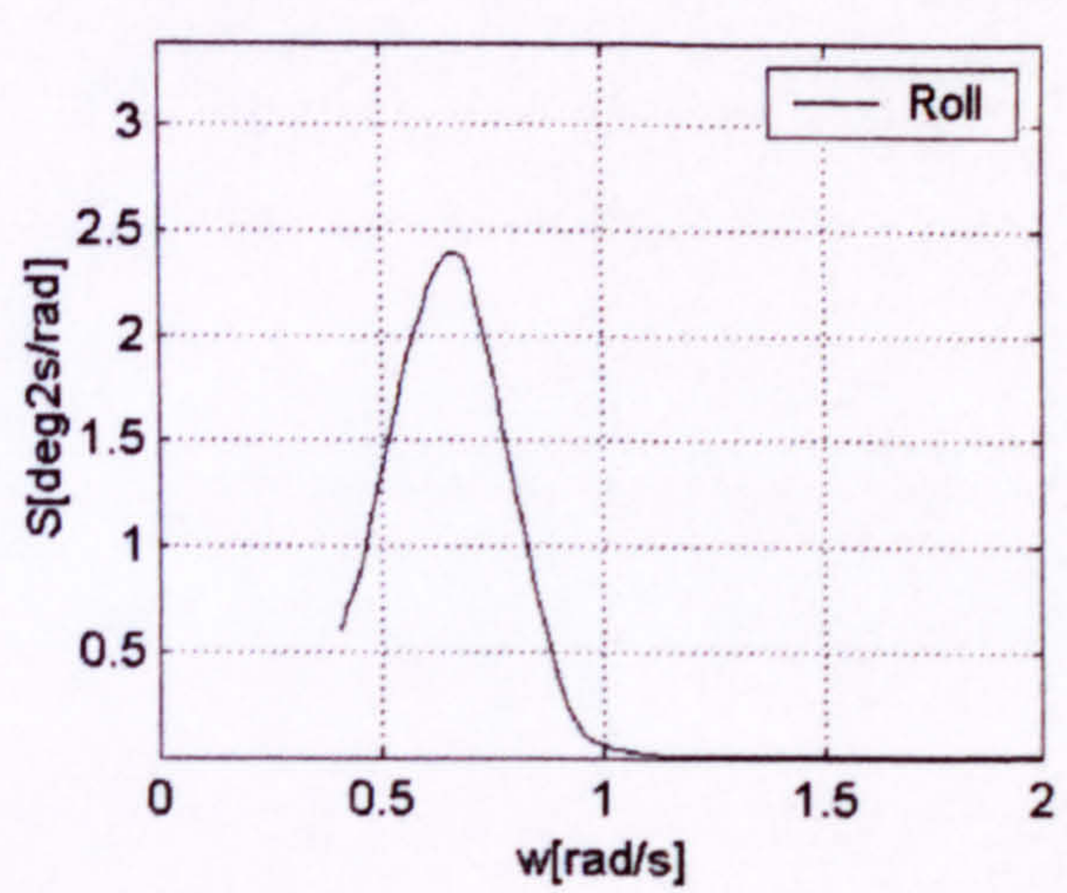

Figure 12 Experiment, Hs=4.50m

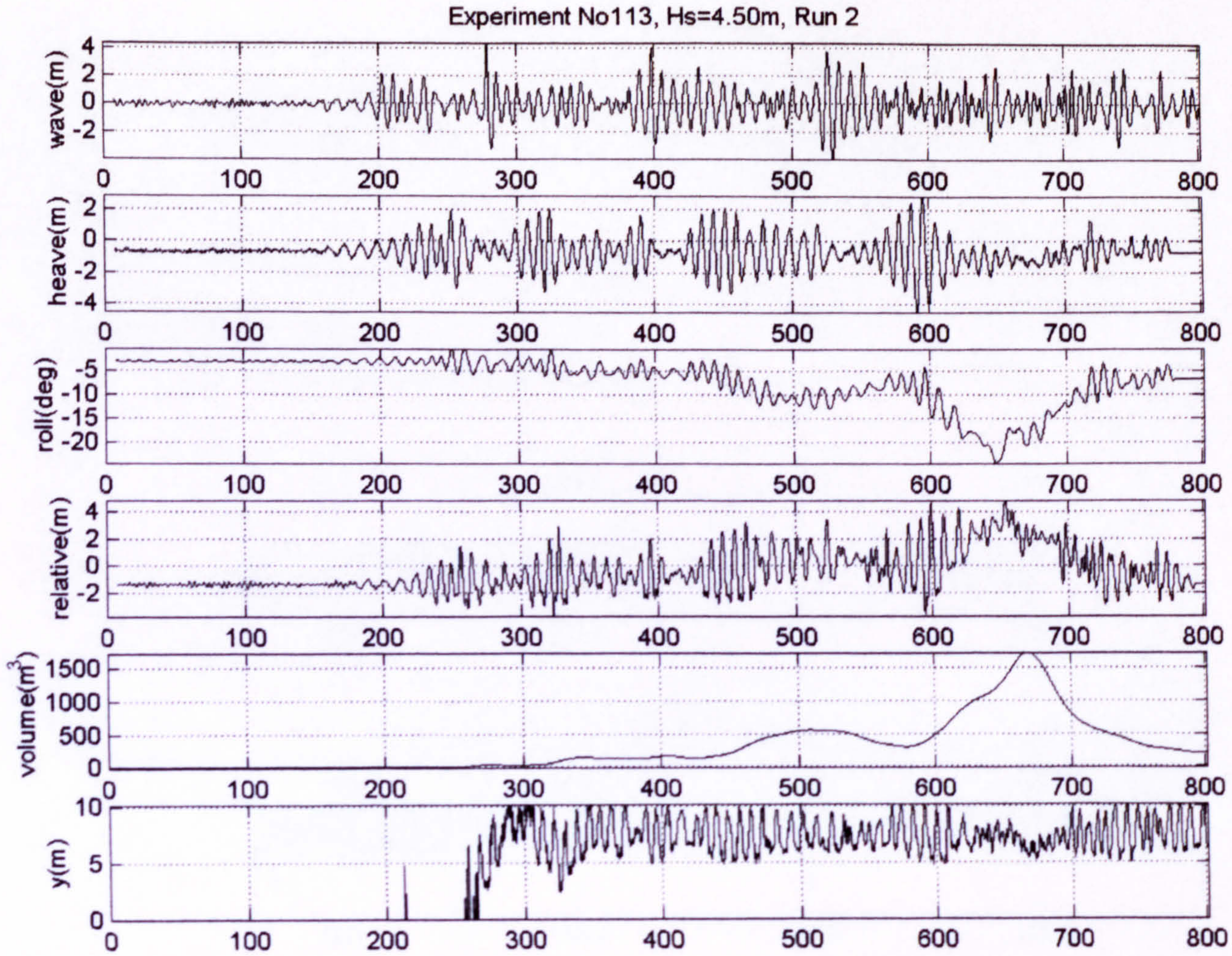

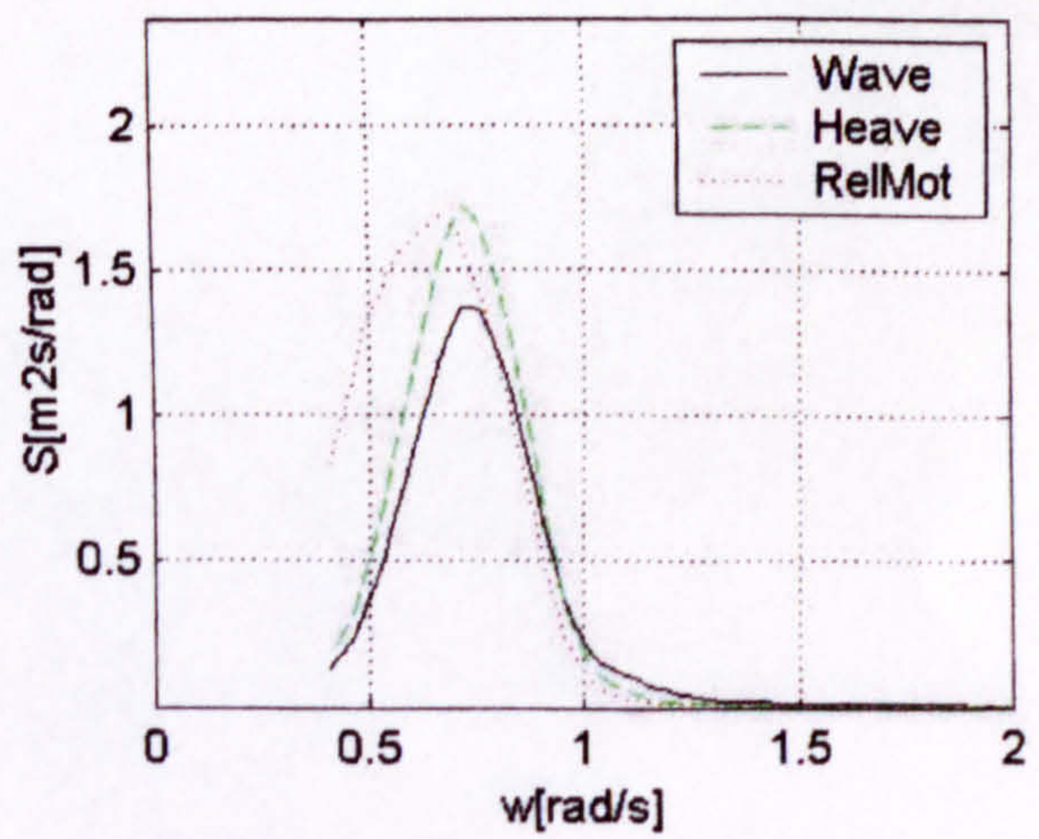

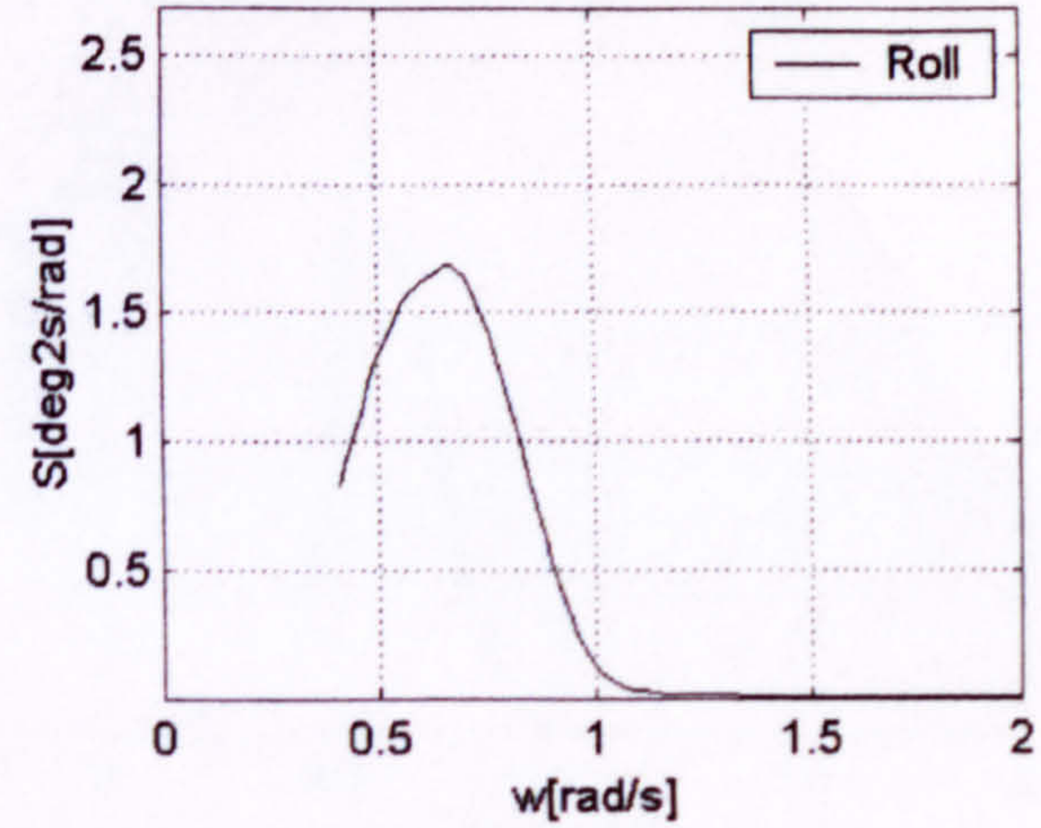

Figure 13 Experiment, Hs=4.50m

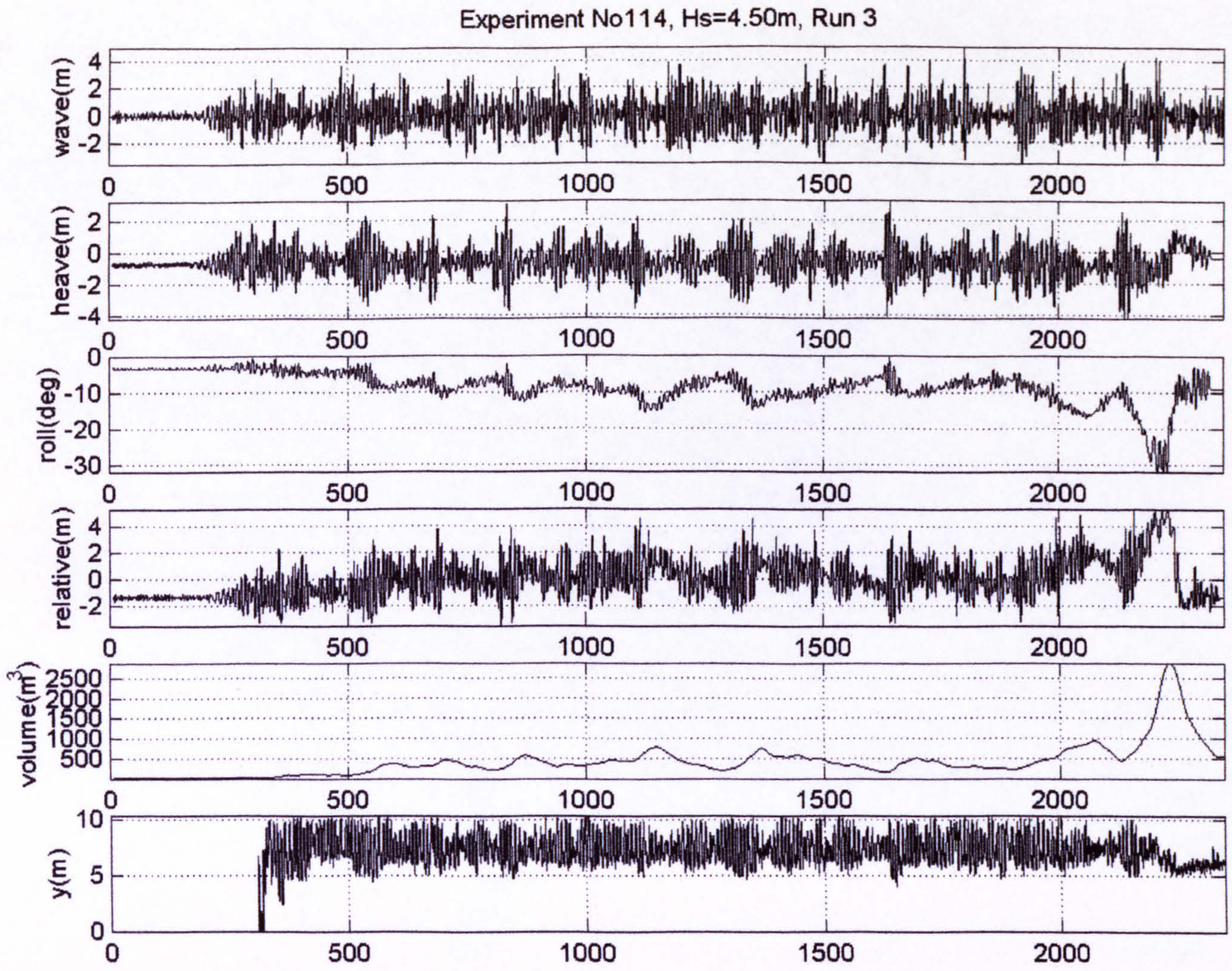

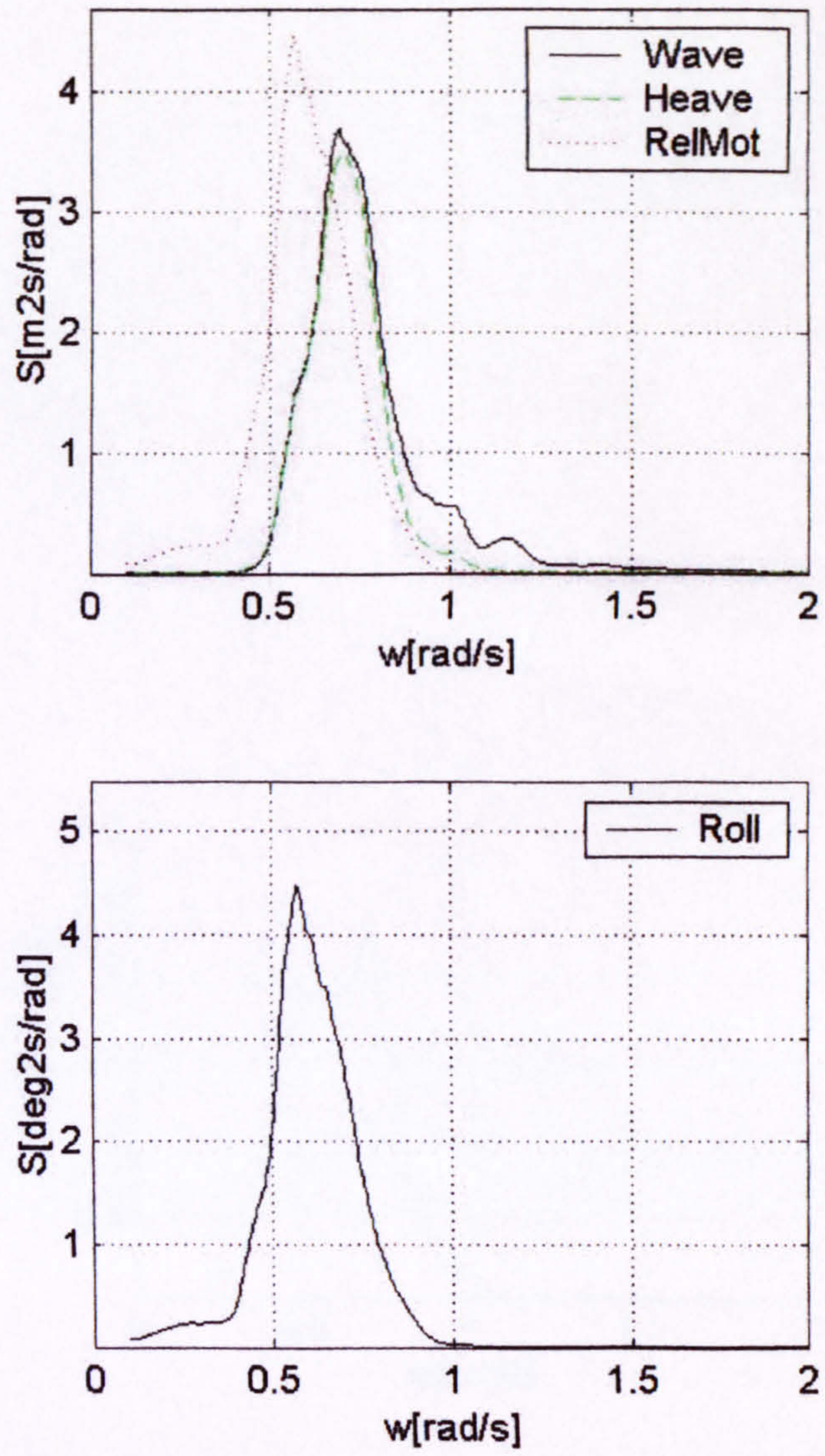

Figure 14 Experiment, Hs=4.50m

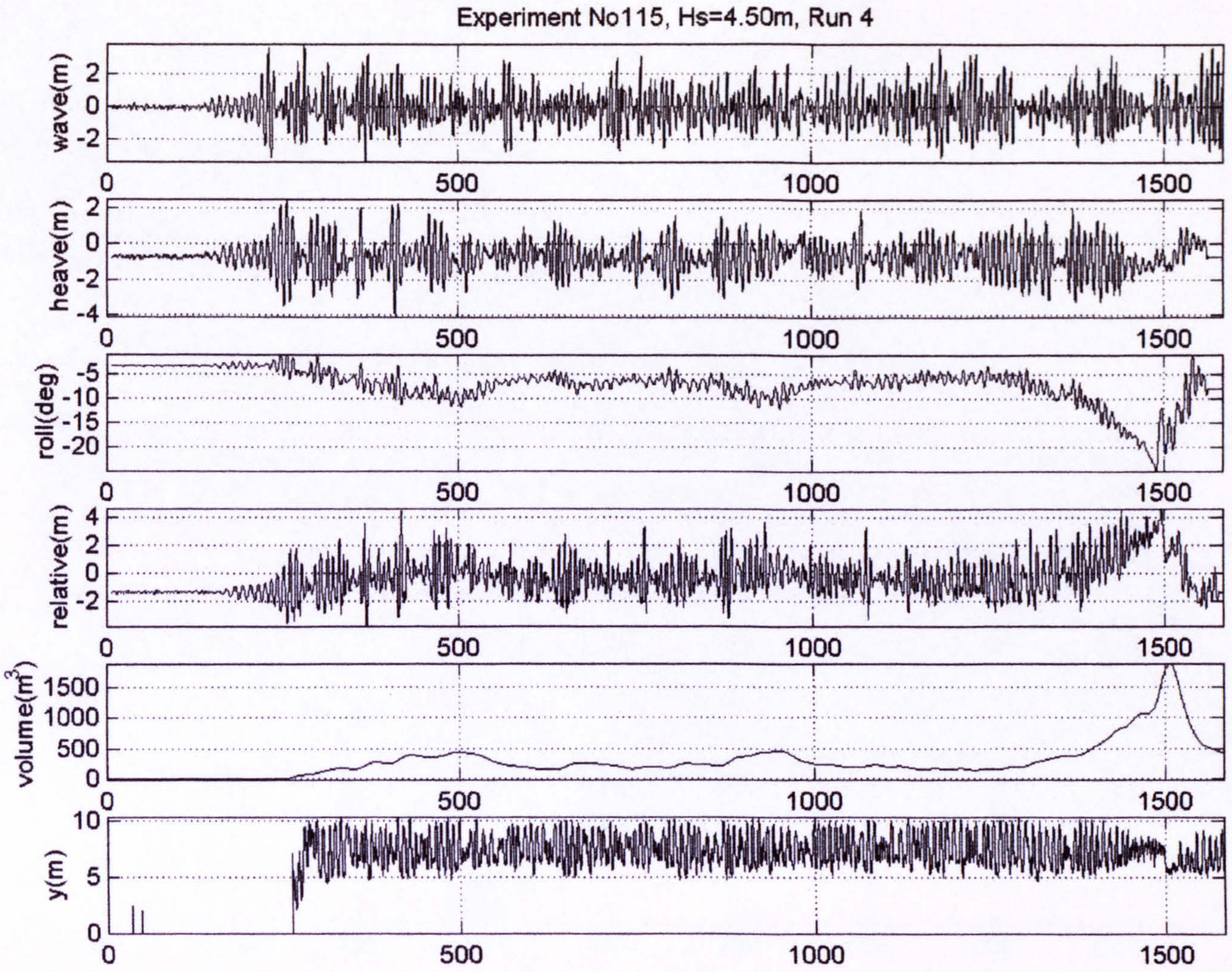

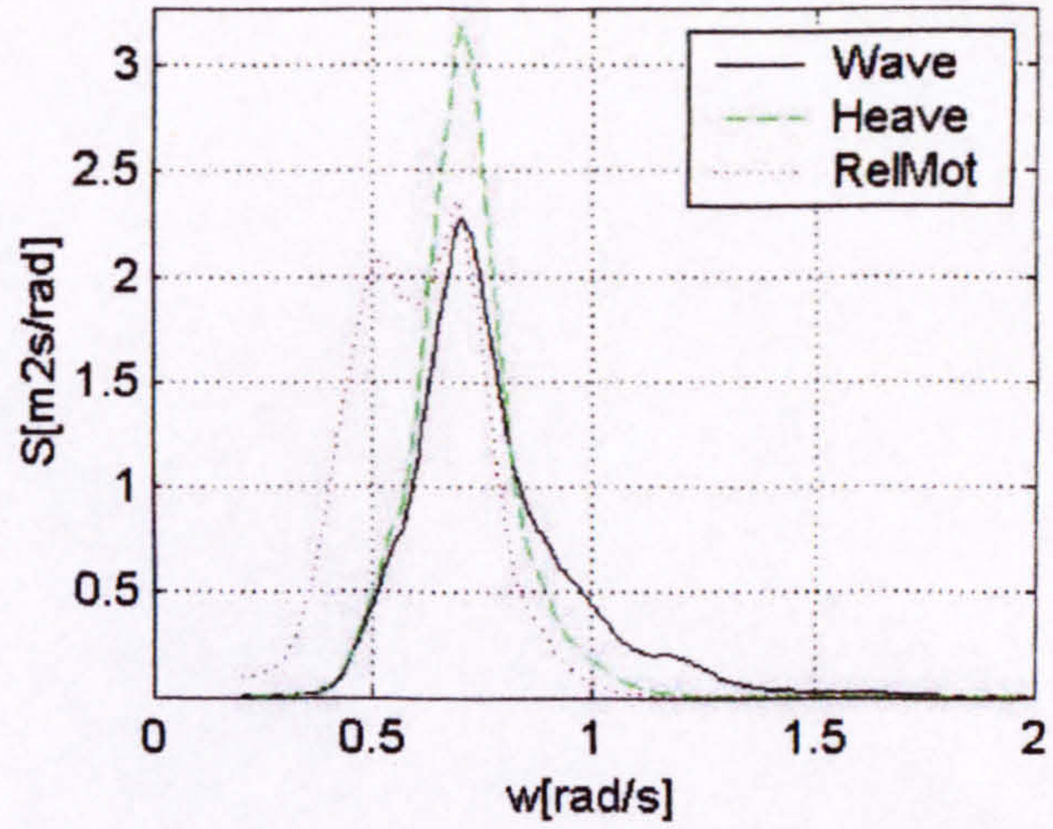

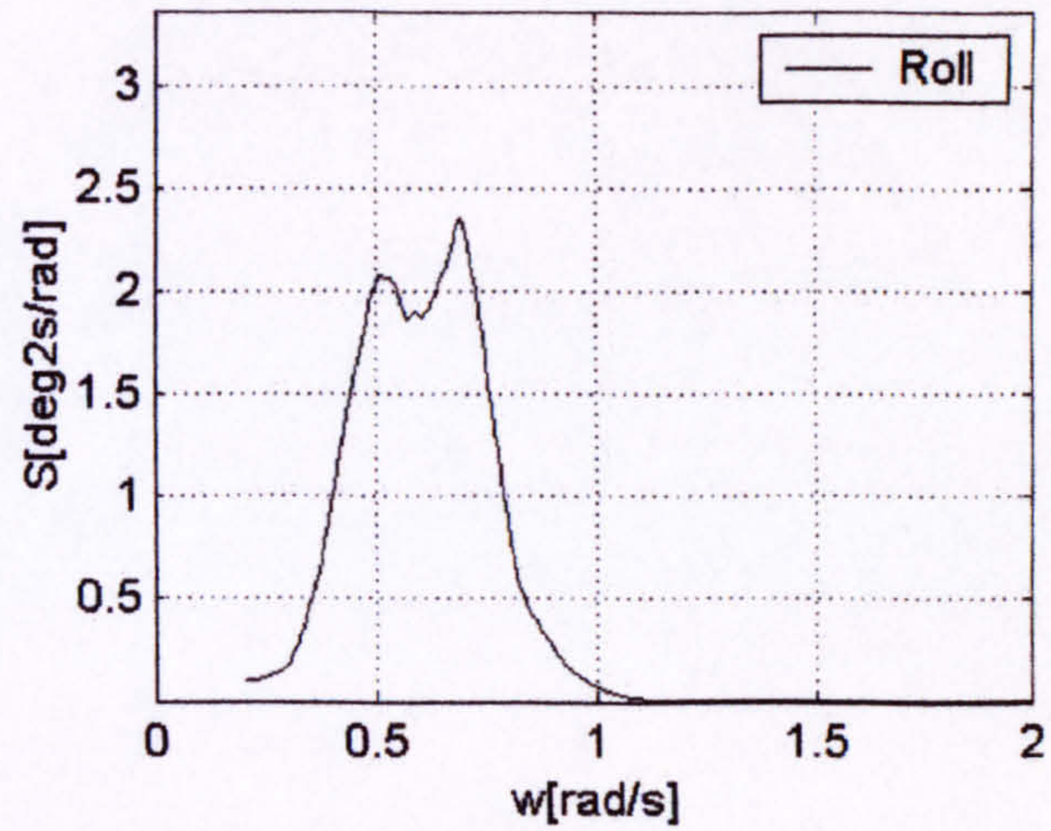

Figure 15 Experiment, Hs=4.50m

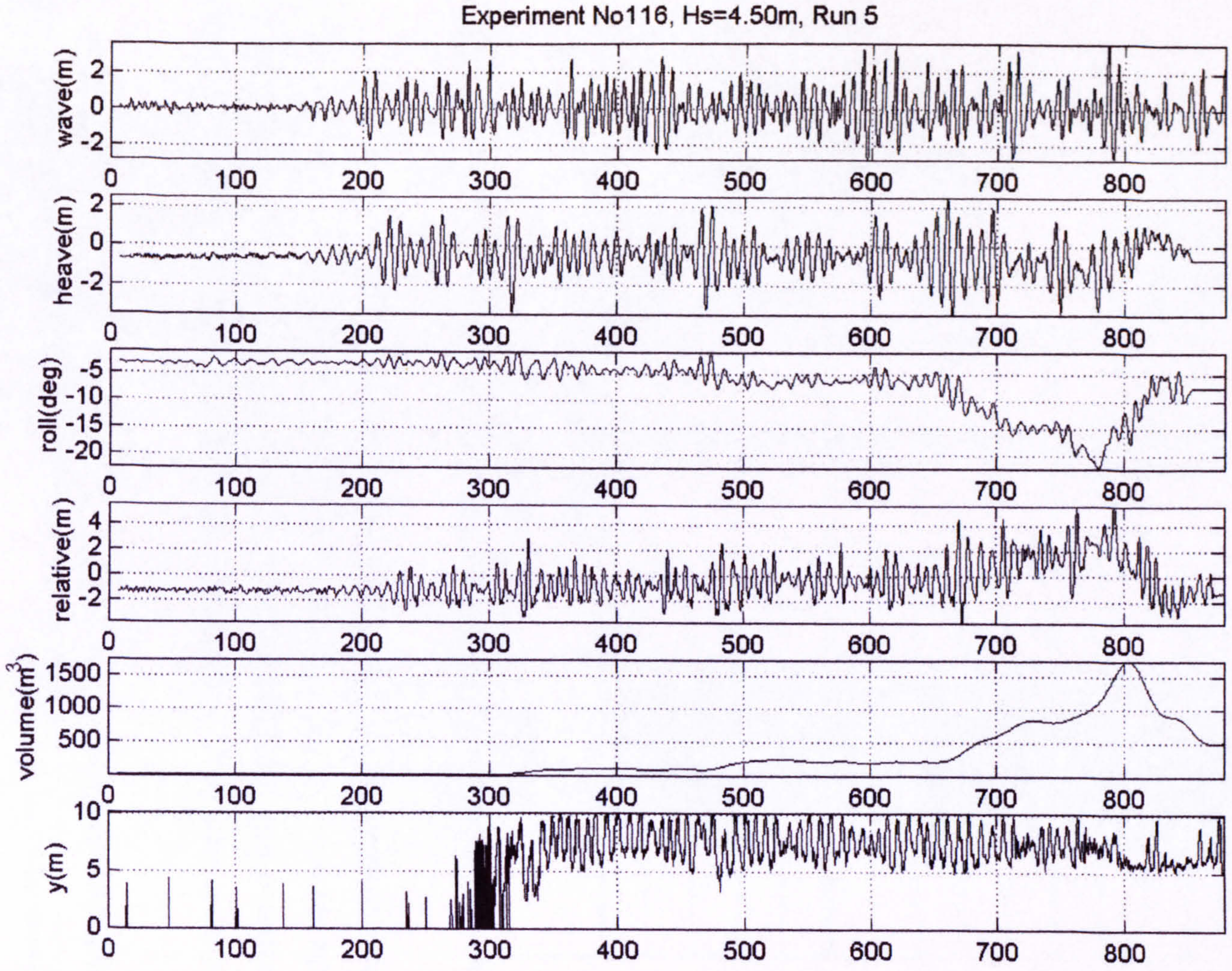

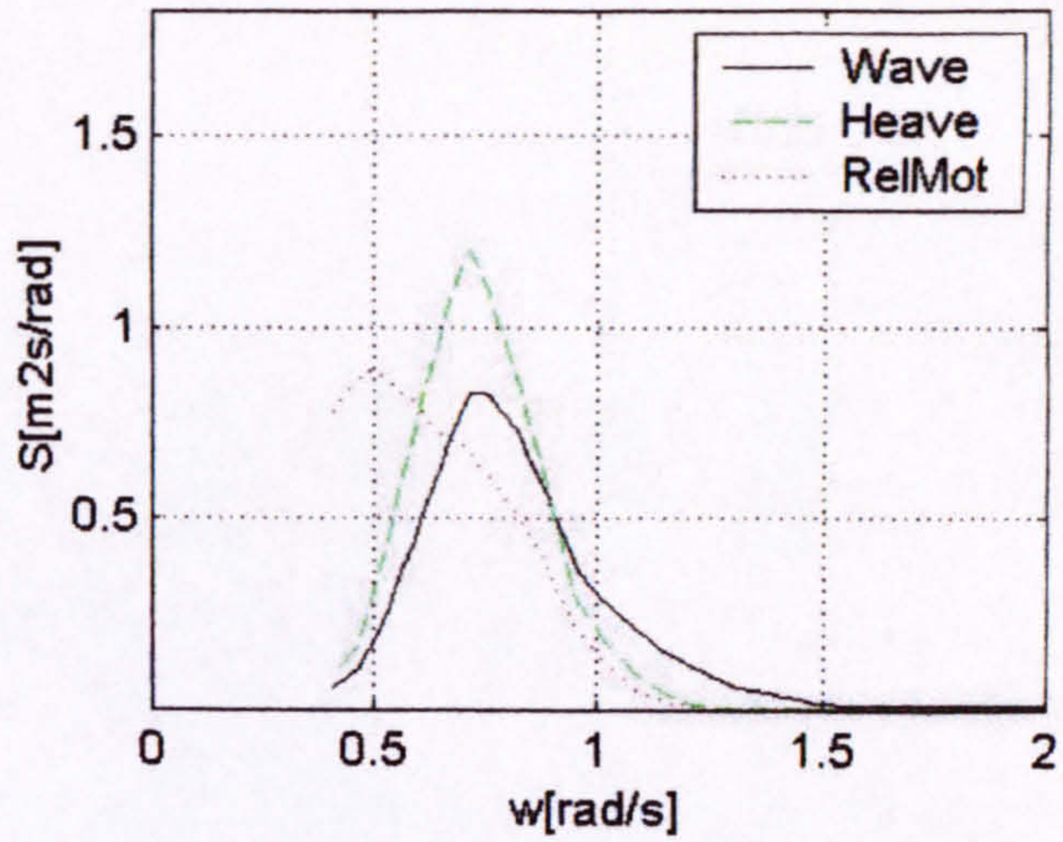

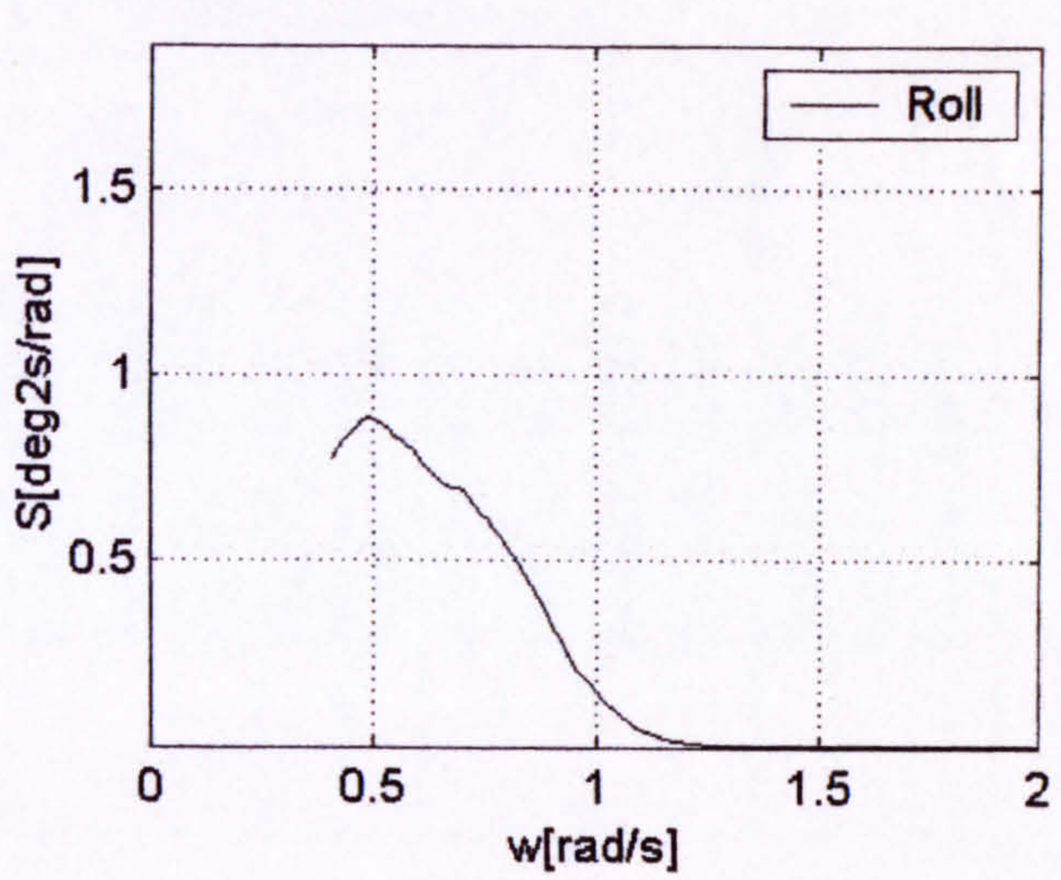

Figure 16 Experiment, Hs=4.50m

2 Numerical simulations

For the purpose of demonstration of the predictions of damaged ship behaviour, a series of numerical simulations is performed with the use of numerical code developed in this thesis. Summary of the survivability for the study case 2, Table 2, is given in the following Table 3, followed by graphical display of the sample simulated ship responses with Fourier analyses of the motions.

Table 3 Numerical testing of survivability of PRR1, wave steepness 1/25, Case2 in Table 2

Run No.	Target Wave Height Hs(m)	Comments
Run386-H350-1	3.50	**Survive**
Run386-H350-2	3.50	**Survive**
Run386-H350-3	3.50	**Survive**
Run386-H350-4	3.50	**Survive**
Run386-H350-5	3.50	**Survive**
Run386-H375-1	3.75	**Capsize**
Run386-H375-2	3.75	**Capsize**
Run386-H375-3	3.75	**Survive**
Run386-H375-4	3.75	**Survive**
Run386-H375-5	3.75	**Capsize**
Run386-H400-1	4.00	**Capsize**
Run386-H400-2	4.00	**Survive**
Run386-H400-3	4.00	**Survive**
Run386-H400-4	4.00	**Survive**
Run386-H400-5	4.00	**Survive**
Run386-H425-1	4.25	**Survive**
Run386-H425-2	4.25	**Capsize**
Run386-H425-3	4.25	**Capsize**
Run386-H425-4	4.25	**Survive**
Run386-H425-5	4.25	**Capsize**
Run386-H450-1	4.50	**Survive**
Run386-H450-2	4.50	**Capsize**
Run386-H450-3	4.50	**Capsize**
Run386-H450-4	4.50	**Survive**
Run386-H450-5	4.50	**Capsize**
Run386-H475-1	4.75	**Survive**
Run386-H475-2	4.75	**Capsize**
Run386-H475-3	4.75	**Capsize**

Run386-H475-4	4.75	**Capsize**
Run386-H475-5	4.75	**Capsize**
Run386-H500-1	5.00	**Capsize**
Run386-H500-2	5.00	**Capsize**
Run386-H500-3	5.00	**Capsize**
Run386-H500-4	5.00	**Survive**
Run386-H500-5	5.00	**Survive**
Run386-H525-1	5.25	**Survive**
Run386-H525-2	5.25	**Capsize**
Run386-H525-3	5.25	**Capsize**
Run386-H525-4	5.25	**Capsize**
Run386-H525-5	5.25	**Survive**
Run386-H550-1	5.50	**Capsized**
Run386-H550-2	5.50	**Capsized**
Run386-H550-3	5.50	**Capsized**
Run386-H550-4	5.50	**Capsized**
Run386-H550-5	5.50	**Capsized**

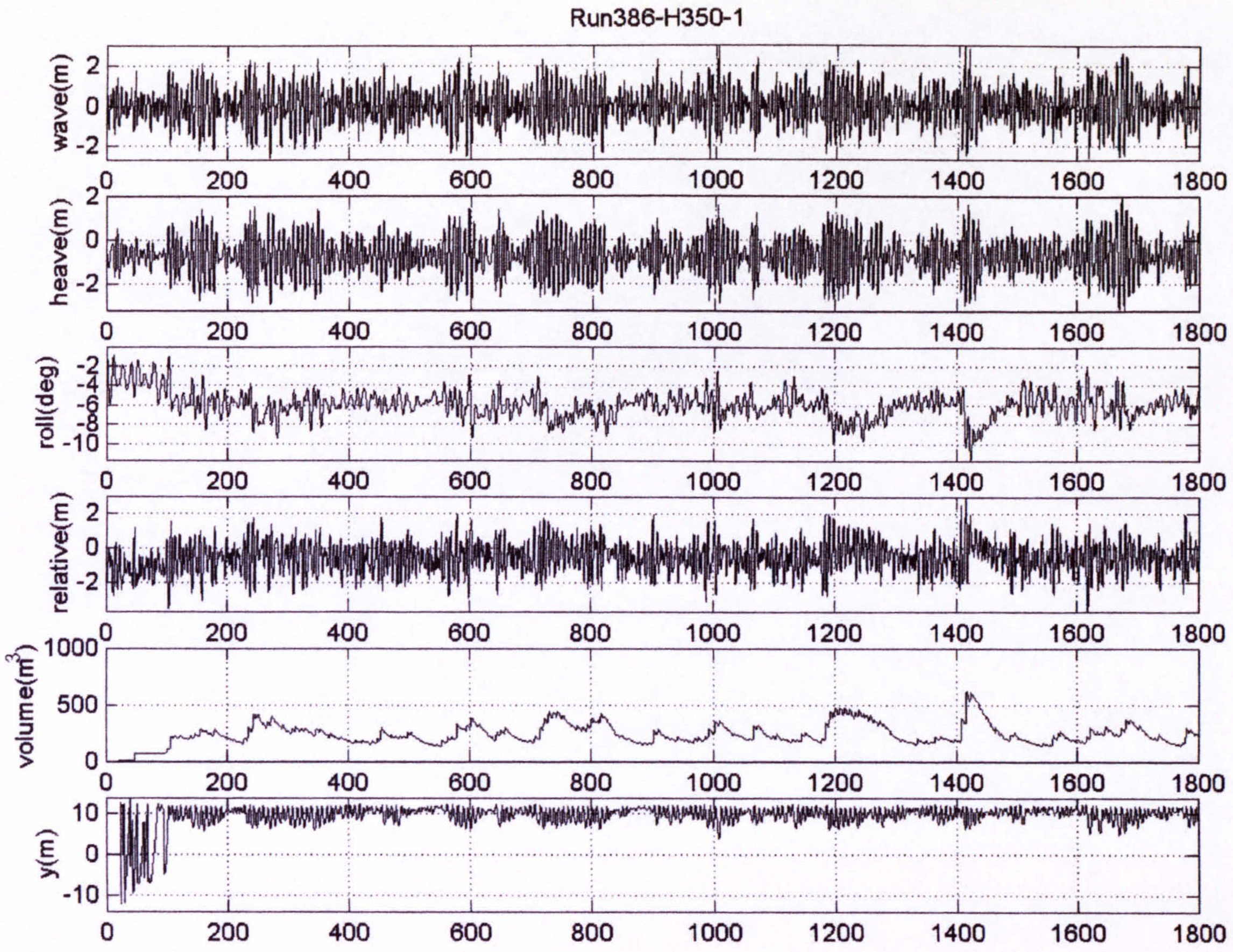

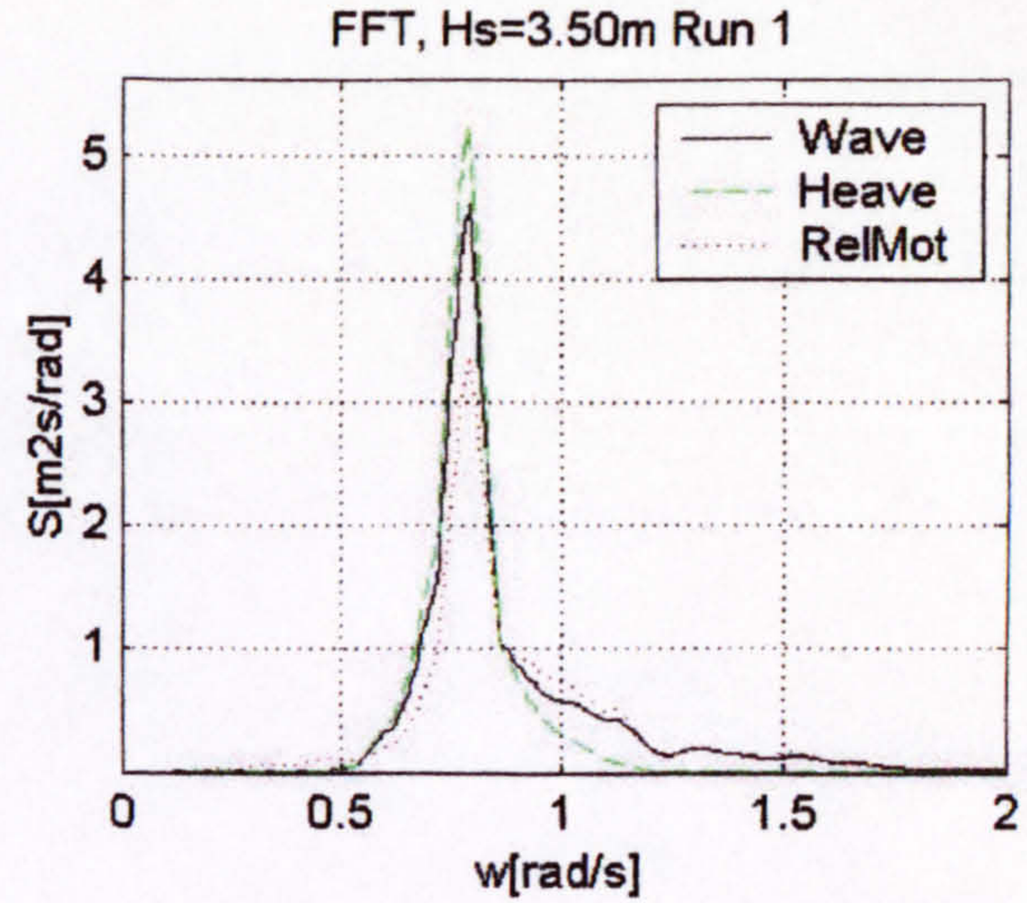

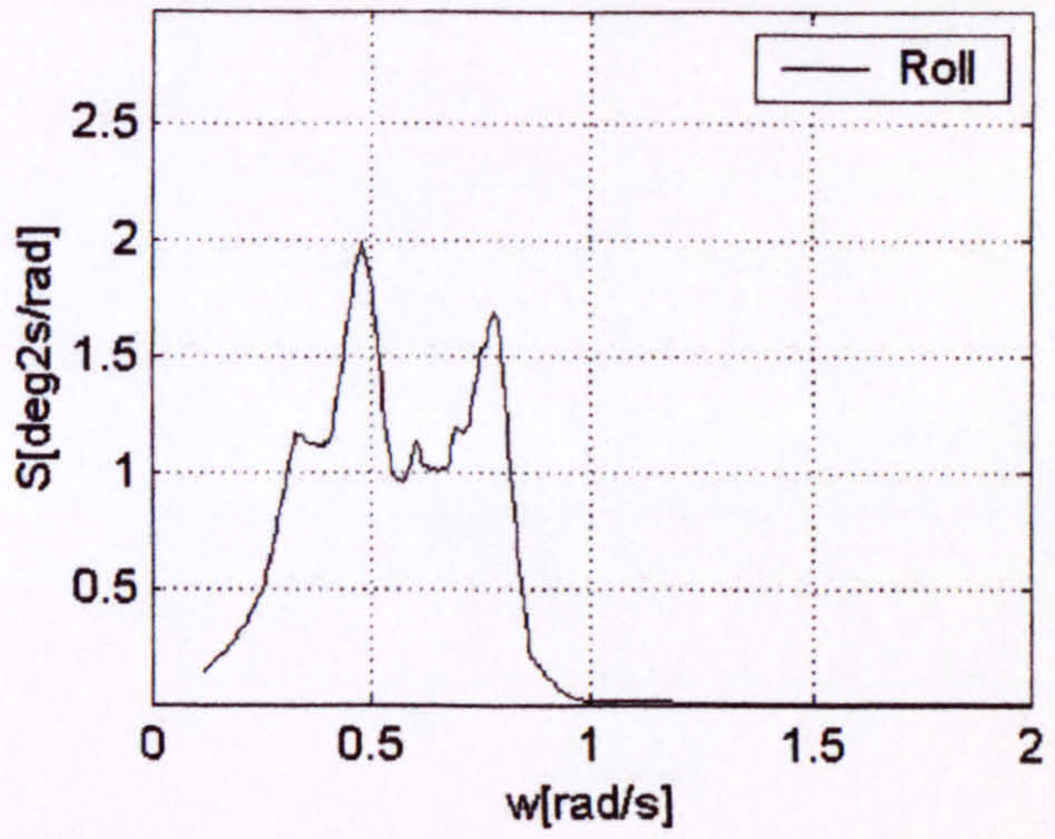

Figure 17 Numerical simulations, PRR1, KG=12.892m, Hs=3.50m

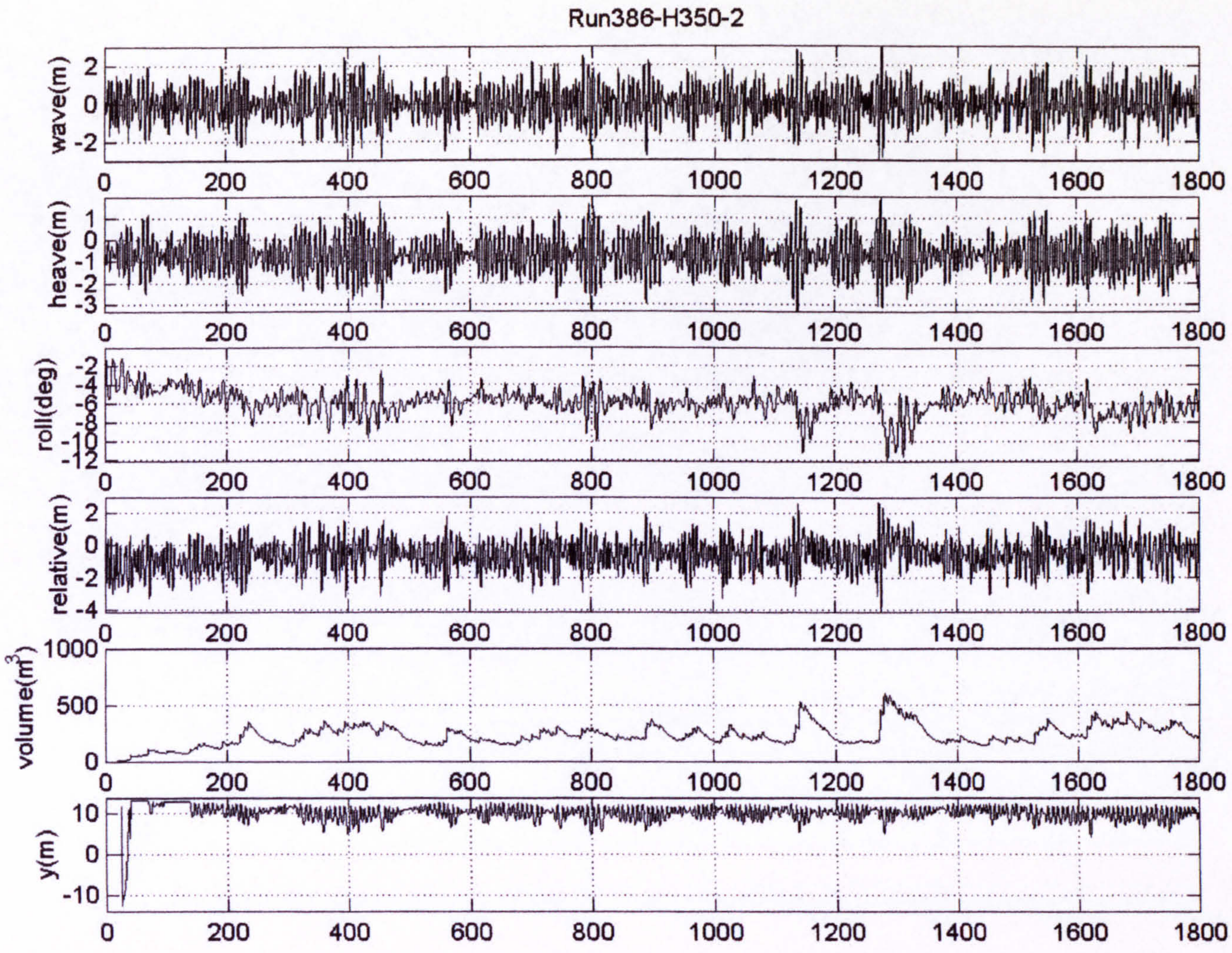

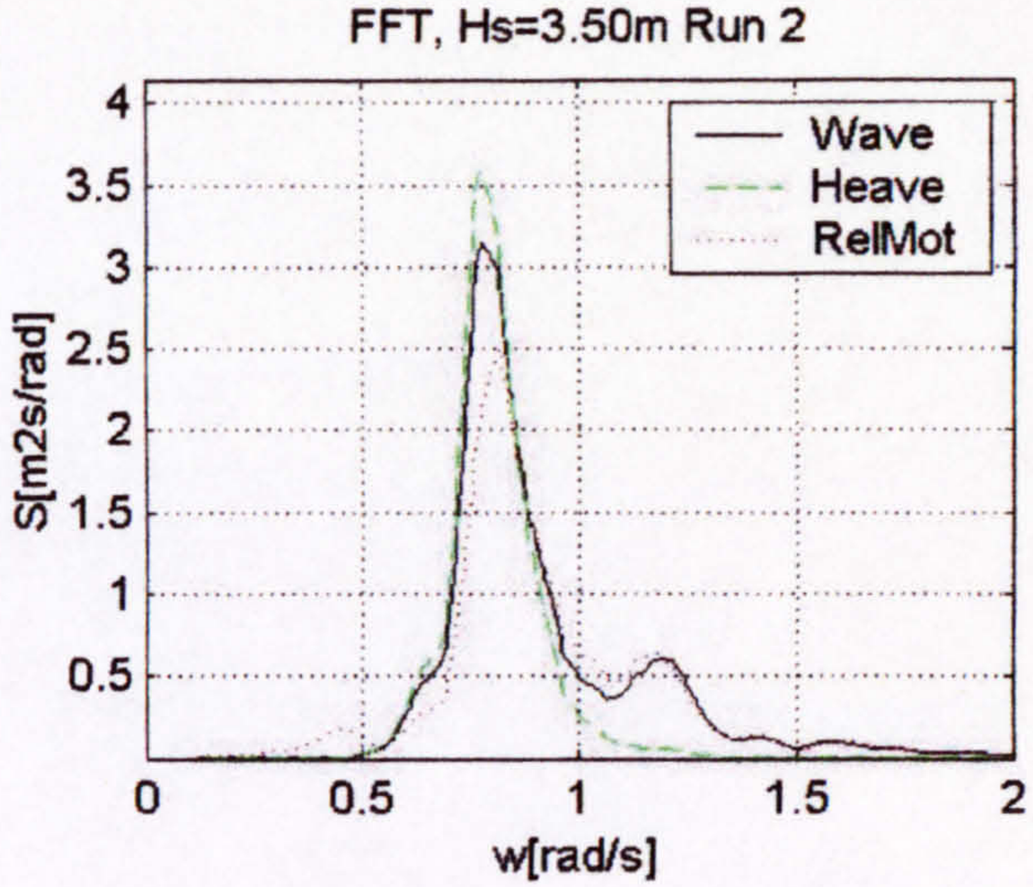

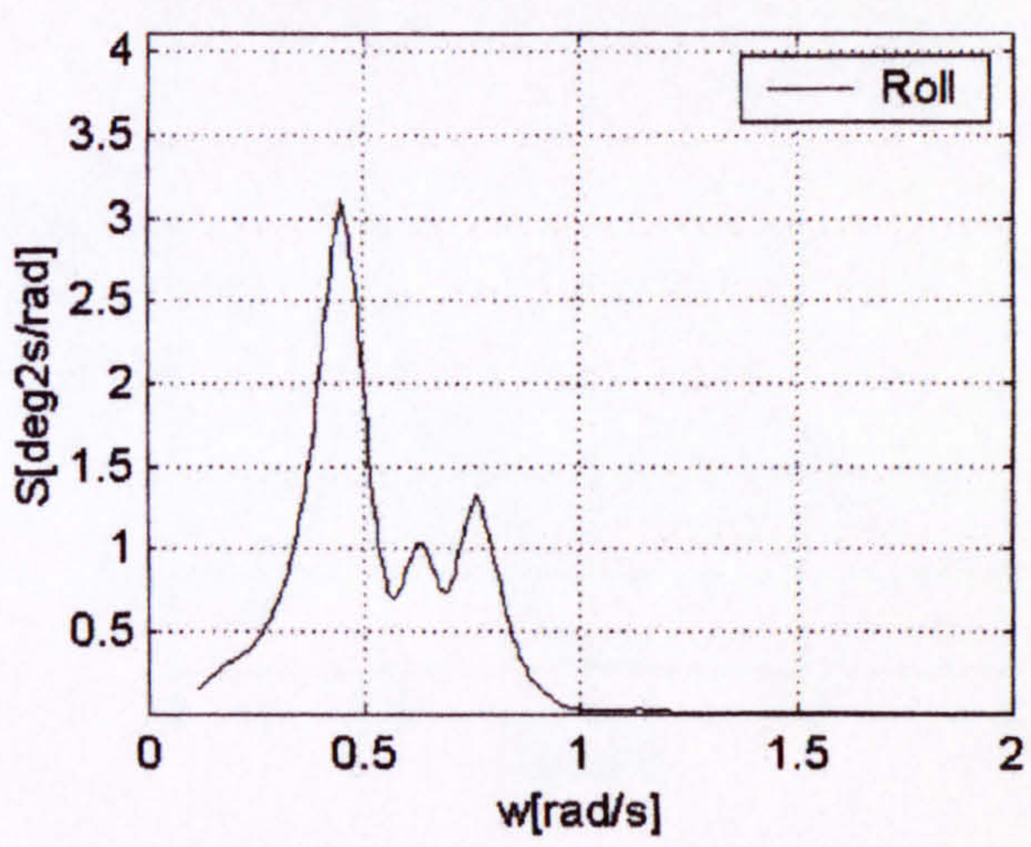

Figure 18 Numerical simulations, PRR1, KG=12.892m, Hs=3.50m

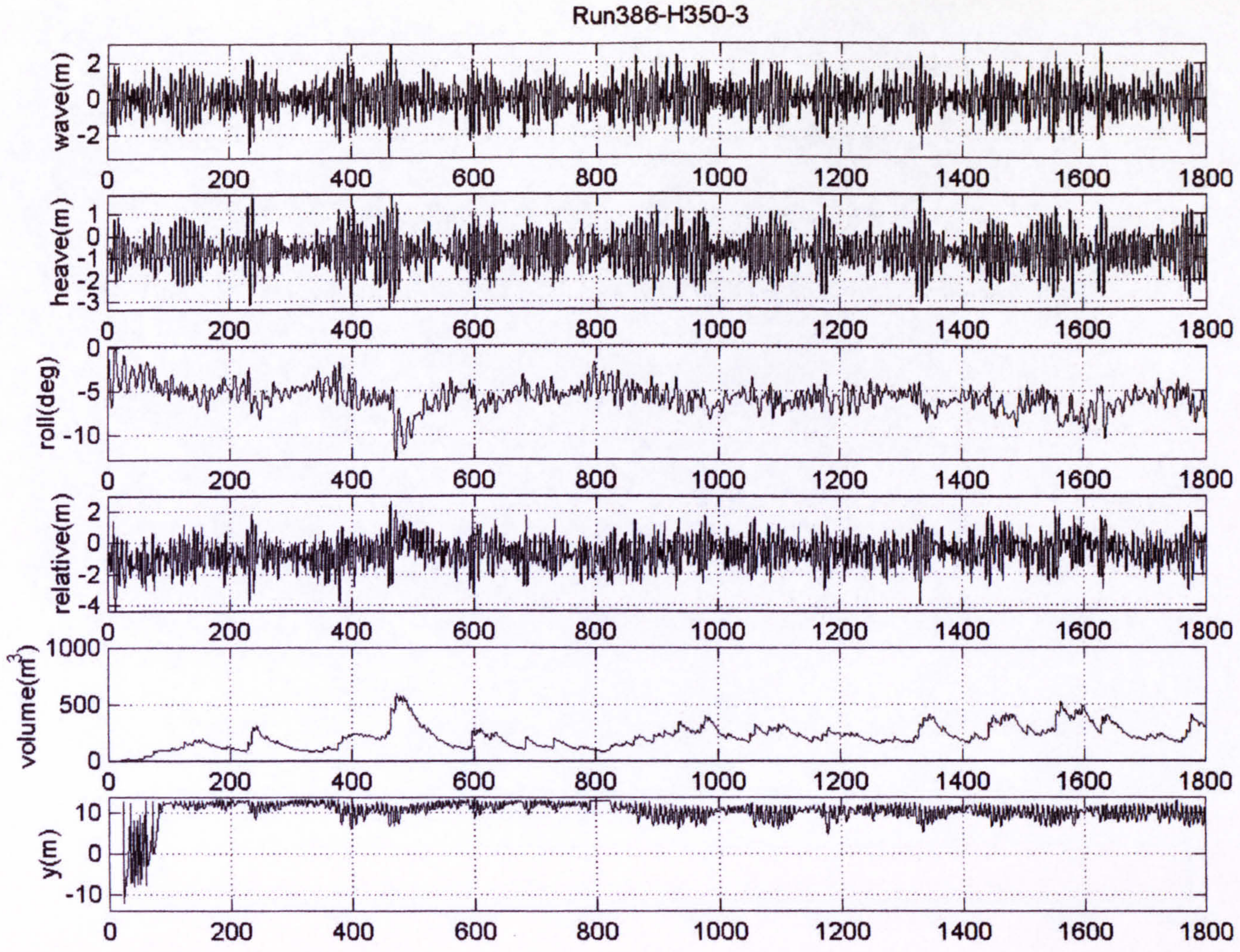

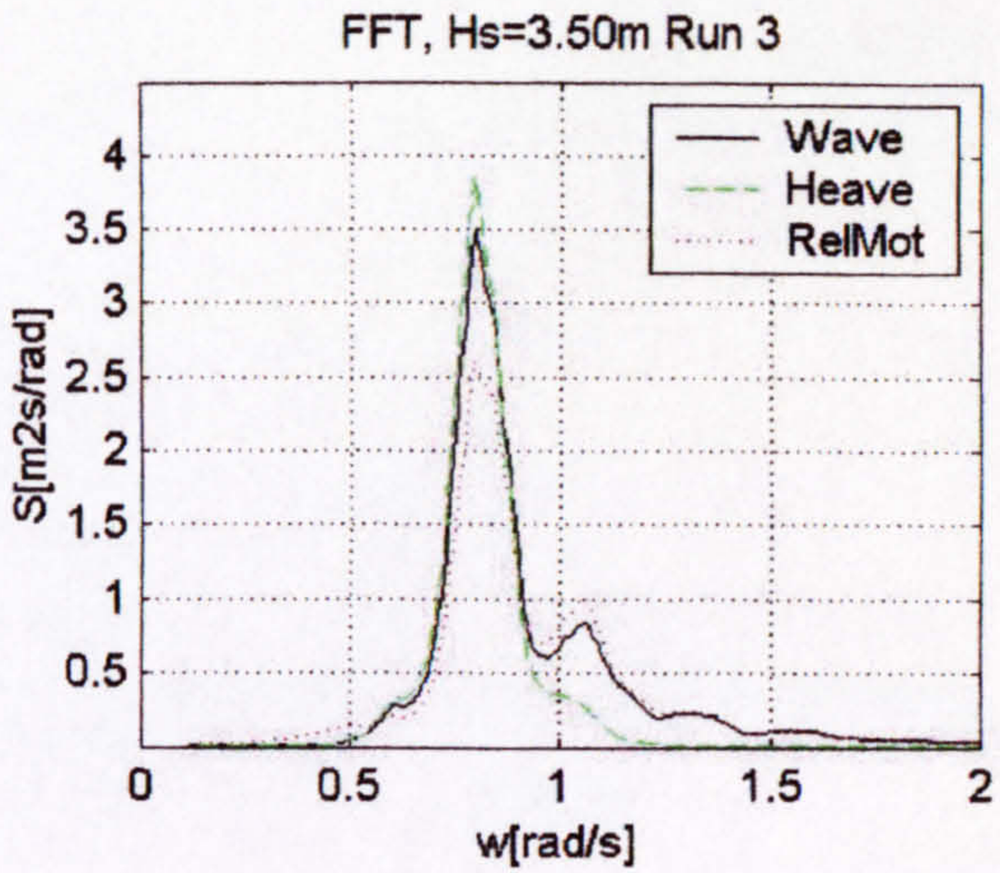

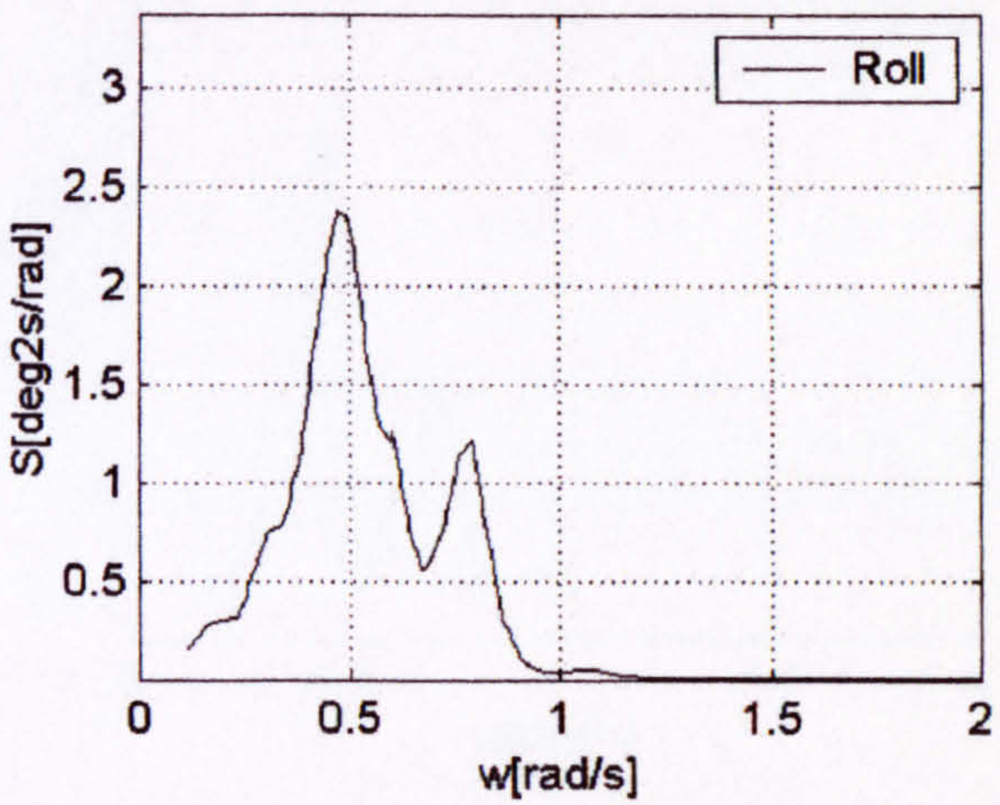

Figure 19 Numerical simulations, PRR1, KG=12.892m, Hs=3.50m

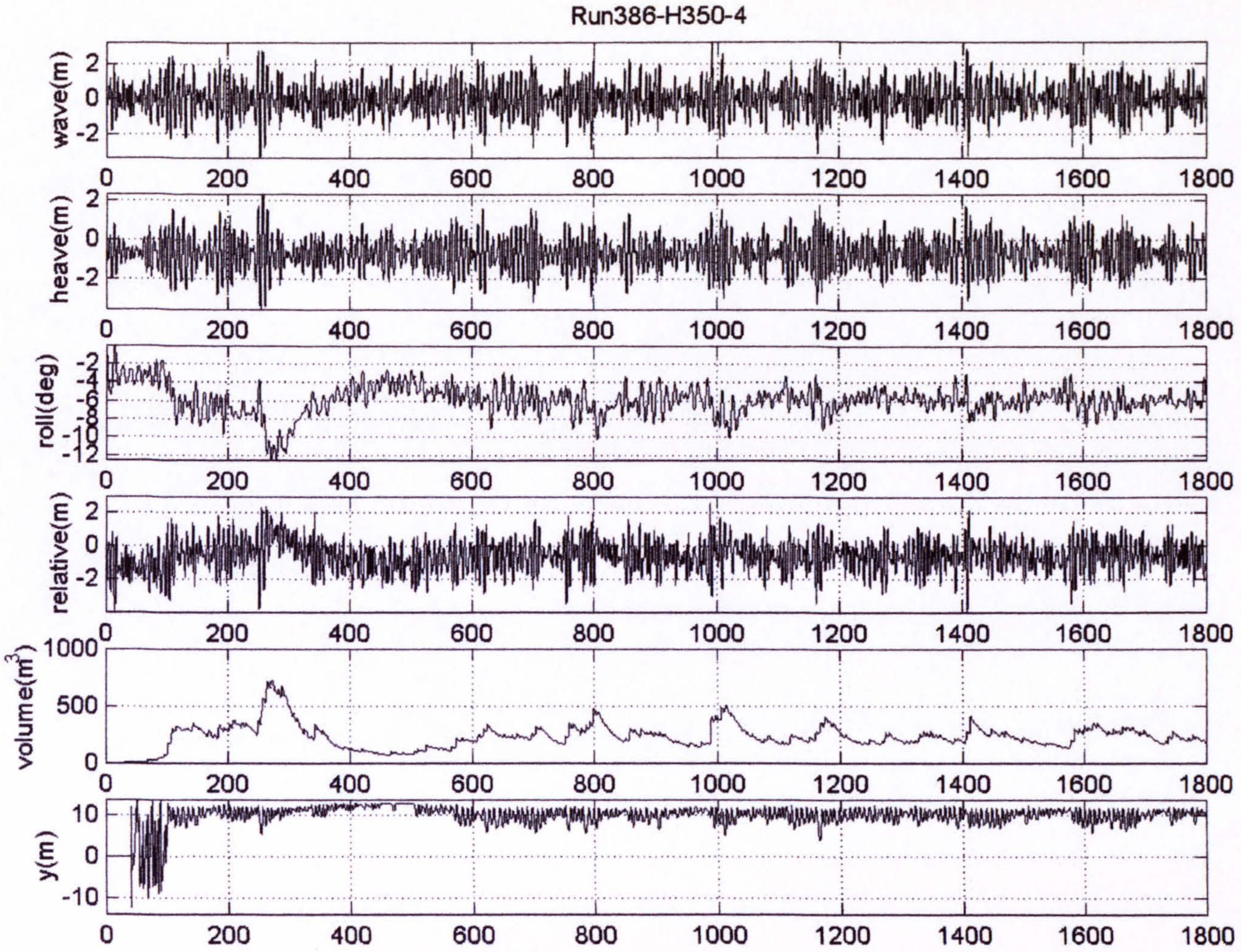

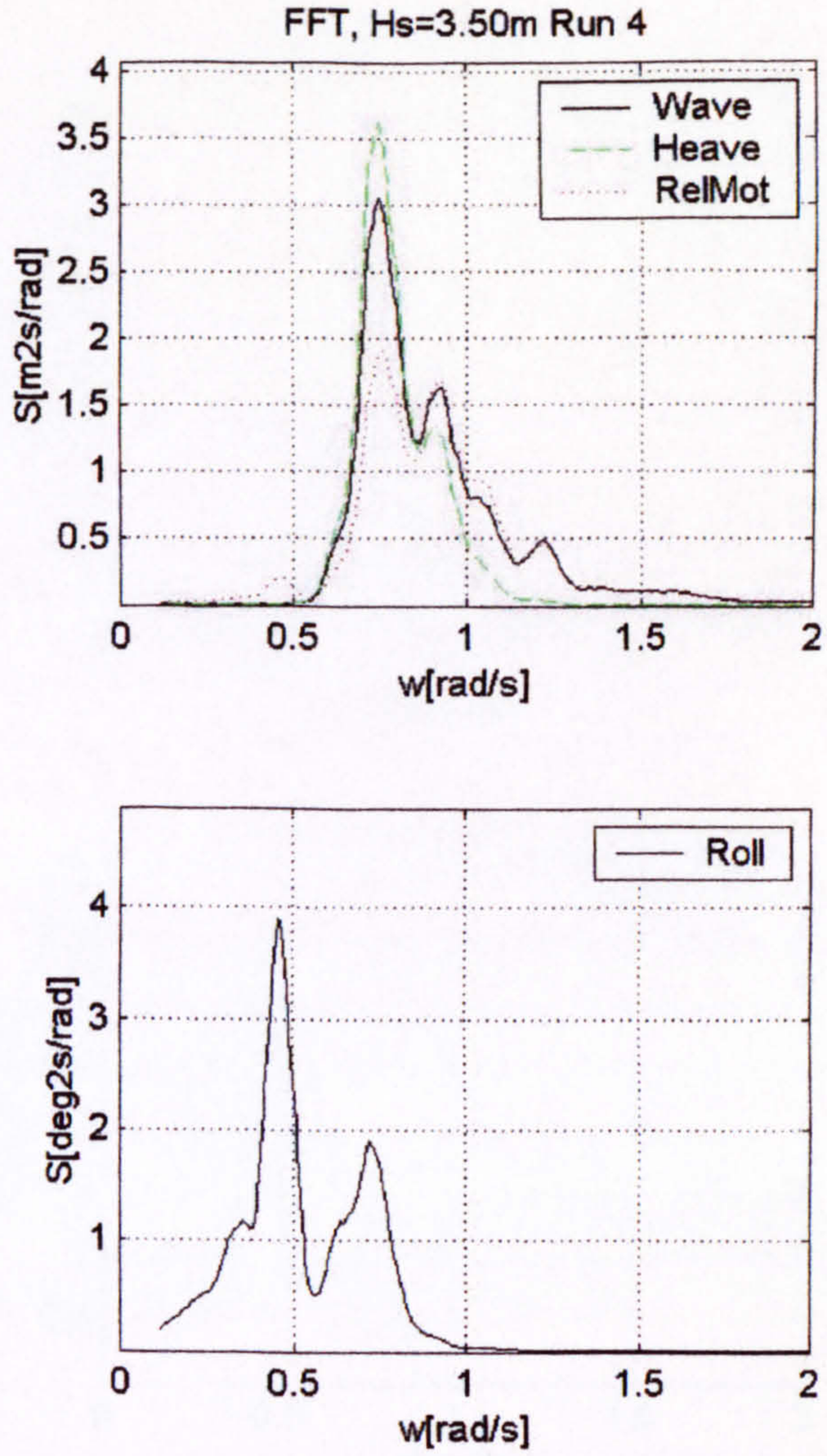

Figure 20 Numerical simulations, PRR1, KG=12.892m, Hs=3.50m

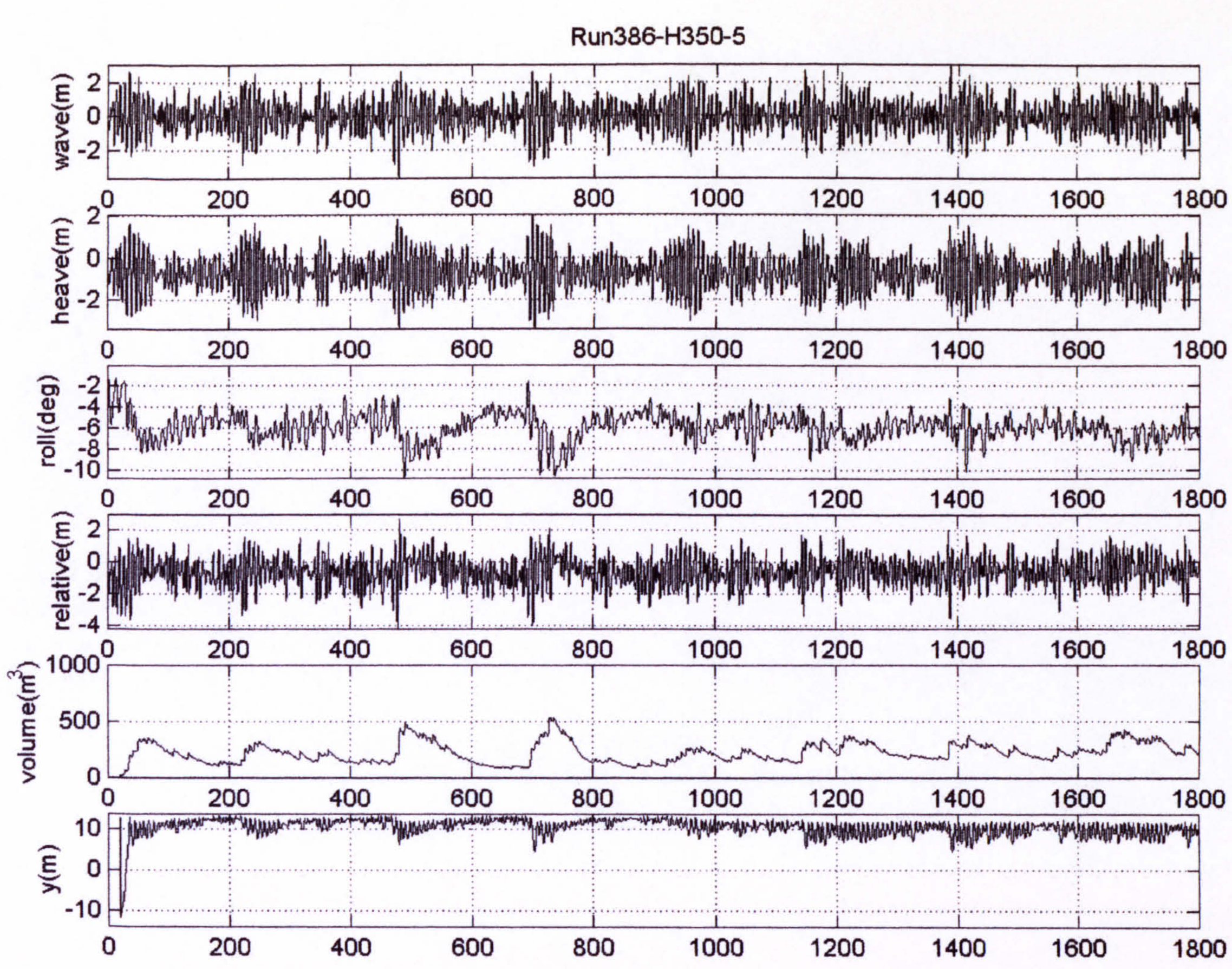

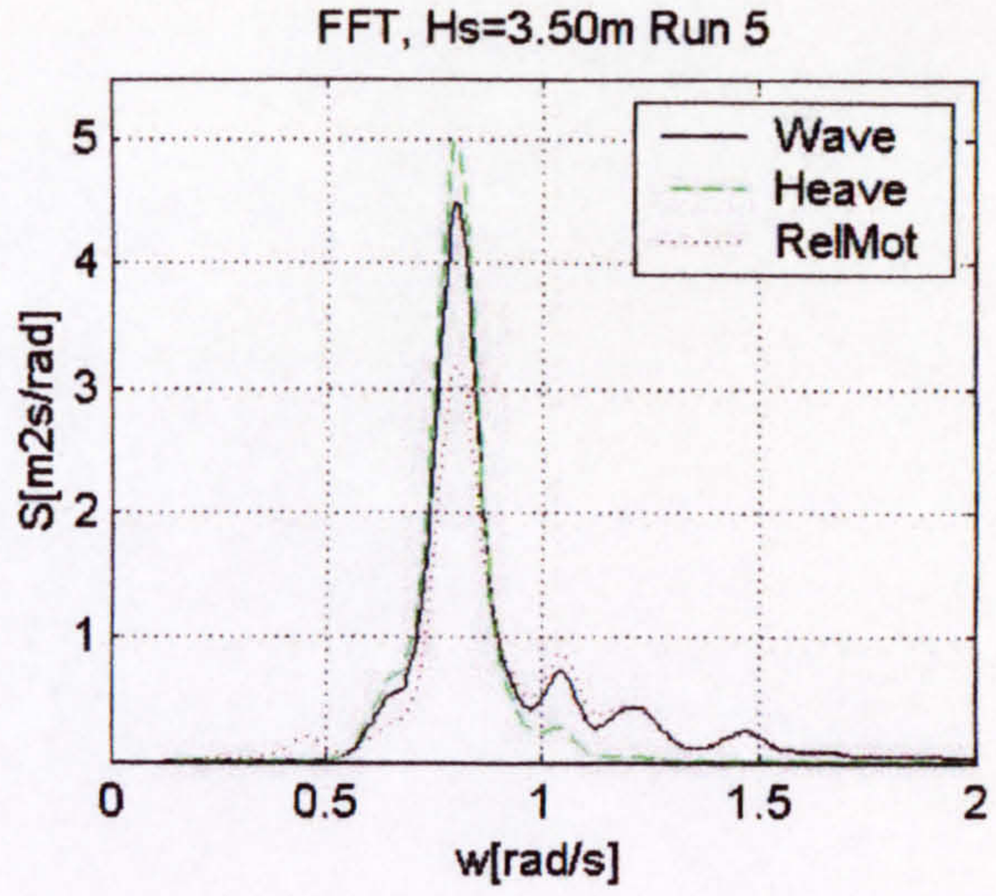

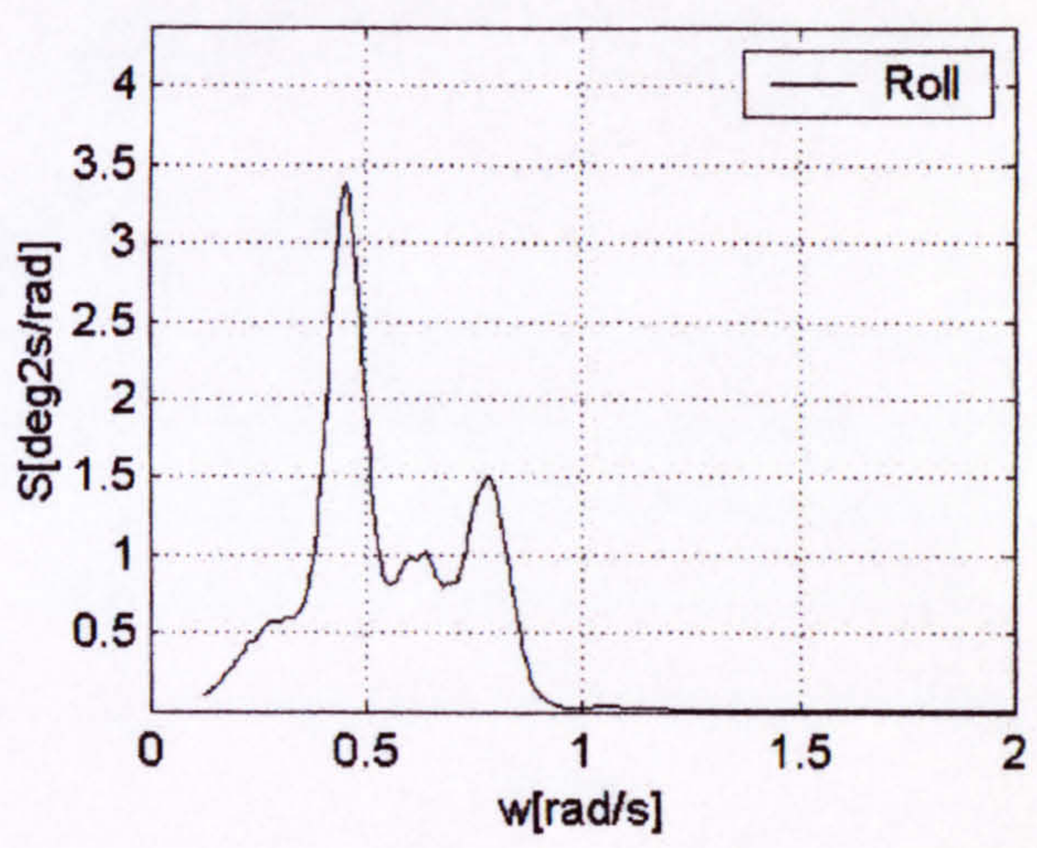

Figure 21 Numerical simulations, PRR1, KG=12.892m, Hs=3.50m

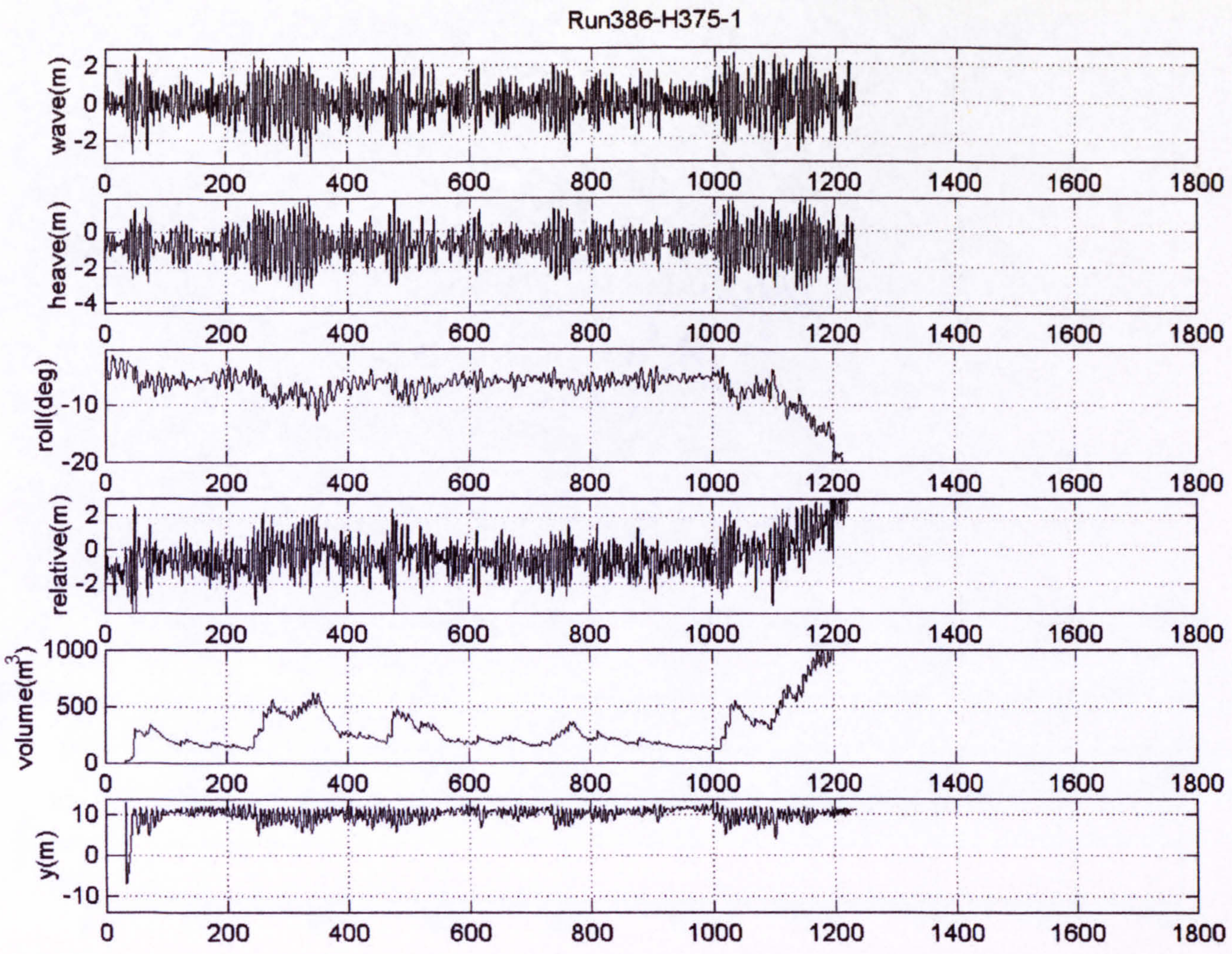

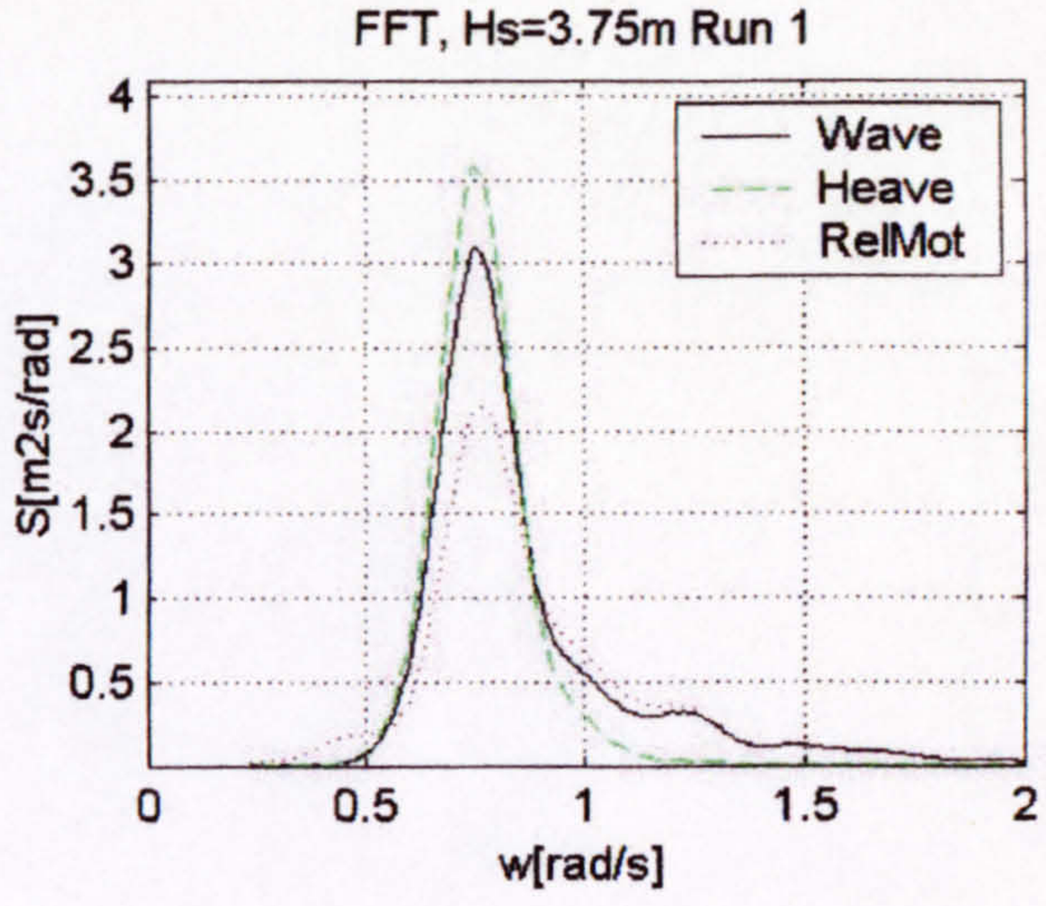

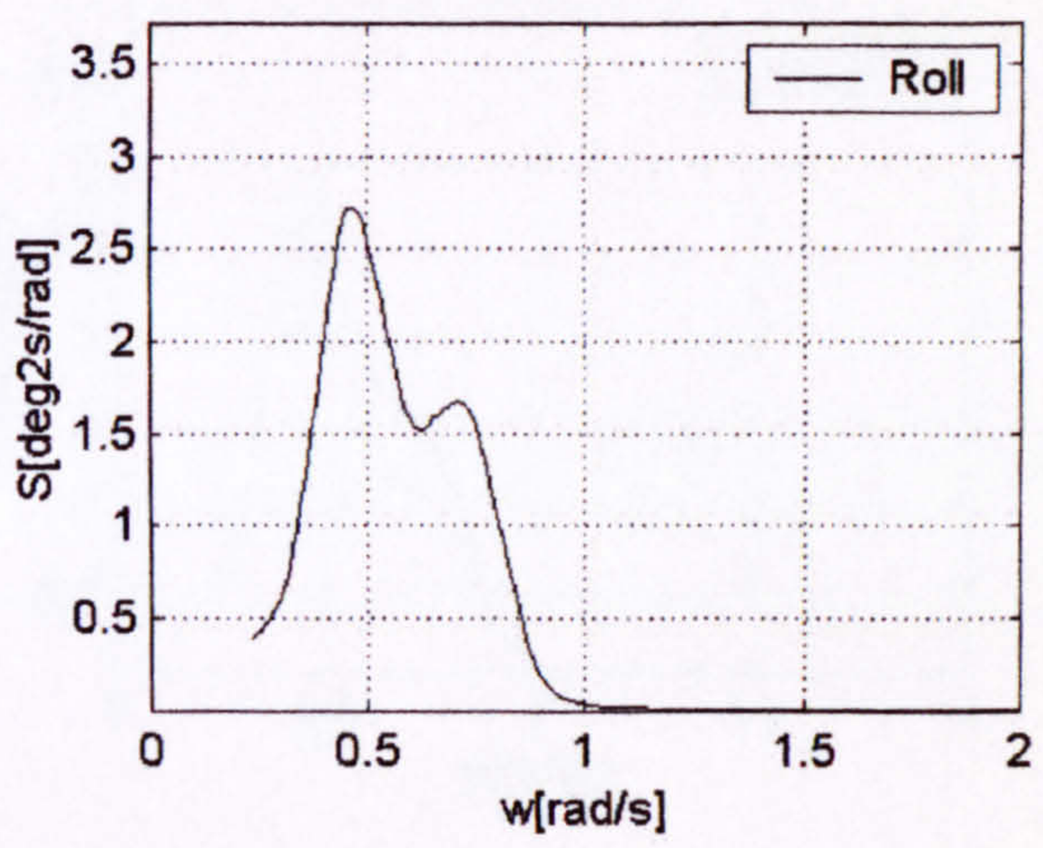

Figure 22 Numerical simulations, PRR1, KG=12.892m, Hs=3.75m

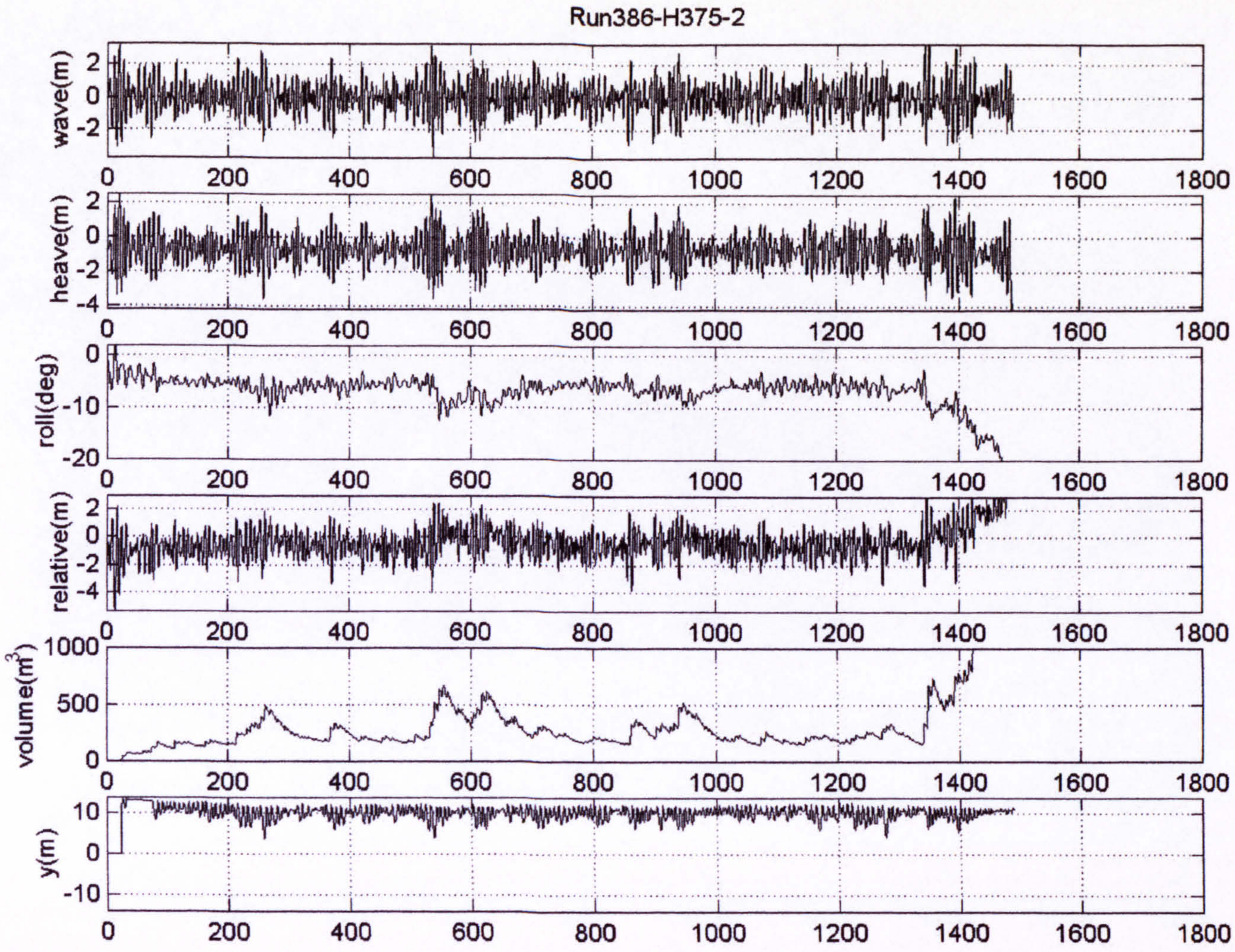

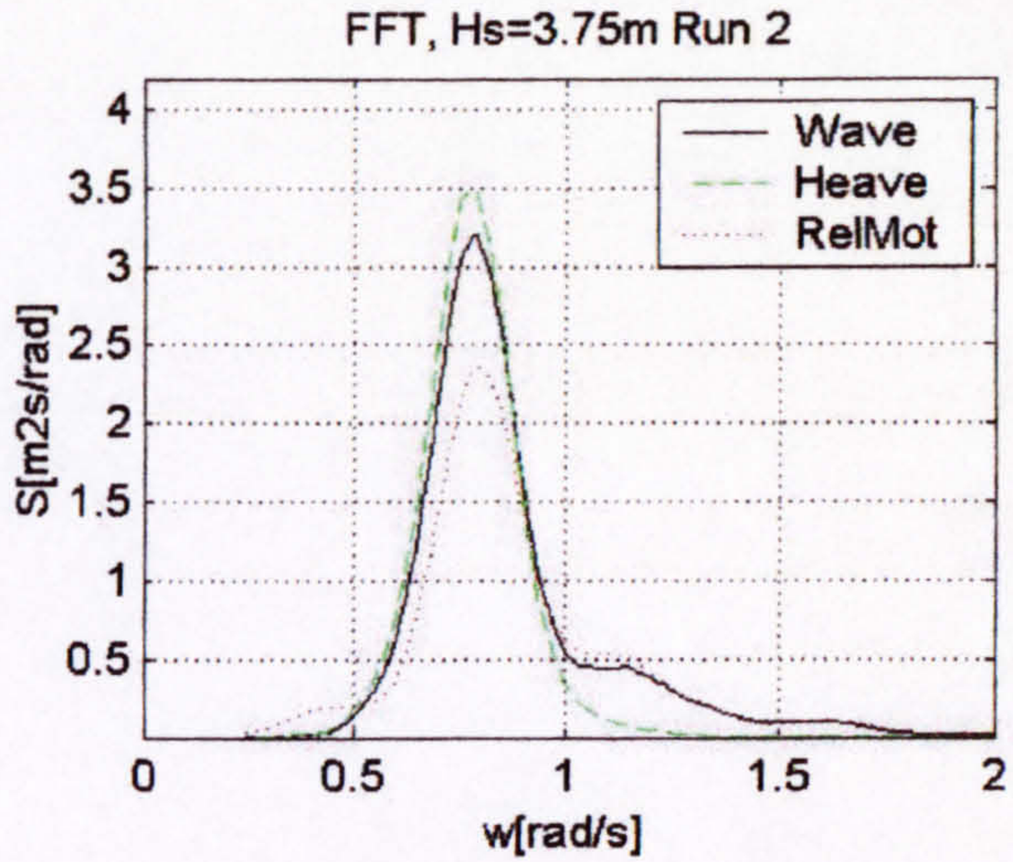

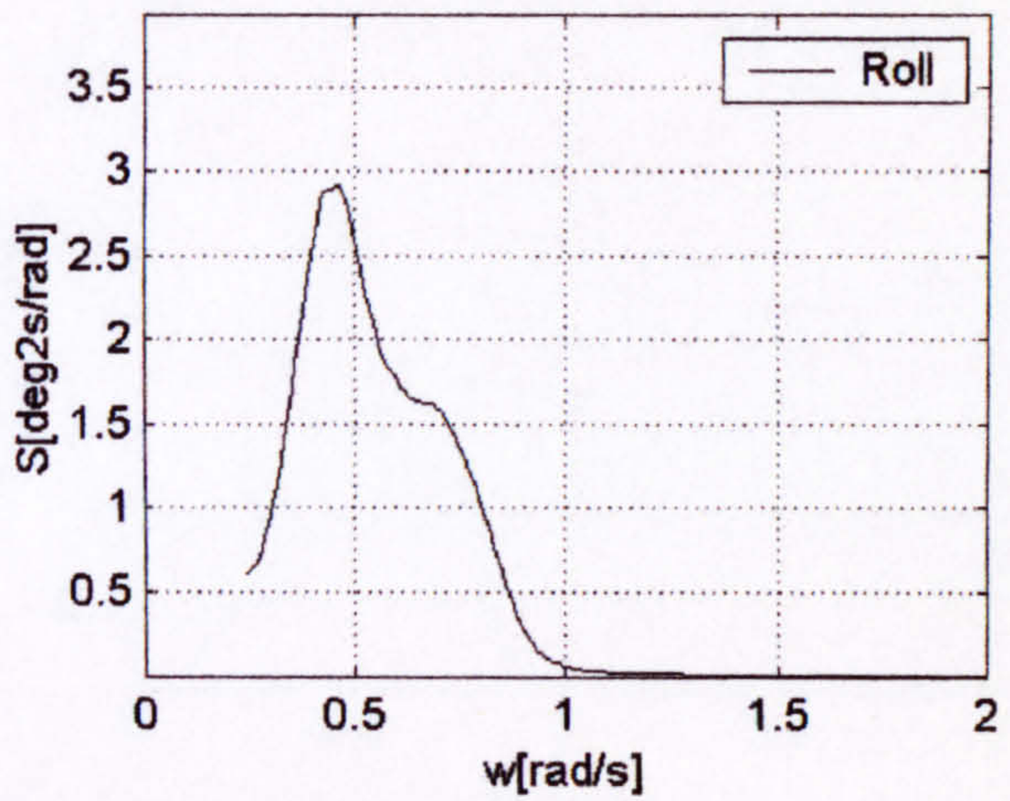

Figure 23 Numerical simulations, PRR1, KG=12.892m, Hs=3.75m

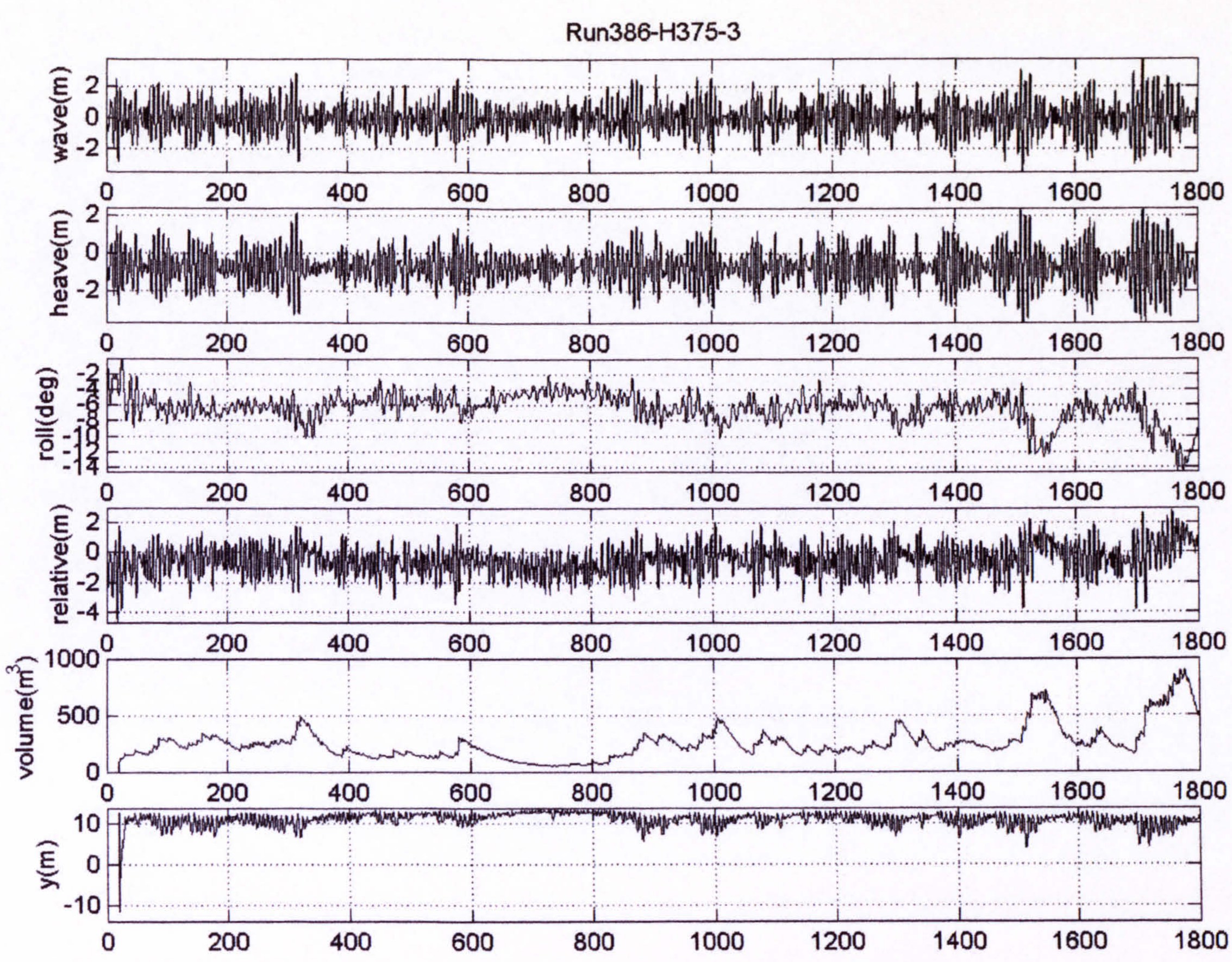

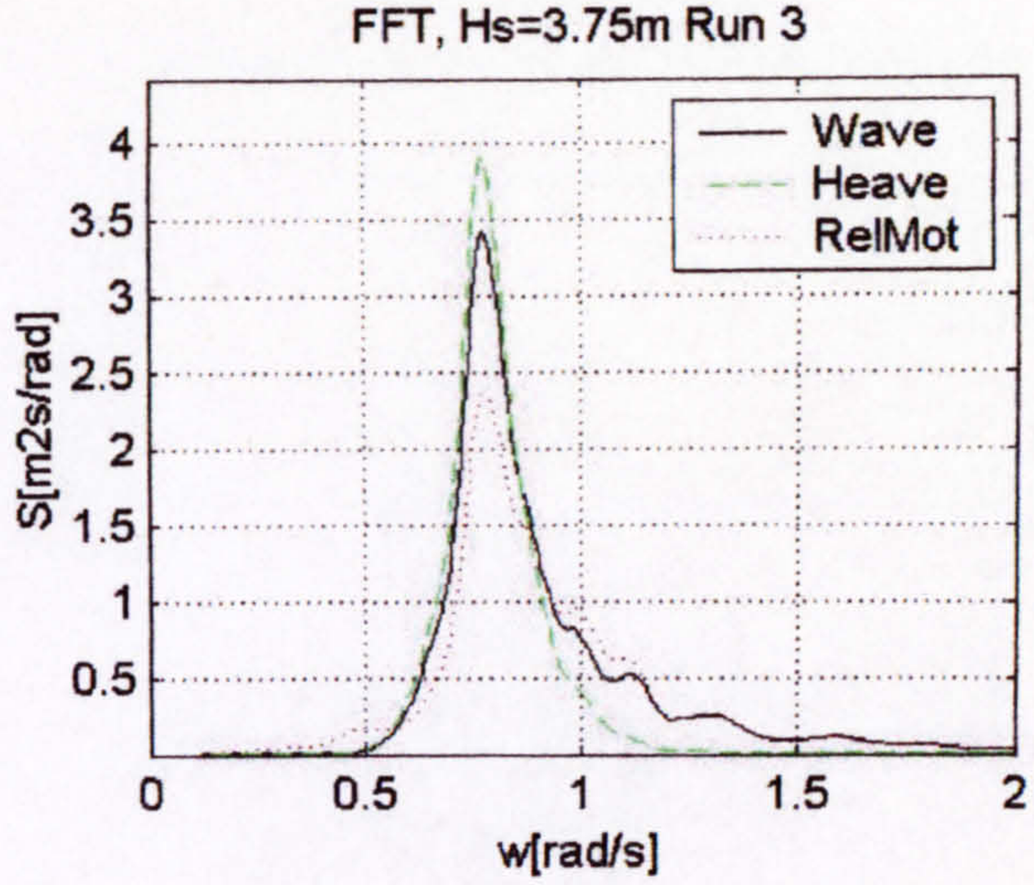

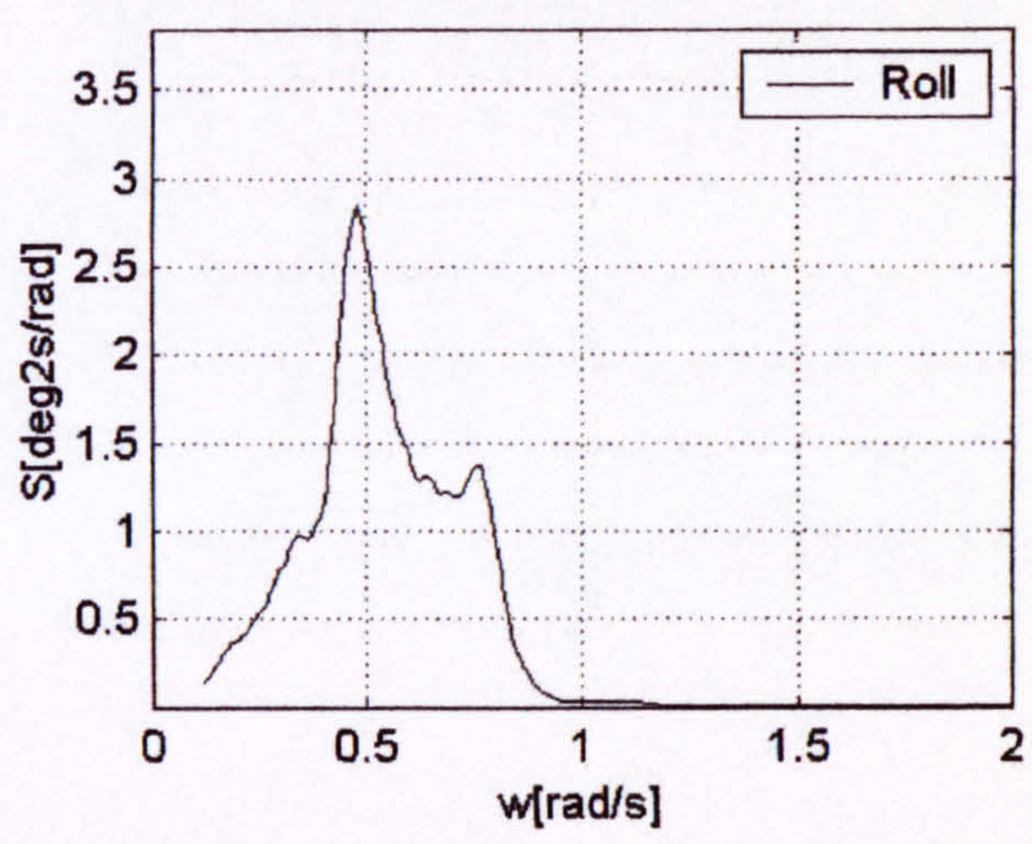

Figure 24 Numerical simulations, PRR1, KG=12.892m, Hs=3.75m

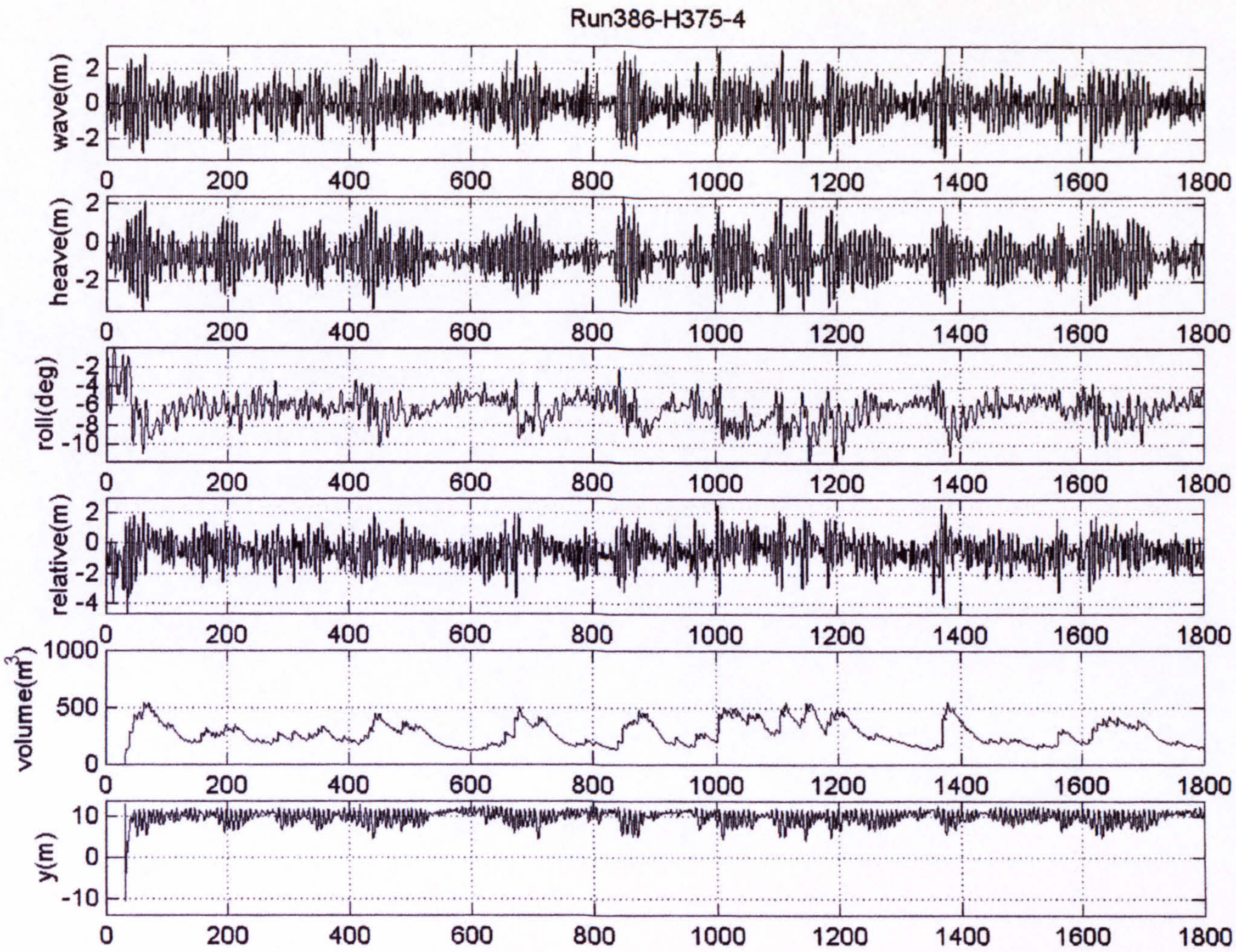

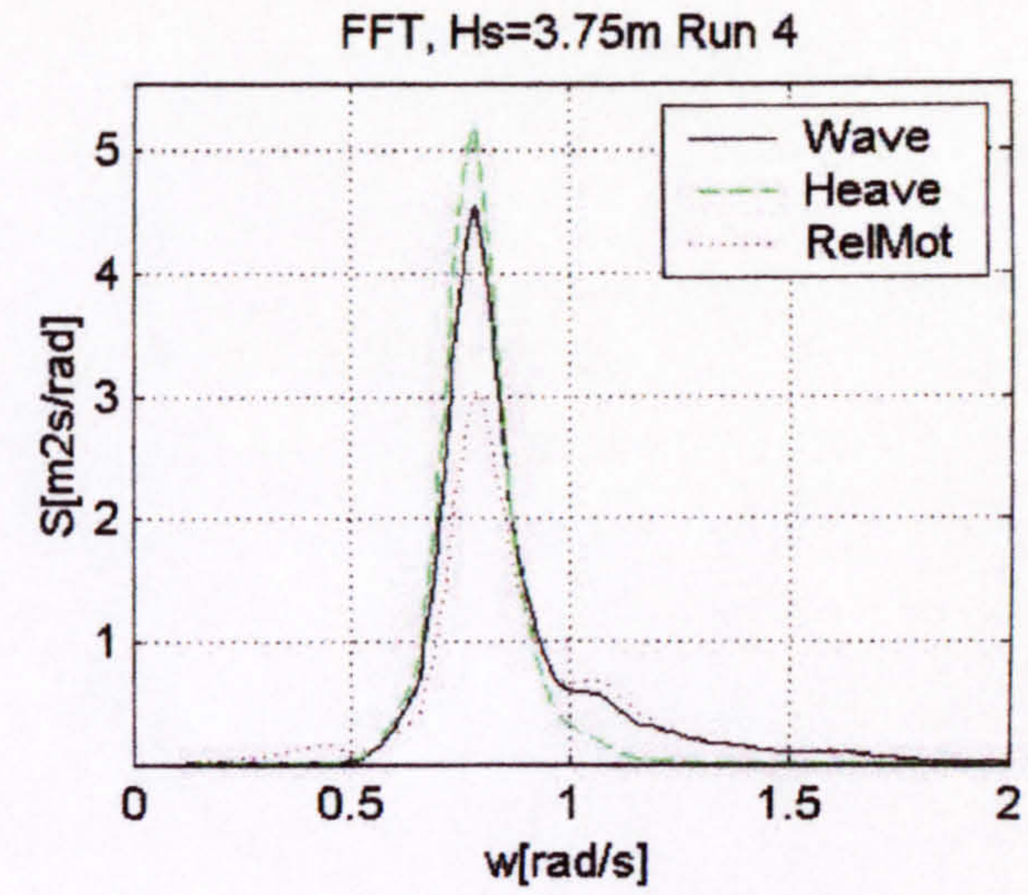

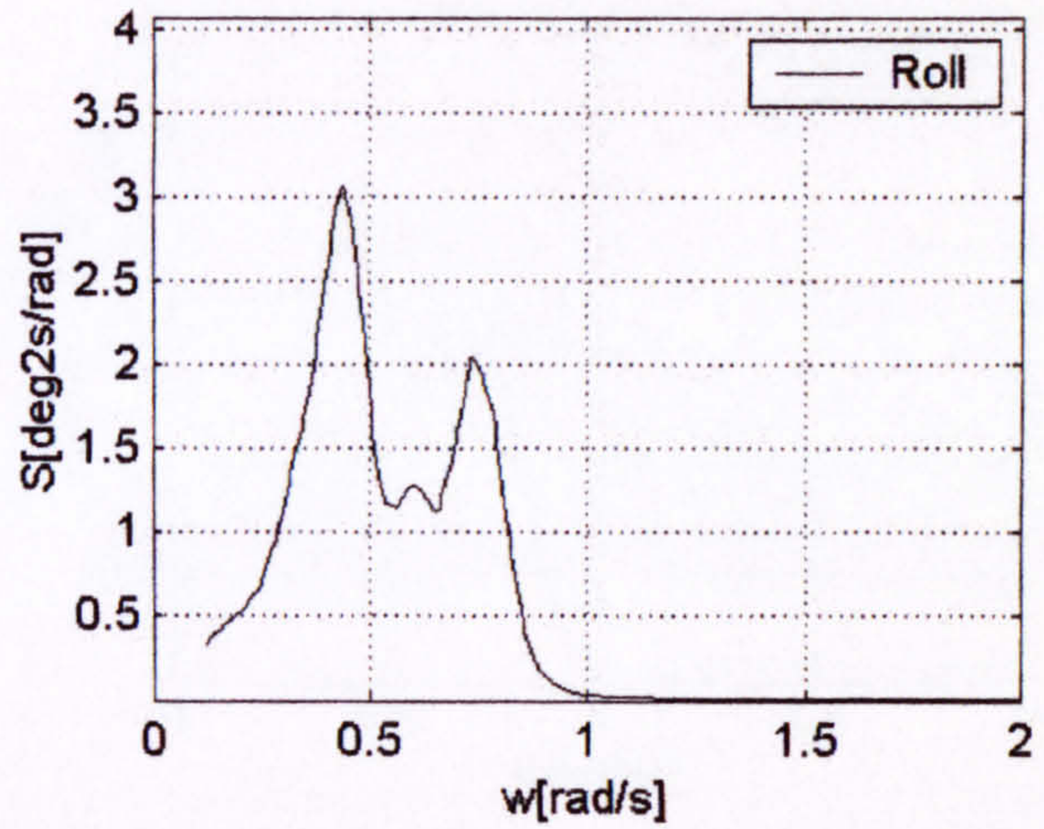

Figure 25 Numerical simulations, PRR1, KG=12.892m, Hs=3.75m

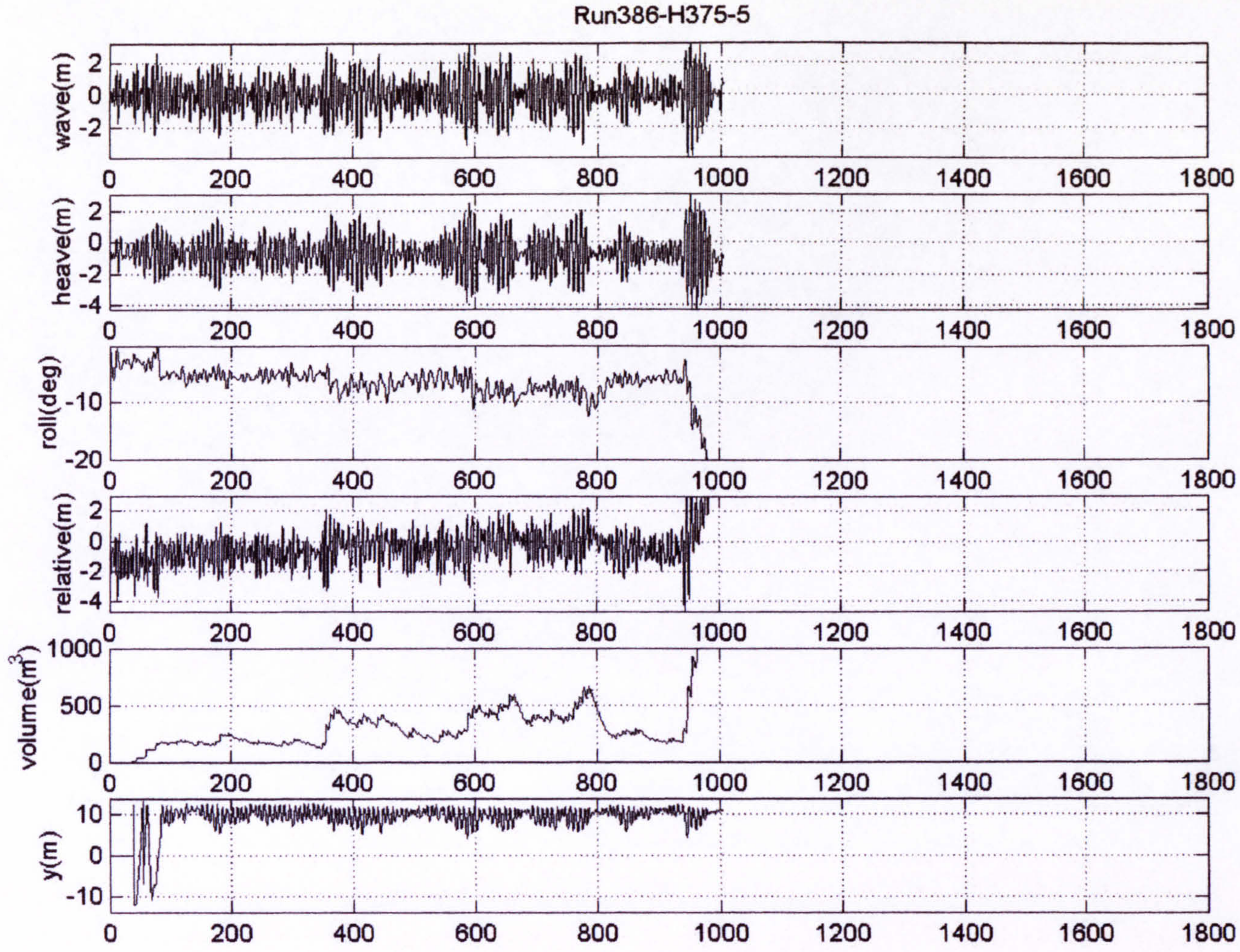

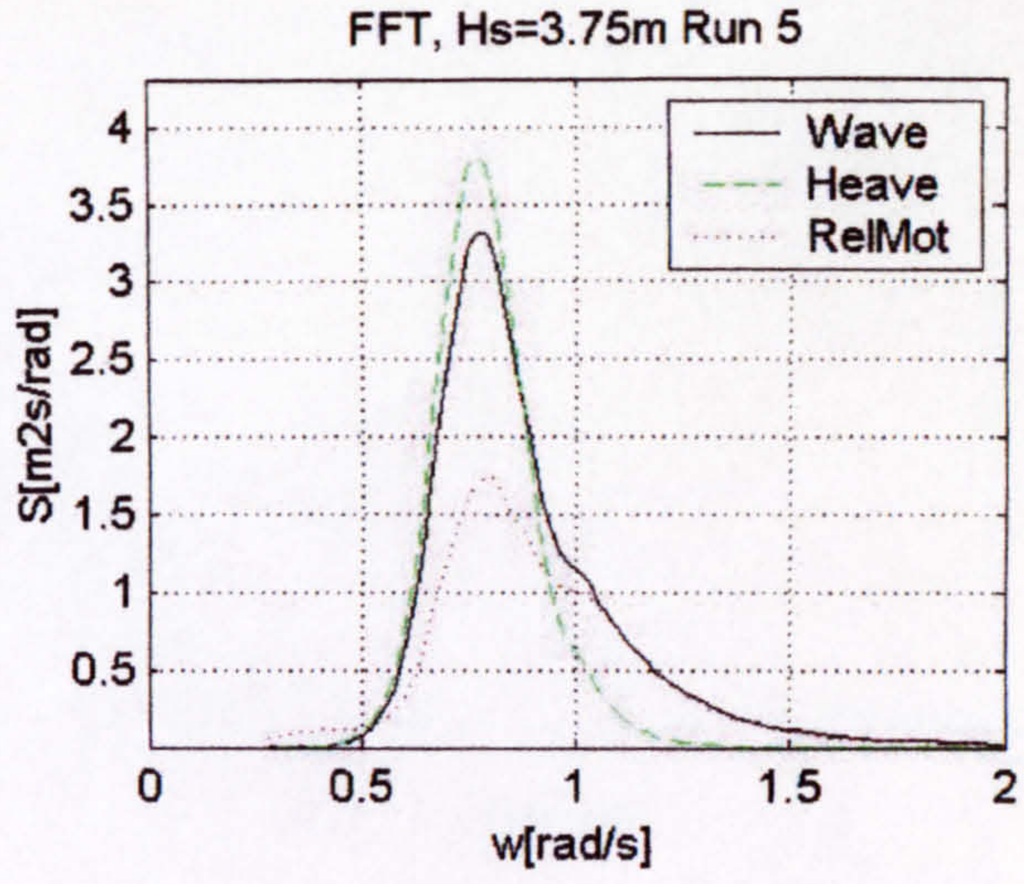

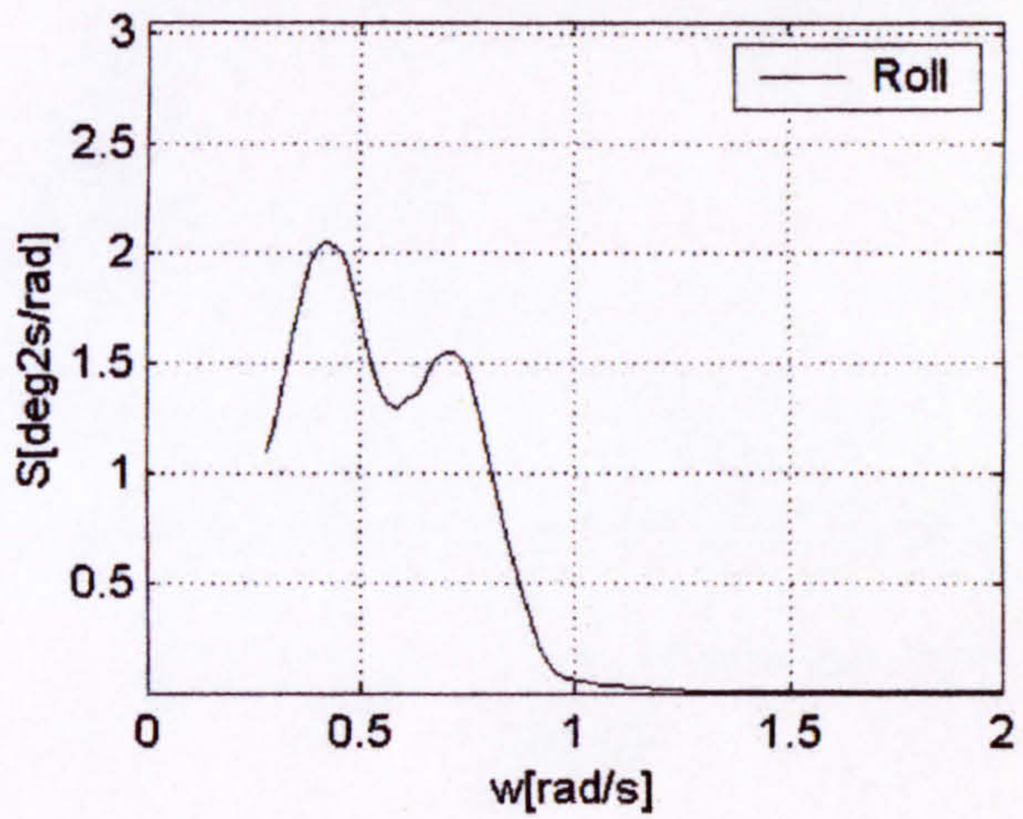

Figure 26 Numerical simulations, PRR1, KG=12.892m, Hs=3.75m

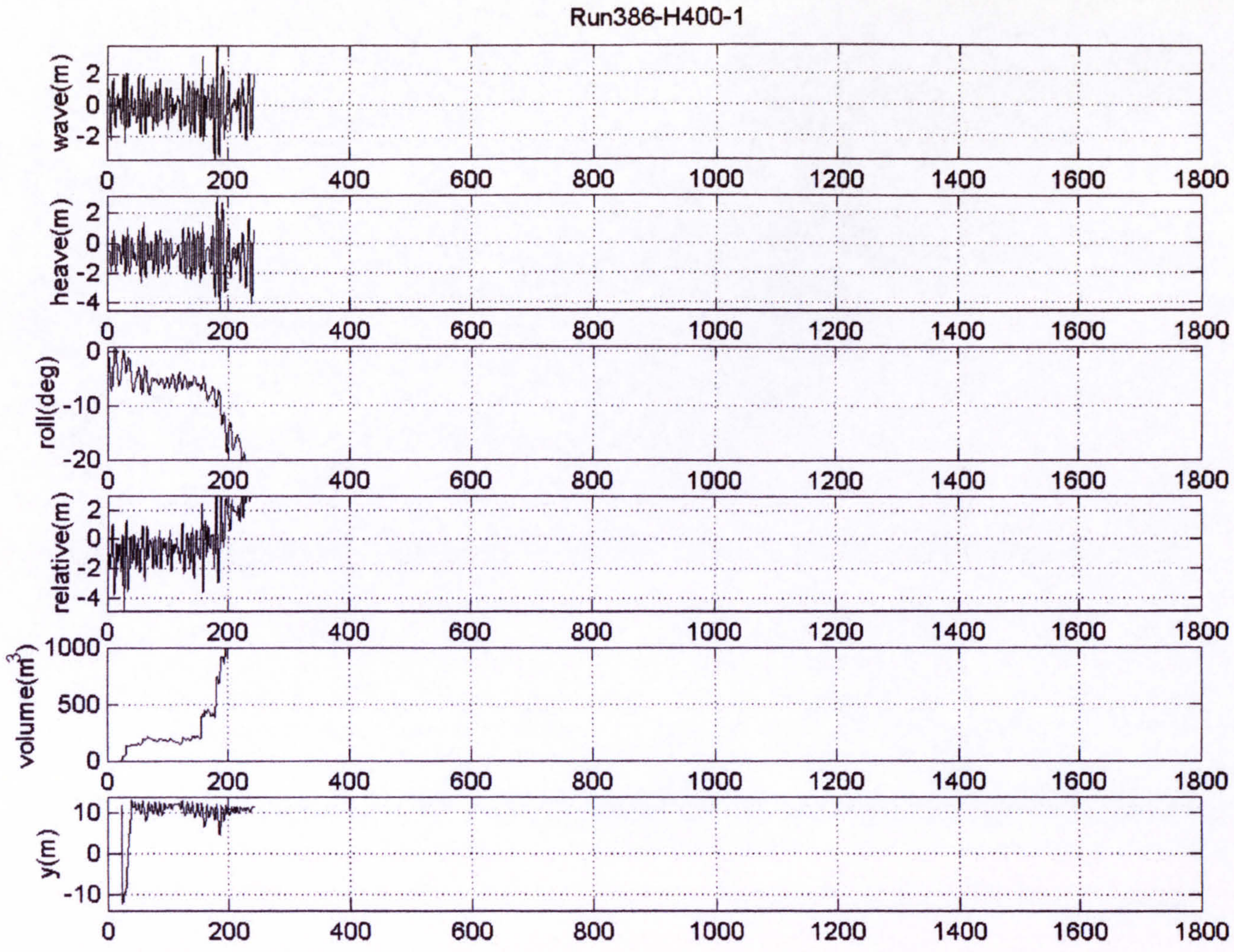

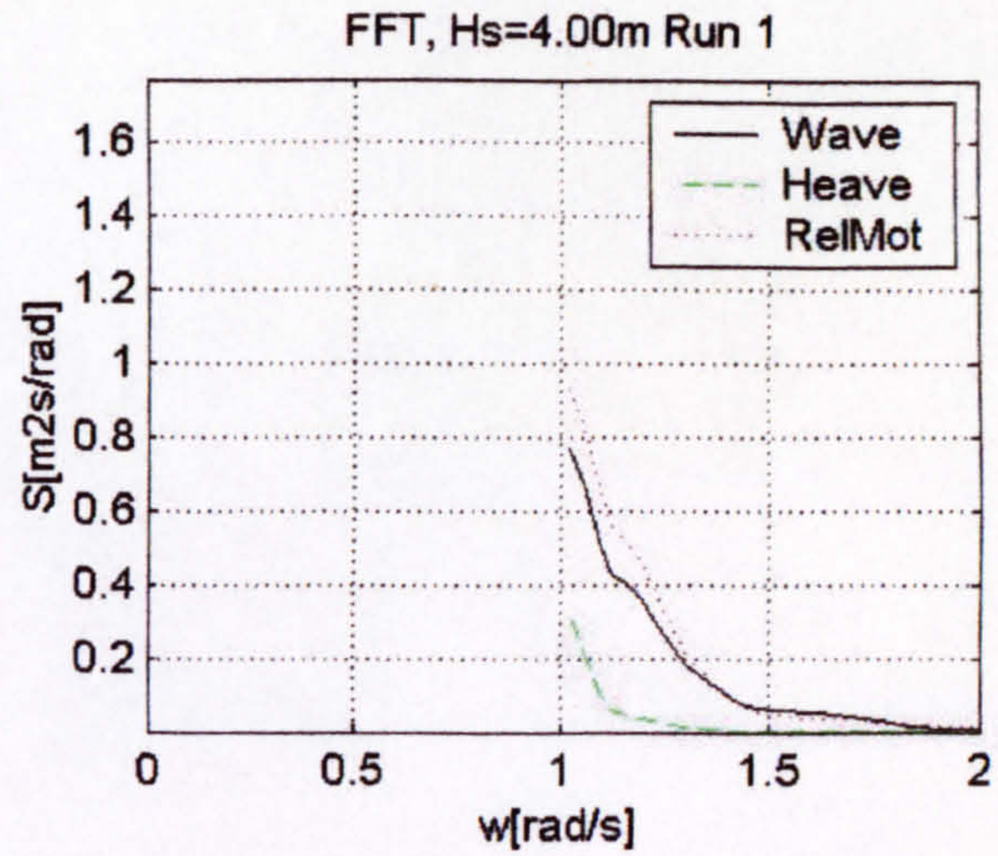

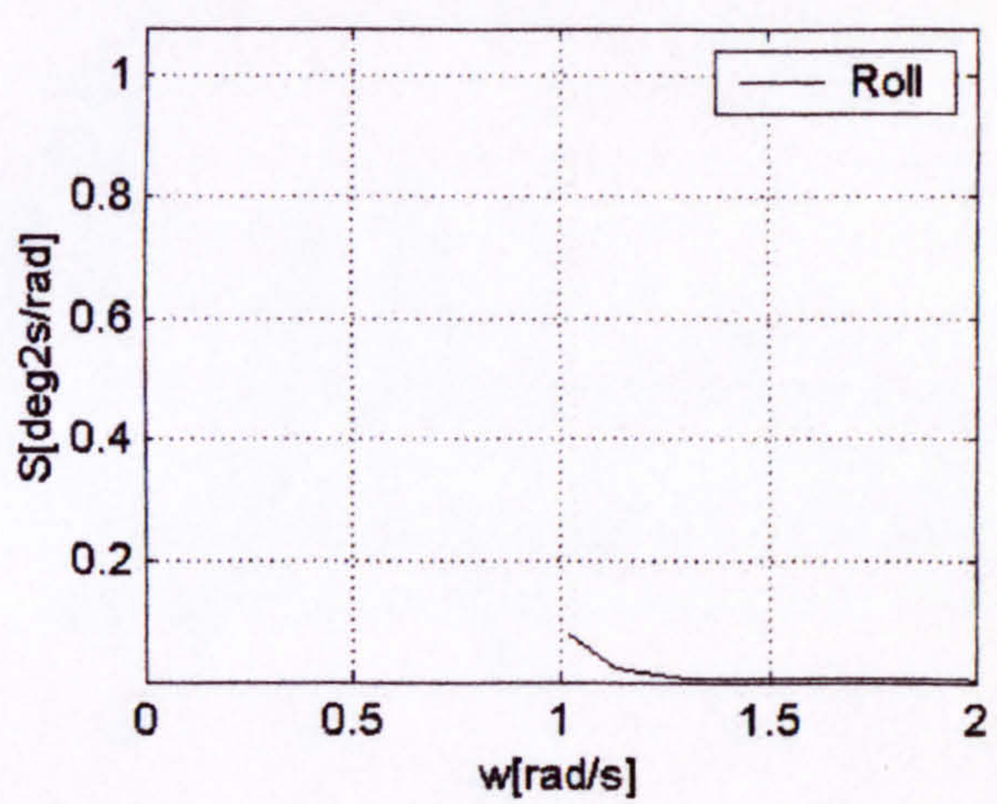

Figure 27 Numerical simulations, PRR1, KG=12.892m, Hs=4.00m

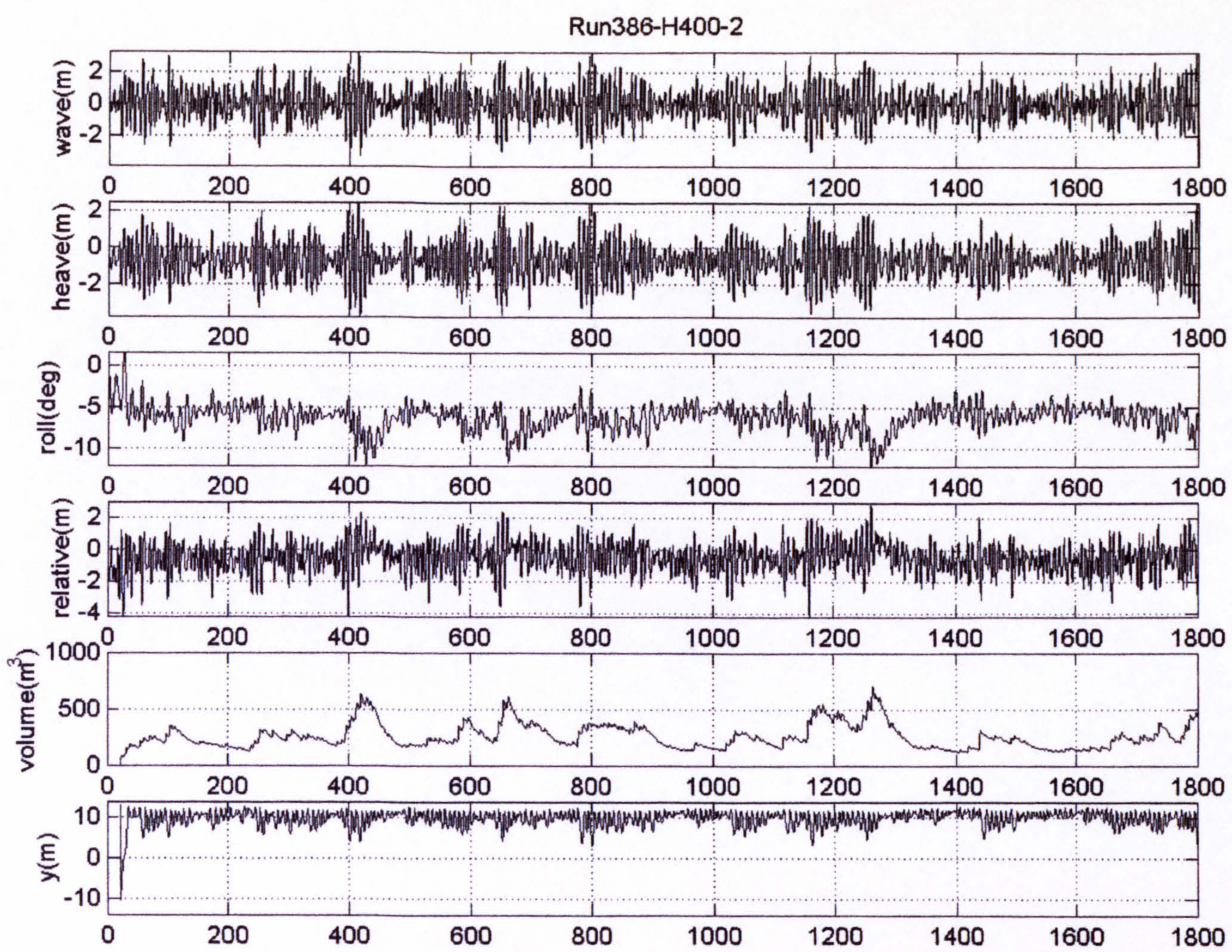

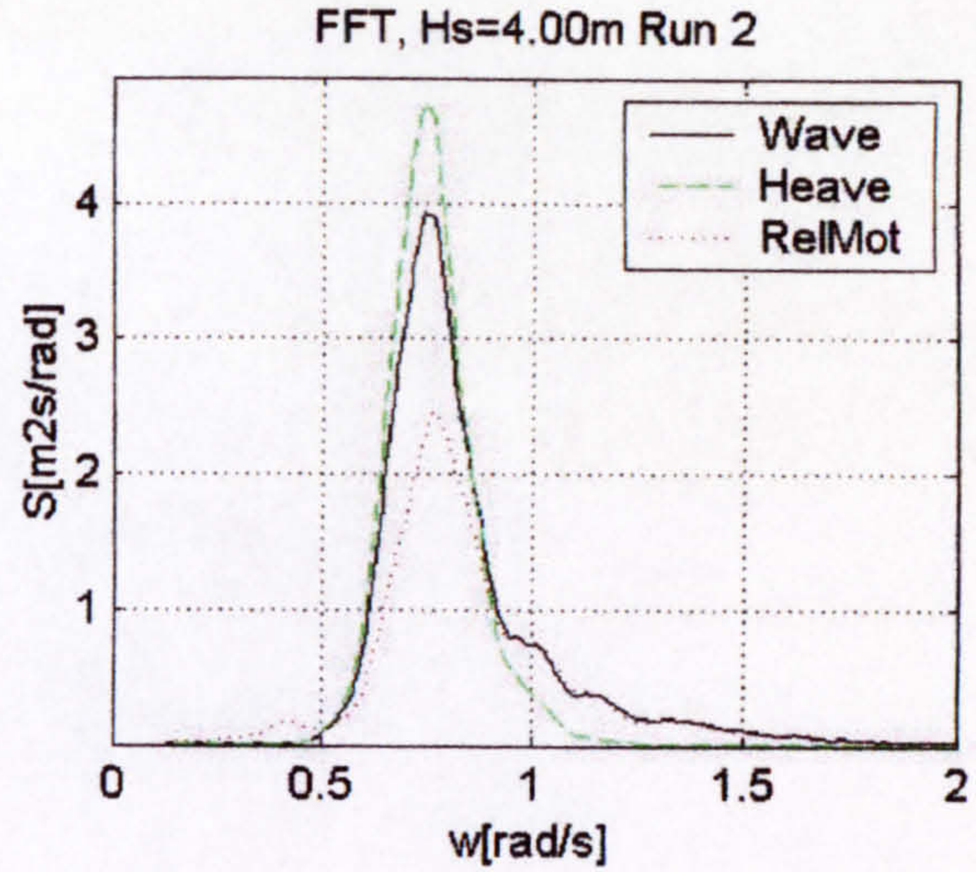

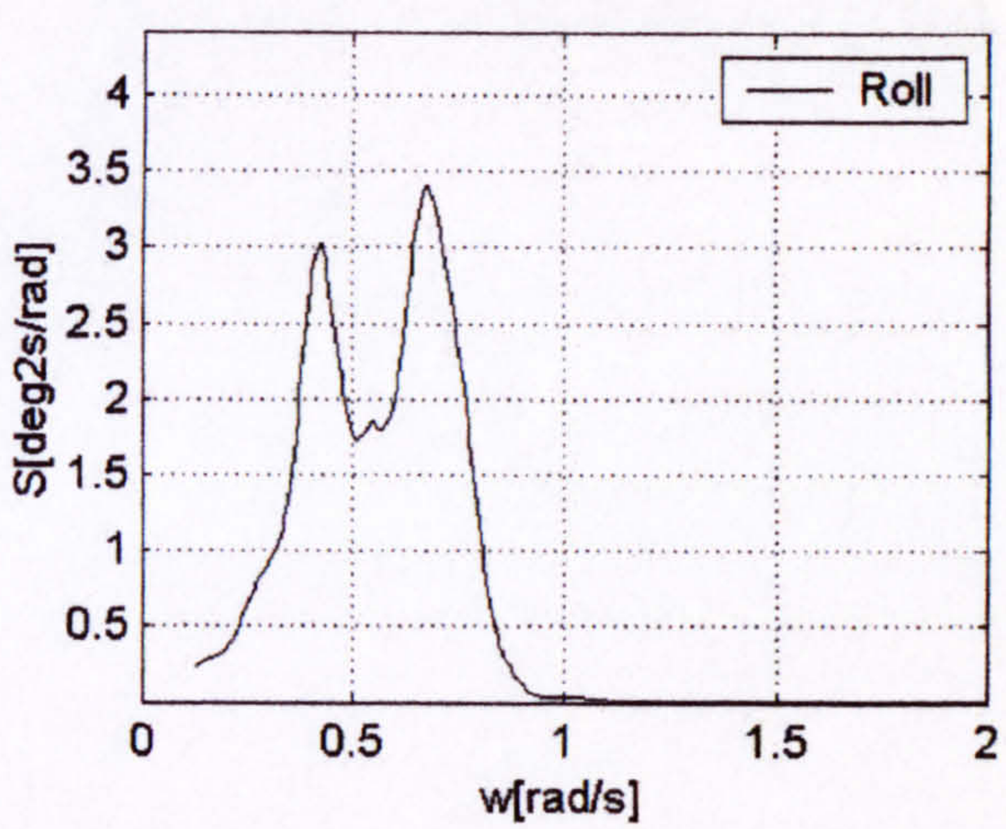

Figure 28 Numerical simulations, PRR1, KG=12.892m, Hs=4.00m

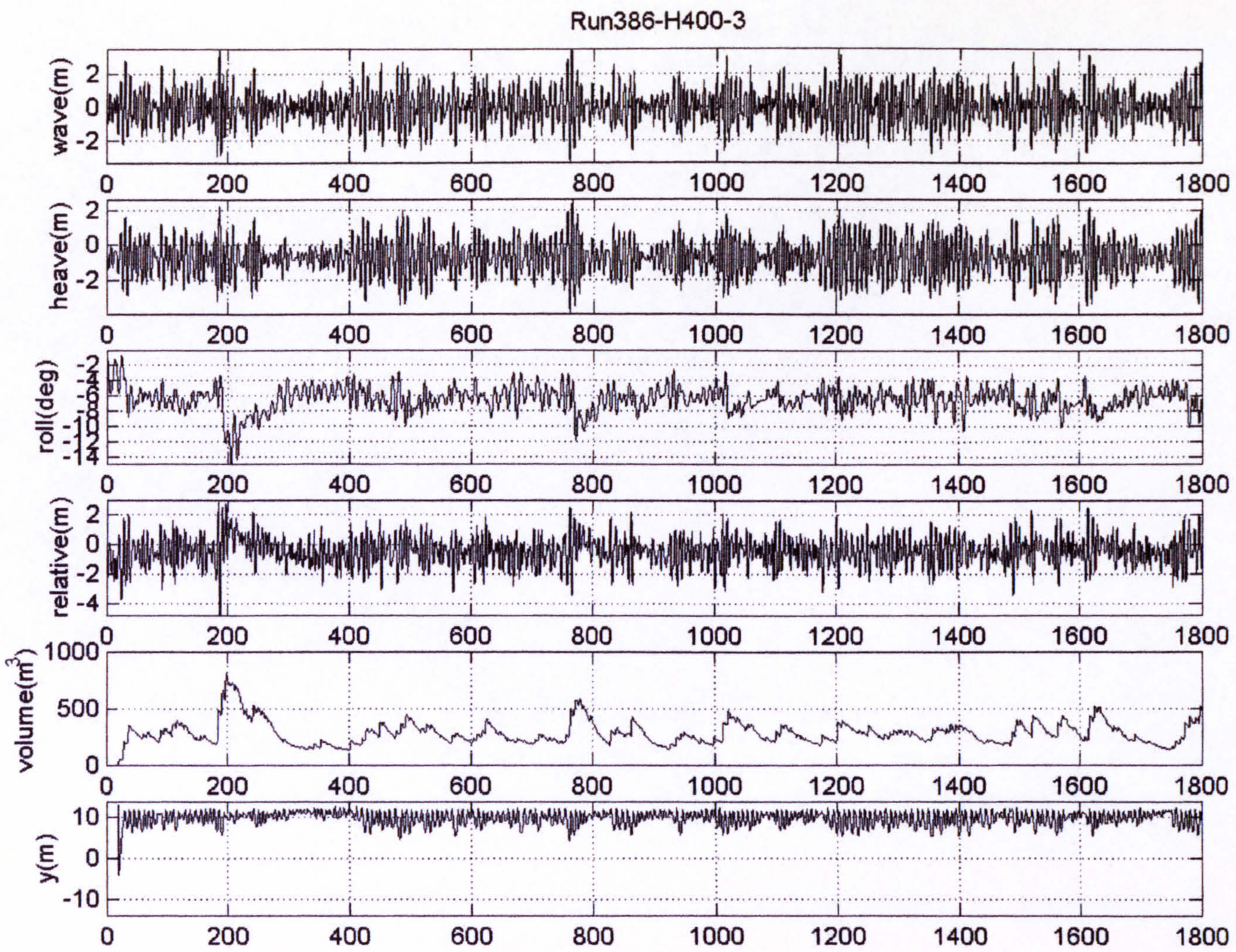

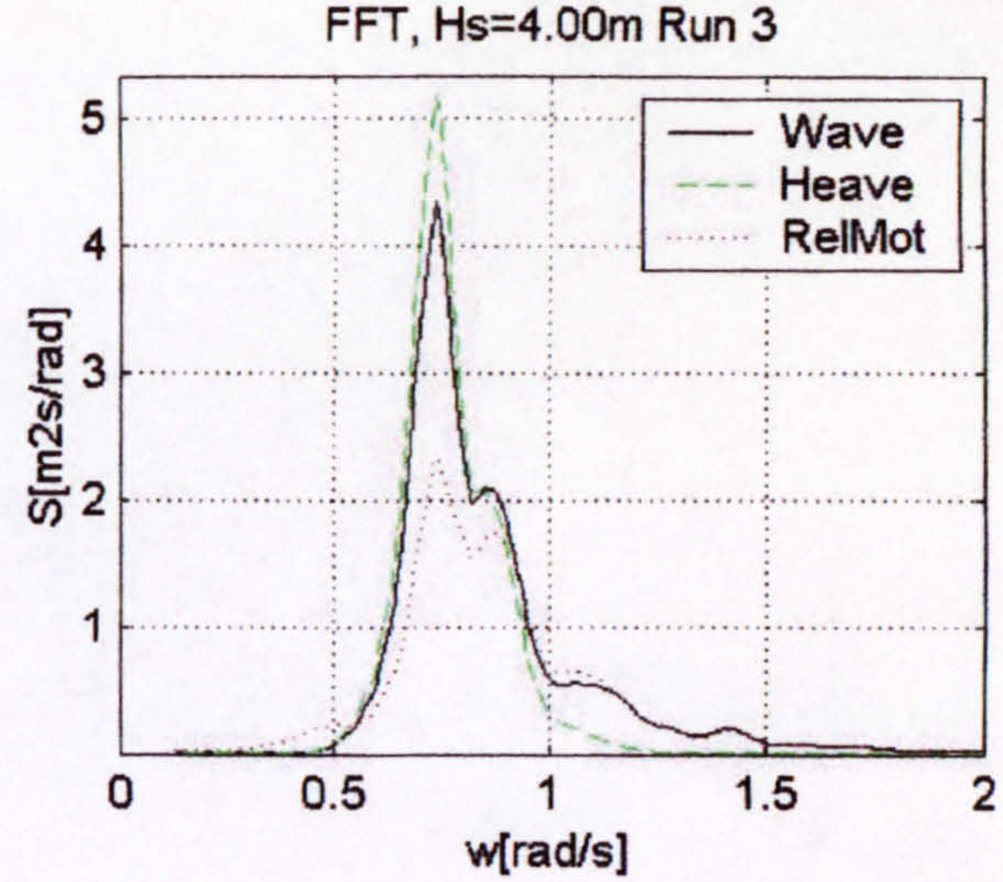

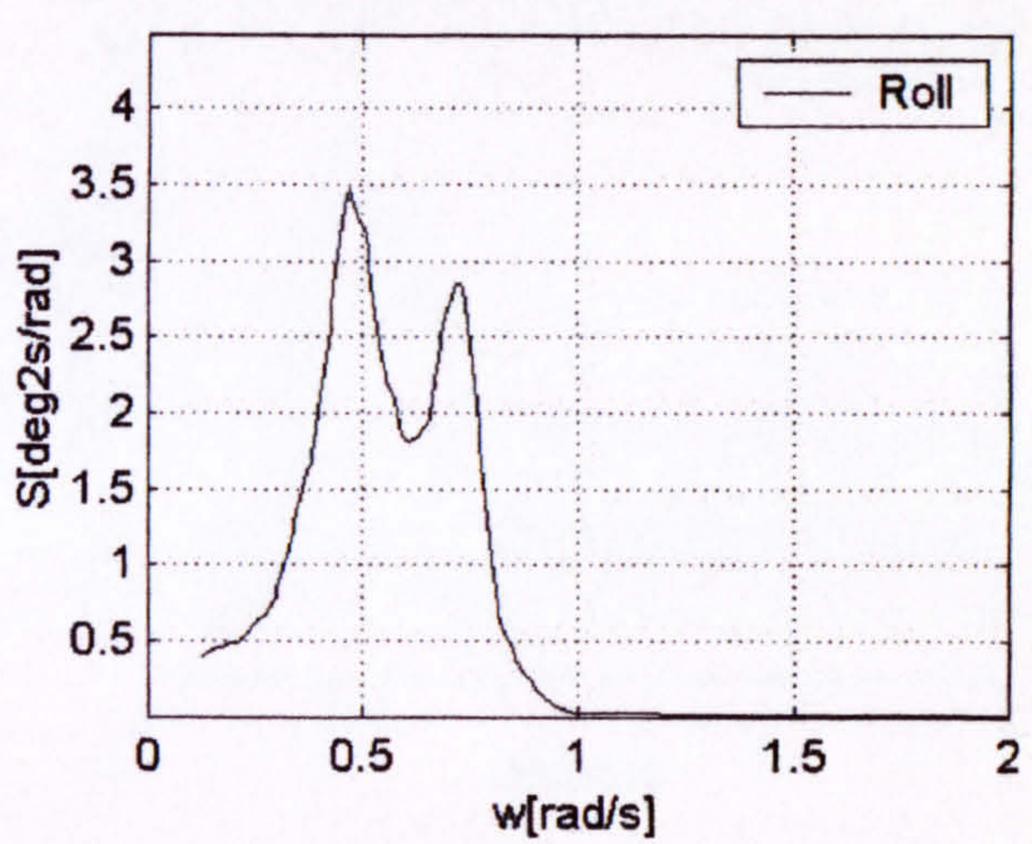

Figure 29 Numerical simulations, PRR1, KG=12.892m, Hs=4.00m

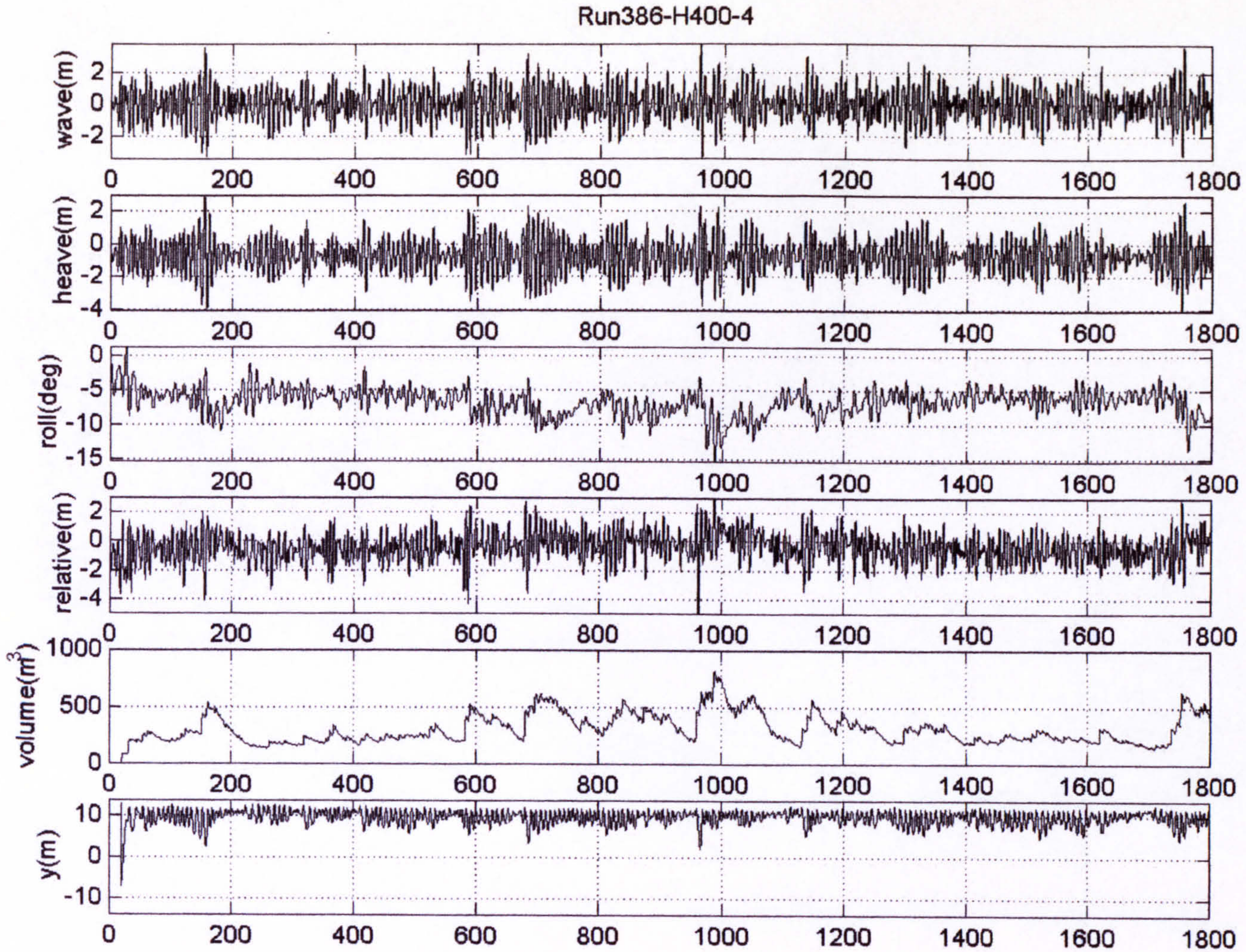

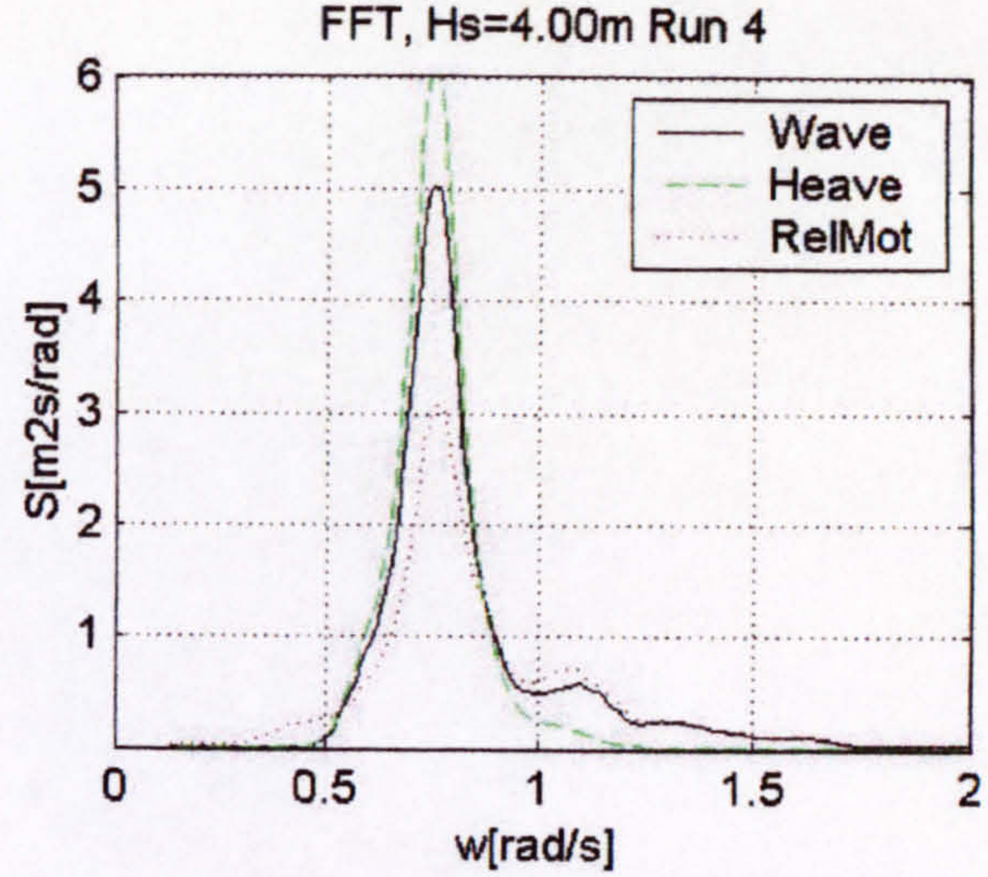

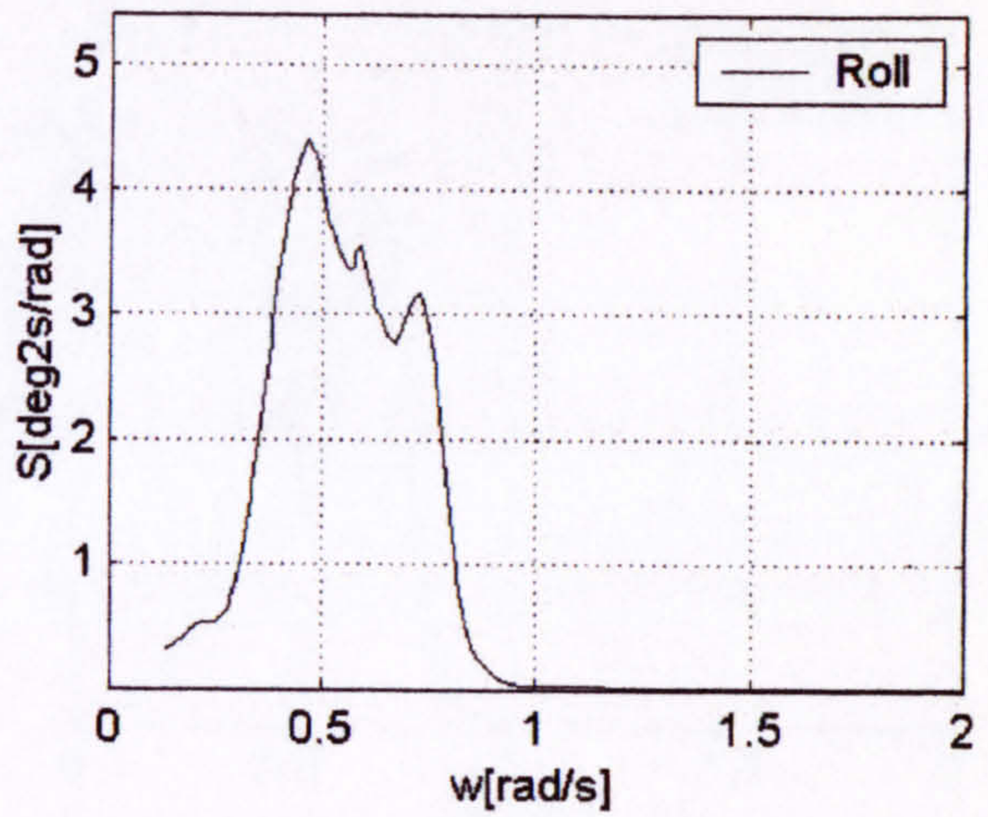

Figure 30 Numerical simulations, PRR1, KG=12.892m, Hs=4.00m

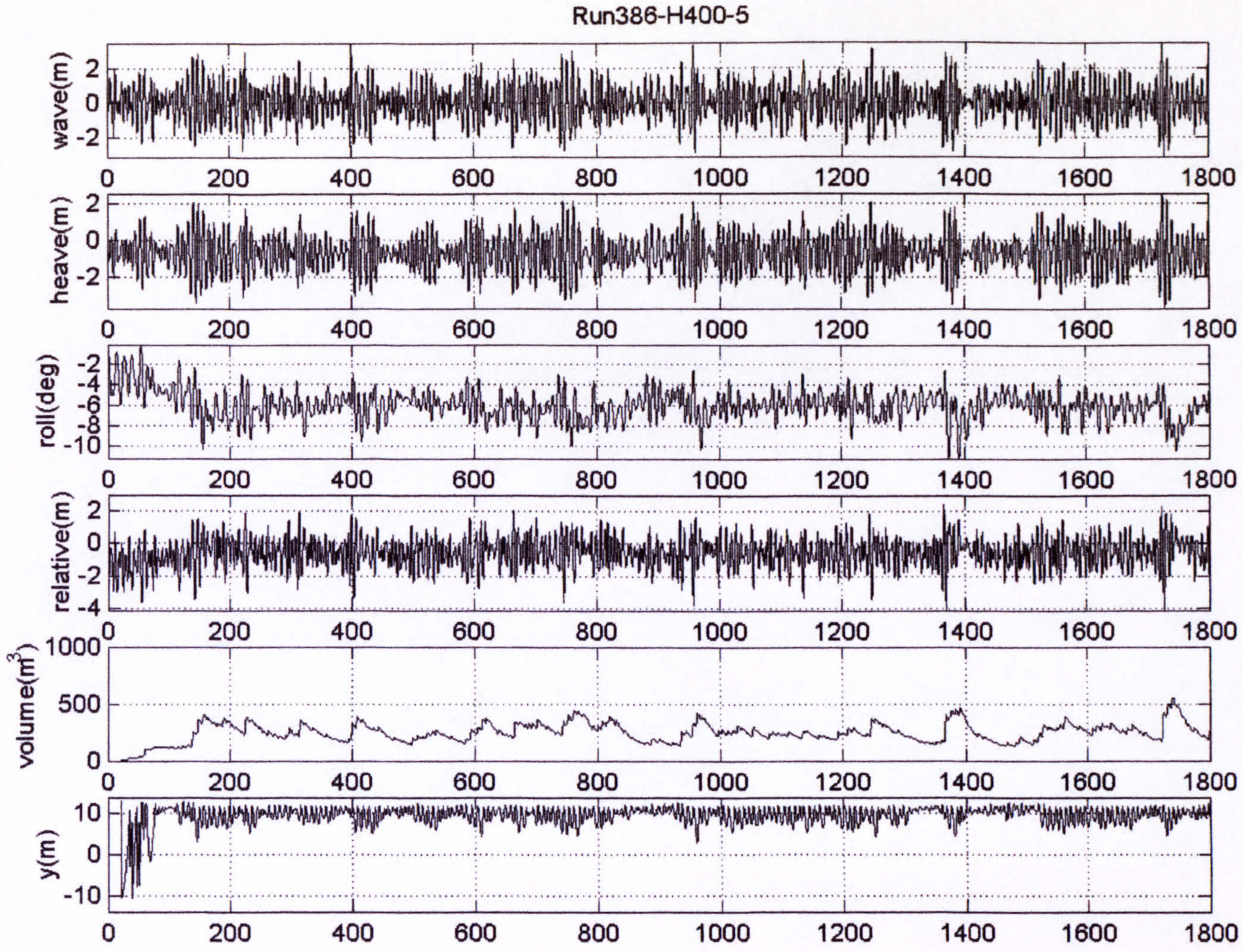

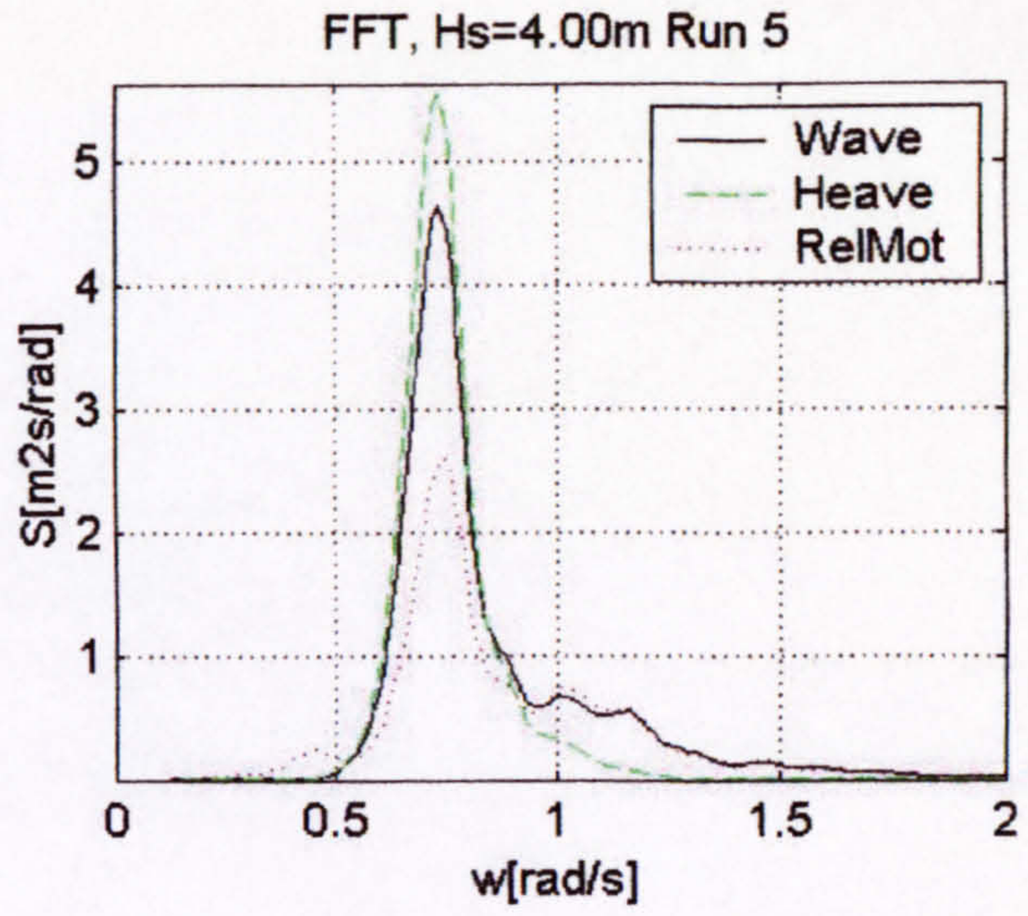

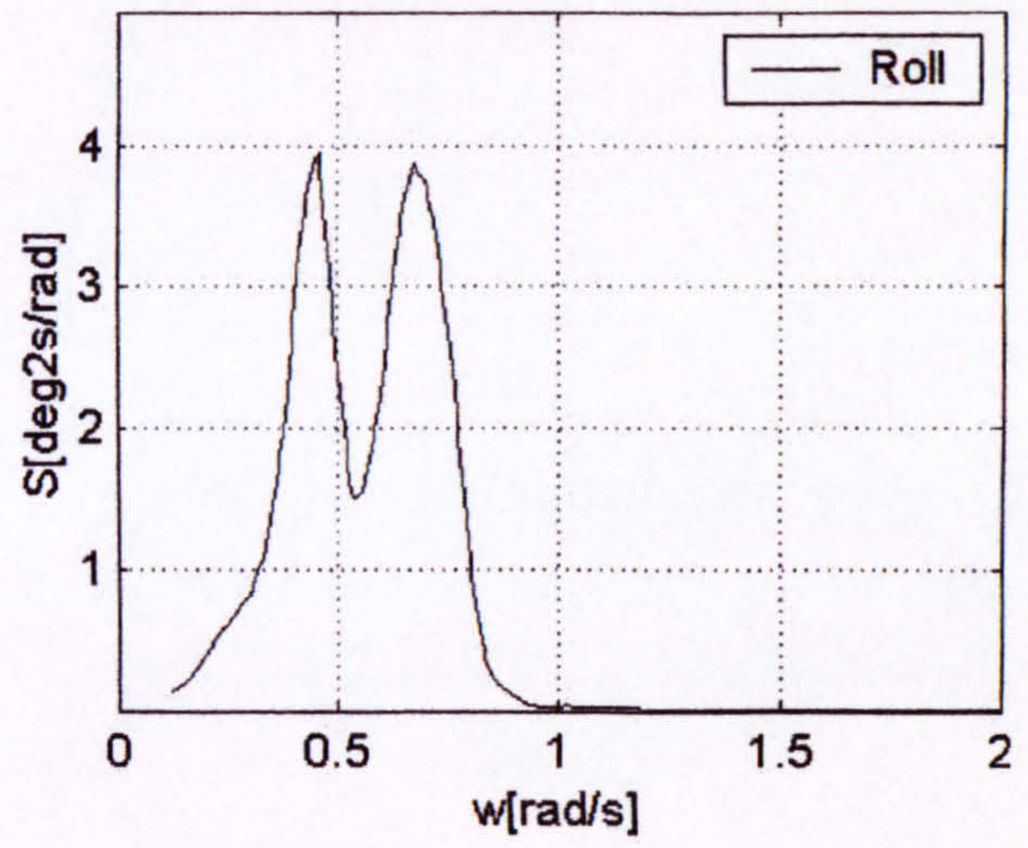

Figure 31 Numerical simulations, PRR1, KG=12.892m, Hs=4.00m

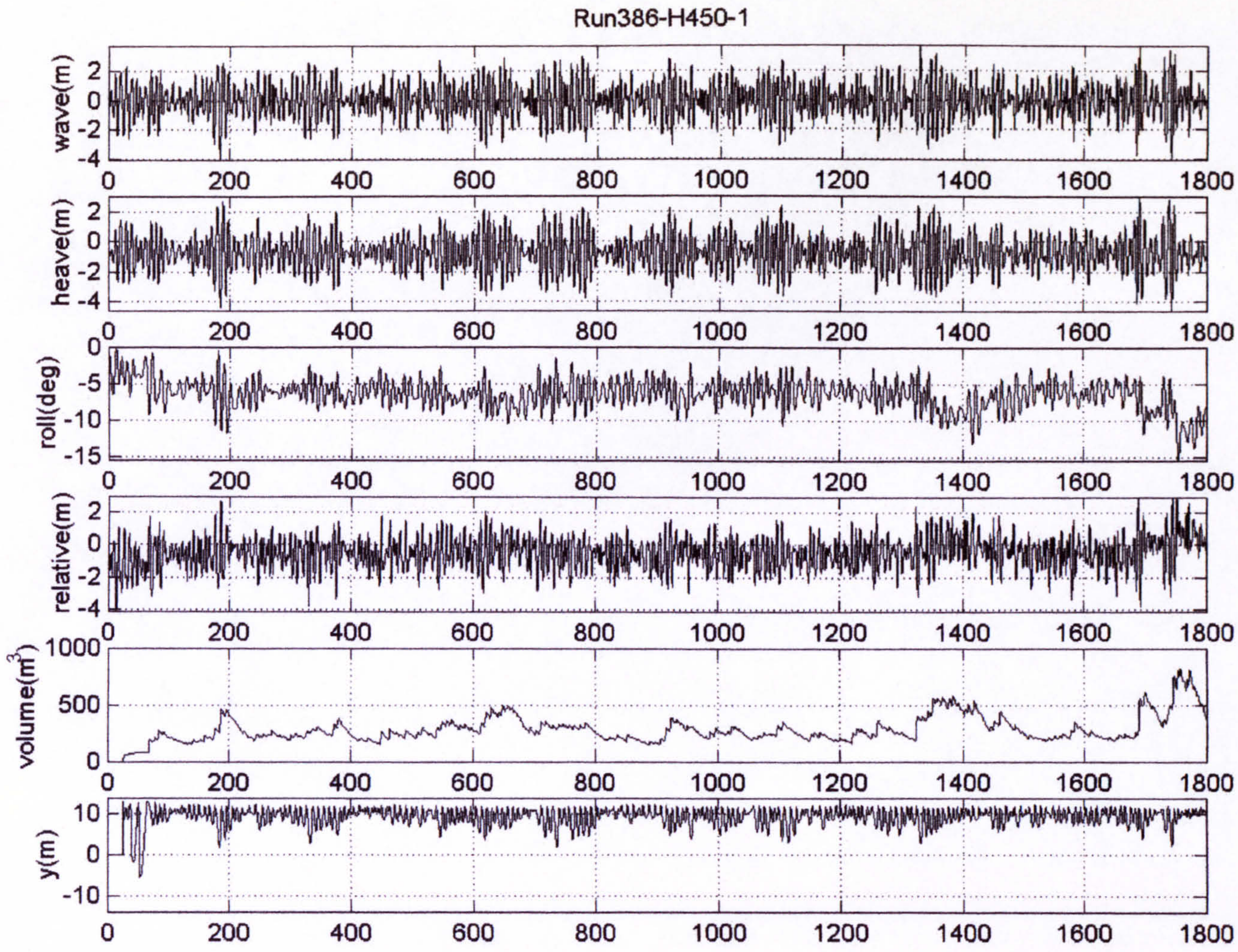

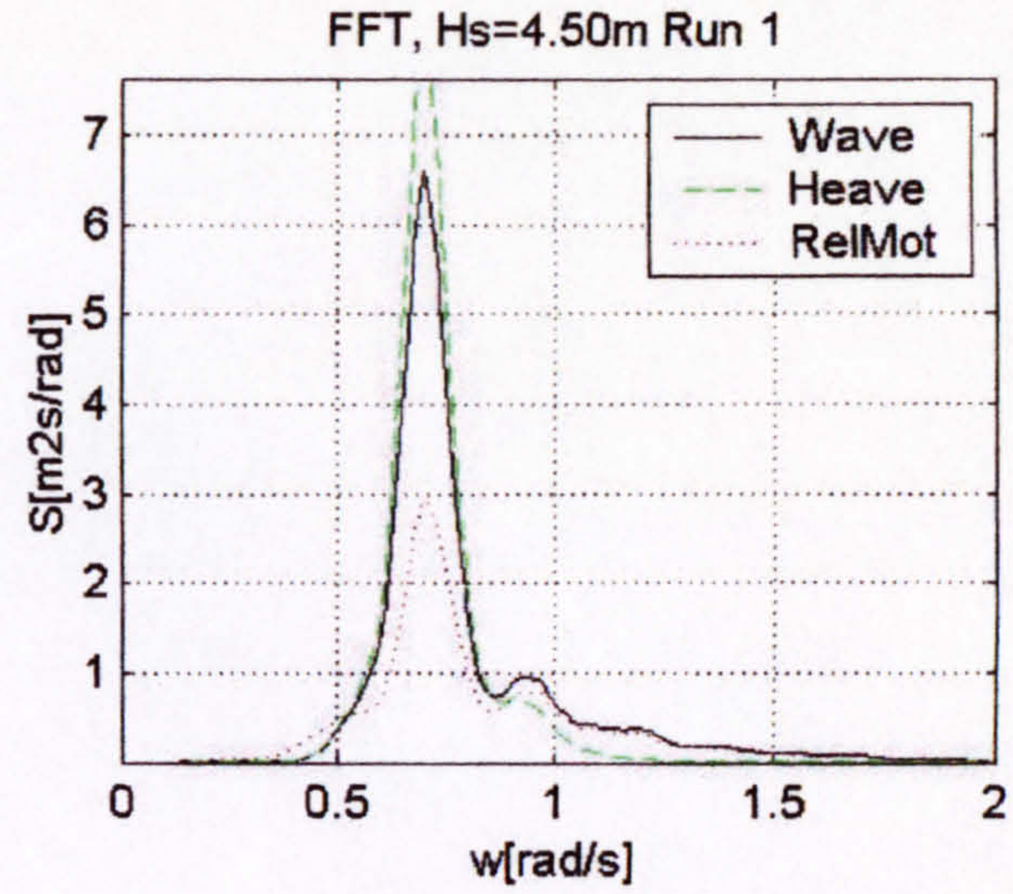

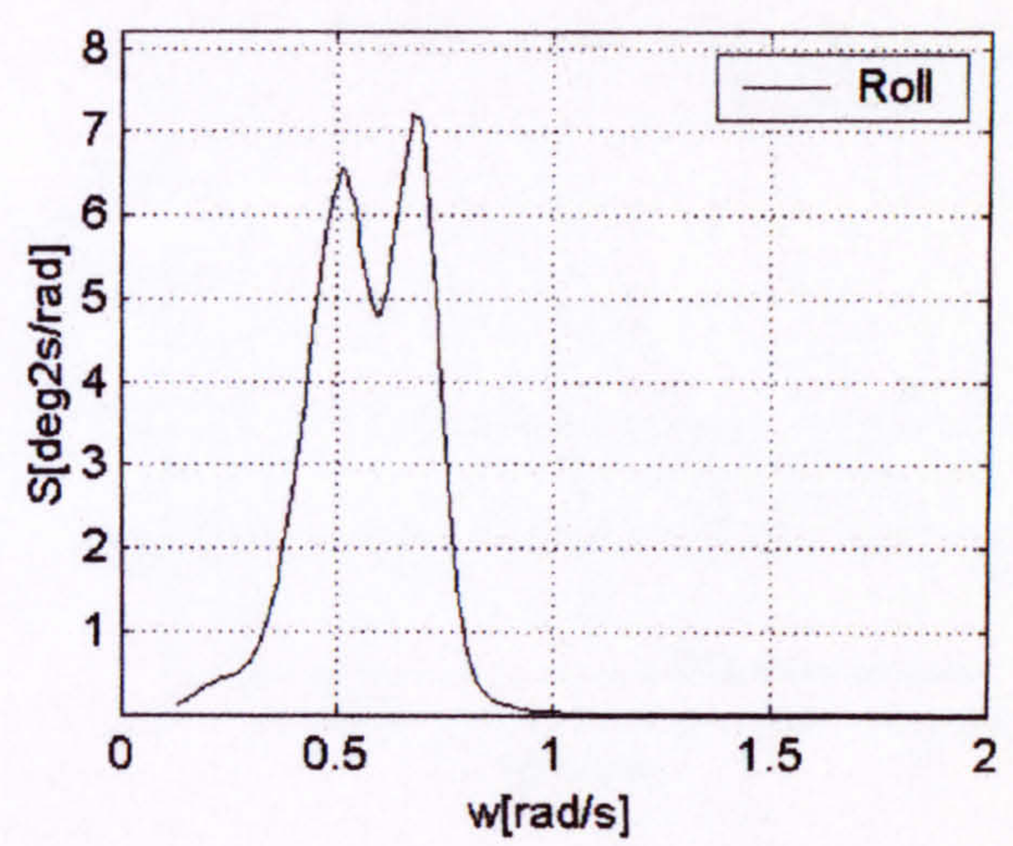

Figure 32 Numerical simulations, PRR1, KG=12.892m, Hs=4.50m

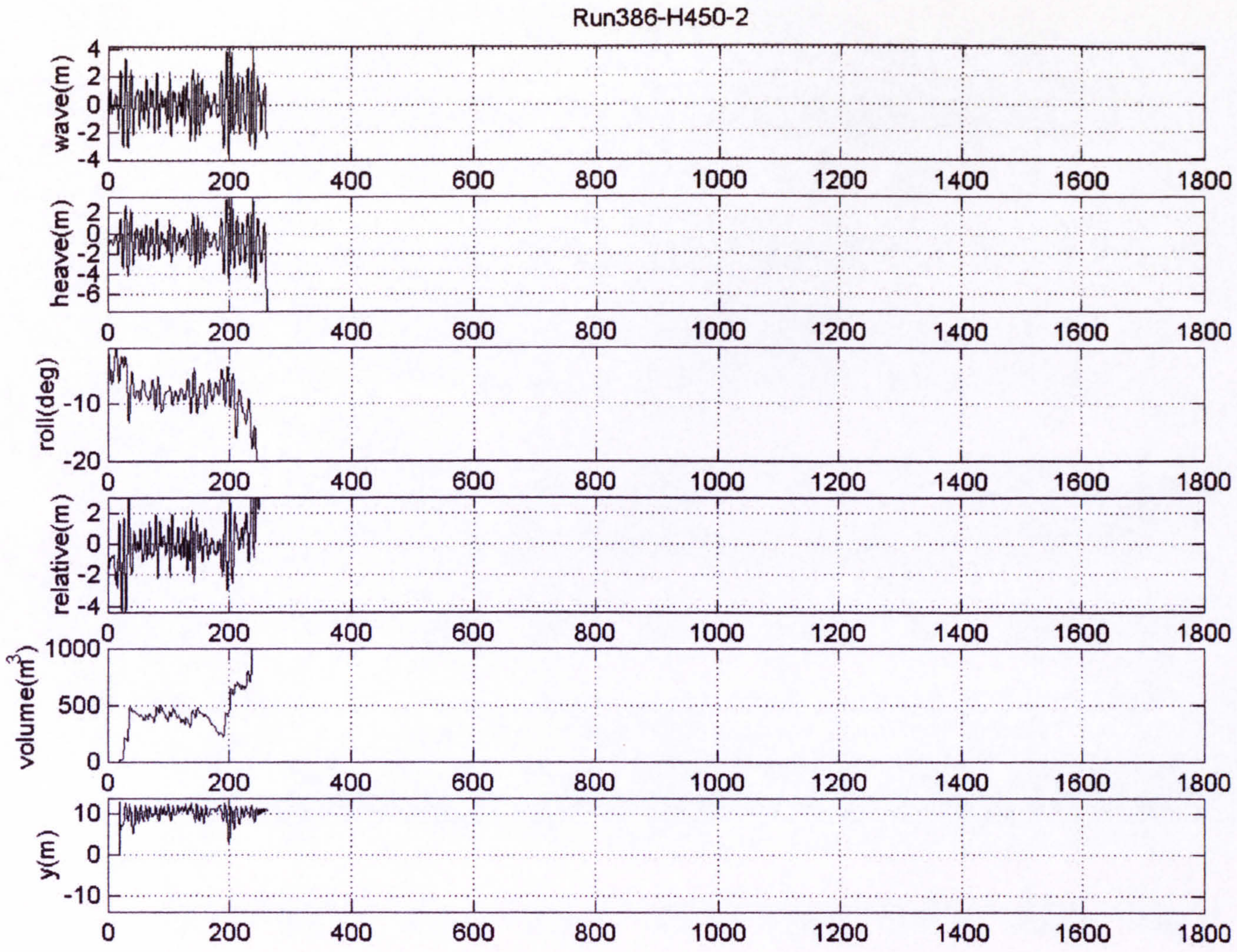

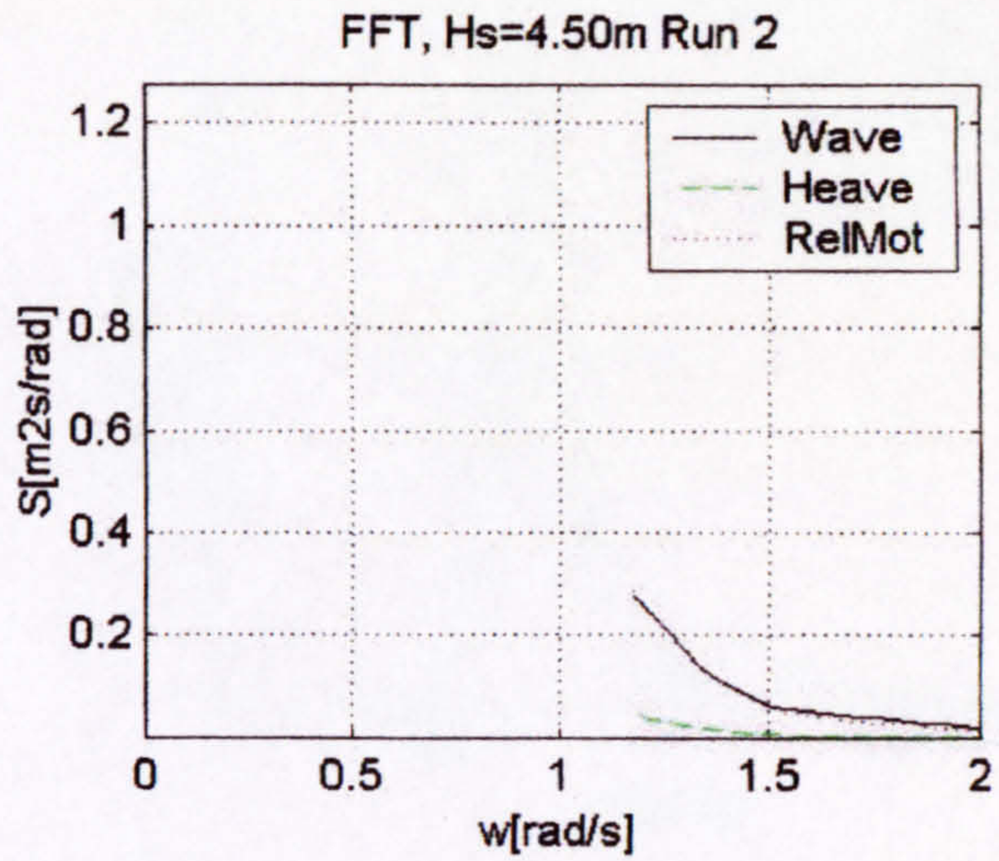

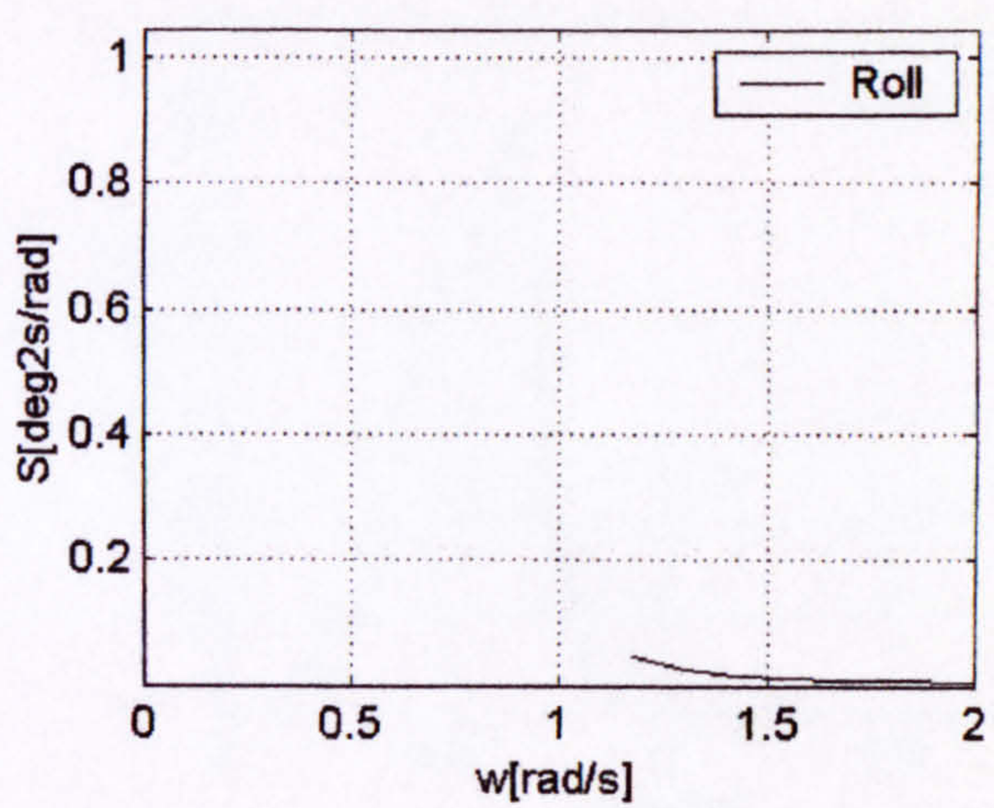

Figure 33 Numerical simulations, PRR1, KG=12.892m, Hs=4.50m

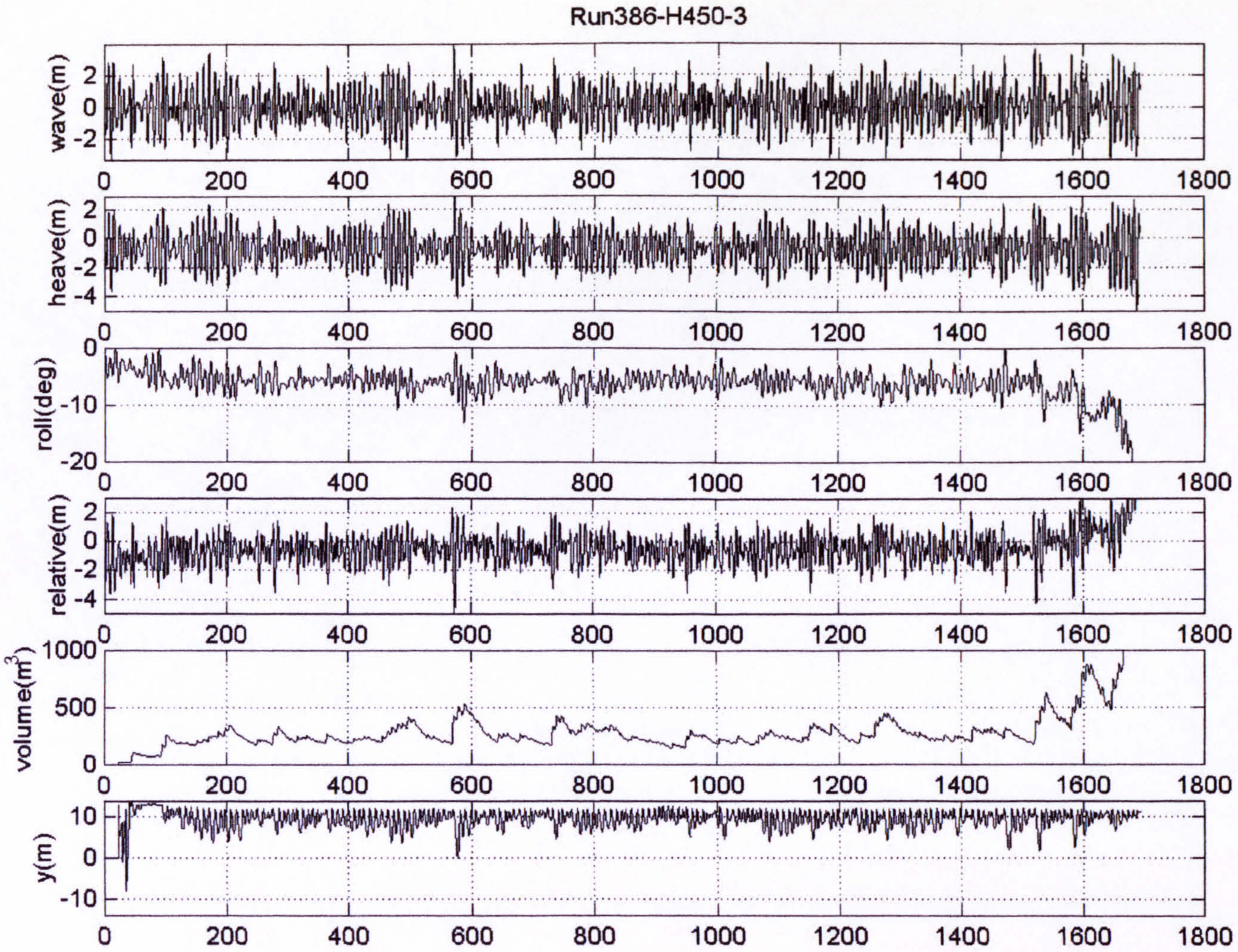

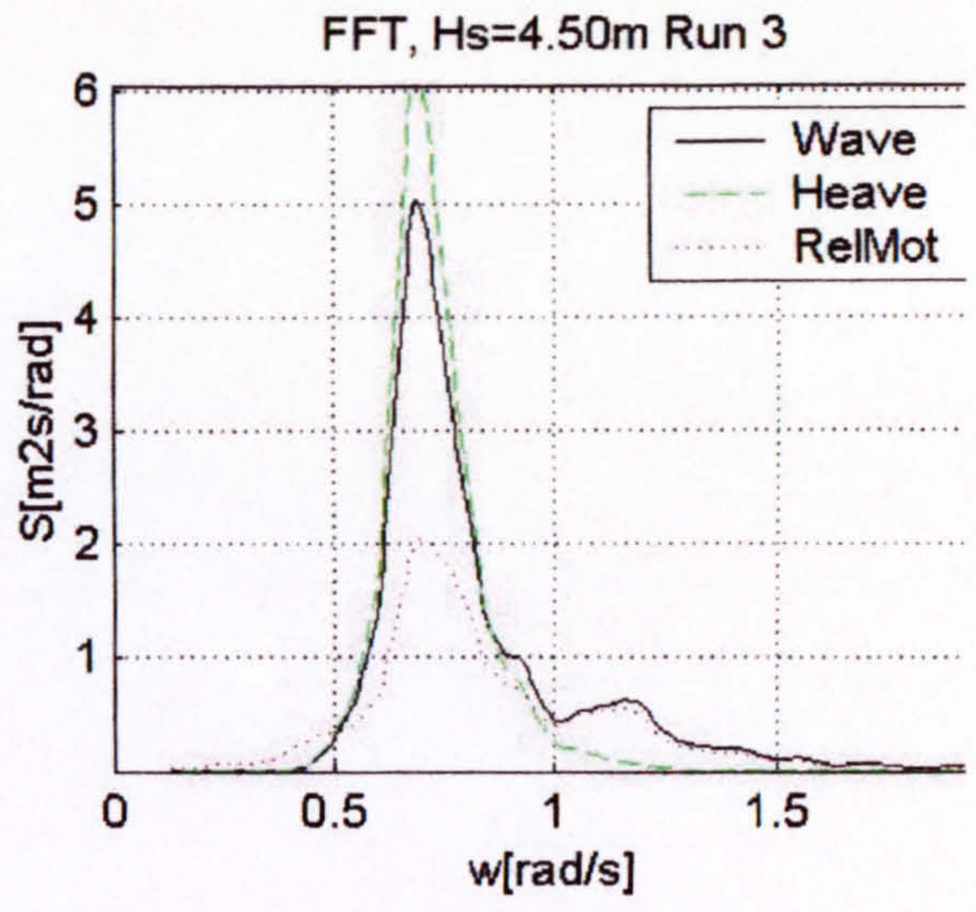

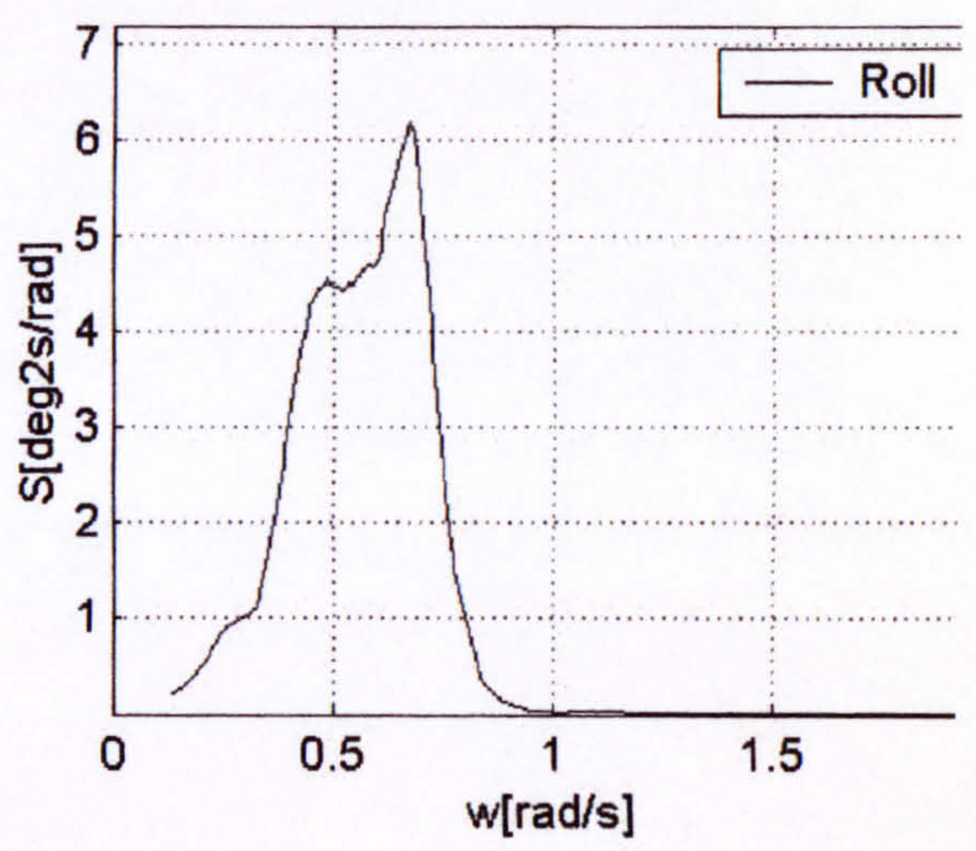

Figure 34 Numerical simulations, PRR1, KG=12.892m, Hs=4.50m

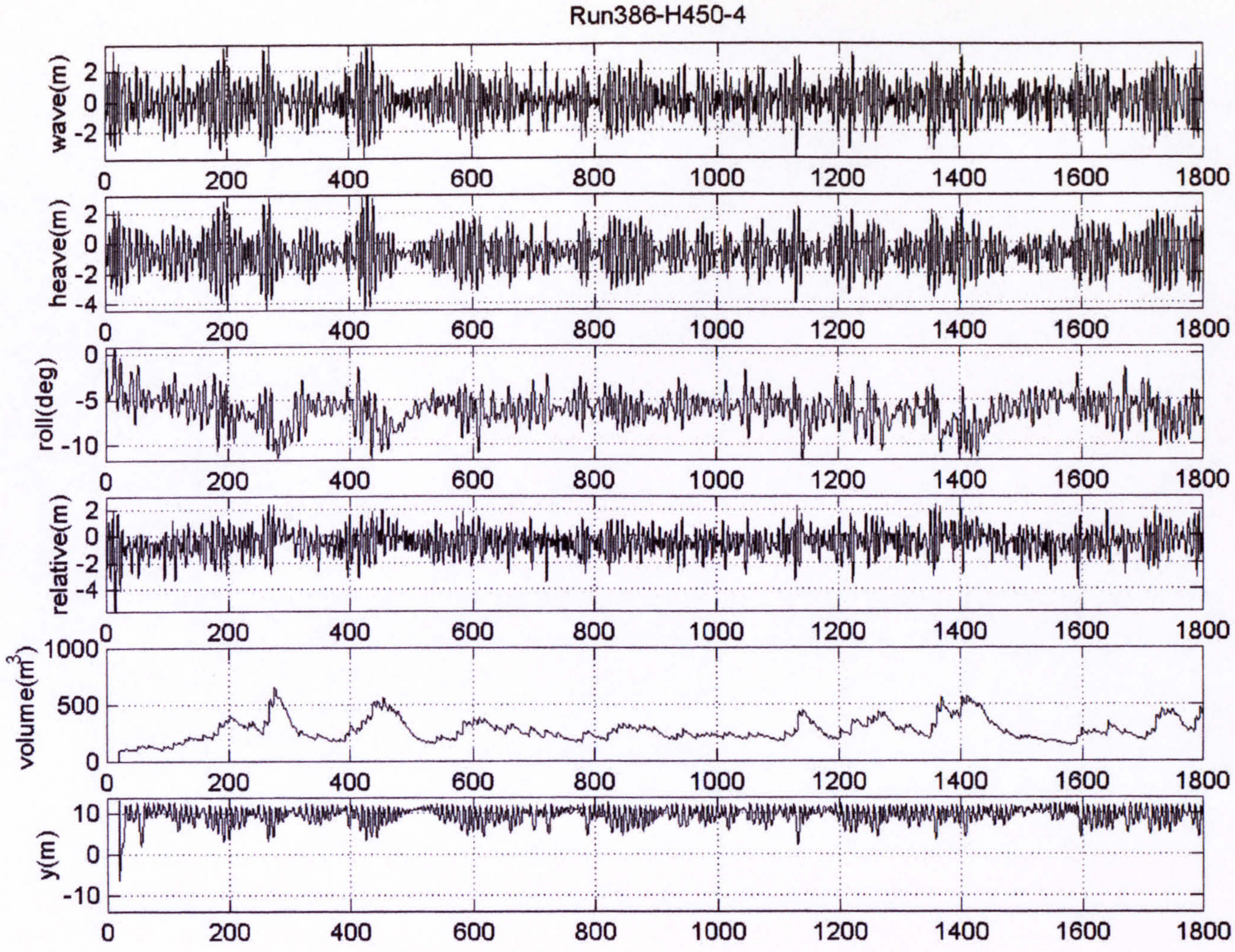

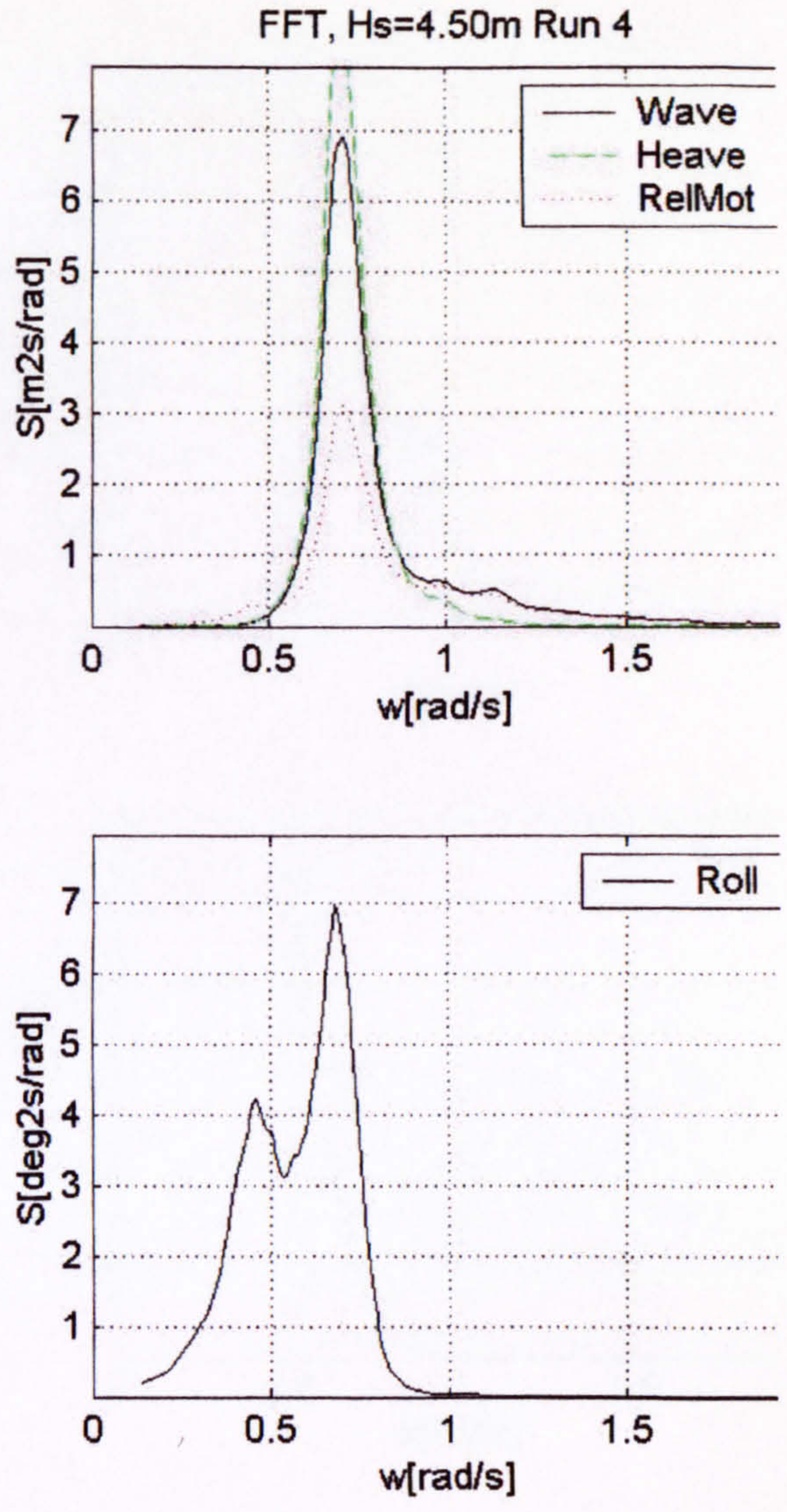

Figure 35 Numerical simulations, PRR1, KG=12.892m, Hs=4.50m

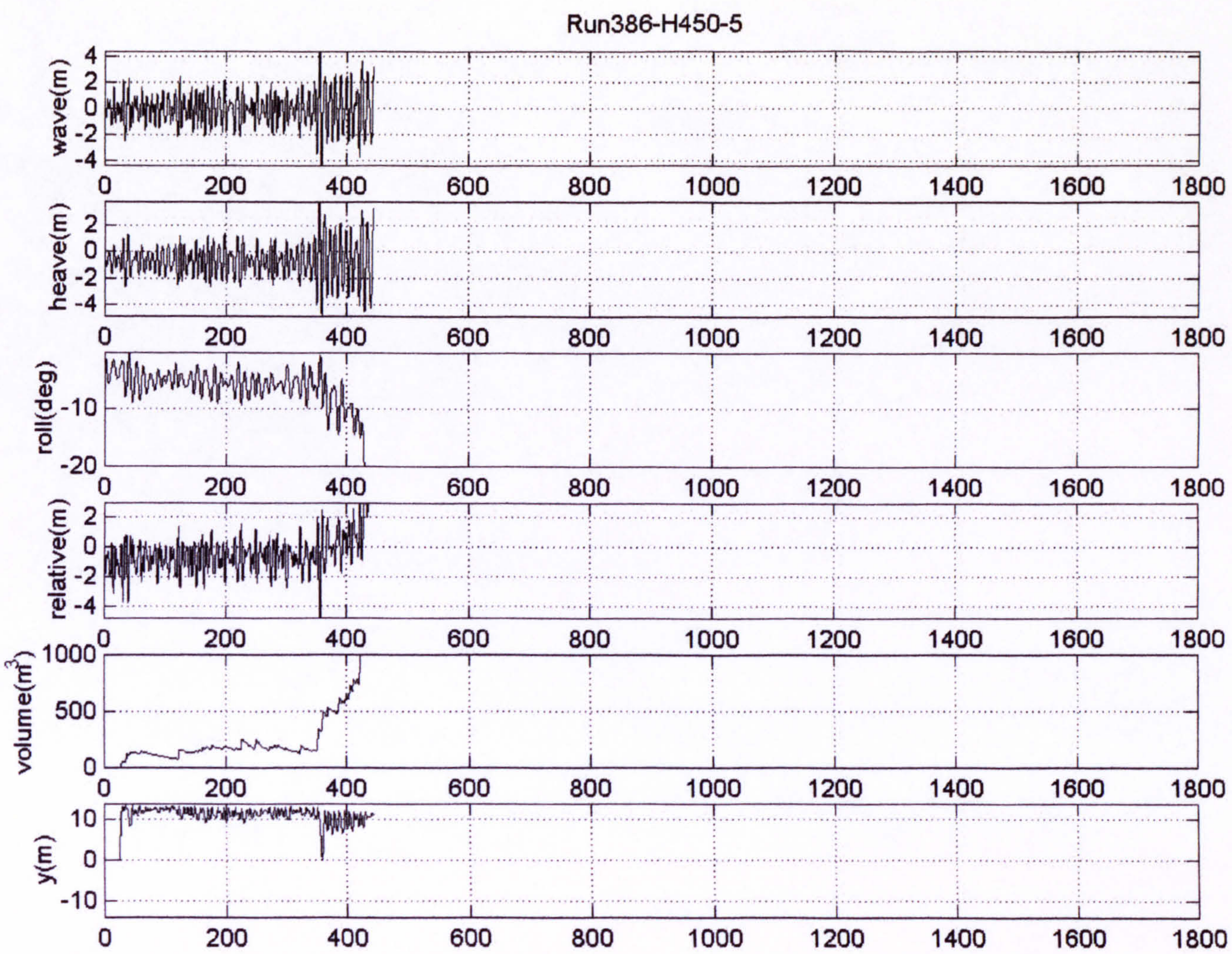

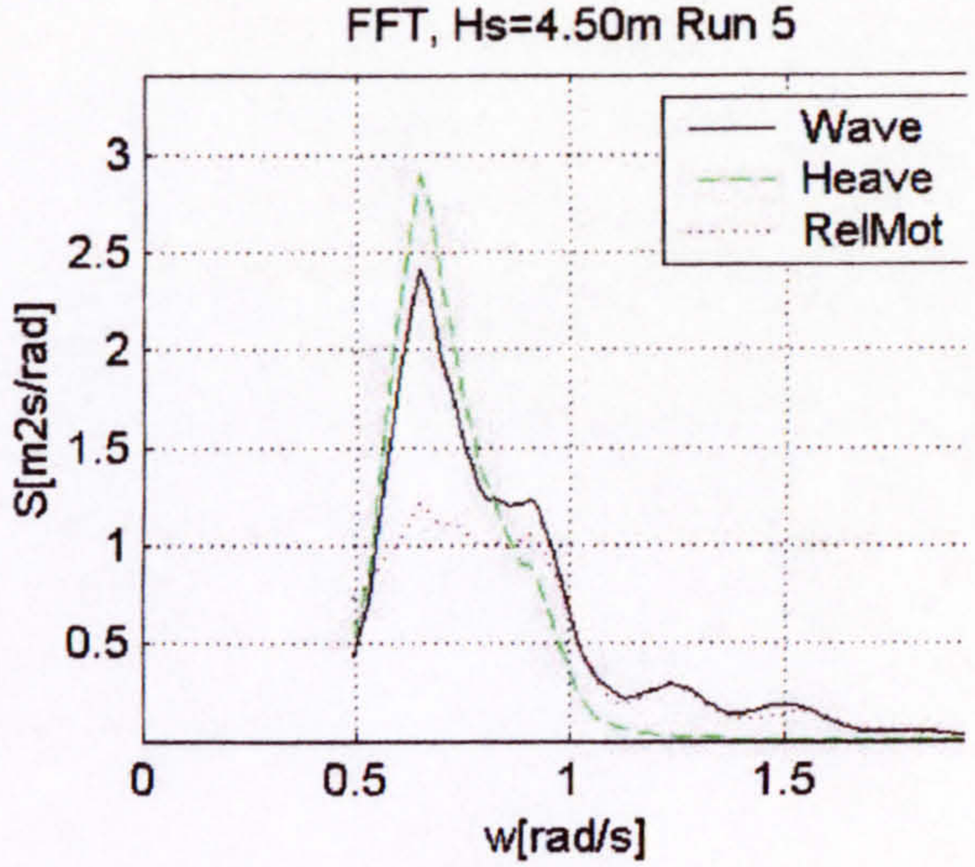

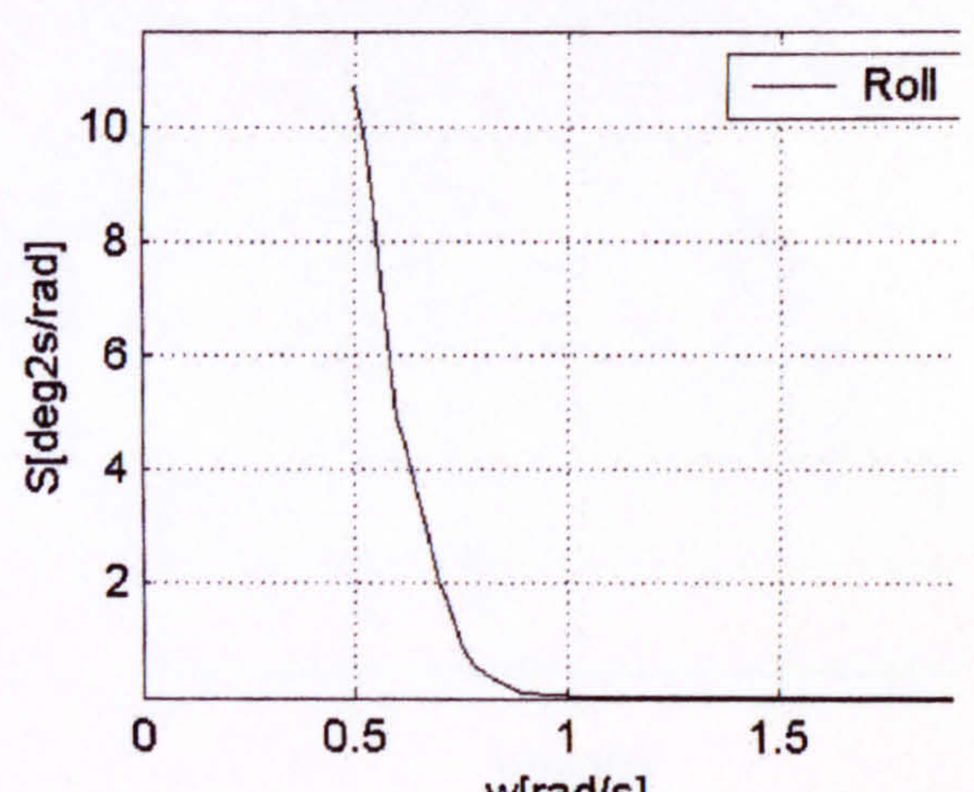

Figure 36 Numerical simulations, PRR1, KG=12.892m, Hs=4.50m

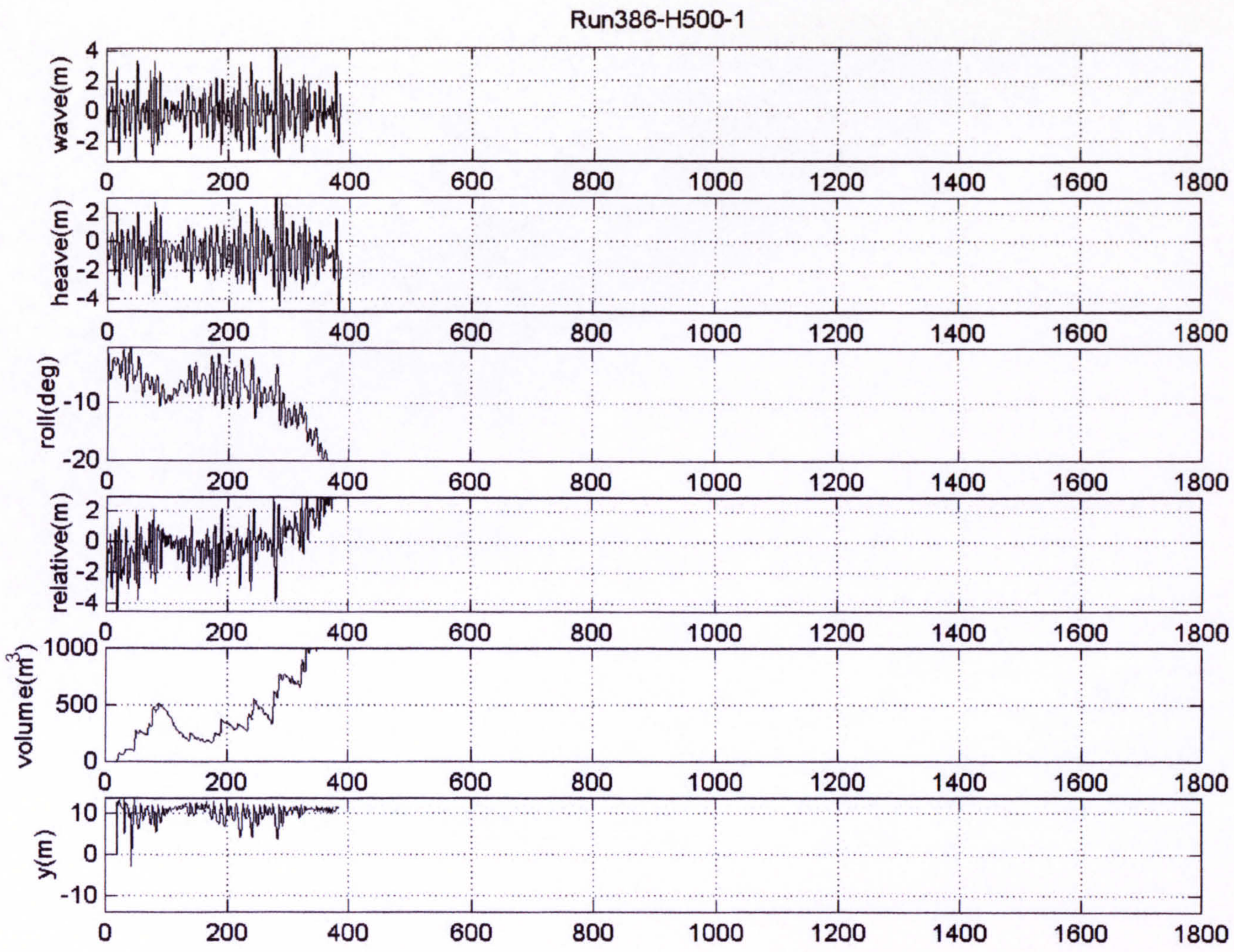

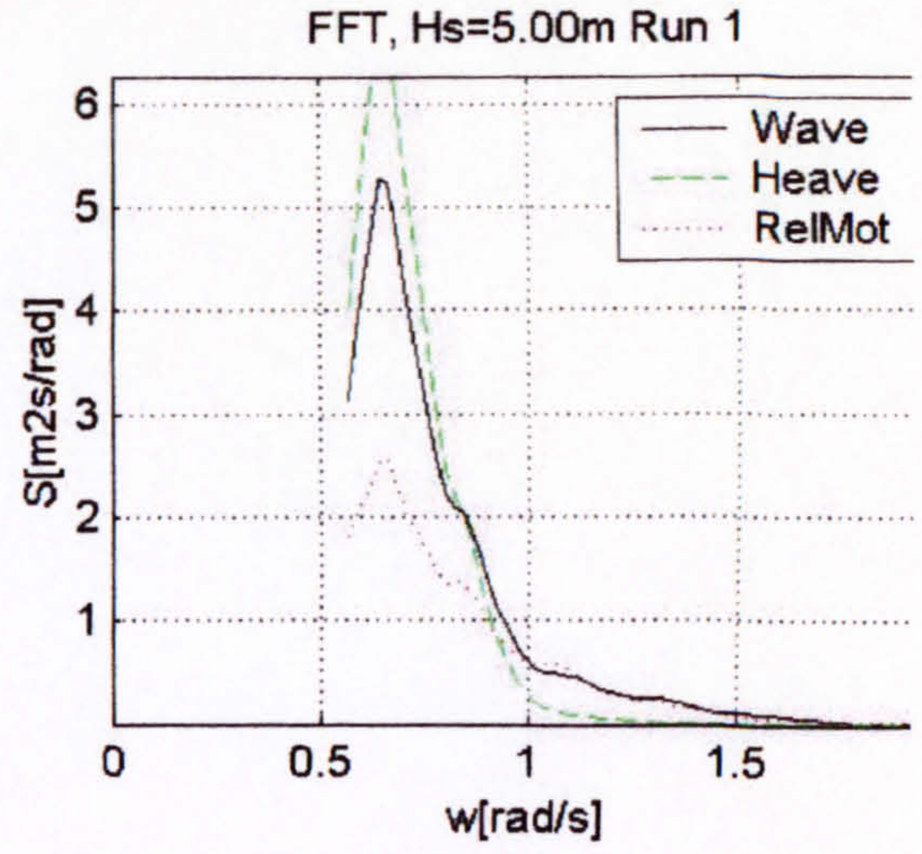

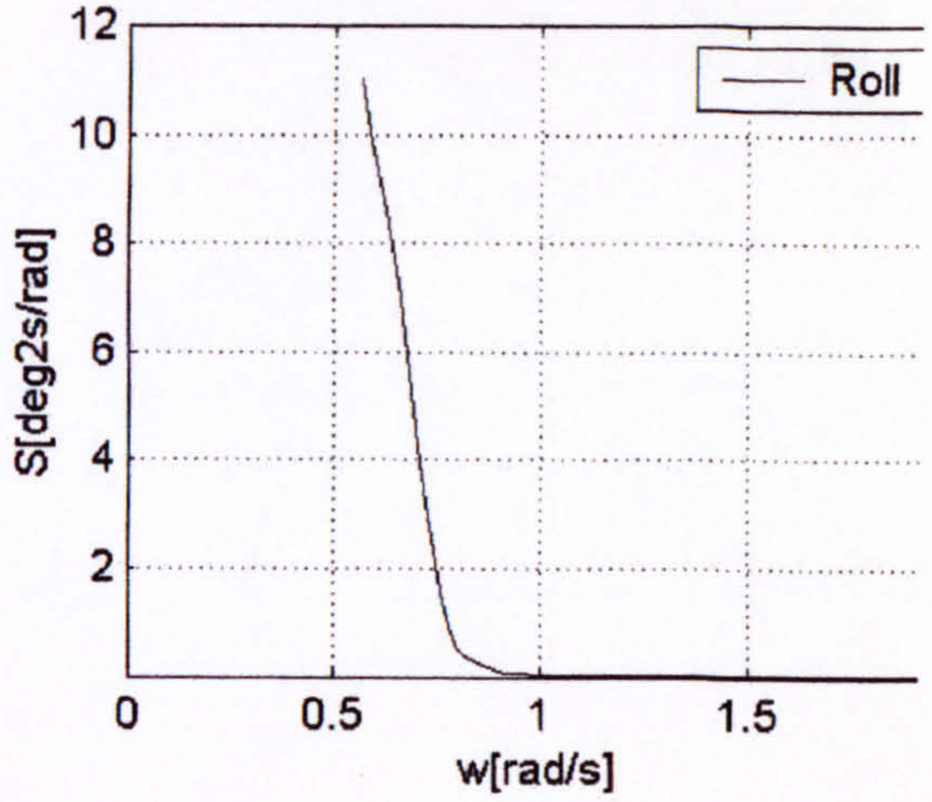

Figure 37 Numerical simulations, PRR1, KG=12.892m, Hs=5.00m

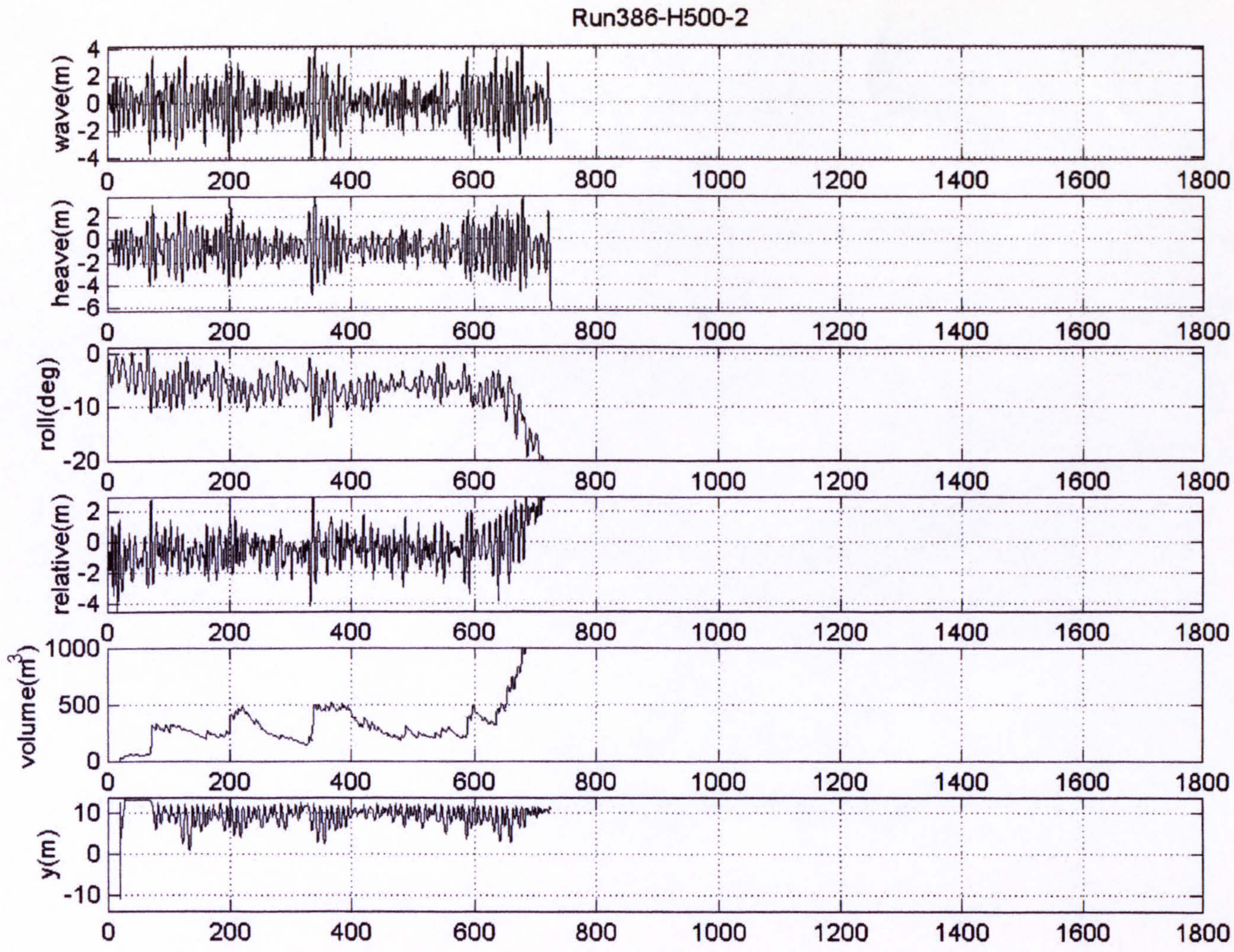

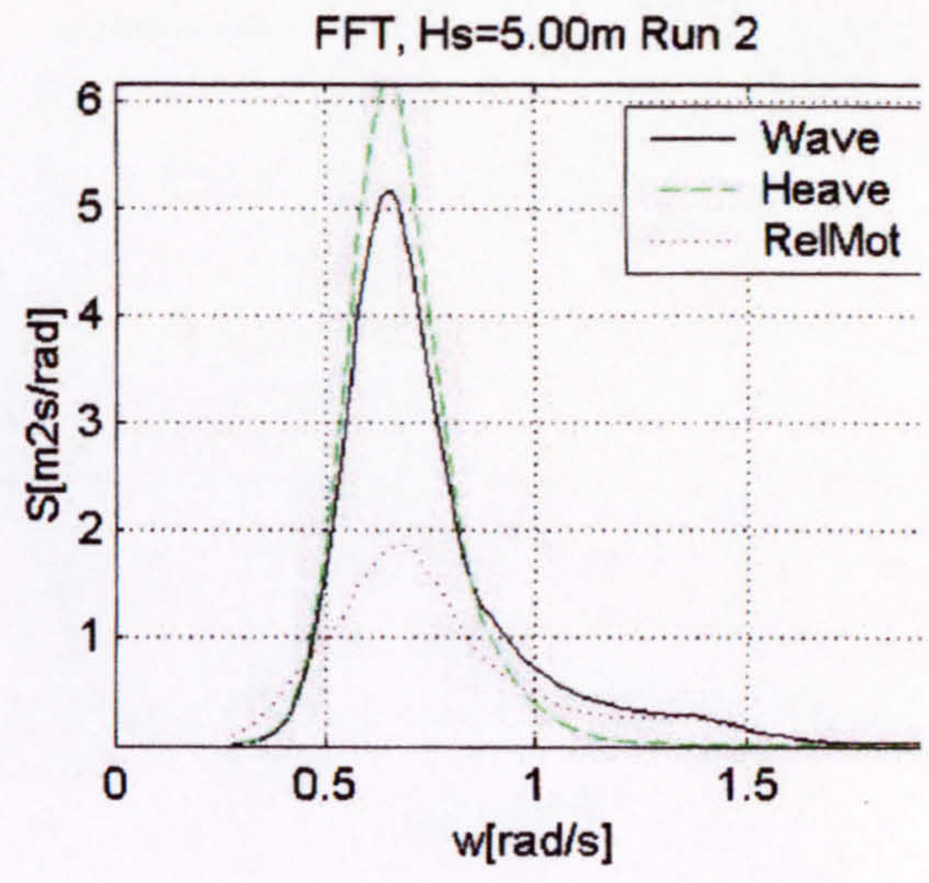

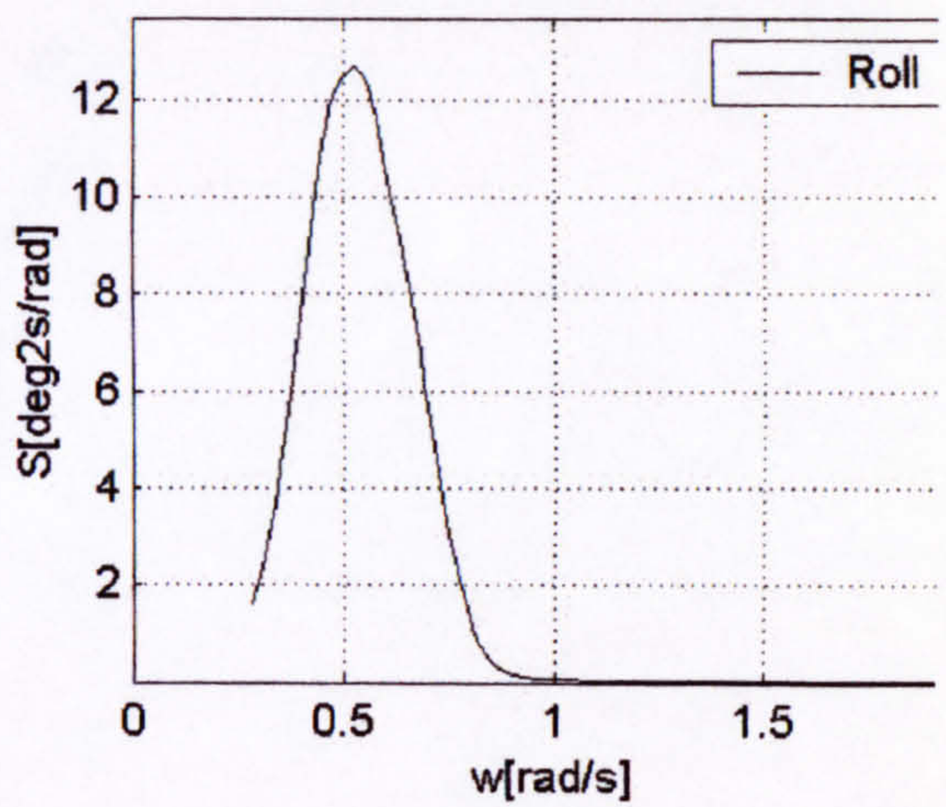

Figure 38 Numerical simulations, PRR1, KG=12.892m, Hs=5.00m

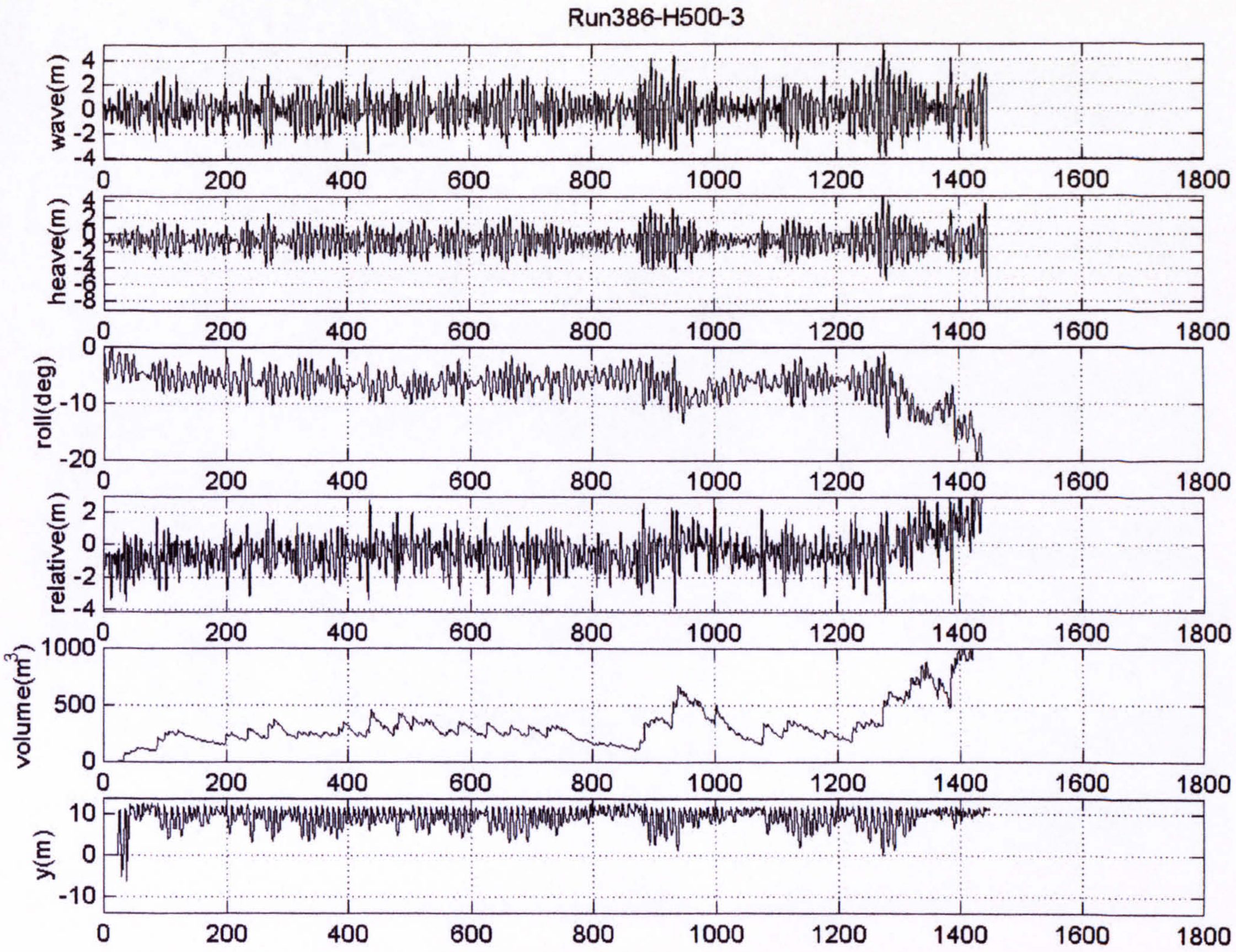

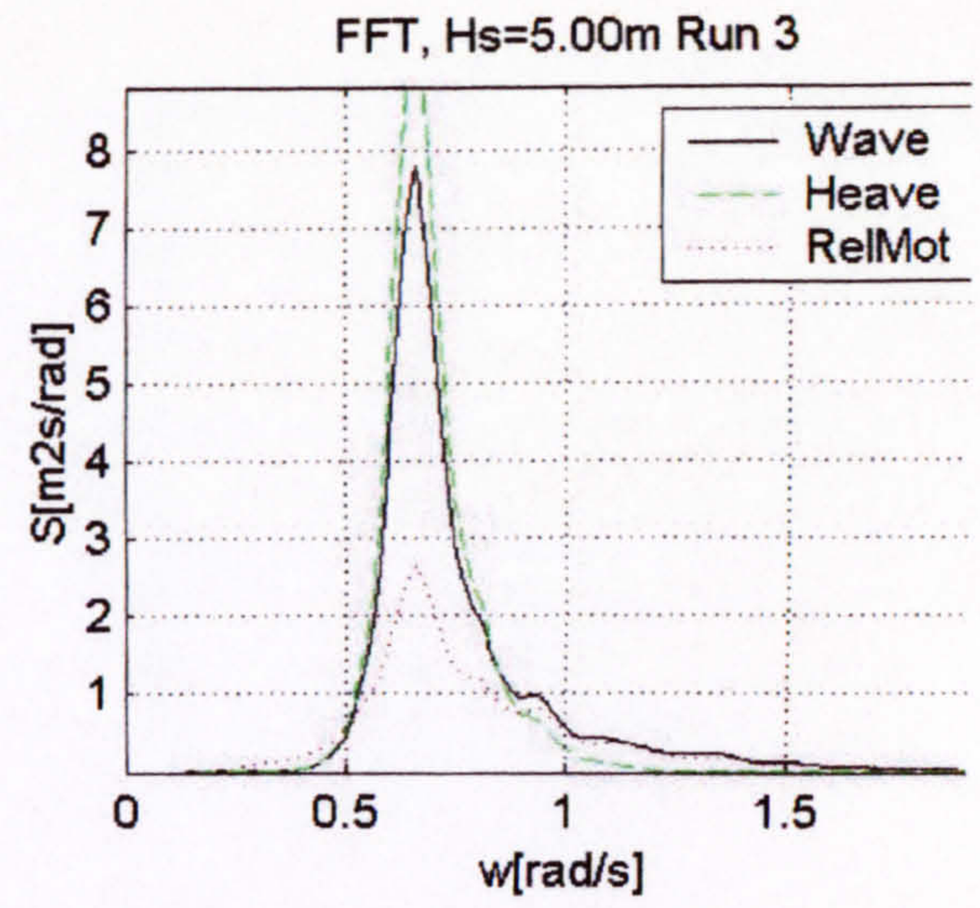

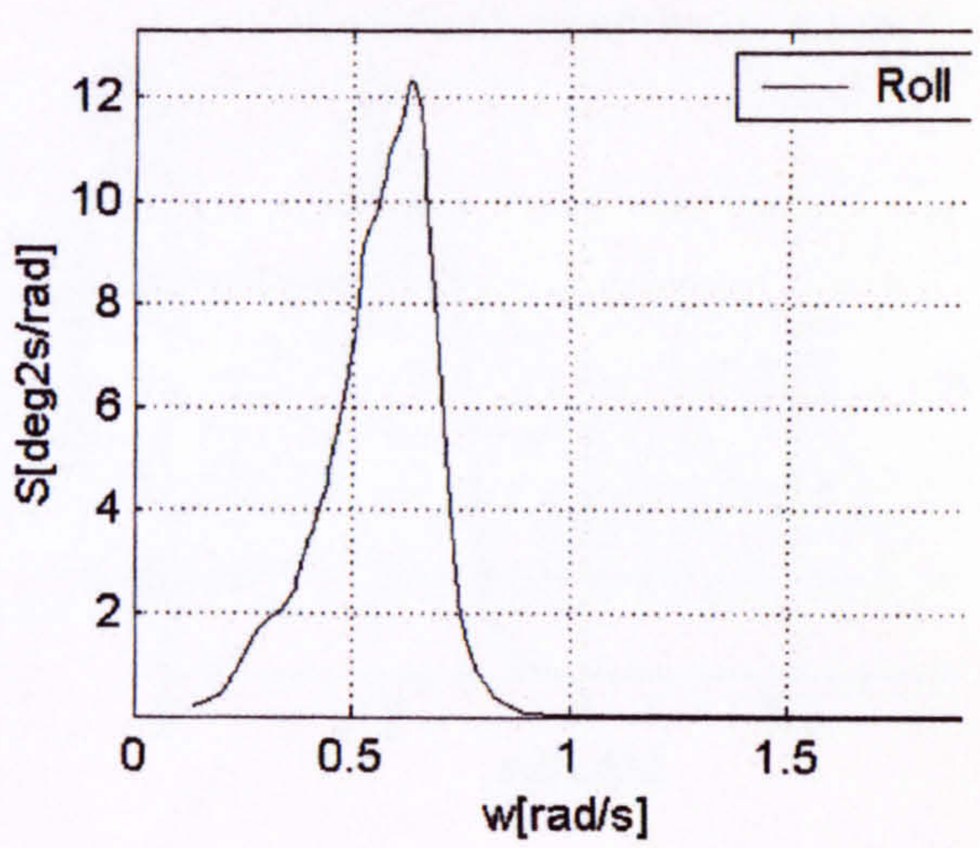

Figure 39 Numerical simulations, PRR1, KG=12.892m, Hs=5.00m

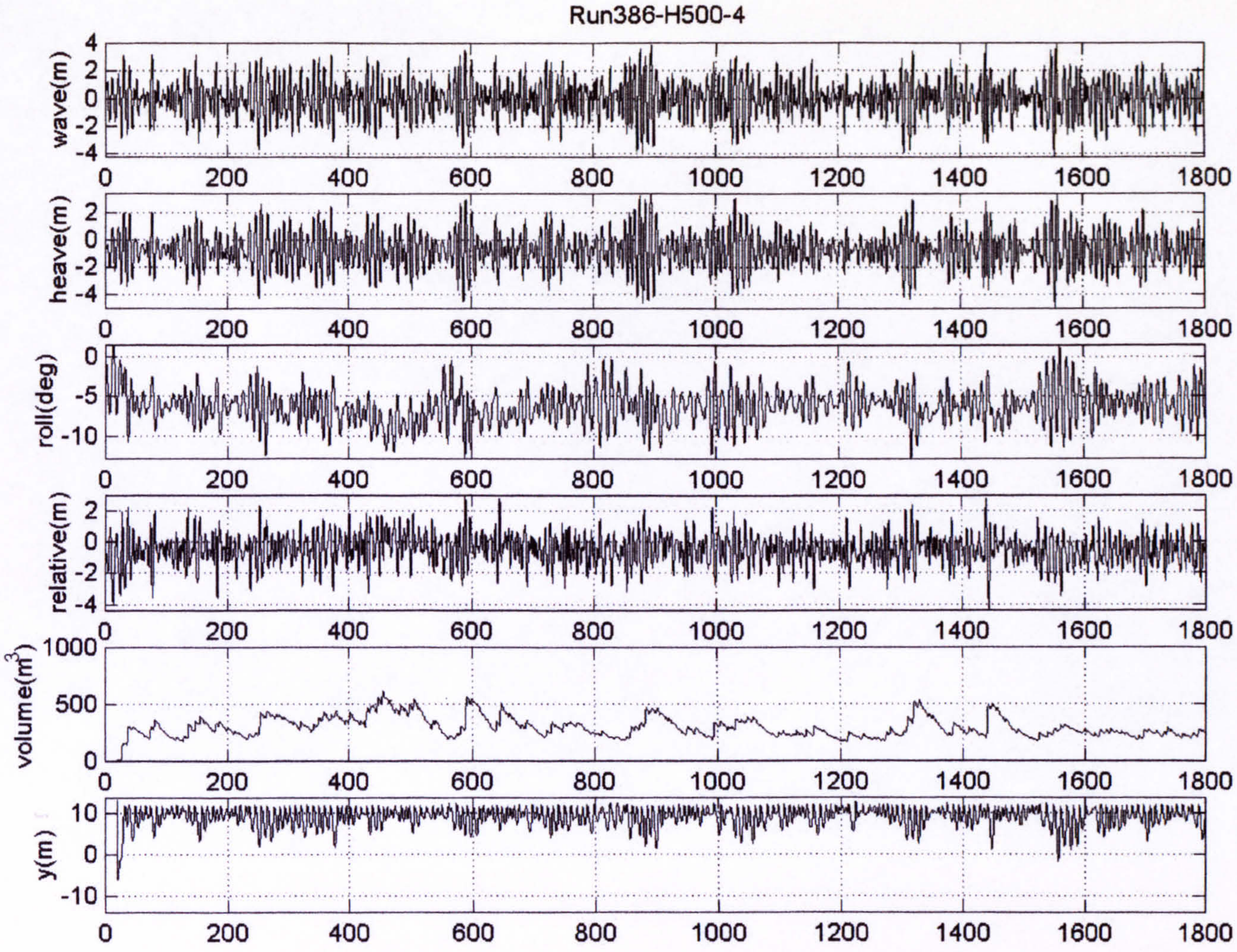

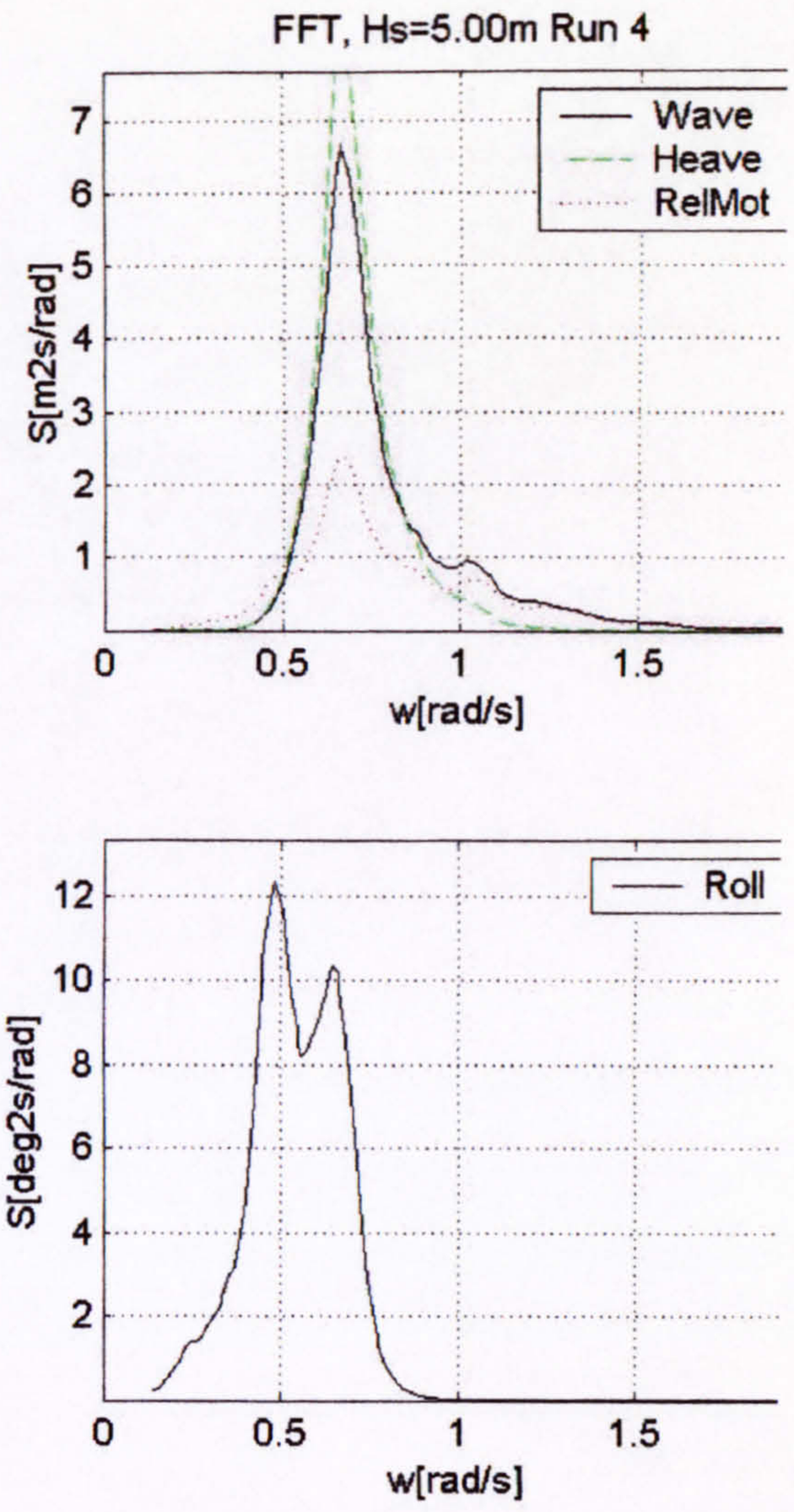

Figure 40 Numerical simulations, PRR1, KG=12.892m, Hs=5.00m

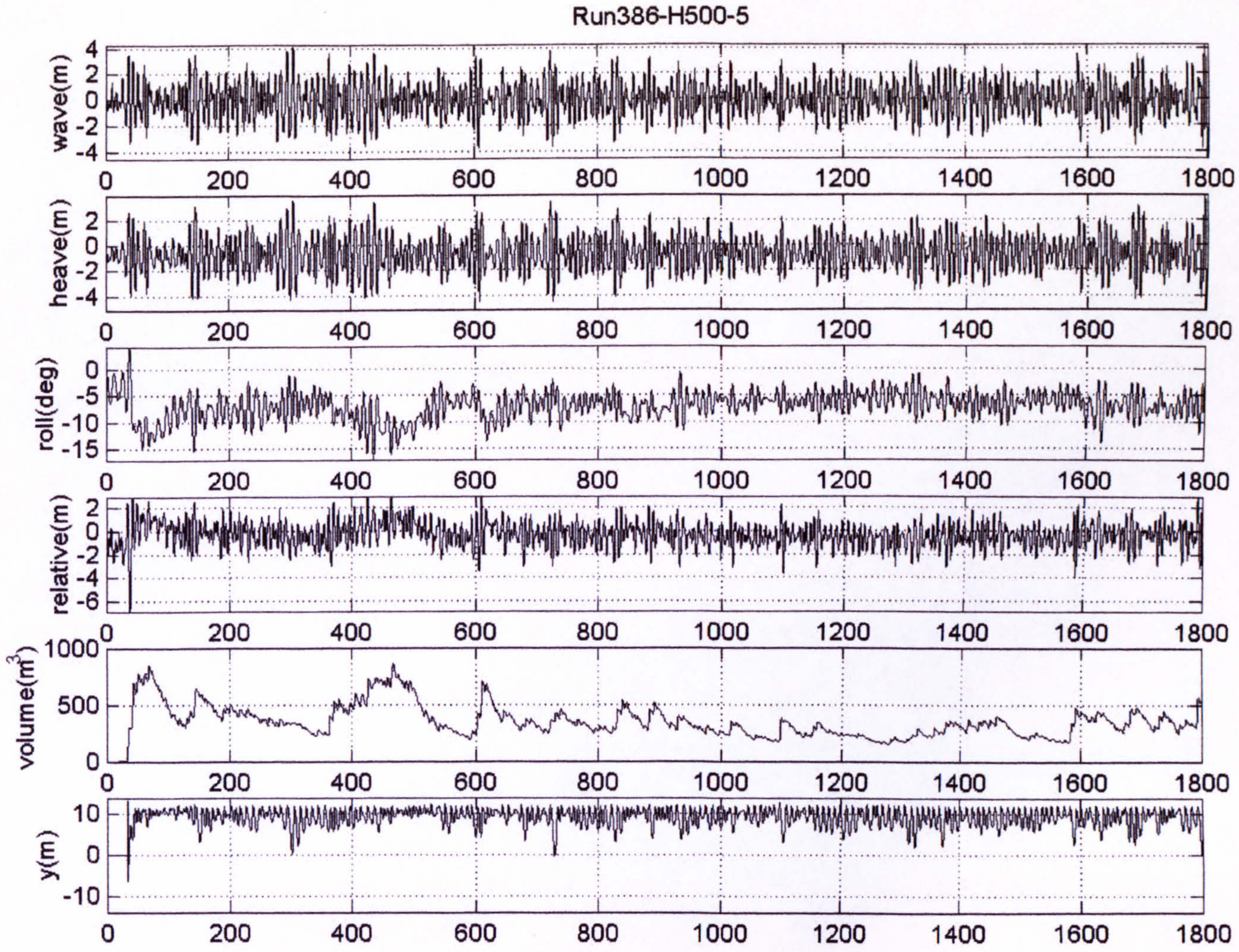

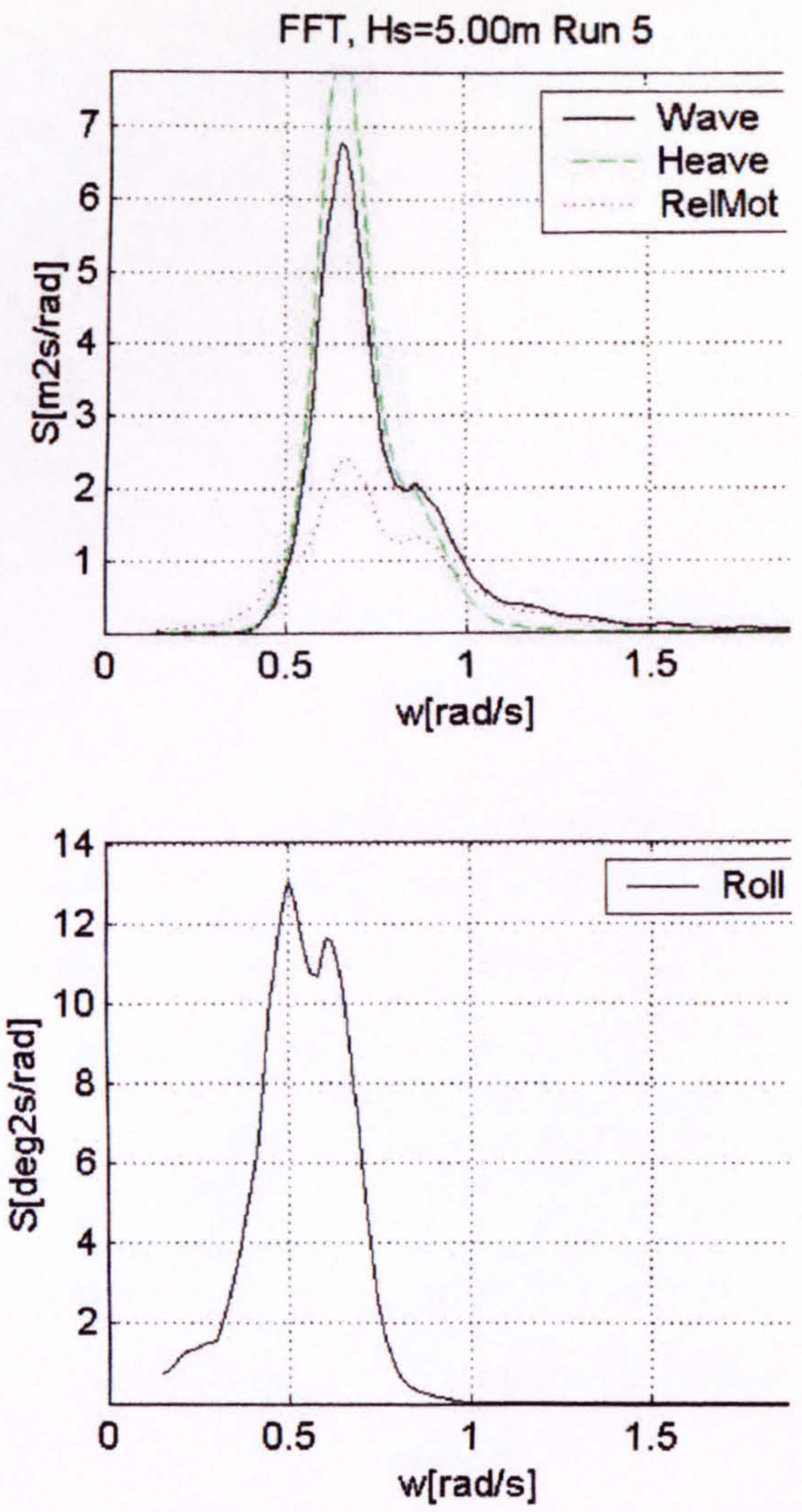

Figure 41 Numerical simulations, PRR1, KG=12.892m, Hs=5.00m

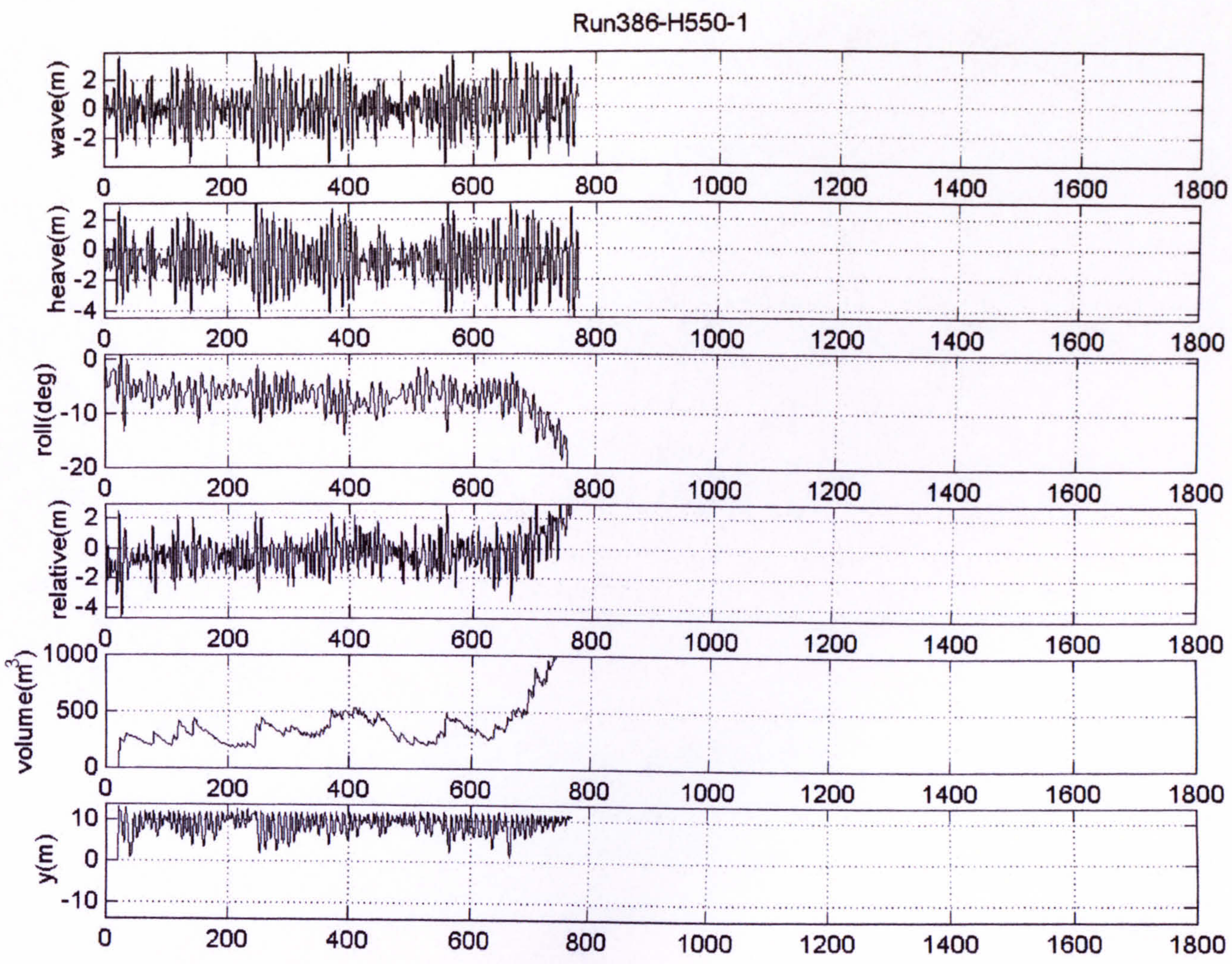

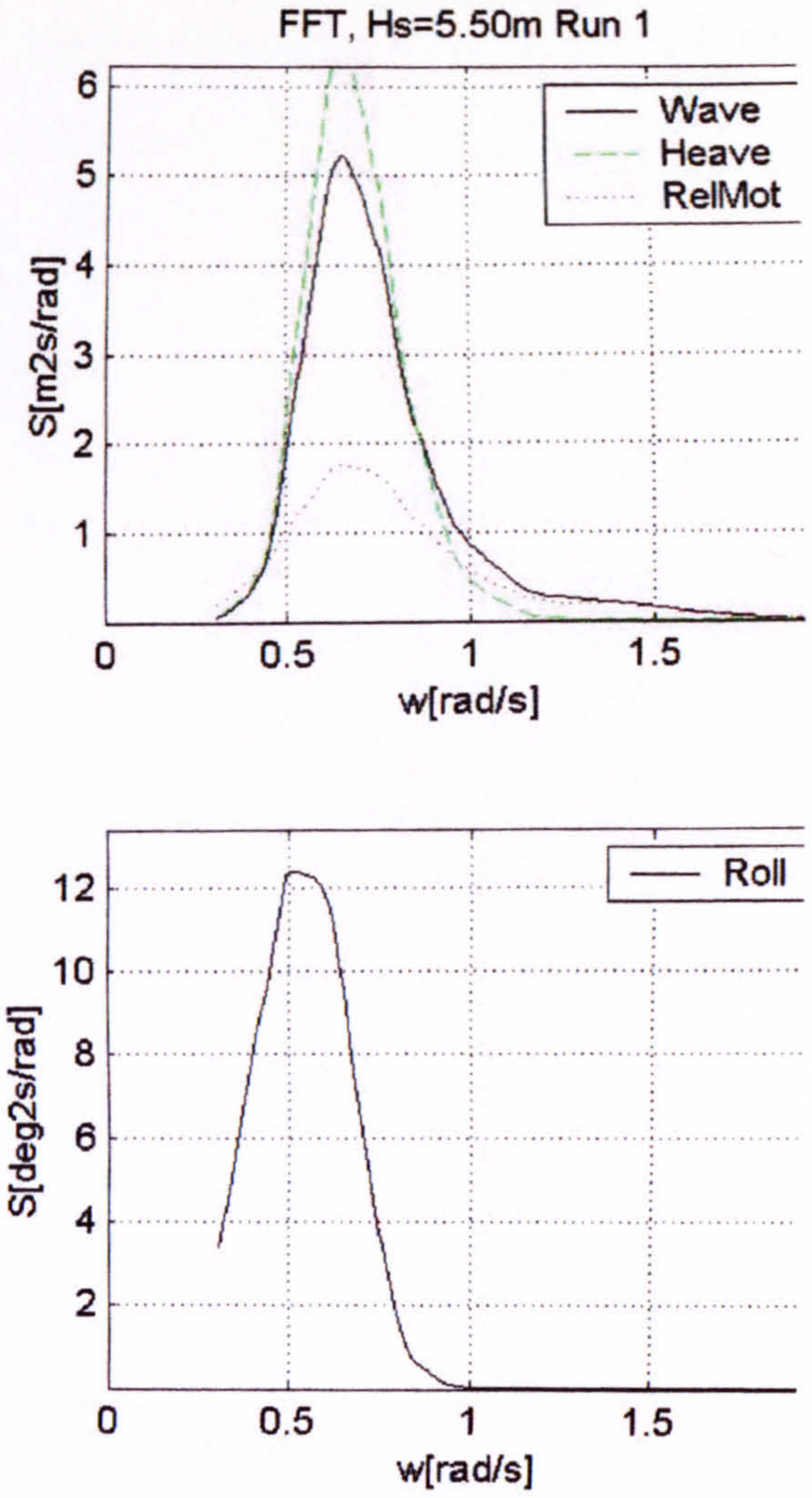

Figure 42 Numerical simulations, PRR1, KG=12.892m, Hs=5.50m

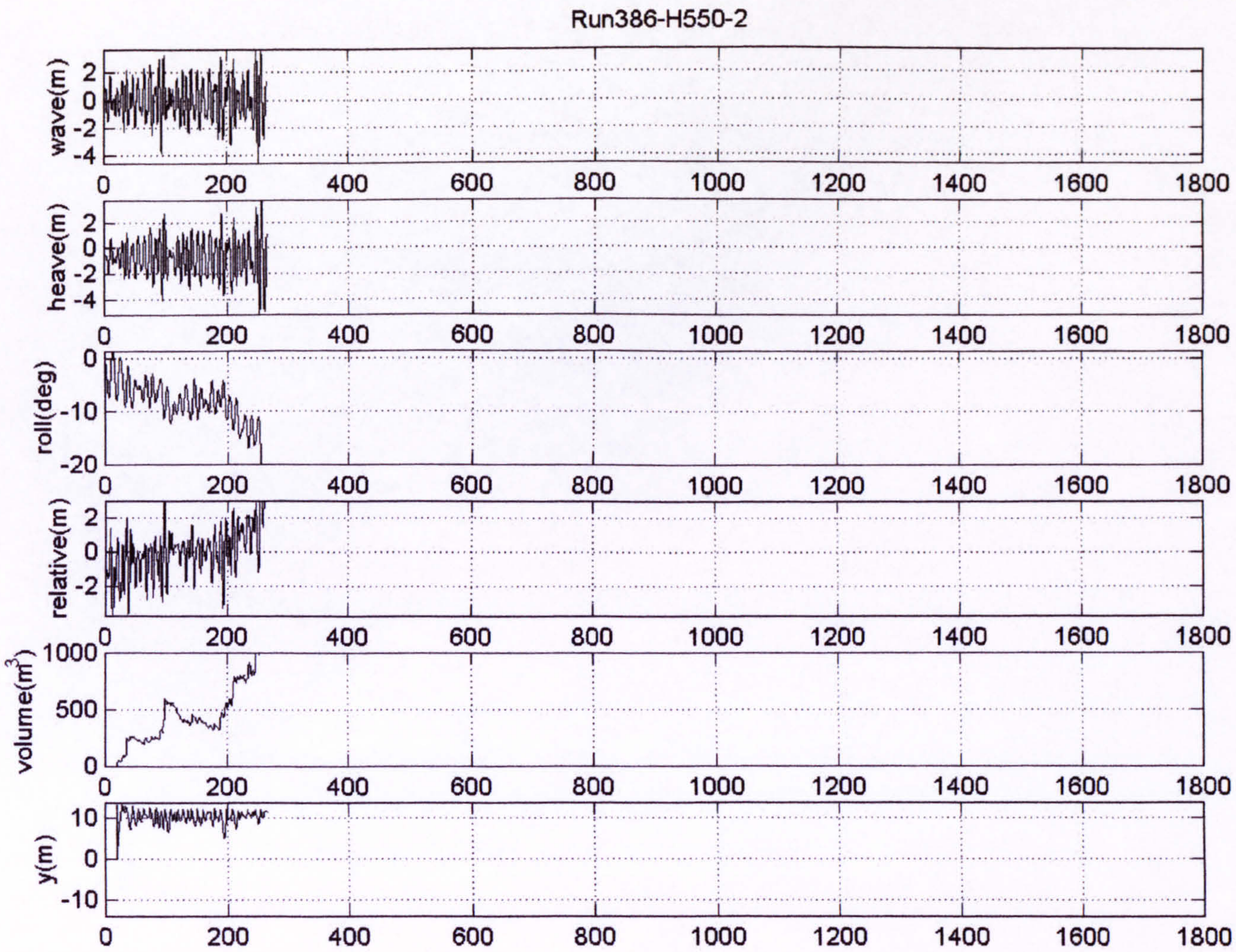

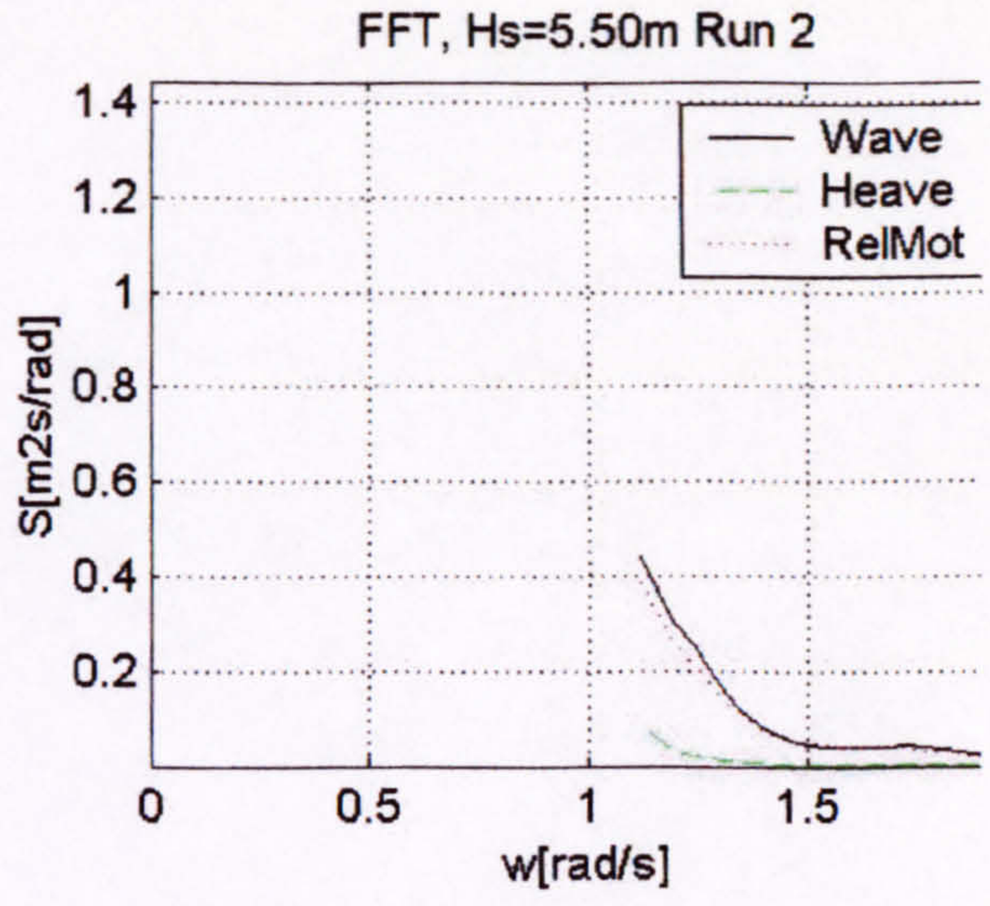

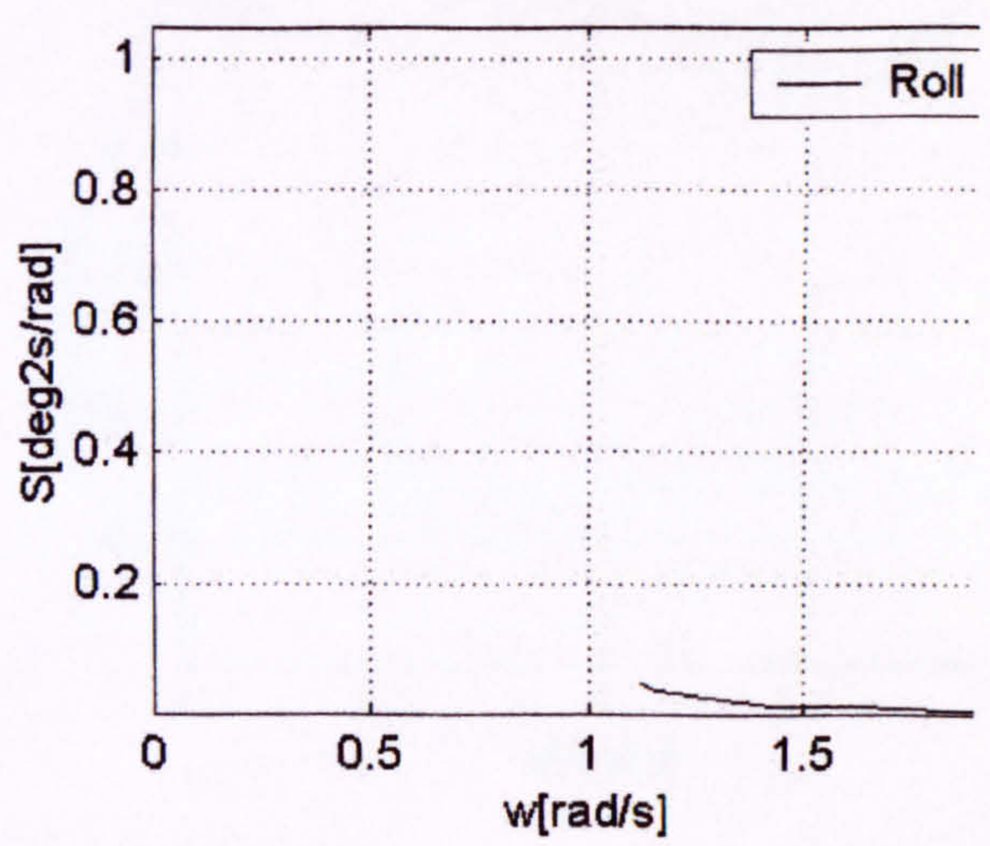

Figure 43 Numerical simulations PRR1, KG=12.892m, Hs=5.50m

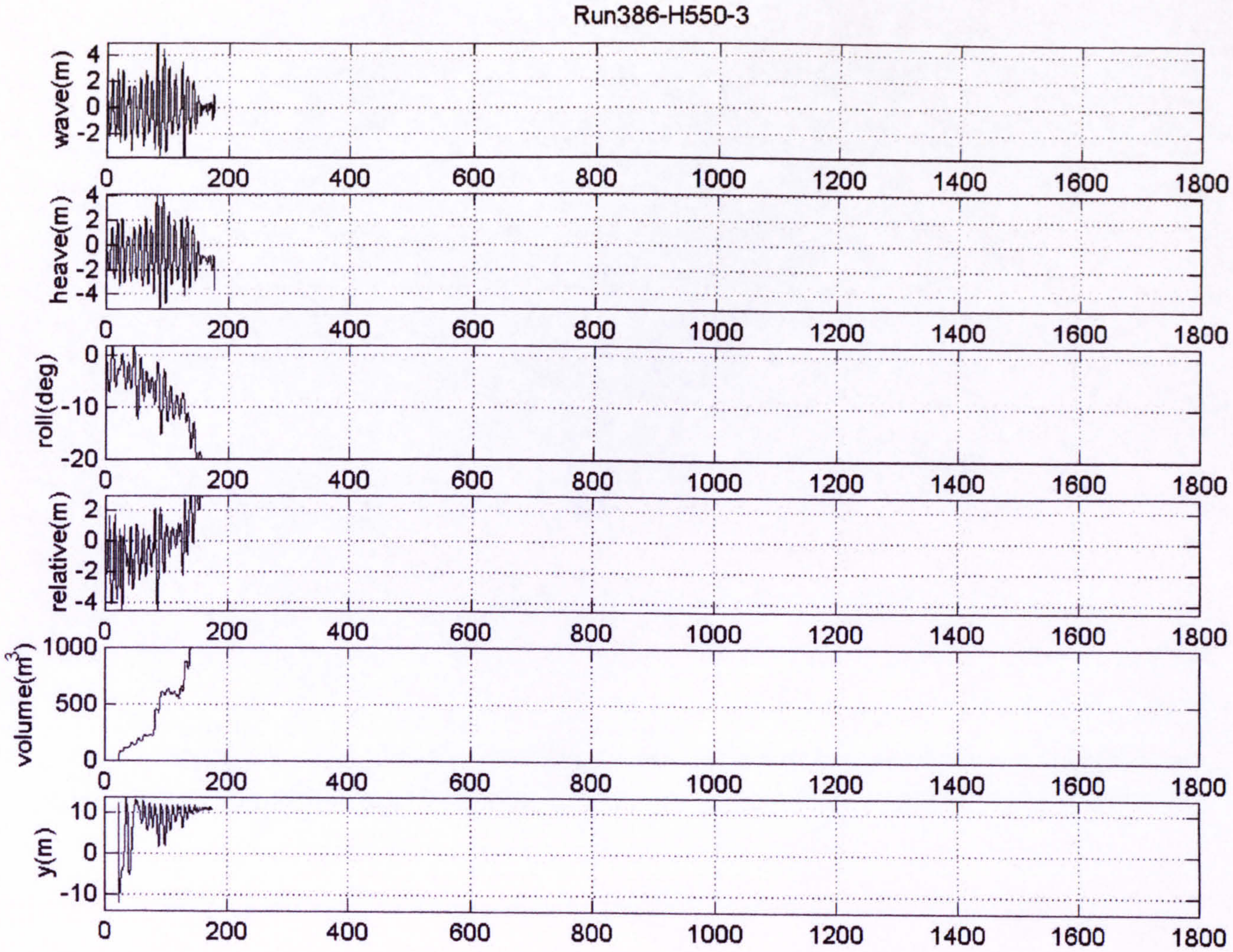

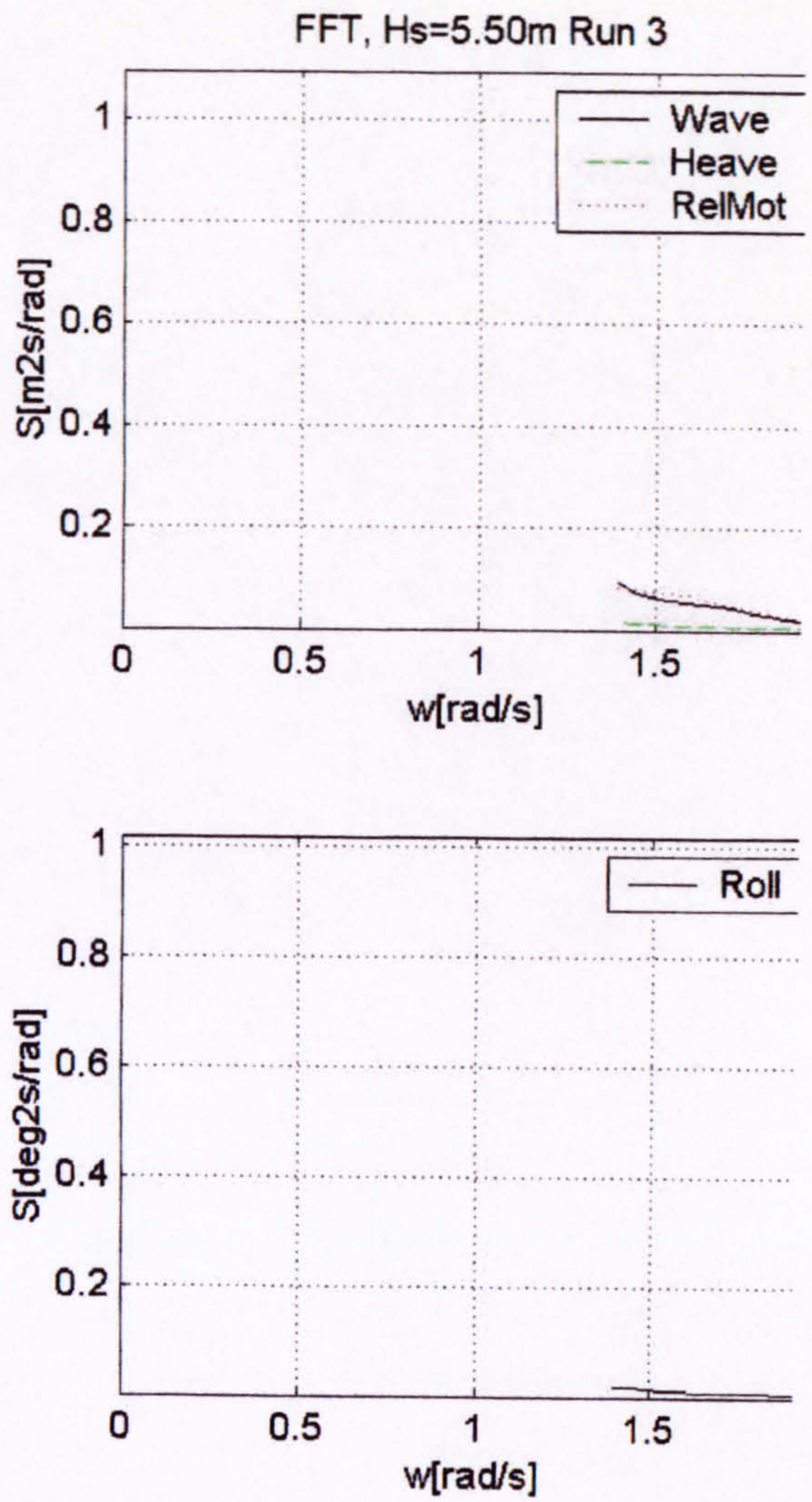

Figure 44 Numerical simulations PRR1, KG=12.892m, Hs=5.50m

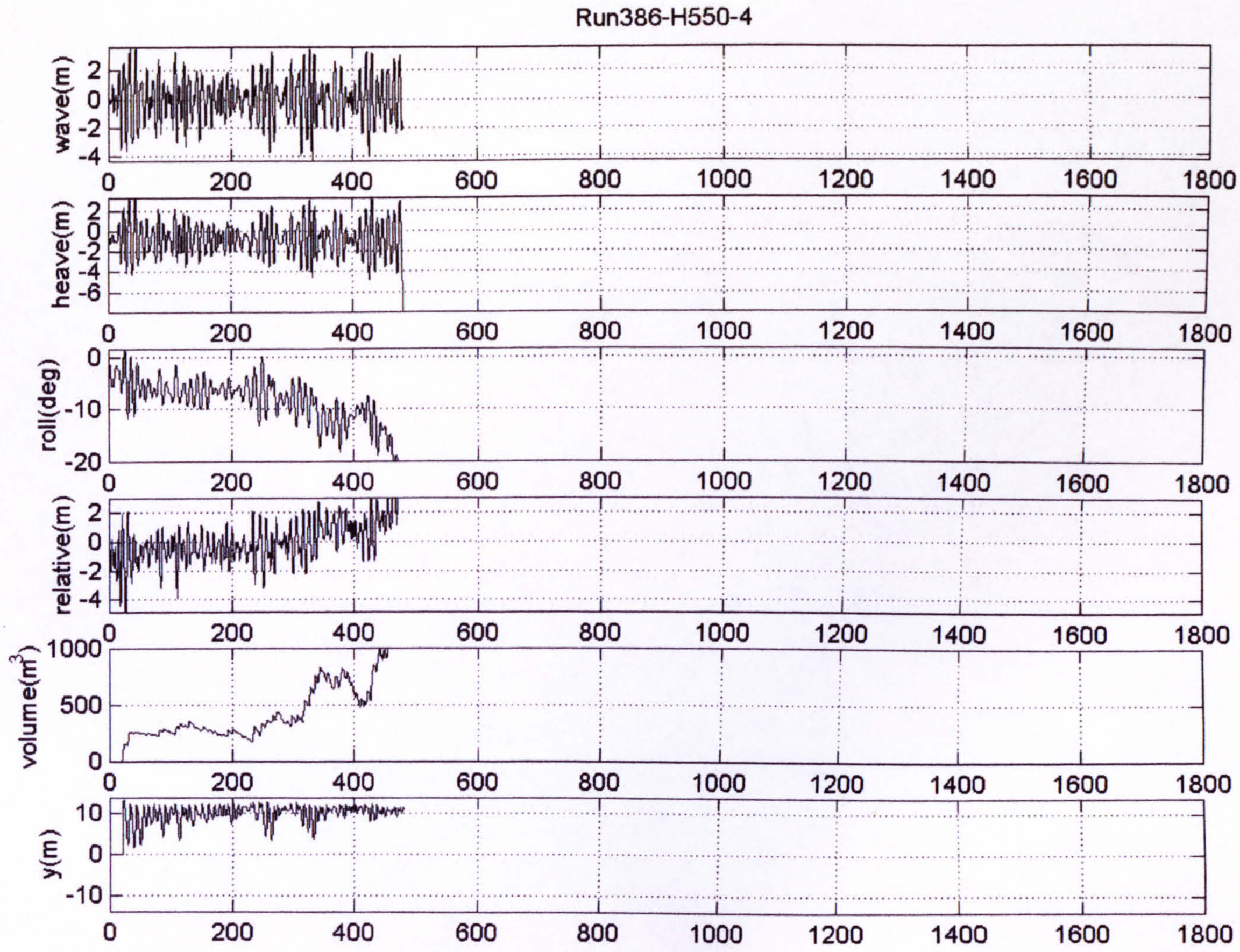

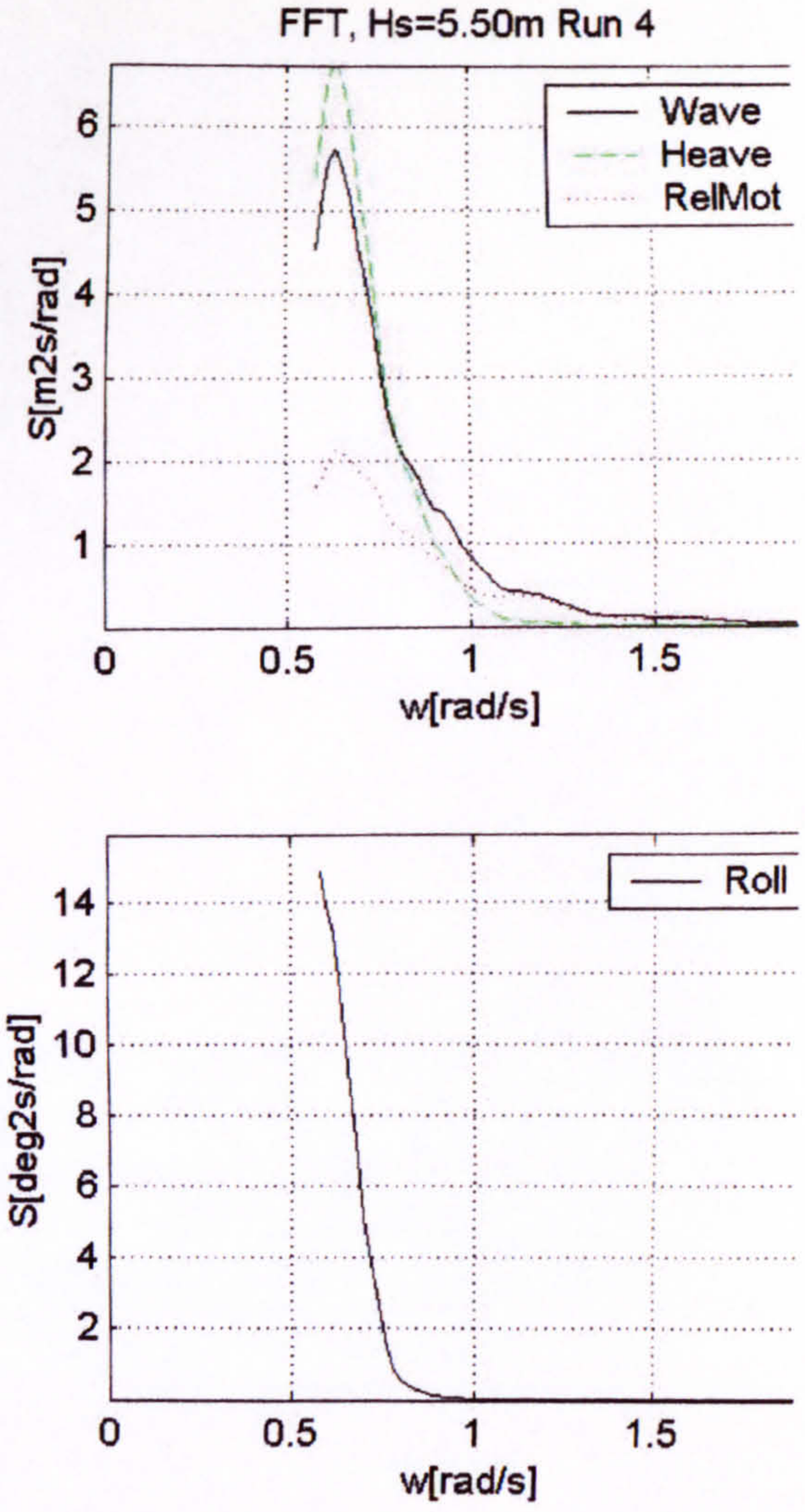

Figure 45 Numerical simulations PRR1, KG=12.892m, Hs=5.50m

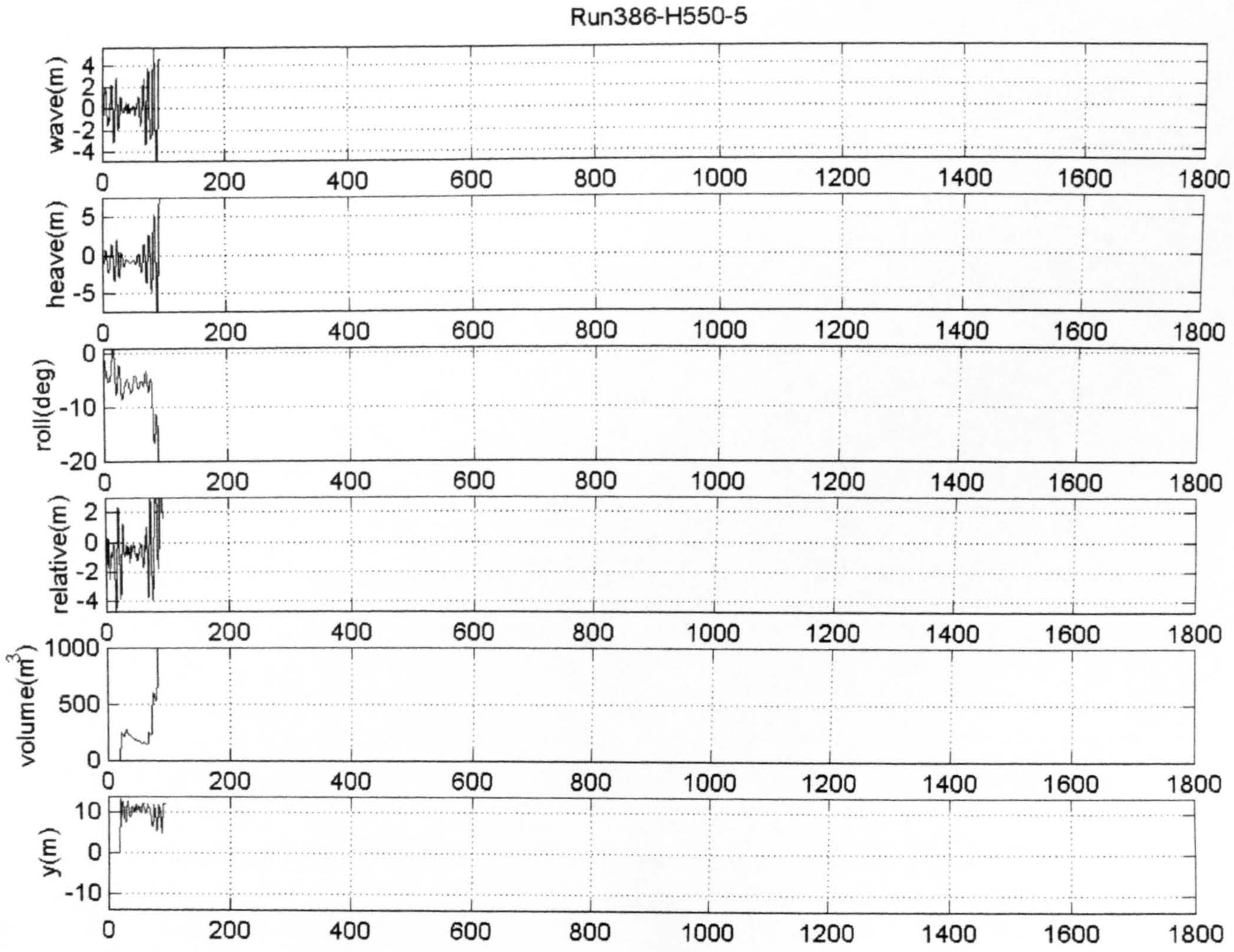

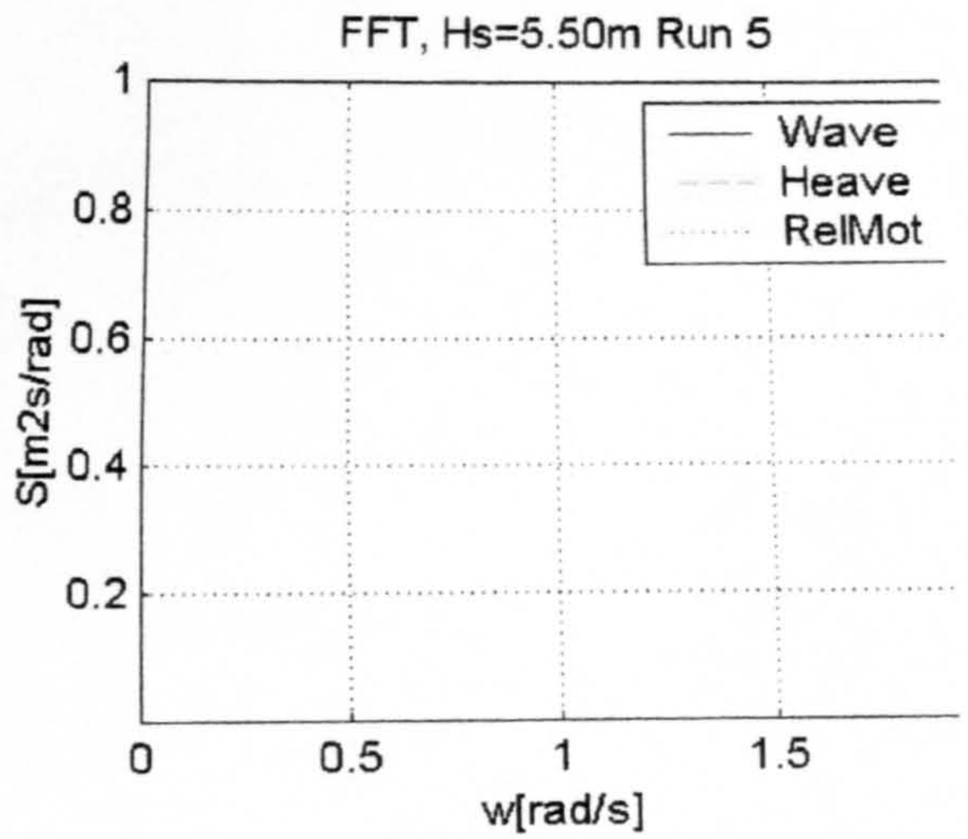

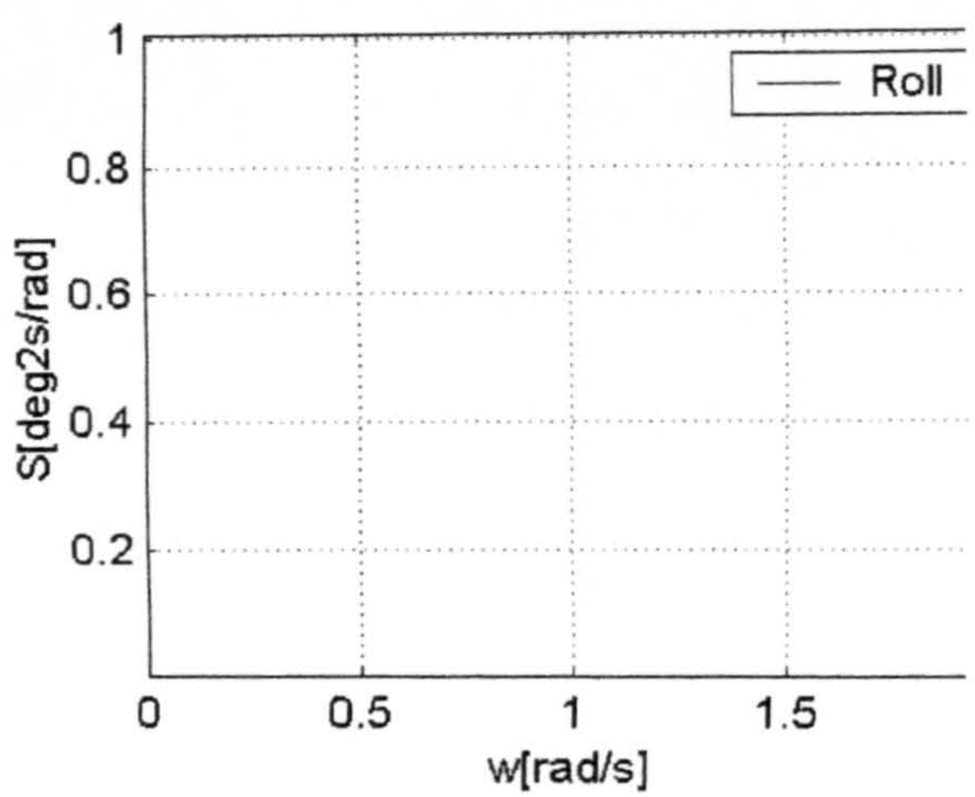

Figure 46 Numerical simulations PRR1, KG=12.892m, Hs=5.50m